Appendix A

APPENDIX A

A summary of drilling, geophysical testing, and seismic monitoring activities at the Moodus borehole site.

MOODUS BOREHOLE TASK DESCRIPTIONS

INTRODUCTION

As part of a continuing program to study crustal stresses and their relation to earthquake generation, a 1.5 km borehole was drilled near Moodus in central Connecticut. This program was established by the Empire State Electric Research Corporation, and for this project, co-sponsored by Northeast Utilities and the Electric Power Research Institute. The primary goal of the project was to determine the state of stress in southern New England by using the hydraulic fracturing technique and through analysis of borehole breakouts. Knowledge of the state of stress was expected to allow testing of hypotheses concerning the spatial distribution of domains in which the orientation of the stress field was uniform.

The project consisted initially of two phases. First, a borehole was drilled to a depth of 1.5 km in the crystalline rocks of the Moodus area. The resulting well is probably the deepest to be drilled in New England. Second, an extensive suite of geophysical surveys was run in the borehole, and hydraulic fracturing tests were conducted. at the end of the geophysical testing phase, an earthquake swarm began less than 0.5 km from the borehole. This prompted the research program to be expanded to take advantage of this unusual opportunity. A third phase was initiated in which the earthquake swarm was monitored for a five-week period.

This appendix provides an overview of the three phases of the Moodus project. First, the drilling activities are summarized. This is followed by a description of the geophysical surveys and hydraulic fracture testing. Finally, the seismic monitoring effort is briefly described.

BOREHOLE DRILLING: PHASE 1

The Moodus borehole is located in Middlesex county, Connecticut at 41° 31.68' N latitude and 72° 26.56' W longitude (Figure A-1). The site is in a small sand and gravel pit, about 3 km north of the town of Moodus on property owned by Mr. John Dill. The site was selected because of its location in southern New England, the results of previous stress measurements in the area, and for its proximity to the epicentral region of recent earthquake swarms.

The borehole was drilled by Warren George, Inc. using air-rotary equipment and percussion hammerbits. Drilling began on 21 March 1987 and ended on 12 June 1987. The borehole has a nominal diameter of 165 mm (6.5 in), and reached a final depth of 1.49 km (4,874 ft). Nine runs of 3 m (10 ft) core were recovered from the borehole at approximately 0.15 km (500 ft) intervals.

Drilling Equipment

A Schramm model "T64H-B Rotadrill" rig with a truck-mounted 425 cubic-feet per minute (cfm)/250 pounds per square inch (psi) compressor was used for drilling and coring. In addition, as drilling progressed, an auxiliary 850 cfm/350 psi Schramm air compressor, an Ingersoll-Rand 755 cfm/355 psi air compressor, and a Joy W12B booster were used to deliver the air pressure needed to drive the hammer bit and to clean the borehole of rock cuttings.

The drill string was composed of several elements to help ensure the borehole remained vertical. The bottom of the string consisted of the hammerbit with a stabilizer collar and two 20-foot-long stabilizer rods. The stabilizers were constructed to inhibit deviation of the bit from a vertical direction. The rest of the drill string consisted of 20-foot-lengths of nominally 4-inch (outside diameter) drill pipe.

Cores were recovered with a 10 ft core barrel of 3 in inside diameter. The entire drill string was needed during coring operations since the core barrel was not a wire-line tool, but rather attached to the drill pipe. Thus, to perform a single core run, the drill string was first pulled and the core barrel attached to the bottom of the string. The string was then lowered and core was drilled. When coring was finished, the string was pulled once more to recover the core. Finally, the string was again lowered with a new hammerbit to continue drilling. These tasks became more time-consuming as drilling depths became greater. The importance of the core to understanding and interpreting the borehole logging data, however, justified the time and expense of periodic rock sampling.

Hole Deviation Surveys

Borehole verticality is important to a hydraulic fracturing experiment because the technique assumes that one of the principal stress directions is vertical. If the borehole is not plumb, this assumption is violated. In addition, many geophysical logging tools cannot operate in a borehole that has a large inclination. Thus, borehole deviation surveys were run at frequent intervals, and corrective actions were implemented if the inclination grew larger than a few degrees.

During drilling, a single-shot Pajari model compass/inclinometer was used to monitor deviation. After completion of the borehole, a Schlumberger wireline compass/inclinometer was used in the borehole. Data from both tools are in good agreement and show that the borehole deviated less than five degrees from vertical.

During drilling, the borehole migrated consistently to the northwest. For depths ranging from 355 to 2,435 ft, the borehole drifted within the azimuth range of 312 to 356 degrees. Below 2,500 ft, the direction of borehole migration stayed within a few degrees of 320 degrees (Table A-1). The slight inclination of the borehole results in the bottom of the well being about 290 ft northwest of its top

(Figure A-2). The northwest direction of migration has no apparent relation to any rock fabric mapped in the borehole. The cause of the consistent drift direction is unclear.

Technical Difficulties

The Moodus research borehole is the deepest to be drilled in the crystalline rocks of New England. Problems associated with a hole of this type were mostly anticipated because of experience in drilling a similar hole at Kent Cliffs, New York. The drill-string hardware was carefully customized to extend bit-life and to minimize bit wandering. Stabilizer wear was monitored to ensure drilling was proceeding smoothly. Minor hardware problems and breakdowns were dealt with quickly, and delays related to them were minimal.

The only major problem during drilling occurred at a depth of 1.07 km (3,500 ft). At that depth the borehole intersected a fracture, or set of fractures, that produced water at an estimated rate of about 150 gallons per minute. This rate of water production was too great to be blown out of the borehole, and when the water pressure exceeded the pressure differential of about 300 psi that is needed to operate the hammer, the hammer stalled.

To alleviate this problem, the fractured interval was sealed and re-drilled. Cement was pumped down the drill-string and allowed to set for several days. The cement was then drilled until bedrock was again reached. At that point no further water entered the hole so drilling proceeded. No other major fracture zones producing large volumes of water were encountered.

Drilling Chronology

The following is a brief chronology of drilling activities for the Moodus Borehole Research Project:

On 23 December 1986, a Failing model 1500 drill rig was mobilized to the site. Overburden, consisting of sands, gravel, and boulders, was penetrated to a depth of 11 m (36 ft) at which point competent bedrock was reached. To confirm and analyze the nature of the bedrock, a 2.3 m (7.5 ft) core was taken.

Following the Christmas holidays, the borehole was reamed with a 12 in bit, and 10 in casing was installed through the overburden to the top of bedrock. The top of the well was capped and secured. Drilling activities were then suspended for several months because of adverse weather and site conditions.

Drilling resumed on March 23 1987. The borehole was extended to 14.3 m (47 ft), and 8 in casing was installed. Subsequently, a borehole deviation survey indicated that the hole was not plumb. Rather than trying to modify the existing hole, it was decided to abandon the first hole and start a new one.

The new borehole reached a depth of 152 m (500 ft) on 10 April 1987. In the upper 30 m (100 ft), 8 in casing was installed. At a depth of 152 m (500 ft), the first core was recovered. Drilling proceeded over the next week until a depth of 457 m (1,500 ft) was obtained. At this depth the second core was taken. Drilling activities were then suspended for several days over the Easter holiday.

After the break, drilling resumed and proceeded smoothly. By 1 May 1987, a depth of 610 m (2,000 ft) had been reached, and two more cores recovered. By May 11, the borehole was at a depth of 914 m (3,000 ft), and the fifth and sixth cores had been recovered. One week later the borehole reached 1,067 m (3,500 ft) and the seventh core was taken.

At this point in the drilling, a highly conductive fracture or fracture set was intersected. The water produced into the borehole stalled the hammer. It was necessary, therefore, to seal the water-bearing zone. About 4.5 m^3 (1,200 gallons) of cement were pumped through the drill-string to the fractured interval. After allowing the cement to set for several days, approximately 150 m (500 ft) of cement was reamed. Drilling continued in bedrock on 23 May 1987.

On 5 June the borehole reached 1,219 m (4,000 ft) and the eighth core was obtained. One week later the borehole reached 1,402 m (4,600 ft) and the ninth and final core was taken. Drilling continued to a depth of 1,458 m (4,784 ft) on the following day. At this point, technical requirements for the borehole had been fulfilled. Drilling activities were terminated to accommodate scheduling constraints for the geophysical logging and hydraulic fracturing experiments. On 13 June 1987, the drill rig was demobilized, and preliminary geophysical surveys started.

GEOPHYSICAL TESTING: PHASE 2

A comprehensive suite of geophysical data was recorded in the Moodus borehole by Schlumberger Wireline Services, the Lamont-Doherty Borehole Research Group, and Schlumberger-Doll Research. The data include analog and digital borehole televiewer logs, multichannel sonic logs, formation microscanner logs, natural gamma logs, density and neutron porosity logs, dual laterologs, geochemical logs, temperature logs, caliper logs, and digital borehole deviation logs.

Hydraulic Fracturing Test Equipment

In the hydraulic fracturing method of stress measurement, an interval of the borehole is isolated and hydraulically pressurized until a fracture is induced in the borehole wall. Preliminary televiewer logs are used to identify intervals that are unfractured prior to testing so that the test will create a new fracture, not open a pre-existing fracture. For these tests the borehole interval was isolated by inflatable straddle packers. The packers consisted of two inflatable elements, top and bottom, that were separated by an approximately 1.5 m (4 to 5 ft) interval. When the elements were inflated, they formed a tight seal with the borehole wall, and isolated the interval from the rest of the borehole. Packers manufactured by Tam International were used in the Moodus experiment.

The orientation of the mimimum compressive stress is determined from the orientation of the hydraulically induced fracture. The fracture will open up perpendicular to the direction of minimum compressive stress. Impression packers are one method used to determine the orientation of the induced fractures. The impression packer consists of a single inflation element that is wrapped with soft rubber. When the packer is lowered in the borehole and the element inflated, the soft rubber coating is impressed into the sides of the borehole. The packer is then deflated and recovered. The impressions made in the soft rubber by the features of the borehole wall can then be studied to learn their orientation. It is also hoped that the packer will leave some of its soft rubber in the induced fractures so that their contrast and visibility during subsequent televiewer logging will be enhanced. The televiewer records are also used to study the orientations of the induced fractures.

The straddle and impression packers were connected to 9 to 10.5 m (30 to 35 ft) lengths of high-pressure tubing. As the string was lowered to the desired depth interval, additional lengths of tubing were added. When the proper depth was reached, the packers were inflated. Then the entire hydrofrac string was pressurized using a water-oil fluid and high-pressure pumps.

Testing Chronology

Geophysical logging surveys began on 13 June 1988. A borehole televiewer (BHTV) log was recorded immediately after drilling to determine the extent of borehole spalling (breakouts) and to identify unfractured intervals that would be suitable for the hydraulic fracturing tests.

Borehole surveys were then temporarily suspended to analyze the BHTV data for fracture densities and distributions, breakout distribution and orientation, and for preliminary estimates of in-situ stress orientation. Borehole surveys resumed on 22 July 1987. Schlumberger Wireline Services and Schlumberger-Doll Research

began a full suite of geophysical logs. Logging continued on a 24 hour basis and ended on 26 July.

Hydraulic fracturing experiments began on 27 July 1987. By the following day 4 successful hydraulic fracturing tests were completed at depths ranging from 107 to 192 m (350 to 630 ft) and at breakdown pressures of 2,000 to 5,000 psi. On the fifth test at a depth of 360 m (1,180 ft), the inflation element on the bottom packer ruptured at a pressure of nearly 6,000 psi.

On 29 July, the hydrofrac string developed a leak during the sixth test at a depth of 619 m (2,030 ft). The rest of the day was spent pulling the string and searching for the leak. On the following day the packers were lowered to a depth of 447 m (1,465 ft). The interval was pressurized to about 6,000 psi but the rock did not fracture. The pressure was held for a half an hour but the rock still did not fracture. This test was then abandoned to avoid damaging the equipment. The packers were lowered to a depth of 853 m (2,795 ft) and a fracture was induced at a pressure of 2,500. This test, however, did not provide useful data because the low breakdown pressure indicated that a horizontal fracture (as opposed to a vertical fracture) was induced. Horizontal fractures only provide information about the lithostatic pressures (weight of the overburden) and little about tectonic stresses.

On 31 July three successful tests were made spanning a depth range of 820 to 1,070 m (2,700 to 3,500 ft) and at pressures ranging from 4,300 to 5,700 psi. These were the ninth, tenth, and eleventh tests, respectively.

On 2 August, after a day of equipment maintenance, a fracture was successfully induced at a depth of 819 m (2,688 ft). Here, the interval was pressurized to 6,000 psi, but the rock did not rupture immediately. The pressure was then reduced and cycled back up to 6,000 psi. After a few seconds of pressure diffusion, the rock finally broke. The packers were then going to be lowered to a depth of 1,370 m (4,500 ft) for the next test, but as the string was being lowered,

the packers became stuck at a depth of 1,356 m (4,450 ft). Efforts to move the string either up or down were unsuccessful.

For the next several days, efforts were made to pull the string out of the hole. When this failed it was decided to attempt a hydraulic fracturing test. This test failed because the packers apparently could not be inflated properly and fluid leaked out of the fracture interval. It was then decided that the most expedient method to extract the string would be to use an explosive charge to cut the high pressure tubing at the connection with the packer.

On 8 August 1987, a Schlumberger technician arrived on site and used a "tube-cutter" explosive that separated the tubing from the top of the packer. Consequently, the packer was left in the borehole; the top of the packer is at a depth of 1,353 m (4,438 ft) and the lower section of the borehole is presently not accessible.

After a brief suspension of activities, borehole-impression surveys were run from August 20 to August 23. The impression packer was lowered to the depths of the induced hydraulic fractures to attempt to impress some of the soft rubber into the fractures. During the next two days, the LDGO Borehole Research Group televiewered the borehole to locate and orient the induced fractures, and to check if further breakout development had occurred.

On 25 August, three additional hydraulic fractures were induced at depths ranging from 1,183 to 1,283 m (3,880 to 4,210 ft) and at pressures ranging from 3,000 to 5,500 psi. On 26 August, the packer was lowered to a depth of 1,109 m (3,640 ft) and inflated to a pressure of 5,500. Before a fracture could be induced, however, the bottom inflation element ruptured. It was then decided to conclude the hydraulic fracturing experiments. The next few days were spent in site demobilization and general clean-up activities. A summary log of the hydraulic fracturing tests is shown in Figure A-3.

SEISMIC MONITORING: PHASE 3

Approximately two weeks after the completion of the geophysical testing phase, another in the recurring series of earthquake swarms began at Moodus. This swarm initiated with a magnitude 2.3 (m_C) earthquake on 11 September 1987. Because of the goals of the Moodus Borehole Research Project, to measure tectonic stress at Moodus and relate it to the potential for earthquake occurrence, it was decided to expand the project to include monitoring of the new swarm.

The characteristics of past earthquake swarms suggested that activity would continue for an extended period of time. Thus, rather than quickly install an array of independent portable stations, a telemetered network was deployed. Data were radioed to the borehole site and recorded on magnetic tape along with a common time signal. This allowed accurate timing of seismic phase arrivals needed to determine accurate locations.

The array was installed beginning beginning five days after the initial event on 17 September 1987. Personnel worked through the night to deploy four stations so that preliminary locations could be determined. This information was then used to adjust the network configuration such that the region of activity was surrounded. The final network configuration consisting of eight stations was established on 1 October 1987.

The network operated continuously for five weeks. Over 160 earthquakes were recorded and located. The detection threshold within the array was about -2.0 (m_C). All stations monitored the vertical component of ground motion, except at the borehole site where a three-component seismometer was deployed. Network operation ended on 23 October 1987.

TABLE A-1

MOODUS, CT, BOREHOLE DEVIATION SURVEY
Schlumberger and Warren-George (Pajari readings)

All readings to true north

DEPTH (feet)	INCLINATION (degrees)	DEVIATION (degrees)	DEPTH (feet)	INCLINATION (degrees)	DEVIATION (degrees)
100 PAJARI	0	0	2500	4.3	320
200 PAJARI	1	005	2600	4.7	325
300	1.5	001	2700	5.0	325
355 PAJARI	1	344	2800	5.0	320
400	2.0	340	2800 PAJARI	5	331
497 PAJARI	2	347	2900	5.0	320
500	2.2	340	3000	4.8	320
600	2.4	340	3100	4.7	320
700	2.6	330	3200	4.6	320
740	2	356	3300	4.7	320
800	2.5	330	3400	4.8	320
900	2.2	320	3450 PAJARI	4	322
1000	2.5	320	3500	4.7	320
1000 PAJARI	2	329	3600	4.9	320
1100	2.0	320	3700	4.6	320
1200	1.5	320	3800	4.5	320
1200 PAJARI	1	334	3900	4.5	320
1300	1.6	317	4000	4.5	320
1400	2.0	312	4100	4.8	320
1500	2.0	325	4100 PAJARI	4	326
1500	2	356	4200	5.0	325
1600	2.5	340	4300	4.8	325
1700	2.6	340	4400	4.6	320
1700 PAJARI	1	335	4500	4.6	320
1800	2.8	340	4600	4.5	320
1900	3.0	335	4700	4.3	320
2000	3.0	335	4770	4.4	320
2000 PAJARI	2	341	end borehole 4784 feet		
2100	3.0	335			
2200	3.0	330			
2300	3.2	325			
2400	4.0	325			
2435 PAJARI	3	339			

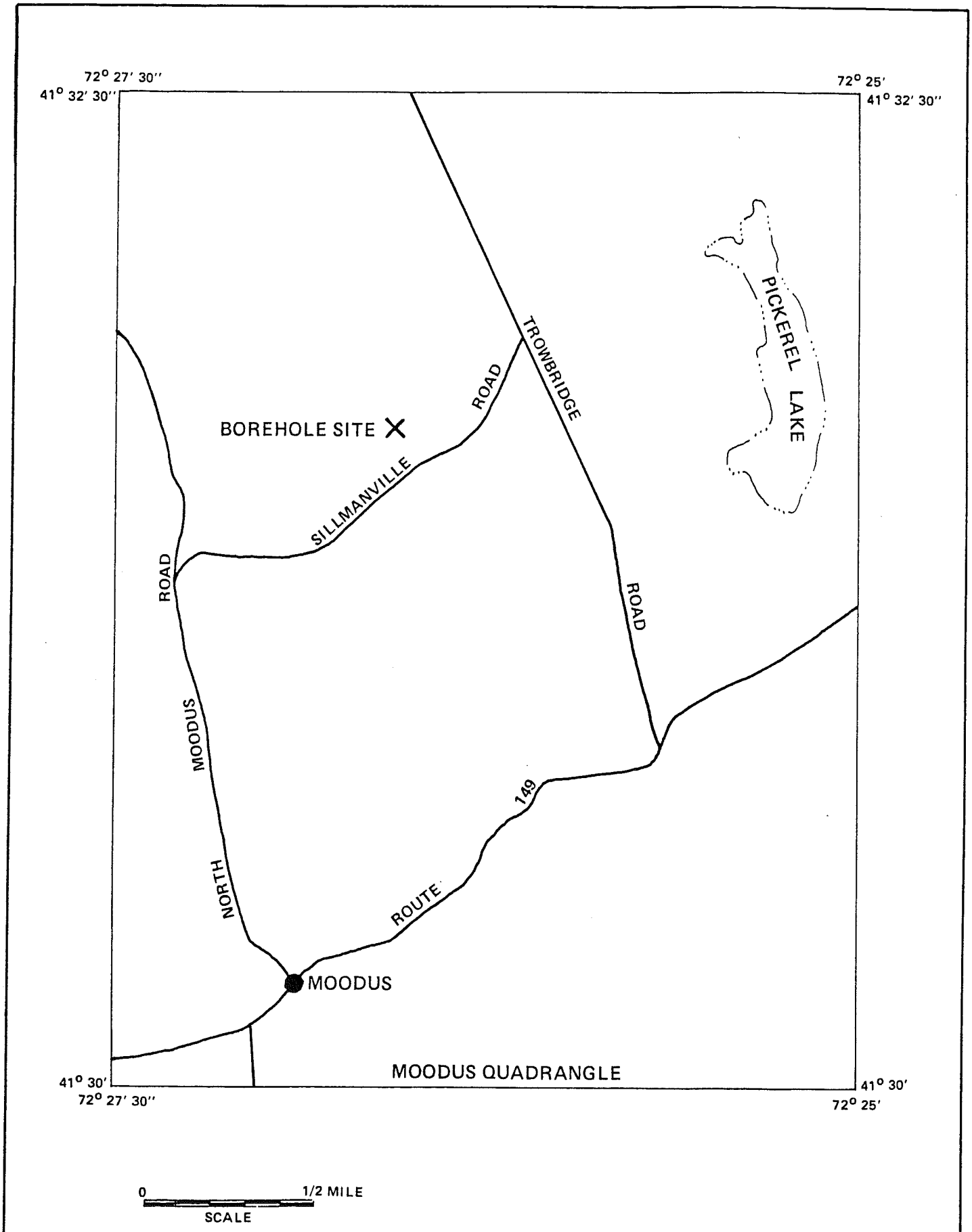

Figure A – 1 Site location map.

86C4111

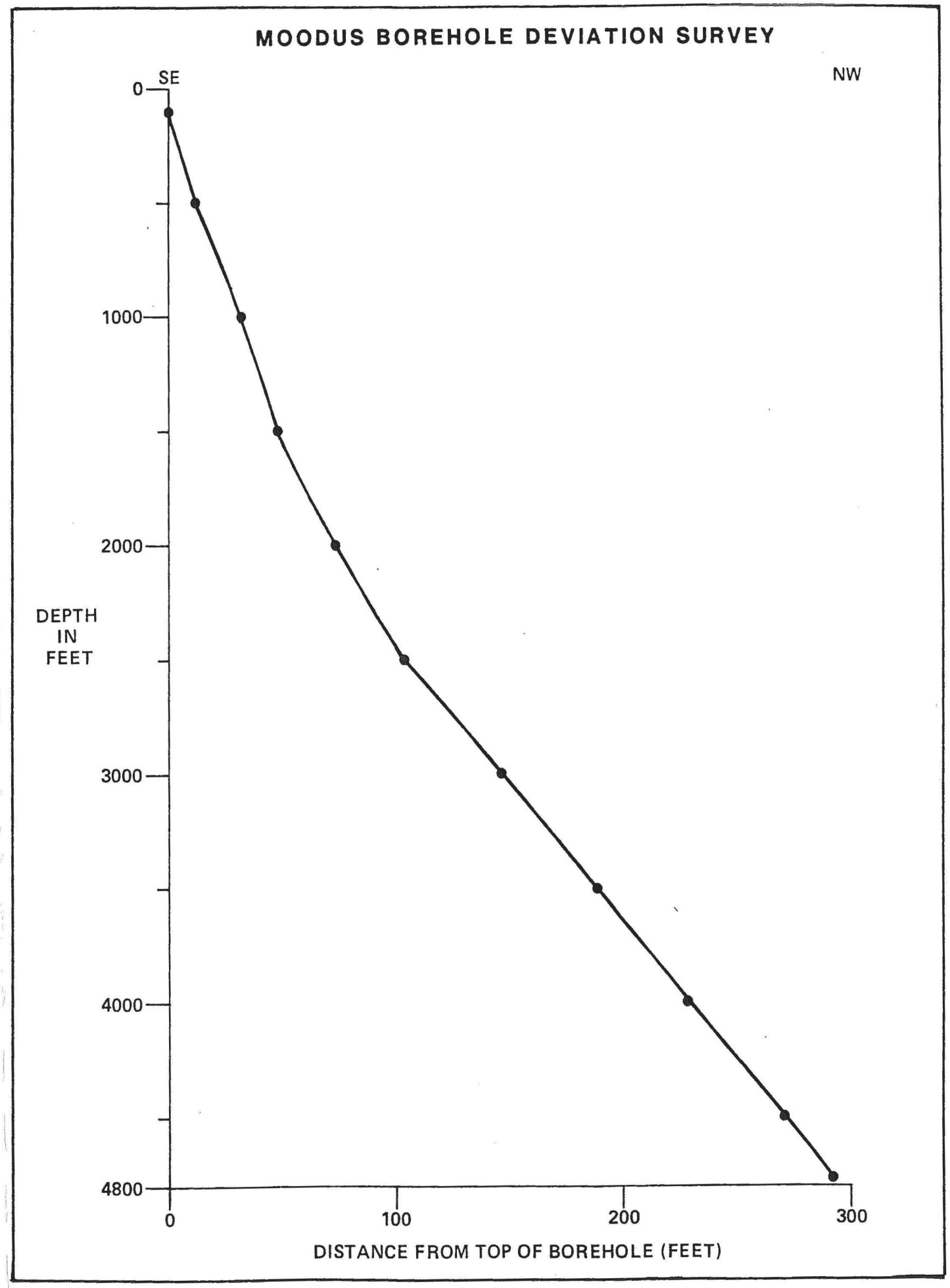

Figure A – 2 Borehole deviation survey.

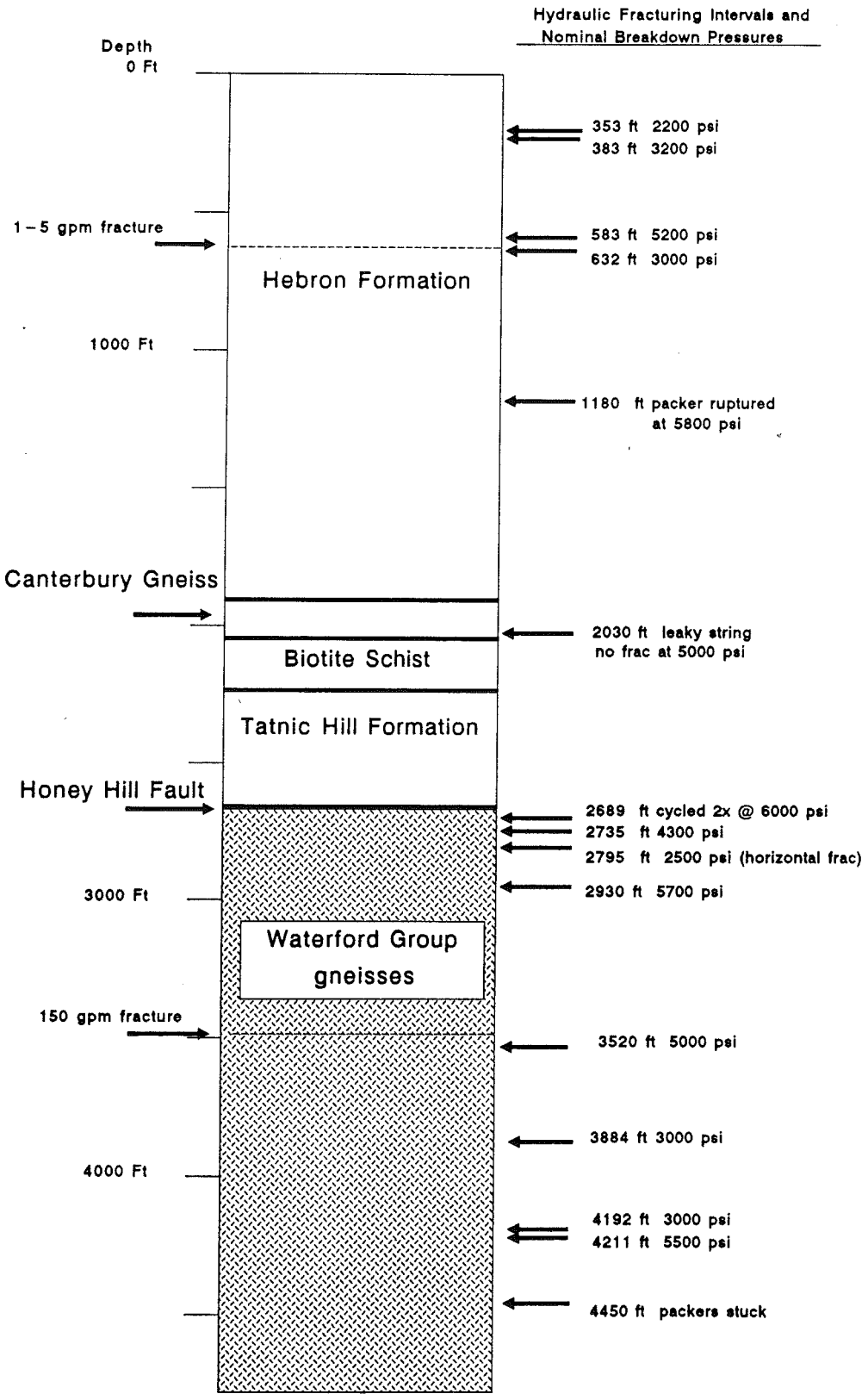

End Borehole 4,784 Feet

Figure A-3 Summary log of the hydraulic fracturing tests.

Appendix B

APPENDIX B

Results of the rock chip, rock core, and thin section analyses. Samples of rock chip, selection sections of core, and thin sections are archived at Woodward-Clyde Consultants, Wayne, N.J.

BOREHOLE GEOLOGY

SECTION 1
INTRODUCTION

Appendix B is separated into 4 sections. Section 1 describes the regional geologic setting of the Moodus area and presents the results of analyses of borehole rocks. Section 2, 3, and 4 contain the detailed descriptions of rock chips, rock core, and thin sections of borehole rocks, respectively.

Regional Geologic Setting

Rocks in east-central Connecticut belong to several geologic provinces. In the easternmost part of the state, the Avalon zone (Williams, 1978) is characterized by metamorphosed volcanic rocks and abundant intrusive plutonic bodies that were formed in the late Precambrian era (Figure B-1) about 600 million years ago (Rast, 1980). This province extends northward through Nova Scotia and into eastern Newfoundland. It is thought to be an ancient microcontinent that collided with North America during the Paleozoic era (e.g., Robinson and Hall, 1980; Williams and Hatcher, 1983).

West of the Avalon zone, another belt of rocks forms the Merrimack synclinorium. This geologic province is characterized by a distinct suite of metamorphosed clastic marine sediments. The ages of the rocks in the Merrimack belt are not well constrained, but they are believed to be early Paleozoic in age based on correlations with fossiliferous units found to the north (Rogers, 1985). The Nashoba and Bronson Hill provinces are also located in east-central Connecticut, and form a complex terrain of igneous, sedimentary, and metamorphic rocks (Figure B-2). The Moodus borehole was drilled through the Merrimack zone into rocks of the Avalon terrane which underlies the Merrimack rocks at this site.

The boundary between the Merrimack and Avalon zones is a major ductile fault system that extends from south-central Connecticut to northern Massachusetts. Segments of this fault are known as the Honey Hill, Lake Char, and Clinton-Newbury faults. Collectively, these segments compose the Honey Hill fault system. Past motion along this fault system was primarily thrusting directed to the southeast (Wintsch and Sutter, 1986).

Tectonic models to account for the accretion of these structural blocks are speculative, and the timing of major geologic events is not well constrained. Most models involve the closing of the ancestral Atlantic ocean (Iapetus) during the late Paleozoic (Permian) with associated movement along the Honey Hill fault system. Large displacements along these faults, however, is not proved. The exact relationship among these crustal blocks is still uncertain.

There is little direct evidence for dating major tectonic events in southeastern Connecticut. For example, the dominant amphibolite-grade of metamorphism observed in the Merrimack and Avalon rocks is commonly assumed to be Acadian (Devonian) in age. This conclusion is based primarily on correlations with well-dated rock units in northern New England (Dixon and Lundgren, 1968). Such a correlation is not unreasonable, however, because early Devonian strata are deformed in southeastern Connecticut (Dixon and Lundgren, 1968), indicating that an intense metamorphic event occurred after the early-Devonian.

Based on these correlations with rock units to the north, Robinson and Hall (1980) present a model in which the Acadian orogeny is attributed to the collision of the Avalon plate with the already assembled package of North America and Bronson Hill rocks. Wintsch and Aleinikoff (1987), however, argue that isotopic ages of selected gneisses in the Avalon zone show no evidence of metamorphism between the late Precambrian and the Permian. They suggest that the Avalon terrane escaped the Acadian metamorphism recorded in other parts of New England because it was not yet accreted to North America. Thus, in their model,

the Acadian Orogeny resulted from interactions among the North American plate, the Bronson Hill zone, and the Merrimack zone, while the Avalon zone collided with North America at a later date.

Although the effects of Acadian deformation are poorly understood in southeastern Connecticut, post-Acadian deformation is well documented for this area. Zartman and Naylor (1970) discuss a "thermal disturbance" in the Permain that affected rocks of southeastern New England. Fossiliferous Pennsylvanian sediments in the Narragansett basin of Rhode Island exhibit low-grade metamorphism. Thus, a regional orogenic event, subsequent to the Acadian orogeny, is documented in southeastern New England (Day and others, 1980). This late Paleozoic tectonic event is called the Alleghanian orogeny, and it is generally attributed to the final "docking" of the Avalonian microplate to North America (Skehan and Murray, 1980; Wintsch and Aleinikoff, 1987).

Following the collisional tectonics of the late Paleozoic, an extensional phase of deformation affected east-central Connecticut. A series of basins was created as the present-day Atlantic ocean began to open. These basins, including the Connecticut Triassic basin, presently contain unmetamorphosed clastic sediments. The lack of metamorphism indicates that major tectonic deformation of the region had ceased by Triassic time.

Geology of the Moodus Area

The Moodus borehole is located near the junction of four major structural and stratigraphic zones (Zartman and Naylor, 1984). The rocks in these zones reflect different geologic histories, suggesting that they evolved independently and then later juxtaposed. All of these zones are bounded by major ductile faults. The borehole itself is located near the southwestern edge of the Merrimack synclinorium, a structural and lithologic zone that extends from near Long Island Sound northward into central Maine. The synclinorium is bordered to the west by the Bronson Hill zone, to the east by the Nashoba zone, and to the south by the Avalon zone (Figure B-2).

The Moodus borehole penetrated rocks of two of these zones, those of the Merrimack synclinorium and the underlying rocks of the Avalon zone. Synclinorium rocks generally consist of metasedimentary sequences of schists and calcsilicate gneisses, as well as metaigneous granitic gneisses and younger granites. The schists occasionally contain sillimanite-muscovite and sillimanite-muscovite-garnet mineral assemblages showing that the rocks were metamorphosed up to middle-amphibolite grade. The ages of these units are based primarily on correlations with fossiliferous units found in less deformed areas to the north, and are generally considered to be early Paleozoic in age (Rogers, 1985). The Canterbury gneiss, a granite unit within the sedimentary sequence, has been radiometrically dated at about 390 Ma (Mega-anno or millions of years before present), indicating it is early Devonian in age (Zartman and Naylor, 1984).

Avalon rocks consist of various interlayered metaigneous granitic gneisses, dioritic gneisses, amphibolites, and granites. The metamorphic grade of these rocks also reflect amphibolite facies pressure/temperature conditions. Based on radiometric age determinations, these rocks are late Precambrian in age (620 Ma) (Wintsch and Aleinikoff, 1987).

The Merrimack and the Avalon zones are separated by a major ductile thrust fault called the Honey Hill fault (Lundgren and Ebblin, 1972). Rocks of the upper plate of the fault consist of the Merrimack units while the Avalon gneisses form the lower plate. Past motion along this fault was generally thrusting directed to the southeast (Wintsch and Lefort, 1984), but the amount of displacement is not well constrained .

The Honey Hill fault is actually a zone, up to several hundred meters wide, of intensely crushed, milled, and sheared rock. Rock exposures south of the borehole show that the Honey Hill fault dips moderately to the north and underlies most, if not all, of the southern part of the Merrimack synclinorium. North of the borehole, the fault again intersects the surface at the Willimantic dome (Wintsch

and Fout, 1982) forming a window that exposes the underlying rocks of the Avalon zone. Most of the mineral assemblages associated with the fault zone show that the dominant ductile fabric developed under amphibolite-grade metamorphic conditions. Minor mylonitic zones of greenschist facies metamorphism, however, indicate that some brittle fault reactivation occurred at shallower crustal levels, presumably during regional uplift.

The preservation of the brittle fabrics indicate that the high-grade ductile deformation preceded the brittle faulting. The age of the two phases of movement, however, is uncertain. Most investigators associate the high-grade deformation with deep-seated movement during the Acadian orogeny (Zartman and Naylor, 1984) since there is only limited documentation of high-grade deformation during the Alleghanian orogeny in the Permian. The Alleghany orogeny would appear to correlate with the low-grade, brittle episode of movement along the Honey Hill fault. There is no evidence of movement along the Honey Hill fault since the late Paleozoic.

Methods of Research

The geology of the borehole was determined primarily from grab samples of rock cuttings, and from microscopic and megascopic analysis of rock cores. Geophysical logs, recorded by Schlumberger Wireline Services, Schlumberger-Doll Research, and Lamont-Doherty Borehole Research group also provided very detailed geologic information.

Rock chips blown from the well during drilling operations were collected at 20-foot intervals. These chips provide a continuous geologic record for the entire length of the borehole and constitute a form of calibration for subsequent interpretation of the geophysical logs. Thin sections were made from a number of the rock chips for microscopic analysis.

Nine cores, three inches in diameter and roughly 10 feet in length, were recovered at 500 foot intervals. At least one core was recovered from every major lithologic unit intersected by the borehole. The cores were not oriented, but accurate foliation, lineation, and fracture orientation were determined from the very detailed Formation Microscanner logs (FMS) and Borehole Televiewer logs recorded by Schlumberger. Sections of the core were distributed to selected laboratories to determine mechanical properties such as tensile strength, thermal conductivity, and microfabric parameters of borehole rocks.

Core and Cutting Descriptions

The major rock units penetrated by the Moodus borehole are, from top to bottom, the Hebron Formation, Canterbury Gneiss, Tatnic Hill Formation, and Avalonian gneisses of the Waterford Group. The Honey Hill fault zone, generally centering along the contact between the Tatnic Hill Formation and the Waterford gneisses, was also intersected by the borehole.

The protoliths of the Hebron and Tatnic Hill rocks are considered to be silts, limey silts, and shales (Lundgren, 1963). The Canterbury gneiss was probably originally a sill-like intrusive body that was emplaced in the sedimentary units (Lundgren and others, 1971). The stratigraphic position of the Canterbury gneiss appears to vary throughout the Merrimack synclinorium and lies either totally within the Hebron Formation or along the Hebron-Tatnic Hill contact (Lundgren and others, 1971; Zartman and Naylor, 1984). Protoliths of the Waterford gneisses are interpreted to be extrusive volcanic tuffs and ash flows (Wintsch and others, 1987).

Descriptions of the various rock types are presented below. A summary lithologic chip and core log of the Moodus borehole is presented in Figure B-3 and the depths of the recovered core are shown in Figure B-4. A more detailed mineralogical description of the rock chips, rock core, and thin sections are presented in Sections 2, 3, and 4, respectively. The distribution of minerals that

are distinct and contribute to the identification of formation boundaries is shown in Figure B-5.

Overburden

The borehole site is located in a small sand and gravel pit north of the town of Moodus. The borehole penetrated 37 feet of overburden which consisted of sands and silts with occasional boulders concentrating near the top of bedrock. The overburden is predominantly derived from glacial outwash, although the overlying sands and gravels are remnant deposits of the ancient Moodus river.

Hebron Gneiss

From a depth of 40 feet to the contact with the Canterbury gneiss at a depth of approximately 1,900 feet (Figure B-5), the Hebron Formation is predominantly a black fine- to medium-grained quartz-plagioclase-biotite-pyroxene calcsilicate granofels and schist. Accessory minerals include amphibole, calcite, scapolite, sphene, and apatite. Locally, the calcsilcates are interlayered with a white medium- to coarse-grained plagioclase-quartz-biotite gneiss. In addition to the interlayered granite gneiss, the borehole penetrated a 300-foot-thick bluish-white, coarse-grained, plagioclase-quartz-biotite-muscovite gneiss. This particular unit has been southwest of the borehole (London, in press) and is informally called the Silver Bullet gneiss (London, personal communication). Another distinctive unit of the Hebron Formation is a biotite-muscovite-sillimanite schist. This unit occurs from a depth of 1,400 feet to 1,700 feet where it is interlayered with the more typical pyroxene-bearing units.

Just above the contact with the Canterbury gneiss at a depth of 1,900 feet, a white, coarse-grained, garnet-bearing plagioclase-quartz-biotite $\pm$ muscovite granite locally becomes common in the Hebron schists.

A mineralogically-distinct unit occurs just below the Canterbury gneiss. This unit is about 140 feet thick, and it is predominantly a black medium-grained, sphene- and sulphide-bearing quartz-plagioclase-biotite schist that is interlayered with abundant white, medium- to coarse-grained, garnet-bearing plagioclase-quartz-biotite gneiss. Lithologically, this unit differs from the Hebron Formation rocks that overlie the Canterbury gneiss in that pyroxene and other calcsilicate minerals are not present. This unit is also compositionally different than the typical Tatnic Hill rocks that are described below. Thus it is unclear whether this unit is part of the Hebron Formation or the Tatnic Hill Formation. The compositional differences between the units immediately above and below the Canterbury gneiss, however, suggest that there might be a stratigraphic positioning of the Canterbury gneiss, as opposed to an intrusive and cross- cutting relationship with the country rock.

Canterbury Gneiss

The Canterbury gneiss occurs from a depth of 1,900 feet to approximately 2,090 feet. It is a pink to white colored, medium- to coarse-grained quartz-plagioclase-k-feldspar-biotite granite gneiss. The foliation is generally poorly to moderately defined. Muscovite, garnet, and epidote may be present in minor amounts. The upper contact of this unit is fairly sharp, although there does appear to be some interlayering between the Canterbury gneiss and the Hebron schists at depths of around 1,880 to 1,900 feet. The lower contact with the biotite schist, however, appears more gradational. From a depth of about 2,090 feet, where chips of 100% granitic gneiss end, to a depth of about 2,224 feet, the biotite schist is interlayered with a granitic gneiss that is compositionally similar to the Canterbury gneiss.

Tatnic Hill Schist

The top of the typical Tatnic schist is here considered to occur at a depth of approximately 2,224 feet. This is the depth at which the interlayered biotite

schist and granitic gneisses end, and muscovite, and soon after, amphibole make their first appearance. The rocks here are black, fine- to medium-grained quartz-plagioclase-biotite-muscovite schists that are typically interlayered with a medium-grained quartz-plagioclase-amphibole-biotite schist. At a depth of about 2,380 feet the mineralogy of the rocks change. Garnet and sillimanite locally become abundant in the biotite schist, although the biotite-amphibole schist is still present. The core recovered from the Tatnic Hill Formation shows well-developed augen and blastomylonitic textures indicating that much of the unit underwent major ductile shearing.

Waterford Gneisses

The layered granitic gneisses and amphibolites found from the Tatnic Hill contact to the bottom of the borehole are not differentiated and are here lumped together as the Waterford Group gneisses. The gneisses are generally white to pink, medium- to coarse-grained rocks with compositional layers of biotite-rich alternating with felsic-rich layers that are poorly to moderately developed. Amphibole is generally present in moderate amounts. The foliation is generally moderately to well-defined by aligned flakes of biotite and amphibole.

Amphibolite occurs locally as thin units throughout the bottom of the borehole, but are most abundant from depths of 3,740 to about 4,200 feet. These units, as seen in core and in the rock chips, are at most a few feet in width.

Orientation of Foliation

The orientation of borehole structures were measured from the FMS logs of Schlumberger Wireline Services.. However, because the FMS tool maps borehole rocks on the basis of electrical resistivities, the sharpest images only occur in those rock formations that have a small amount of natural porosity that contains fluids capable of conducting electrical current. Rocks of the Merrimack synclinorium apparantly contain some amounts of fluids because the FMS images

of these rocks are excellent in quality. Waterford group gneisses, however, are shown to have some of the highest resistivities ever to be recorded (Anderson et al., this volume). This resulted in poor-quality images and prevented measurements of borehole structures in this group of rocks.

The foliation of Moodus borehole rocks generally have moderate dips that rarely exceed 20 degrees. The strikes of the borehole rocks, however, can be quite variable. A contour plot of the orientation of all borehole rocks shows a maxima that indicates most of the borehole rocks have shallow dips to the northeast (Figure B-6). The contour plot of only Hebron Formation rocks shows a similar pattern. Although the strikes of Hebron rocks can be variable, the bulk of the rocks dip to the northeast (Figure B-7).

Tatnic Hill Formation rocks also generally have shallow to moderate dips, but they occasionally steepen considerably. The bulk of the rocks, however, as seen in the contour plot, have shallow dips to the east and southeast (Figure B-8). The well-defined girdle seen in Figure B-8 is the result of the presence of a few recumbent folds at a depth of about 2,460 feet. One of these folds is seen in both a section of core recovered from that interval (section 3) and in the Schlumberger FMS logs. The fold has a subhorizontal hinge surface and a hinge that trends north-northeast/south-southwest. The subhorizontal orientation of this fold suggests that it may be related to movement along the Honey Hill fault.

Honey Hill Fault

The Honey Hill fault is a major ductile fault zone that centers along the contact between the Tatnic Hill Formation and the gneisses of the Waterford Group. Traditionally, the trace of the fault plane is placed along the contact between the two units (e.g. Lundgren and Ebblin, 1972; Rodgers, 1985), but deformation attributed to the fault actually took place across a fairly wide zone. In the Moodus borehole, evidence for major ductile faulting is not found in the chip samples of the Waterford Group. The gneissic chips recovered from intervals

just below the Tatnic Hill/Waterford contact do not display penetrative cataclastic or mylonitic fabrics typically associated with major faulting. In addition, core number 6, recovered from less than 300 feet below the Tatnic Hill-Waterford Group contact shows no significant ductile/brittle fabrics. Instead, the slight undulose extinction of the felsic minerals indicates that only minor strain affected rocks at this level. Ductile fabrics are better developed and more widespread in rock of the Tatnic Hill Formation, as indicated by the presence of recumbent folds, augen structure, and blastomylonitic fabrics. This suggests that much of the deformation attributed to the Honey Hill fault zone took place within the Tatnic Hill schist.

Some minor mylonitic zones are present in the borehole but they are widely spaced and fairly evenly distributed throughout the lower sections of the borehole (Figure B-9). The rock chips recovered from these minor mylonite zones are usually phyllonitic and rich with chlorite, indicating that deformation took place under greenschist facies metamorphism. The contrast between the higher-grade amphibolite facies deformation, best seen in the Tatnic schist and the lower grade of metamorphism in these minor mylonite zones, indicates that the Honey Hill fault has been reactivated at shallower crustal levels and over a relatively long time span.

Fractures and Borehole Hydrology

During borehole drilling, at least two water-bearing zones were intersected. When the borehole was less than 500 feet deep, the borehole was dry. When the borehole reached a depth of about 750 feet, water entered the hole at a rate of about 1 gallon per minute (GPM) so it was apparent that somewhere between 500 and 750 feet a conductive fracture or set of fractures was intersected. A subsequent review of borehole televiewer logs, caliper logs, and formation microscanner logs revealed a set of open fractures spanning a depth of 615 to 620 feet. The clearest fracture of the set has a strike of about 000 to 010 degrees and a dip of 30 to 35 degrees to the east.

A major conductive fracture zone was intersected at a depth of about 3,500 feet. Here, water entered the borehole at an estimated rate of 150 GPM. A review of the geophysical logs shows that the orientations of these fractures are similar to the shallower open fracture; a strike of about 340 degrees and a dip of 30 degrees to the east. Because drilling could not continue with so much water entering the borehole, this set of fractures was sealed with cement.

It is not known whether other water-bearing fractures were intersected by the borehole. If other conductive fractures do occur, their flow rate can not exceed a few GPM or they would have been detected during drilling.

The static water level in the borehole has been measured several times after drilling activities ended. The differences in depth may reflect, in part, seasonal influences on ground water.

278 feet	22 July 1987
220 feet	23 August 1987
190 feet	13 February 1988

The water table in the overburden, however, is for all practical purposes at the ground surface as seen by the swamp-like and marshy conditions immediately around the borehole. Water in the overburden, however, cannot enter the borehole because the well is cased and grouted to a depth of 100 feet.

Stress-Induced (Brittle) Borehole Deformation

After drilling activities concluded, a borehole televiewer survey showed that stress-induced borehole spalling was occurring. In addition to the logs, an on-going spalling process was indicated by thin 1-inch-long slivers of rock that were commonly brought to the surface on the logging tools. In one case, a 4-inch-long spall was recovered. These spalls, or breakouts, lead to borehole elongation

through brittle deformation and have been shown to correlate with the orientation of stress. Breakouts in the Moodus borehole continued to such an extent that by a month after drilling, the bottom 25 feet of the borehole were filled with spalled rock chips, and chips were still being caught on the geophysical logging tools. The gneissic mineralogy and texture of all the recovered rock chips show that they spalled from the Waterford Group gneisses. This is also supported by borehole televiewer logs which show that the breakouts are best developed below depths of about 3,500 feet, and thus occur predominantly in the Waterford rocks.

Another type of stress-induced deformation that occurred is a phenomenon known as core "disking" (Obert and Duvall, 1967). This was best seen in core number 8, removed from a depth of 3,985 feet. When the core was removed from the core barrel, it came out as 1/4 to 1/2 inch wide disks, essentially resembling poker chips. This disking results from stress relaxation as the vertical and horizontal stresses are relieved once the core is freed from the in-situ stress environment by the core bit. This fabric is best developed in core number eight probably because the foliation is subhorizontal, and the foliation surfaces act as planes of weakness during core relaxation. This disking is also present in core number 9, the deepest core, but the fabric is not as well developed. In this core the foliation is steeper, and consequently at a greater angle to the vertical stress so that the layering of the rock does not act as weakness planes. The amphibolite portion of the core, however, has a well-developed disking fabric, probably resulting from the fine-grained and homogeneous texture of the rock.

CONCLUSIONS

Rock formations penetrated by the Moodus borehole are part of a stratigraphic sequence that is similar to sequences exposed both to the north in the Willimantic dome and to the south near the surface trace of the Honey Hill fault. Although the borehole is within a few kilometers of the Bronson Hill zone, rocks of that zone were not intersected by the borehole. Instead, only gneisses of the Waterford Group were penetrated, indicating that the Avalon basement and

the Honey Hill fault zone extend through the subsurface as far west as Moodus. Although the boundary between the Bronson Hill zone and the Merrimack zone has been mapped as a steep, ductile fault (London, 1988), the relationship between Bronson Hill rocks, Avalon rocks, and the Honey Hill fault is not determinable.

Deformation that is attributed to the Honey Hill fault occurred under ductile to semi-ductile conditions and indicates that the fault operated under a range of metamorphic conditions. Ductile fabrics are best developed in the schists of the Tatnic Hill Formation and typically consist of flasers, augen, and minor recumbant folds. The occurrence of folded augen (Section 3) indicates that several high-grade pulses occurred along the Honey Hill fault; at least one event resulted in the formation of the flasers and augen and another pulse folded these features. Although the more ductile features appear to concentrate in the Tatnic Hill Formation, the more brittle features such as the greenschist phyllonitic zones are evenly distributed throughout the borehole.

Geologic time scale

AGE (Ma)	ERA	PERIOD	EVENTS
0.0	Cenozoic	Quaternary	
1.6		Tertiary	
66.4	Mesozoic	Cretaceous	
144		Jurassic	
208		Triassic	
245	Paleozoic	Permian	Alleghanian
286		Pennsylvanian	
320		Mississippian	
360		Devonian	Acadian
408		Silurian	
438		Ordovician	Taconic
505		Cambrian	
570	Precambrian	Proterozoic	Avalonian
2500		Archean	
4600			

Figure B – 1 Geologic time scale and timing of orogenic events.

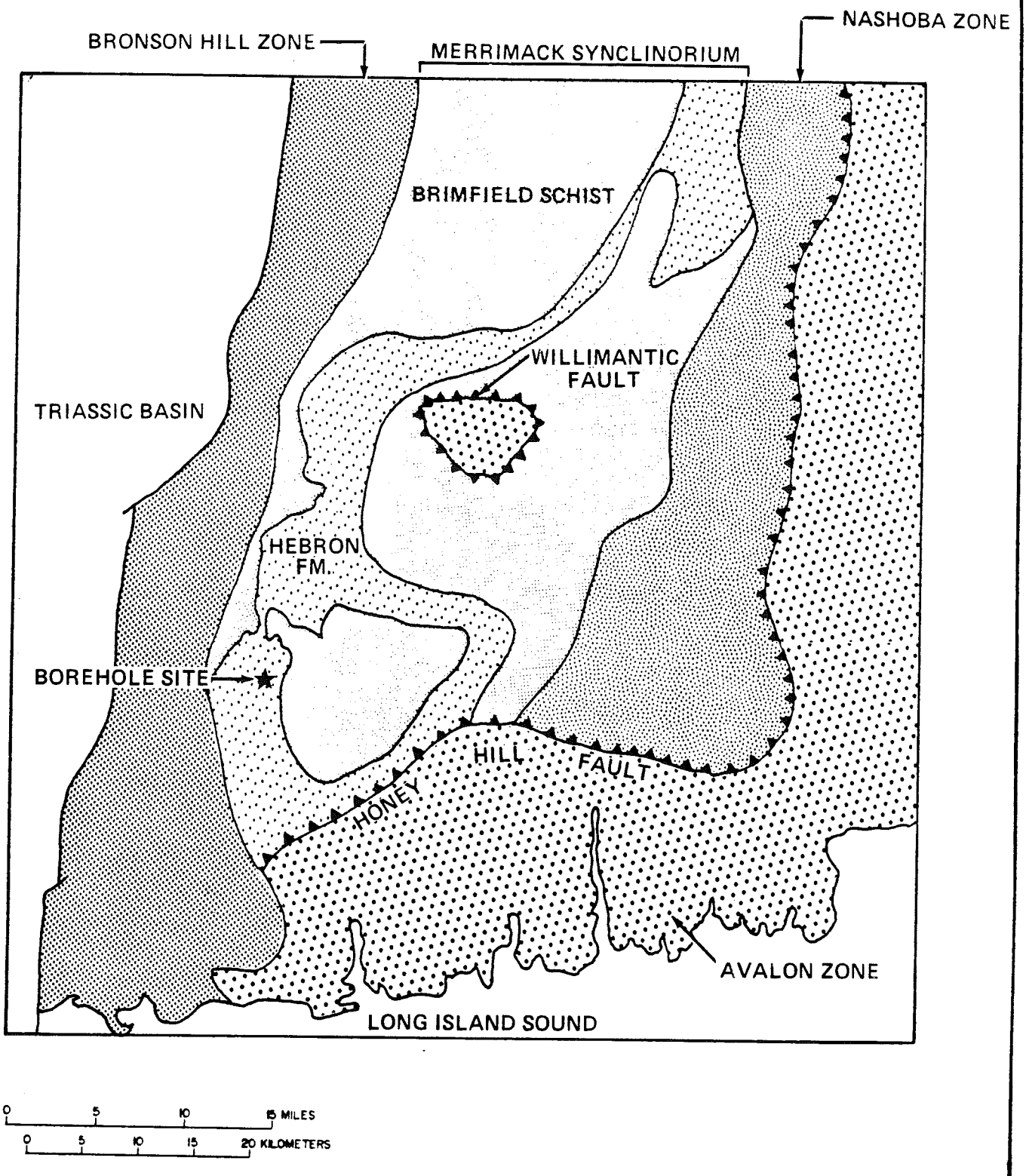

Figure B – 2 Geologic setting of the Moodus borehole.

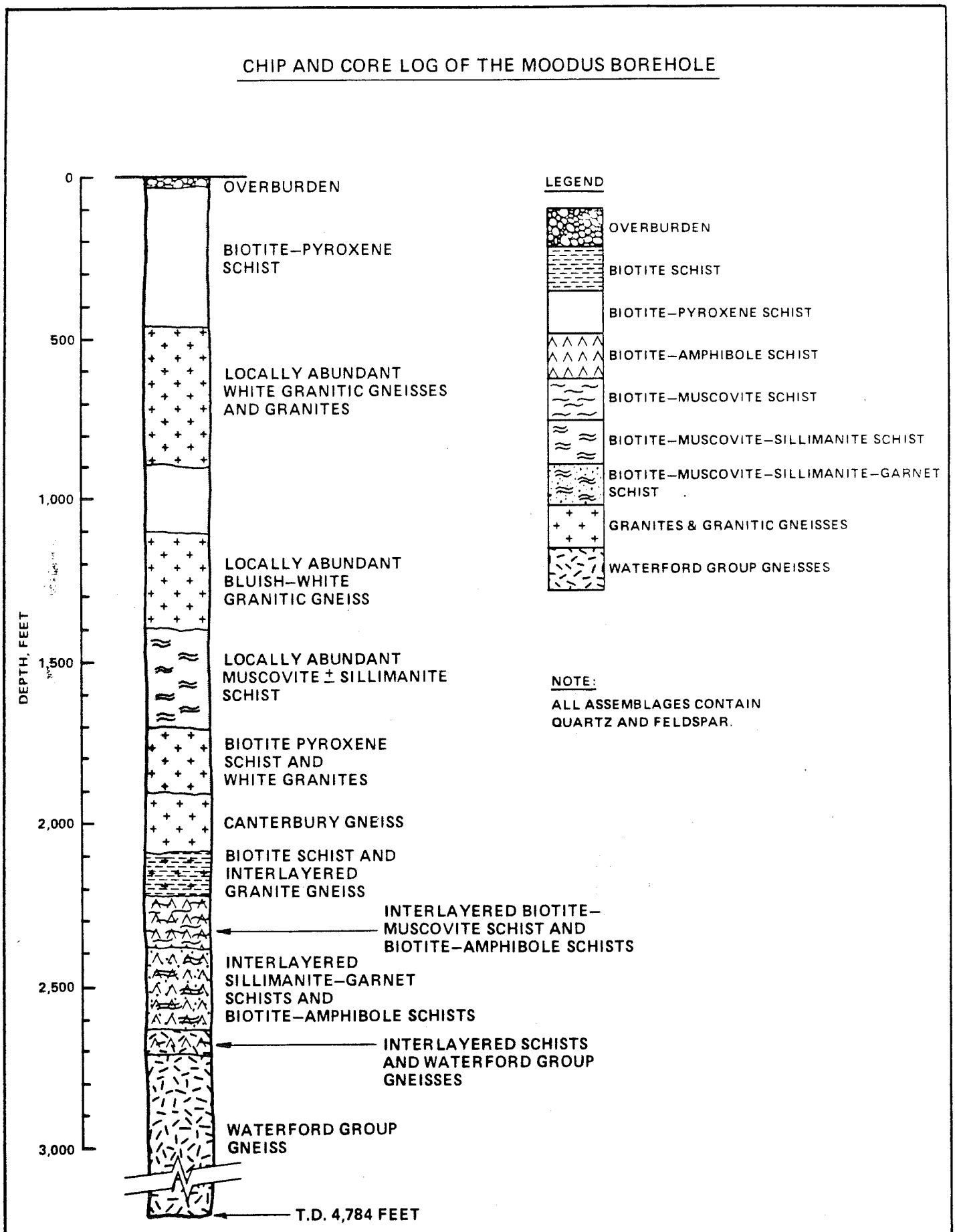

Figure B – 3 Lithologic units in the Moodus borehole.

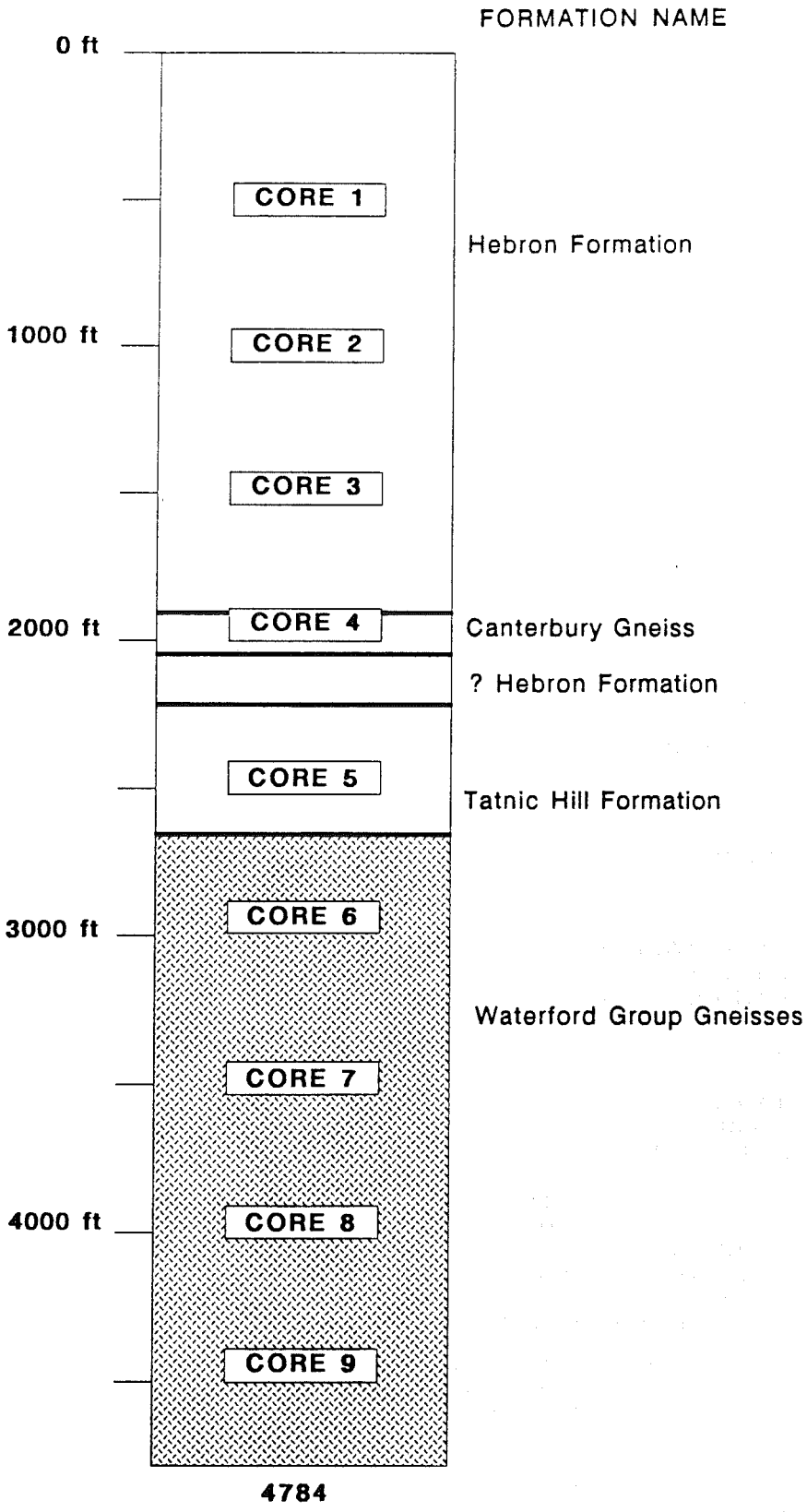

Figure B–4 Location of cored intervals.

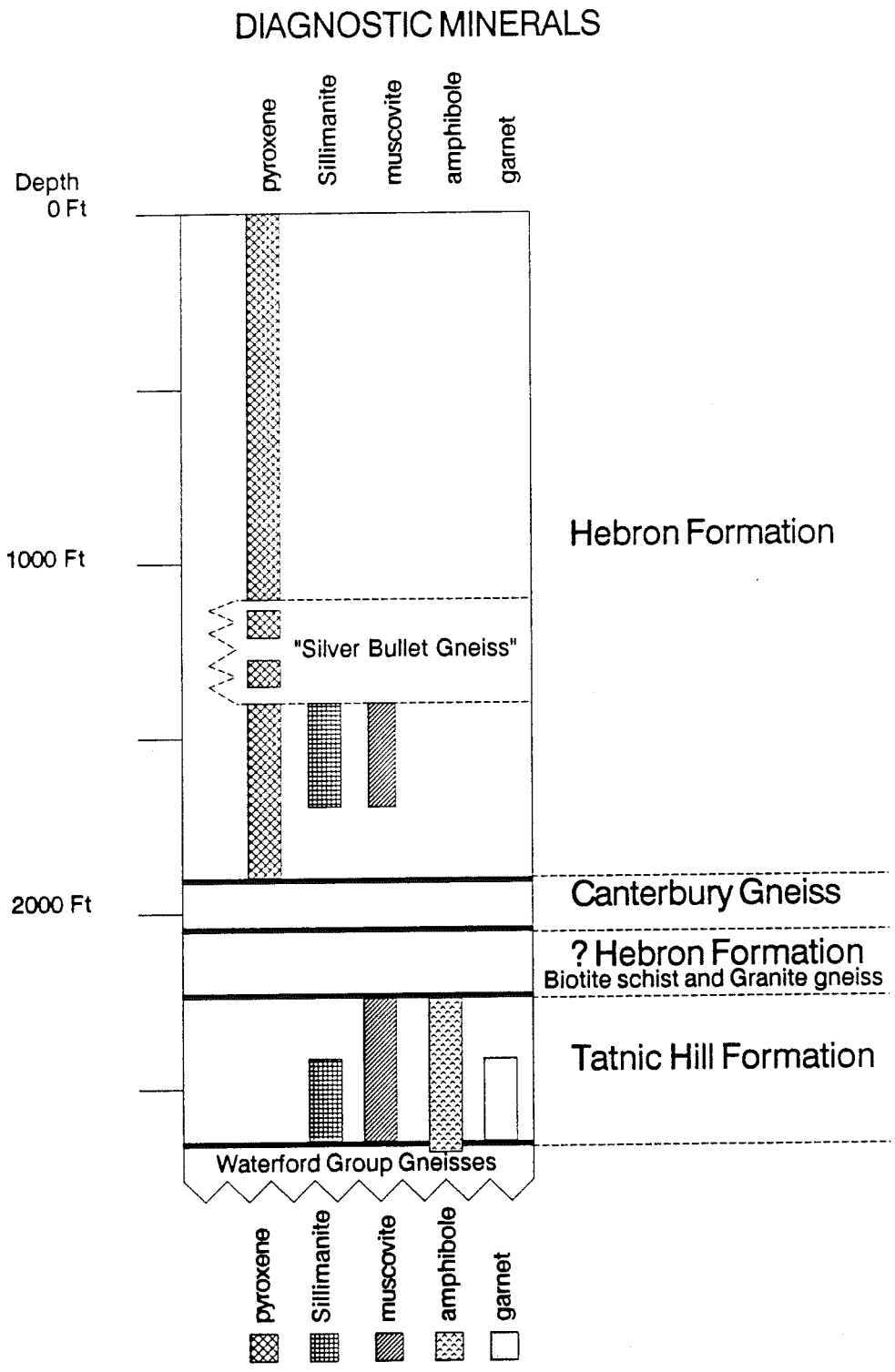

Figure B–5 Distribution of diagnostic minerals and location of formation boundaries.

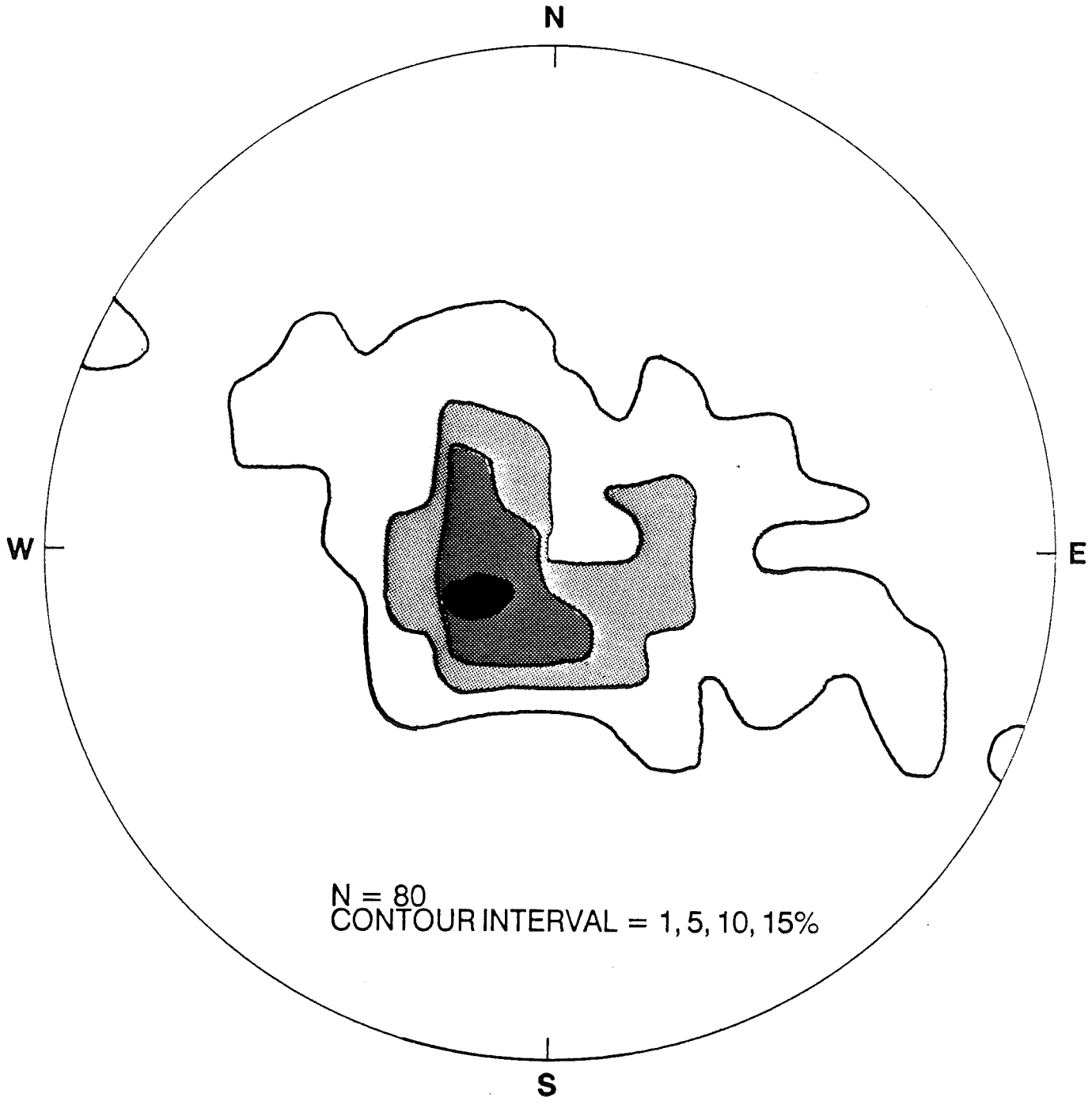

CONTOURED PLOT OF ROCK FOLIATION – MERRIMACK SYNCLINORIUM

Figure B – 6 Contoured plot of rock foliation – Merrimack zone rocks.

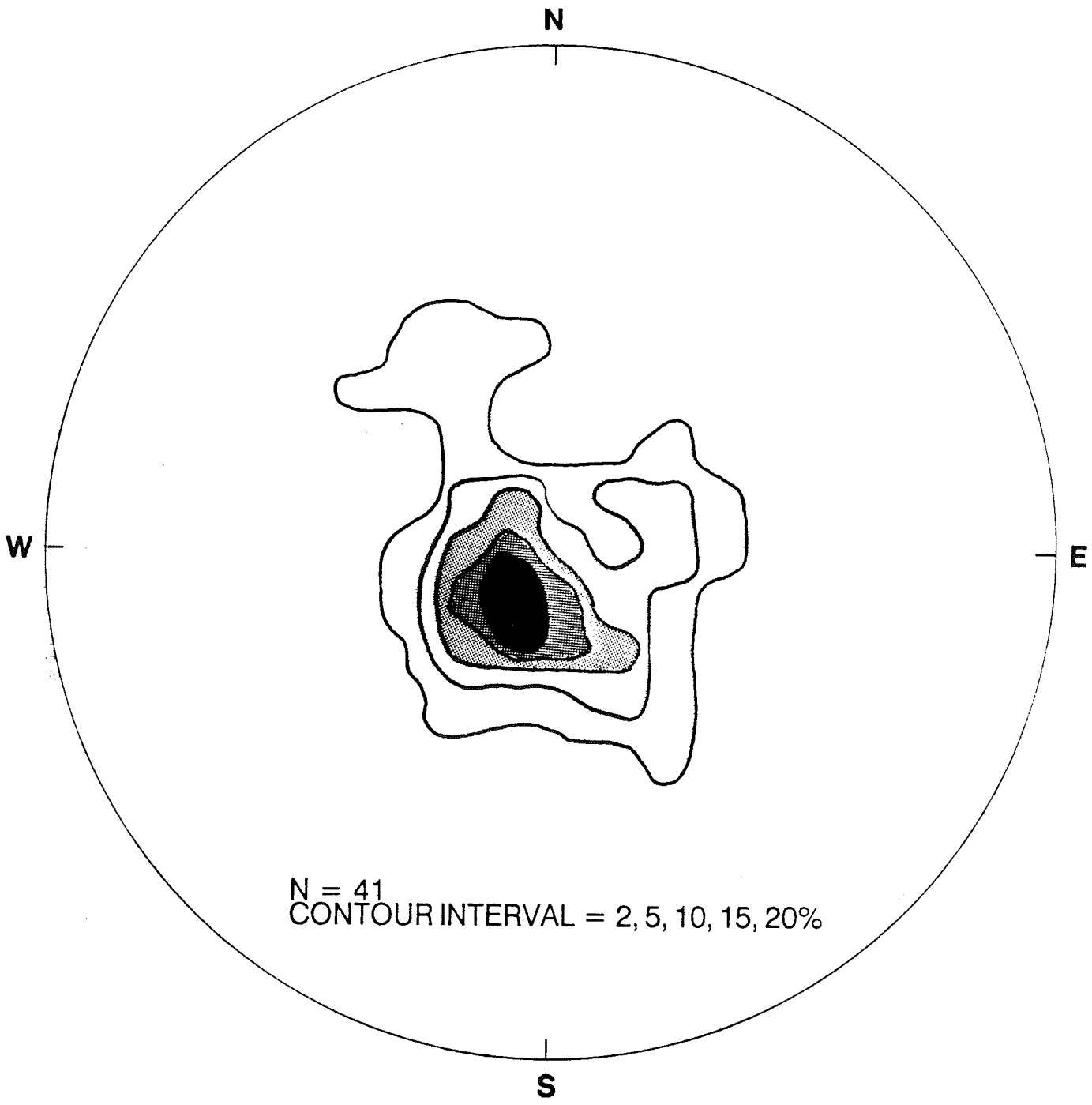

CONTOURED PLOT OF ROCK FOLIATION – HEBRON FORMATION

Figure B – 7 Contoured plot of rock foliation – Hebron Formation.

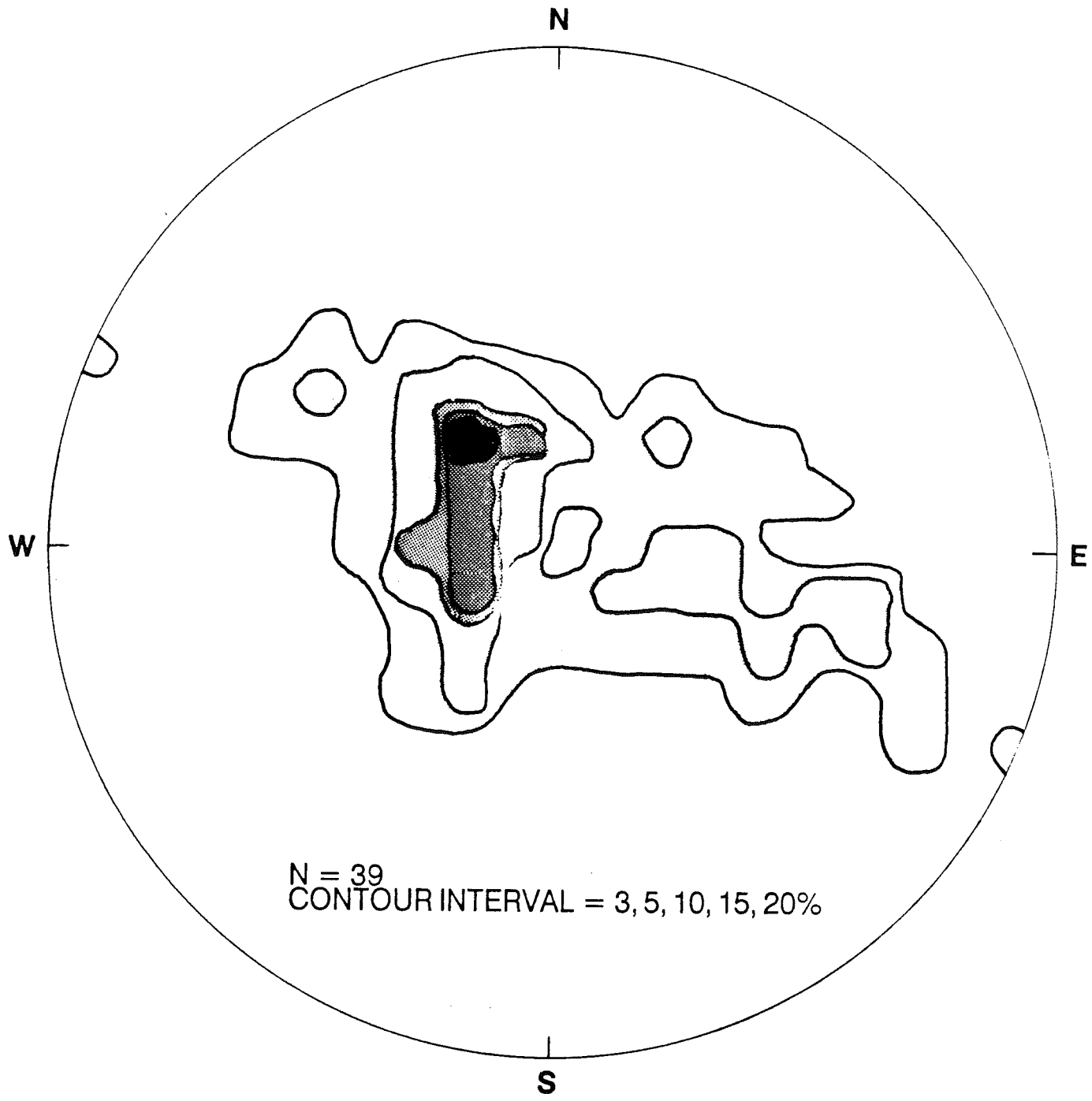

CONTOURED PLOT OF ROCK FOLIATION – TATNIC HILL FORMATION

Figure B – 8 Contoured plot of rock foliation – Tatnic Hill Formation.

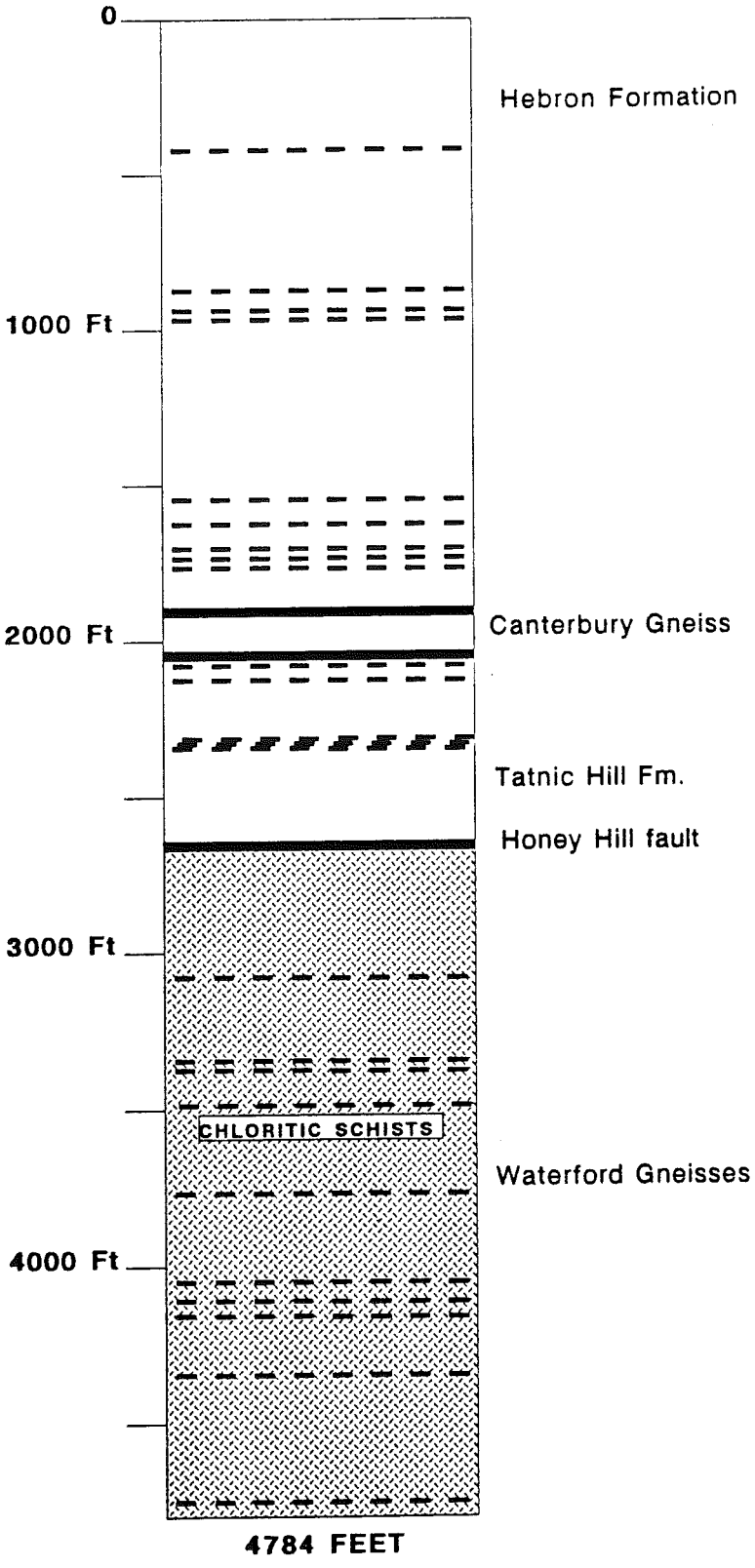

Figure B–9 Distribution of brittle and chloritic zones.

REFERENCES

Day, H.W., Brown, V.M., and Abraham, K., 1980, Precambrian (?) Crystallization and Permian (?) Metamorphism of Hypersolvus Granite in the Avalonian Terrane of Rhode Island, Geological Society of America Bulletin, Part II, v. 91, p. 1669-1741.

Dixon, H.R., and Lundgren, L.W., Jr., 1968, Structure of Eastern Connecticut in Zen, E-an, White, W.S., Hadley, J.B., and Thompson, J.B., Jr., eds., Studies of Appalachian Geology: Northern and Maritime, New York Wiley-Interscience, p. 219-229.

London, D., 1988, Characteristics and Regional Significance of the Cremation Hill Ductile Fault Zone at the Bronson Hill-Merrimack Boundary, South-Central Connecticut, American Journal of Science, v. 288, p. 353-375.

London, D., in press, Bedrock Geology of the Moodus Seismic Area, South-Central Connecticut, Report of Investigations, Connecticut Geological and Natural History Survey, 49 p.

Lundgren, L., Jr., 1963, The Bedrock Geology of the Deep River Quadrangle With Map, State Geological and Natural History Survey of Connecticut, Quadrangle Report No. 13, 42 p.

Lundgren, L., Jr., Ashmead, L., and Snyder, G.L., 1971, The Bedrock Geology of the Moodus and Colchester Quadrangles with Maps, State Geological and Natural History Survey of Connecticut, Quadrangle Report No. 27, 24 p.

Lundgren, L., and Ebblin, C., 1972, Honey Hill Fault in Eastern Connecticut: Regional Relations, Geological Society of America Bulletin, v. 83, p. 2773-2794.

REFERENCES
(continued)

Obert, L., and Duvall, W.I., 1967, Rock Mechanics and the Design of Structures in Rock, New York, John Wiley and Sons.

Rast, N., 1980, The Avalonian Plate in the Northern Appalachians and Caledonides, in Wones, D.R., ed., The Caledonides in the USA, I.G.C.P. Project 27: Caledonide Orogen, Virginia Polytechnic Institute and State University Memoir 2, p. 63-66.

Robinson, P., and Hall, L.M., 1980, Tectonic Synthesis of Southern New England, in Wones, D.R., ed., The Caledonides in the USA, I.G.C.P. Project 27: Caledonide Orogen, Virginia Polytechnic Institute and State University Memoir 2, p. 73-82.

Rogers, J., 1985, Bedrock Geological Map of Connecticut, Connecticut Geological and Natural History Survey, Scale 1:125,000.

Skehan, S.J., J.W., and Murray, D.P., 1980, A Model for the Evolution of the Eastern Margin (EM) of the Northern Appalachians, in Wones, D.R., ed., The Caledonides in the USA, I.G.C.P. Project 27: Caledonide Orogen,Virginia Polytechnic Institute and State University Memoir 2, p. 67-72.

Williams, H., 1978, Tectonic Lithofacies Map of the Appalachian Orogen, Memorial University of Newfoundland, Map No. 1, Scale 1:1,000,000.

Williams, H., and Hatcher, R.D., Jr., 1983, Appalachian Suspect Terranes, in Hatcher, R.D., Jr., Williams, H., and Zietz, I., eds., Contributions to the Tectonics and Geophysics of Mountain Chains, Geological Society of America Memoir 158, p. 33-53.

REFERENCES
(continued)

Wintsch, R.P., and Sutter, J.F., 1986, A Tectonic Model for the Late Paleozoic of Southeastern New England, Journal of Geology, v. 94, p. 459-472.

Wintsch, R.P., and Aleinikoff, J.N., 1987, U-Pb Isotopic and Geologic Evidence for Late Paleozoic Anatexis, Deformation, and Accretion of the Late Proterozoic Avalon Terrane, Southcentral Connecticut, American Journal of Science, v. 287, p. 107-126.

Wintsch, R.P., and Leffort, J.-P., 1984, A Clockwise Rotation of Variscan Strain Orientation in SE New England and Regional Implications, in Hutton, D.H.W., and Sanderson, D.J., eds., Variscan Tectonics of the North Atlantic Region, Oxford, Blackwell Scientific Publications, p. 245-251.

Wintsch, R.P, and Fout, 1982, Structure and Petrology of the Willimantic Dome and the Willimantic Fault, Eastern Connecticut, in Joesten, R., and Quarrier, S.S., eds., Guidebook for Fieldtrips in Connecticut and South Central Massachusetts, New England Intercollegiate Geological Conference, 74th Annual Meeting, The University of Connecticut, Storrs, Connecticut, p. 465-482

Wintsch, R.P., Webster, J.R., Bernitz, J.A., and Fout, J.S., 1987, Subdivision of Rope Ferry Gneiss, Avalon Terrane, and Structural Implications, Geological Society of America, Abstract with Programs, v. 19, p. 66.

Woodward-Clyde Consultants, 1986, Regional Crustal Stress Study: Tectonic Stress in Southeastern New York State, Prepared for Empire State Electric Energy Research Corporation, Research Report EP 84-27.

REFERENCES
(continued)

Zartman, R.E., and Naylor, R.S., 1984, Structural Implications of Some Radiometric Ages of Igneous Rocks in Southeastern New England, Geological Society of America Bulletin, v. 95, p. 522-539.

Zartman, R.E., Hurley, P.M., Krueger, H.W., and Giletti, B.J., 1970, A Permian Disturbance of K-Ar Radiometric Ages in New England: Its Occurrence and Cause, Geological Society of America Bulletin, v. 81, p. 3359-3374.

SECTION 2

This section consists of a chip log of the Moodus borehole. Only the upper 2,700 feet were logged in detail. This is the approximate depth where rocks of the Merrimack zone end and the rocks of the Avalon zone begin. The Avalon zone rocks have not been differentiated in this report and are grouped together as granitic gneisses of the Waterford Group.

CHIP LOG OF THE MOODUS BOREHOLE

DEPTH (feet)	DESCRIPTION
38-45 feet	Top of bedrock-NX core. Black fine grained quartz-plagioclase-biotite-pyroxene granofels
62	black fine-grained quartz-plagioclase-biotite +- pyroxene (diopside) granofels.
82	black fine-grained quartz-plagioclase-biotite-pyroxene granofels.
105	black fine-grained quartz-plagiolcase-biotite-pyroxene granofels.
122	70% white coarse-grained plagioclase-quartz-biotite-muscovite granite.
	30% black fine-grained sulphide-bearing quartz-plagioclase-biotite-pyroxene granofels.
142	98% black fine-grained sulphide-bearing quartz-plagioclase-biotite-pyroxene +- amphibole schist.
	2% white coarse-grained plagioclase-quartz-biotite granite.
162	black fine-grained sulphide-bearing quartz-plagioclase-biotite-pyroxene schist.
182	black fine-grained sulphide-bearing quartz-plagioclase-biotite-pyroxene schist.
202	black fine-grained sulphide-bearing quartz-plagioclase-biotite schist.
222	black fine-grained sulphide- and sphene-bearing quartz-plagioclase-biotite-pyroxene schist.
242	98% black fine-grained quartz-plagioclase-biotite-pyroxene schist.
	2% white coarse-grained plagioclase-quartz +- sulphide +- garnet granite.
262	98% black fine-grained quartz-plagioclase-biotite-pyroxene schist.
	2% white coarse-grained plagioclase-quartz +- sulphide +- garnet granite.
282	black fine-grained quartz-plagioclase-biotite-pyroxene granofels.
302	90% black fine-grained quartz-plagioclase-biotite-pyroxene +- amphibole schist.
	10% white fine- to medium-grained sulphide-bearing plagioclase-quartz-biotite segregations.
322	black fine-grained sulphide-bearing quartz-plagioclase-biotite-amphibole +- pyroxene schist.
342	black fine-grained quartz-plagioclase-biotite +- pyroxene granofels.
362	black fine-grained quartz-plagioclase-biotite +- pyroxene granofels.
382	black fine-grained sulphide-bearing quartz-plagioclase-biotite-pyroxene granofels.
402	black fine-grained quartz-plagioclase-biotite-pyroxene granofels.
422	95% black fine-grained quartz-plagioclase-biotite +- pyroxene granofels

5% white medium- to coarse-grained plagioclase-quartz +- biotite +- muscovite +- sulphide ?segregation

442 black fine-grained sulphide-bearing quartz-plagioclase-biotite-amphibole pyroxene granofels.

462 80% light gray medium-grained plagioclase-quartz-biotite gneiss.

20% black fine-grained quartz-plagioclase-biotite granofels.

482 60% black fine-grained quartz-plagioclase-biotite-amphibole schist.

40% white medium-grained sulphide-bearing plagioclase-quartz-biotite gneiss

CORE No.1 501 to 511 feet black medium-grained quartz-plagioclase-biotite-pyroxene +- amphibole schist.

524 95% black medium-grained quartz-plagioclase-biotite-pyroxene-amphibole schist.

5% white medium-grained plagioclase-quartz-biotite gneiss.

544 85% black fine-grained quartz-plagioclase-biotite-pyroxene granofels.

15% white medium-grained plagioclase-quartz-biotite gneiss.

564 black fine- to medium-grained quartz-plagioclase-biotite-pyroxene schist.

584 90% black sphene-bearing quartz-plagioclase-biotite-pyroxene +- amphibole schist.

10% white medium-grained plagioclase-quartz-biotite gneiss.

604 95% black medium-grained quartz-plagioclase-biotite-pyroxene schist.

5% white medium-grained plagioclase-quartz-biotite gneiss.

624 black fine-grained quartz-plagioclase-biotite-pyroxene granofels.

644 90% black medium-grained quartz-plagioclase-biotite-pyroxene schist.

10% greenish-white sulphide- and sphene-bearing plagioclase-quartz-pyroxene gneiss (compositional layers).

664 85% black medium-grained quartz-plagioclase-biotite-pyroxene schist.

15% white fine-grained plagioclase-quartz-biotite gneiss.

684 black medium-grained quartz-plagioclase-biotite-pyroxene schist.

704 60% white coarse-grained plagioclase-rich -quartz-biotite "granite".

40% black medium-grained quartz-plagioclase-biotite-pyroxene schist.

724 95% black fine- to medium-grained quartz-plagioclase-biotite-pyroxene schist.

5% white medium-grained plagioclase-quartz-biotite gneiss.

744 60% black fine-grained quartz-plagioclase-biotite-pyroxene +- amphibole granofels.

40% white fine-grained plagioclase-quartz-biotite gneiss.

764 black medium-grained quartz-plagioclase-biotite-pyroxene schist.

784 50% black medium-grained quartz-plagioclase-biotite-pyroxene schist.

50% whitish-gray medium-grained sulphide-bearing quartz-plagioclase-biotite gneiss.

804 black fine-grained sulphide- and sphene-bearing quartz-plagioclase-biotite-pyroxene granofels.

824 90% black medium-grained quartz-plagioclase-biotite-pyroxene schist.

10% bluish-white fine-grained sulphide-bearing plagioclase-quartz +- pyroxene +- biotite gneissic segregations

844 50% black fine-grained sulphide-bearing quartz-plagioclase-biotite-pyroxene granofels.

50% bluish-white medium- to coarse-grained garnet-bearing plagioclase-quartz-muscovite (coarse plates) granite.

864 black fine-grained quartz-plagioclase-biotite-pyroxene granofels.

884 black fine-grained quartz-plagioclase-biotite-pyroxene granofels. Some zeolite? mineralization on fracture surfaces.

904 bluish-white coarse-grained garnet-bearing plagioclase-quartz-muscovite (coarse plates) granite.

924 black fine-grained quartz-plagioclase-biotite-pyroxene granofels. Some zeolite mineralization on fracture surfaces.

944 black fine-grained quartz-plagioclase-biotite-pyroxene granofels. Some zeolite mineralization on fracture surfaces.

964 black fine-grained quartz-plagioclase-biotite-pyroxene granofels. Some zeolite mineralization on fracture surfaces.

984 black fine-grained quartz-plagioclase-biotite-pyroxene granofels.

CORE No.2 1001-1011 feet black fine- to medium-grained quartz-plagioclase-biotite-pyroxene +- calcite +- scapolite calcsilicate granofels.

1024 black fine-grained sulphide-bearing quartz-plagioclase-biotite-pyroxene granofels.

1044 black fine-grained sulphide- and sphene-bearing quartz-plagioclase-biotite-pyroxene granofels.

1064 97% black fine-grained quartz-plagioclase-biotite-pyroxene granofels.

3% white medium-grained sulphide-bearing plagioclase-quartz-biotite +- muscovite gneiss.

1084 90% black fine- to medium-grained quartz-plagioclase-biotite-pyroxene schist.

10% white fine-grained sulphide-bearing plagioclase-quartz-biotite gneiss.

1104 85% black fine-grained quartz-plagioclase-biotite-pyroxene granofels.

15% white medium- to coarse-grained garnet-bearing plagioclase-quartz granite

1124 85% black fine-grained quartz-plagioclase-biotite-pyroxene granofels.

15% white fine-grained plagioclase-quartz-biotite +-pyroxene gneiss.

1144 80% black fine-grained quartz-plagioclase-biotite-pyroxene granofels.

20% white fine-grained plagioclase-quartz-biotite +-pyroxene gneiss.

1164 bluish-white coarse-grained plagioclase-muscovite-quartz-biotite granite.

1184 98% black fine-grained sulphide-bearing quartz-plagioclase-biotite +- pyroxene granofels.

2% white fine-grained sulphide-bearing plagioclase-quartz-biotite gneiss.

1204 80% black fine-grained quartz-plagioclase-biotite +- pyroxene granofels.

20% white fine-grained plagioclase-quartz-biotite gneiss.

1215 bluish-white fine-grained plagioclase-k-feldspar-quartz gneiss.

1224 95% bluish-white medium-grained plagioclase-kspar-quartz-muscovite gneiss.

5% black fine-grained quartz-plagioclase-biotite granofels.

1244 50% bluish-white sulphide-bearing plagioclase-kspar-quartz-muscovite gneiss.

50% black fine-grained quartz-plagioclase-biotite granofels.

1264 bluish-gray medium-grained plagioclase-(kspar?)-quartz-biotite-muscovite gneiss.

1284 70% black fine-grained quartz-plagioclase-biotite +- pyroxene granofels.

30% bluish-white fine-grained sulphide-bearing plagioclase-quartz-biotite gneiss.

1304 90% black fine-grained quartz-plagioclase-biotite granofels.

10% white fine-grained garnet-bearing plagioclase-quartz-muscovite-biotite gneiss.

1324 bluish-gray medium-grained garnet- and sulphide-bearing plagioclase-quartz-biotite gneiss.

1344 85% black fine-grained quartz-plagioclase-biotite-pyroxene granofels
interlayered with
15% bluish-white fine- to medium-grained plagioclase-quartz-gneiss.
Some zeolite mineralization on fracture surfaces.

1364 95% black fine-grained quartz-plagioclase-biotite-pyroxene granofels.

5% bluish-white fine-grained plagioclase-quartz +- bioite gneiss.

1384 60% black fine-grained quartz-plagioclase-biotite-pyroxene granofels.

40% white fine- to medium-grained sulphide-bearing plagioclase-quartz +- biotite gneiss.

1404 black fine-grained quartz-plagioclase-biotite-pyroxene granofels.

1424 black fine-grained quartz-plagioclase-biotite-pyroxene granofels.

1444 black fine-grained quartz-plagioclase-biotite-pyroxene granofels.

1464 black fine-grained quartz-plagioclase-biotite-pyroxene granofels.

1484 black medium-grained quartz-plagioclase-biotite-muscovite schist.

CORE No.3 1500-1510 feet black fine-grained garnet-bearing quartz-plagioclase-biotite-muscovite-sillimanite schist.

1524 black medium-grained sulphide-bearing biotite-muscovite-garnet schist.

1544 black fine-grained quartz-plagioclase-biotite granofels.

1564 black fine-grained quartz-plagioclase-biotite +- pyroxene granofels.

1584 black fine-grained sulphide-bearing quartz-plagioclase-biotite-pyroxene granofels.

1604 black fine-grained quartz-plagioclase-biotite granofels.

1624 black fine-grained quartz-plagioclase-biotite granofels.

1644 black fine- to medium-grained biotite-muscovite +- sillimanite schist.

1664 black fine-grained quartz-plagioclase-biotite granofels.

1684 95% black fine-grained quartz-plagioclase-biotite granofels.

5% black garnet-bearing biotite-muscovite +- sillimanite schist.

1704 95% black fine-grained quartz-plagioclase-biotite granofels.

5% white medium-grained sulphide-bearing plagioclase-quartz-muscovite-biotite granite.

1724 95% black medium-grained biotite-muscovite-sillimanite schist.

5% white medium-grained garnet-bearing plagioclase-quartz-muscovite granite.

1744 black fine-grained sulphide-bearing quartz-plagioclase-biotite granofels.

1764 50% black fine-grained quartz-plagioclase-biotite +- amphibole granofels.

50% white medium- to coarse-grained plagioclase-quartz-biotite granite.

1784 50% black fine-grained quartz-plagioclase-biotite-pyroxene-amphibole granofels.

50% white coarse-grained plagioclase-quartz-biotite granite.

1804 90% black fine-grained quartz-plagioclase-biotite-pyroxene-amphibole granofels.

10% white coarse-grained garnet bearing plagioclase-quartz-biotite-muscovite granite.

1824 90% black fine-grained quartz-plagioclase-biotite-pyroxene granofels.

10% white coarse-grained garnet-bearing plagioclase-quartz +- muscovite granite.

1844 black fine-grained quartz-plagioclase-biotite-pyroxene granofels.

1864 85% black fine-grained sulphide-bearing quartz-plagioclase-biotite-pyroxene-amphibole granofels.

15% white medium- to coarse-grained plagioclase-quartz-biotite granite.

1884 50% black fine-grained quartz-plagioclase-biotite-pyroxene-amphibole granofels.

50% white and black medium-grained garnet-bearing plagioclase-quartz-biotite gneiss.

1904 black and white medium-grained garnet-bearing plagioclase-quartz-kspar biotite gneiss.

1924 black and white medium-grained garnet-bearing plagioclase-quartz-kspar-biotite gneiss.

1944 pinkish gray medium- to coarse-grained garnet-bearing plagioclase-quartz-kspar-biotite gneiss.

CORE No.4 1960-1966 feet pinkish-gray medium-grained garnet-bearing quartz-plagioclase-kspar-biotite gneiss.

1984 grayish salmon medium- to coarse-grained garnet-bearing kspar-quartz-plagioclase-biotite gneiss.

2004 pinkish gray medium-grained garnet-bearing quartz-kspar-plagioclase-biotite gneiss.

2024 light gray medium-grained garnet-bearing quartz-plagioclase-?kspar-biotite gneiss.

2044 light pinkish gray medium-grained garnet-bearing quartz-plagioclase-kspar-biotite-muscovite gneiss.

2064 60% black fine- to medium-grained sphene-bearing plagioclase-quartz-biotite-kspar schist.

40% pinkish gray medium-grained quartz-plagioclase-kspar-biotite gneiss.

2084 90% light gray quartz-plagioclase-biotite gneiss with locally abundant pink k-spar grains. Medium-grained.

8% black calcsilicate biotite-amphibole schist. Medium-grained.

2% Light green chloritic/mylonitic chips. Fine-grained.

2104 70% black fine-grained sulphide-bearing quartz-plagioclase-biotite-amphibole schist.

30% light pinkish gray medium- to coarse-grained garnet-bearing plagioclase-quartz-kspar gneiss.

2124 50% black and white medium- to coarse-grained quartz-plagioclase-biotite gneiss. Local coarse muscovite and bioite.

50% black fine to medium sphene-bearing quartz-plagioclase-biotite schist.

2144 50% white and black medium- to coarse-grained garnet-bearing quartz-plagioclase-kspar-biotite gneiss.

50% black medium-grained sphene- and sulphide-bearing quartz-plagioclase-biotite schist.

2164 80% pinkish white medium- to coarse-grained garnet- and pyrite-bearing quartz-plagioclase-kspar gneiss.

20% black medium-grained sphene-bearing quartz-plagioclase-biotite schist.

2184 70% steel gray fine-grained quartz-plagioclase-biotite gneiss. Greenish discoloration around black unidentified minerals.

30% black medium-grained sulphide-bearing quartz-plagioclase-biotite schist.

2204 85% black mylonitic fine- to medium-grained sulphide-bearing quartz-plagioclase-biotite schist. Mylonitic areas are very fine grained and massive and greenish in color.

15% white coarse-grained quartz-plagioclase-biotite sulphide-bearing gneiss

2224 60% black fine- to medium-grained sulphide-bearing quartz-plagioclase-biotite-muscovite schist.

40% white medium-grained locally garnet-bearing plagioclase-quartz-muscovite-biotite gneiss

2244 95% black fine- to medium-grained quartz-plagioclase-biotite-muscovite schist.

5% white coarse-grained quartz-plagioclase segregations/compositional layers.

2264 80% black medium-grained quartz-plagioclase-biotite +- pyroxene (diopside) schist.

20% coarse white plagioclase-quartz-biotite segregations?/compositional layering?

2284 80% black fine-grained sulphide-bearing quartz-plagioclase-biotite-muscovite schist. Muscovite-rich surfaces are usually well lineated. Some granofels present.

20% white fine-grained garnet-bearing plagioclase-quartz-muscovite segregations/compositional layers.

2304 70% same-as-above black schist and granofels.

30% white medium-grained plagioclase-quartz-muscovite-biotite seg/comp.

2324 90% black fine-grained sulphide-bearing quartz-plagioclase-biotite schist.

10% white medium- to coarse-grained plagioclase-quartz-biotite seg/comp.

2344 95% black medium-grained sulphide-bearing quartz-plagioclase-biotite-amphibole schist. Some smeared and well lineated surfaces present. Some sulphide smearing.

5% misc. rocks- some medium-grained white granitic chips; some more leucocratic schists, some greenish mylonitic sulphide-rich chips.

2364 95% black medium-grained quartz-plagioclase-biotite-muscovite and quartz-plagioclase-biotite-amphibole schists.

5% misc. - some vein quartz; some smeared mylonitic sulphitic surfaces.

2384 70% black medium-grained sulphide- and garnet-bearing quartz-plagioclase-biotite-muscovite schist

30% white medium-grained garnet-bearing quartz-plagioclase-muscovite gneiss.

2404 90% black medium-grained sulphide-bearing quartz-plagioclase-biotite-

muscovite +- garnet +- sillimanite schist.

10% white medium- to coarse-grained quartz-plagioclase-muscovite gneiss.

2424 85% black sulphide- and garnet-bearing quartz-plagioclase-biotite-muscovite schist.

5% black medium-grained amphibole-plagioclase-quartz gneiss.

10% white quartz-plagioclase +- k-feldspar granite.

2444 85% black medium-grained sulphide-bearing quartz-plagioclase-biotite schist.

10% black medium-grained amphibole-plagioclase-quartz-pyroxene gneiss.

5% white coarse-grained quartz-plagioclase granite.

CORE No.5 2460-2465 feet black medium-grained quartz-plagioclase-biotite augen schist.

2484 90% black medium-grained sulphide- and sphene-bearing quartz-plagioclase-biotite-amphibole schist.

10% white quartz-plagioclase-biotite gneiss.

2504 70% black medium-grained sulphide- and garnet-bearing quartz-plagioclase-biotite-muscovite schist (one chip contained sillimanite).

30% white medium-grained quartz-plagioclase-muscovite granite.

2524 95% black fine-grained sulphide-bearing quartz-plagioclase-amphibole-biotite gneiss.

5% white coarse-grained quartz-plagioclase granite.

2544 85% black medium-grained sulphide-bearing quartz-plagioclase-biotite-muscovite-garnet schist.

15% white medium-grained quartz-plagioclase-muscovite granite.

2564 80% black medium-grained sulphide- and garnet-bearing quartz-plagioclase-biotite-muscovite schist.

15% black medium-grained biotite-amphibole-plagioclase-quartz-pyroxene gneiss.

10% white medium-grained quartz-plagioclase-muscovite granite.

2584 95% black fine- to medium-grained sulphide-bearing quartz-plagioclase-biotite-muscovite-sillimanite-garnet schist.

5% white coarse quartz-plagioclase-muscovite granite.

2604 85% black fine- to medium-grained sulphide-bearing quartz-plagioclase-biotite-muscovite-sillimanite-garnet schist.

15% white medium-grained quartz-plagioclase-muscovite granite.

some greenish mylonitic chips present.

2624 70% black medium-grained quartz-plagioclase-biotite-muscovite-sillimanite-garnet schist.

10% black medium-grained amphibole-biotite-plagioclase-quartz gneiss.

20% white medium-grained quartz-plagioclase granite.

2634 60% white and pink medium- to coarse-grained magnetite-bearing quartz-kspar-plagioclase gneiss.

40% black medium-grained quartz-plagioclase-amphibole-biotite gneiss.

2644 60% pinkish-white coarse-grained magnetite-bearing quartz-k-feldspar-plagioclase-biotite gneiss.

40% black medium-grained quartz-plagioclase-biotite-amphibole schist.

2664 35% black medium-grained sulphide-bearing quartz-plagioclase-biotite-amphibole +- pyroxene schist

35% black medium-grained quartz-plagioclase-biotite-muscovite schist.

30% white medium-grained sulphide-bearing quartz-plagioclase-biotite gneiss.

2684 60% light gray fine- to medium-grained quartz-plagioclase-biotite-magnetite gneiss.

40% black medium-grained sulphide-bearing quartz-plagioclase-biotite schist.

2704 light gray fine-grained quartz-plagioclase-biotite gneiss.

2724-4784 feet undifferentiated quartz-plagioclase-biotite-amphibole gneisses of the Waterford Group.

SECTION 3

This section consists of a core log of the 9 cores recovered from the Moodus borehole. The cores were logged on a 1:2 scale. The logs also show the locations of thin sections used for microscopic analyses.

Logged by: P.G. Naumoff Date: 4/16/87

CORE LOG

Project Moodus borehole 86c4111

Run 1 of 9

Depth, ft	Sketch Scale = 1:2	Thin Section	Foliation Strike/Dip	Rock Fabric		Remarks
				Strike/Dip	Description	
501						Calcsilicate gneiss of the Hebron Formation. Dark – grey to black, fine – to medium grained, biotite – quartz – feldspar rock. Foliation well defined by parallel biotite flakes and by alternating mafic/felsic layers. Leucocratic (felsic) layers range from 1/10 inch to several inches thick.
0.1						
0.2						
0.3						
0.4						
0.5	TOP OF CORE FELSIC SEGREGATION BIOTITE-RICH LAYER					
0.6						
0.7						
0.8			Foliation 15 degree dip			
0.9						
502						

Logged by: P.G. Naumoff Date: 4/16/87

CORE LOG

Project Moodus borehole 86c4111

Run 1 of 9

Page 2 of 11

Depth, ft 502	Sketch Scale = 1:2	Thin Section	Foliation Strike/Dip	Rock Fabric		Remarks
				Strike/Dip	Description	
0.1						
0.2					nebulous, non – continuous felsic segregations.	
0.3						
0.4						
0.5	LEUCOCRATIC SEGREGATION				core break	
0.6						
0.7	QF		Foliation 5 degree dip		wide quartzo – feldspathic band.	
0.8						
0.9						
503						

Logged by: P.G. Naumoff Date: 4/16/87

CORE LOG

Project Moodus borehole 86c4111

Run 1 of 9

Depth, ft 503	Sketch Scale = 1:2	Thin Section	Foliation Strike/Dip	Rock Fabric		Remarks
				Strike/Dip	Description	
0.1			Foliation 20 degree dip		Layering well developed	
0.2						
0.3						
0.4						
0.5						
0.6						
0.7					layering less well – developed; segregations not continuous, nebulous	
0.8						
0.9						
504						

Logged by: P.G. Naumoff Date: 4/16/87

CORE LOG

Project Moodus borehole 86c4111

Run 1 of 9

Depth, ft 504	Sketch Scale = 1:2	Thin Section	Foliation Strike/Dip	Rock Fabric		Remarks
				Strike/Dip	Description	
0.1	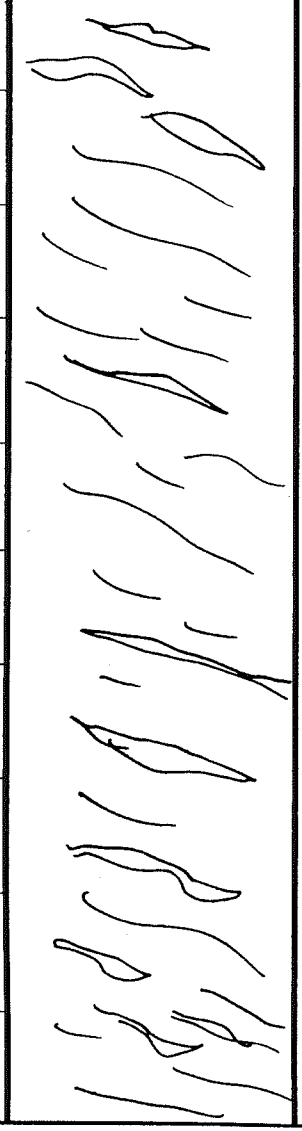				Swirly, nebulous layering; augen – like	
0.2						
0.3						
0.4						
0.5					Layering becomes sub – horizontal	
0.6						
0.7						
0.8						
0.9						
505						

Logged by: P.G. Naumoff Date: 4/16/87

CORE LOG

Project Moodus borehole 86c4111

Run 1 of 9

Depth, ft 505	Sketch Scale = 1:2	Thin Section	Foliation Strike/Dip	Rock Fabric		Remarks
				Strike/Dip	Description	
0.1	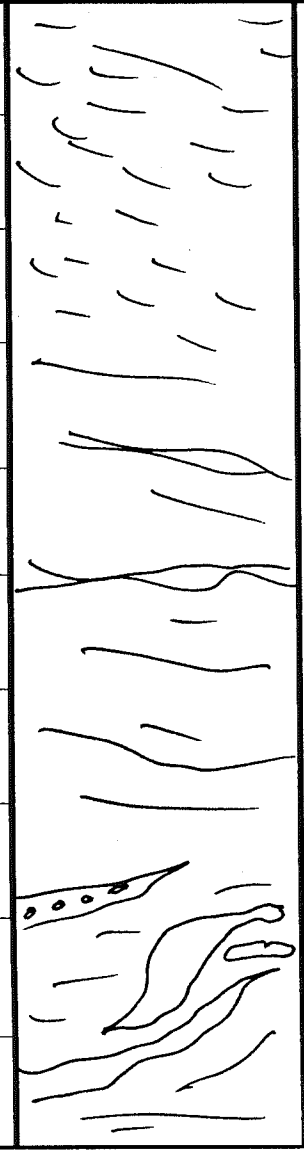				Nebulous, augen – like layering.	
0.2						
0.3					Layering becomes better developed.	
0.4						
0.5						
0.6						
0.7					Quartzo – feldspathic segregation with garnet.	
0.8					Folded quartzo – feldspathic segregation.	
0.9						
506						

Logged by: P.G. Naumoff Date: 4/16/87

CORE LOG

Project Moodus borehole 86c4111

Run 1 of 9

Depth, ft 506	Sketch Scale = 1:2	Thin Section	Foliation Strike/Dip	Rock Fabric		Remarks
				Strike/Dip	Description	
0.1	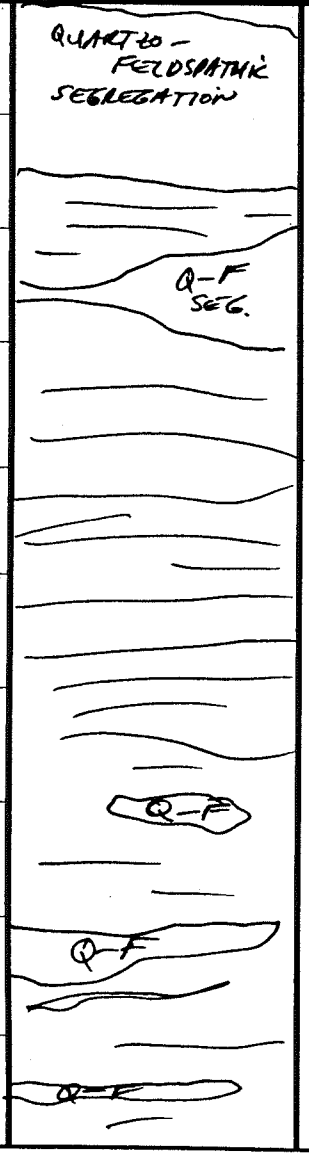				Quartzo – feldspathic segregations become less prominant.	
0.2						
0.3						
0.4						
0.5						
0.6						
0.7						
0.8						
0.9						
507						

Logged by: P.G. Naumoff Date: 4/16/87

CORE LOG

Project Moodus borehole 86c4111

Run 1 of 9

Page 7 of 11

Depth, ft 507	Sketch Scale = 1:2	Thin Section	Foliation Strike/Dip	Rock Fabric		Remarks
				Strike/Dip	Description	
0.1	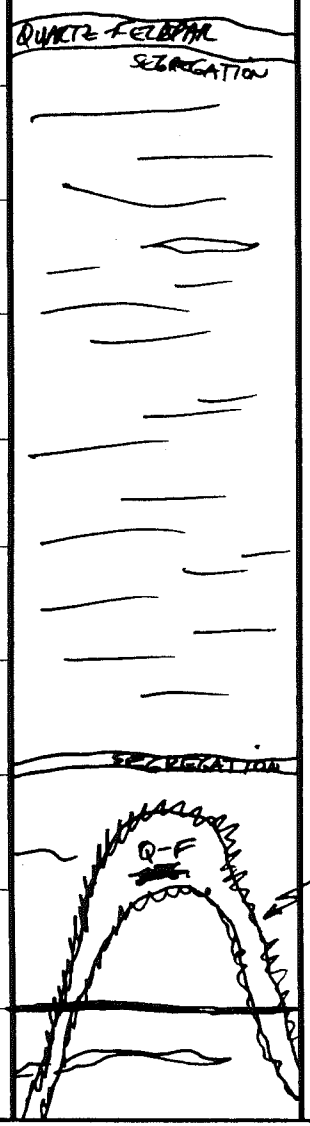		Horizontal foliation.		A). Cross – cutting vein; contains quartz – feldspar and greenish alterations along vein edges. Extends down to 509.8 feet. Vein is 2/10 to 3/10 inch wide.	
0.2						
0.3						
0.4						
0.5						
0.6						
0.7						
0.8						
0.9						
508					Fresh core break.	

Logged by: P.G. Naumoff Date: 4/16/87

Run 1 of 9

CORE LOG

Project Moodus borehole 86c4111

Depth, ft 508	Sketch Scale = 1:2	Thin Section	Foliation Strike/Dip	Rock Fabric		Remarks
				Strike/Dip	Description	
0.1	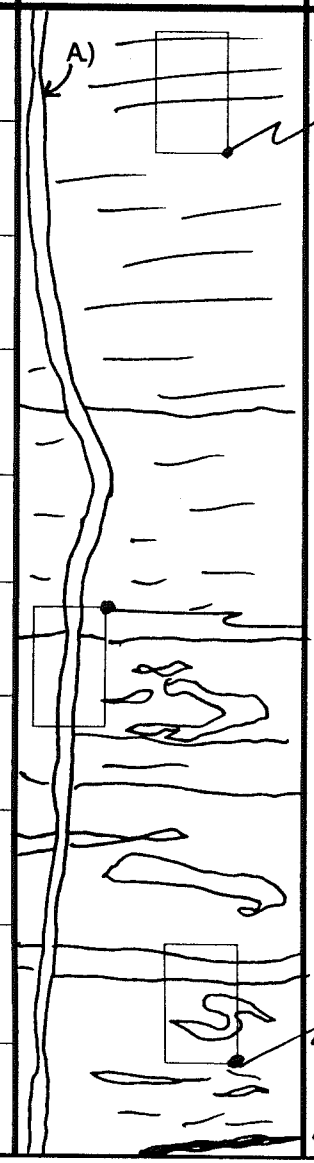				A.) Cross – cutting quartzo – feldspathic vein.	
0.2						
0.3						
0.4					Wide white quartzo – feldspathic layer.	
0.5						
0.6					Swirly ptygmatic folding.	
0.7						
0.8						
0.9					B.) Fracture has slicked calcite paste and elongate voids that contain very fine euhedral crystals. - CALCITE	
509						

Logged by: P.G. Naumoff Date: 4/16/87

CORE LOG

Project Moodus borehole 86c4111

Run 1 of 9

Depth, ft 509	Sketch Scale = 1:2	Thin Section	Foliation Strike/Dip	Rock Fabric		Remarks
				Strike/Dip	Description	
0.1	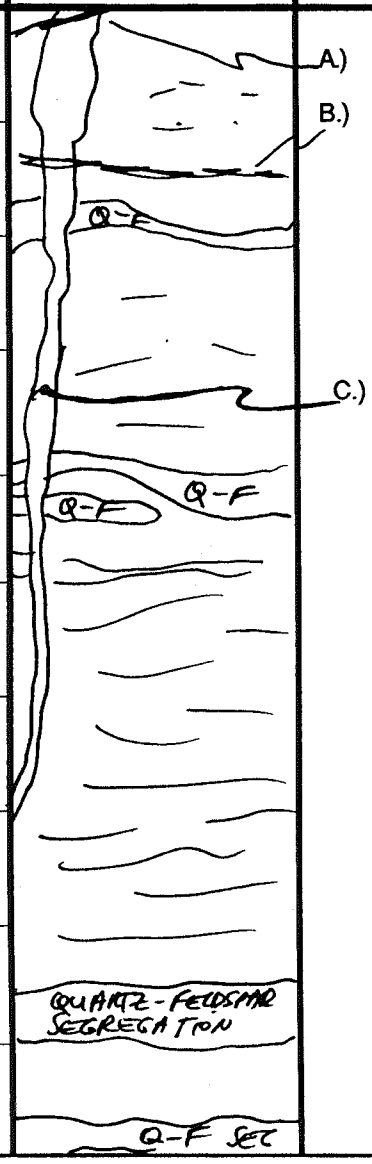		Subhorizontal foliation.	A.) Fracture dips 15 degrees. B.) horizontal fracture.	Lineations of slicked calcite well developed. Slicked with calcite paste. C.) Vein with alteration.	
0.2						
0.3						
0.4						
0.5						
0.6						
0.7						
0.8						
0.9						
510						

Logged by: P.G. Naumoff Date: 4/16/87

CORE LOG

Project Moodus borehole 86c4111

Run 1 of 9

Depth, ft 510	Sketch Scale = 1:2	Thin Section	Foliation Strike/Dip	Rock Fabric		Remarks
				Strike/Dip	Description	
0.1						
0.2					Foliation not that well developed except for the quartz – feldspar segregations.	
0.3	Q-F. QUARTZ FELDSPAR SEG.					
0.4						
0.5					Drill break – fresh	
0.6						
0.7						
0.8					Foliation gets a bit swirly.	
0.9	Q-F					
511						

Logged by: P.G. Naumoff Date: 4/16/87

CORE LOG

Project Moodus borehole 86c4111

Run 1 of 9

Depth, ft	Sketch Scale = 1:2	Thin Section	Foliation Strike/Dip	Rock Fabric		Remarks
				Strike/Dip	Description	
511						
0.1	QF		Horizontal foliation.		Quartzo–feldspathic layer.	
0.2						
0.3						
0.4	END CORE 511.38 ft					
0.5						
0.6						
0.7						
0.8						
0.9						
512						

Logged by: P.G. Naumoff Date: 4/23/87

CORE LOG

Project Moodus borehole 86c4111

Run 2 of 9

Page 1 of 10

Depth, ft	Sketch Scale = 1:2	Thin Section	Foliation Strike/Dip	Rock Fabric		Remarks
				Strike/Dip	Description	
1001	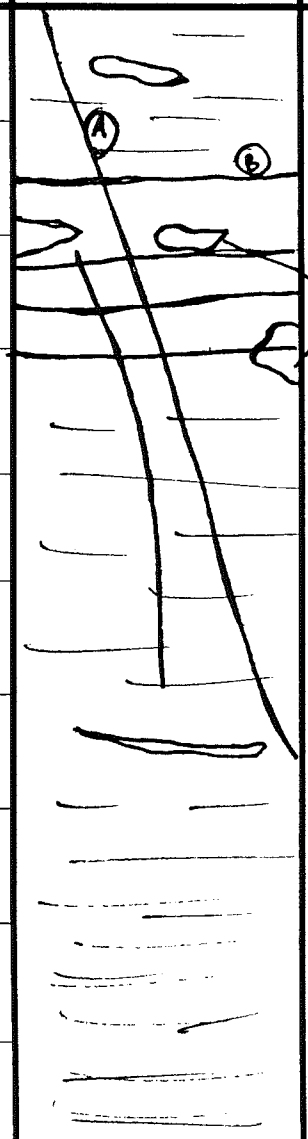		Subhorizontal foliation.	A.) 65 degrees	A.) Quartz – feldspar fracture cuts the foliation – has a thinner sub – parallel vein associated with it. B.) Horizontal breaks along slightly weathered surfaces; biotites weathered to a lighter color. Foliation massive – looking; homogeneous gneiss. No quartz – feldspar segregations.	Grayish biotite gneiss of the Hebron Formation. Fine – to medium – grained with occasional quartz – diopside (CPX) knots and segregations.
1002						

Logged by: P.G. Naumoff Date: 4/23/87

CORE LOG

Project Moodus borehole 86c4111

Run 2 of 9

Depth, ft	Sketch Scale = 1:2	Thin Section	Foliation Strike/Dip	Rock Fabric		Remarks
				Strike/Dip	Description	
1002						
0.1						
0.2			Subhorizontal foliation.			
0.3		qtz – cpx – feldspar knots.				
0.4						
0.5						
0.6					Amorphous felsic and cpx knots with biotite selvages.	
0.7		MC 1002				
0.8						
0.9						
1003						

Logged by: P.G. Naumoff Date: 4/23/87

CORE LOG

Project Moodus borehole 86c4111

Run 2 of 9

Page 3 of 10

Depth, ft	Sketch Scale = 1:2	Thin Section	Foliation Strike/Dip	Rock Fabric		Remarks
				Strike/Dip	Description	
1003	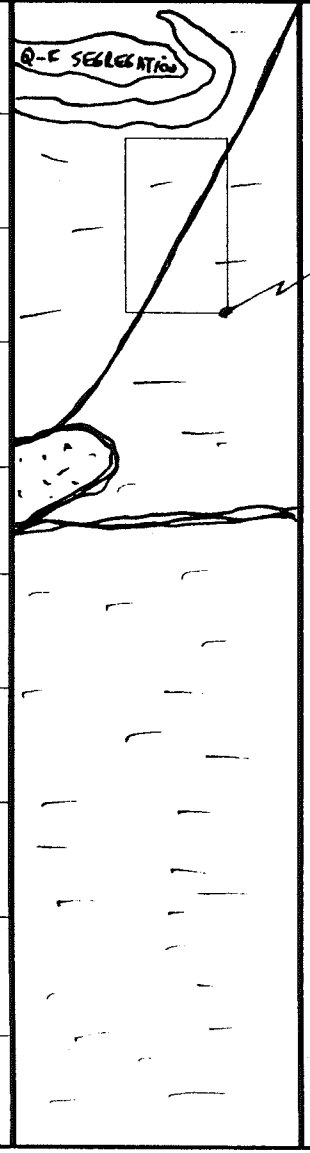	MC 1003	Horizontal foliation.	65 deg. dip	Cross–cutting quartz–feldspar fracture. cpx–rich greenish band.	
0.1						
0.2						
0.3						
0.4						
0.5						
0.6						
0.7						
0.8						
0.9						
1004						

Logged by: P.G. Naumoff Date: 4/23/87

CORE LOG

Project Moodus borehole 86c4111

Run 2 of 9

Page 4 of 10

Depth, ft	Sketch Scale = 1:2	Thin Section	Foliation Strike/Dip	Rock Fabric		Remarks
				Strike/Dip	Description	
1004	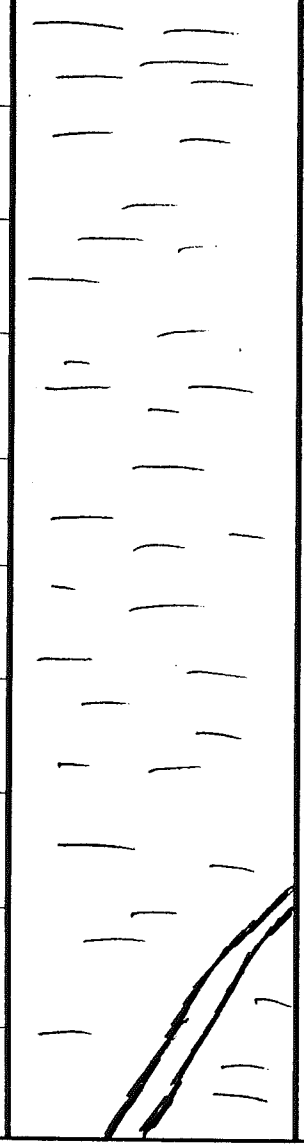		Horizontal foliation.	Fracture dips 50 degs.	Quartz – feldspar – cpx fracture with biotite selvages.	
0.1						
0.2						
0.3						
0.4						
0.5						
0.6						
0.7						
0.8						
0.9						
1005						

Logged by: P.G. Naumoff Date: 4/23/87

CORE LOG

Project Moodus borehole 86c4111

Run 2 of 9

Page 5 of 10

Depth, ft	Sketch Scale = 1:2	Thin Section	Foliation Strike/Dip	Rock Fabric		Remarks
				Strike/Dip	Description	
1005	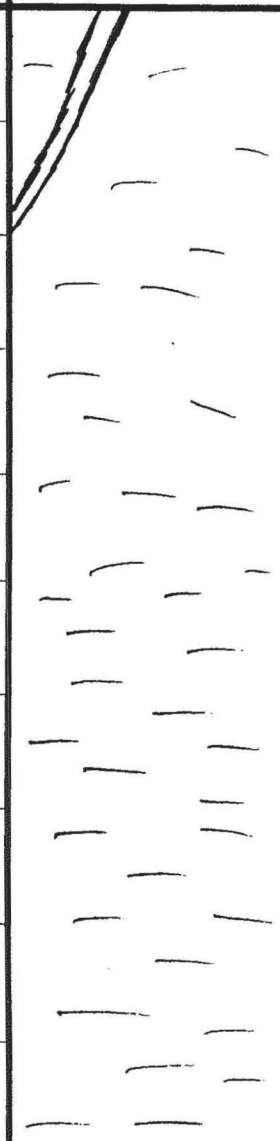			Fracture dips 50 degs.	Quartz – feldspar – cpx fracture with biotite selvages.	Homogeneous biotite gneiss.
0.1						
0.2						
0.3						
0.4						
0.5						
0.6			Horizontal foliation.			
0.7						
0.8						
0.9						
1006						

Logged by: P.G. Naumoff Date: 4/23/87

CORE LOG

Project Moodus borehole 86c4111

Run 2 of 9

Page 6 of 10

Depth, ft	Sketch Scale = 1:2	Thin Section	Foliation Strike/Dip	Rock Fabric		Remarks
				Strike/Dip	Description	
1006	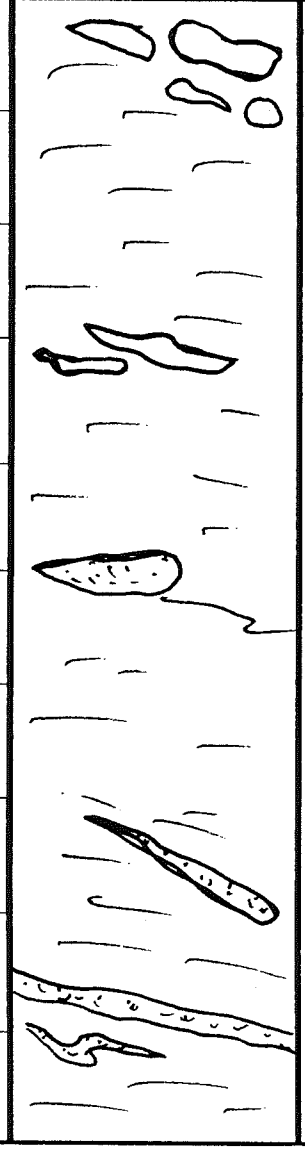	cpx – rich knots.	Horizontal foliation.		Quartz – feldspar +/– cpx knots.	
0.1						
0.2						
0.3						
0.4						
0.5						
0.6						
0.7						
0.8					Knot cross – cuts the foliation ?	
0.9						
1007						

Logged by: P.G. Naumoff Date: 4/23/87

CORE LOG

Project Moodus borehole 86c4111

Run 2 of 9

Depth, ft 1007	Sketch Scale = 1:2	Thin Section	Foliation Strike/Dip	Rock Fabric		Remarks
				Strike/Dip	Description	
0.1	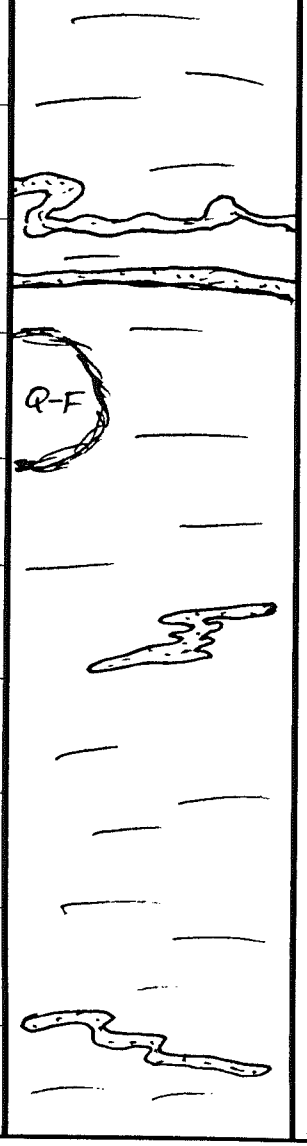				Quartz – feldspar – cpx rich layers.	
0.2						
0.3					Some slight convoluted folding of segregations.	
0.4					Quartz – feldspar segregation with biotite – cpx selavage.	
0.5						
0.6					Diopside – rich (cpx) layers appear to define some intra – folial folding.	
0.7						
0.8						
0.9						
1008						

Logged by: P.G. Naumoff Date: 4/23/87

CORE LOG

Project Moodus borehole 86c4111

Run 2 of 9

Depth, ft	Sketch Scale = 1:2	Thin Section	Foliation Strike/Dip	Rock Fabric		Remarks
				Strike/Dip	Description	
1008	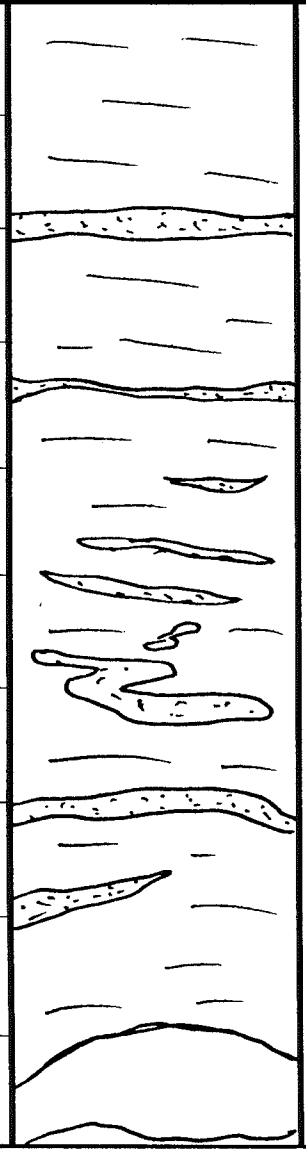		Subhorizontal foliation.		Cpx–rich layers becoming more abundant.	
0.1						
0.2						
0.3						
0.4					Some chaotic isoclinal folds defined by cpx layers.	
0.5						
0.6						
0.7						
0.8						
0.9					Large, coarse qtz +/– cpx segregation.	
1009						

Logged by: P.G. Naumoff Date: 4/23/87

CORE LOG

Project Moodus borehole 86c4111

Run 2 of 9

Depth, ft	Sketch Scale = 1:2	Thin Section	Foliation Strike/Dip	Rock Fabric		Remarks
				Strike/Dip	Description	
1009	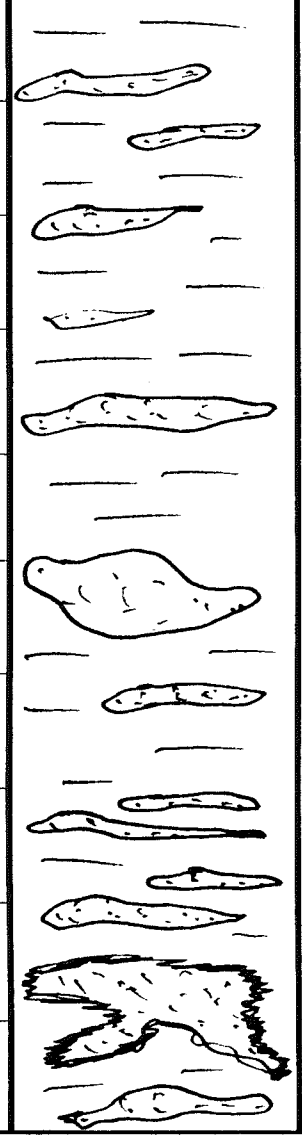					Greenish – white diopside (cpx) – rich layers abundant, but generally not a penetrative fabric.
0.1						
0.2						
0.3						
0.4						
0.5					Wispy, cpx – rich flasers.	
0.6						
0.7						
0.8						
0.9					Some biotite selvages associated with the segregations.	
1010						

Logged by: P.G. Naumoff Date: 4/23/87

CORE LOG

Project Moodus borehole 86c4111

Run 2 of 9

Depth, ft	Sketch Scale = 1:2	Thin Section	Foliation Strike/Dip	Rock Fabric		Remarks
				Strike/Dip	Description	
1010	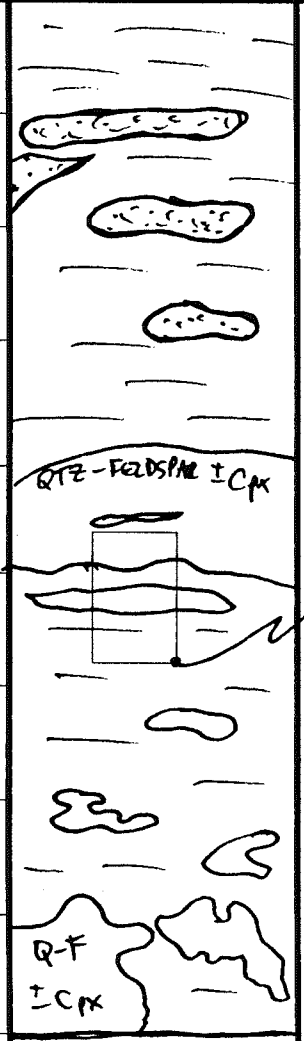				Abundant white quartz – feldspar and greenish cpx – rich segregations.	
	END CORE 1010.90 ft.					
1011						

Logged by: P.G. Naumoff Date: 4/25/87

CORE LOG

Project Moodus borehole 86c4111

Run 3 of 9

Page 1 of 10

Depth, ft	Sketch Scale = 1:2	Thin Section	Foliation Strike/Dip	Rock Fabric		Remarks
				Strike/Dip	Description	
1500	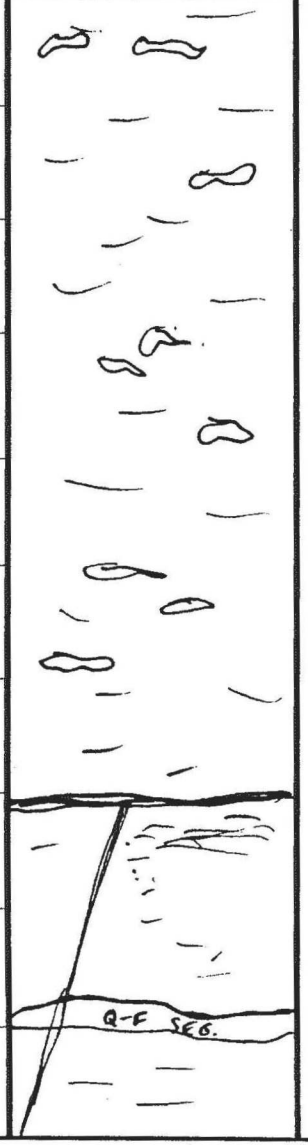	Generalized sketch of core.	Subhorizontal foliation.		Core breaks – slightly punky zone; some kaolinized feldspars.	Grayish – black, blotchy, muscovite – biotite – sillimanite schist, medium – to coarse – grained. Blotchy texture results from irregular pods and knots of quartzo – feldspathic segregations associated with biotite selvages. Trace garnet. Sillimanite associated with muscovite rich layers.
0.1						
0.2						
0.3						
0.4						
0.5						
0.6						
0.7						
0.8						
0.9						
1501						

Logged by: P.G. Naumoff Date: 4/25/87

CORE LOG

Project Moodus borehole 86c4111

Run 3 of 9

Depth, ft	Sketch Scale = 1:2	Thin Section	Foliation Strike/Dip	Rock Fabric		Remarks
				Strike/Dip	Description	
1501		Generalized sketch of core.				
0.1					Core break.	
0.2						
0.3						
					Irregular quartz – feldspar segregations	
0.4						
0.5						
0.6						
0.7						
0.8						
0.9					Core break.	
1502						

Logged by: P.G. Naumoff Date: 4/25/87

CORE LOG

Project Moodus borehole 86c4111

Run 3 of 9

Page 3 of 10

Depth, ft	Sketch Scale = 1:2	Thin Section	Foliation Strike/Dip	Rock Fabric		Remarks
				Strike/Dip	Description	
1502	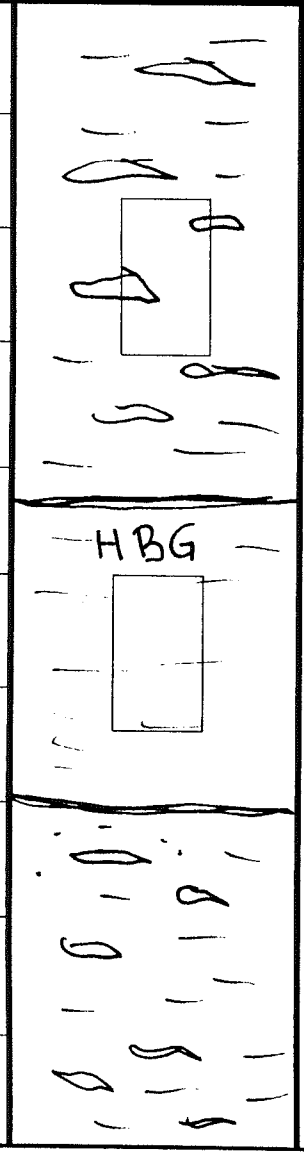	Generalized sketch of core.				
0.1						
0.2		MC 1502 A				
0.3						
					Core break.	
0.4					HBG	Textural change – rock becomes more homogeneous, no segregations. Fine biotite gneiss (HGB)
0.5	HBG					
		MC 1502 B				
0.6						
0.7						
0.8						
0.9						
1503						

Logged by: P.G. Naumoff Date: 4/25/87

CORE LOG

Project Moodus borehole 86c4111

Run 3 of 9

Page 4 of 10

Depth, ft	Sketch Scale = 1:2	Thin Section	Foliation Strike/Dip	Rock Fabric		Remarks
				Strike/Dip	Description	
1503		Generalized sketch of core.				
0.1						
0.2	HBG					
0.3						
0.4						
0.5						
0.6						
0.7	HGB					
0.8						
0.9						
1504						

Logged by: P.G. Naumoff Date: 4/25/87

CORE LOG

Project Moodus borehole 86c4111

Run 3 of 9

Depth, ft	Sketch Scale = 1:2	Thin Section	Foliation Strike/Dip	Rock Fabric		Remarks
				Strike/Dip	Description	
1504		Generalized sketch of core.				
0.1						
0.2	HBG					
0.3						
		MC 1504				
0.4						
0.5						
0.6						
0.7						
0.8						
0.9						
1505						

Logged by: P.G. Naumoff Date: 4/25/87

CORE LOG

Project Moodus borehole 86c4111

Run 3 of 9

Depth, ft	Sketch Scale = 1:2	Thin Section	Foliation Strike/Dip	Rock Fabric		Remarks
				Strike/Dip	Description	
1505		Generalized sketch of core.				
0.1						
0.2						
0.3						
0.4						
0.5						
0.6						
0.7						
0.8						
0.9						
1506						

Logged by: P.G. Naumoff Date: 4/25/87

CORE LOG

Project Moodus borehole 86c4111

Run 3 of 9

Depth, ft	Sketch Scale = 1:2	Thin Section	Foliation Strike/Dip	Rock Fabric		Remarks
				Strike/Dip	Description	
1506	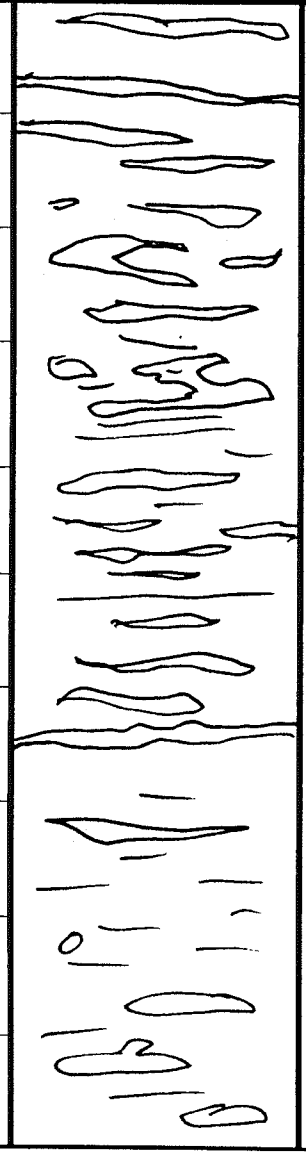	Generalized sketch of core.			Well developed segregations.	
0.1						
0.2						
0.3						
0.4						
0.5						
0.6						
0.7						
0.8						
0.9						
1507						

Logged by: P.G. Naumoff Date: 4/25/87

CORE LOG

Project Moodus borehole 86c4111

Run 3 of 9

Depth, ft	Sketch Scale = 1:2	Thin Section	Foliation Strike/Dip	Rock Fabric		Remarks
				Strike/Dip	Description	
1507	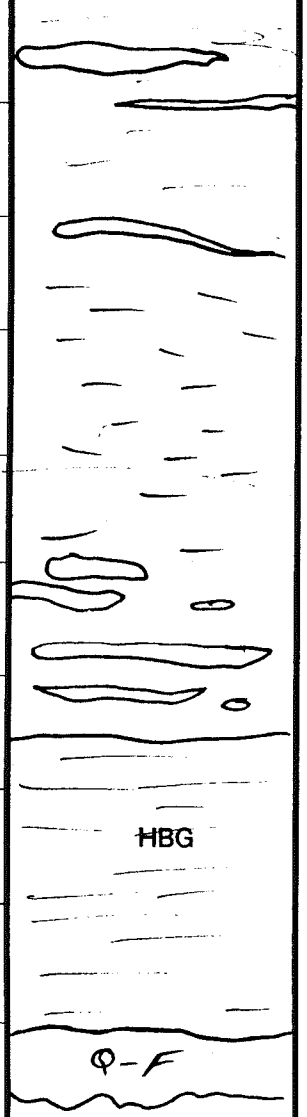	Generalized sketch of core.				
0.1						
0.2						
0.3						
0.4						
0.5						
0.6						
0.7						
0.8						
0.9						
1508					Quartz – feldspar segregation.	

Logged by: P.G. Naumoff Date: 4/25/87

CORE LOG

Project Moodus borehole 86c4111

Run 3 of 9

Page 9 of 10

Depth, ft	Sketch Scale = 1:2	Thin Section	Foliation Strike/Dip	Rock Fabric		Remarks
				Strike/Dip	Description	
1508	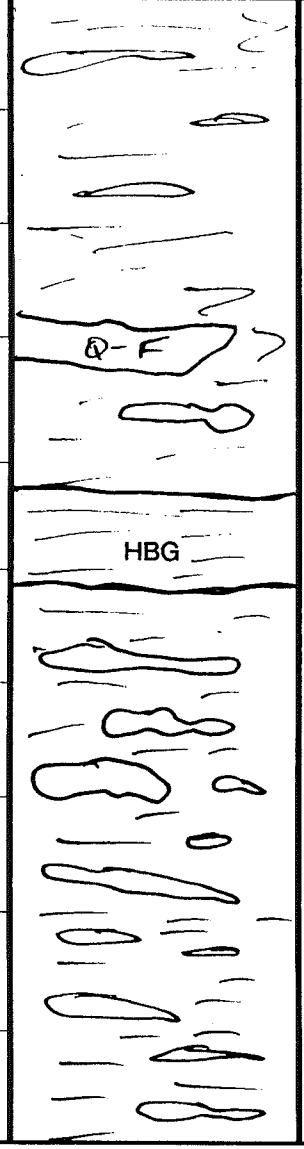	Generalized sketch of core.			Quartz – feldspar segregation.	
0.1						
0.2						
0.3						
0.4						
0.5						
0.6						
0.7						
0.8						
0.9						
1509						

Logged by: P.G. Naumoff Date: 4/25/87

CORE LOG

Project Moodus borehole 86c4111

Run 3 of 9

Depth, ft	Sketch Scale = 1:2	Thin Section	Foliation Strike/Dip	Rock Fabric		Remarks
				Strike/Dip	Description	
1509		Generalized sketch of core.				
0.1						
0.2	HBG					
0.3						
0.4					Quartz – feldspar segregation.	
0.5						
0.6						
0.7						
0.8						
0.9	END CORE 1509.82 ft					
1510						

Logged by: P.G. Naumoff Date: 5/01/87

CORE LOG

Project Moodus borehole 86c4111

Run 4 of 9

Depth, ft	Sketch Scale = 1:2	Thin Section	Foliation Strike/Dip	Rock Fabric		Remarks
				Strike/Dip	Description	
1960			Subhorizontal foliation.		Homogeneous – layering not well developed. Some blotchy and streaky pink, leucocratic segregations.	Light gray and pink granitic gneiss, containing quartz, pink k – feldspar, plagioclase, biotite, and minor garnet. Some well – developed compositional layering rich in k – feldspar present. Canterbury Gneiss. Core was recovered in two runs; upper 1.45 feet can not be oriented with respect ot the lower section of core.
0.1						
0.2						
0.3						
0.4						
0.5						
0.6						
0.7						
0.8						
0.9						
1961						

Logged by: P.G. Naumoff Date: 5/01/87

CORE LOG

Project Moodus borehole 86c4111

Run 4 of 9

Depth, ft	Sketch Scale = 1:2	Thin Section	Foliation Strike/Dip	Rock Fabric		Remarks
				Strike/Dip	Description	
1961	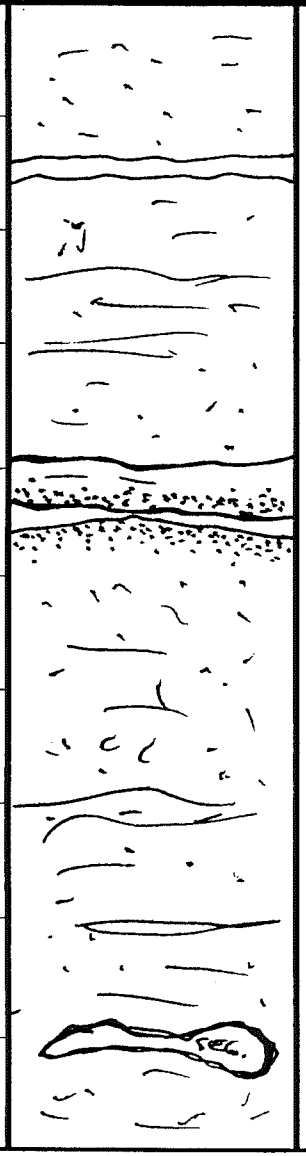		Subhorizontal foliation.		Pink compositional layer.	
0.1						
0.2						
0.3					Drilling crack.	Core was pulled for rig repair; upper and lower pieces not oriented with respect to each other.
0.4						
0.5						
0.6						
0.7					Compositional layers become a little better defined.	
0.8						
0.9					K–feldspar segregations with biotite selvages.	
1962						

Logged by: P.G. Naumoff Date: 5/01/87

CORE LOG

Project Moodus borehole 86c4111

Run 4 of 9

Page 3 of 7

Depth, ft 1962	Sketch Scale = 1:2	Thin Section	Foliation Strike/Dip	Rock Fabric		Remarks
				Strike/Dip	Description	
0.1	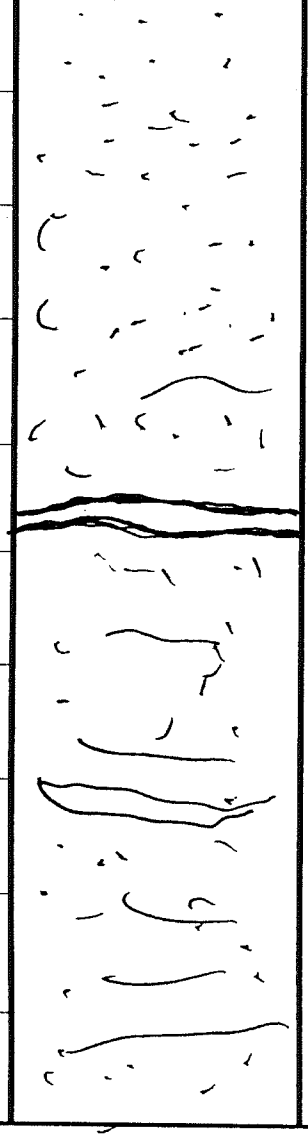		Subhorizontal foliation.			
0.2					Fairly homogeneous; layering poorly defined.	
0.3						
0.4						
0.5					K–feldspar–garnet segregation and biotite selvages.	
0.6						
0.7					K–feldspar rich layer.	
0.8						
0.9						
1963						

Logged by: P.G. Naumoff Date: 5/01/87

CORE LOG

Project Moodus borehole 86c4111

Run 4 of 9

Depth, ft	Sketch Scale = 1:2	Thin Section	Foliation Strike/Dip	Rock Fabric		Remarks
				Strike/Dip	Description	
1963						
0.1						
0.2						
0.3					Pinkish fine – grained layer.	
0.4						
0.5					K – feldspar – garnet rich layer.	
0.6						
0.7						
0.8						
0.9					K – feldspar rich layer.	
1964						

Logged by: P.G. Naumoff Date: 5/05/87

CORE LOG

Project Moodus borehole 86c4111

Run 4 of 9

Depth, ft	Sketch Scale = 1:2	Thin Section	Foliation Strike/Dip	Rock Fabric		Remarks
				Strike/Dip	Description	
1964	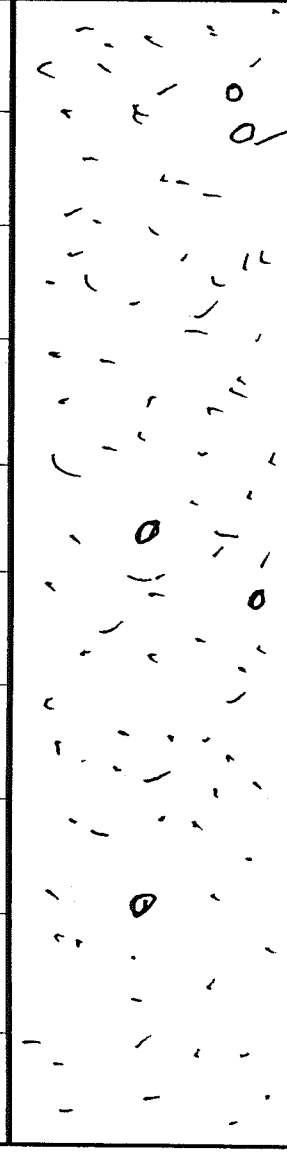	Garnets.	Subhorizontal foliation.		Homogeneous granitic gneiss; layering not well – developed.	
0.1						
0.2						
0.3						
0.4						
0.5						
0.6						
0.7						
0.8						
0.9						
1965						

Logged by: P.G. Naumoff Date: 5/05/87

CORE LOG

Project Moodus borehole 86c4111

Run 4 of 9

Page 6 of 7

Depth, ft 1965	Sketch Scale = 1:2	Thin Section	Foliation Strike/Dip	Rock Fabric		Remarks
				Strike/Dip	Description	
0.1	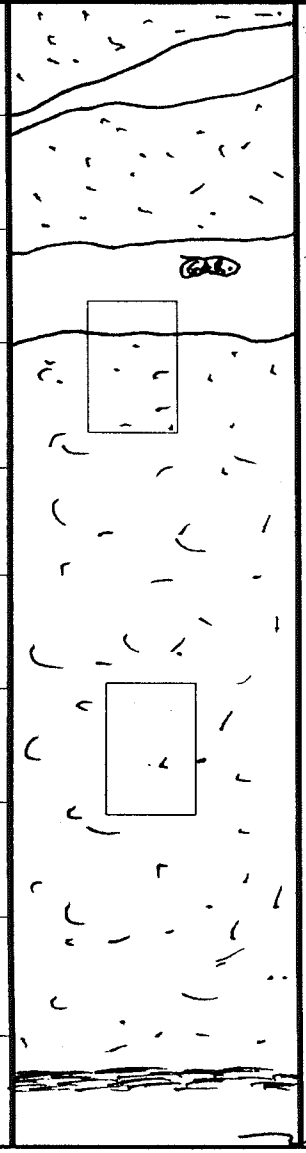				K–spar rich layer.	
0.2					K–feldspar–quartz–garnet segregation.	
0.3		MC 1966 A				
0.4						
0.5						
0.6		MC 1966 B				
0.7						
0.8						White gneiss; homogeneous, medium–to coarse–grained containing quartz feldspar, biotite (about 10%), and trace garnet. Some pinkish feldspar, but not as much as in the overlying unit. Layering poorly developed but some foliation is moderately developed with biotite.
0.9					Biotite–rich layer forms the contact between pink and white granitic gneisses.	
1966		WHITE GNEISS				

Logged by: P.G. Naumoff Date: 5/05/87

CORE LOG

Project Moodus borehole 86c4111

Run 4 of 9

Depth, ft 1966	Sketch Scale = 1:2	Thin Section	Foliation Strike/Dip	Rock Fabric		Remarks
				Strike/Dip	Description	
0.1	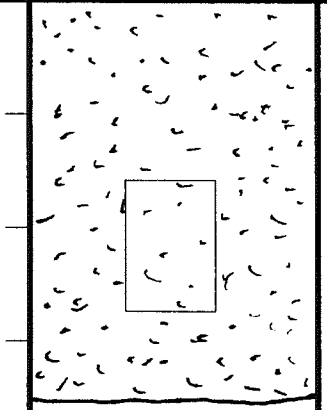	MC 1966 C			White homogeneous granitic gneiss.	
0.2						
0.3						
0.4	END CORE 1966.35 ft					
0.5						
0.6						
0.7						
0.8						
0.9						
1967						

Logged by: P.G. Naumoff Date: 5/11/87

CORE LOG

Project Moodus borehole 86c4111

Run 5 of 9

Page 1 of 6

Depth, ft	Sketch Scale = 1:2	Thin Section	Foliation Strike/Dip	Rock Fabric		Remarks
				Strike/Dip	Description	
2460	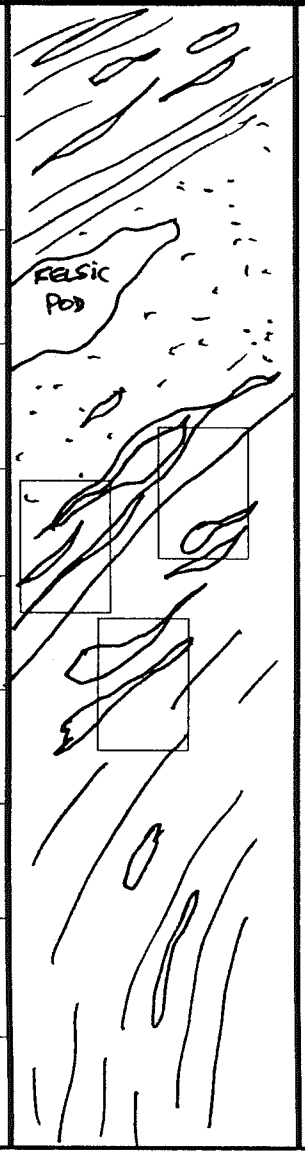		35 deg. dip.		Streaky layers with augen.	Black, fine – to medium – grained augen schist containing biotite, quartz, and plagioclase.
0.1						
0.2					Finer grained matrix; not as streaky. Some augen; slightly lighter in color.	
0.3						
0.4		MC 2460 A				
0.5		MC 2460 B				
0.6		MC 2460 C				
0.7					More homogeneous fabric; less augen.	
0.8						
0.9			Foliation steepens 90 deg. dip.			
2461						

Logged by: P.G. Naumoff Date: 5/11/87

CORE LOG

Project Moodus borehole 86c4111

Run 5 of 9

Depth, ft	Sketch Scale = 1:2	Thin Section	Foliation Strike/Dip	Rock Fabric		Remarks
				Strike/Dip	Description	
2461	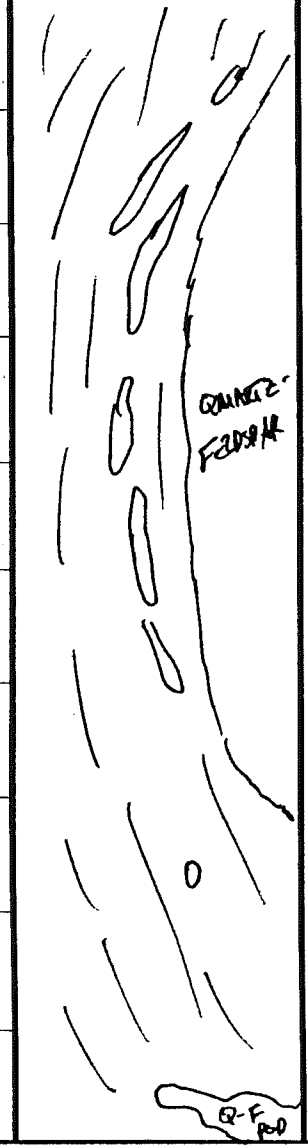		90 deg. dip.			
0.1						
0.2						
0.3						
0.4					K – feldspar – quartz knot; foliation wraps around it.	Augen are associated with the quartz – feldspar pod.
0.5						
0.6						
0.7			Foliation swings to the opposite direction.			
0.8					Well – developed schistosity.	
			35 deg. dip.			
0.9						
2462						

Logged by: P.G. Naumoff Date: 5/11/87

CORE LOG

Project Moodus borehole 86c4111

Run 5 of 9

Depth, ft	Sketch Scale = 1:2	Thin Section	Foliation Strike/Dip	Rock Fabric		Remarks
				Strike/Dip	Description	
2462						
0.1					irregular quartz – kspar pod.	
0.2						
0.3						
0.4			50 deg. dip.		Coarse quartz – feldspar pods	
0.5	Q-F					
0.6						
0.7			0 deg. dip.			
0.8						
0.9						
2463			30 deg. dip.			

Logged by: P.G. Naumoff Date: 5/11/87

CORE LOG

Project Moodus borehole 86c4111

Run 5 of 9

Depth, ft	Sketch Scale = 1:2	Thin Section	Foliation Strike/Dip	Rock Fabric		Remarks
				Strike/Dip	Description	
2463	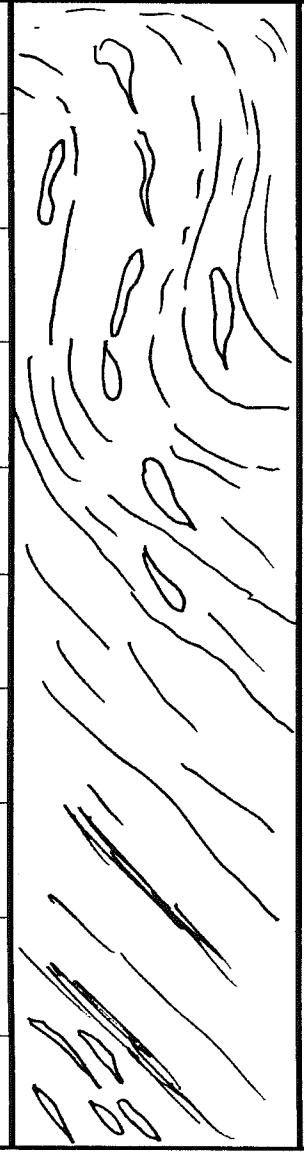					
0.1					Augen associated with, as well as folded by a tight fold. Layers are felsic – rich.	
0.2						
0.3					About 50 – 50 felsic and mafic (biotite) layers.	
0.4						
0.5			30 deg. dip.			
0.6						
0.7					Biotite – rich layers	
0.8			50 deg. dip.			
0.9					Felsic – rich layers.	
2464					Augen very well developed.	

Logged by: P.G. Naumoff Date: 5/11/87

CORE LOG

Project Moodus borehole 86c4111

Run 5 of 9

Depth, ft	Sketch Scale = 1:2	Thin Section	Foliation Strike/Dip	Rock Fabric		Remarks
				Strike/Dip	Description	
2464						
0.1						
0.2					Augen texture is very well developed.	
0.3						
0.4						
0.5			65 deg. dip.			
0.6						
0.7						
0.8						
0.9					Biotite – rich layers.	
2465						

Logged by: P.G. Naumoff Date: 5/11/87

CORE LOG

Project Moodus borehole 86c4111

Run 5 of 9

Depth, ft	Sketch Scale = 1:2	Thin Section	Foliation Strike/Dip	Rock Fabric		Remarks
				Strike/Dip	Description	
2465					Ptygmatic – like folds.	
0.1						
0.2	END CORE 2465.15 ft					
0.3						
0.4						
0.5						
0.6						
0.7						
0.8						
0.9						
2466						

Logged by: P.G. Naumoff Date: 5/12/87

CORE LOG

Project Moodus borehole 86c4111

Run 6 of 9

Page 1 of 8

Depth, ft	Sketch Scale = 1:2	Thin Section	Foliation Strike/Dip	Rock Fabric		Remarks
				Strike/Dip	Description	
2920	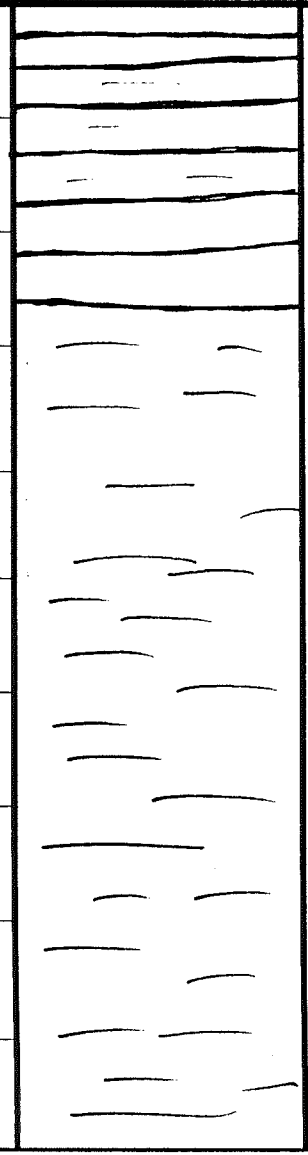		Partings along subhorizontal foliation.		Numerous subhorizontal partings along fresh surfaces; possibly a stress – relaxation phenomena.	A whitish – gray, medium – grained granitic gneiss containing quartz, plagioclase, biotite, and amphibole. Compositional layering is not well developed. Rock is about 60% felsic and 40% mafic. Biotite and amphibole form discontinuous "streaks" in the rock. Fairly homogeneous in texture. A streaky biotite – amphibole gneiss.
0.1						
0.2						
0.3						
0.4						
0.5						
0.6						
0.7						
0.8						
0.9						
2921						

Logged by: P.G. Naumoff Date: 5/12/87

CORE LOG

Project Moodus borehole 86c4111

Run 6 of 9

Depth, ft	Sketch Scale = 1:2	Thin Section	Foliation Strike/Dip	Rock Fabric		Remarks
				Strike/Dip	Description	
2921	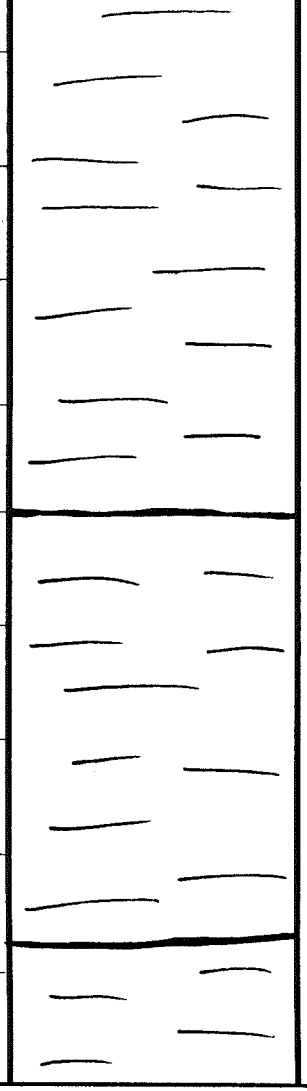		Subhorizontal foliation.		Homogeneous streaky biotite–amphibole gneiss.	
0.1						
0.2						
0.3						
0.4						
0.5			Parting.			
0.6						
0.7						
0.8						
			Parting.			
0.9						
2922						

Logged by: P.G. Naumoff Date: 5/12/87

CORE LOG

Project Moodus borehole 86c4111

Run 6 of 9

Depth, ft	Sketch Scale = 1:2	Thin Section	Foliation Strike/Dip	Rock Fabric		Remarks
				Strike/Dip	Description	
2922	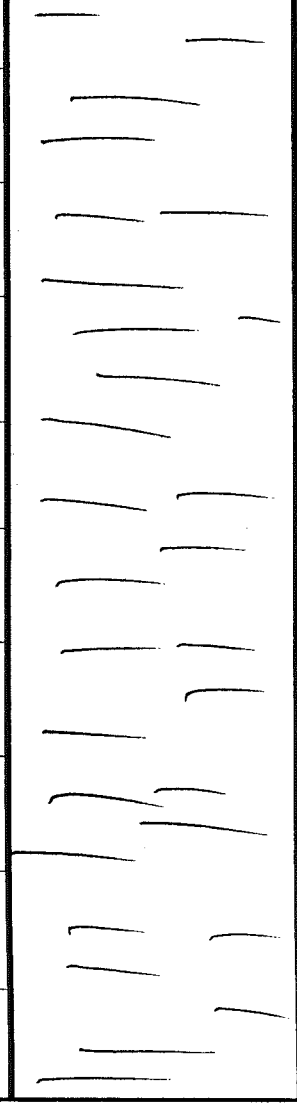		Subhorizontal foliation.		Homogeneous streaky biotite–amphibole gneiss.	
0.1						
0.2						
0.3						
0.4						
0.5						
0.6						
0.7						
0.8						
0.9						
2923						

Logged by: P.G. Naumoff Date: 5/12/87

CORE LOG

Project Moodus borehole 86c4111

Run 6 of 9

Page 4 of 8

Depth, ft	Sketch Scale = 1:2	Thin Section	Foliation Strike/Dip	Rock Fabric		Remarks
				Strike/Dip	Description	
2923						
0.1						
0.2						
0.3					Homogeneous streaky biotite – amphibole gneiss.	
0.4			Parting.			
0.5			Subhorizontal foliation.			
0.6						
0.7						
0.8						
			Parting.			
0.9	Φ-F SEG				Coarser quartz – feldspar segregation.	
2924						

Logged by: P.G. Naumoff Date: 5/12/87

CORE LOG

Project Moodus borehole 86c4111

Run 6 of 9

Page 5 of 8

Depth, ft 2924	Sketch Scale = 1:2	Thin Section	Foliation Strike/Dip	Rock Fabric		Remarks
				Strike/Dip	Description	
0.1	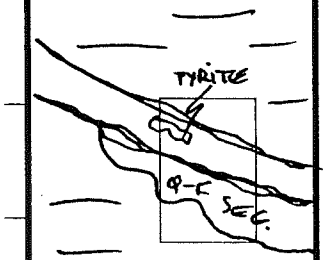	MC 2924 A			Quartz vein with biotite selvages and associated with pyrite.	
0.2						
0.3					Homogeneous streaky biotite – amphibole gneiss.	
0.4		MC 2924 B				
0.5						
0.6						
0.7					Parting.	
0.8						
0.9						
2925						

Logged by: P.G. Naumoff Date: 5/12/87

CORE LOG

Project Moodus borehole 86c4111

Run 6 of 9

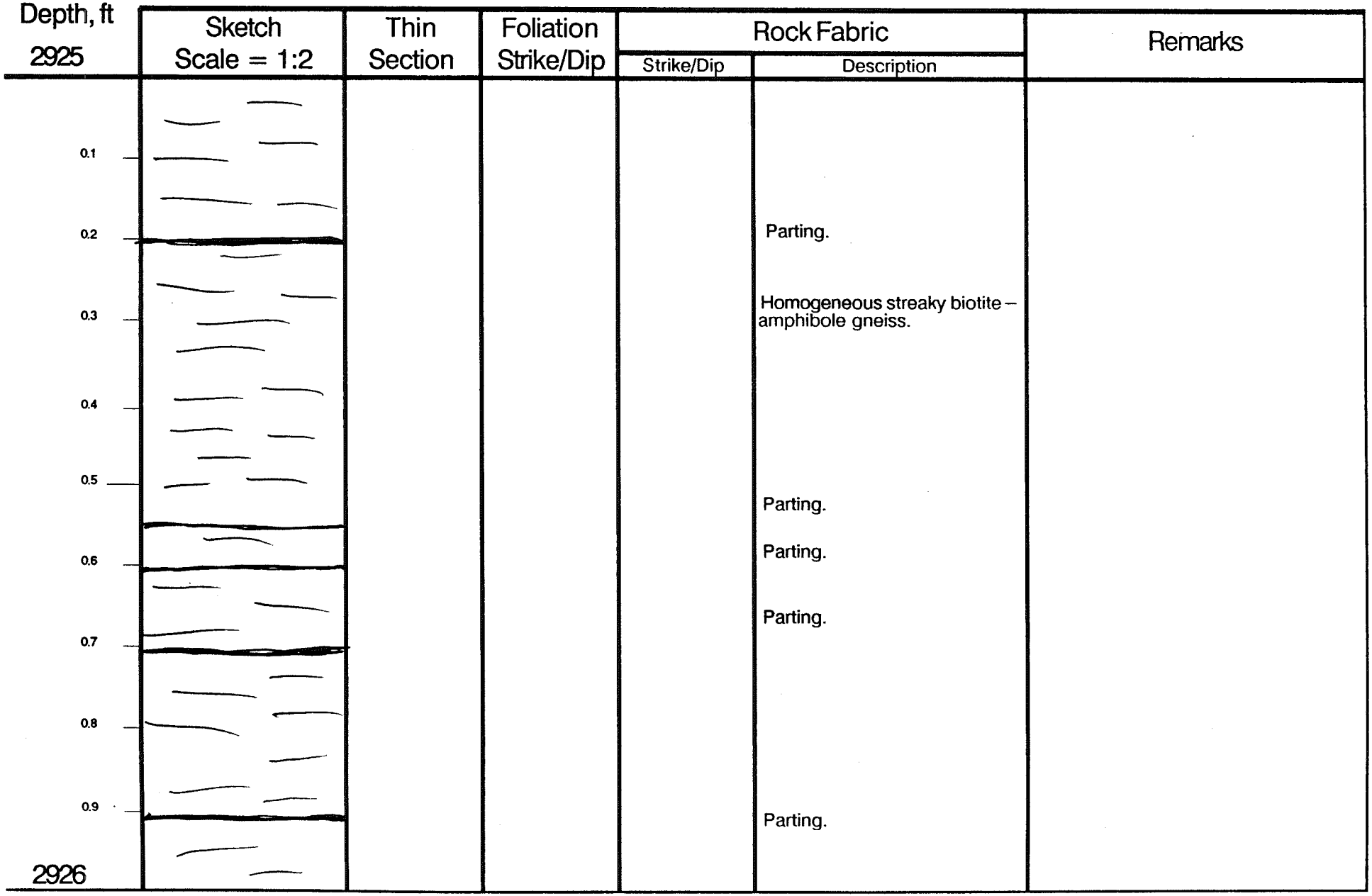

Logged by: P.G. Naumoff Date: 5/12/87

CORE LOG

Project Moodus borehole 86c4111

Run 6 of 9

Depth, ft	Sketch Scale = 1:2	Thin Section	Foliation Strike/Dip	Rock Fabric		Remarks
				Strike/Dip	Description	
2926	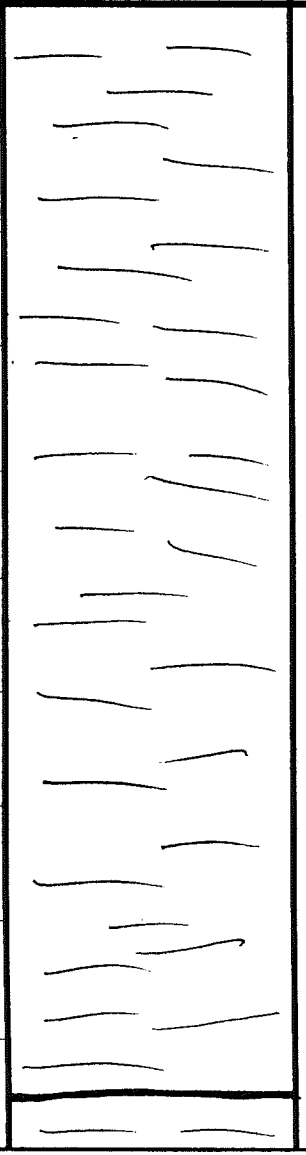		Subhorizontal foliation.		Homogeneous streaky biotite–amphibole gneiss.	
0.1						
0.2						
0.3						
0.4						
0.5						
0.6						
0.7						
0.8						
0.9						
2927					Parting.	

Logged by: P.G. Naumoff Date: 5/12/87

CORE LOG

Project Moodus borehole 86c4111

Run 6 of 9

Depth, ft	Sketch Scale = 1:2	Thin Section	Foliation Strike/Dip	Rock Fabric		Remarks
				Strike/Dip	Description	
2927	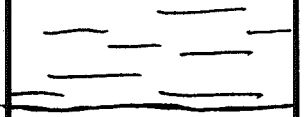		Subhorizontal foliation.			
0.1	END CORE 2927.10 ft					
0.2						
0.3					Homogeneous streaky biotite – amphibole gneiss.	
0.4						
0.5						
0.6						
0.7						
0.8						
0.9						
2928						

Logged by: P.G. Naumoff Date: 5/20/87

CORE LOG

Project Moodus borehole 86c4111

Run 7 of 9

Depth, ft	Sketch Scale = 1:2	Thin Section	Foliation Strike/Dip	Rock Fabric		Remarks
				Strike/Dip	Description	
3494						A gray, medium – grained biotite – amphibole – plagioclase – kspar – quartz gneiss. Streaky with occasional augen. Compositional layers not well developed, but some quartzo – feldspathic flasers and layers present. Some thin amphibolite layers are present.
0.1						
0.2						
0.3						
0.4						
0.5						
	TOP OF CORE 3494.66					
0.6						
0.7	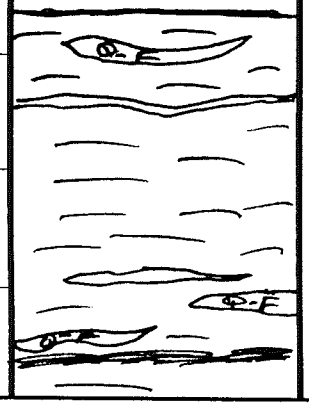		Subhorizontal foliation.		Quartzo – feldspathic (Q – F) segregations	
0.8						
0.9					Horizontal break with slicks; blackish – green smeared surface; chloritic.	
3495						

Logged by: P.G. Naumoff Date: 5/20/87

CORE LOG

Project Moodus borehole 86c4111

Run 7 of 9

Depth, ft	Sketch Scale = 1:2	Thin Section	Foliation Strike/Dip	Rock Fabric		Remarks
				Strike/Dip	Description	
3495	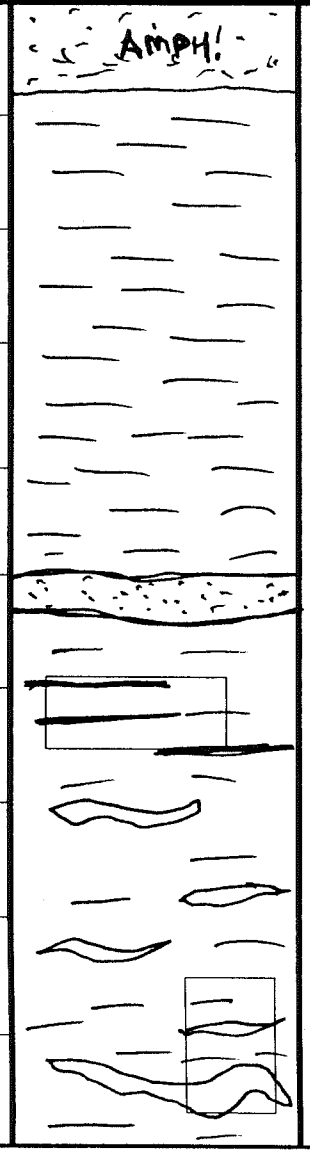				Amphibolite.	
0.1						
0.2						
0.3					Compositional layering not well – developed.	
0.4						
0.5					Amphibolite. Greenish chloritic paste on surface; slicks.	
0.6		MC 3495			Some non – penetrative subhorizontal partings; core relaxtion?	
0.7						
0.8						
0.9		MC 3496			Quartzo – feldspathic flasers and augen.	
3496						

Logged by: P.G. Naumoff Date: 5/20/87

CORE LOG

Project Moodus borehole 86c4111

Run 7 of 9

Depth, ft	Sketch Scale = 1:2	Thin Section	Foliation Strike/Dip	Rock Fabric		Remarks
				Strike/Dip	Description	
3496						
0.1						
0.2					(POOR RECOVERY LAYER)	
0.3					Probable "blown – out" amphibolite layer Break with some greenish chloritic paste.	
0.4						
0.5						
0.6						
0.7						
0.8						
0.9					Non – penetrative fracture.	
3497						

Logged by: P.G. Naumoff Date: 5/20/87

CORE LOG

Project Moodus borehole 86c4111

Run 7 of 9

Depth, ft	Sketch Scale = 1:2	Thin Section	Foliation Strike/Dip	Rock Fabric		Remarks
				Strike/Dip	Description	
3497	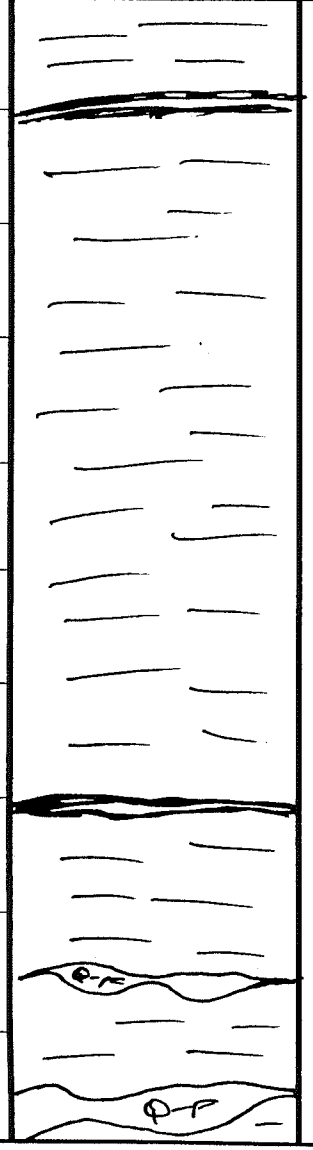		Subhorizontal foliation.		Fracture with green – and salmon – colored weathered paste; probable "blown – out" amphibolite layer ? "Blown – out" amphibolite layer. Large quartzo – feldspathic layer.	
0.1						
0.2						
0.3						
0.4						
0.5						
0.6						
0.7						
0.8						
0.9						
3498						

Logged by: P.G. Naumoff Date: 5/20/87

CORE LOG

Project Moodus borehole 86c4111

Run 7 of 9

Depth, ft	Sketch Scale = 1:2	Thin Section	Foliation Strike/Dip	Rock Fabric		Remarks
				Strike/Dip	Description	
3498						
0.1					Drilling break.	
0.2	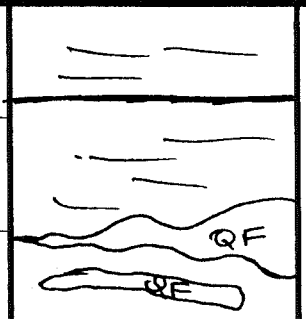				Pinkish quartzo – feldspathic (Q – F) segregations.	
0.3						
0.4						
0.5			Subhorizontal foliation.			
0.6						
0.7						
0.8						
0.9						
3499						

Logged by: P.G. Naumoff Date: 5/20/87

CORE LOG

Project Moodus borehole 86c4111

Run 7 of 9

Depth, ft	Sketch Scale = 1:2	Thin Section	Foliation Strike/Dip	Rock Fabric		Remarks
				Strike/Dip	Description	
3499						
0.1					Homogeneous streaky gneiss.	
0.2						
0.3						
0.4						
0.5			Subhorizontal foliation.			
0.6						
0.7						
0.8						
0.9	QF				Amphibolite; slightly vuggy; calcite coming out? Break along greenish chloritic surface. Some coarse and lineated calcite.	
3500						

Logged by: P.G. Naumoff Date: 5/20/87

CORE LOG

Project Moodus borehole 86c4111

Run 7 of 9

Page 7 of 11

Depth, ft	Sketch Scale = 1:2	Thin Section	Foliation Strike/Dip	Rock Fabric		Remarks
				Strike/Dip	Description	
3500	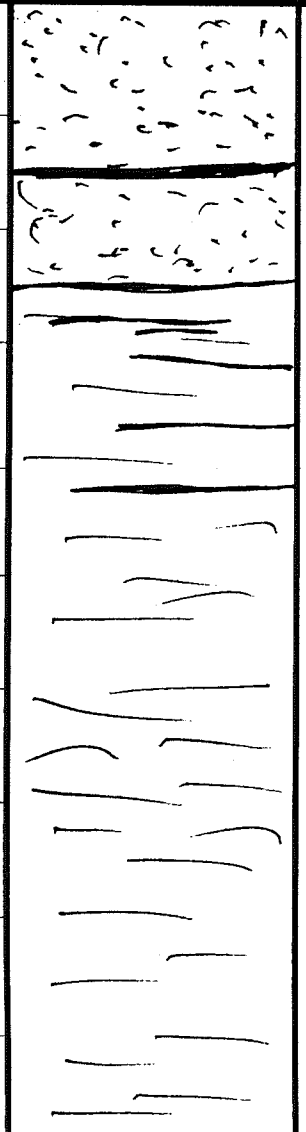		Subhorizontal foliation.		Amphibolite. Green, pasty surface. Non – penetrative subhorizontal surfaces. Homogeneous streaky gneiss.	
0.1						
0.2						
0.3						
0.4						
0.5						
0.6						
0.7						
0.8						
0.9						
3501						

Logged by: P.G. Naumoff Date: 5/20/87

CORE LOG

Project Moodus borehole 86c4111

Run 7 of 9

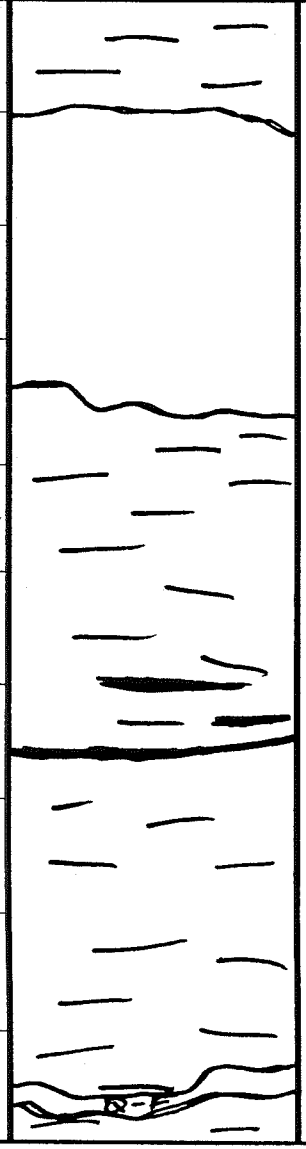

Depth, ft	Thin Section	Foliation Strike/Dip	Rock Fabric		Remarks
			Strike/Dip	Description	
3501					
0.1					
0.2				Large, coarse, pink kspar – rich felsic knot.	
0.3					
0.4					
0.5		Subhorizontal foliation.		Streaky gneiss.	
0.6				non – penetrative fractures. Well lineated green chloritic surface.	
0.7					
0.8					
0.9				Quartzo – feldspathic layer.	
3502					

Logged by: P.G. Naumoff Date: 5/20/87

CORE LOG

Project Moodus borehole 86c4111

Run 7 of 9

Depth, ft	Sketch Scale = 1:2	Thin Section	Foliation Strike/Dip	Rock Fabric		Remarks
				Strike/Dip	Description	
3502	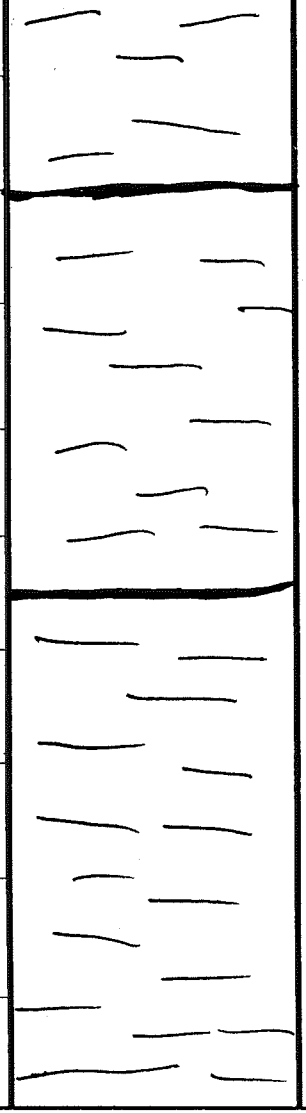				Streaky gneiss.	
0.1						
0.2						
0.3					Breaks with slight greenish weathering.	
0.4						
0.5			Subhorizontal foliation.			
0.6						
0.7						
0.8						
0.9						
3503						

Logged by: P.G. Naumoff Date: 5/20/87

CORE LOG

Project Moodus borehole 86c4111

Run 7 of 9

Page 10 of 11

Depth, ft	Sketch Scale = 1:2	Thin Section	Foliation Strike/Dip	Rock Fabric		Remarks
				Strike/Dip	Description	
3503	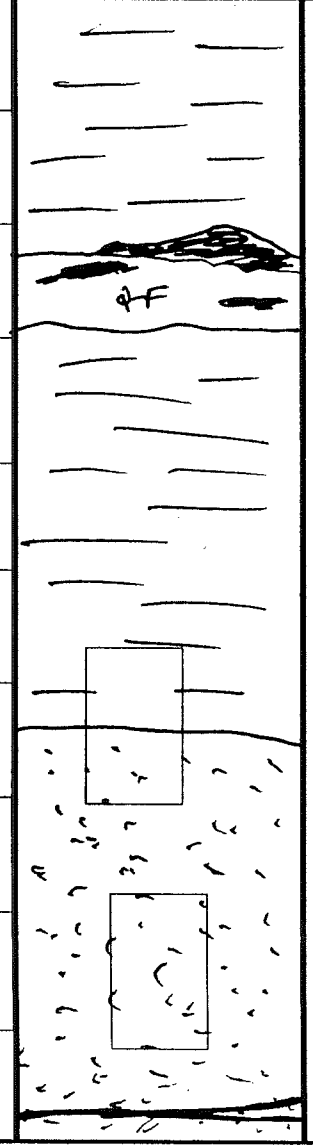					
0.1						
0.2					Pinkish quartz – feldspar layer associated with coarse amphibole.	
0.3						
0.4						
0.5			Subhorizontal foliation.			
0.6		MC 3503 A				
0.7					Amphibolite.	
0.8		MC 3503 B				
0.9						
3504					Well – lineated surface; some greenish paste.	

Logged by: P.G. Naumoff Date: 5/20/87

CORE LOG

Project Moodus borehole 86c4111

Run 7 of 9

Depth, ft	Sketch Scale = 1:2	Thin Section	Foliation Strike/Dip	Rock Fabric		Remarks
				Strike/Dip	Description	
3504	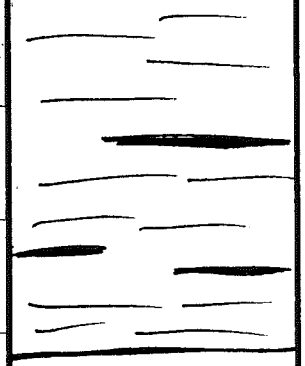				Some non – penetrative fractures.	
0.1						
0.2						
0.3						
	END CORE 3504.32 ft					
0.4						
0.5						
0.6						
0.7						
0.8						
0.9						
3505						

Logged by: P.G. Naumoff Date: 6/18/87

CORE LOG

Project Moodus borehole 86c4111

Run 8 of 9

Depth, ft	Sketch Scale = 1:2	Thin Section	Foliation Strike/Dip	Rock Fabric		Remarks
				Strike/Dip	Description	
3985						Core was removed from barrel as 1/4" – to 1/2" – wide disks; probably due to subhorizontal foliation and core relaxation along those planes. Rock consists of primarily 4 lithologic and texturally distinct interlayered gneisses. BPG = a fine bluish – gray homogeneous biotite – plagioclase – quartz gneiss. Compositional layering not well developed. AMPH = a fine – grained, black, biotite – bearing amphibolite. PGG = a medium – grained, pinkish – white granitic gneiss. Foliation poorly defined by minor biotite and other minor mafic minerals; magnetite bearing also. BAG = a mottled black and white, medium – grained biotite – amphibole – plagioclase – quartz gneiss. Biotite and amphibole form discontinuous streaks and clots that define the foliation.
0.1						
0.2						
0.3	TOP OF CORE 3985.33					
0.4						
0.5	BPG		Subhorizontal foliation.			
0.6						
0.7						
0.8						
0.9					Biotite – rich layer.	
3986	BPG				Start amphibolite 3985.99 ft; sharp contact.	

Logged by: P.G. Naumoff Date: 6/18/87

CORE LOG

Project Moodus borehole 86c4111

Run 8 of 9

Depth, ft	Sketch Scale = 1:2	Thin Section	Foliation Strike/Dip	Rock Fabric		Remarks
				Strike/Dip	Description	
3986	AMPH	MC 3986 B				
0.1						
0.2	BPG	MC 3986 A			Sharp contacts.	
0.3	AMPH					
0.4	BAG				Finer BAG grades into BPG.	
0.5			Subhorizontal foliation.			
0.6	BPG					
0.7						
0.8						
0.9						
3987						

Logged by: P.G. Naumoff Date: 6/18/87

CORE LOG

Project Moodus borehole 86c4111

Run 8 of 9

Depth, ft	Sketch Scale = 1:2	Thin Section	Foliation Strike/Dip	Rock Fabric		Remarks
				Strike/Dip	Description	
3987						
0.1						
0.2	BPG					
0.3						
0.4						
0.5			Subhorizontal foliation.		Sharp contacts.	
0.6	AMPH					
0.7						
0.8	BPG					
0.9					Rock becomes segregated; irregular coarse – grained, white feldspar – quartz blebs and dark biotite – rich layers.	
3988						

Logged by: P.G. Naumoff Date: 6/18/87

CORE LOG

Project Moodus borehole 86c4111

Run 8 of 9

Depth, ft	Sketch Scale = 1:2	Thin Section	Foliation Strike/Dip	Rock Fabric		Remarks
				Strike/Dip	Description	
3988						
0.1	BPG					
0.2						
0.3					Sharp contact.	
0.4	PGG					
0.5			Subhorizontal foliation.			
0.6						
0.7						
0.8						
0.9					Biotite – rich layer.	
					More biotite coming in; grading into thinly layered gneiss.	
3989						

Logged by: P.G. Naumoff Date: 6/18/87

CORE LOG

Project Moodus borehole 86c4111

Run 8 of 9

Page 5 of 10

Depth, ft	Sketch Scale = 1:2	Thin Section	Foliation Strike/Dip	Rock Fabric		Remarks
				Strike/Dip	Description	
3989					Well – developed thin compositional layers of biotite and felsic minerals; grades into BPG.	
0.1						
0.2	BPG					
0.3					Sharp contacts.	
0.4	PGG					
0.5	BPG		Subhorizontal foliation.			
0.6						
0.7	PGG					
0.8						
0.9						
3990						

Logged by: P.G. Naumoff Date: 6/18/87

CORE LOG

Project Moodus borehole 86c4111

Run 8 of 9

Depth, ft	Sketch Scale = 1:2	Thin Section	Foliation Strike/Dip	Rock Fabric		Remarks
				Strike/Dip	Description	
3990						
0.1	PGG					
0.2						
0.3	BAG					
0.4						
0.5			Subhorizontal foliation.			
0.6						
0.7						
0.8						
0.9					Fine – grained biotite – amphibole rich layer.	
3991						

Logged by: P.G. Naumoff Date: 6/18/87

CORE LOG

Project Moodus borehole 86c4111

Run 8 of 9

Page 7 of 10

Depth, ft	Sketch Scale = 1:2	Thin Section	Foliation Strike/Dip	Rock Fabric		Remarks
				Strike/Dip	Description	
3991						
0.1					Fine – grained biotite – amphibole rich layers.	
	BAG					
0.2						
0.3		MC 3991				
0.4						
0.5			Subhorizontal foliation.			
0.6	BAG					
0.7						
0.8						
0.9	BAG					
3992						

Logged by: P.G. Naumoff Date: 6/18/87

CORE LOG

Project Moodus borehole 86c4111

Run 8 of 9

Depth, ft	Sketch Scale = 1:2	Thin Section	Foliation Strike/Dip	Rock Fabric		Remarks
				Strike/Dip	Description	
3992						
0.1	BAG					
0.2					Fine – grained biotite amphibole layer.	
0.3	Q-F PGG				Gradational contact with pink granitic gneiss.	
0.4						
					Sharp contact.	
0.5	BAG		Subhorizontal foliation.			
0.6						
0.7						
0.8	AMPH				Sharp contacts.	
					Quartz – feldspar (Q – F) segregation.	
0.9						
3993	BAG					

Logged by: P.G. Naumoff Date: 6/18/87

CORE LOG

Project Moodus borehole 86c4111

Run 8 of 9

Page 9 of 10

Depth, ft	Sketch Scale = 1:2	Thin Section	Foliation Strike/Dip	Rock Fabric		Remarks
				Strike/Dip	Description	
3993	BAG				Sharp contacts between all rock types.	
0.1						
0.2	PGG					
0.3						
0.4						
0.5			Subhorizontal foliation.	Fracture dips 70 degs.	Fracture 1/10" to 2/10" wide. Fracture defined by pinkish weathered zone; hematite in kspar?	
0.6						
0.7	BPG					
0.8						
0.9	PGG					
3994						

Logged by: P.G. Naumoff Date: 6/18/87

CORE LOG

Project Moodus borehole 86c4111

Run 8 of 9

Depth, ft 3994	Sketch Scale = 1:2	Thin Section	Foliation Strike/Dip	Rock Fabric		Remarks
				Strike/Dip	Description	
0.1	PGG	MC 3994			Sharp contacts between rock types.	
0.2						
0.3	BPG		Subhorizontal foliation.			
0.4	PGG					
0.5						
0.6	END CORE 3994.56 ft Some broken pieces on bottom.					
0.7						
0.8						
0.9						
3995						

Logged by: P.G. Naumoff Date: 6/18/87

CORE LOG

Project Moodus borehole 86c4111

Run 9 of 9

Page 1 of 9

Depth, ft	Sketch Scale = 1:2	Thin Section	Foliation Strike/Dip	Rock Fabric		Remarks
				Strike/Dip	Description	
4440	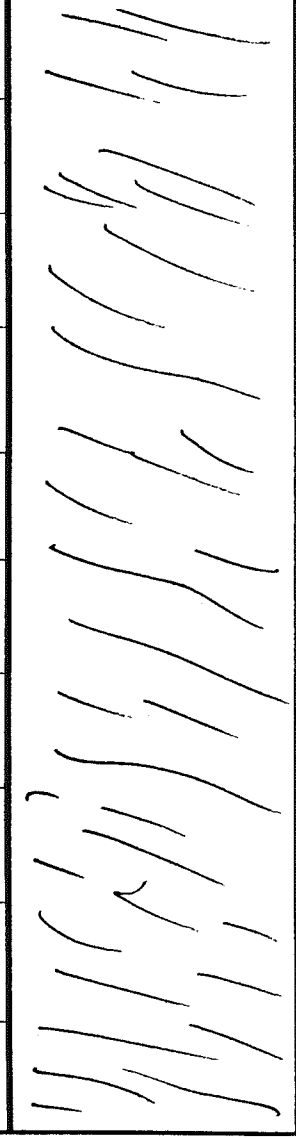		Foliation dips 13 degrees.			A dark gray, medium – grained biotite – amphibole gneiss. Compositional layering not well developed, but felsic layers are irregular and streaky. Incipient and penetrative subhorizontal cracks present, but not as well – developed as in core #8. Evenly spaced cracks occur in the lower amphibolite unit.
0.1						
0.2						
0.3						
0.4						
0.5						
0.6						
0.7						
0.8						
0.9						
4441						

Logged by: P.G. Naumoff Date: 6/18/87

CORE LOG

Project Moodus borehole 86c4111

Run 9 of 9

Page 2 of 9

Depth, ft	Sketch Scale = 1:2	Thin Section	Foliation Strike/Dip	Rock Fabric		Remarks
				Strike/Dip	Description	
4441						
0.1					A more leucocratic layer.	
0.2						
0.3						
0.4					A coarse quartz – plagioclase? – kspar knot with minor biotite.	
0.5			Foliation dips 12 degrees.			
0.6						
0.7						
0.8						
0.9						
4442	QF				Quartzo – feldspathic (Q – F) segregation.	

Logged by: P.G. Naumoff Date: 6/18/87

CORE LOG

Project Moodus borehole 86c4111

Run 9 of 9

Depth, ft	Sketch Scale = 1:2	Thin Section	Foliation Strike/Dip	Rock Fabric		Remarks
				Strike/Dip	Description	
4442	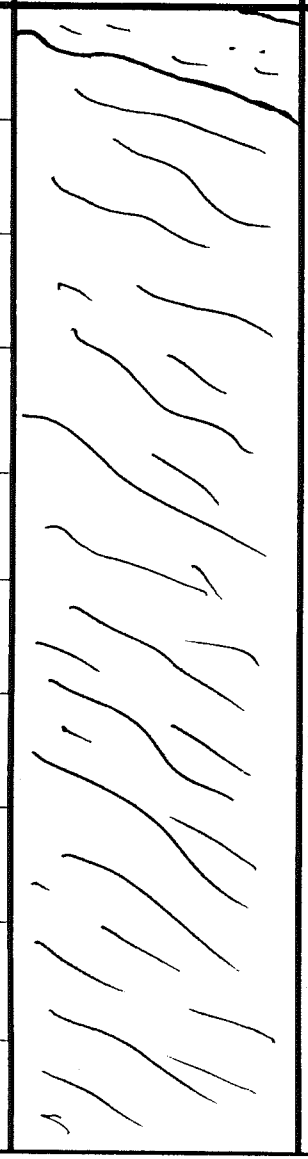				Quartzo – feldspathic (Q – F) segregation.	
0.1						
0.2						
0.3						
0.4						
0.5			Foliation dips 15 degrees.			
0.6						
0.7						
0.8						
0.9						
4443						

Logged by: P.G. Naumoff Date: 6/18/87

CORE LOG

Project Moodus borehole 86c4111

Run 9 of 9

Page 4 of 9

Depth, ft	Sketch Scale = 1:2	Thin Section	Foliation Strike/Dip	Rock Fabric		Remarks
				Strike/Dip	Description	
4443	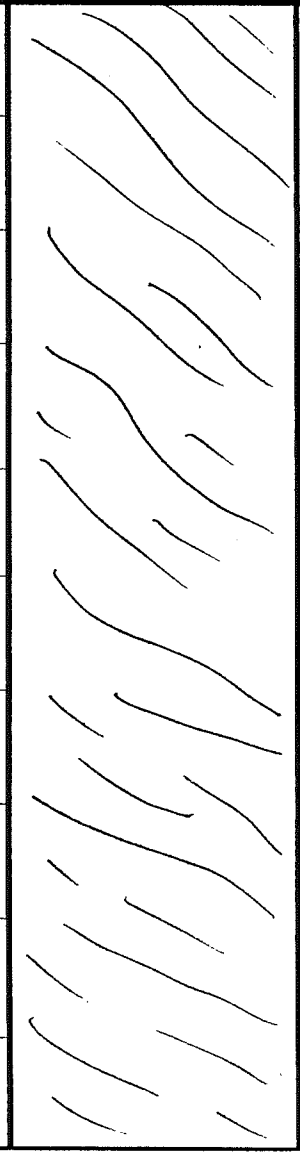		Foliation dips 15 degrees.			
0.1						
0.2						
0.3						
0.4						
0.5						
0.6						
0.7						
0.8						
0.9						
4444						

Logged by: P.G. Naumoff Date: 6/18/87

CORE LOG

Project Moodus borehole 86c4111

Run 9 of 9

Depth, ft	Sketch Scale = 1:2	Thin Section	Foliation Strike/Dip	Rock Fabric		Remarks
				Strike/Dip	Description	
4444						
0.1						
0.2						
0.3						
0.4						
0.5			Foliation dips 25 degrees.			
0.6	QF				A coarse quartzo – feldspathic layer.	
0.7						
0.8						
0.9						
4445						

Logged by: P.G. Naumoff Date: 6/18/87

CORE LOG

Project Moodus borehole 86c4111

Run 9 of 9

Page 6 of 9

Depth, ft	Sketch Scale = 1:2	Thin Section	Foliation Strike/Dip	Rock Fabric		Remarks
				Strike/Dip	Description	
4445	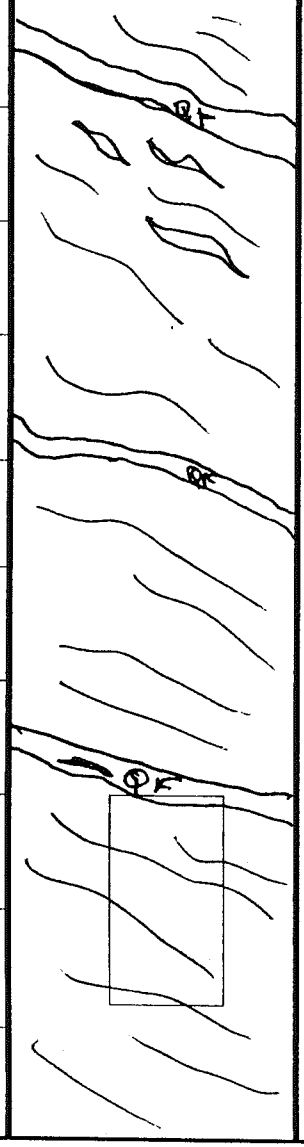	MC 4445	Foliation dips 15 degrees.		Wider quartzo – feldspathic (Q – F) layers become better defined; banding more prominant. Rock appears more blotchy with nebulous layering.	
0.1						
0.2						
0.3						
0.4						
0.5						
0.6						
0.7						
0.8						
0.9						
4446						

Logged by: P.G. Naumoff Date: 6/18/87

CORE LOG

Project Moodus borehole 86c4111

Run 9 of 9

Page 7 of 9

Depth, ft	Sketch Scale = 1:2	Thin Section	Foliation Strike/Dip	Rock Fabric		Remarks
				Strike/Dip	Description	
4446	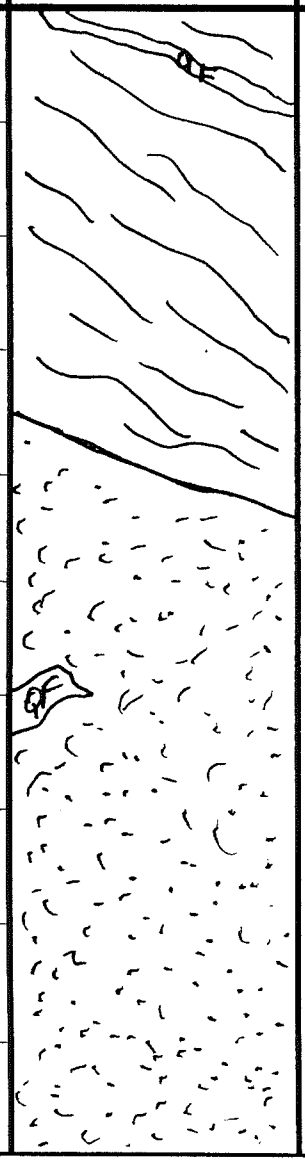		Foliation dips 15 degrees.		a fine – grained, black, homogeneous biotite – chlorite bearing amphibolite. Layering poorly defined. Quartz – feldspar (Q – F) segregation.	
0.1						
0.2						
0.3						
0.4						
0.5						
0.6						
0.7						
0.8						
0.9						
4447						

Logged by: P.G. Naumoff Date: 6/18/87

CORE LOG

Project Moodus borehole 86c4111

Run 9 of 9

Depth, ft	Sketch Scale = 1:2	Thin Section	Foliation Strike/Dip	Rock Fabric		Remarks
				Strike/Dip	Description	
4447	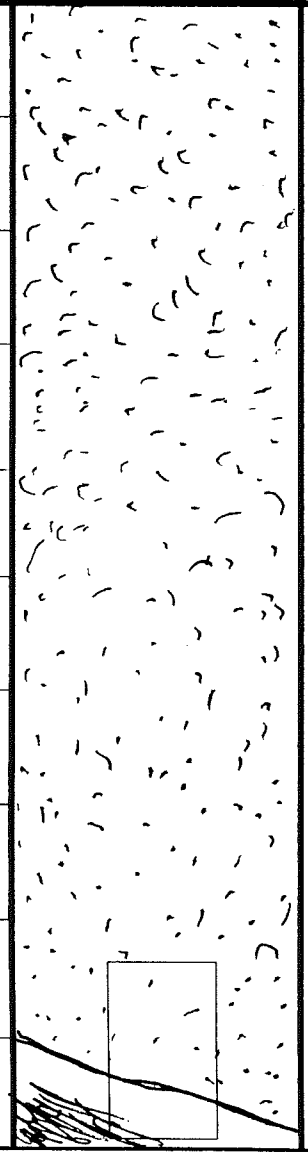					
0.1					a fine – grained, black, homogeneous biotite – chlorite bearing amphibolite. Layering poorly defined.	
0.2						
0.3						
0.4						
0.5						
0.6						
0.7						
0.8						
0.9		MC 4448	Foliation dips 20 degrees.			
4448					Biotite – amphibole gneiss.	

Logged by: P.G. Naumoff Date: 6/18/87

CORE LOG

Project Moodus borehole 86c4111

Run 9 of 9

Page 9 of 9

Depth, ft	Sketch Scale = 1:2	Thin Section	Foliation Strike/Dip	Rock Fabric		Remarks
				Strike/Dip	Description	
4448	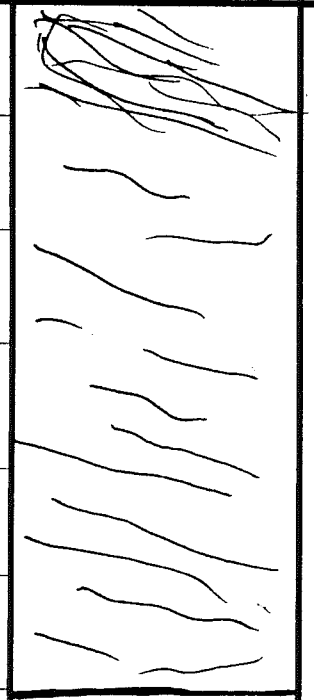					
0.1					Epidote and quartz – rich gneiss	
0.2						
0.3						
0.4					Biotite – amphibole gneiss.	
0.5						
0.6	END CORE 4448.60 ft					
0.7						
0.8						
0.9						
4449						

SECTION 4

This section is a log of thin sections made from selected chip samples and sections of core. The prefix before the section number "MC" means the section was made from core. The prefix "M" means the section was made from a chip sample.

THIN SECTION DESCRIPTION: MOODUS BOREHOLE

Described by: P.G. Naumoff Date: 2/18/88 Project number: 86C4111

A. HAND SPECIMEN | COLOR | TEXTURE

Hebron Gneiss | Black | Equigranular

B. MINERAL IDENTIFICATION; SECTION NUMBER MC 508 A

	MINERAL	OTHER PROPERTIES	GRAIN SIZE, SHAPE, ETC	%
ESSENTIAL	Quartz		estimated percentages >	35
	Plagioclase			35
	Biotite			20
	Pyroxene			9
	Amphibole			1
ACCESSORY	Calcite			Trace
	Apatite			Tr
	Zircon			Tr
	Opaques			Tr

C. THIN SECTION DESCRIPTION:

A medium-grained equigranular biotite schist. Grain size about 0.5 mm. Foliation well defined by aligned biotites and somewhat defined by flattened quartzo-feldspathic minerals. Q-f minerals predominantly form a granoblastic-polygonal network. Diopside generally occurs in discrete layers.

THIN SECTION DESCRIPTION: MOODUS BOREHOLE

Described by: P.G. Naumoff Date: 2/19/88 Project number: 86C4111

A. HAND SPECIMEN

HAND SPECIMEN	COLOR	TEXTURE
Hebron Gneiss	Black/white	Contact between schist and quartzo-feldspatic layer

B. MINERAL IDENTIFICATION; SECTION NUMBER MC 508 B

	MINERAL	OTHER PROPERTIES	GRAIN SIZE, SHAPE, ETC	%
ESSENTIAL	Quartz		estimated >	25
	Plagioclase			25
	K-feldspar			20
	Biotite		bio concentrated in schist	30
	Muscovite			Trace
	Pyroxene			Tr
	Amphibole			Tr
ACCESSORY	Calcite			Trace
	Zircon			Tr
	Monazite			Tr
	Opaque			Tr

C. THIN SECTION DESCRIPTION:

Contact between quartzo-feldspathic layer and biotite schist. Schist is a fine, granoblastic rock with grain size ≈ 0.4 mm. Foliation well defined by aligned biotite. Quartzo-feldspathic layer (from core) is about 2" thick and consists of a fine granoblastic network of quartz, plag, and k-feldspar. A ≈ 5mm-wide fracture cuts both layers. Fracture contains coarse (up to 3 mm) and undulatory grains of quartz, plag, k-spar and opaques.

THIN SECTION DESCRIPTION: MOODUS BOREHOLE

Described by: P.G. Naumoff Date: 2/19/88 Project number: 86C4111

A. HAND SPECIMEN | COLOR | TEXTURE

Hebron Gneiss | Black | Variable: Granoblastic and strained

B. MINERAL IDENTIFICATION; SECTION NUMBER MC 508 C

	MINERAL	OTHER PROPERTIES	GRAIN SIZE, SHAPE, ETC	%
ESSENTIAL	Quartz		estimated >	35
	Plagioclase			40
	Biotite			25
	Amphibole			Trace
ACCESSORY	Zircon			Trace
	Apatite			Tr
	Opaques			Tr

C. THIN SECTION DESCRIPTION:

Rock is predominantly a fine-grained ($\approx$ 0.5mm) granoblastic biotite schist. Foliation well-defined by thin quartzo-feldspathic layers and aligned biotite crystals. Rock is strained, however, evidenced by undulatory quartzo-feldspathic grains, moderately-developed mortar texture, and convolute folding of thin quartzo-feldspathic layers.

THIN SECTION DESCRIPTION: MOODUS BOREHOLE

Described by: P.G. Naumoff Date: 2/19/88 Project number: 86C4111

A. HAND SPECIMEN | COLOR | TEXTURE

Hebron Gneiss | Black | Granoblastic-polygonal

B. MINERAL IDENTIFICATION; SECTION NUMBER MC 1002

	MINERAL	OTHER PROPERTIES	GRAIN SIZE, SHAPE, ETC	%
ESSENTIAL	Quartz		estimated >	35
	Plagioclase			35
	Biotite			25
	Pyroxene			3
	Calcite			1
ACCESSORY	Zircon			Trace
	Opaque			1
	Apatite			Tr

C. THIN SECTION DESCRIPTION:

Bulk of the rock is a fine-grained (0.25 mm) biotite schist with a granoblastic polygonal texture. Foliation defined by aligned biotite crystals. Pyroxene is evenly disseminated throughout the section. Section also contains one "flaser" or pod of coarse quartz and feldspar crystals (up to 1.0 mm) with coarse biotite selvages. Plagioclase here is extensively twinned (deformation twins ?) and lightly sericitized. Minor amounts of calcite and pyroxene are associated with flaser.

THIN SECTION DESCRIPTION: MOODUS BOREHOLE

Described by: P.G. Naumoff Date: 2/22/88 Project number: 86C4111

A. HAND SPECIMEN | COLOR | TEXTURE

Hebron Gneiss | Black | Granoblastic-polygonal

B. MINERAL IDENTIFICATION; SECTION NUMBER MC 1003

	MINERAL	OTHER PROPERTIES	GRAIN SIZE, SHAPE, ETC	%
ESSENTIAL	Quartz		estimated >	35
	Plagioclase			38
	Biotite			20
	Pyroxene			3
	Calcite			2
	Scapolite			1
ACCESSORY	Zircon			Trace
	Opaques			1
	Tourmaline			Tr
	Rutile (?)	uniaxial +, slight reddish pleochroism		Tr

C. THIN SECTION DESCRIPTION:

Rock is predominantly a fine granoblastic-polygonal biotite schist. Grain size is about 0.2 mm and the foliation defined by aligned biotite grains. A granitic veins cuts the foliation. It contains coarse grains of quartzo-feldspathic minerals as well as minor amounts of tourmaline, calcite, scapolite, pyroxene, and (?) rutile. The larger feldspar grains show sutured contacts and undulose extinction.

THIN SECTION DESCRIPTION: MOODUS BOREHOLE

Described by: P.G. Naumoff Date: 2/22/88 Project number: 86C4111

A. HAND SPECIMEN	COLOR	TEXTURE
Hebron Gneiss	Black	Flasered

B. MINERAL IDENTIFICATION; SECTION NUMBER MC 1010

	MINERAL	OTHER PROPERTIES	GRAIN SIZE, SHAPE, ETC	%
ESSENTIAL	Quartz		estimated >	32
	Plagioclase			32
	Biotite			20
	Pyroxene	cpx		10
	Scapolite			2
	Calcite			2
	Amphibole			Trace
ACCESSORY	Zircon			Trace
	Opaques			1
	Beryl			1
	Rutile (?)			Tr

C. THIN SECTION DESCRIPTION:

Section is from a flasered portion of calcsilicate gneiss. The typical fine granoblastic fabric (grain size about 0.2 mm) is over-printed by pods of coarse quartzo-feldspathic grains (up to 5.0 mm). In these pods, poikiloblastic pyroxene and feldspar are common and development of incipient mortar texture is evident. Selvages of coarse biotite occasionally define the pods. The flasers also locally contain concentrations of beryl, calcite, scapolite, amphibole, and pyroxene. Many of the coarser felsic grains exhibit undulose extinction.

THIN SECTION DESCRIPTION: MOODUS BOREHOLE

Described by: P.G. Naumoff Date: 2/24/88 Project number: 86C4111

A. HAND SPECIMEN — COLOR — TEXTURE

Hebron Gneiss "Silver Bullet Gneiss" — Bluish-gray — Equigranular and homogeneous

B. MINERAL IDENTIFICATION; SECTION NUMBER M 1215

	MINERAL	OTHER PROPERTIES	GRAIN SIZE, SHAPE, ETC	%
ESSENTIAL	Quartz		estimated >	30
	Plagioclase			35
	K-felspar			35
	Biotite			Tr
	Muscovite			Tr
ACCESSORY	Apatite			Trace
	Chlorite			Tr
	Opaques			Tr

C. THIN SECTION DESCRIPTION:

Rock is a homogeneous and equigranular granite gneiss. K-feldspar grains are lightly to moderately sericitized. Grain size is about 0.3 mm.

THIN SECTION DESCRIPTION: MOODUS BOREHOLE

Described by: P.G. Naumoff Date: 2/24/88 Project number: 86C4111

A. HAND SPECIMEN | COLOR | TEXTURE

Hebron Gneiss | Black | Granoblastic-polygonal

B. MINERAL IDENTIFICATION; SECTION NUMBER M 1464

	MINERAL	OTHER PROPERTIES	GRAIN SIZE, SHAPE, ETC	%
ESSENTIAL	Quartz		estimated >	40
	Plagioclase			40
	Biotite			20
	Pyroxene			Trace
	Amphibole			Tr
	Calcite			Tr
ACCESSORY	Zircon			Trace
	Opaques			Tr
	Chlorite			Tr

C. THIN SECTION DESCRIPTION:

A fine (0.2 mm) granoblastic-polygonal biotite schist. Small flakes of aligned biotites moderately define the foliation.

THIN SECTION DESCRIPTION: MOODUS BOREHOLE

Described by: P.G. Naumoff Date: 2/24/88 Project number: 86C4111

A. HAND SPECIMEN | COLOR | TEXTURE

Hebron Gneiss | Black | Schistose

B. MINERAL IDENTIFICATION; SECTION NUMBER MC 1502 A

	MINERAL	OTHER PROPERTIES	GRAIN SIZE, SHAPE, ETC	%
ESSENTIAL	Quartz		estimated >	33
	Plagioclase			35
	Biotite			20
	Muscovite			8
	Sillimanite			3
	Garnet			1
ACCESSORY	Zircon			Trace
	Apatite			Tr
	Tourmaline			Tr
	Opaques			Tr

C. THIN SECTION DESCRIPTION:

Rock is a medium grained (about 0.75 mm) biotite-muscovite-sillimanite schist with coarse (up to 3. 5 mm) quartzo-feldspathic segregations. The Q-F minerals in the segregations appear to overprint the schistose fabric; relicts of the schistosity are still visable. Biotite, muscovite, and sillimanite are intergrown and form a well-developed schistosity.

THIN SECTION DESCRIPTION: MOODUS BOREHOLE

Described by: P.G. Naumoff Date: 2/22/88 Project number: 86C4111

A. HAND SPECIMEN | COLOR | TEXTURE

Hebron Gneiss | Black | Granoblastic

B. MINERAL IDENTIFICATION; SECTION NUMBER MC 1502 B

	MINERAL	OTHER PROPERTIES	GRAIN SIZE, SHAPE, ETC	%
ESSENTIAL	Quartz		estimated >	35
	Plagioclase			43
	Biotite			20
	Muscovite			2
	Garnet			Trace
ACCESSORY	Zircon			Trace
	Apatite			Tr
	Tourmaline			Tr
	Opaques			Tr

C. THIN SECTION DESCRIPTION:

A fine-grained (about 0.3 mm) granoblastic biotite schist. Small flakes of biotite (0.3 mm) are moderately aligned to moderately define the foliation. Some of the plagioclase crystals are well twinned.

THIN SECTION DESCRIPTION: MOODUS BOREHOLE

Described by: P.G. Naumoff Date: 2/24/88 Project number: 86C411

A. HAND SPECIMEN | COLOR | TEXTURE

Hebron Gneiss | Black | Granofels with a coarse schistose layer

B. MINERAL IDENTIFICATION; SECTION NUMBER MC 1504

	MINERAL	OTHER PROPERTIES	GRAIN SIZE, SHAPE, ETC	%
ESSENTIAL	Quartz		estimated >	30
	Plagioclase			34
	Biotite			25
	Muscovite			10
	Garnet			1
	Sillimanite			Trace
ACCESSORY	Zircon			Trace
	Opaques			Tr
	Apatite			Tr

C. THIN SECTION DESCRIPTION:

Rock is generally a equigranular biotite schist with a moderately defined foliation of aligned biotite flakes. Grain size is about 0.2 mm. Section is cut by a coarse schistose layer that contains muscovite, garnet, biotite, and traces of sillimanite. A coarse quartzo-feldspathic layer (grain size up to 5 mm) is associated with this layer.

THIN SECTION DESCRIPTION: MOODUS BOREHOLE

Described by: P.G. Naumoff Date: 2/25/88 Project number: 86C4111

A. HAND SPECIMEN	COLOR	TEXTURE
Hebron Gneiss	Black	Schistose

B. MINERAL IDENTIFICATION; SECTION NUMBER M 1804

	MINERAL	OTHER PROPERTIES	GRAIN SIZE, SHAPE, ETC	%
ESSENTIAL	Quartz		estimated >	37
	Plagioclase			37
	Biotite			15
	Pyroxene			5
	Amphibole			5
	Calcite			1
ACCESSORY	Zircon			Trace
	Apatite			Tr
	Opaques			Tr
	Rutile (?)			Tr
	Sphene			Tr

C. THIN SECTION DESCRIPTION:

Rock is a fine- to medium-grained schistose calcsilicate. Grain size ranges from about 0.2 mm to 1.0 mm. Schistosity is well developed and defined by aligned biotite grains and trains of elongate quartzo-feldspathic minerals. The Q-F minerals show sutured contacts. Amphibole and pyroxene are evenly disseminated throughout the section.

THIN SECTION DESCRIPTION: MOODUS BOREHOLE

Described by: P.G. Naumoff Date: 2/24/88 Project number: 86C4111

A. HAND SPECIMEN	COLOR	TEXTURE
Canterbury Gneiss	Pinkish-gray	Granitic

B. MINERAL IDENTIFICATION; SECTION NUMBER MC 1966 A

	MINERAL	OTHER PROPERTIES	GRAIN SIZE, SHAPE, ETC	%
ESSENTIAL	Quartz		estimated >	34
	Plagioclase			32
	K-feldspar			32
	Biotite			2
ACCESSORY	Apatite			Trace
	muscovite			Tr
	epidote			Tr
	Chlorite			Tr

C. THIN SECTION DESCRIPTION:

Rock is a medium grained granitic gneiss with a faint folition imparted by aligned micas. Section also contains a contact between two texturally different granites; a pinkish-rock having grain size of about 2.0 mm and K-feldspar grains that are pink (in hand sample) and a whitish gray rock where the K-felspar grains are not altered. Grain size in the white granite is smaller (about 1.0 mm), and biotite is a little more abundant.

THIN SECTION DESCRIPTION: MOODUS BOREHOLE

Described by: P.G. Naumoff Date: 2/25/88 Project number: 86C4111

A. HAND SPECIMEN | COLOR | TEXTURE

Canterbury Gneiss | Light grey | Granitic

B. MINERAL IDENTIFICATION; SECTION NUMBER MC 1966 B

	MINERAL	OTHER PROPERTIES	GRAIN SIZE, SHAPE, ETC	%
ESSENTIAL	Quartz		estimated >	34
	Plagioclase			31
	K-feldspar			30
	Biotite			5
ACCESSORY	Muscovite			Trace
	Apatite			Tr
	Chlorite			Tr
	Epidote			Tr

C. THIN SECTION DESCRIPTION:

Section is a medium-grained (about 1.0 mm) granitic gneiss with a foliation moderately defined by small flakes of aligned mica.

THIN SECTION DESCRIPTION: MOODUS BOREHOLE

Described by: P.G. Naumoff Date: 2/25/88 Project number: 86C4111

A. HAND SPECIMEN | COLOR | TEXTURE

Canterbury Gneiss | White | Granitic

B. MINERAL IDENTIFICATION; SECTION NUMBER MC 1966 C

	MINERAL	OTHER PROPERTIES	GRAIN SIZE, SHAPE, ETC	%
ESSENTIAL	Quartz		estimated >	34
	Plagioclase			32
	K-feldspar			32
	Biotite			1
	Muscovite			1
	Garnet			Tr
ACCESSORY	Chlorite			Trace
	Epidote			Tr
	Apatite			Tr

C. THIN SECTION DESCRIPTION:
A medium- to coarse-grained (average about 2.5 mm) garnet-bearing granitic gneiss. A slight development of compositional layering and small flakes of aligned micas weakly defines the foliation.

THIN SECTION DESCRIPTION: MOODUS BOREHOLE

Described by: P.G. Naumoff Date: 2/25/88 Project number: 86C4111

A. HAND SPECIMEN	COLOR	TEXTURE
(?) Hebron Gneiss	Black	Schistose

B. MINERAL IDENTIFICATION; SECTION NUMBER M 2104

	MINERAL	OTHER PROPERTIES	GRAIN SIZE, SHAPE, ETC	%
ESSENTIAL	Quartz		estimated >	30
	Plagioclase			40
	Biotite			15
	Amphibole	Brown to green pleochroic hornblende		15
ACCESSORY	Sphene			1
	Apatite			Trace
	Opaques			Tr

C. THIN SECTION DESCRIPTION:

Section is of a medium-grained biotite-hornblende calcsilicate. Grain size averages about 1.0 mm in size. Large crystals of sphene (0.5 mm) are fairly abundant. Foliation well-developed and defined by aligned biotite and amphibole crystals.

THIN SECTION DESCRIPTION: MOODUS BOREHOLE

Described by: P.G. Naumoff Date: 2/25/88 Project number: 86C4111

A. HAND SPECIMEN	COLOR	TEXTURE
Calcsilicate	Black	Schistose

B. MINERAL IDENTIFICATION; SECTION NUMBER M 2324

	MINERAL	OTHER PROPERTIES	GRAIN SIZE, SHAPE, ETC	%
ESSENTIAL	Quartz		estimated >	30
	Plagioclase			35
	Biotite			20
	Amphibole	Light brown to green pleochroic hornblende		15
ACCESSORY	Zircon			Trace
	Opaques			Tr
	Apatite			Tr
	Sericite	Out of Plagioclase		Tr
	Epidote			Tr
	Calcite			Tr
	(?) Rutile			Tr

C. THIN SECTION DESCRIPTION:

A well-foliated medium-grained calcsilicate schist. Grain size is about 0.75 mm. Plagioclase is generally well twinned and has an anorthite content of at least An 54 (labradorite).

THIN SECTION DESCRIPTION: MOODUS BOREHOLE

Described by: P.G. Naumoff Date: 2/26/88 Project number: 86C4111

A. HAND SPECIMEN	COLOR	TEXTURE
Tatnic Hill Formation	Black	Blastomylonitic/Augenoid

B. MINERAL IDENTIFICATION; SECTION NUMBER MC 2460 A

	MINERAL	OTHER PROPERTIES	GRAIN SIZE, SHAPE, ETC	%
ESSENTIAL	Quartz		estimated >	30
	Plagioclase			40
	Biotite			30
ACCESSORY	Zircon			Trace
	Apatite			Tr
	Muscovite			Tr

C. THIN SECTION DESCRIPTION:
A coarse-grained (felsic minerals up to 10.0 mm) biotite schist. Coarse lathes of biotite define quartzo-feldspathic augen.

THIN SECTION DESCRIPTION: MOODUS BOREHOLE

Described by: P.G. Naumoff Date: 2/26/88 Project number: 86C4111

A. HAND SPECIMEN	COLOR	TEXTURE
Tatnic Hill Formation	Black	Blastomylonite

B. MINERAL IDENTIFICATION; SECTION NUMBER MC 2460 B

	MINERAL	OTHER PROPERTIES	GRAIN SIZE, SHAPE, ETC	%
ESSENTIAL	Quartz		estimated >	32
	Plagioclase			35
	Biotite			30
	Muscovite			3
ACCESSORY	Zircon			Trace
	Apatite			Tr
	Opaques			Tr
	Epidote			Tr

C. THIN SECTION DESCRIPTION:

A medium- to coarse-grained biotite-muscovite schist with grain size ranging from about 0.5 mm to over 3.0 mm. Foliation is well defined by thin layers of aligned biotite and biotite-muscovite intergrowths. A 1.5-cm-wide quartzo-feldspathic layer is present. Here, an incipient mortar texture is developed; coarse grains of undulatory quartz and plagioclase are surrounded by fine felsic grains.

THIN SECTION DESCRIPTION: MOODUS BOREHOLE

Described by: P.G. Naumoff Date: 2/26/88 Project number: 86C4111

A. HAND SPECIMEN	COLOR	TEXTURE
Tatnic Hill Formation	Black	Cataclastic

B. MINERAL IDENTIFICATION; SECTION NUMBER MC 2460 C

	MINERAL	OTHER PROPERTIES	GRAIN SIZE, SHAPE, ETC	%
ESSENTIAL	Quartz		estimated >	30
	Plagioclase			35
	Biotite			35
ACCESSORY	Zircon			Trace
	Apaptite			Tr
	Opaques			Tr
	Muscovite			Tr

C. THIN SECTION DESCRIPTION:

A medium- to coarse-grained biotite schist with grain size ranging from about 0.5 mm to 3.0 mm. Foliation is well defined by aligned biotite flakes. Some cataclasis is present, seen by granulated felsic mineral and larger grains that show undulose extinction.

THIN SECTION DESCRIPTION: MOODUS BOREHOLE

Described by: P.G. Naumoff Date: 2/25/88 Project number: 86C4111

A. HAND SPECIMEN | COLOR | TEXTURE

Calcsilcate | Black | Schistose

B. MINERAL IDENTIFICATION; SECTION NUMBER M 2524

	MINERAL	OTHER PROPERTIES	GRAIN SIZE, SHAPE, ETC	%
ESSENTIAL	Quartz		estimated >	30
	Plagioclase			40
	Biotite			15
	Amphibole	Actinolite		15
ACCESSORY	Apatite			Trace
	Calcite			Tr
	Epidote			Tr
	Opaques			Tr
	Zircon			Tr
	(?) Rutile			Tr

C. THIN SECTION DESCRIPTION:

A medium-grained (about 1.0 mm) calcsilicate schist with occasional large (up to 7.0 mm) poikiloblastic grains of actinolite. Foliation is well developed and predominantly defined by aligned biotite flakes. Feldspar grains are generally well-twinned and have an anorthite content of at least An 60 (labradorite).

THIN SECTION DESCRIPTION: MOODUS BOREHOLE

Described by: P.G. Naumoff Date: 2/26/88 Project number: 86C4111

A. HAND SPECIMEN	COLOR	TEXTURE
Waterford Group	Gray	Gneissic

B. MINERAL IDENTIFICATION; SECTION NUMBER MC 2924 A

	MINERAL	OTHER PROPERTIES	GRAIN SIZE, SHAPE, ETC	%
ESSENTIAL	Quartz		estimated >	40
	Plagioclase			47
	Biotite			10
	Amphibole	Hornblende		Trace
ACCESSORY	Opaques	Sulphide		Trace
	Tourmaline	Associated with quartzo-feldspathic vein		3
	Calcite			Tr
	Muscovite			Tr
	Epidote			Tr
	Sphene			Tr
	Apatite			Tr

C. THIN SECTION DESCRIPTION:

A coarse-grained plagioclase-quartz-biotite gneiss. Grain size is about 1.0 to 1.5 mm. Foliation moderately defined by streaky clots of aligned biotite and evenly dispersed individual flakes of biotite. A 1-cm-wide plagioclase-quartz vein cuts the gneiss. Concentrations of sulphides and tourmaline occur along the walls of the vein and within the vein. Vein felsics are very coarse (up to 1 cm) and show undulose extinction.

THIN SECTION DESCRIPTION: MOODUS BOREHOLE

Described by: P.G. Naumoff Date: 2/29/88 Project number: 86C4111

A. HAND SPECIMEN | COLOR | TEXTURE

Warterford Gneiss | Gray | Gneissic

B. MINERAL IDENTIFICATION; SECTION NUMBER MC 2924 B

	MINERAL	OTHER PROPERTIES	GRAIN SIZE, SHAPE, ETC	%
ESSENTIAL	Quartz		estimated >	37
	Plagioclase			38
	Amphibole	Hornblende		10
	Biotite			15
ACCESSORY	Apatite			Trace
	Sphene			Tr
	Epidote			Tr
	Monazite (?)			Tr

C. THIN SECTION DESCRIPTION:

The section is of a coarse-grained quartz-plagioclase-biotite-hornblende gneiss. Grain size reaches 3.0 mm. Foliation is well defined by streaky clots of biotite or biotite and amphibole. These clots are evenly disseminated. Grains of ? monazite reach 1.0 mm in size.

THIN SECTION DESCRIPTION: MOODUS BOREHOLE

Described by: P.G. Naumoff Date: 3/1/88 Project number: 86C4111

A. HAND SPECIMEN | COLOR | TEXTURE

Waterford gneiss | Whitish-gray | Gneissic

B. MINERAL IDENTIFICATION; SECTION NUMBER M 3004

	MINERAL	OTHER PROPERTIES	GRAIN SIZE, SHAPE, ETC	%
ESSENTIAL	Quartz		estimated >	34
	Plagioclase			55
	Biotite			10
	Amphibole	Hornblende		1
ACCESSORY	Opaques			Trace
	Chlorite			Tr
	Muscovite			Tr
	Sphene			Tr
	Apatite			Tr

C. THIN SECTION DESCRIPTION:

Rock is a fine- to medium-grained plagioclase-quartz-biotite gneiss. Grain size ranges from about 0.2 mm to 2.0 mm. Foliation is defined by moderately developed compositional layering that consists of predominantly felsic layers alternating with biotite-rich layers.

THIN SECTION DESCRIPTION: MOODUS BOREHOLE

Described by: P.G. Naumoff Date: 3/2/88 Project number: 86C4111

A. HAND SPECIMEN | COLOR | TEXTURE

Waterford Gneiss | Dark gray | Gneissic

B. MINERAL IDENTIFICATION; SECTION NUMBER M 3244

	MINERAL	OTHER PROPERTIES	GRAIN SIZE, SHAPE, ETC	%
ESSENTIAL	Quartz		estimated >	30
	Plagioclase			40
	Amphibole			20
	Biotite			10
ACCESSORY	Apatite			Trace
	Opaque			Tr
	Calcite			Tr
	Sphene			Tr

C. THIN SECTION DESCRIPTION:

Rock is a medium-grained plagioclase-quartz-amphibole-biotite gneiss. Foliation is defined by moderately developed compositional layers consisting of felsic layers alternating with biotite- plus amphibole-rich layers. Grain size is about 1.0 mm.

THIN SECTION DESCRIPTION: MOODUS BOREHOLE

Described by: P.G. Naumoff Date: 3/1/88 Project number: 86C4111

A. HAND SPECIMEN | COLOR | TEXTURE

Gneiss | Dark gray | Gneissic

B. MINERAL IDENTIFICATION; SECTION NUMBER M 3264

	MINERAL	OTHER PROPERTIES	GRAIN SIZE, SHAPE, ETC	%
ESSENTIAL	Quartz		estimated >	30
	Plagioclase			40
	Amphibole			15
	Biotite			15
ACCESSORY	Apatite			Trace
	Epidote			Tr
	Calcite			Tr
	Sphene			Tr
	Chlorite			Tr

C. THIN SECTION DESCRIPTION:

Rock is a medium- to coarse-grained plagioclase-quartz-amphibole-biotite gneiss with an average grain size of about 0.5 mm. Foliation is well defined by oriented biotite and amphibole grains. Epidote, chlorite, and calcite are relatively abundant as alteration products of amphibole and biotite.

THIN SECTION DESCRIPTION: MOODUS BOREHOLE

Described by: P.G. Naumoff Date: 3/2/88 Project number: 86C4111

A. HAND SPECIMEN | COLOR | TEXTURE

Gneiss | Gray | Gneissic

B. MINERAL IDENTIFICATION; SECTION NUMBER M 3284

	MINERAL	OTHER PROPERTIES	GRAIN SIZE, SHAPE, ETC	%
ESSENTIAL	Quartz		estimated >	30
	Plagioclase			40
	Biotite			20
	Amphibole	Hornblende		10
ACCESSORY	Apatite			Trace
	Epidote			Tr
	Sphene			Tr

C. THIN SECTION DESCRIPTION:

Rock is a medium- to coarse-grained gniess with an average grain size of about 0.5 mm. Foliation is well defined by oriented biotite and amphibole grains and flattened quartzo-felspathic minerals.

THIN SECTION DESCRIPTION: MOODUS BOREHOLE

Described by: P.G. Naumoff Date: 2/29/88 Project number: 86C4111

A. HAND SPECIMEN	COLOR	TEXTURE
Gneiss	Gray	Gneissic

B. MINERAL IDENTIFICATION; SECTION NUMBER MC 3495

	MINERAL	OTHER PROPERTIES	GRAIN SIZE, SHAPE, ETC	%
ESSENTIAL	Quartz		estimated >	40
	Plagioclase			42
	Biotite			10
	Amphibole	Hornblende		8
ACCESSORY	Calcite			Trace
	Epidote			Tr
	Apatite			Tr
	Sphene			Tr

C. THIN SECTION DESCRIPTION:
Section is a medium-grained (about 0.75 mm) gneiss. Foliation is moderately defined by small flakes of aligned amphibole and biotite.

THIN SECTION DESCRIPTION: MOODUS BOREHOLE

Described by: P.G. Naumoff Date: 2/29/88 Project number: 86C4111

A. HAND SPECIMEN	COLOR	TEXTURE
Gneiss	Gray	Augen gneiss

B. MINERAL IDENTIFICATION; SECTION NUMBER MC 3496

	MINERAL	OTHER PROPERTIES	GRAIN SIZE, SHAPE, ETC	%
ESSENTIAL	Quartz		estimated >	40
	Plagioclase			40
	Biotite			10
	Amphibole	Hornblende		10
ACCESSORY	Sphene			Trace
	Epidote			Tr
	Apatite			Tr
	Calcite			Tr
	Muscovite			Tr
	K-feldspar			Tr

C. THIN SECTION DESCRIPTION:

Rock is a medium-grained (0.5 mm) quartz-plagioclase-biotite-amphibole gneiss. Foliation is moderately defined by aligned biotite and amphibole grains. Section contains 0.5- to 1.0-cm-wide augen of very coarse felsic minerals (grain size up to 1 cm). Some grains of K-feldspar are associated with the augen; the grains are generally lightly sericitized and contain opaque inclusions (hematite). All of the felsic minerals exhibit udulose extinction.

THIN SECTION DESCRIPTION: MOODUS BOREHOLE

Described by: P.G. Naumoff Date: 2/29/88 Project number: 86C4111

A. HAND SPECIMEN | COLOR | TEXTURE

Gneiss | Black | Gneiss/amphibolite contact

B. MINERAL IDENTIFICATION; SECTION NUMBER MC 3503 A

	MINERAL	OTHER PROPERTIES	GRAIN SIZE, SHAPE, ETC	%
ESSENTIAL	Quartz	amphibolite/gneiss combined estimate >		25
	Plagioclase			25
	Amphibole	Hornblende		40
	Biotite			10
ACCESSORY	Sphene			Trace
	Epidote			Tr
	Opaques			Tr

C. THIN SECTION DESCRIPTION:

One half of the section is a medium- to coarse-grained amphibolite. Foliation is very well defined by aligned biotite and amphibole crystals. Average grain size is about 0.75 mm. Quartz and plagioclase grains are generally separated by biotite and amphibole. The contact between the amphibolite and gneiss is gradational; the quartzo-feldspathic content increases substantially and the amount of biotite and amphibole decreases. The foliation of the gneiss is moderately developed by aligned biotite and amphibole.

THIN SECTION DESCRIPTION: MOODUS BOREHOLE

Described by: P.G. Naumoff Date: 2/29/88 Project number: 86C4111

A. HAND SPECIMEN	COLOR	TEXTURE
Amphibolite	Black	Schistose

B. MINERAL IDENTIFICATION; SECTION NUMBER MC 3503 B

	MINERAL	OTHER PROPERTIES	GRAIN SIZE, SHAPE, ETC	%
ESSENTIAL	Amphibole	Hornblende	estimated >	50
	Quartz			15
	Plagioclase			20
	Biotite			15
ACCESSORY	Sphene			Trace
	Apatite			Tr
	Opaques			Tr

C. THIN SECTION DESCRIPTION:

Section is a medium-grained amphibolite. Grain size is about 0.5 mm. Foliation is very well developed and defined by oriented biotite and amphibole grains. Felsic minerals occur as individual grains.

THIN SECTION DESCRIPTION: MOODUS BOREHOLE

Described by: P.G. Naumoff Date: 3/2/88 Project number: 86C4111

A. HAND SPECIMEN	COLOR	TEXTURE
Gneiss	Pink	Gneissic

B. MINERAL IDENTIFICATION; SECTION NUMBER M 3583

	MINERAL	OTHER PROPERTIES	GRAIN SIZE, SHAPE, ETC	%
ESSENTIAL	Quartz		estimated >	30
	Plagioclase			35
	K-feldspar			35
ACCESSORY	Opaque			Trace

C. THIN SECTION DESCRIPTION:

Rock is a medium- to coarse-grained granitic gneiss with grain size averaging about 1.0 mm. Foliation is well defined by flattened and aligned quartzo-feldspathic minerals.

THIN SECTION DESCRIPTION: MOODUS BOREHOLE

Described by: P.G. Naumoff Date: 2/29/88 Project number: 86C4111

A. HAND SPECIMEN — COLOR — TEXTURE

Gneiss — Light gray — Gneissic

B. MINERAL IDENTIFICATION; SECTION NUMBER MC 3986 A

	MINERAL	OTHER PROPERTIES	GRAIN SIZE, SHAPE, ETC	%
ESSENTIAL	Quartz		estimated >	40
	Plagioclase			50
	Biotite			10
ACCESSORY	Apatite			Trace
	? Rutile			Tr
	Opaques			Tr

C. THIN SECTION DESCRIPTION:

Rock is a fine grained plagioclase-quartz-biotite gneiss with an average grain size of about 0.3 mm. Foliation is moderately to poorly defined by individual flakes of aligned biotite and occasional flattened quartzo-feldspathic minerals.

THIN SECTION DESCRIPTION: MOODUS BOREHOLE

Described by: P.G. Naumoff Date: 2/29/88 Project number: 86C4111

A. HAND SPECIMEN | COLOR | TEXTURE

Amphibolite | Black | Schistose

B. MINERAL IDENTIFICATION; SECTION NUMBER MC 3986 B

	MINERAL	OTHER PROPERTIES	GRAIN SIZE, SHAPE, ETC	%
ESSENTIAL	Amphibole	Hornblende	estimated >	50
	Quartz			15
	Plagioclase			24
	Biotite			10
ACCESSORY	Opaque			Trace
	Apatite			Tr
	Sphene			1

C. THIN SECTION DESCRIPTION:

Rock is a medium-grained (about 0.75 mm), very well foliated amphibolite. Foliation defined by oriented plates of biotite and amphibole. Quartz and plagioclase occur mainly as individual crystals that are surrounded by amphibole and biotite. Small grains of sphene are evenly disseminated throughout the section.

THIN SECTION DESCRIPTION: MOODUS BOREHOLE

Described by: P.G. Naumoff Date: 3/1/88 Project number: 86C4111

A. HAND SPECIMEN	COLOR	TEXTURE
Gneiss	Light gray with black "streaks"	Gneissic

B. MINERAL IDENTIFICATION; SECTION NUMBER MC 3991

	MINERAL	OTHER PROPERTIES	GRAIN SIZE, SHAPE, ETC	%
ESSENTIAL	Quartz		estimated >	34
	Plagioclase			40
	Amphibole	Hornblende		20
	Biotite			5
ACCESSORY	Opaque			Trace
	Sphene			1
	Apatite			Tr
	Calcite			Tr

C. THIN SECTION DESCRIPTION:

Rock is a coarse-grained plagioclase-quartz-hornblende-biotite gneiss with an average grain size of about 1.0 mm. Amphibole and biotite usually occur in lens-shaped clots that define the foliation. Concentrations of sphene are associated with these clots. Some flattened quartzo-feldspathic minerals also define the foliation.

THIN SECTION DESCRIPTION: MOODUS BOREHOLE

Described by: P.G. Naumoff Date: 3/1/88 Project number: 86C4111

A. HAND SPECIMEN | COLOR | TEXTURE

Gneiss | Pinkish-white | Gneissic

B. MINERAL IDENTIFICATION; SECTION NUMBER MC 3994

	MINERAL	OTHER PROPERTIES	GRAIN SIZE, SHAPE, ETC	%
ESSENTIAL	Quartz		estimated >	33
	Plagioclase			33
	K-feldspar			34
ACCESSORY	Opaques	Magnetite		Trace
	Chlorite			Tr
	Garnet			Tr
	Allanite			Tr
	Sphene			Tr
	Muscovite			Tr

C. THIN SECTION DESCRIPTION:

Rock is a medium- to coarse-grained granitic gneiss with grain size ranging from about 0.2 mm to over 2.5 mm. Foliation is very poorly defined although there is some alignment of small streaks of opaque minerals and flattened quartzo-feldspathic minerals.

THIN SECTION DESCRIPTION: MOODUS BOREHOLE

Described by: P.G. Naumoff Date: 3/2/88 Project number: 86C4111

A. HAND SPECIMEN — COLOR — TEXTURE

Phyllonite — Greenish-black — Mylonitic

B. MINERAL IDENTIFICATION; SECTION NUMBER M 4103

	MINERAL	OTHER PROPERTIES	GRAIN SIZE, SHAPE, ETC	%
ESSENTIAL	Chlorite		estimated >	50
	Biotite			20
	Plagioclase			26
ACCESSORY	Apatite			1
	Opaques			1
	Sphene			1
	Calcite			1

C. THIN SECTION DESCRIPTION:

Rock is a fine-grained phyllonite with grain sizes not exceeding 0.4 mm. Felsic grains are extensively crushed, flattened, and cracked. Biotite laths are bent and broken.

THIN SECTION DESCRIPTION: MOODUS BOREHOLE

Described by: P.G. Naumoff Date: 3/1/88 Project number: 86C4111

A. HAND SPECIMEN — COLOR — TEXTURE

Gneiss — White and black — Gneissic

B. MINERAL IDENTIFICATION; SECTION NUMBER MC 4445

	MINERAL	OTHER PROPERTIES	GRAIN SIZE, SHAPE, ETC	%
ESSENTIAL	Quartz		estimated >	30
	Plagioclase			45
	Amphibole	Hornblende		15
	Biotite			10
ACCESSORY	Opaques	Magnetite		Trace
	Sphene			Tr
	Apatite			Tr

C. THIN SECTION DESCRIPTION:

Rock is a medium-grained plagioclase-quartz-amphibole-biotite gneiss with a grain size of about 0.4 mm. Foliation is well defined by aligned biotite-amphibole crystals as well as moderately developed compositional layers consisting of alternating felsic-rich and biotite- plus amphibole-rich layers.

THIN SECTION DESCRIPTION: MOODUS BOREHOLE

Described by: P.G. Naumoff Date: 3/1/88 Project number: 86C4111

A. HAND SPECIMEN

Gneiss

COLOR

Black and white

TEXTURE

Contact between amphibolite and gneiss

B. MINERAL IDENTIFICATION; SECTION NUMBER MC 4448

	MINERAL	G=gneiss A=amphibolite >		% G	% A
ESSENTIAL	Quartz		estimated >	30	14
	Plagioclase			40	25
	Amphibole			10	40
	Biotite				20
	Epidote			20	
	Pyroxene			Trace	
ACCESSORY	Apatite			Tr	Tr
	Opaque			Tr	Tr
	Sphene			Tr	1
	Zircon			Tr	Tr
	Chlorite				Tr
	Calcite				Tr

C. THIN SECTION DESCRIPTION:

The amphibolite is a black, coarse-grained rock. Amphibole crystals reach up to 3.0 mm in size. Quartz and plagioclase generally occur as individual grains in between plates of amphibole.

At the contact with the gneiss, grain size of amphibole diminishes abruptly to about 0.4 mm, although some larger grains occur. General grain size in the gneiss is about 0.5 mm and the rock texture becomes granoblastic-polygonal. Euhedral epidote crystals occur in small aggregates and appear to be secondary alterations of pyroxene. Foliation is poorly defined by aligned and disseminated amphibole.

THIN SECTION DESCRIPTION: MOODUS BOREHOLE

Described by: P.G. Naumoff Date: 3/2/88 Project number: 86C4111

A. HAND SPECIMEN

COLOR	TEXTURE
Gneiss	Black and white	Gneissic

B. MINERAL IDENTIFICATION; SECTION NUMBER M 4644

	MINERAL	OTHER PROPERTIES	GRAIN SIZE, SHAPE, ETC	%
ESSENTIAL	Quartz		estimated >	40
	Plagioclase			52
	Biotite			5
	Amphibole	Hornblende		3
ACCESSORY	Opaque			Trace
	Epidote			Tr
	Calcite			Tr
	Apatite			Tr
	Sphene			Tr
				Tr

C. THIN SECTION DESCRIPTION:

Rock is a coarse-grained (average grain size about 0.75 mm) gneiss. Foliation is defined by aligned biotite and amphibole and by slight flattening of felsic minerals.

THIN SECTION DESCRIPTION: MOODUS BOREHOLE

Described by: P.G. Naumoff Date: 3/2/88 Project number: 86C4111

A. HAND SPECIMEN | COLOR | TEXTURE

Gneiss | Light gray | Gneissic

B. MINERAL IDENTIFICATION; SECTION NUMBER M 4764

	MINERAL	OTHER PROPERTIES	GRAIN SIZE, SHAPE, ETC	%
ESSENTIAL	Quartz		estimated >	33
	Plagioclase			33
	K-feldspar			34
ACCESSORY	Opaque			Trace
	Calcite			Tr
	Muscovite			Tr
	Epidote			Tr

C. THIN SECTION DESCRIPTION:

Rock is a fine-grained equigranular granite gneiss. Grain size is about 0.2 mm. Rock has a granoblastic-polygonal texture. K-feldspar grains are are moderately to extensively sericitized.

Appendix C

APPENDIX C

Results of the hydraulic fracturing experiments and other geophysical surveys. Copies of borehole televiewer logs are archived at Woodward-Clyde Consultants, Wayne, N.J.

IN SITU STRESS, NATURAL FRACTURE AND SONIC VELOCITY MEASUREMENTS IN THE MOODUS, CONNECTICUT SCIENTIFIC RESEARCH WELL

Report Submitted to

Woodward-Clyde Consultants
210 Willowbrook Blvd.
Wayne, New Jersey 07470

Submitted by

Mark D. Zoback
Daniel Moos

Department of Geophysics
Stanford University
Stanford, California 94305

April 25, 1988

Executive Summary

This report presents an analysis and interpretation of a series of in situ stress, natural fracture and sonic velocity measurements conducted in the 4784 ft (1.46 km) deep Moodus, Conn. research well drilled by Woodward-Clyde Consultants for the Empire State Electrical Energy Research Corporation. The principal scientific objective of this project was to study the in situ stress field in this area and to attempt to relate the magnitude and orientation of the in situ stress field to the occurence of shallow earthquakes in this region. The field measurements analysed in this report were conducted in July and August, 1987 and principally involved (1) a series of hydraulic fracturing in situ stress measurements, (2) ultrasonic borehole televiewer surveys that were used to pick optimal intervals for the hydraulic fracturing tests and to study stress-induced wellbore breakouts and natural fractures and possible faults encountered in the well, and (3) full-waveform sonic velocity logs. All of these data are presented and discussed in this report.

The principal scientific findings of this study are that over the depth range of study (0.1 to 1.3 km), (1) the direction of maximum horizontal compression is essentially E-W ($N86^{o}E$), (2) the least principal stress is vertical and equal to the weight of the overburden, (3) in the context of frictional faulting theory, the magnitude of the greatest horizontal stress is sufficiently greater than the vertical stress that well-oriented reverse faults are potentially active (such faults would be expected to strike approximately N-S and dip about 30^{o}, either to the east or west), and (4) there is no apparent relationship between either the stress field or the pattern of natural fractures and the Honey Hill fault, a major, presumably inactive low-angle fault that passes through the well at a depth of 2630 ft (802 m). In other words, the orientation of the maximum horizontal principal stress, the relative magnitudes of the principal stresses and the distribution and orientations of natural fracture planes are essentially the same above and below the Honey Hill.

These findings are in remarkable agreement with the focal mechanisms of shallow earthquakes that ocurred in the region of the hole just a few weeks after

the stress measurements were completed. In addition to observing the appropriate stress field for the occurrence of these earthquakes in the upper 1.3 km, the borehole televiewer revealed numerous planar features with the appropriate orientation to be potential reverse faults. However, a possibly important observation is that such features seem to be absent in the lower part of the hole.

The observation of high horizontal stresses in the upper km in this area and the occurrence of small-magnitude shallow-depth reverse-faulting earthquakes is quite similar to many intraplate areas around the world with a similar tectonic settings and local geology (i.e., areas which have crystalline rock exposed at the surface). It is clear in a number of these areas tha the relatively high horizontal stresses in the near-surface do not continue to greater depth because of the rapid increase in the weight of the vertical stress resulting from the overburden. In other words, the vetical stress increases with depth more rapidly than the horizontal stresses and thus there is not sufficient differential stress to cause reverse faulting with depth. In these areas, it clear, therefore, that the high horizontal stress field and small-magnitude, near-surface earthquakes that occur at shallow depth are essentially unrelated to the possible occurrence of deeper, potentially more damaging seismicity. Such may be the case at Moodus.

An important element of the Moodus experimental program was advancement of the state-of-the-art for making, analysing and interpreting measurements of the types described here. Advancements include (1) development of new field equipment for safe and efficient hydraulic fracturing operations at high pressure, (2) theoretical derivation of a new hydraulic fracturing breakdown equation for tight crystalline rock, (3) development of new interactive analysis techniques of hydraulic fracturing pressure-time data that are especially useful at sites like Moodus whg breakouts and natural fractures. All of these advancements have contributed measurably to the success of the Moodus stress measurement project and are briefly described in this report.

Acknowledgements

The Moodus field measurement program was the result of cooperative efforts between individuals at Stanford University and Lamont-Doherty Geological Observatory. We would like to thank Roger Anderson and Eric Scholz of Lamont-Doherty for making their field equipment available and their assistance with the tests. We would also like to thank Joerg Baumgaertner of Stanford for assistance with the field tests and analysis of the hydraulic fracturing data and Doug Schmitt of Stanford for his work on derivation of a new hydraulic fracturing equation and measurements on core samples. We also appreciate the assistance of Peter Naumoff of Woodward-Clyde who helped make the field measurement program go smoothly.

Table of Contents

Section I. Geologic and Tectonic Setting

The Moodus wellbore is located in the southwestern edge of the Merrimack synclinorium (fig. 1). This lithogical and structural province occupies an area extending from near Long Island Sound northward into central Maine (Dixon and Lundgren, 1968). The Merrimack synclinorium is bordered by two large thrust faults on the south and east, the west dipping Lake Cahr fault on the east and the north-northwest dipping Honey Hill fault on the south. Dip angles of these fault planes vary strongly from 10 W (Lake Char fault) to 20^{o}NW - 55^{o}N (Honey Hill fault, increasing dip angle from west to east). The western boundary of the synclinorium is formed by the Monson anticline.

Wintsch and Fout (1982) describe another major south dipping thrust fault within the synclinorium which is exposed to the surface about 25 km north of the Moodus drill site. They believe this fault to be an extension of the Honey Hill Fault which would suggest that most of the synclinorium is underlain by this fault zone.

All rocks within the synclinorium show metamorphism to staurolite grade or higher (Dixon and Lundgren, 1968). Major geological units in the Moodus area are the Hebron gneiss and the Brimfield schist formations. In contact zones about 0.5 km east of the Moodus drill site, older Brimfield schists structurally overlie the Hebron formation. Barosh et al. (1985) attribute this to simple thrust movements. The Moodus wellbore starts within the Hebron gneiss formation. Below 1900 ft (579 m) the borehole penetrates the Canterbury Gneiss as well as gneiss and biotite-muscovite schists of the Tatnic Hill formation. The Honey Hill thrust fault is intersected at a depth of about 2630 ft (802 m).

The surface trace of this fault is mapped only 15 km south of the Moodus drill site. Below this depth, the borehole continues in gneiss formations probably belonging to the Waterford group. The hole was drilled with a nominal 6 1/2" diameter and cores were cut periodically.

Interest in the stress field of the Moodus area stems from the history of recurrent micro-earthquakes in this region. The name Moodus was derived from the Indian word

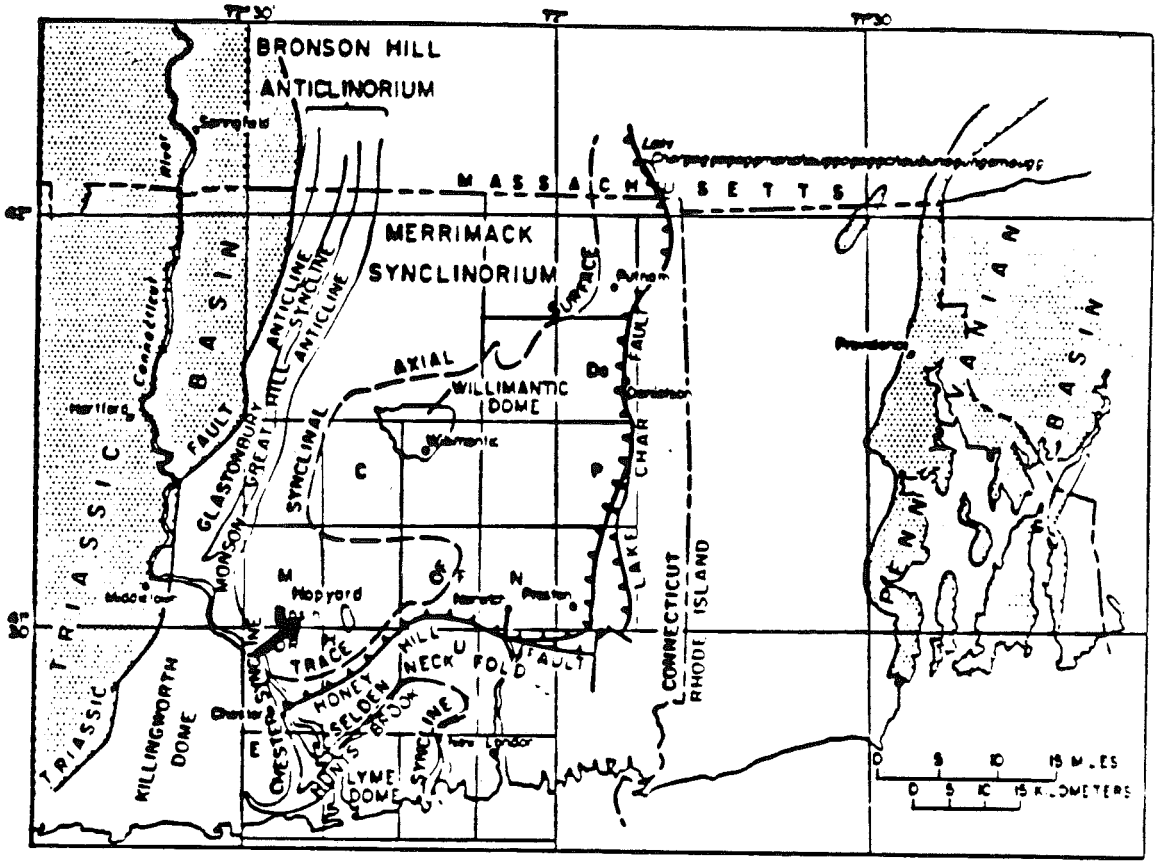

Figure 1. Simplified structural map of eastern Connecticut. Quadrangle names: C, Columbia; Da, Danielson; DR, Deep River; E, Essex; F, Fitchville; H, Hamburg; M, Moodus; N, Norwich; P, Plainfield; U, Uncasville. The Moodus deep borehole location is marked by an arrow. Map from Dixon and Lundgren (1968).

"Morehemoodus", meaning "the place where noises come from the ground" (Brigham, 1871). The name indicates that many events in the area around the village of Moodus can literally be heard. Recent earthquake activity recorded in this area appeared to occur in swarms. A swarm of more than 500 events in 1981 was reported by Ebel et al. (1982). The largest event in this series had a magnitude of 2.1. All events could be tracked back to hypocenters at very shallow depth. Calculated depths for the 1981 earthquakes are in the order of 1 km or even less (Ebel et al.,1982).

Consequently the Moodus deep drilling project offered a unique opportunity to drill in a thrust faulting environment into a seismic active depth range. The hydraulic fracturing technique was then used to determine a stress-depth profile from shallow depth down to depths greater than the hypocenter depths calculated for the 1981 swarm.

In terms of active regional tectonics, the Moodus site is within a large area of compressional tectonics in which earthquake focal mechanisms indicated predominately reverse, with some strike-slip faulting (see review of New England focal mechanisms by Gephart and Forsyth (1985). Fig. 2 presents a synthesis of maximum horizontal compressive stress orientation data (from Zoback and Zoback, 1988). A relatively uniform ENE-WSW to NE-SW directed maximum compression is observed to the west of the site in New York and the surrounding region. However, there is such a considerable scatter of earthquake focal mechanisms in New England (see Gephart and Forsyth, 1985) that the maximum horizontal stress orientation east of New York appears to be highly variable. Stress-induced wellbore breakouts in wells on the continental shelf about 400 km east of Moodus indicate a more E-W direction of maximum horizontal compression.

A series of hydraulic fracturing stress measurements in the Moodus area were made in two shallow boreholes (<1500 ft) by Engineers International, Inc. and sponsored by the U.S. Nuclear Regulatory Commission. A total of five successful hydrofracs are reported out of twenty-three attempted tests (Engineers Intl., 1986). They report extremely high horizontal stresses in which both horizontal principal

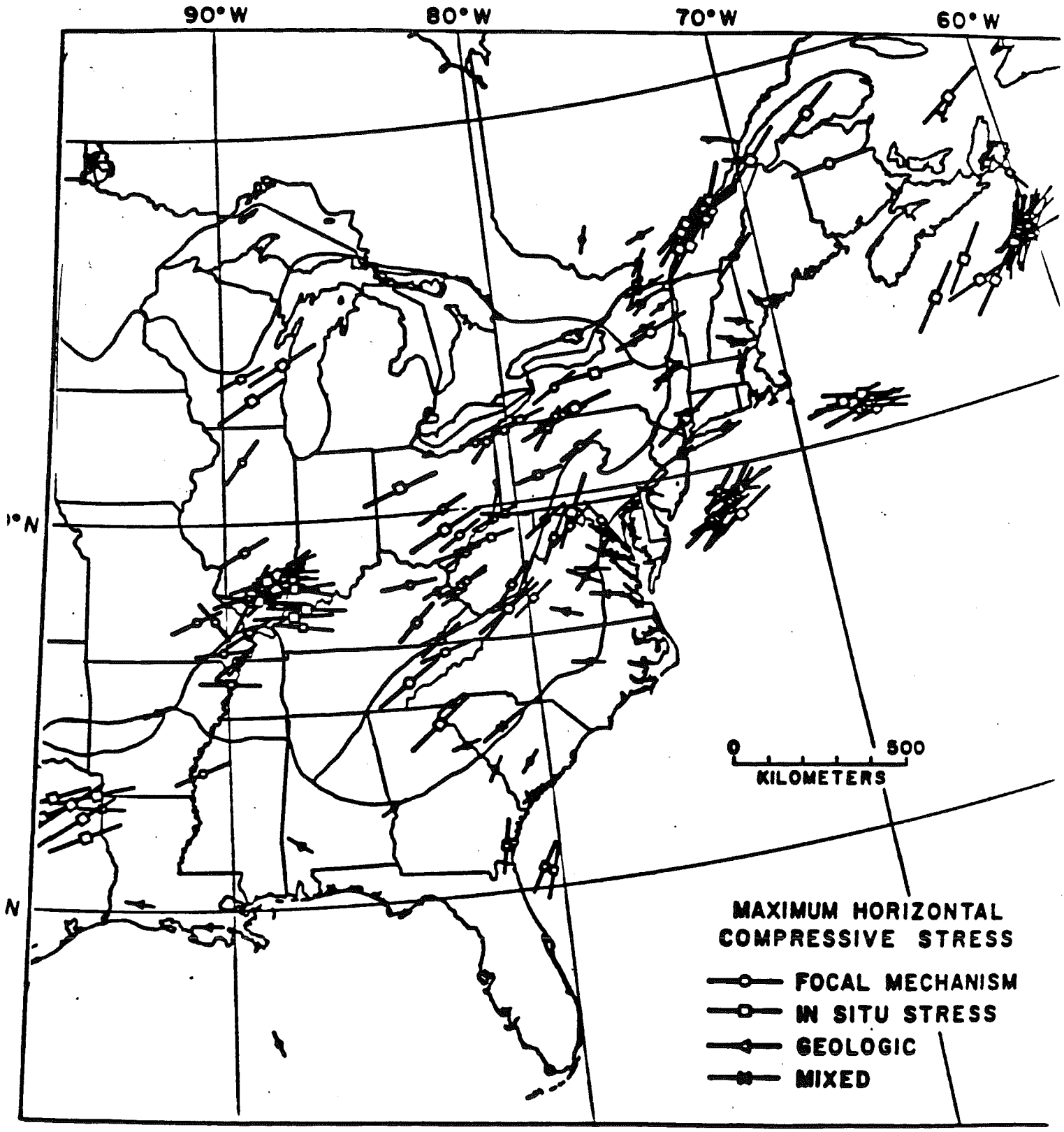

Figure 2. Map of directions of maximum horizontal principal stress direction gathered from a variety of sources. The different symbols represent the type of data and the lengths of the arrows indicate the data quality (from Zoback and Zoback, 1988).

stresses greatly exceed the vertical stress. Four hydraulic fracture impressions were used for determining the orientation of maximum horizontal compression- these indicated an average direction of N62^{o}W. While this direction is quite unusual as it is nearly orthogonal to the direction of maximum horizontal compression observed at Kent Cliffs and many other sites to the west, it can not be ruled out out-of-hand in light of the focal mechanism variability in New England (note that two focal mechanisms in eastern New Hampshire indicate WNW-ESE compression). As mentioned above, however, the direction of maximum horizontal compression that we determined from the Moodus well at greater depths differs from the EEI direction by about 30^{o}.

Section II. Overview of Experimental Program

Hydraulic fracturing stress measurements were made in the Moodus borehole only after a thorough suite of logs by Schlumberger, several borehole televiewer surveys and a multi-component full-wave sonic log were run in the hole. All of the data (with the exception of the Schlumberger logs) are described in this report.

Hydraulic Fracturing Testing Procedure

Optimal test sections for hydraulic fracturing were selected by careful inspection of borehole televiewer logs (BHTV) as well as by analyzing a variety of other logs (caliper, sonic ..), inspection of the core and consideration of the optimal distribution of measurements in the hole.

The hydraulic fracturing tests were conducted using a 6 cm i.d. (2 3/8") tubing and a 14 cm (5 1/2") straddle packer assembly manufactured by TAM International, Houston. The straddle length was 5.6 ft (1.7 m). In addition to conventional packer elements, rated for differential pressures up to a maximum of 41 MPa (6000 psi), new stiffer, high pressure elements (maximum differential pressure of 68.5 MPa (10,000 psi) were tested in the lower part of the hole. The mechanically driven hydraulic pump was capable of injection rates up to approximately 52 l/min. The pressurization fluid used was water. The measuring and recording system on the surface included two turbine flowmeters (injection rate as well as flow back were recorded) and two pressure transducers. One pressure gauge was a high precision digital quartz gauge that was recorded at a rate of 5 samples/sec. Due to the rather low flow rates (average injection rate into a fracture was 15 - 30 l/min) viscous pressure losses in the tubing were negligible, on the order of 0.1 - 0.3 MPa. For fast and safe valve operation at high pressures, a fully automatic surface manifold rated for fluid pressures up to 68.5 MPa was developed by Eric Scholz of Lamont Doherty Geological Observatory. The system uses electrically-activated air driven valves. All flow and pressure data were digitally recorded on a MASSCOMP computer system in the logging/hydrofrac truck and later

transferred onto a Macintosh computer for interpretation. A summary of the results of the hydraulic fracturing tests is presented in Section III. In Section VI, we present each hydraulic fracturing pressure-time curve for the twelve successful measurements and in Section VII, we present a thorough discussion of the interpretation techniques applied to these data.

In a typical hydrofrac test, the inflatable packers were pre-set at pressures between 10 and 15 MPa. Packer pressures for the straddle assembly used, dynamically increase to values always slightly larger than the injection pressure in the test interval. As shown in Fig. 1, each fracture was extended in several repeated pressurization cycles (at least 4 cycles) until shut-in pressure values P_{isip} stabilized. During each cycle, a volume of about 30 - 50 l was injected. Upon completion of each test, recovery of fluid upon flow-back varied between 15 and 50 %. After all fracturing was completed and prior to a post-fracturing BHTV log, several shallow fractures were re-pressurized with an impression packer. The intent of this procedure was to mechanically widen the fracture opening at the wellbore wall by loosening small particles and increasing thus the potential for fracture detection during a BHTV logging. As indicated in Section IV, the post-frac data confirm that vertical fractures were induced at the wellbore, as predicted by hydraulic fracturing theory.

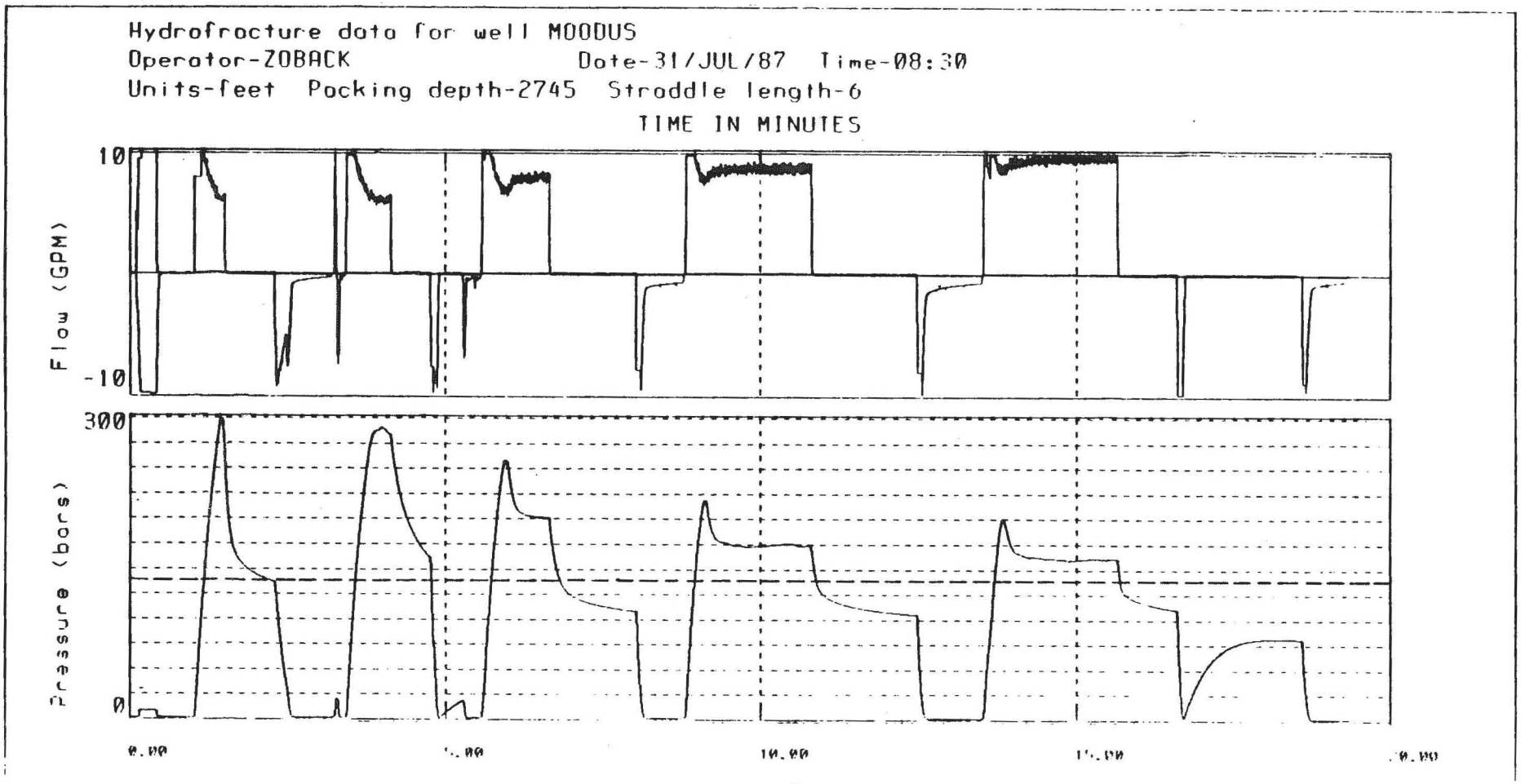

Figure 1. Complete hydrofrac test sequence at 2745 ft. in the Moodus wellbore. Pressure values are given in 'bar'. Flow rates are given in GPM.

Section III. Summary of Hydraulic Fracturing Data

Twelve successful hydraulic fracturing experiments were conducted in the Moodus borehole in the depth range between 354- 4211 feet (108-1284 m). Due to the high least horizontal compressive stress and high tensile strength of the rock no hydraulic fractures could be initiated in the lower part of the Hebron Gneiss (650-2000 feet, or 200 - 600 m). In this depth range, breakdown pressures exceeded the maximum differential sealing pressure of the conventional inflatable packers. Tests with the higher-rated packer elements were not carried out at this depth because of rather strict time constraints for the whole series of experiments and the higher priority of obtaining data near the bottom of the borehole.

The most important pressure values used for stress computations, the instantaneous shut-in pressure P_{isip} and fracture re-opening pressure P_r, increase with depth (see Tables in Section VII) and are consistently equal to or larger than the overburden pressure (an average rock density 2.61 g/cm^3 has been used). At three depths (2795 ft/852 m, 3884 ft/1184 m and 4192 ft/1277 m) it is clear that we opened subhorizontal planes of weakness- the shut-in pressure values P_{isip} at the end of the first cycle, were only slightly larger than the overburden pressure and the post-fracturing televiewer log showed that low-angle fractures had been opened at the wellbore (dip angles: about 16^o- 27^o). At 2688 ft (819 m), the system was shut-in at the maximum differential pressure supported by the packer elements until a weakness plane in the borehole wall was opened. As it turned out later, this plane was oriented nearly normal to the maximum horizontal compression, S_H, and the shut-in pressure from this test is an approximate measure of S_H.

Interpretation of the pressure records at this site is based on the following principles appropriate for tests in a thrust faulting environment:

1.) If a subhorizontal fracture plane was opened, the last shut-in pressure

1.) If a subhorizontal fracture plane was opened, the last shut-in pressure observed was taken as a measure of the overburden stress. As mentioned previously, all fractures were extended in repeated cycles until the shut-in pressure values stabilized.

2.) The tubing/packer system incorporated a relatively large fluid volume (between about 0.4 m^3 and 3.7 m^3 depending on the test depth). This increase in fluid volume causes a remarkable loss of system stiffness (defined by the gradient of dP/dV) with depth. The pressure gradient increase with injected fluid volume (dP/dV) drops from about 53 bar/l (20.0 MPa/gallon) at 108 m to about 7 bar/l (2.6 MPa/gallon) at 1284 m. At the same time, the already large amount of potential energy stored in the pressurized system at shallow depth increases from roughly 0.2 * 10^3 Nm/MPa to about 1.4 * 10^3 Nm/Mpa at 1.2 km depth. With water as fracturing fluid, friction losses are extremely small during fracture extension. Thus, most of the stored potential energy will be used to create new surface. As a result, the first fracture initiation cycle will then create a fairly large fracture extending beyond the stress concentration around the wellbore. On the basis of these arguments, in all cases where new vertical fractures could be induced at the wellbore wall, the shut-in pressure of the first pressurization cycle was taken as a measure of the minimum horizontal compression S_h. This technique may involve a slight overestimation of S_h due to the remaining increment of rock tensile strength at short fracture lengths. However, it offers the highest probability of not including the fracture re-orientation process in the stress estimation.

3.) If a test sequence shows sharply decreasing pressure levels (fracture extension pressure, instantaneous shut-in pressure) between two successive fracture extension cycles, a complete re-orientation of the fracture plane was assumed. In those cases the last shut-in pressure was comparable to the calculated overburden stress and we were thus able to estimate all three principal stresses.

4.) To minimize the possibility of underestimating the fracture opening pressure, due to an incompletely closed fracture system, the fracture re-opening pressure values P_r used for stress computations were consistently determined from the second

pressurization cycle.

At 819 m depth the shut-in pressure of the second pressurization cycle was regarded to represent the stress component normal to the fracture trace observed at the wellbore wall. As already mentioned above, a pre-existing weakness plane was opened at this depth when the system was shut-in at the maximum pressure sealed by the packer elements.

A nearly complete fracture re-orientation (no. 3, above) could be observed only during two tests at 383 ft (117 m) in the Hebron Gneiss and 2745 ft (837 m) in the Waterford Gneiss. At both depths, the last re-opening and fracture extension pressure(s) measured was (were) equal to or lower than the shut-in pressure of the first cycle(s) (fig. 2). This suggests that the first vertical part of the fracture could not completely close anymore upon shut-in and we were essentially able to determine the stress normal to the near-horizontal plane. Conversely, in several test sequences where decreasing shut-in pressure values were recorded, the shut-in pressure stabilized above the overburden stress. This was apparently because the "rolled-over" fracture was not hydraulically communicating with the wellbore. Thus, even though the fracture had rolled-over into a near-horizontal plane, it was not possible to determine the overburden stress in the borehole.

The stress values derived from the above described analysis procedure are presented in Table I and shown in Fig. 1. The estimation of the maximum horizontal compressive stress, S_H, is done in a somewhat unusual way. By applying an "exact" effective stress law (Nur and Byerlee, 1971) we have re-derived the hydraulic fracture breakdown equation (Section VIII). To utilize this new equation, appreciable information is needed on the elastic properties of the rock and preliminary measurements are described in that section on the Moodus core. However, it is straight forward to utilize the new formulation and simply put bounding values on S_H. We do this by utilizing the simplified form of the the breakdown equation that is commonly used and that was originally derived by Haimson and Fairhurst (1967) after Hubbert and Willis' (1957) pioneering work and subsequently modified by Bredehoeft

TABLE I
Summary of Hydraulic Fracturing Stress Measurements

Depth (ft.)	Depth (m)	S_h (MPa)	S_H (Upper Bound) (MPa)	S_H (Lower Bound) (MPa)	S_V* (MPa)
353	108	8.0	13.1	12.0	
383	117	9.2	12.6	11.4	4.2
584	178	14.1	26.7	24.9	
632	193	12.2	21.8	19.9	
2688	819			45.2	
2745	837	27.4	48.5	14.3	21.3
2795	852				21.8
2920	890	28.6	59.3	50.6	
3530	1076	39.1	81.1	70.5	
3884	1184				31.7
4192	1277				30.7
4211	1284	44.6	92.8	80.2	

* A value is given for the cases in which this was measurable from the hydraulic fracturing data. At other depths it is assumed to approximately correlate with the theoretical weight of the overburden. For a density of 2.61 g/cm^3 this corresponds to a gradient of about 26 MPa/km.

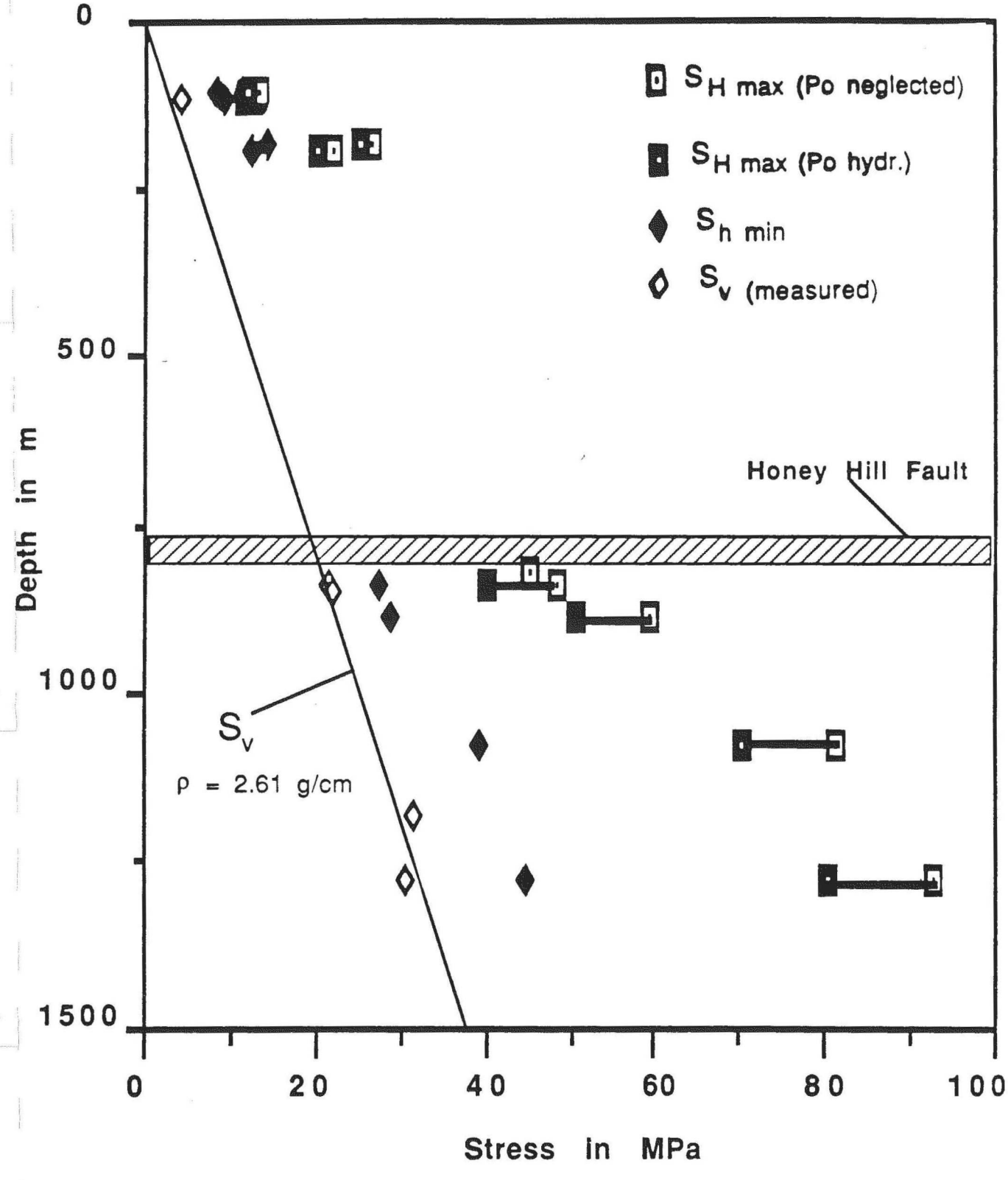

Figure 1. Principal horizontal stresses S_H and S_h as a function of depth in the Moodus deep borehole. The thick solid line indicates the overburden stress S_v ($\rho = 2.61$ g/cm^3). P_o is the pore pressure.

et. al (1976):

$$S_H = 3S_h - P_r - P_o$$

where P_r is the fracture re-opening pressure and P_o is the pore pressure. As shown in Section VIII, we obtain the upper and lower limits for S_H by simply using P_o as the estimated pore pressure (for an upper bound) and $P_o = 0$ (for a lower bound). As seen in Fig. 1, this variation in values is not large and does not reduce our ability to interpret the results.

Section IV. Analysis of Borehole Televiewer and Sonic Velocity Data

Specialty logs at Moodus analyzed by the Stanford group include (a) an acoustic borehole televiewer (BHTV) log recorded before hydraulic fracturing operations from the water table at 428 to 4750 feet, and from 600 to 90 feet by backfilling the borehole with water, (b) a BHTV log recorded after hydraulic fracturing experiments were completed from 4350 to 250 feet, and (c) a 12-receiver digitally recorded full waveform sonic log from 76 to 4728 feet.

Televiewer Logging

The acoustic borehole televiewer (BHTV) is a well logging tool that produces an image of the reflectivity of the borehole wall as a function of azimuth and depth in the borehole (Figure 1). The BHTV is an acoustic device containing a piezoelectric transducer mounted on a shaft rotating 3 times per second, which emits and receives an ultrasonic pulse 1800 times a second. The televiewer is pulled up the borehole at 5 feet per minute while the transducer assembly rotates. The resulting helical path is sampled approximately 600 times around the circumference of the well and every 1/3 inch in depth. The images are oriented w.r.t. magnetic North using a flux-gate magnetometer mounted on the transducer assembly. The reflected pulses are recorded during the log, and the data is digitized later to determine the reflected amplitude and the time of flight of each acoustic pulse. The finite width of the acoustic beam results in complete coverage of the well bore. A three-dimensional image of the shape and reflectivity of the borehole wall can therefore be analyzed using the digitized data. In the subsequent analysis all orientations are with respect to true North, unless otherwise stated.

Two BHTV logs were recorded in the Moodus well. A pre-hydrofracture BHTV log was recorded shortly after the completion of drilling in early June, 1987. This log was recorded from the water table at 428 feet to a total depth of 4750 feet; while filling the hole with water a second pass was run from 600 feet to about 90 feet. Intervals for hydraulic fracturing were chosen on the basis of this data. However, although numerous breakouts (zones of stress-induced wellbore spalling) and natural fractures were observed, a miss-alignment of the magnetic compass on the BHTV prevented the accurate determination of their

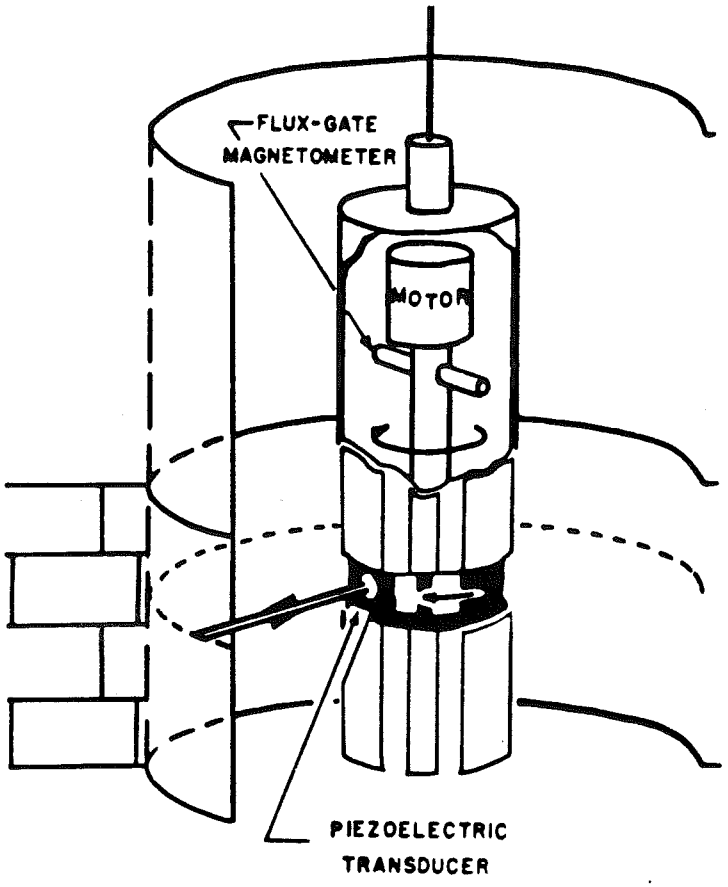

Figure 1: Schematic of the operation of the borehole televiewer, after Zemanek et al., 1969.

orientation. The televiewer was sent to the factory to be re-calibrated after this logging run.

At the completion of the hydraulic fracturing experiments a second log was run, to image the hydrofractures and also to log the orientation of the breakouts and fractures observed in the previous run. The orientation calibration was checked before and after the log. The second log was recorded from the then-static water level at 220 feet to a depth of 4350 feet, as a packer was lost during an attempted hydrofrac experiment immediately below that depth. At the conclusion of the experiments both of these logs were digitized from the analog data. The discussion below is from analysis of only the second of the two logs.

Four different analyses of the BHTV data were conducted. The first involved determining the orientation and width of stress-induced wellbore breakouts. The second was an analysis of the shape and average reflectivity of the well-bore, to study subtle ellipticity possibly related to stresses, and variations in reflectivity associated with lithologic changes. The third was the analysis of the post and pre fracturing logs within the successful hydrofrac intervals, to observe the direction of the induced fractures. The fourth was a determination of the orientation and width of natural fractures and foliation planes intersecting the well.

Stresses and breakouts

Borehole breakouts are enlarged sections of a wellbore caused by brittle failure of the rock surrounding the borehole at the azimuth of the minimum horizontal stress (Zoback et al., 1985). The width of the breakout is a function of rock strength and the magnitude of the horizontal stresses. Breakouts are easily observed in BHTV images, typically as dark bands 180 degrees apart. In analyzing the breakouts their orientation yields the direction of the minimum horizontal principal stress, and their width provides a measure of the stress magnitudes.

Figure 2 shows a zone of breakouts in the Moodus well, over the interval from 4287 to 4273; the figure is a copy of the computer graphics screen produced during interactive analysis of the breakouts. On the right is a plot of travel-time as a function of azimuth and depth. As the interior surface of a breakout is concave, reflections from the sides are generally not returned to the crystal, and they are apparent as black bands on the image. However, where the center of the breakout is sufficiently smooth a reflection is returned, allowing

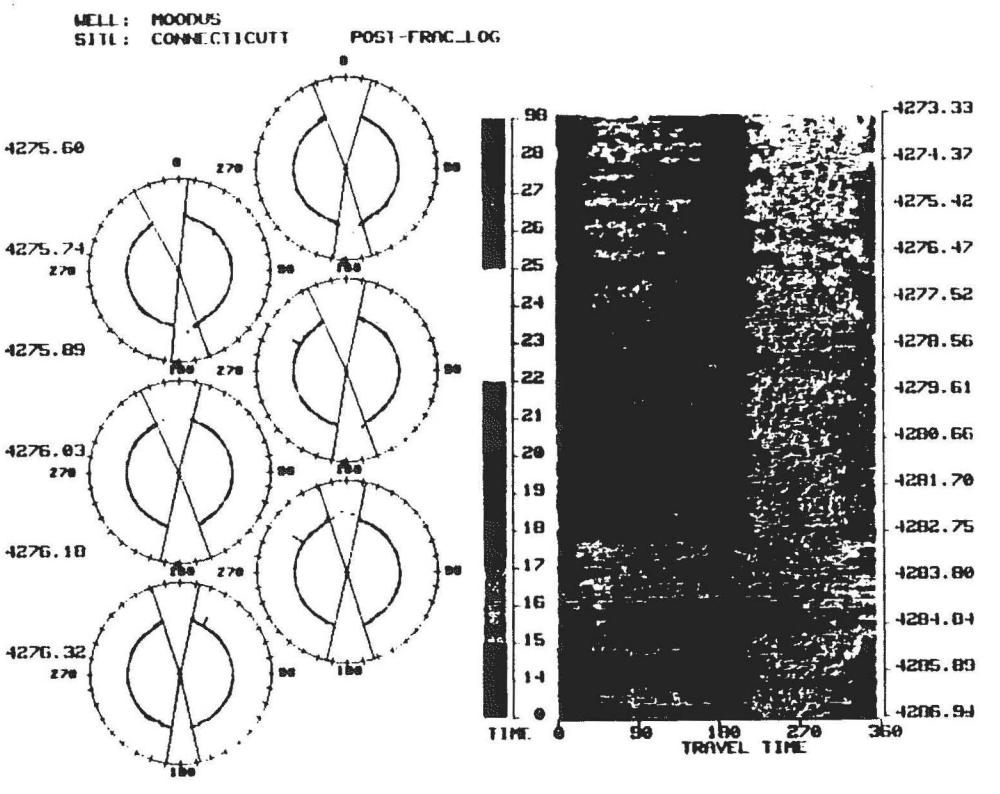

Figure 2: Section of the Moodus borehole from 4287 to 4273 feet, showing a typical breakout zone. On the right is a travel-time image of the borehole, oriented with respect to magnetic North. On the left are a series of cross-sections formed by the superposition of 5 scan lines. The breakouts are the dark bands in the televiewer image. Note that the breakout continues below the bottom of the dark band as somewhat enlarged bands (green on the otherwise blue image) connecting the zone at 4283.5 feet to the more continuous zone above that depth. The cross-sections show that the breakouts are only approximately 180 degrees apart, and that the precise orientation and width vary along the breakout length.

the determination of the breakout's depth. On the left are a series of borehole cross-sections produced by superimposing 5 scan lines. Each cross-section covers about 4 cm depth. The edges of the breakout chosen interactively are displayed on the cross-sections as radial lines from which the width and orientation of the breakout over each 4-cm interval is recorded. The selection criteria required that the breakout must be clearly visible on the image, and that the cross-section must allow unambiguous determination of both edges of the feature. Furthermore, if the feature did not appear to occur on both sides of the well-bore, or extend from a feature above or below that did, it was eliminated from consideration. These overly restrictive criteria certainly resulted in some loss of data, but the orientation and width data remaining are thus unquestionably measurements of true breakouts.

These data are stored during analysis, and the average orientation and width are determined statistically. Figure 3 shows a compressed section of the Moodus well from 3450 to 4350 feet. Although numerous breakouts are observed below 3650 feet, few are present above that depth. Almost no breakouts were observed above 3450 feet, although at shallow depths the borehole exhibited some ellipticity roughly coincident with the orientations of the breakouts deeper in the well (see below).

The breakout orientations are remarkably consistent through most of the Moodus borehole. The mean for the entire section is N88.6E with a standard deviation of 5 degrees. The average width is about 40 degrees +/- 5.5 degrees. Examination of Figure 3 does however reveal a slight rotation in the breakout azimuth from approximately E-W below 3910 feet, about 10 degrees counter-clockwise from 3860 to 3750 (excepting the interval around 3770), back to E-W above 3750 feet. This effect may be related to a true systematic change in stress orientation, or to the interaction of the stresses with the rock's intrinsic anisotropy. Measurements of core properties should help differentiate between these possibilities.

Caliper and reflected amplitude

The televiewer images accurately represent the shape and reflectivity of the borehole, but are difficult to deal with quantitatively. For example, the average reflectivity of the intact rock should be a function of mineralogy grain size and the surface roughness of the borehole wall, as intrinsic impedance contrasts and scattering control the reflected amplitudes. The travel-time images can be reduced to the parameters defining a best-fitted ellipse through

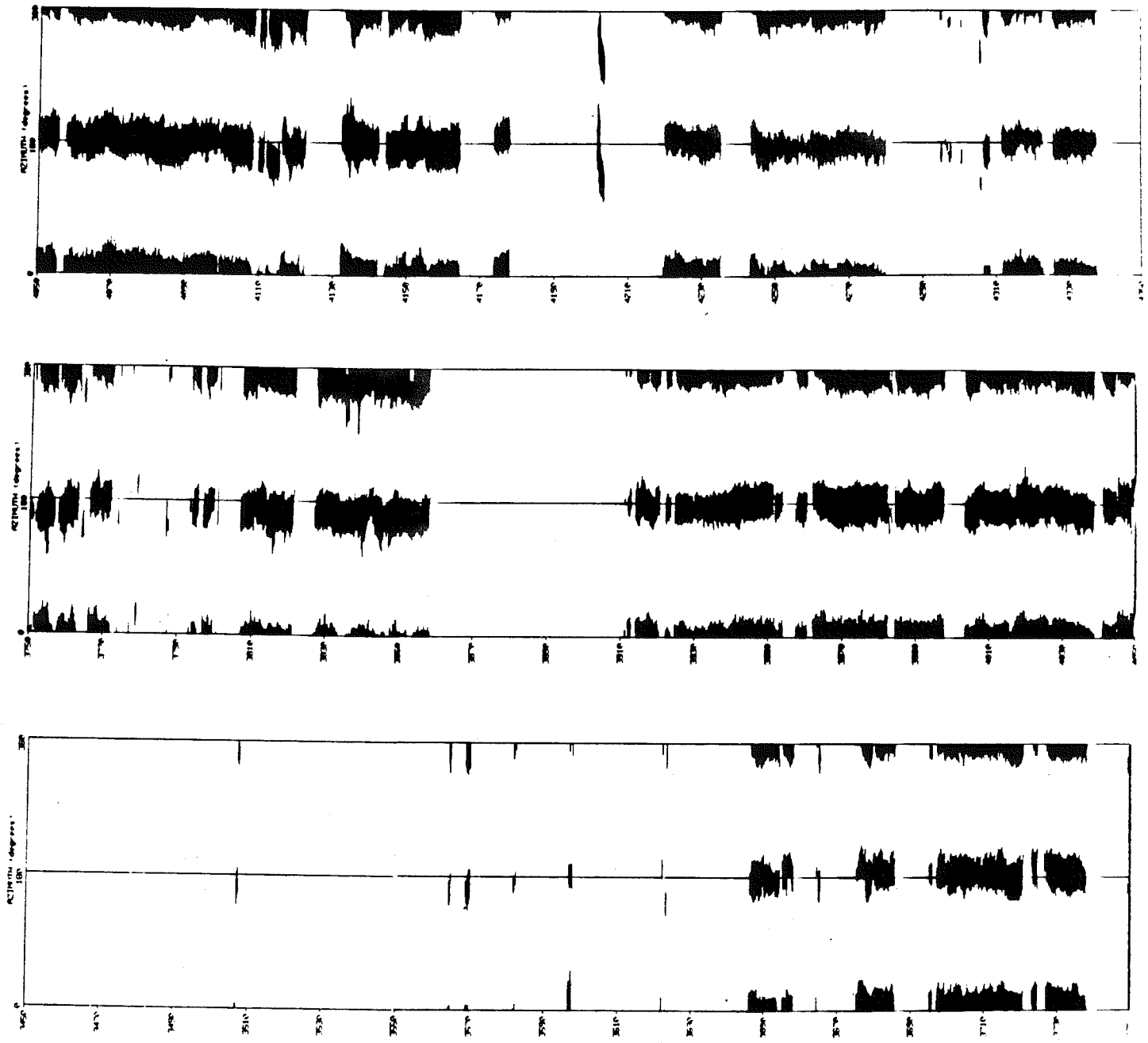

Figure 3: A compressed image of the Moodus borehole, showing the results of the breakout analysis over the interval from 4350 to 3450 feet. The interval above 3450 feet contained few breakouts and therefore is not shown in this figure. Breakouts are shown as shaded zones, roughly 180 degrees apart. The width of the dark band is the breakout width determined by interactive analysis, as shown in Figure 2. The results are displayed with respect to true North.

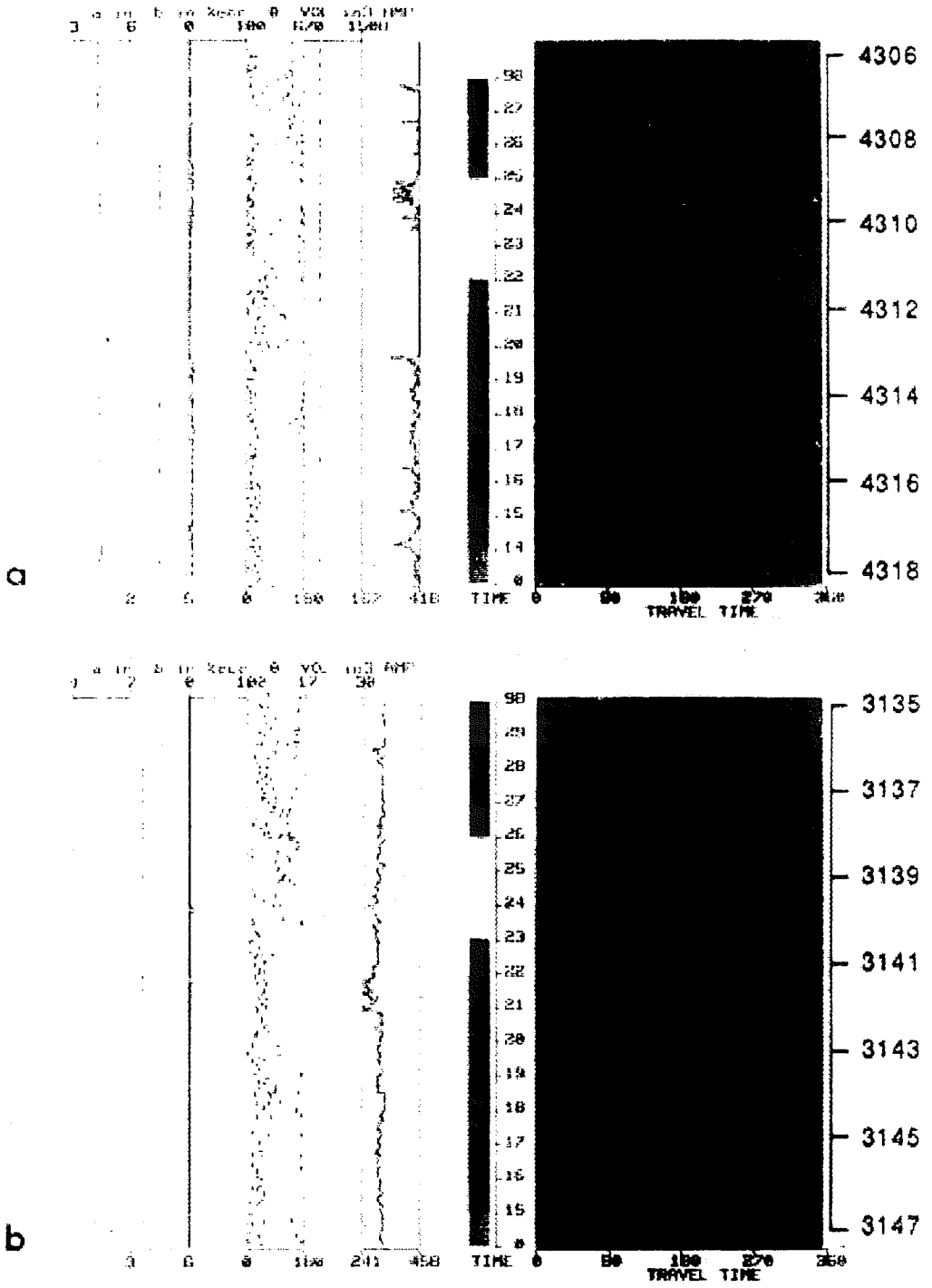

Figure 4: Illustration of the caliper / amplitude analysis of data across (a) a breakout interval from 4318 to 4306 feet (b) a fracture at 3140 feet. On the right are travel-time images, oriented w.r.t. magnetic N. On the left are the log curves. **A** and **b** are the major and minor radii in inches. **E** is the eccentricity in percent. Theta θ is the orientation of the major axis. Hole **VOL**ume is the product of the cross-sectional area and the distance between scans. **AMP** is the average of the uppermost 500 amplitudes recorded by the digitizer. The amplitudes are not calibrated for changes in gain settings during data collection, and should be treated as relative values only.

the data, i.e. the major and minor axis lengths and the orientation of the major axis. Figure 4 illustrates this procedure. Shown are two sections of the Moodus borehole showing the effect of breakouts and fractures on the geometry and reflectivity results. Travel-time images are shown on the right. The curves on the left show major (a) and minor (b) axes, eccentricity, the orientation of the major axis, and the amplitude computed by averaging the largest 500 values. Figure 4a shows an interval with well-developed breakouts within the Lower Avalon. Within the broken-out interval the major axis is larger and the minor axis somewhat smaller than in the undisturbed hole, leading to a finite eccentricity. The major axis is consistently aligned with the breakout azimuth, and more random where no breakouts occur. Amplitudes are consistently greater than 400, but are measurably decreased within the broken-out interval. Thus breakouts are clearly located by an averaging scheme that includes almost all of the amplitudes. Figure 4b shows a fracture within the Lower Avalon section at shallower depth. Small breakouts immediately below the fracture create measurable eccentricity, and again the orientation of the major axis is quite consistent. However, even where the breakouts are quite small (e.g. below 3143 feet) the azimuth of the major axis is often aligned with the breakout direction. The fracture severely distorts the borehole, causing a kick in the eccentricity, and sharply reduces the averaged reflectivity. The averaged amplitudes are lower throughout this interval due to a gain reduction during recording, which illustrates the difficulty in using the uncalibrated amplitudes for lithologic discrimination. However, the breakout interval again has lower amplitudes than the adjacent rock. Breakouts can be differentiated from fractures by the consistent azimuth of the major axis and by their finite length.

The correlation between breakout orientation and the orientation of the major axis of the best-fit ellipse is not surprising, as the distortion in the borehole is largely due to the formation of breakouts. To study this effect quantitatively histograms of the direction of maximum compression inferred from breakout directions and from the major axis azimuths are compared in Figure 5. The direction of maximum horizontal compression (N88.6E) is shown above the histograms. The tight grouping of the inferred axis of maximum compression from breakout orientations is remarkable. However, the azimuth of the major axis of the best-fit ellipse also clusters around the maximum stress direction. This data includes the entire well, not just the locations of breakouts. Thus, although there is considerably more scatter in the ellipse data the major axis is

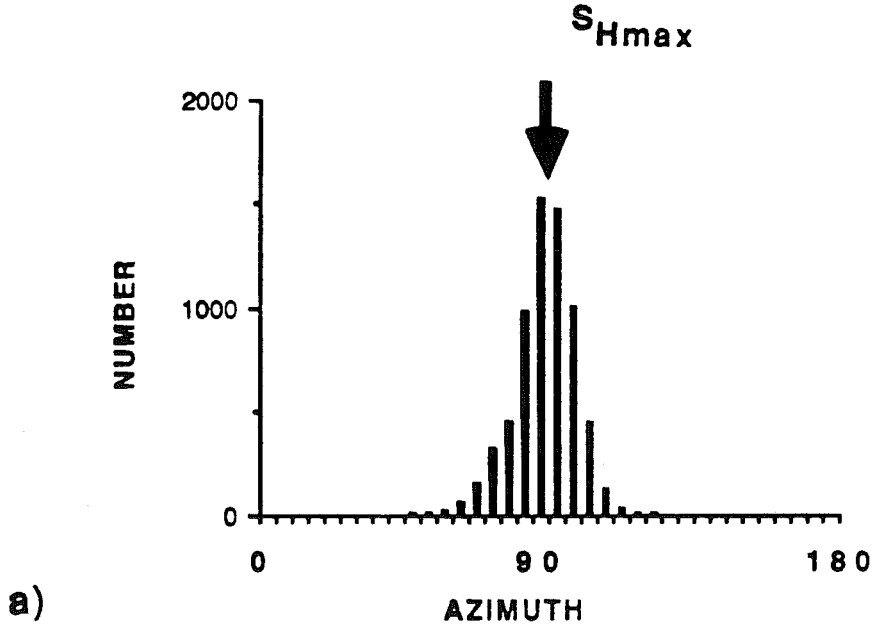

a)

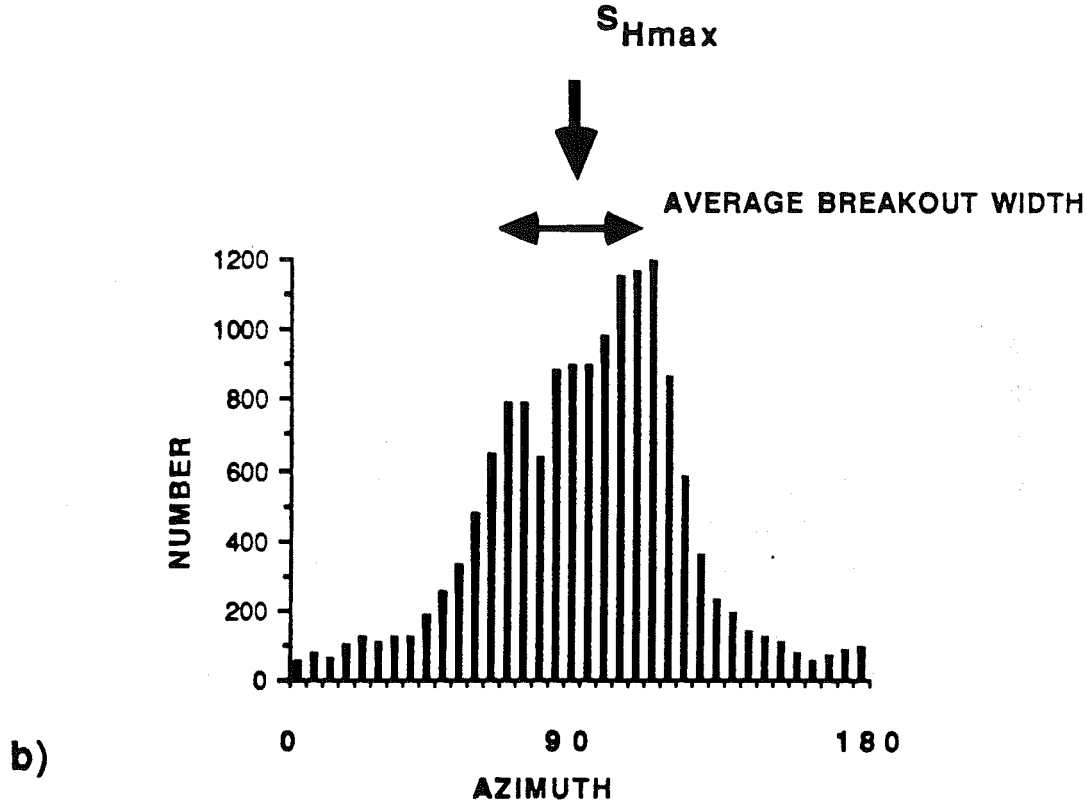

b)

Figure 5: Histograms of the expected orientation of S_{Hmax} from breakout orientation (a), and from the orientation of the major axis of the ellipse fitted to the televiewer travel-time data (b), from 4350 to 250 feet in the Moodus borehole. The data are plotted w.r.t. true North. The average breakout width is also plotted, to illustrate the effect of the missing data from within the breakouts on the caliper analysis.

apparently related to the direction of greatest horizontal compression. However, the distribution of axis orientations is bimodal. Neither of the peaks is actually in the breakout direction, although a significant number of orientations are. In fact, the miss-alignment of the ellipse axis is related to the breakout width; the ellipse axis is pointing to the "edge" of the breakout. This is due to the absence of data within the breakout, as seen in the televiewer data discussed above, which causes the algorithm to select one or the other breakout edge as the furthest point from the tool and thus as the orientation of the major axis. Where data is present within the breakouts, the true breakout direction is selected. This will occur even where no breakout is apparent by visual inspection of the image.

Orientation of Hydraulically Induced Fractures

Although the breakout orientations in the Moodus borehole define the direction of the minimum and maximum horizontal principal stresses, accurate orientation of the hydraulically induced fractures is necessary in order to confirm the fact that vertical hydraulic fractures were induced. Hydrofractures are very difficult to locate. We therefore ran a post-fracturing impression packer in several shallow test intervals. The hydrofrac at each depth was reopened by inflating the impression packer to a pressure above the fracture reopening pressure recorded during the test. This allows a small amount of impression rubber to extrude into the fracture, and damages the fracture walls, thus enhancing the reflectivity contrast and increasing the likelihood that the fracture will be visible in the post-fracturing televiewer image. We then compared the borehole televiewer images recorded before and after hydraulic fracturing within each successful test interval to locate the newly created hydrofracs.

Evidence was found at three depths of near vertical fractures generated during the hydrofracture experiments. The fracture induced at 4211 feet strikes N60E and dips 82 degrees SE. The test at 584 feet generated a near-vertical fracture, but the fracture was not continuous enough on the televiewer image to allow its orientation. At 3884 feet a new vertical fracture was also observed, approximately 90 degrees from the breakouts above and below the test interval. No other induced fractures were located in the BHTV images.

There is ample evidence from other experiments that hydraulic fracturing produces near-vertical fractures aligned perpendicular to breakout directions. Impression packers revealed breakouts oriented 90 degrees to near-vertical hydraulic fractures in the Kent Cliffs well (Woodward-Clyde, 1986) and at Cajon

Pass (Healey and Zoback, in press). Furthermore, near-vertical hydraulic fractures revealed by oriented impression packers in a well in Auburn NY were 90 degrees to the breakout direction in that well (Hickman et al., 1985). The orientation of the new fracture created at 4211 feet is 33 degrees from the expected orientation, based on a breakout zone immediately below this depth which yields a maximum compression direction of N87W. This is somewhat surprising, as the breakout orientations do not change more than 10 degrees from the average orientation, throughout the total depth of the well.

BHTV Log Curves

The above analyses provide quantitative measurements from the BHTV images. This information includes the parameters which describe the shape of the wellbore, the magnitude and variation in wellbore reflectivity, and the orientation, shape and extent of wellbore breakouts. These logs allow the comparison of BHTV-derived properties with those from the other logs. For example, in order to relate breakout width to stress magnitude the rock strength must be known. Furthermore, variations in breakout orientation can be related to changes in the principal stress orientations only after the effects of anisotropy are taken into account. Finally, variations in reflected amplitude and its statistical distribution can be related to lithology and the degree of foliation.

Figures 6-8 summarize the televiewer analysis in the Moodus borehole. Shown are the major and minor axis lengths (a and b), the eccentricity in percent, the picked edges of observed breakouts (aleft, bleft, aright, bright), the amplitudes of the largest 400 and 200 reflected pulses for each 360 degree scan (a400 and a200), the normalized difference between a400 and a200 (anorm = (a200-a400)/(a400·a200), and the widths of the 180 degree opposed breakouts (awidth and bwidth), in Tracks 1 through 6 respectively.

Figure 6 shows an 800 foot interval with no breakouts around the large open fracture at 620 feet. The fracture sharply reduces the average amplitudes, and greatly increases the normalized amplitude difference. Eccentricity is much greater within the fractured interval. Thus, although the best-fit ellipse major axis is often aligned with the minimum stress direction, it can also be affected by fracturing. The lithologic and sonic logs help to discriminate between these effects (for instance, at this fracture sonic amplitudes decrease, density and resistivity are lower and porosity increases).

Figure 7 illustrates the results over the interval 3700 to 3800 feet in the borehole, where breakouts are large continuous features separated by short

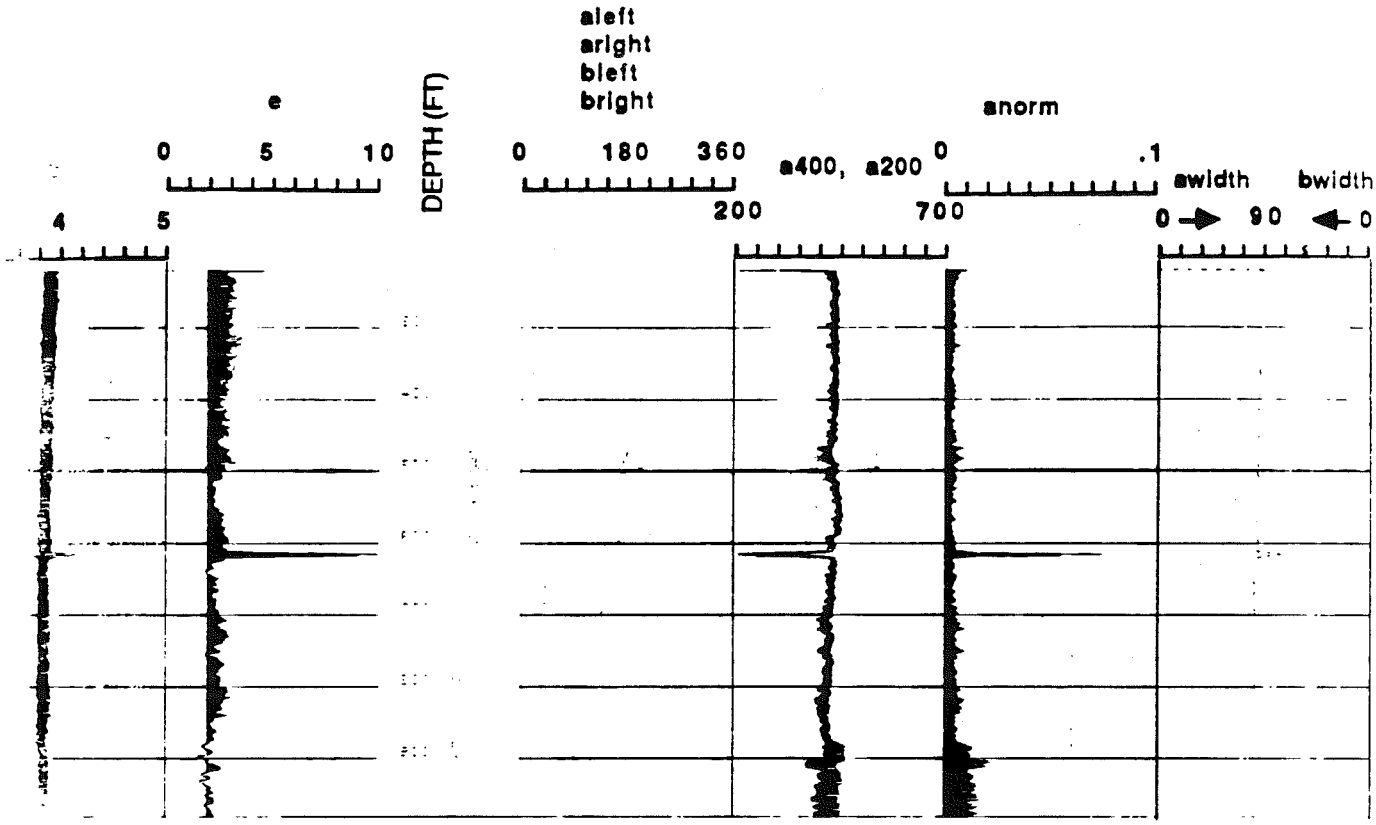

Figure 6: Borehole televiewer log curves across a large open fracture at 625 feet in the Moodus borehole. Shown are the major and minor radii in inches in Track 1, the eccentricity in percent (shaded above 2%) in Track 2, the right and left edges of picked breakouts in Track 3 (w.r.t. magnetic North), the average amplitudes of the 200 and 400 largest values for each scan line in Track 4, the normalized amplitude difference in Track 5, and the widths of the measured breakouts in degrees in Track 6. No breakouts were present in this interval, so the 3rd and 6th track are empty.Aside from the position of the fracture, eccentricity is quite low and the two amplitude averages are approximately equal.

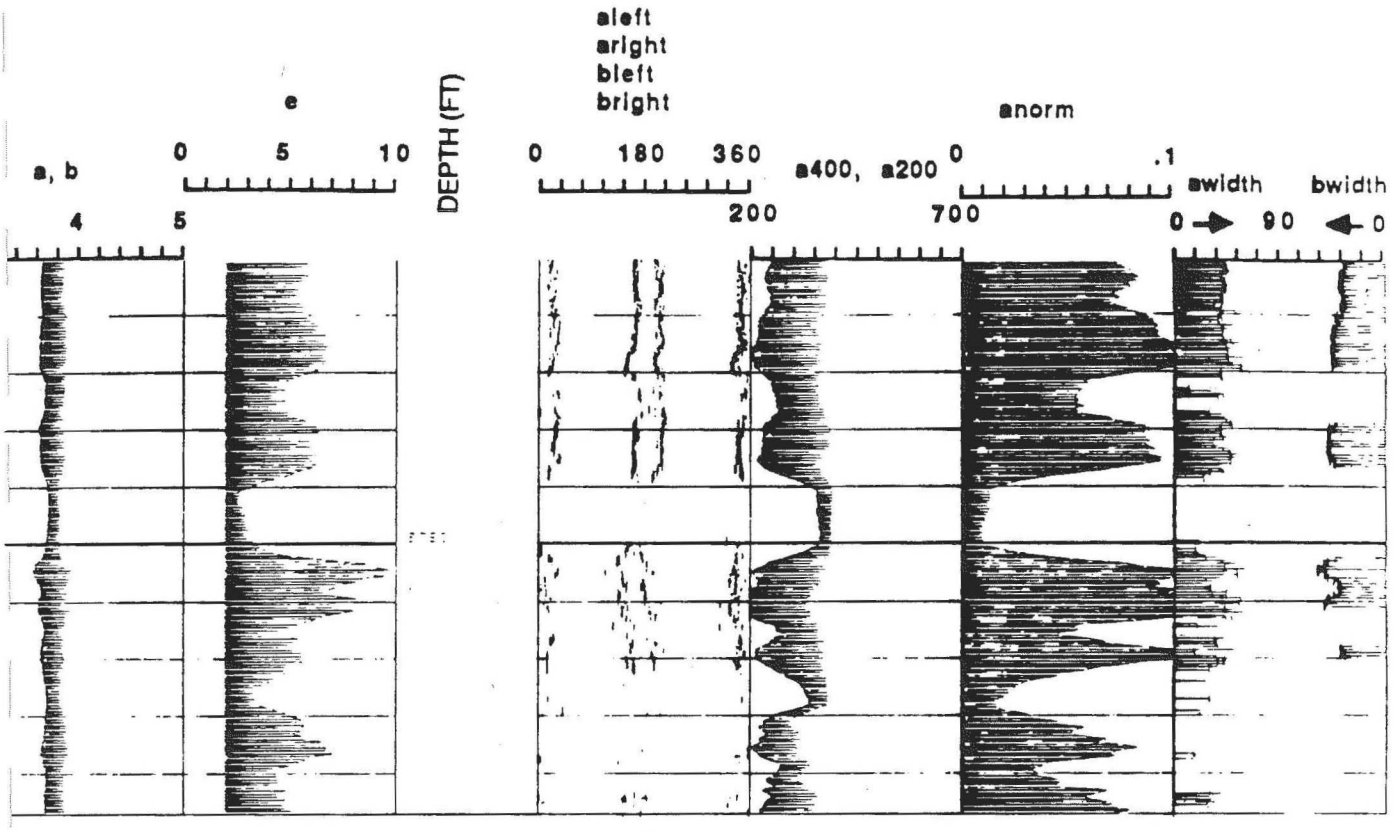

Figure 7: Borehole televiewer log curves across a zone of discontinuous breakouts (3700 - 3800 feet). Shown are the major and minor radii in inches in Track 1, the eccentricity in percent (shaded above 2%) in Track 2, the right and left edges of picked breakouts in Track 3 (w.r.t. magnetic North), the average amplitudes of the 200 and 400 largest values for each scan line in Track 4, the normalized amplitude difference in Track 5, and the widths of the measured breakouts in degrees in Track 6. Breakouts are revealed by increased eccentricity, and a large difference in the amplitude averages. The amplitude difference generally increases with breakout width.

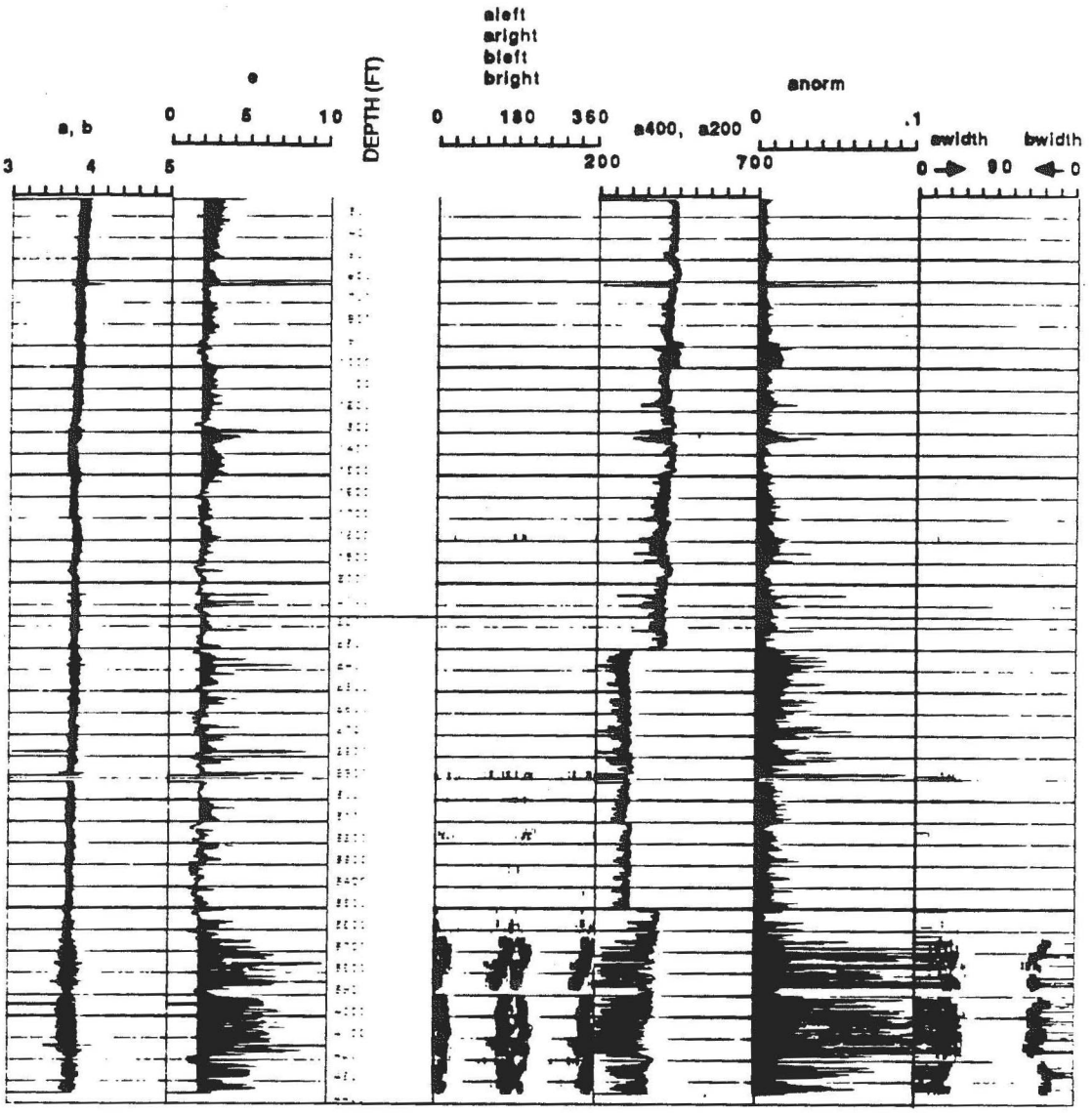

Figure 8: Summary borehole televiewer log curves for the entire Moodus well. Shown are the major and minor radii in inches in Track 1, the eccentricity in percent (shaded above 2%) in Track 2, the right and left edges of picked breakouts in Track 3 (w.r.t. magnetic North), the average amplitudes of the 200 and 400 largest values for each scan line in Track 4, the normalized amplitude difference in Track 5, and the widths of the measured breakouts in degrees in Track 6. Changes in televiewer gain can be seen clearly in the amplitude averages (e.g. at 3500, 2300, 1000, and 880 feet). Away from major fractures and breakout zones the eccentricity is generally less than 4% and the amplitude difference is quite small. Fractures and breakouts can typically be distinguished by the length of the affected interval.

sections of intact rock. The breakouts can be seen clearly in Track 3, spanning the intervals around magnetic N and S, over the depth intervals 3700-3739 and 3750-3773, and are less well developed in the remainder of the interval. Within the breakout intervals the a and b axis difference is larger (Track 1) leading to a pronounced increase in eccentricity (Track 2). The difference between the two amplitude measurements is much greater (Tracks 4 and 5). There appears to be a correlation between breakout width (Track 6) and the normalized amplitude difference (Track 5), particularly in the interval 3700 to 3720 feet, where both the width and the difference increase with depth.

Figure 8 shows the televiewer results for the entire well. The relationships illustrated in Figures 6 and 7 are clearly expressed here. Trends in the data with depth are also apparent. For example, hole size generally decreases with depth. The large change in average amplitude at 3500 and again at 2300 is due to changes in the recording parameters, as is the smaller change from 1000 to 880 feet. Otherwise, fractures and breakouts can be recognized by decreased average BHTV amplitude and increased measured eccentricity. Breakouts can be generally recognized by their continuity as illustrated in Figure 7 and by the tendency of the ellipticity to be more coherently oriented as illustrated in Figure 4.

Natural Fractures

Fracture analysis of the Moodus BHTV data was conducted interactively on the digitized images. Figure 9 shows a large fracture at 1937 feet, and a series of features truncated by this high-angle fracture, and therefore developed at a later time. Both travel-time and amplitude images are presented. A feature which could possibly be miss-identified as a breakout is seen to be due to spalling of the material between the borehole wall and a less well-developed second high-angle fracture just below the first. Variations in reflected amplitude, such as the high-amplitude band at 1940 feet, are due to changes in lithology.

Fracture orientation and apparent aperture were selected interactively, as illustrated in Figure 10. On the right is an image of the reflectivity of the wellbore over the interval 3525 to 3512 feet, including two well-developed low-angle fractures and a set of less clear co-planar features. Cross-sections across the uppermost fracture at 15 degree intervals along the wellbore are shown on the left. The minimum "width" of the fracture can be picked from the cross-sections, to allow for the geometrical effect of the fracture intersection with

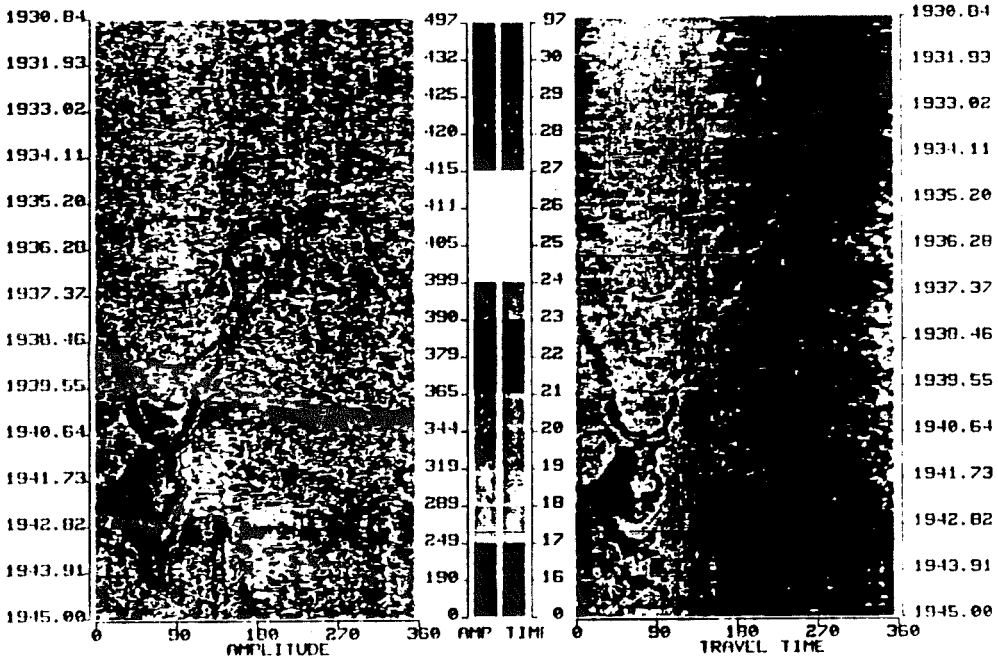

Figure 9: Travel-time and amplitude images of a high-angle fracture at about 1938 feet in the Moodus borehole. The images are oriented w.r.t. magnetic North. Variations in amplitude are due to fine scale changes in lithology.

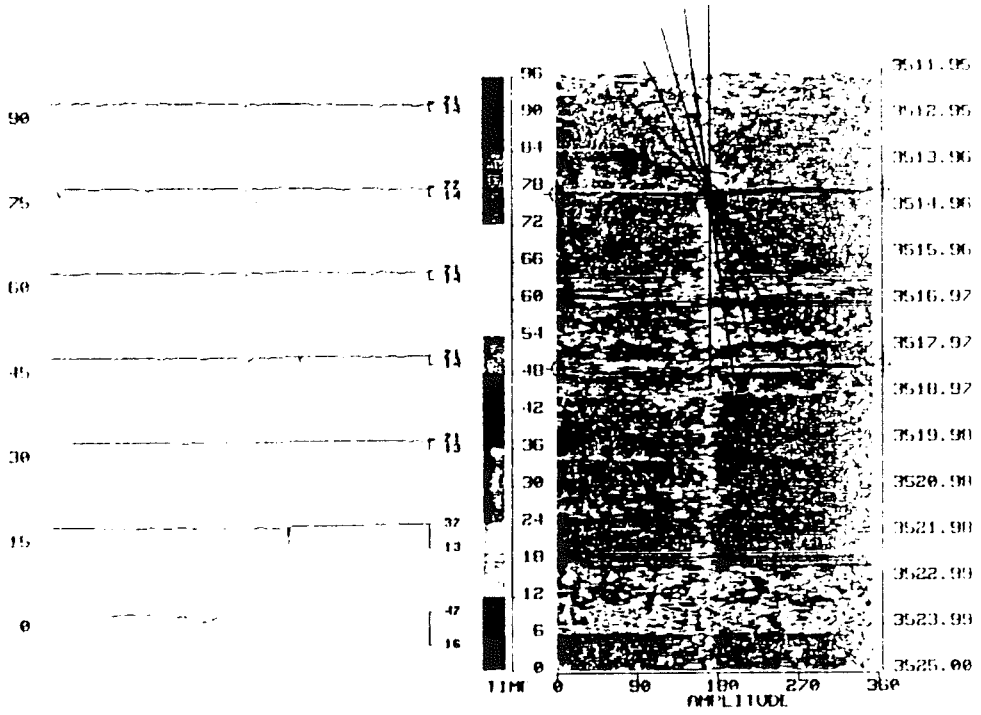

Figure 10: Illustration of interactive fracture analysis of one of a series of shallowly dipping fractures. The width of the fracture is the minimum value in cross-sections drawn along the borehole intersecting the fracture. Numerous features sub-parallel to the two finite-width fractures suggest that they are foliation-parallel features.

the hole. The presence of the finer features suggests that the fractures shown here occur along foliation planes, rather than having developed at high angles to the rock fabric.

Figures 11-13 present the results of the fracture analysis. Figure 11 shows fracturing and foliation as a function of depth in the well. Figure 11a presents a simple fracture count as a function of depth, whereas 11b is a plot of the apparent aperture of fractures in each 2-foot depth interval. The uniform density of fracturing throughout the logged interval illustrated by the fracture count is quite different from the more tightly clustered fracture apertures. This suggests that the majority of the fractures, for which no aperture could be calculated, are probably foliation planes. With a few notable exceptions these are apparently quite evenly distributed in the Moodus well. Comparison of the elastic properties as shown in Figures 15-17 and the fracturing confirms the hypothesis that the 0-aperture features are foliation, as the velocities and coherence are much more strongly affected by those fractures with measurable apertures (e.g. at 620 feet).

Figure 12 presents a series of lower hemisphere equal-area (Schmidt) stereographic projections of the poles to fracture planes over each lithologic section in the Moodus borehole. The predominance of low-angle features is evident in the figure. However, higher-angle features striking roughly NNE-SSW occur in the Canterbury Gneiss (b, 1900-2240 feet) and the Tatnic Hill Fm (c, 2240-2630) above the Honey Hill Fault and less clearly in the Waterford Group immediately below the fault. A cluster of high-angle (>60 degrees) NW-SE striking fractures occurs in the Hebron Gneiss (a). Figure 9 shows a series of sub-parallel fractures dipping steeply NE within the Canterbury Gneiss, possibly equivalent to a fault set recognized by Dixon and Lundgren (1968). Although this fracture set is not well expressed within the Canterbury Gneiss, a cluster of steeply NE-dipping fractures can be seen on the stereo-plot (Figure 12b) within the Hebron Gneiss. Interestingly, very few features strike EW.

The predominance of features with EW to ESE-trending dips suggests a fold set generated by compression oriented along the dip direction. These features may be the consequence of ESE-directed recumbant folding of earlier structures, as described by Dixon and Lundgren (1968). The cluster of fractures in the Waterford Group dipping 20-30 degrees E is perpendicular to present-day maximum horizontal compression. These fractures are optimally

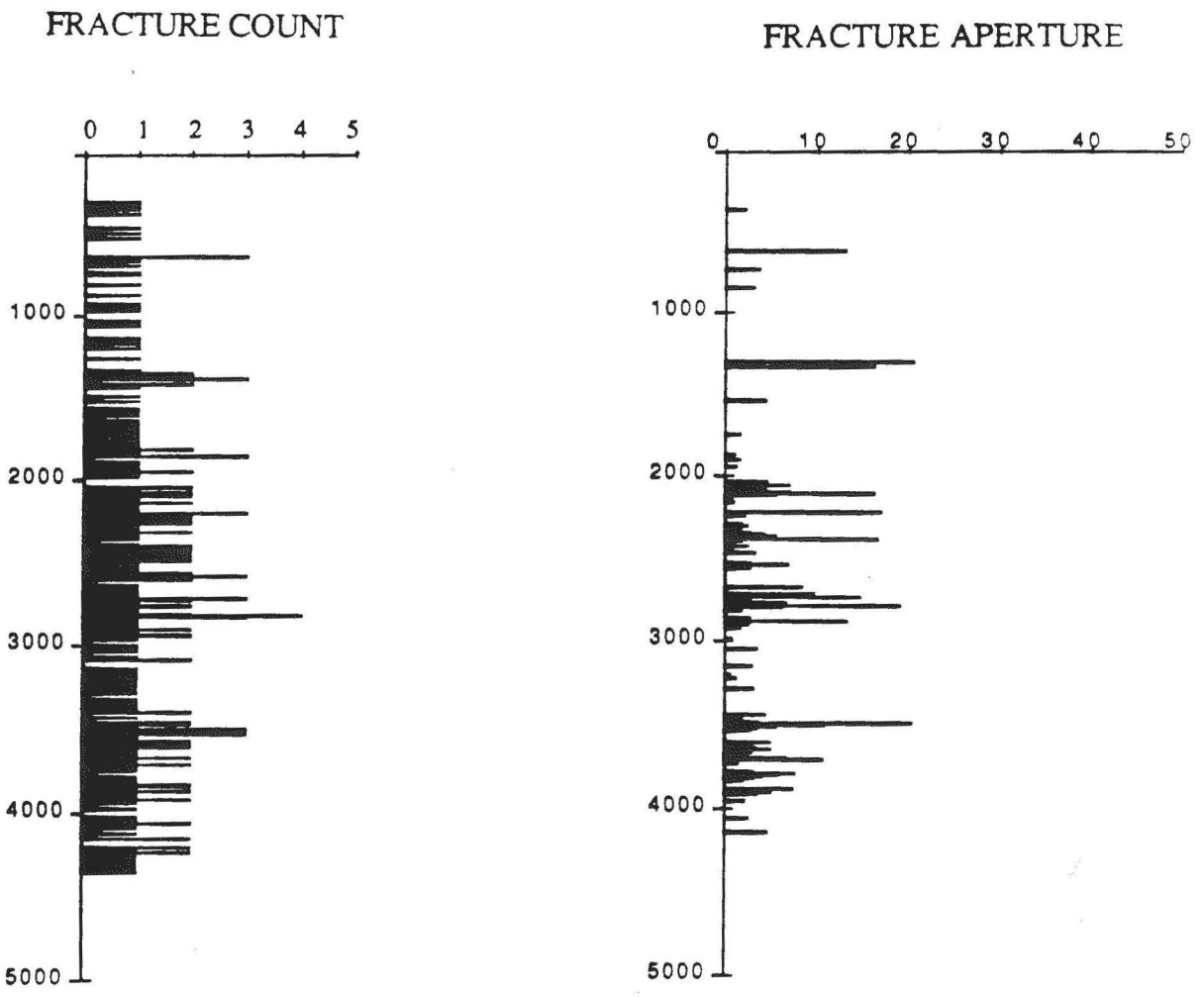

Figure 11: Fractures and foliation intersecting the Moodus borehole as a function of depth. (a) a simple count of fracture density. (b) Cumulative fracture aperture. Although the density of observed features is relatively constant, the apertures are clustered within narrower depth intervals. The features without a measurable width are foliation planes, distributed fairly uniformly within the well.

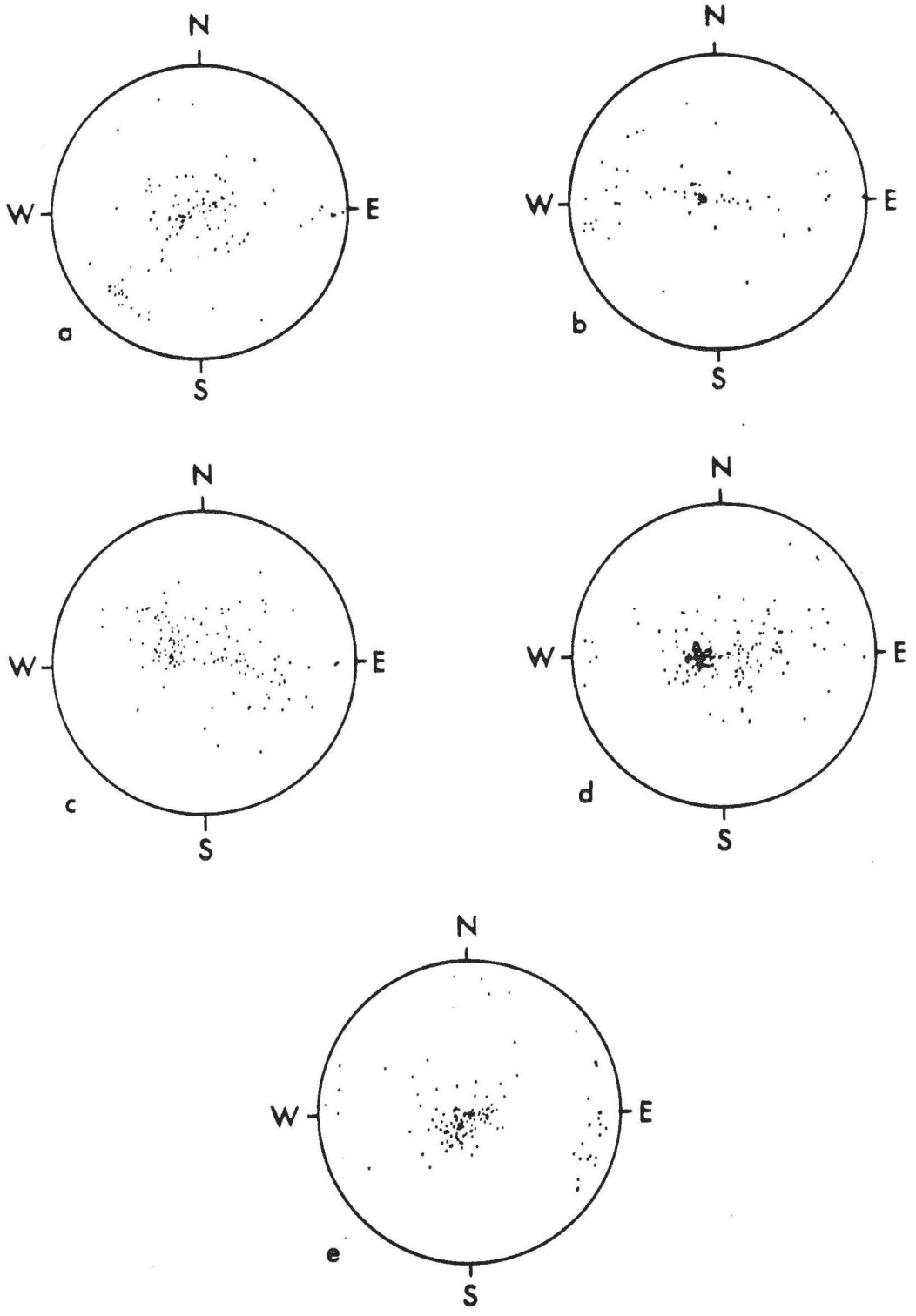

Figure 12: Fracture orientations as a function of rock type in the Moodus borehole. Shown are the poles to the fracture planes on a lower hemisphere equal area projection. The depth ranges correspond to (a) Hebron Gneiss, (b) Canterbury Gneiss, (c) Tatnic Formation, (d) Waterford Group, and (e) Lower Avalon. Fractures are not subdivided by aperture. From 1900 to 2630 feet the fracture poles describe a girdle running roughly EW, typical of structures formed by EW compression. The Waterford Group has a cluster of fractures dipping roughly 20-30 degrees E, aligned optimally for thrust motion in the current stress field. Within the Lower Avalon and the Hebron Gneiss (excluding a cluster of steeply NNE-dipping features) few high-angle features are observed, and orientations are more random.

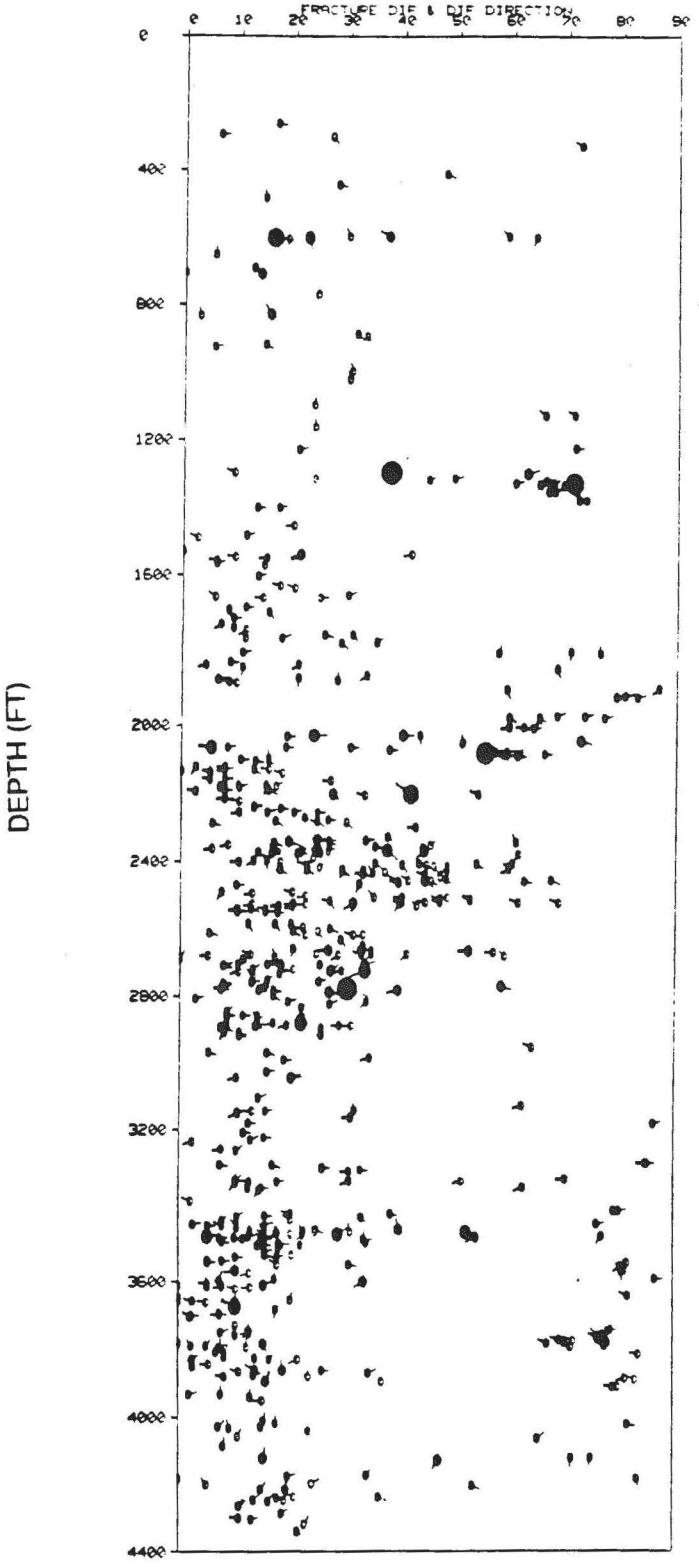

Figure 13: Fracture orientations as a function of depth in the Moodus borehole. Fractures with measurable apertures are shown as filled symbols whose size is proportional to the fracture width. Open circles are those fractures for which no width could be determined. The ordinate indicates fracture dip. The tail points in the downdip azimuth. This figure locates the fractures shown on the stereonet. For example, the steeply dipping features in the Hebron Gneiss are within the interval 1200 to 1400 feet.

oriented for movement in the current stress field, and may well be reactivated to account for much of the current seismicity.

Figure 13 illustrates fracture orientations as a function of depth using a tadpole plot, where dip angle is plotted along the horizontal axis and dip direction is the orientation of the "tail". The size of the "head" is proportional to the fracture aperture; those features with no measurable aperture are plotted with open circles. This figure locates the anomalous fracture orientation clusters as a function of depth. For example, the cluster of high-angle fractures in the Hebron Gneiss are all located within the interval from 1200 to 1400 feet, their pattern suggests drag on a roughly W-directed thrust fault at the base of the zone. Similar steeply E-dipping fractures are present at about 1900 to 2100 feet.

Although there is no systematic change in the distribution of dips as a function of depth, there does appear to be a bimodal distribution of dips, with large numbers of low-angle features and a smaller number of high-angle features, except within the interval 2000 to 3000 feet, where fracture dips of the low-angle set increase to 40 to 50 degrees. The low-angle features are probably foliation. The same relative proportion of high and low angle features have measurable apertures.

The E-dipping fracture cluster within the Waterford Group (Figure 12d) is located by this plot in the interval 3400 to 3600 feet. This is approximately the epicentral depth for many of the low-magnitude seismic events within the region. Thus we may have penetrated within this depth interval a series of active microfaults.

Sonic Velocity Logging

The multi-channel sonic log, run in the Moodus borehole from 4728 to 76 feet, recorded at 2-foot depth intervals in the well a set of 12 full waveforms from a single source multi-receiver logging tool. Figure 14 shows a schematic of the multi-channel sonic tool. A magnetostrictive source is mounted 6.25 feet above a group of 12 piezoelectric receivers spaced at 0.5 foot intervals. The receiver section therefore spans a 5.5 ft interval centered about 10 feet below the source. Also shown in Figure 14 are a set of waveforms recorded with the source at a common depth. The principal received phases are (1) a first-arriving P-wave refracted along the borehole wall, (2) a second-arriving S-wave refracted along the borehole wall which is followed by a ringing pseudo-Rayleigh phase, and (3) a low frequency Stoneley guided wave. Compressional and shear velocities are computed from the linear moveouts across the receiver array of the P and S waves. The Poisson's ratio can be computed from Vp/Vs, and the elastic moduli can be computed from the velocities if the density is known. The Stoneley guided wave velocity and amplitude provides information about fracturing and fracture permeability.

Results

Figure 15 shows the final results of the velocity analyses: compressional and shear velocity logs, semblance, and Vp/Vs, along with the results of fracture analysis of the BHTV data discussed above and a geologic column. The details of the waveform variations and the processing by a modified semblance technique are presented below. Fractures are separated into those with finite apparent apertures, and those without finite apparent apertures. Compressional velocities are about 5 km/s above the water table at about 420 feet; no coherent shear arrival is present within this interval. Below 420 feet compressional velocities within the Hebron Gneiss are approximately 5.5 km/s, increasing slightly with increasing depth; shear velocities are above 3.1 km/s. Vp/Vs decreases from 1.8 to 1.75 with increasing depth in this interval. The Canterbury Gneiss has high velocities (Vp 5.7-5.9 km/s; Vs 3.3-3.4 km/s) and constant Vp/Vs ~ 1.73. The gneisses and schists of the Tatnic Hill Formation directly above the Honey Hill Fault have lower and more variable compressional velocities, averaging about 5.5 km/s, and more variable Vp/Vs. The Waterford Group and the Lower Avalon have high compressional velocities

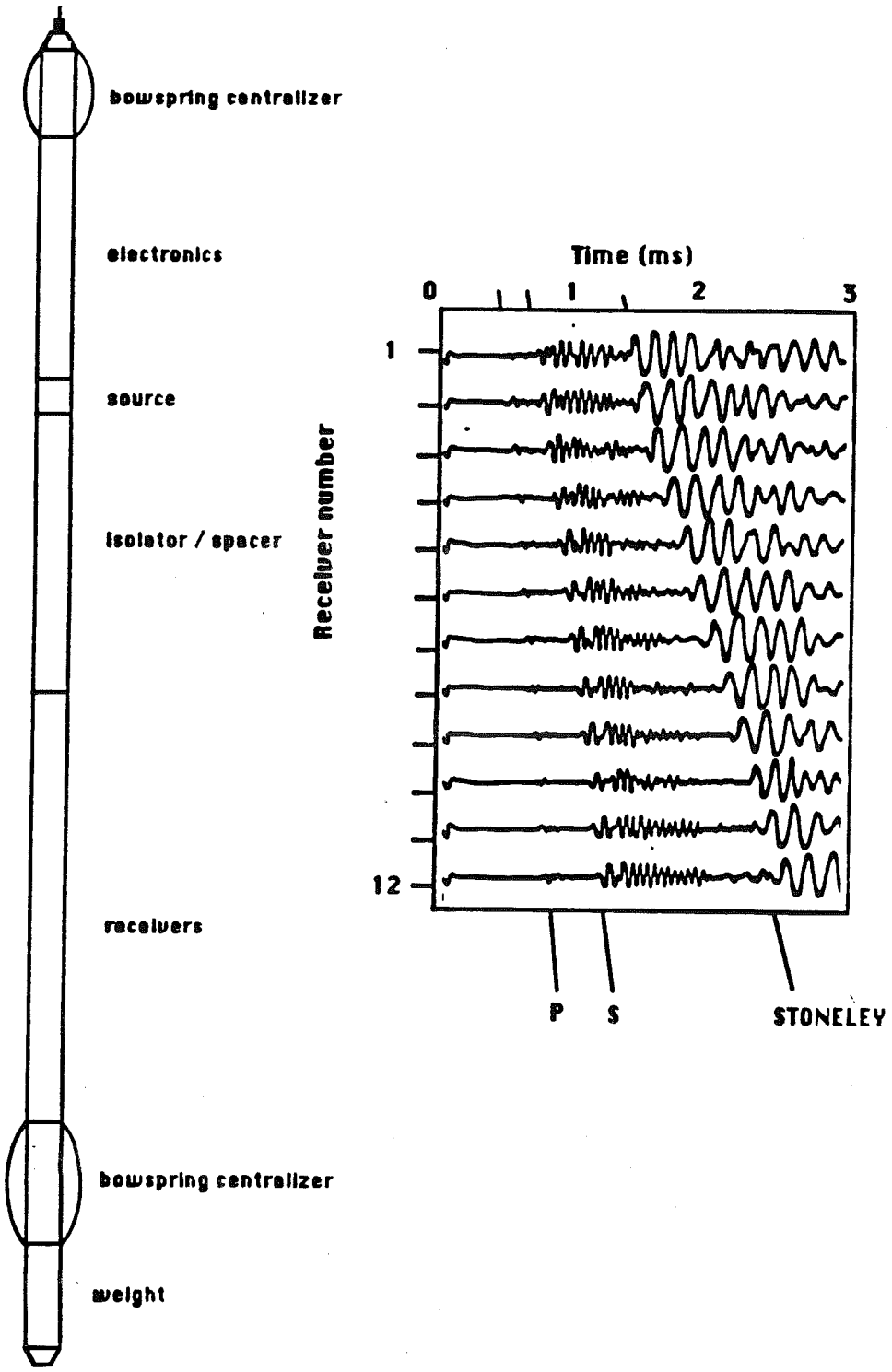

Figure 14: Schematic of the 12 receiver single source multi-channel sonic logging sonde, showing a typical set of waveforms recorded in crystalline rock. The first arrival P-wave is followed by a shear and ringing pseudo-Rayleigh wave packet. The low frequency high energy arrival following the shear is the Stoneley interface wave.

(5.9-6.0 km/s) and fairly constant Vp/Vs (~1.70 - 1.73). Shear velocities are above 3.4 km/s.

Both large aperture fractures and foliation affect the coherence and propagation velocities of the refracted waves. For example, two intervals within the Tatnic Hill Fm have low coherence and a high "fracture" density. Only the lower interval has increased Vp/Vs; this interval also contains measurably "open" fractures. The Honey Hill Fault itself is coincident with a low coherence zone at 2760 feet; although velocities are not strongly affected by the fault, the juxtaposition of the low-velocity Tatnic Hill Fm over the much higher velocity Waterford Group should generate seismic reflections there. The large fractures at 170, 620, and 2375 feet and the cluster of large aperture fractures at about 3495 feet reduce waveform coherence, although with the exception of the interval at 3495 feet the velocities are not strongly affected.

Waveforms and semblance processing

Figure 16 shows the sonic waveforms from the near-offset receiver (6.25 feet from the source) for the entire depth range of the experiment. The three wave modes (P, S, and Stoneley) can be seen clearly throughout most of the logged interval. Above the water table at 420 feet the shear arrival is not seen. This and other evidence suggests that an unsaturated alteration zone extends from ground surface to this depth. Narrow intervals of reduced coherence and amplitude are evidence of large fractures intersecting the well (for instance at 170, 620, 2375, and 2760 feet). At these depths all three wave modes are affected. Smaller fractures (for instance at 990 or 1170 feet, among others) affect only the refracted waves. Changes in the otherwise uniform character of the waveforms are due to changes in rock type. For instance, the very high amplitude section at about 890 feet has very high gamma activity and elevated gamma spectroscopy determined silicon (a pegmatite?). Waveform variations at other depths also correlate with lithologic changes. The intersection of the well with the Honey Hill Fault at about 2760 feet is coincident with a zone of low wave-mode amplitudes, as mentioned above.

The compressional and shear sonic wave velocities shown in Figure 15 are calculated from the 12 received waveforms by a modified semblance technique. Semblance for a given wave mode is defined as the energy-normalized maximum coherence, and is calculated as a function of velocity as the sum of the cross-correlations of the windowed waveforms divided by the sum of the autocorrelations within each window. The time delay to each

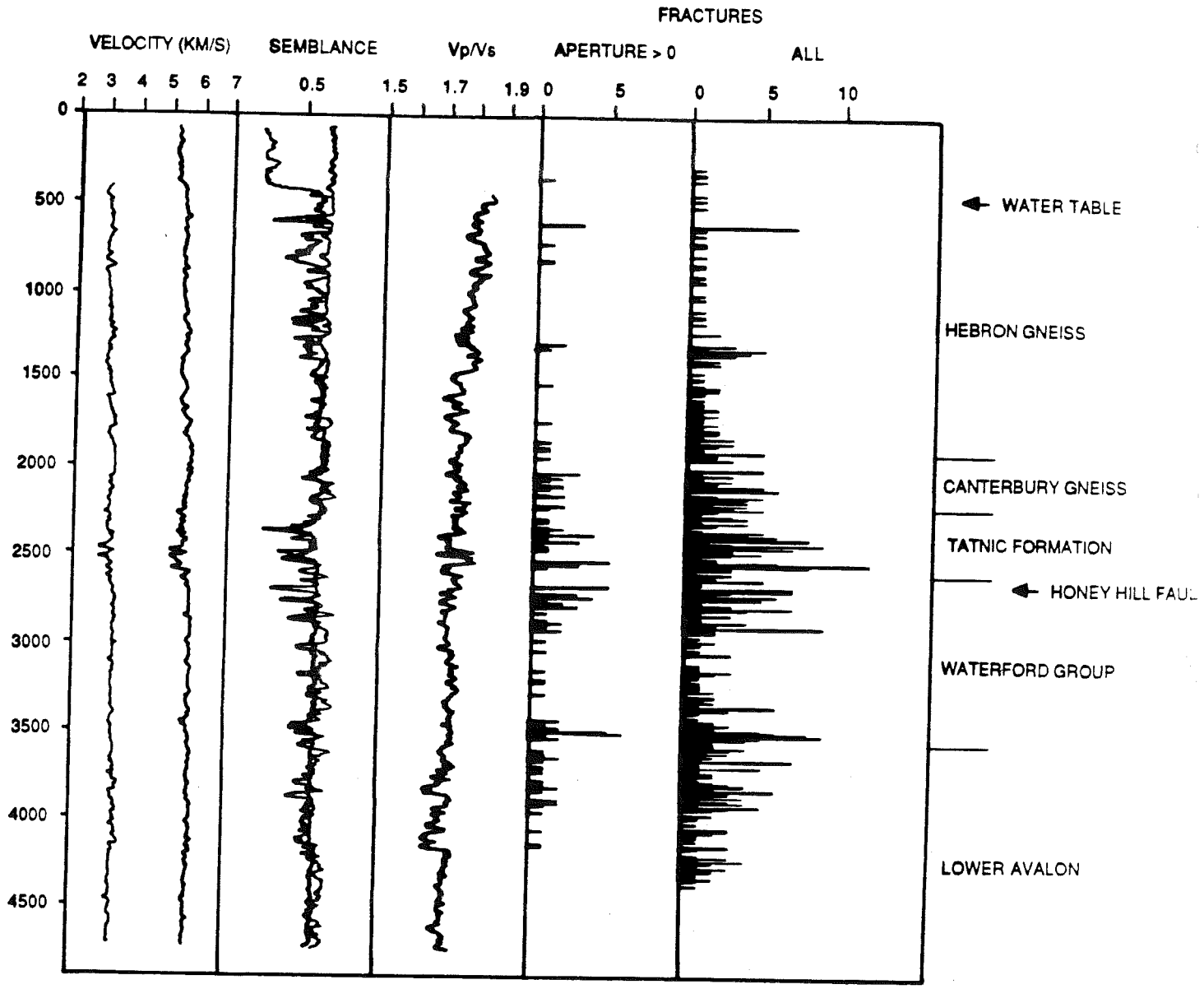

Figure 15: Compressional and shear velocities, the velocity ratio, and coherence as a function of depth computed from semblance calculations across the 5.5 foot receiver array, from 76 to 4728 feet, along with fracture density and aperture and a simplified geologic column. The inferred location of the Honey Hill Fault at about 2760 feet is indicated by the arrow.

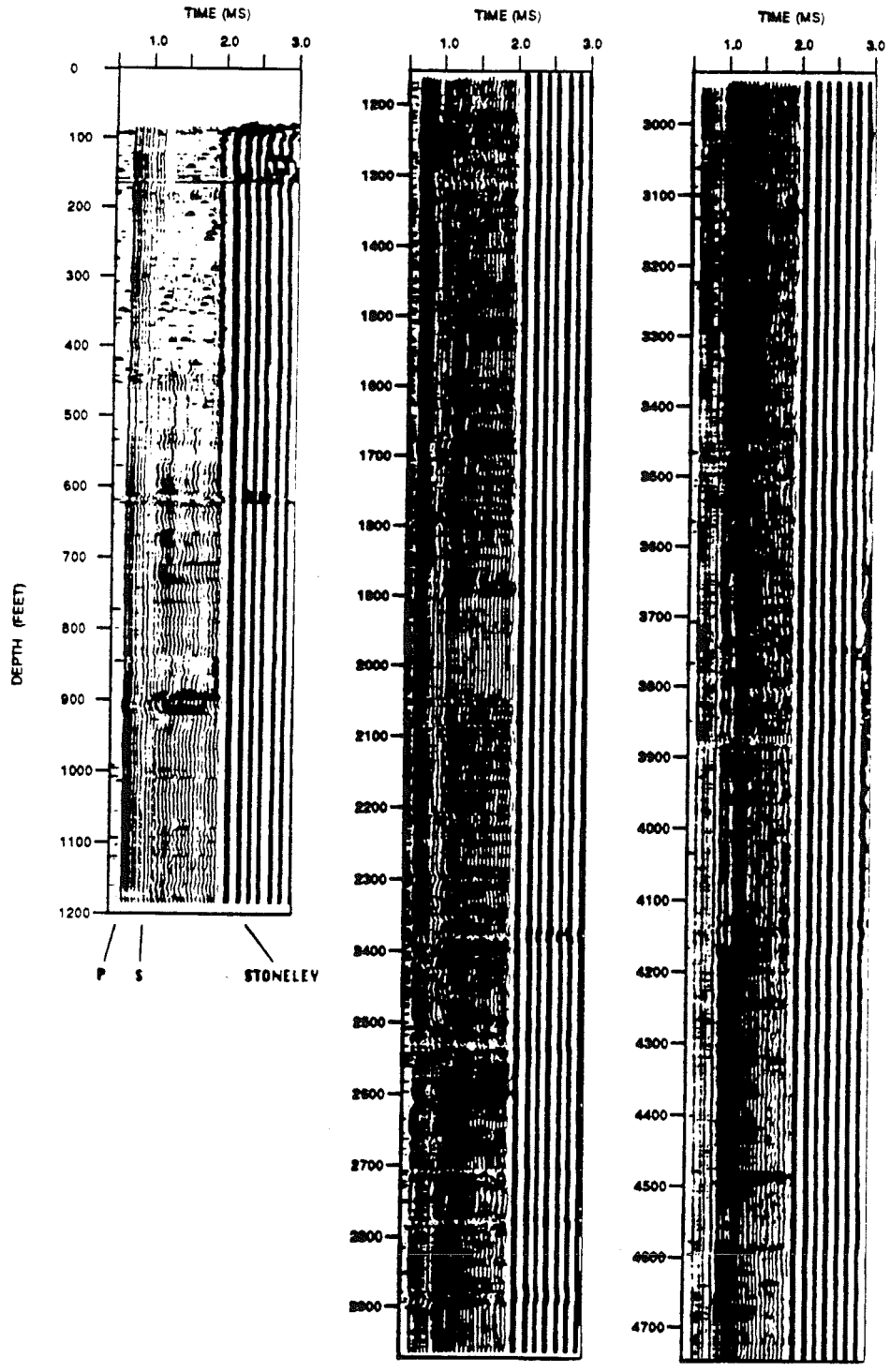

Figure 16: Waveforms recorded in the Moodus well, from an elevated water table at 78 feet to a depth of 4730 feet. Three milliseconds of data recorded by the first receiver at 2-foot intervals are shown. The three arrivals seen in Figure 1 are also evident in this display. Variations in arrival time are due to changes in elastic-wave velocity and hole size; variations in amplitude indicate regions where energy is lost due to fracturing, foliation, or intrinsic attenuation.

window is the product of the receiver offset from the source and the inverse velocity or slowness. The window length is selected so that several full cycles of data are included. The maximum semblance is obtained when the velocity used in the calculation is equal to the wave mode propagation velocity. Since the receiver section spans a 5.5-foot interval in the well, the velocity result will be approximately equal to the average velocity over that interval. If the velocity variations occur at a finer scale the coherence will be lower, and the result will be weighted by the length of each constant velocity section. Thus foliated intervals will have somewhat lower coherence, even though the calculated velocity may be identical to that in an unfoliated interval.

Figure 17 shows the results of the semblance calculation for the entire logged section. The magnitude of the semblance is plotted as a function of inverse velocity. Peaks in the semblance corresponding to the compressional and shear modes are shaded. Throughout most of the well the Stoneley wave propagates too slowly to be seen in this plot. Towards the bottom of the well, however, the Stoneley semblance peak can be seen at the extreme right-hand edge of the plot. Variations in amplitude and arrival time seen in the waveforms (Figure 16) are seen here as variations in coherence (semblance magnitude) and velocity. For example, as mentioned above, from the top of the log to 420 feet no coherent shear arrivals are observed. Fracture zones with low amplitudes also have low coherence, as seen at 620, 890,1160, and other depths. The approximate location of the Honey Hill Fault at 2760 corresponds to a zone of lower coherence, but the velocity is not strongly affected. The Honey Hill Fault is clearly not the most disrupted zone in the borehole. In general, shear coherence and velocity are more variable than compressional coherence and velocity. Changes in lithology (for instance, the degree of foliation) cause changes in the coherence.

Below 4190 feet shear and compressional coherence and velocity are quite uniform, excepting the location of a prominent fracture at 4470 feet. From 4190 to 3400 feet intervals of decreased coherence and variable velocity are interspersed with short sections with more uniform properties. From 3400 to about 2760-70 feet semblance is higher, although several thin intervals of low semblance occur (3310, 3200, 3120, 2980, 2870-90, 2825, and 2760-70). The latter is the expression of the Honey Hill fault. From 2760 to 2040 velocities are quite variable and semblance is lower, particularly for shear. From 2050 to

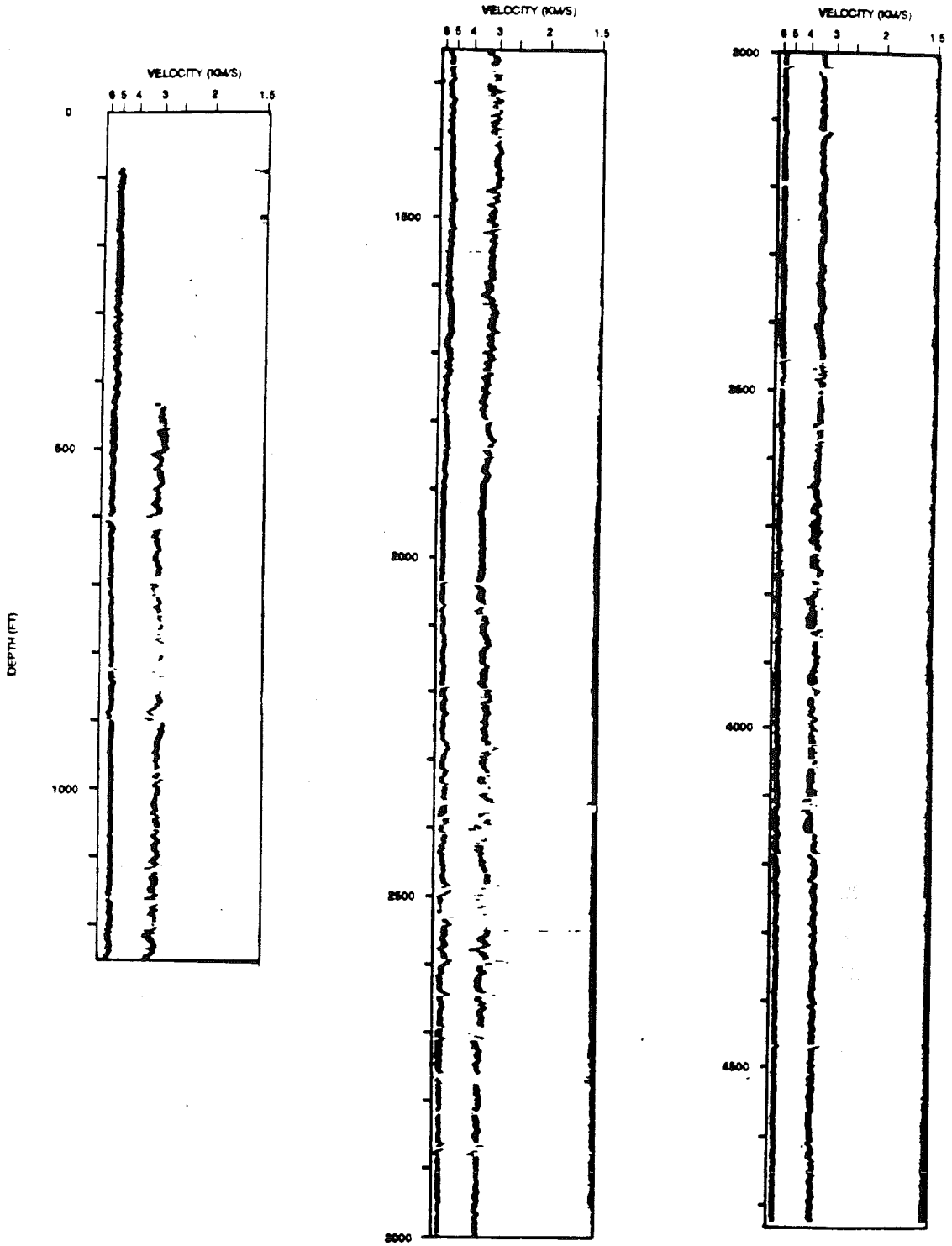

Figure 17: Semblance analysis of the multi-channel sonic data recorded within the Moodus well. The energy-normalized coherence of the arrivals travelling across the receiver array is displayed as a function of inverse velocity (slowness). The compressional arrival (about 5 to 6 km/s) and the shear arrival (about 2.5 to 3.5 km/s) exhibit high coherence and relatively constant velocity. The Stoneley arrival travels at more than 205 microseconds per foot, and is barely visible at the extreme right of the figure. The decrease in coherence of the direct arrivals within fracture zones is evident in this display (e.g. at 620 feet).

1880 a very coherent interval occurs; above this depth to 420 feet shear semblance is quite variable with numerous low coherence intervals.

Summary

Breakouts in the Moodus well yield a remarkably consistent N88.6E (+/- 5 degrees) azimuth for the maximum horizontal principal stress. The breakout direction rotates about 10 degrees counterclockwise within the interval from 3860 to 3750 feet but is consistent with the average direction above and below this interval.

Reduction of the BHTV data to logs provides a summary look at the data. The BHTV "log curves" indicate the presence of large fractures and breakouts, and can be presented in a consistent form for comparisons of the data between different depth intervals within this well, and in the future between this well and others.

More than 700 planar features were identified in the BHTV data. Most of these are foliation planes and have fairly shallow dips (less than 45 degrees). However, a significant number of high angle fractures intersect the well. Few of these strike EW. Numerous fractures intersecting the Moodus borehole above 3500 feet strike roughly NS, perpendicular to the maximum horizontal principal stress. As this is a reverse faulting stress regime, a significant number of these fractures may in fact be reverse faults: the fracture cluster at 3300-3600 feet is within the active seismic zone. Below 3600 feet the number of such fractures decreases.

Some features observed in the Moodus borehole can be related to past tectonic events. For example, the zone at 1290 to 1330 feet is characterized by consistently ENE dipping features whose dip increases with depth. This characteristic signature suggests drag on an ENE-dipping reverse fault. Thus these features are the downhole expression of the northwest-trending, steeply dipping faults within the hanging wall of the Honey Hill Fault observed by Dixon and Lundgren (1968).

Compressional and shear sonic velocities and wavemode coherence were calculated for the entire open hole interval. No refracted shear wave was recorded in the unsaturated zone above 420 feet; compressional velocity is about 5 km/s. Compressional velocities in the Hebron Gneiss are about 5.5 km/s, and increase slightly with depth. Vp/Vs decreases from 1.80 to 1.75 in this

interval. The Canterbury Gneiss has high velocities (Vp 5.7-5.9 km/s; Vs 3.3-3.4 km/s) and constant Vp/Vs ~ 1.73. The gneisses and schists of the Tatnic Hill Formation directly above the Honey Hill Fault have lower and more variable compressional velocities, averaging about 5.5 km/s, and more variable Vp/Vs. The Waterford Group and the Lower Avalon have high compressional velocities (5.9-6.0 km/s) and fairly constant Vp/Vs (~1.70 - 1.73). Shear velocities are above 3.4 km/s.

Variations in shear and compressional wave velocities and coherence are related to lithologic changes - generally, an increase in schistocity or foliation decreases the coherence and velocities. The velocity ratio generally decreases with depth within each lithologic unit, consistent with the effect of confining pressure on microcracks. This effect is more pronounced at shallow depths; below about 2630 feet the ratio is essentially constant. Large open fractures reduce the coherence presumably by scattering at the intersection of the fracture and the borehole wall. This effect on the Stoneley wave is one way to estimate the hydraulic conductivity of the fracture. By this method the fractures at 170, 620, 2375 and 2760 are hydraulically conductive, whereas the majority of the other fractures are not.

Section V. Interpretation of Local Stress Field

As illustrated in Section IV, the wellbore breakouts encountered in the lower part of the borehole show that the direction of maximum principal stress is N88.6°E. As mentioned in Section II, E-W compression is consistent with offshore wellbore breakouts in wells located several hundred km to the east of Moodus, but such a compressive stress direction denotes an apparent clockwise swing in the direction of maximum horizontal compression between this site and Kent Cliffs, approximately 100 km to the west. With the large scatter in P-axis orientation of earthquake focal mechanisms in New England, perhaps the discrepancy between Kent Cliffs and Moodus should not be surprising.

The primary purpose of this section of the report is to demonstrate that we have not only succeeded in characterizing the local stress field in the Moodus area, we have also measured directly the stress field associated with the shallow earthquake swarm that occurred within 1 km of the Moodus borehole shortly after the field measurements described in this report were completed. These focal mechanisms indicated reverse faulting on N-S striking planes and E-W compression (T. Statton, pers. comm.). As documented above, we have (1) unequivocally determined that the direction of maximum horizontal compresssion is essentially E-W, consistent with the focal mechanisms, (2) showed in Section III that the least principal stress is vertical, a requirement for reverse faulting (Anderson, 1951), and (3) in Section IV, demonstrated the existence of potential N-S striking, moderately-dipping fault planes.

With these three requirements satisfied, we can evaluate the magnitude of the maximum horizontal principal stress required to cause reverse faulting along favourably oriented fault planes from a simple two-dimensional Coulomb friction model. The critical stress ratio is then given by Jaeger and Cook, (1969):

$$(S_H - P_0)/(S_V - P_0) = ((\mu^2+1)^{1/2} + \mu)^2$$

where P_o is the pore pressure and μ the friction coeficient. S_v corresponds to the overburdon stress. Interpretation of friction measurements by Byerlee (1978) suggests that friction coefficients in rocks may vary between 0.6 and 1.0 depending on the rock type and the magnitude of normal stress across the friction plane. Comparing the stress magintudes measured in the Moodus well with the critical limits for the maximum horizontal compression S_H (Fig. 1) demonstrates that the stress magnitude at all measured depths in the Moodus borehole indicate that favorably-oriented fault planes have sufficient shear stress to cause reverse faulting. Thus, there is remarkable agreement between the nature of the near-by seismicity that occurred at shallow depth and the measured stress field in the Moodus borehole.

As the depth of the seismicity was limited to depths comparable to that of the borehole (T. Statton, pers. comm.) it is important to address the question whether such seismicity is potentially related to the occurrence of deeper earthquakes. While it is possible that the absence of favorably-oriented planes in the lower part of the well (Fig. 12, Section IV) is related to the lack of seismicity at greater depth, it is perhaps more important that at numerous sites around the world shallow seismicity similar to that at Moodus occurs that is totally unrelated to the potential for deeper seismicity. These cases include the deep mines of South Africa where a reverse faulting stress regime such as that at Moodus is observed to a depth slightly less than 1 km, but an normal stress field is observed at greater depth (Brace and Kohlstedt, 1980). In other words, while S_H is much greater than S_v at shallow depth, it is actually less than S_v at greater depths. A very similar case (reverse faulting at shallow depth and normal faulting at greater depth) has been documented at Oroville, CA (Anderson and Zoback, 1988). The state of stress in Fennoscandia (Stephansson et al., 1986) on the Canadian shield (Brace and Kohlstedt, 1980) and near Monticello Reservoir in South Carolina (Zoback and Hickman, 1982) all show very high horizontal stresses in the upper ~1 km that does not extend to greater depths.

From the available data it cannot be said with certainty that Moodus is such a case, but the shallow nature of the recent seismicity (as well as that previously reported

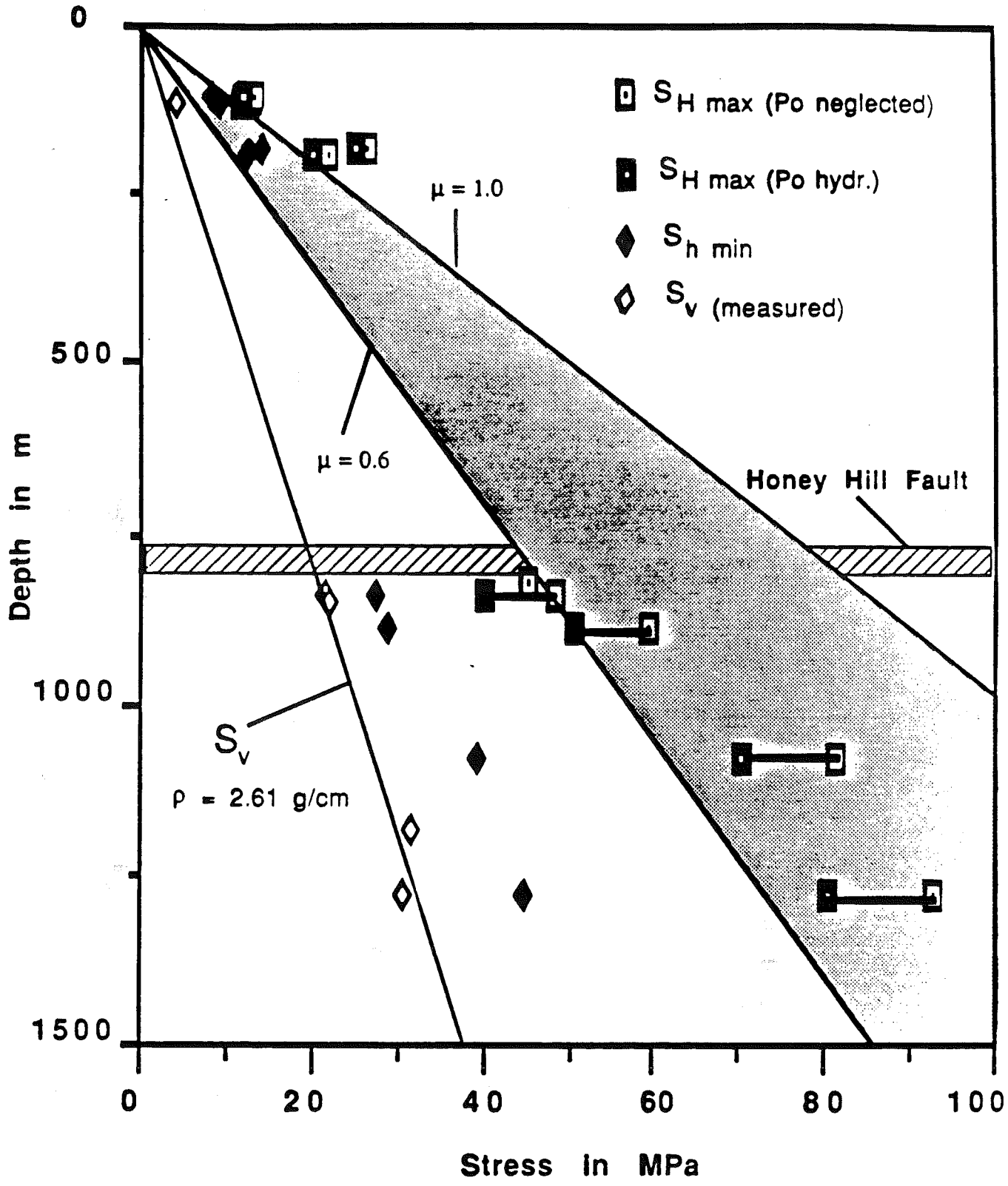

Figure 1. Principal horizontal stresses S_H and S_h as a function of depth in the Moodus deep borehole. The thick solid line indicates the overburden stress S_v (ρ = 2.61 g/cm^3). P_o is the pore pressure. The shaded zone represents the range of calculated critical values of the maximum horizontal stress S_H (friction coefficients μ = 0.6-1.0), i.e. the region in which the magnitude of S_H would be sufficiently high to activate thrust faulting on favourably oriented fault planes.

by Ebel et al., 1982) and the historic record indicating that many of the earthquakes in this region have been heard, all suggest that Moodus may indeed be an area where only shallow, small-magnitude seismicity occurs, similar to the other areas mentioned above. Careful monitoring of future earthquake hypocentral depths is critical to testing this hypothesis.

Of available hypotheses to explain magnified shallow stresses, the denudation model of Voight and St. Pierre (1974) seems most capable explaining why shallow horizontal principal stresses may be locally magnified with respect to the vertical stress. A common feature of all of the areas of "shallow-only" seismicity cited above is that they are areas where hard, crystalline rock is exposed at the surface. As the denudation effect is a function of the rocks elastic properties, this would seem to be consistent with the Voight and St. Pierre hypothesis. In fact, of the 10 boreholes in which we have measured stress in eastern North America (2 holes at Monticello, 2 near Charleston, 3 in northwestern South Carolina, Auburn, Kent Cliffs, and Moodus), the only holes in which a state of stress dissimilar to that at Moodus has been observed are those in which sedimentary rocks are present (Auburn and Charleston). Thus, the high horizontal stresses at shallow depth in these areas may largely depend on the ability of the near-surface rocks to magnify the magnitude of the tectonic stresses.

Section VI. Hydraulic Fracturing Pressure-Time Data

In this section we present each of the hydraulic fracturing pressure and flow records obtained in the field. Each record represents pressure (in bars) and flow rate (in gpm) plotted as function of time (in minutes). Flow-back after an injection cycle is represented as negative flow rate in the upper part of the plots. The pressure was recorded on the surface with a highly accurate digital pressure transducer manufactured by Seling, Inc. and recorded on the MASSCOMP in the hydrofrac/logging truck at a rate of 5 samples/sec. To compute the downhole pressure, one must add the weight of water in the borehole (see Table I, Section III). The depth, date and time of each measurement is also indicated on each plot.

For reference, the pressure equivalent to the vertical stress is shown on each record as a horizontal dashed line using a theoretical lithostat corresponding to density of 2.61 g/cm^3. In other words, as discussed in Section III, the proximity of the pumping or shut-in pressure to this line was evidence of a near-horizontal fracture.

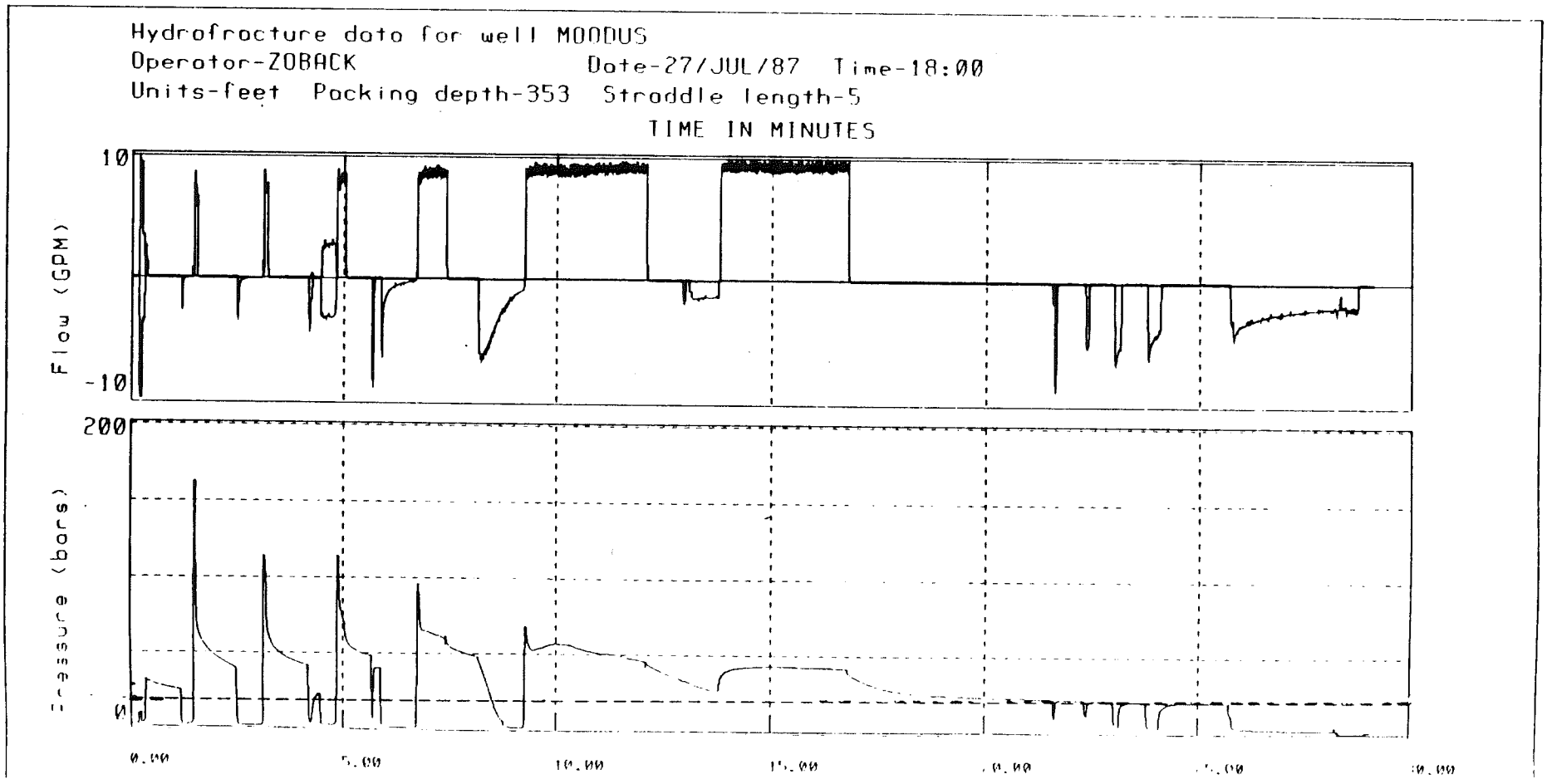
Hydrofracture data for well MODDUS
Operator-ZOBACK
Date-27/JUL/87 Time-18:00
Units-feet Packing depth-353 Straddle length-5
TIME IN MINUTES
10
-10
Flow (GPM)
200
0
Pressure (bars)
0.00
5.00
10.00
15.00
20.00
25.00
30.00

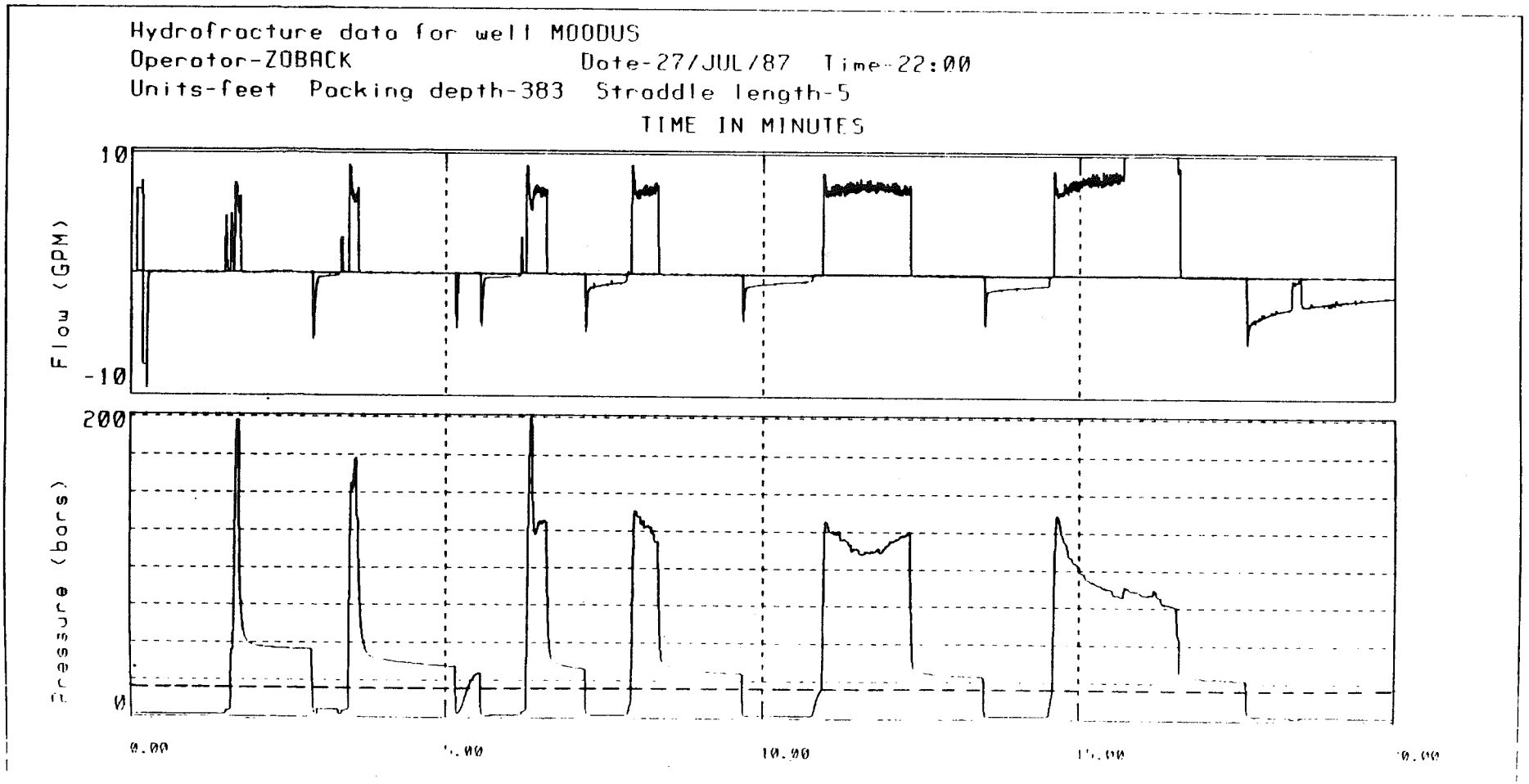
Hydrofracture data for well MOODUS
Operator-ZOBACK
Date-27/JUL/87 Time-22:00
Units-feet Packing depth-383 Straddle length-5
TIME IN MINUTES
10
-10
Flow (GPM)
200
0
Pressure (bars)
0.00
10.00
20.00

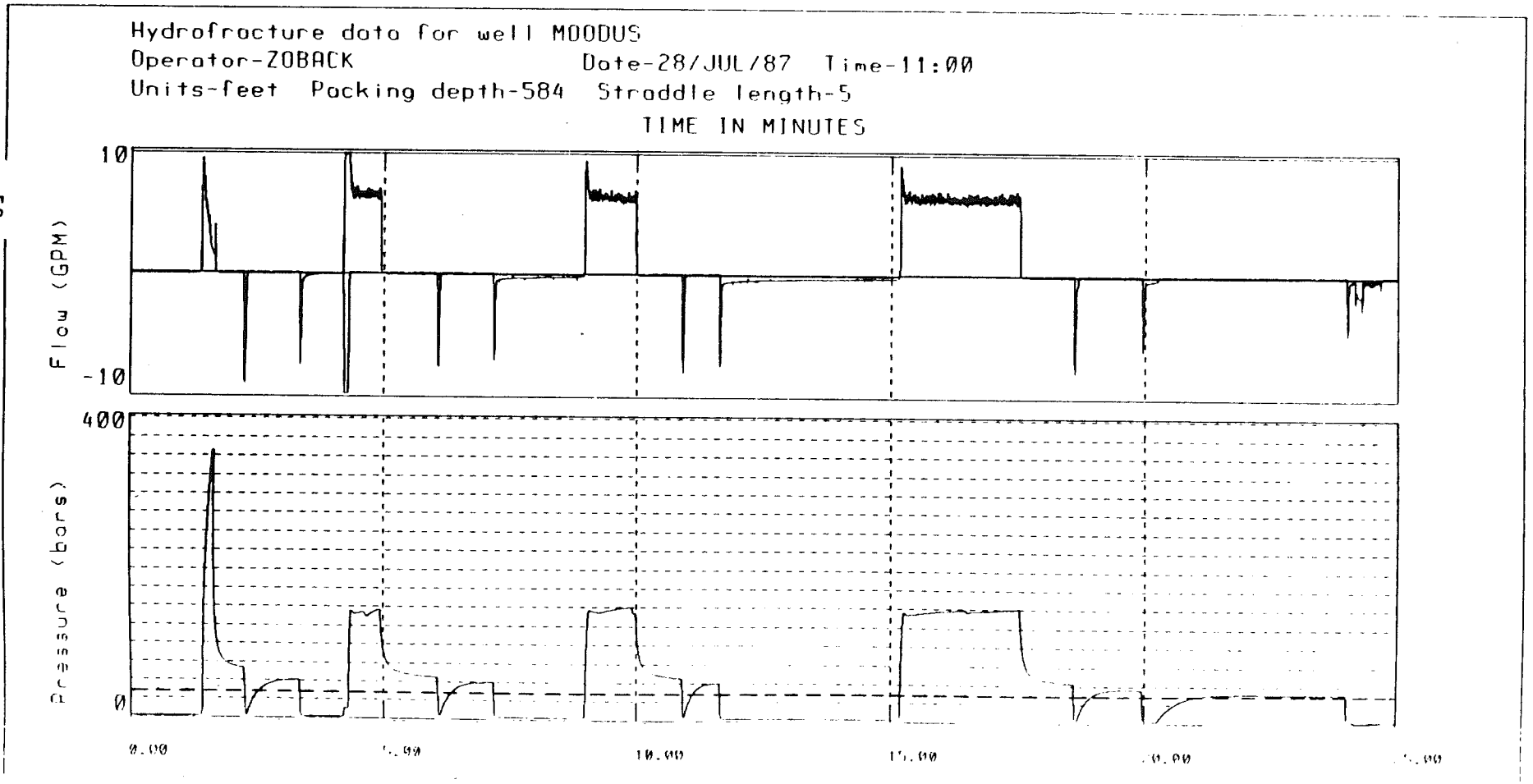
Hydrofracture data for well MOODUS
Operator-ZOBACK
Date-28/JUL/87 Time-11:00
Units-feet Packing depth-584 Straddle length-5
TIME IN MINUTES
10
-10
Flow (GPM)
400
0
Pressure (bars)
0.00
10.00

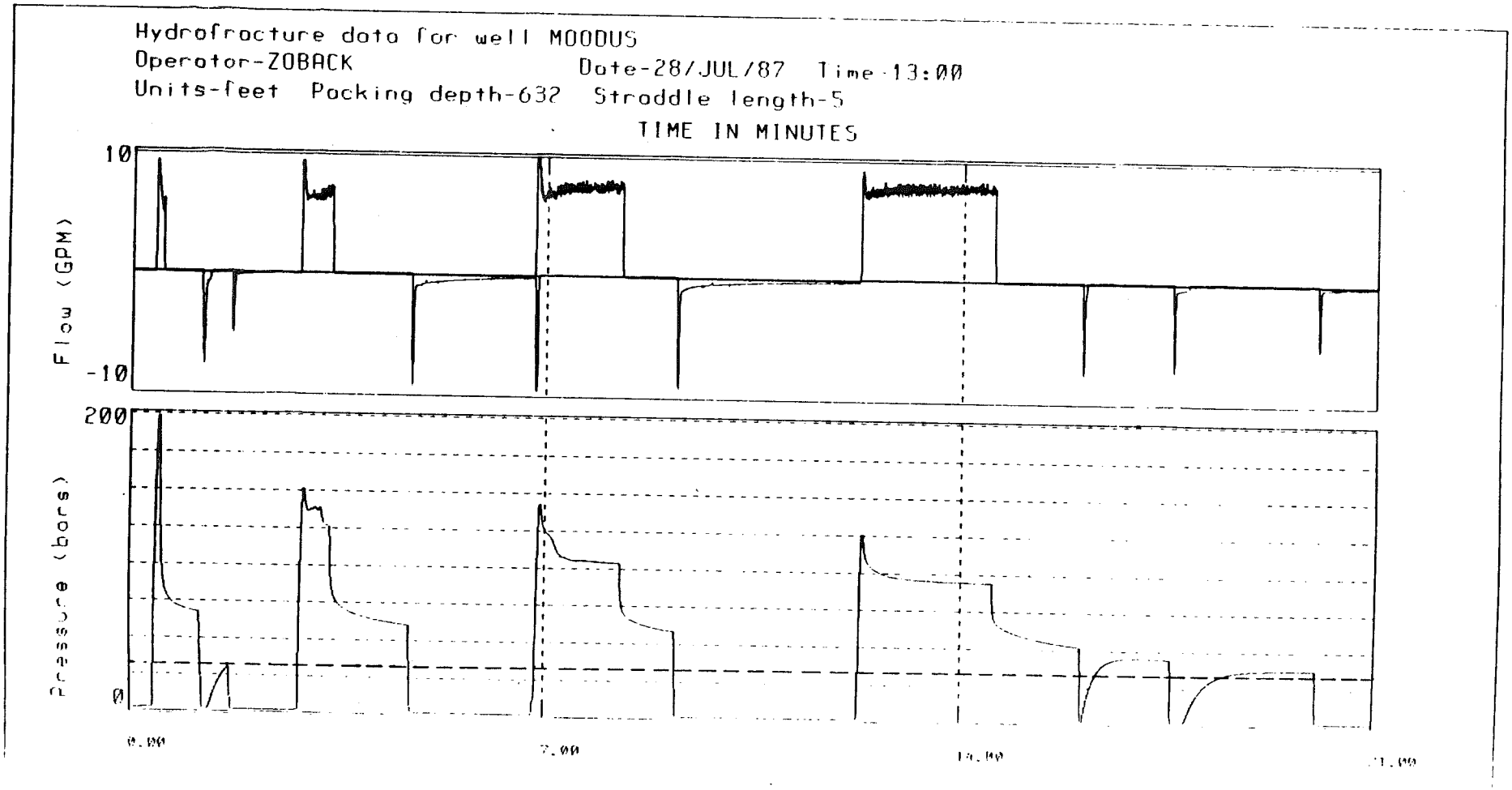
Hydrofracture data for well MOODUS
Operator-ZOBACK
Date-28/JUL/87 Time-13:00
Units-feet Packing depth-632 Straddle length-5
TIME IN MINUTES
10
-10
Flow (GPM)
200
0
Pressure (bars)
0.00
7.00
14.00
21.00

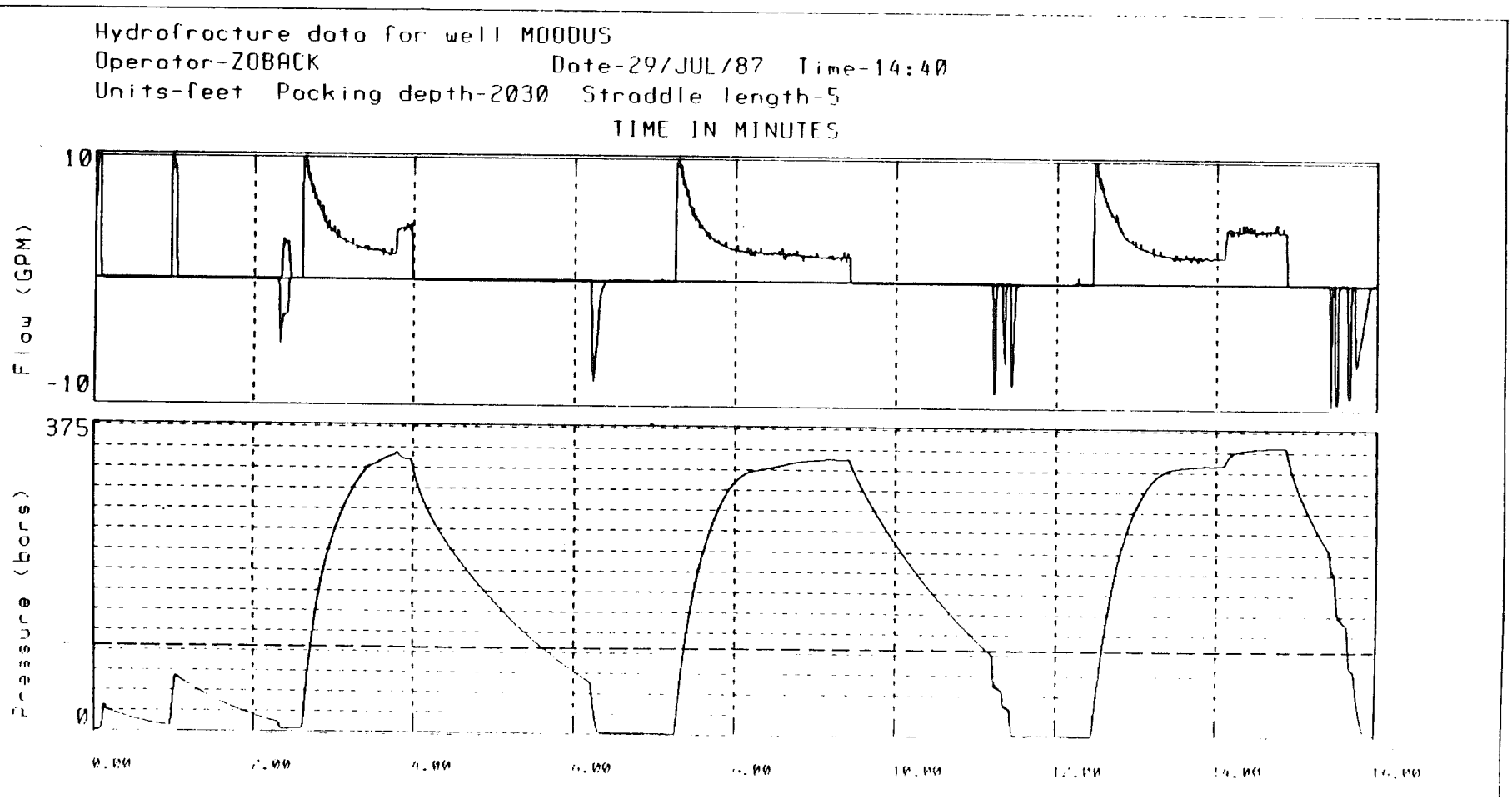
Hydrofracture data for well MOODUS
Operator-ZOBACK
Date-29/JUL/87 Time-14:40
Units-feet Packing depth-2030 Straddle length-5
TIME IN MINUTES
10
-10
Flow (GPM)
375
0
Pressure (bars)

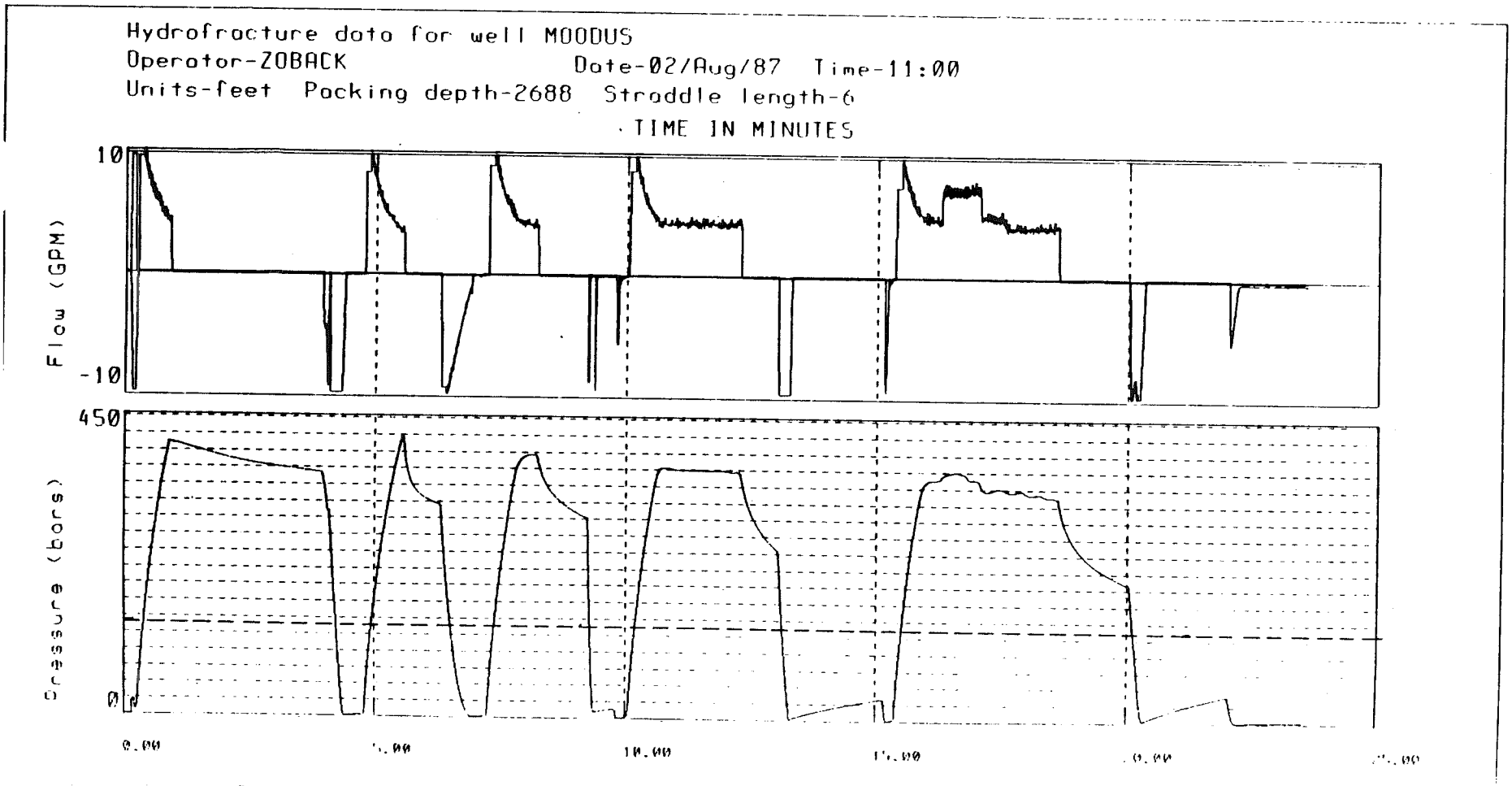
Hydrofracture data for well MOODUS
Operator-ZOBACK
Date-02/Aug/87 Time-11:00
Units-feet Packing depth-2688 Straddle length-6
TIME IN MINUTES
10
-10
Flow (GPM)
450
0
Pressure (bars)

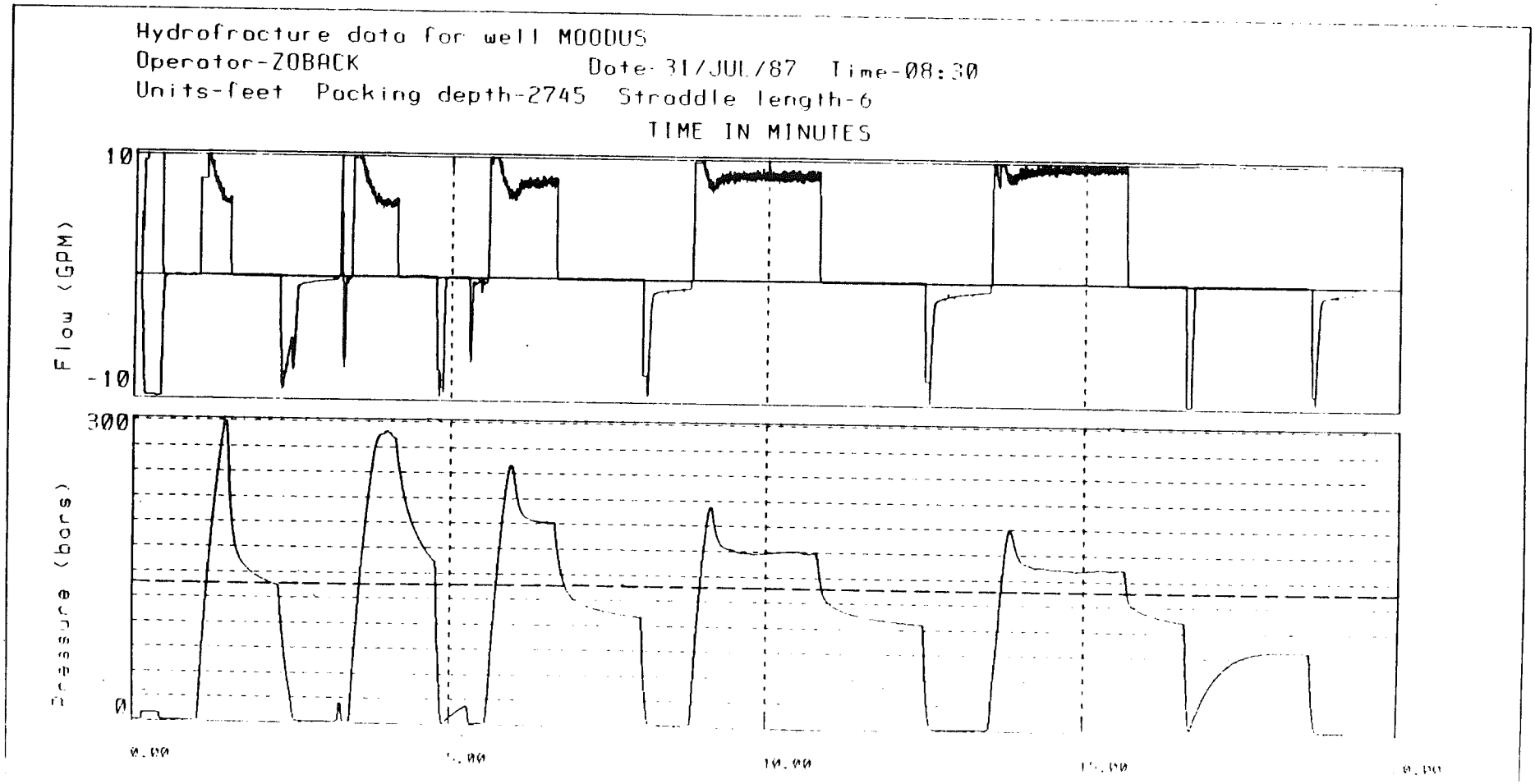
Hydrofracture data for well MOODUS
Operator-ZOBACK
Date-31/JUL/87 Time-08:30
Units-feet Packing depth-2745 Straddle length-6
TIME IN MINUTES
10
-10
Flow (GPM)
300
0
Pressure (bars)

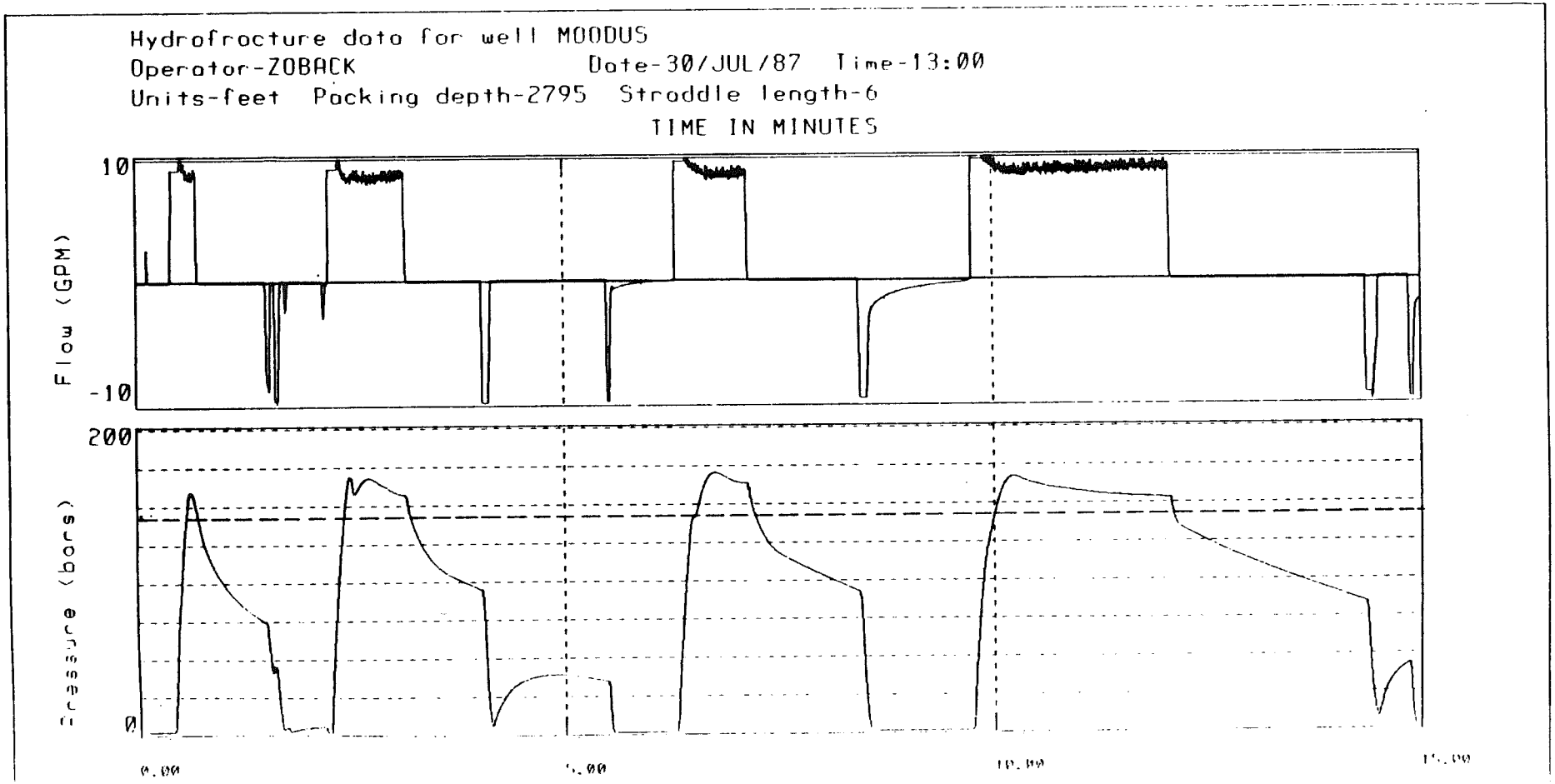
Hydrofracture data for well MOODUS
Operator-ZOBACK
Date-30/JUL/87 Time-13:00
Units-feet Packing depth-2795 Straddle length-6
TIME IN MINUTES
10
-10
Flow (GPM)
200
0
Pressure (bars)
0.00
5.00
10.00
15.00

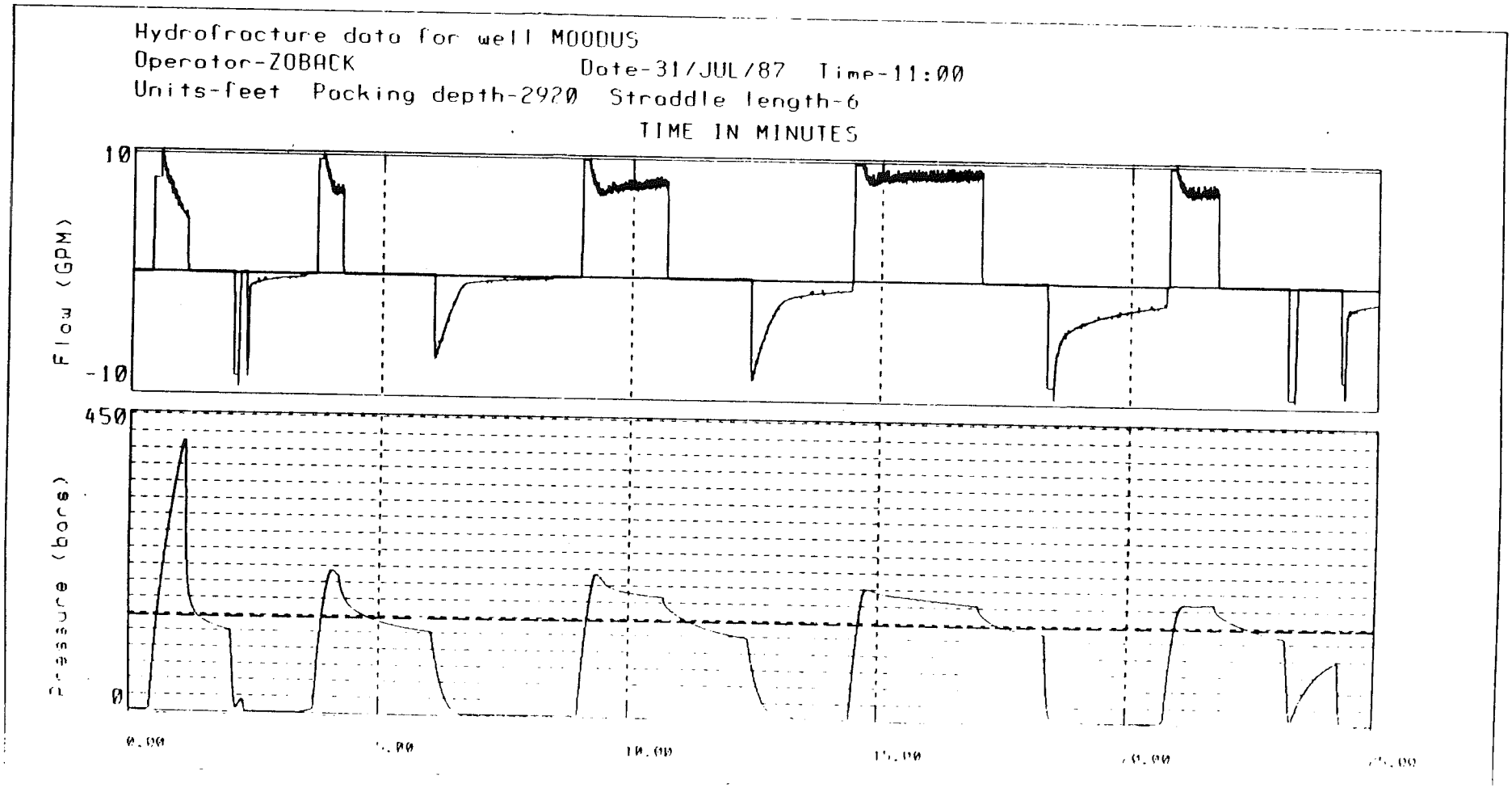
Hydrofracture data for well MOODUS
Operator-ZOBACK
Date-31/JUL/87 Time-11:00
Units-feet Packing depth-2920 Straddle length-6
TIME IN MINUTES
10
-10
Flow (GPM)
450
0
Pressure (bars)
0.00
10.00

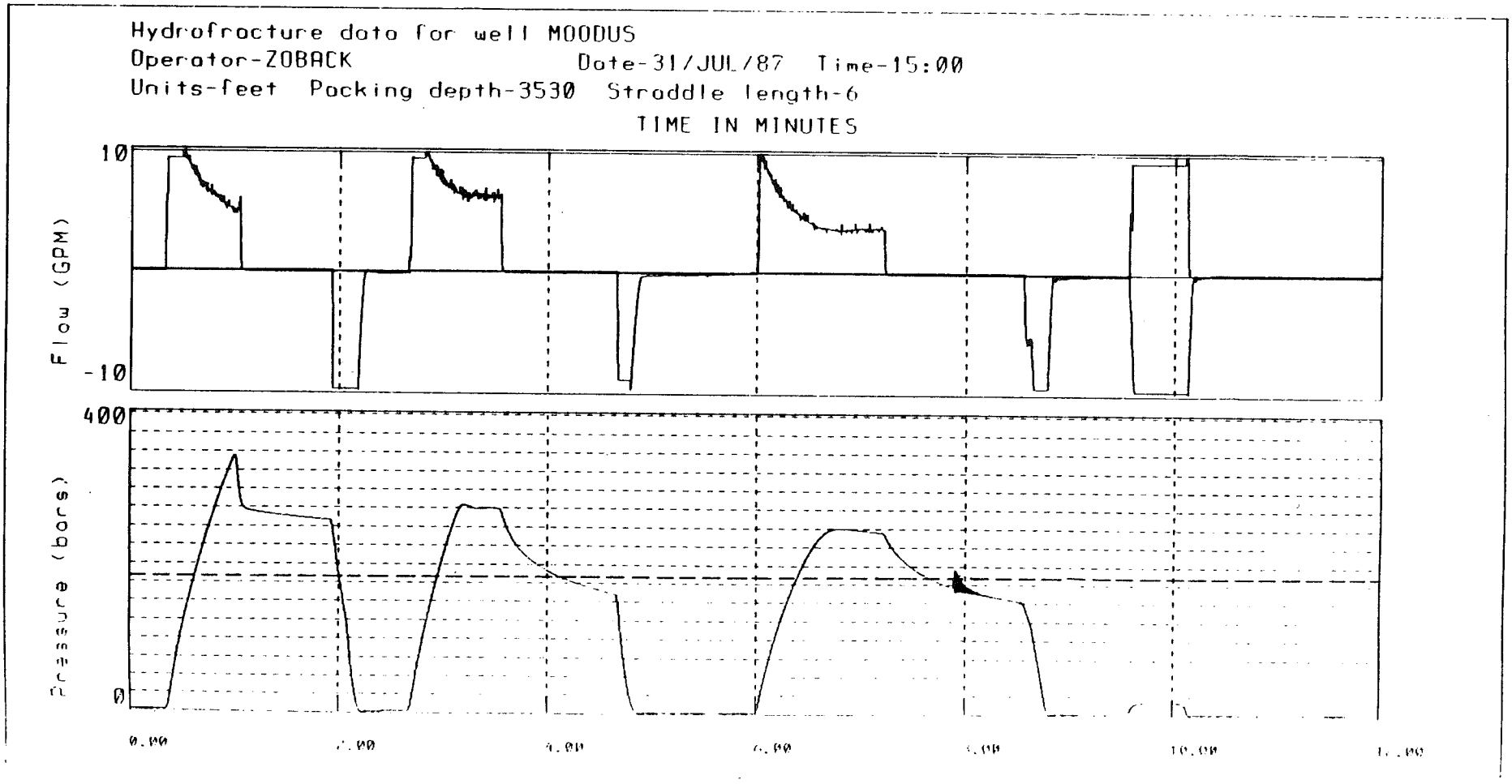
Hydrofracture data for well MOODUS
Operator-ZOBACK
Date-31/JUL/87 Time-15:00
Units-feet Packing depth-3530 Straddle length-6
TIME IN MINUTES
10
-10
Flow (GPM)
400
0
Pressure (bars)
0.00
2.00
4.00
6.00
8.00
10.00

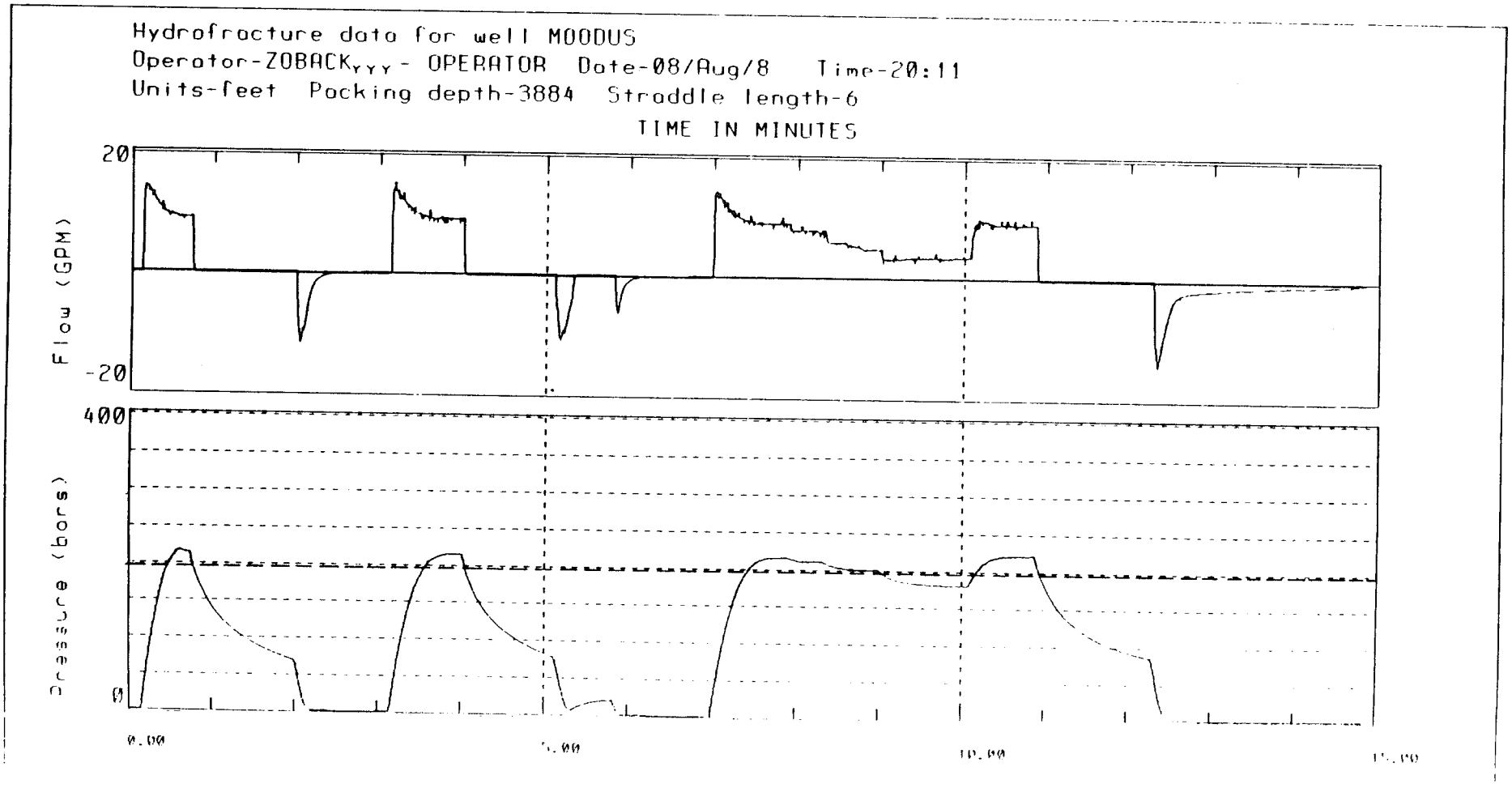
Hydrofracture data for well MOODUS
Operator-ZOBACK$_{YYY}$ - OPERATOR Date-08/Aug/8 Time-20:11
Units-feet Packing depth-3884 Straddle length-6
TIME IN MINUTES
20
-20
Flow (GPM)
400
0
Pressure (bars)
0.00
5.00
10.00
15.00

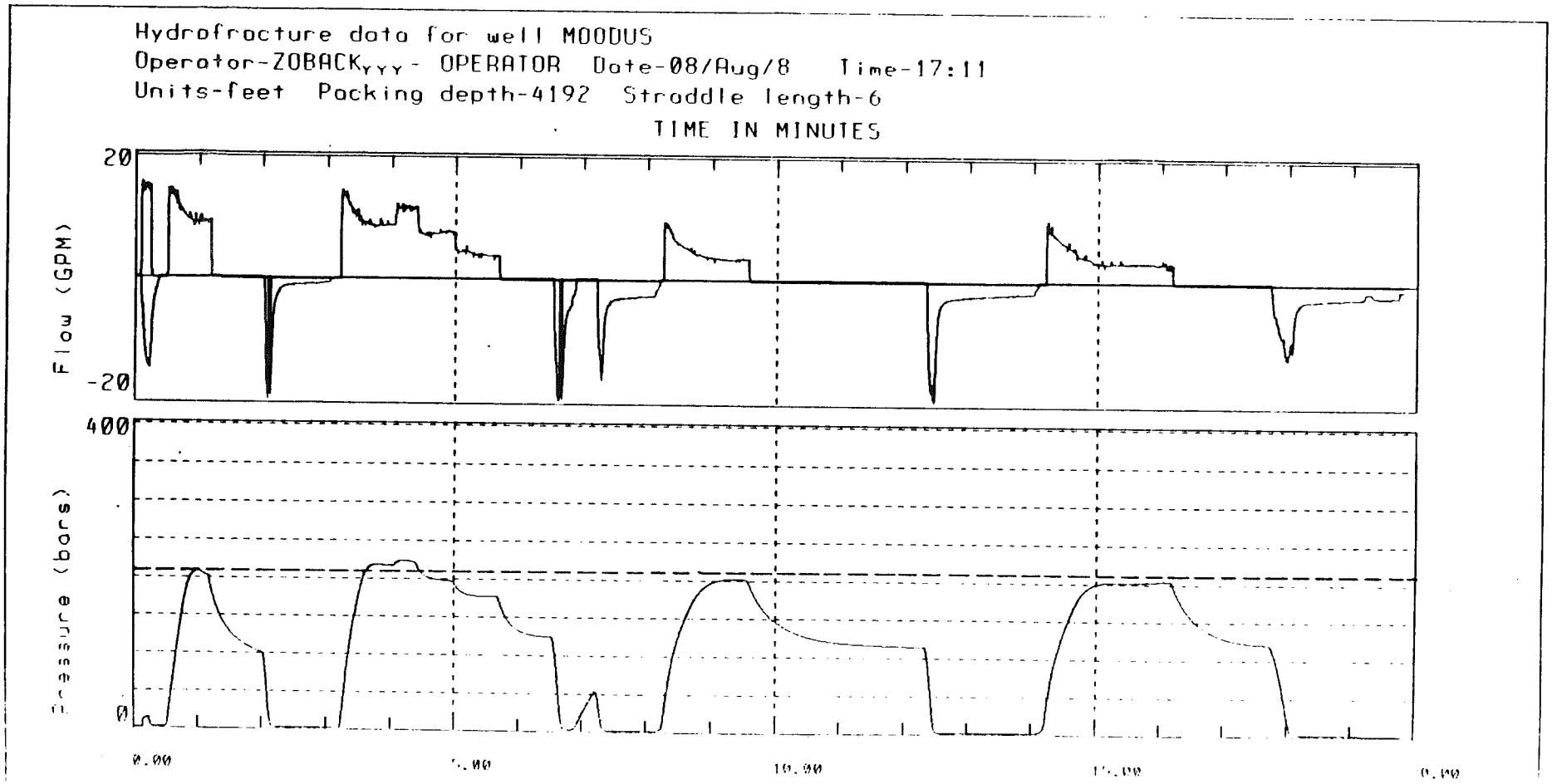
Hydrofracture data for well MOODUS
Operator-ZOBACK$_{YYY}$- OPERATOR Date-08/Aug/8 Time-17:11
Units-feet Packing depth-4192 Straddle length-6
TIME IN MINUTES
20
-20
Flow (GPM)
400
0
Pressure (bars)
0.00
10.00

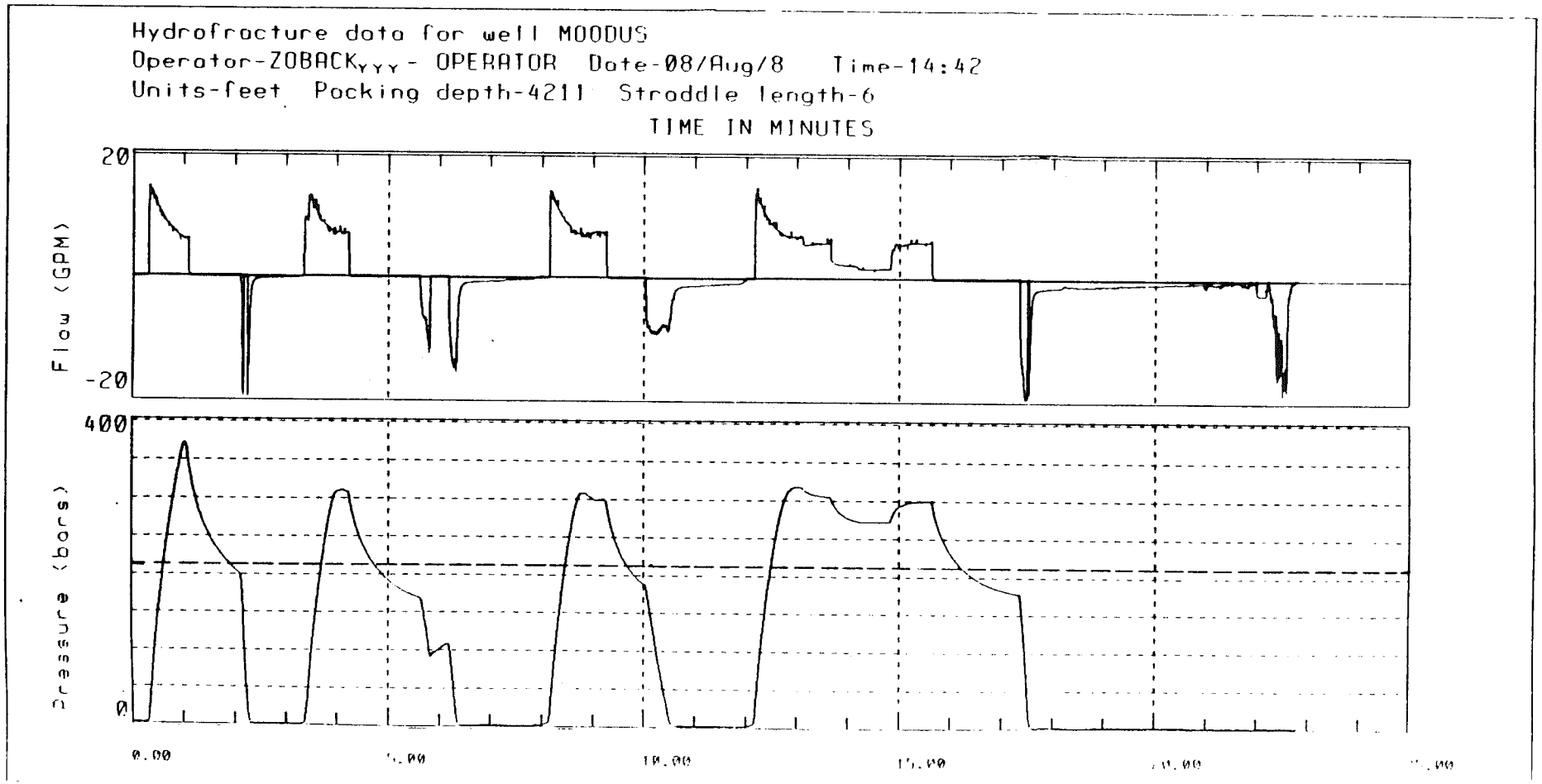
Hydrofracture data for well MOODUS
Operator-ZOBACK$_{YYY}$ - OPERATOR Date-08/Aug/8 Time-14:42
Units-feet Packing depth-4211 Straddle length-6
TIME IN MINUTES
20
-20
Flow (GPM)
400
0
Pressure (bars)
0.00
10.00

Section VII. New Hydraulic Fracturing Interpretation Methodology

Since Haimson and Fairhurst (1967) and v. Schoenfeldt (1970) introduced hydraulic fracturing as a stress measuring method in the late 1960's, it has become a widely used technique for deep in situ stress measurements (see review by Zoback and Haimson, 1983a; Rummel et al., 1986; Stephannson, 1986). Recent technical developments such as high pressure, high temperature sealing elements and high temperature downhole data recording units make hydraulic fracturing the only current direct in situ stress measuring technique discussed for use in ultra-deep boreholes. However, these technical and theoretical developments were not accompanied by a comparable development of interpretation techniques. Pressure/time records are still often analyzed by visual inspection, by graphical methods such as Gronseth and Kry's (1983) tangent method used, to identify the inflection point in the pressure decay after shut-in (instantaneous shut-in pressure P_{isip}) or using Hickman and Zoback's (1983) comparison of pre-reopening pressure-time curves for determination of fracture re-opening pressures. Some more sophisticated methods, as summarized by Zoback and Haimson (1983b) have been applied only to very few scientific field cases - probably largely due to the additional requirements for data interpretation and processing.

An enhanced interpretation procedure, packaged in a simple and convenient analysis program was developed for the Moodus project. The hydraulic fracturing data analysis program (ANFRAC) includes 7 different procedures to present pressure and flow data. Fracture re-opening and shut-in pressure values can be derived by at least four different methods. Instantaneous shut-in pressures are logically and consistently determined by analyzing graphs of:

- pressure [P] versus time [t] (detailed expanded plots),
- pressure [P] versus injection rate [Q],
- pressure [P] versus pressure change [dP/dt],
- pressure change [dP/dt] and pressure [P] versus time [t],

- pressure change [dP/dt] and pressure [P] versus log(t).

The fracture re-opening pressure at the borehole wall can be determined by means of:

- detailed pressure [P] versus time [t] plots,
- graphs of pressure [P] versus accumulated volume [V],
- graphs of pressure [P] versus system stiffness [dP/dV],
- graphs of pressure [P] versus a normalized pressure change [dP/dt] (to compensate for pressure-dependent flow rates [dP/dt] has to be normalized by the injection rate [Q]).

In the following, the test sequence at 2745 ft (837 m) which, as mentioned above, resulted in a completely re-oriented fracture plane, is used to demonstrate the interpretation package. This record is reproduced in this section as Fig. 1 for convenience.

Determination of the instantaneous shut-in pressure Pisip:

Figures 2a,b and 2a,b are pressure-time plots of the first (fig. 2a,b) and the last pressurization cycle (fig. 3a,b) at 837 m. On these plots annotated values were picked either visually or by applying Gronseth and Kry's tangent method for a first analysis of the pressure time charts recorded in the field. Expanded graphs of the pressure decay after shut-in (fig. 2b, 3b) were in many cases of only limited help in accurately determining an inflection point.

Plots of pressure versus injection rate provide a reliable way to identify the pressure level at which the injection pump was actually stopped and the system closed. Figure 2c and 3c show that there was always - regardless of whether slow (manual) or fast (air pressure-operated) valves were used, a short period of about 1 to 2 seconds after the pump drive was disengaged during which flow into the system occurred while the pressure was dropping. The final pressure level, at which the injection was shut-off completely, can then be regarded as an upper pressure boundary for the instantaneous shut-in pressure.

If the injection pressure is plotted as a function of the pressure gradient after

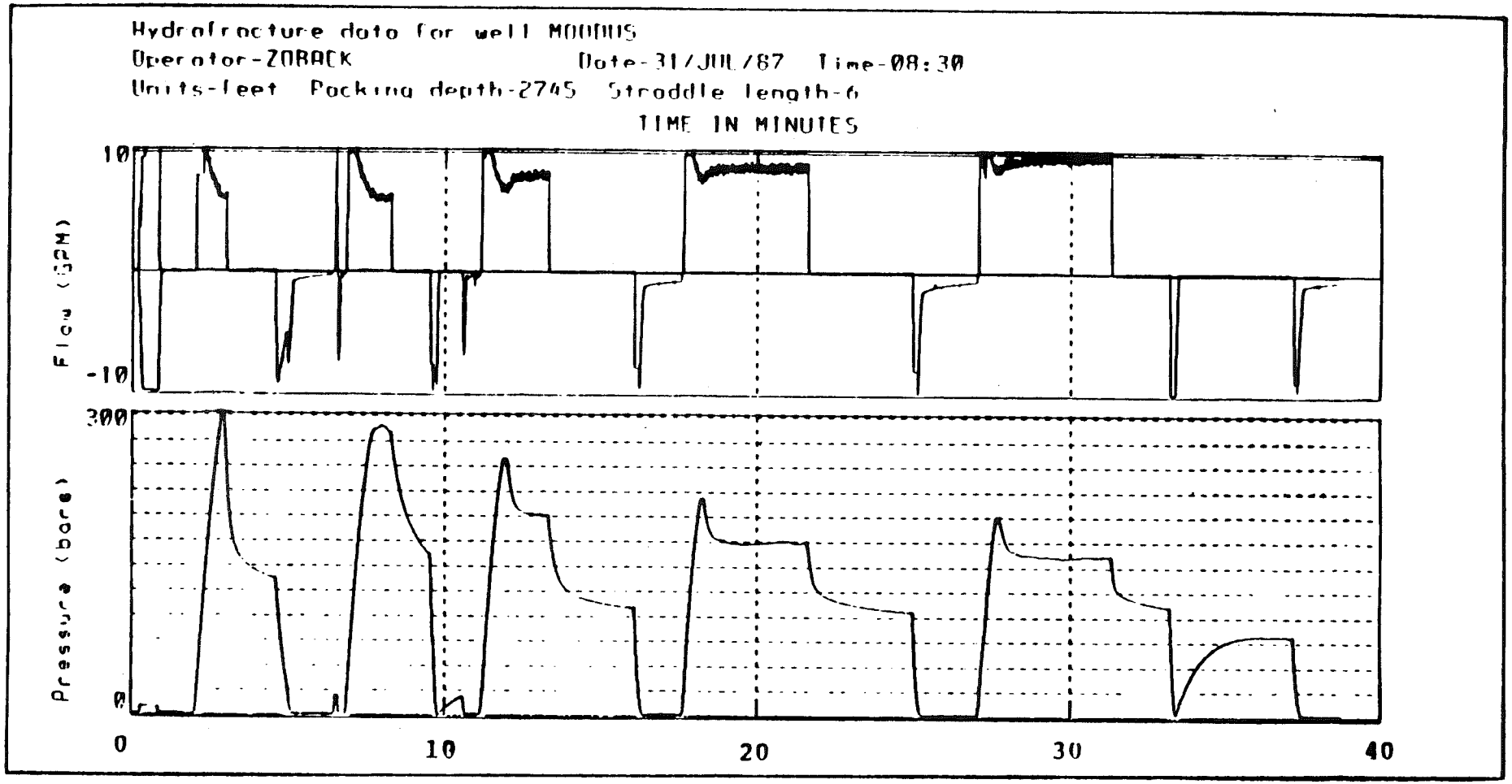

Figure 1. Complete hydrofrac test sequence at 2745 ft. in the Moodus wellbore. Pressure values are given in 'bar'. Flow rates are given in GPM.

Figure 2. Interactive interpretation of hydrofrac pressure and flow data. Shown is the determination of the instantaneous shut-in pressure of the first pressurization cycle during the test sequence at 837 m. All pressure values are given in bars. Divide by 10 to obtain MPa. Injection rates and fluid volume are given in (US) GPM or Gallon. Divide by 3.785 to obtain fluid flow in 1/min or volume in 1, respectively. *: Each star corresponds to a sampling point; the sampling rate was 2.5 Hz. --->: Arrows indicate inflection points after shut-in.

a,b: P_{isip} values shown in these pressure/time plots were determined during a first analysis of the pressure/time charts recorded in the field.

c: Fluid pressure [P] as a function of the injection rate [Q].

d: Fluid pressure [P] as a function of the pressure change [dP/dt].

e: Pressure change [dP/dt] and pressure [P] versus time [t].

f: Pressure change [dP/dt] and pressure [P] versus log(t).

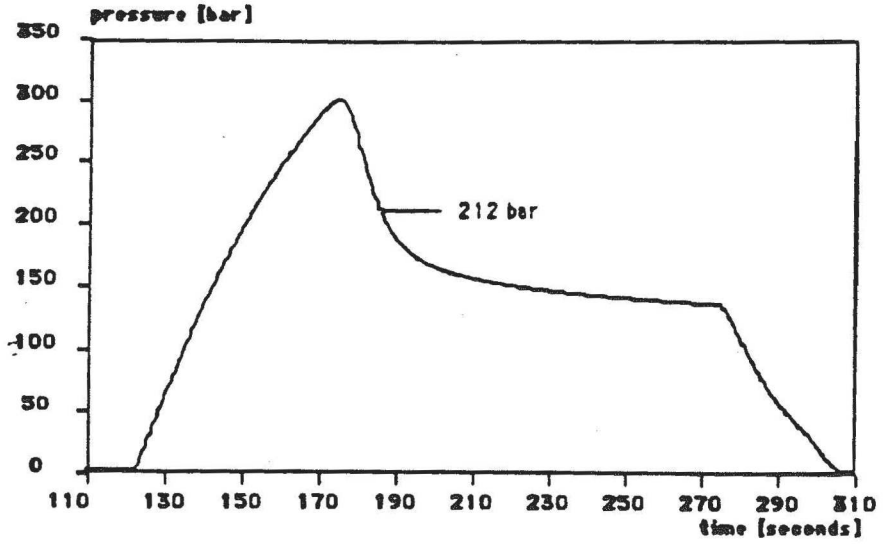
pressure [bar]
350
300
250
200
150
100
50
0
212 bar
110
130
150
170
190
210
230
250
270
290
310
time [seconds]

a

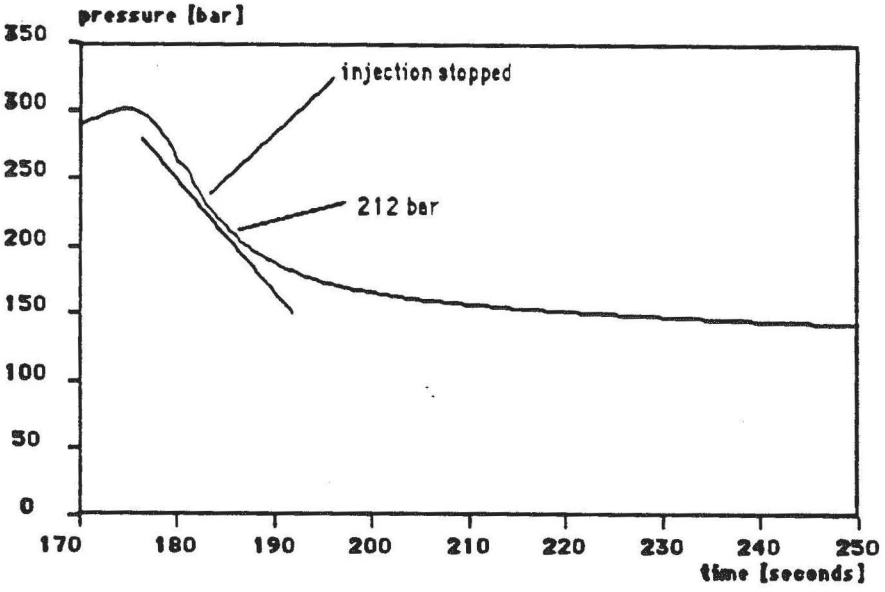
pressure [bar]
350
300
250
200
150
100
50
0
injection stopped
212 bar
170
180
190
200
210
220
230
240
250
time [seconds]

b

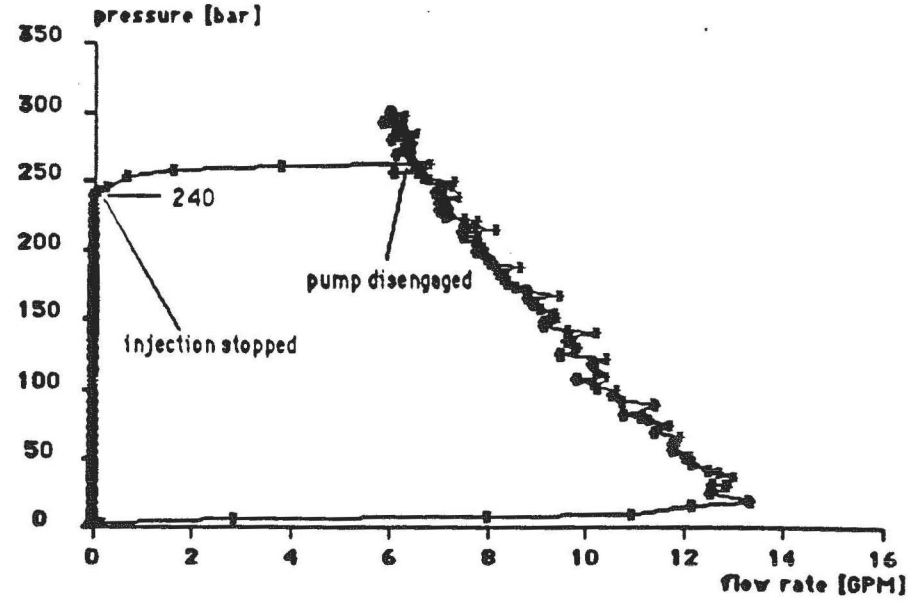
pressure [bar]
350
300
250
200
150
100
50
0
240
pump disengaged
injection stopped
0
2
4
6
8
10
12
14
16
flow rate [GPM]

c

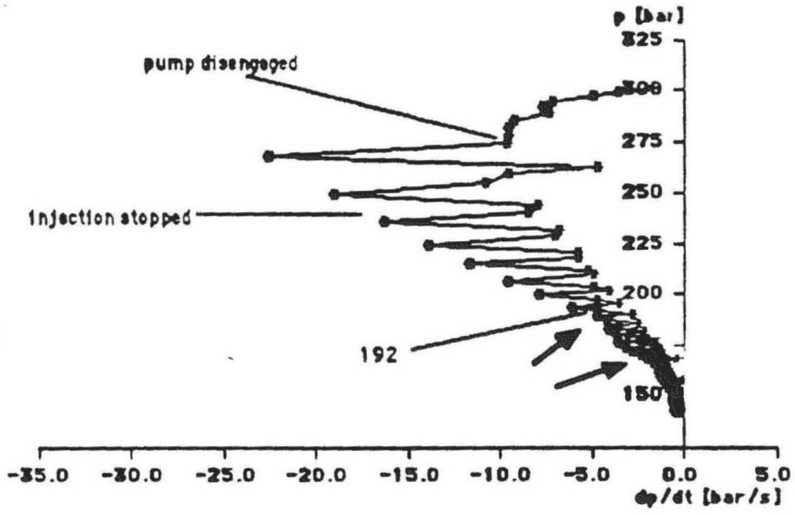
p [bar]
pump disengaged
injection stopped
192
325
300
275
250
225
200
150
-35.0
-30.0
-25.0
-20.0
-15.0
-10.0
-5.0
0.0
5.0
dp/dt [bar/s]

d

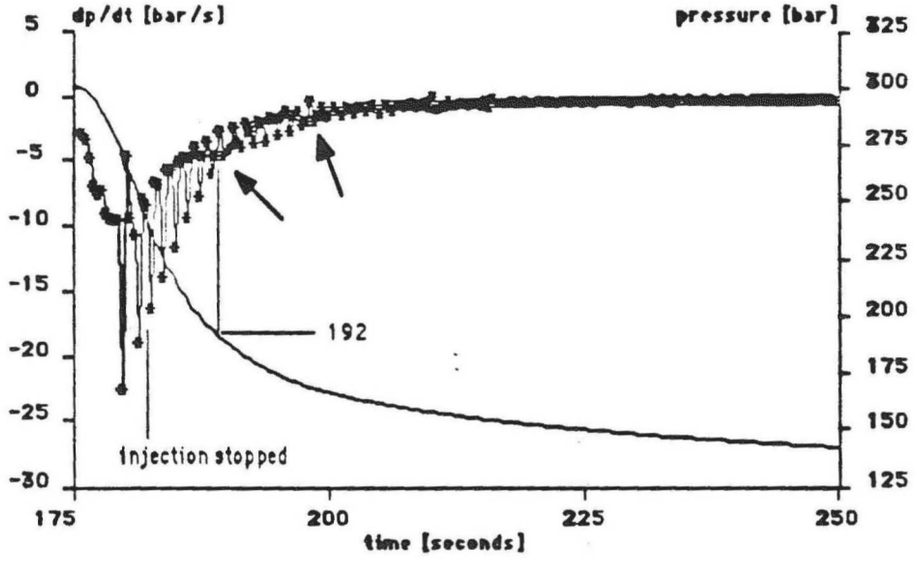
dp/dt [bar/s]
pressure [bar]
5
0
-5
-10
-15
-20
-25
-30
325
300
275
250
225
200
175
150
125
192
injection stopped
175
200
225
250
time [seconds]

e

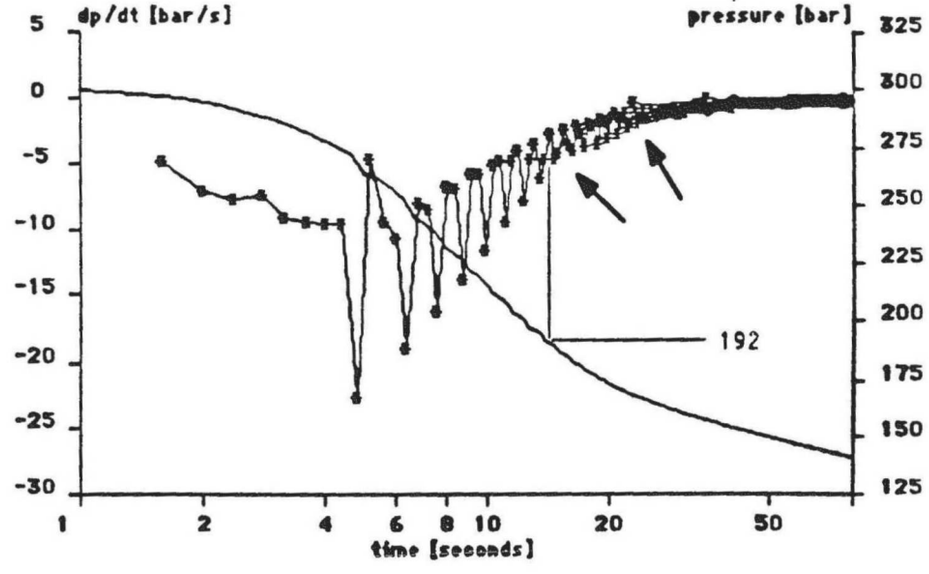
dp/dt [bar/s]
pressure [bar]
5
0
-5
-10
-15
-20
-25
-30
325
300
275
250
225
200
175
150
125
192
1
2
4
6
8
10
20
50
time [seconds]

f

Figure 3. Interactive interpretation of hydrofrac pressure and flow data. Shown is the determination of the instantaneous shut-in pressure of the fifth pressurization cycle during the test sequence at 837 m. All pressure values are given in bar. Divide by 10 to obtain MPa. Injection rates and fluid volume are given in (US) GPM or Gallon. Divide by 3.785 to obtain fluid flow in 1/min or volume in 1, r espectively. *: Each star corresponds to a sampling point; the sampling rate was 2.5 Hz. --->: Arrows indicate inflection points after shut-in.

a,b: P_{isip} values shown in these pressure/time plots were determined during a first analysis of the pressure/time charts recorded in the field.

c: Fluid pressure [P] as a function of the injection rate [Q].

d: Fluid pressure [P] as a function of the pressure change [dP/dt].

e: Pressure change [dP/dt] and pressure [P] versus time [t].

f: Pressure change [dP/dt] and pressure [P] versus log(t).

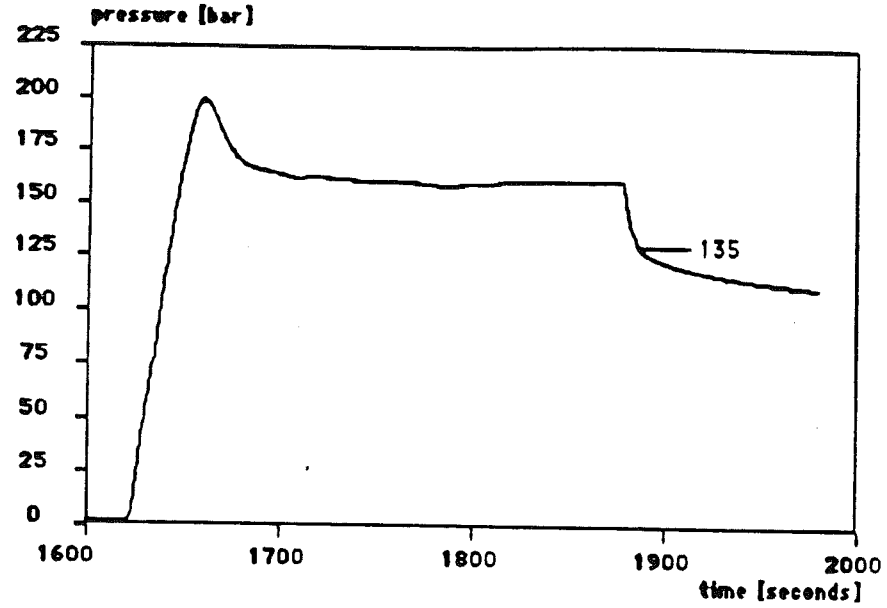
pressure [bar]
225
200
175
150
125
100
75
50
25
0
1600
1700
1800
1900
2000
time [seconds]
135

a

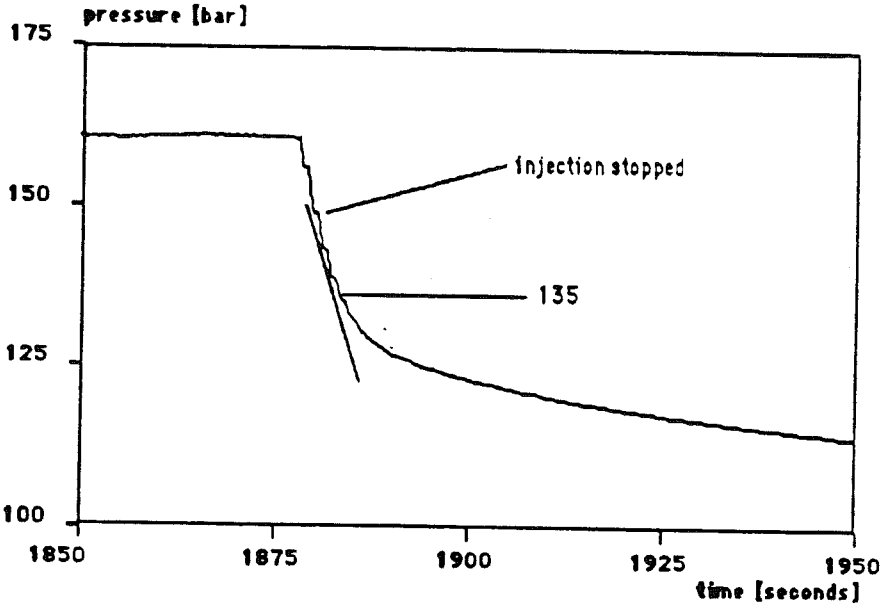
pressure [bar]
175
150
125
100
1850
1875
1900
1925
1950
time [seconds]
injection stopped
135

b

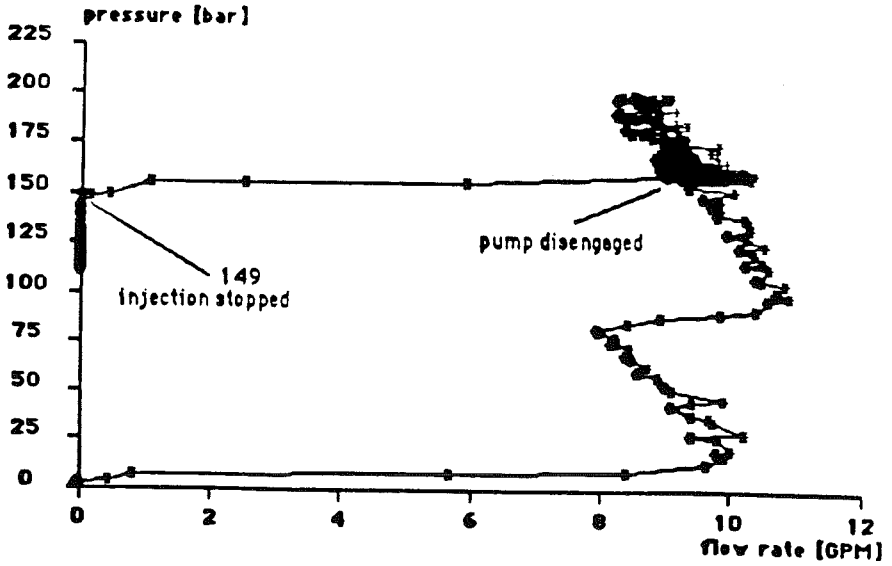
pressure [bar]
225
200
175
150
125
100
75
50
25
0
0
2
4
6
8
10
12
flow rate [GPM]
149
injection stopped
pump disengaged

c

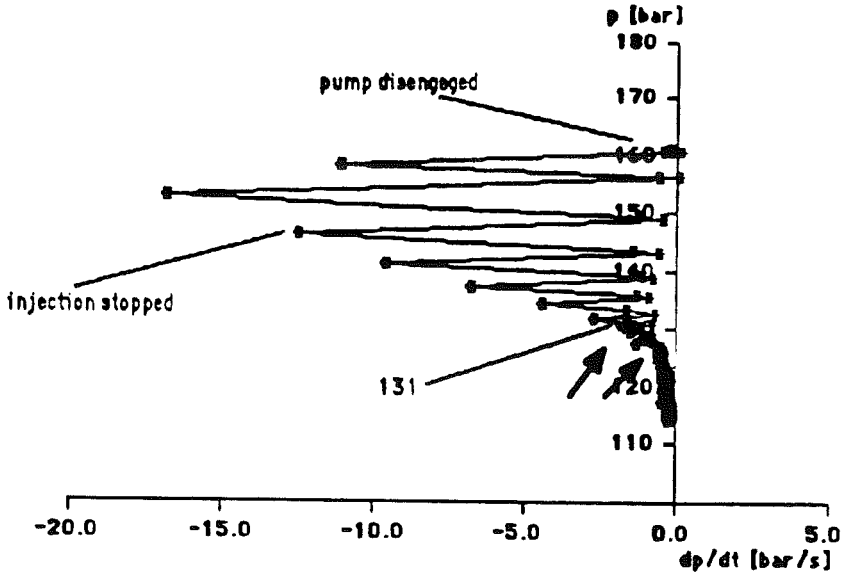
p [bar]
180
170
160
150
140
130
120
110
pump disengaged
injection stopped
131
-20.0
-15.0
-10.0
-5.0
0.0
5.0
dp/dt [bar/s]

d

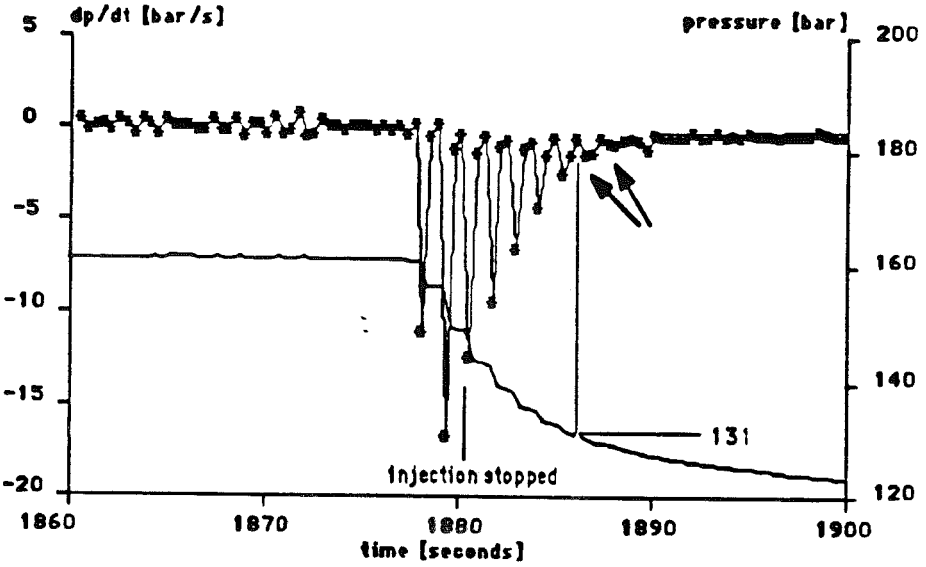
dp/dt [bar/s]
pressure [bar]
5
0
-5
-10
-15
-20
200
180
160
140
120
131
injection stopped
1860
1870
1880
1890
1900
time [seconds]

e

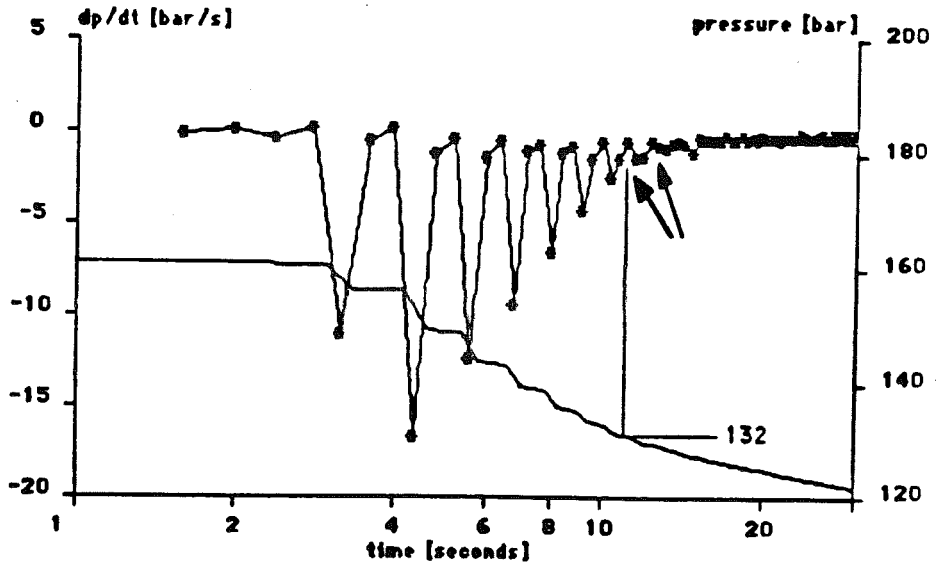
dp/dt [bar/s]
pressure [bar]
5
0
-5
-10
-15
-20
200
180
160
140
120
132
1
2
4
6
8
10
20
time [seconds]

f

shut-in (P versus dP/dt), the pressure gradient curve shows a first slope change as soon as the pressure dropped to the instantaneous shut-in pressure P_{isip} (fig. 2d; fig. 3d). (The rapid swings in Fig. 2 d,e,f and subsequent figures results from differentiating relatively coarsely sampled data. These are bothersome but do not seriously degrade our ability to interpret the data In the next set of analysis programs being developed these will be removed by an nait-aliasing filter.) The second slope change observed in fig. 2d and fig. 3d is probably related to the so-called "closure pressure" at which a first contact between the fracture planes occurs (see arrows in fig. 2d,e,f and 3d,e,f). Both inflection points are more easily seen if the pressure gradient and the injection pressure after shut-in are simultaneously plotted on a real time basis or a logarithmic time basis (fig. 2e,f; fig. 3e,f). The advantage of these time-based graphs is that they allow a direct correlation of those P_{sisp}-values which were picked during the first visual and graphical analysis of the pressure decay and the exact pressure gradient slope.

Determination of fracture re-opening pressure values P_r

Fracture re-opening pressure values P_r used to estimate the maximum horizontal compression were first determined by comparing the beginning of the first and second pressurization cycle as proposed by Hickman and Zoback (1983) and marking the pressure level at which both pressurization curves deviate. This value is given in the pressure-time graphs of the second pressurization cycle at 837 m in fig. 4a and fig. 4b.

The second step in an evaluation of P_r is a plot of the accumulated injected volume versus injection pressure (fig. 4c), used as a first order estimate of the pressure level at which the system stiffness is reduced when the fracture opens at the borehole wall and the fracture volume is connected to the hydraulic system. These graphs also allowed an estimate of the fluid volume which remained in the formation after the hydraulic system was drained. It should be noted that this is not a completely accurate measurement because the turbine flowmeters used could not register flow rates below about 1 GPM (3.75 l/min).

Figure 4. Interactive interpretation of hydrofrac pressure and flow data. Shown is the determination of the fracture re-opening pressure of the second pressurization cycle during the test sequence at 837 m. All pressure values are given in bar. Divide by 10 to obtain MPa. Injection rates and fluid volume are given in (US) GPM or Gallon. Divide by 3.785 to obtain fluid flow in 1/min or volume in 1, respectively. *: Each star corresponds to a sampling point, the sampling rate was 2.5 HZ. --->: Arrows indicate inflection points after shut-in.

a,b: P_r values shown in these pressure/time plots were determined during a first analysis of the pressure/time charts recorded in the field.

c: Fluid pressure [P] as a function of the accumulated volume [V].

d: Fluid pressure [P] as a funciton of the pressure change [dP/dt] normalized by the injection rate [Q].

e: Fluid pressure [P] as a function of the system stiffness [dP/dV].

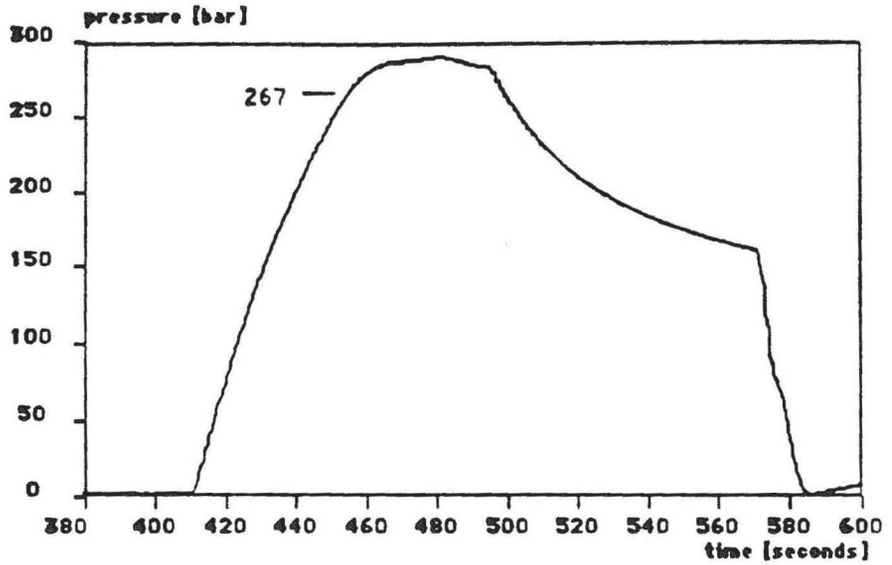
pressure [bar]
300
250
200
150
100
50
0
267
380
400
420
440
460
480
500
520
540
560
580
600
time [seconds]

a

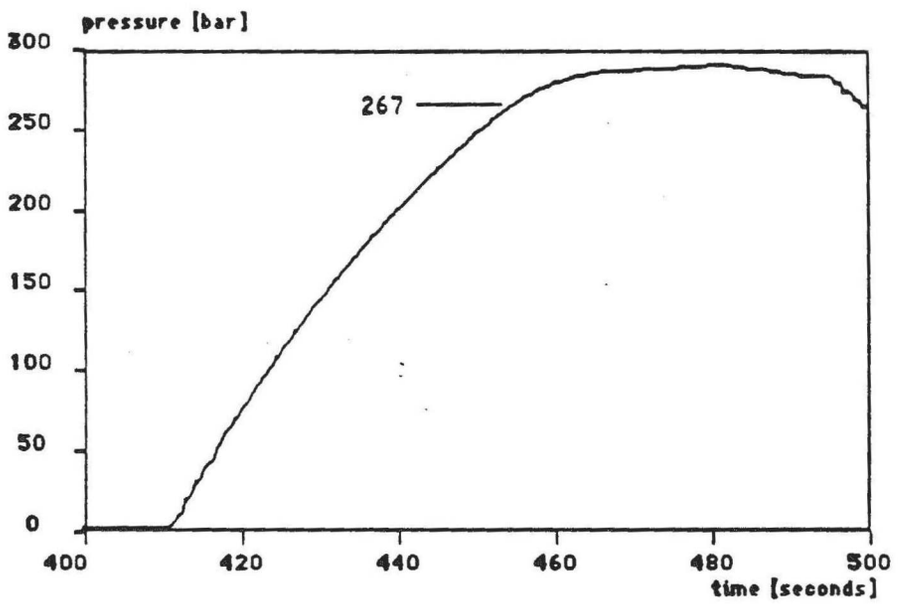
pressure [bar]
300
250
200
150
100
50
0
267
400
420
440
460
480
500
time [seconds]

b

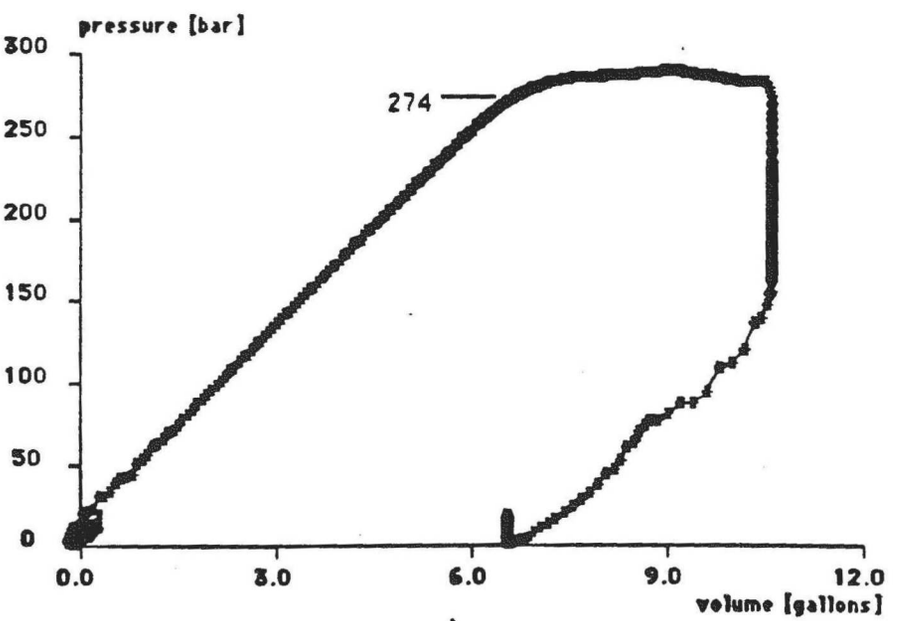
pressure [bar]
300
250
200
150
100
50
0
274
0.0
3.0
6.0
9.0
12.0
volume [gallons]

c

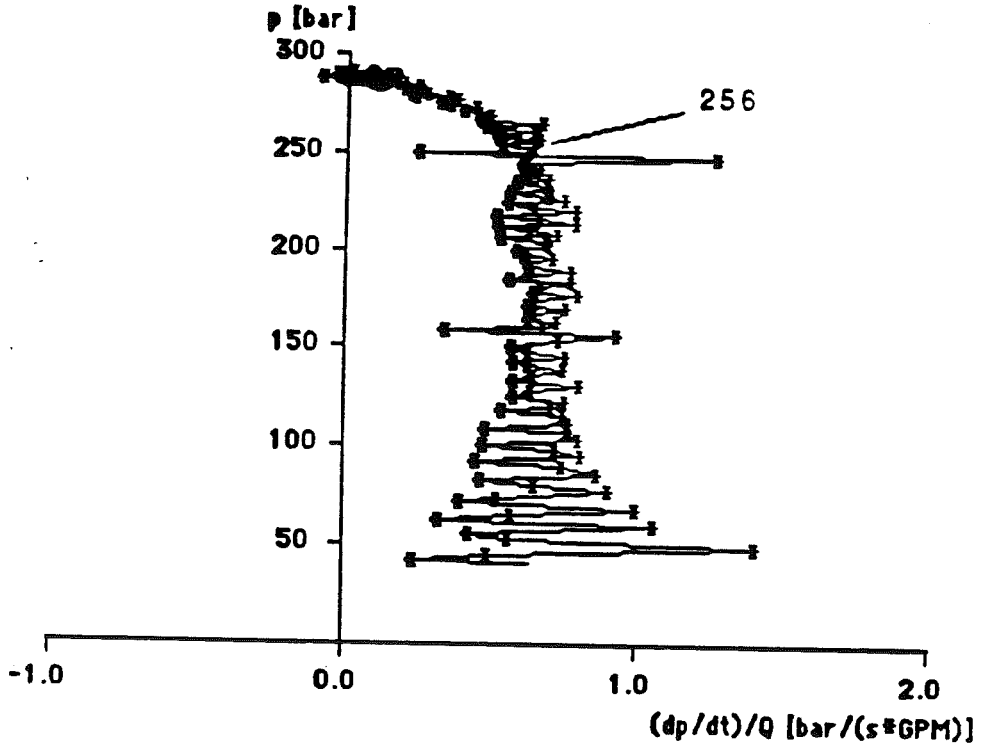
p [bar]
300
250
200
150
100
50
256
-1.0
0.0
1.0
2.0
(dp/dt)/Q [bar/(s*GPM)]

d

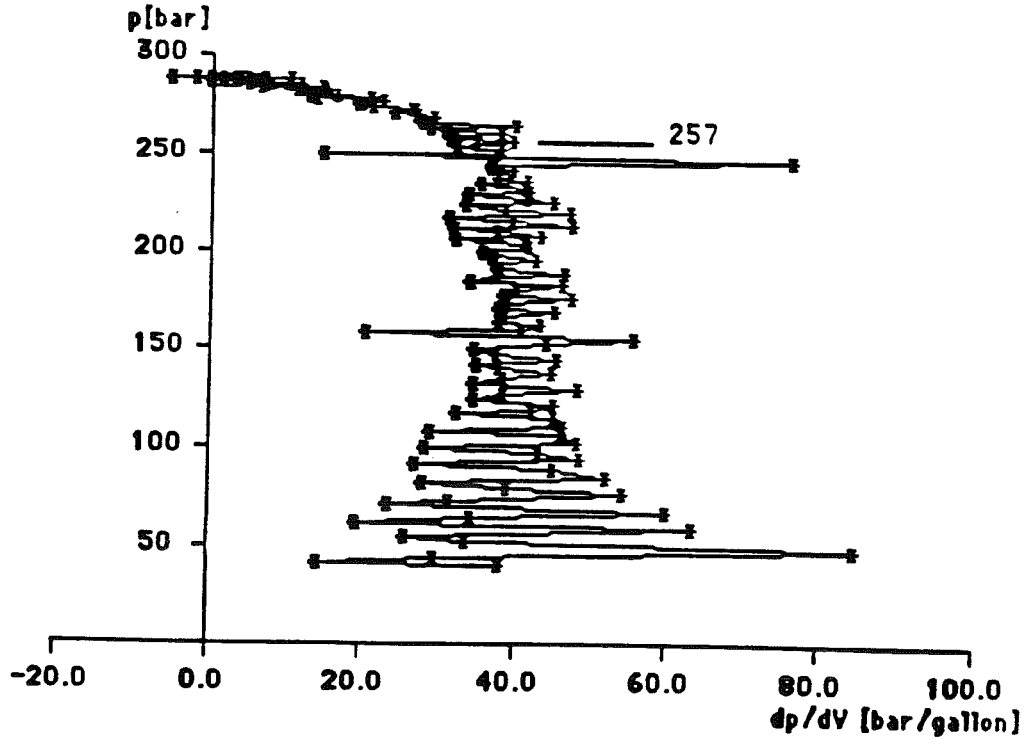
p[bar]
300
250
200
150
100
50
257
-20.0
0.0
20.0
40.0
60.0
80.0
100.0
dp/dV [bar/gallon]

e

A much more exact identification of the re-opening pressure value is possible if the change of pressure with injected volume (dp/dV) is plotted as function of the injection pressure. The fracture opening pressure is then characterized by a sharp slope change (fig. 4e). The same picture can be obtained from a graph of the pressure gradient versus injection pressure. Because of the pressure-dependent injection rate, the pressure gradient (dP/dt) had to be normalized by the injection rate Q (fig. 4d). Both techniques proved to be very reliable and sensitive methods to determine the fracture re-opening pressure P_r.

Tables I and II present the values determined for the Moodus tests. These values were used in the stress computations presented in Table I of Section III.

depth/m	cycle no.	class	hydr.	P --> t *)	P --> Q	P --> dP/dt	P,dP/dt -> t	P,dP/dt > log(t)
108	1	F	1.1	7.1	<= 7.6	6.8	6.9	7.0
117	1	F+	1.2	8.2	<= 8.7	7.8	8.1	~ 8.0
117	6	F+	1.2	3.0	<= 3.2	3.0	3.1	3.0
178	1	F	1.8	11.9	<= 13.7	12.3	12.3	12.2
193	1	F	1.9	9.8	<= 11.1	10.2	10.3	10.4
819	2	PX	8.0	37.4	<= 38.7	36.0	37.2	37.3
837	1	F+	8.2	21.2	<= 24.0	19.2	19.2	19.2
837	5	F+	8.2	13.5	<= 14.9	13.1	13.1	13.2
852	4	PX	8.4	13.6	<= 14.9	13.6	13.4	13.4
890	1	F	8.7	20.1	<= 40.5	19.9	19.9	19.7
1076	1	F	10.6	27.6	<= 28.7	28.5	28.5	28.7
1184	3	PX	11.6	20.0	<= 20.9	20.2	20.0	20.2
1277	4	PX	12.5	18.4	<= 19.9	18.3	18.1	18.2
1284	1	F	12.6	31.5	<= 35.1	32.0	32.0	31.8

TABLE I.

Summary of Pressure Data from Hydrofrac Tests in the Moodus Wellbore

Instantaneous shut-in pressure values P_{isip} determined during the analysis procedure described in the text. All pressure values are given in MPa. The following symbols and abbreviations are used: P, Fluid pressure; Q, Injection rate; t, time; hydr., Hydrostatic pressure at test depth; *), These pressure values were determined during a first preliminary analysis of the pressure time charts recorded in the field. The tests were classified applying the following criteria: F, a vertical fracture was initiated at the wellbore wall; re-orientation of the fracture plane, however, was not complete. F+, a vertical fracture was initiated at the wellbore wall which then rolled over and propagated horizontally; PX, a pre-existing plane of weakness was opened at the wellbore wall. Add hydrostatic pressure to obtain downhole pressure values.

depth/m	cycle no.	class	hydr.	dyn. corr.	P --> t *)	P --> V	P --> dP/dV	P > (dP/dt)/Q
108	2	F	1.1	0	11.5	<= 10.2	9.8	9.8
117	2	F+	1.2	0	15.0	<= 14.7	13.8	13.8
178	2	F	1.8	0	13.8	<= 14.0	13.8	13.8
193	2	F	1.9	0	14.3	<= 14.6	12.8	12.9
837	2	F+	8.2	0.2	26.7	<= 27.4	25.7	25.6
890	2	F	8.7	0.2	17.2	<= 19.8	18.0	18.0
1076	2	F	10.6	0.3	25.3	<= 27.1	26.0	25.8
1284	2	F	12.6	0.3	27.1	<= 29.0	28.8	28.6

TABLE II.

Fracture re-opening Pressure Values P_r

Fracture re-opening pressure values P_r determined during the analysis procedure described in the text. All pressure values are given in MPA. The following symbols and abbreviations are used: P, Fluid pressure; Q, Injection rate; V, Accumulated volume; t, Time; hydr., Hydrostatic pressure at test depth; dyn. corr., Corrections for viscous pressure losses based on the Darcy-Weissbach equation. *), These pressure values were determined during a first preliminary analysis of the pressure time charts recorded in the field. The tests were classified applying the following criteria: F, a vertical fracture was initiated at the wellbore wall; re-orientation of the fracture plane, however, was not complete. F+, a vertical fracture was initiated at the wellbore wall which then rolled over and lpropagated horizontally. Downhole pressure values are obtained by adding the hydrostatic pressure and subtracting the dynamic correction.

Section VIII - New Theory of Hydraulic Fracturing

Summary

The hydrofracture breakdown equation is reformulated using an exact effective stress concept. In practice, the pressure of hydraulic fracture inititation, (i.e., the breakdown pressure), is considered to be only a function of the principal horizontal crustal stresses and the tensile strength of the rock. As in the earlier derivation of Haimson and Fairhurst, however, we have derived a new formula which displays a dependence of the breakdown pressure on the Biot parameter: $a = 1 - K_b/K_m$, and on Poisson's ratio. K_b is the rock bulk modulus and K_m is the bulk modulus of the rock matrix material. The new formula indicates that the effect of ambient pore pressure vanishes in hydrofracture experiments conducted in low porosity rocks for which $a \to 0$. However, recent measurements to 10 MPa yield values of a which range from 0.9 to 0.1 suggest that rock properties should be considered in hydraulic fracture experiments. As applied to the stress measurements at Moodus, we assume that a can be anywhere between 0 and 1 and compute the respective values of S_H in Section III. In terms of the revised hydraulic fracturing theory presented here, this represents the upper and lower bounds for S_H.

Introduction

The appeals of the hydraulic fracturing stress measurement method include the fact that it is the only widely-used stress measurment technique that can be used at great depth in wells and boreholes and the generally accepted simplifying assumption that the measured stresses are independent of the elatic moduli of the rock. The assumption of independence of elastic moduli is used in essentially all hydrofracture experiments and originates from the pioneering theoretical work of Hubbert and Willis (1957) and Haimson and Fairhurst (1967). The simplified theory of Haimson and Fairhurst (1967) assumes finite ambient pore pressure within the rock formation and vanishing permeablity to the hydraulic fracturing fluid. and gives the breakdown formula:

$$P_b = 3S_h - S_H + T - P_o \qquad (1)$$

where P_b is the pressure of fracture initiation or the breakdown pressure, P_o is the ambient pore pressure within the formation prior to the experiment, T is the tensile strength of the rock, and S_H and S_h are the greatest and least total principal horizontal stresses, respectively. Equation (1) is derived assuming

both the borehole axis and a principal stress are vertical, and with a total or confining stress S_{ij} given by the empirical effective stress law (Nur and Byerlee, (1971):

$$S_{ij} = \sigma_{ij} + P_o \tag{2}$$

where σ_{ij} is the effective stress. Note that here compressive stresses have positive sign and $T > 0$.

The utility of Equation (1) lies in its straightforward use in the determination of the greatest principal horizontal stress: S_H. In a hydrofracture experiment both P_b and S_h are directly measured. If the tensile strength T of the rock formation and the ambient pore pressure P_o is known, then S_H may be solved for. In practice T may be eliminated by using fracture reopening pressures (Bredehoeft et. al., (1976), Hickman and Zoback (1983)).

Equation (1) ignores the effect of flow of fluid into a permeable porous rock formation from the sealed interval during a hydraulic fracturing experiment. Hubbert and Willis (1957) noted that the pressure of hydraulic fracture initiation was smaller when low viscosity fracturing fluids were employed suggesting that penetration of fracturing fluid could influence breakdown pressures. Haimson and Fairhurst (1967), based upon the theory of Lubinski (1954), demonstrated that fluids penetrating the borehole wall induce additional stresses which must be accounted for when the greatest horizontal principal stress is to be determined from the breakdown pressure. Their analysis, which employed the empirical effective stress relation of Equation (2), yielded the following breakdown equation:

$$P_b = \frac{3S_h - S_H + T - 2P_o}{K} + P_o. \tag{3}$$

K is given by:

$$K = 2 - \alpha\frac{1-2\nu}{1-\nu} \tag{4}$$

where n is Poisson's ratio and a, and measure of the compliance of a rock and here referred to as the Biot parameter, is given by:

$$\alpha = 1 - \frac{K_b}{K_m}. \tag{5}$$

K_b is the bulk modulus of the rock including the effects of microcracks and pores. K_m is the bulk modulus of the rock matrix material, i.e., the mineral skeleton of the rock. a approaches unity for highly porous rock, especially at low confining pressure; as confining pressure increases, resulting in the

closure of pores and microcracks within a rock, α approaches zero. Thus, at low pressure K is near unity and with increasing pressure K approaches 2. A paradox arises in that equations (1) and (3) predict similar behavior at low pressures or in highly compliant rocks and at high confining pressure equations (1) and (3) predict breakdown pressures which can differ by a factor of 2. Intuition suggests the opposite, i.e., as pressure increases and the porosity and permeability of a rock correspondingly decreases the effect fluid flow into the rock formation should decrease with the result that an expression accounting for this flow should converge with equation (1) as confining pressure increases. Haimson and Fairhurst (1967) also recognized this fact and accounted for it by ignoring the stresses induced by fluid flow at high pressure or low permeabilty which leaves the simpler relationship of equation (1).

The empirical effective stress relation of equation (2) was originally proposed by Terzaghi (1923) to explain deformation in saturated soils. A constant effective stress is that which induces identical behavior (e.g. static deformation or failure strength) in a porous permeable material for a given set of corresponding total (confining) stresses and ambient pore pressures. Measurements on rock samples with varying porosities and compositions (Nur and Byerlee (1971), Zoback (1975), and Coyner (1984)) demonstrate that volumetric strain does not follow the effective stress law of equation (2), i.e., measured volumetric strains in rocks with nonzero pore pressure are larger than would be expected on the basis of the empirical effective stress law. Others have suggested that the effective stress law would take the form:

$$S_{ij} = \sigma_{ij} + \alpha P_o . \qquad (6)$$

In particular, Nur and Byerlee (1971) provide a derivation of equation (6), which they refer to as the exact effective stress law, with α as defined by equation (5) as suggested from the earlier theory of Geertsma (1957) and Biot and Willis (1957). Equation (6) states that as α approaches zero with decreasing porosity the effect of pore pressure on volumetric strain is diminished.

Since it appears that both static defomation and tensile failure are not described by the empirical effective stress law, in this paper we apply the exact effective stress law to a rederivation of the hydraulic fracture breakdown equation. We note that Evans et. al., (1988) have also applied the new effective stress law but have not carried the redierivaiton far enough. Our derilvation

follows closely that of the original derivation of Haimson and Fairhurst (1967).

Rederivation

Our rederivation of the hydraulic fracture breakdown equation follows closely that of Haimson and Fairhurst (1967). The same assumptions are applied, namely:

(1). Rock is linearly elastic, homogeneous, isotropic, porous, permeable.

(2). A deviatoric triaxial state of stress, defined by S_H, S_h, and S_V: the total horizontal greatest, total horizontal least, and total vertical principal stresses, respectively, acts on the rock formation.

(3). The borehole and one principal stress, S_V, are aligned with the vertical.

(4). The borehole is smooth and circular in cross-section.

(5). Darcy's law describes fluid flow through the formation.

Three stress fileds exist in the vicinity of the borehole during hydraulic fracturing: 1) the concentration of the far-rield regional tectonic stresses by the existence of the borehole in the rock mass itself, 2) the axisymmetric stress field induced by pressurization of the sealed off section of the borehole, and 3) the axisymmetric stress field induced by flow of the fracturing fluid into a permeable rock formation. The total stress field near the borehole during a hydrofracture experiment is a superposition of these three.

Figure 1 describes the relationship between the Cartesian co-ordinate system aligned with the principal total stresses S_H, S_h, and S_V and the cylindrical co-ordinate system aligned with the borehole axis with the principal total stresses S_ρ, $S_{\theta\theta}$, and S_V. In this analysis we consider only the azimuthal stress concentrations near the borehole since these concentrations are the only stresses which become tensile and result in the creation of a hydraulic fracture (Hubbert and Willis (1957), Haimson and Fairhurst (1967)).

Having defined the total stress field within the rock mass, the three borehole wall stress fields are now defined. The exact effective stress law as defined by equation (6) is applied as opposed to the empirical effective stress law of equation (2) as used by Haimson and Fairhurst (1967). First, a vertical borehole drilled into the given regional stress regime results in the concentrated total azimuthal stress at the borehole wall of (Kirsch (1898); Timoshenko and Goodier (1970); Hubbert and Willis, (1957); Haimson and Fairhurst (1967):

$$S^1_{\theta\theta} = \sigma_H - \sigma_h - 2(\sigma_H - \sigma_h)\cos(2\theta) + \alpha P_o \qquad (7)$$

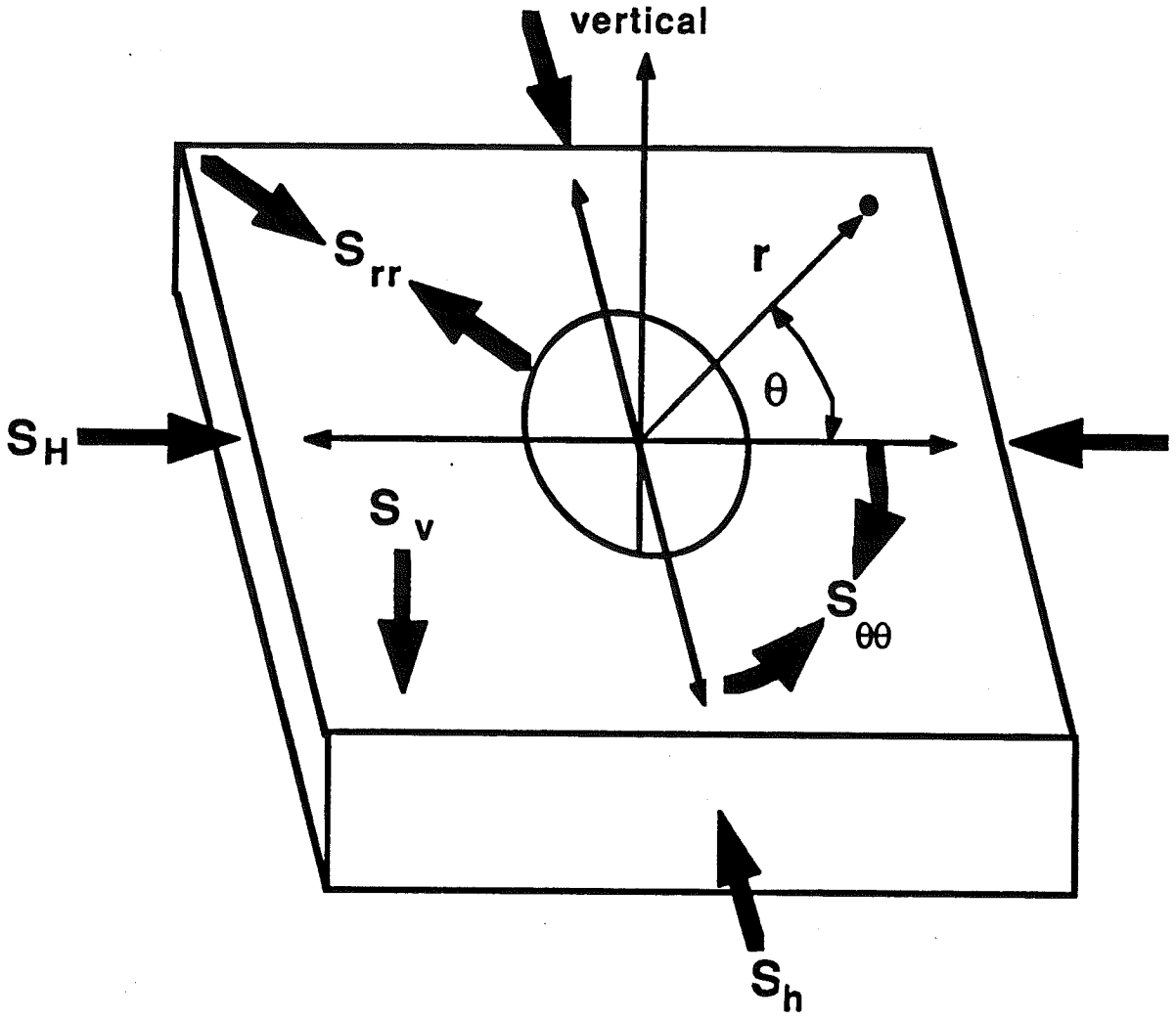

Figure 1. Definition of notation used in text.

Where θ is the counterclockwise angle as measured from the radius of the borehole in the direction of S_H.

The second stress field, induced by increasing pressure in the sealed section of the borehole, at the borehole wall becomes (Timoshenko and Goodier (1970)):

$$S^2_{\theta\theta} = -P_w + \alpha P_o \qquad (8)$$

where P_w is the fracturing fluid pressure within the sealed interval. Note that the effect of this fluid pressure within the interval creates a tensile azimuthal stress at the borehole wall. Evans et. al., (1988) apply equation (2) at this step as in Haimson and Fairhurst's (1967) earlier derivation.

The third stress field is induced by injected fluid into a permeable formation before fracture initiation. By Darcy's Law, for a permeable matrix, fluid must flow into the formation when driven by the pressure gradient between the injection and pore pressures. This flow induces additional stresses within the rock which alter the state of stress near the borehole. This is a diffusion type problem, and as such the solution must be analogous to solutions for problems of heat conduction; results of well known thermal stress problems may be applied with slight modification (Lubinski, (1954); Geertsma, (1957)). The relevant thermoelastic problem is that of heat conduction in a long circular cylinder with a concentric circular hole (Timoshenko and Goodier, (1970); Haimson and Fairhurst, (1967)). In this cylinder the temperature T = T(r) is axisymmetric and independent of position along the cylinder axis. Note that in this solution T is implicitly dependent upon time, i.e., the stresses determined are due to the instantaneous temperature distribution. The solution to this problem is credited to Lorentz and is (Timoshenko and Goodier, 1970):

$$S^3_{\theta\theta} = -\frac{AE}{1-\nu}\frac{1}{r^2}\left[\frac{r^2+a^2}{b^2-a^2}\int_a^b Trdr + \int_a^r Trdr - Tr^2\right] \qquad (9)$$

where A is the thermal expansion co-efficient, E is Young's modulus, and a and b are the inside and outside radii of the cylinder, respectively.

Lubinski (1954) describes the thermal analogy for solving problems of elasticity in porous bodies. To obtain poroelastic expressions from similar thermoelastic problems replace A with a(1 - 2n)/E and T(r) by the flow induced effective pressure distribution p(r) = P(r) - aP_o. Under these circumstances, Equation (9) is converted to:

$$S^3_{\theta\theta} = -\frac{\alpha(1-2\nu)}{1-\nu}\frac{1}{r^2}\left[\frac{r^2+a^2}{b^2-a^2}\int_a^b prdr + \int_a^r prdr - pr^2\right] \quad (10)$$

and here the need for knowledge of the rock elastic moduli is obvious. For a borehole in the Earth, b >> a. Also, at the borehole wall r = a and the integrals vanish to leave:

$$S^3_{\theta\theta} = \frac{\alpha(1-2\nu)}{1-\nu}[P_w - \alpha P_o] \quad (11)$$

The state of stress at the borehole wall results from the superposition of these three total stress fields determined above and is defined as:

$$\begin{aligned} S_{\theta\theta} &= S^1_{\theta\theta} + S^2_{\theta\theta} + S^3_{\theta\theta} \\ &= \sigma_H - \sigma_h - 2(\sigma_H - \sigma_h)\cos(2\theta) - P_w + \frac{\alpha(1-2\nu)}{1-\nu}[P_w - \alpha P_o] + 2\alpha P_o \end{aligned} \quad (12)$$

Hydraulic fracturing initiates at a point on the borehole wall where the effective stress exceeds the tensile strength of the rock. The fracture created will coicide with a plane which is perpendicular to the direction of the least principal stress. Considering only azimuthal dependence, we see $S_{\theta\theta}$ is of maximum tension at $\theta = 0$ and π and at these angles:

$$S_{\theta\theta} = 3\sigma_h - \sigma_H - P_w + \frac{\alpha(1-2\nu)}{1-\nu}[P_w - \alpha P_o] + 2\alpha P_o \quad (13)$$

The borehole wall will fail in tension when the effective azimuthal stress exceeds the rock tensile strength:

$$\begin{aligned} \sigma_{\theta\theta} &= -T \\ &= S_{\theta\theta} - \alpha P_w \\ &= 3\sigma_h - \sigma_H - (1 + \alpha - \frac{\alpha(1-2\nu)}{1-\nu})P_w + \alpha K P_o \end{aligned} \quad (14)$$

where the subtle point that P_w is simultaneously the pore pressure immediately at the borehole wall and the fluid pressure within the sealed interval (Haimson and Fairhurst, (1967)). Note that we have applied the exact effective stress law to the to the system at failure. As reviewed above, We now have information useful for stress measurement, rearranging Equation (14) gives a new hydraulic fracture breakdown formula:

$$P_b = \frac{3\sigma_h - \sigma_H + T + \alpha K P_o}{K + \alpha - 1} \quad (15)$$

$$= \frac{3S_h - S_H + T + \alpha(K-2)P_o}{K + \alpha - 1}$$

where we have substituted the breakdown pressure P_b for P_w at fracture

initiation.

Discussion

At shallow depths (low confining pressures), or in relatively compliant rocks when both a and K are near unity equations (3) and (15) produce similar results. However, at increasing depth or in very low porosity rocks when a vanishes and K approaches 2 the formulas differ by the pore pressure term which can be significant at great depth. For the purpose of applying these results to the Moodus stress measurements, laboratory measurements of α and K were made on a sample from a depth of 890 m and a sample from a depth of 108 m in the Kent Cliffs well. The results of these measurements are shown in Table I along with other key parameters. As shown in table II, the results of using the Schmitt and Zoback equation (equation (15) derived above) has only minor significance for the computed value of S_H for the single Moodus sample tested (with respect to the simple form of Haimson and Fairhurst (1967) (equation (1)) that is commonly used) because of it's relatively high a value (0.57). However, to be conservative, in Section III, we accomodate equation (15) by considering limiting values of 0 and 1 for α, which has the effect of reducing equation (15) to equation (1) without P_o, in the first case, and to exactly equation (1) in the second. Thus, in the absence of a knowing the elastic properties for all the Moodus test intervals, this adequately compensates for any uncertainty in the computed values of S_H caused by the elastic properties. As shown in Section III, this uncertainty is relatively small and does not seriously affect interpretation of the data.

Table I. Specific hydrofracture and rock properties for Moodus and Kent Cliffs Stress Measurement Experiments.

Location	Depth (m)	Reopening Pressure (bars)	Shut-in Pressure (bars)	Pore[a] Pressure (bars)	Lithostatic[b] Pressure (bars)	Biot[c] α	Poisson's[d] Ratio ν	Poroelastic Parameter K
Kent Cliffs	108	164	146	11	28	0.29	0.27	1.82
Moodus	890	286	291	87	321	0.57	0.25	1.62

(a) Estimated using rock density of 2.6 g/cm^3
(b) Estimated using water density of 1.0 g/cm^3
(c) Confining pressure is assumed to be the mean stress: $(S_H + S_h + S_V)/3$
(d) Poisson's ratio estimated from borehole sonic log compressional and shear velocity ratios of 1.80 (Kent Cliffs) and 1.74 (Moodus).

Table II. Comparison of published hydrofracture breakdown equations and results for Moodus and Kent Cliffs.

	Haimson & Fairhurst simple	Haimson & Fairhurst complete	Evans, Engelder & Plumb	Pine, Ledingham & Merrifield	Schmitt & Zoback
S_H =	$3S_h - P_R - P_P$	$3S_h - KP_R + (K-2)P_P$	$3S_h - P_R - \alpha P_P$	$3S_h - P_R$	$3S_h - (K + \alpha - 1)P_R + \alpha(K-2)P_P$
Kent Cliffs	263	138	271	274	255
Moodus	500	377	537	587	513

S_H : Greatest horizontal principal stress, S_h : Least horizontal principal stress, P_R : Reopening pressure, P_P : Pore pressure, K : Poroelastic parameter, α: Biot parameter. See Table 1 for values.

Section IX. References Cited in Text

Anderson, R.N. and M.D. Zoback, Did surface compression arrest propagation of rupture during the Oroville normal faulting earthquake?, in preparation, 1988.

Barosh, P.J., D. London, and J. de Boer, The structural geology of the Moodus seismic area, South Central Connecticut, , in New England Intercollegiate Geological Conference, 74th Annual Meeting, Guidebook for Fieldrtips in Connecticut and South Central Massachusetts,The University of Connecticut, Storrs, Connecticut, 419-451, 1982.

Bernabe, Y., & W.F. Brace, The effect of confining pressure and pore pressure on fracture and deformation of Berea sandstone, abstract in EOS, Trans. Amer. Geoph. Union, 68, pp. 1464, 1987.

Biot, M.A., and D.G. Willis, The elastic coefficients of the theory of consolidation, J. Appl. Mech., 78, 91-96, 1956.

Brace, W.F. and D.L. Kohlstedt, Limits on lithospheric stress imposed by laboratory experiments, Jour. Geophys. Res., 85, 6248-6252, 1980.

Bredehoeft, J.D., R.G. Wolff, W.S. Keys, and E. Shuter, Hydraulic fracturing to determine the regional in situ stress field, Piceance Basin, colorado, Geol. Soc. Am. Bull., 87, 250-258, 1976.

Brigham, W.T., Historical notes on the earthquakes of New England 1638-1869, Reprint from Boston Society of Natural History, Memoir 2, 1871.

Byerlee, J., Friction of rocks, Pure and Applied Geoph., 116, 615-629, 1978.

Coyner, K.B., Effects of stress, pore pressure, and pore fluids on bulk strain, velocity, and permeability in rocks, Ph.D. thesis, Massachusetts Institute of Technology, 361 p., 1984.

Corner, F.H., and B. Valette, In situ stress determination from hydraulic injection test data, J. Geoph. Res., 89, 527-537, 1984.

Dixon H.R. and L. W. Lundgren, Structure of Eastern Connecticut, in Studies of Appalachian Geology: Northern and Maritime,1968.

Ebel, J.E., V. Vudler, and M.Celata, The 1981 micorearthquake swarm near Moodus, Connecticut, Geoph. Res. Lett., 9, 397-400, 1982.

Engineers International, Report to Nuclear Regulatory Commission on Hydraulic Fracturing Stress Measurements in the Eastern U.S., Exact Ref. Unknown, 1986.

Evans, K.F., C.H. Scholz, and T. Engelder, An analysis of horizontal fracture

initiation during hydrofrac stress measurements in granite at North Conway, New Hampshire, Geoph. J. R. astr. Soc. in press, 1988.

Geertsma, J., The effect of fluid pressure decline on volumetric changes of porous rocks, Trans. AIME, 210, 331-340, 1957.

Gephart, J.W. and D.D. Forsyth, On the state of stress in New England as determined from earthquake focal mechanisms, Geology, 13, 70-76, 1985.

Gronseth, J.M., and P.R. Kry, Instantaneous shut-in pressure and its relationship to the minimum in-situ stress, in M.D. Zoback & B.C. Haimson, eds., Hydraulic Fracturing Stress Measurements, Proc. of a Workshop on Hydraulic Fracturing Stress Measurements, U.S. National Committee for Rock Mechanics, National Academy Press, 55-60, 1983.

Haimson, B.C., and C. Fairhurst, Initiation and extension of hydraulic fractures in rock, Soc. Petr. Engin. J., 310-318, 1967.

Healy, J.H. and M.D. Zoback, Hydraulic fracturing to 2.1 km depth at Cajon Pass, Ca., Geophys. Res. Lett.,in press., 1988.

Hickman, S.H., J.H. Healey and M.D. Zoback, In situ stress, natural fracture distribution, and borehole elongation in the Auburn geothermal well, Auburn, New York, J. Geophys. Res., 90, 5497-5512, 1985.

Hickman, S.H., & M.D. Zoback, The interpretation of hydraulic fracturing pressure-time data for in situ stress determinations, in M.D. Zoback and B.C. Haimson, eds., Hydraulic Fracturing Stress Measurements, Proc. of a Workshop on Hydraulic Fracturing Stress Measurements, U.S. National Committee for Rock Mechanics, National Academy Press,. 44-54, 1983.

Hubbert, M.K. & D.G. Willis, Mechanics of hydraulic fracturing, Trans. AIME, 210, 153-163, 1957.

Jeager, J.C. & N.G.W. Cook, Fundamentals of rock mechanics, Chapman and Hall, 1979.

Kirsch, G., Die theorie der elastizitat und die Dedurfnisse der fertigkeirslehre, Zeitschrift der Vereines Deutscher Ingenieure, 42, 797, 1898.

Lubinski, A., The theory of elasticity for porous bodies displaying a strong pore pressure, Proc. 2nd U.S. Natl. Cong. Appl. Mech., 247-256, 1954.

Nur, A. & J.D. Byerlee, An exact effective stress law for elastic deformation of rock with fluids, J.Geoph.Res., 76, 6414-6419, 1971.

Rummel, R., G. G. Mohring-Erdmann, and J. Baumgartner, Stress constraints and hydrofracturing stress data for the continental crust, Pure and Applied

Geoph., 124, 875-895, 1986.

Schoenfeldt, H., An experimental study of open hole hydraulic fracturing as a stress measurement methoed with particular emphasis on field tests, Ph.D. thesis, University of Minnesota, 1970.

Schmitt, D.R., and M.D. Zoback, The effect of an exact effective stress law on the hydrofracture breakdown equations, Submitted to Second International Workshop on Hydraulic Fracturing Stress Measurements, Minneapolis, Minnesota, 1988.

Stephannson, O. ed., Proc. of Intl. Symp. on Rock Stress and Rock Stress Measurements, Stockholm, 1-3 September, 1986, Centek Publ., Lulea, Sweden, 694 pp., 1986.

Stephannson, O., P. Sarkaa and O. Myrvang, State of stress in Fennoscandia, in Proc. of Intl. Symp. on Rock Stress and Rock Stress Measurements, Stockholm, 1-3 September, 1986, Centek Publ., Lulea, Sweden, 694 pp., 1986.

Terzaghi, K. Van, Die berechnung der durchassigkeitsziffer des tones aus dem verlauf der hydrodynamishchen spannungserscheinungun, Sitzungsber Akad. Wiss. Wein Math Nuturwiss. K. Abt. 2A. 132, 105, 1932.

Timoshenko, S.P., and J.N. Goodier, Theory of Elasticity, 3rd Edition, McGraw-Hill, N.Y., 1970.

Wintsch, R.P. and J.S. Fout, Structure and petrology of the Willimantic Dome and the Willimantic Fault, Eastern Connecticut, in New England Intercollegiate Geological Conference, 74th Annual Meeting, Guidebook for Fieldrtips in Connecticut and South Central Massachusetts,The University of Connecticut, Storrs, Connecticut, 419-451, 1982.

Voight, B. and B.H.P. St. Pierre, Stress history and rock stress, in Proc. Third Cong. Intern. Soc. Rock Mech., Denver, 2, 580-582, 1974.

Zemanek, J., E.E. Glen, Jr., L.J. Norton, and R.W. Caldwell, Formation evaluation by inspection with the borehole televiewer, Geophysics, 35, 254-269, 1970.

Zoback, M.D., High pressure deformation and fluid flow in sandstone, granite, and granular materials, Ph.D. thesis, Stanford University, 210 p. , 1975.

Zoback, M.D., D. Moos, L. Mastin, and R.N. Anderson, Well bore breakouts and in situ stress, J. Geophys. Res., 90, 5523-5530, 1985.

Zoback, M.D., and B.C. Haimson, eds., Workshop on hydraulic fracturing stress measurements, U.S. National Committee for Rock Mechanics, National

Academy Press, 44-54, 1983.

Zoback, M.D., and B.C. Haimson, Status of the hydraulic fracturing method for in situ stress measurements, in R.E. Goodman and F.E. Heuze, eds., Issues in Rock Mechanics, 23rd Symp. on Rock Mechanics, Soc. Mining Engineers, New York, 143-156, 1982.

Zoback, M.D. and S. Hickman, In situ study of the physical mechanisms controlling induced seismicity at Monticello Reservoir, South Carolina, Jour. Geophys. Res., 87, 6959-6974, 1982.

Zoback, M.L. and M.D. Zoback, Tectonic stress field of the continental U.S., in Geophysical Framework of the Continental United States, eds. L. Pakiser and W. Mooney, Geol. Soc. Amer. Mem., in press, 1988.

Appendix D

APPENDIX D

Results of the ultrasonic image and stonely wave surveys. Copies of the digital borehole televiewer logs are archived at Woodward-Clyde Consultants, Wayne, N.J.

In-Situ Stress Directions and Permeable Fractures in the Moodus#1 Well: Measurements From Experimental Ultrasonic Image and Stoneley Wave Logs

Draft Report
May 11, 1988

Prepared For
Woodward-Clyde Consultants
Wayne, NJ

Prepared by
Richard. A. Plumb
and
Brian Hornby

Schlumberger-Doll Research
Old Quarry Road
Ridgefield, Ct. 06877

In-Situ Stress Directions and Permeable Fractures in the Moodus #1 Well: Measurements From Experimental Ultrasonic Image and Stoneley Wave Logs

Richard A. Plumb and Brian Hornby

Schlumberger-Doll Research
Old Quarry Road
Ridgefield, CT 06877

Abstract

Schlumberger-Doll Research field tested two research logging tools in the Moodus#1 well. A digital ultrasonic imaging tool was used to map fracture location and orientation, and to determine in-situ stress directions. A digital array sonic tool was run to measure Stoneley wave reflection coefficients from permeable fractures intersecting the well.

The majority of breakouts measured in the Moodus well occur in the Avolonian rocks below the Honey Hill fault. The average azimuth of wellbore breakouts observed in the Moodus well is 346°-166° ± 6 indicating that the contemporary stress direction at Moodus is only slightly different than the mid-continent stress province. Thus we see only a small clockwise rotation of stress direction upon crossing this major tectonic boundary in eastern New England.

Two fracture populations were mapped, shallow dipping fractures (dips= 0°-10°) and steeply dipping fractures (dips = 80°-90°) striking NW. Shallow dipping fractures are consistent with the contemporary stress but the majority of steeply dipping fractures are inconsistent with origin under the contemporary stress field and may be of Mesozoic age. The orientation of a 0.3m thick fracture zone mapped at a depth of 840m could be a thrust fault under the contemporary state of stress.

Borehole Stoneley wave reflections identified in the Moodus well are correlated with the locations of fractures. The strongest reflections are observed from fractures located in zones where the drillers reported significant water influx. Among the known water producing fracture zones the ungrouted fractures produce the largest

reflections. Reflections are often observed at multiply intersecting fractures. In many cases intersecting fractures include shallow dipping fractures intersecting steeply dipping fractures. This geometry is favorable for a highly interconnected fracture network in the region surrounding the well. Permeable fractures and the existence of potential faults are significant tectonic factors consistent with the current seismic activity in the region.

Introduction

The Moodus #1 well was drilled by the Empire State Electric Energy Research Corporation.(ESEERCO) to better understand the state of stress in southern New England and in particular to understand the nature of the local seismicity known as the Moodus Noises. In-situ measurements of the contemporary stress directions and the location and distribution of permeable fractures in seismically active regions of New England are important for understanding the regional tectonic setting.

Studies of the state of stress in New England became more active with the development of nuclear power plants sited in zones of historic seismicity. Early studies of earthquake hazards in eastern North America relied upon earthquake fault plane solutions for clues about the orientation of active faults and the state of stress (Sbar and Sykes, 1973; Sbar and Sykes, 1977; Yang and Agarwal 1981). Seismologists suggested that the maximum horizontal stress was oriented SE-NW near the east coast of North America, but was oriented ENE-WSW in much of the mid-continent of North America. Zoback and Zoback (1980) drew a stress province boundary to the west of New England suggesting that New England was part of a different tectonic province. More recent studies based on in-situ stress measurements and higher quality earthquake fault plane solutions contradict those earlier findings and show instead that stress directions in New England are ENE similar to all mid-plate North America (Seborowski, 1982; Plumb et al., 1984; Gephart and Forsyth, 1985 ; Quittmeyer et al., 1985; Zoback et al., 1985; Evans et al., .1986; Plumb and Cox., 1987; Fang et al., 1988). Stress directions obtained from the Moodus well should help further refine the edge of the mid-continent stress province.

Permeable fractures play a critical role in the earthquake process (Raleigh et al., 1972; Agarwal et al.1975; Costain et al., 1987). However little information on the

geometry of fractures zones or permeability of those zones has been available near hypocentral depths of earthquakes. The nature of permeable fracture zones encountered in the Moodus well is therefore of considerable interest to ESEERCO and seismologists seeking an understanding of the earthquake hazards in New England.

The Moodus well was air drilled to a depth of approximately 1458 m into crystalline rocks of Paleozoic to Precambrian age (Figure 1). The formations and structures penetrated by the well are shown in Figure 2. A lithologic boundary tentatively identified as the Honey Hill fault was crossed at a depth of about 845m. Drillers identified two water producing zones at depths of about 185m and 1064m. Water influx at the deeper zone was great enough that the well had to be grouted from 1067 m to 914 m and redrilled (Naumoff personal communication, 1987).

Schlumberger-Doll Research field tested two research logging tools in the Moodus well on the weekend of July 25 1987. A digital ultrasonic imaging tool was used to map fracture location and orientation, and to determine in-situ stress directions. A digital array sonic tool was run to measure Stoneley wave reflection coefficients from permeable fractures intersecting the well. In the following report we present results of a reconnaissance mapping of the fracture system and wellbore breakouts and a preliminary evaluation of the two water producing fracture zones.

Ultrasonic Imaging

Ultrasonic images of the Moodus well were acquired by a research ultrasonic logging tool based on the borehole televiewer (BHTV) concept developed by Mobil Oil Company. (Zemanek and Caldwell, 1969). Our tool differs from the conventional BHTV in the design of the ultrasonics assembly and the data acquisition electronics. The ultrasonic imaging sonde contains two transducers diametrically opposed on a rotating assembly. Resonant frequencies of the transducers are about 400 kHz and 1.3 mHz. The ultrasonic assembly rotates at a rate of three revolutions per second and one of the two selectable transducers is pulsed 250 times per rotation. Each pulse travels through the borehole fluids and is reflected off the wellbore surface. The tool measures the peak reflected amplitude and the two-way transit time of each ultrasonic pulse using a down-hole digitizer. These two measurements are then transmitted via a standard telemetry cartridge to the logging truck computer. The new

ultrasonics assembly tested in the Moodus well provides a more robust measurement of transit time and amplitude particularly when the tool is eccentered or in a rugose hole for example when logging through breakouts.

Full coverage (360°) images of the wellbore surface are created from the digital amplitude and transit time data by transforming signal strength into a gray scale. Each image pixel on Moodus images spans 2.1mm circumferentially and 7.6 mm axially along the wellbore surface. The axial resolution is controlled by the logging rate of the tool which is about 3 cm/s. The azimuthal position of the active transducer is determined by a flux-gate magnetometer attached to the rotating assembly. To ensure proper orientation of the images the magnetometer is calibrated on site before logging (Appendix 1). The orientation and location of fractures, metamorphic structures and wellbore breakouts are obtained using an interactive computer graphics techniques described in Plumb and Luthi (1986). Ultrasonic images were acquired continuously from 1458m to 182m and also from 122m to about 75m. Interpretations of ultrasonic signals and images presented in this report are all based upon data acquired with the 400 KHz. transducer (Figure 3).

Stoneley Wave Logging

A research array sonic log (DWST) was run in the Moodus well to evaluate the characteristics of Stoneley waves reflected from known water producing fracture zones. The DSWT has an array of sixteen matched receivers and three selectable source excitation functions. For fracture characterization the tool is logged using a low frequency source and data are digitally recorded across the receiver array for 25 ms or more. The low frequency source excites a Stoneley wave with significant energy below 1000 hertz and the long acquisition time provides a strong reflected Stoneley wave signal without direct headwave interference.

Borehole Stoneley waves are dispersive waves that propagate along the fluid solid interface in the well. The lowest order Stoneley mode, also known as a tube wave, propagates like a pressure pulse in the borehole fluid. When the pressure pulse encounters a permeable region on the wellbore surface such as an open fracture part of the Stoneley energy is reflected and part is transmitted across the fracture. Transmitted and reflected Stoneley wave energy is being evaluated as a means of quantifying the flow properties of fractures (Hsu et al., 1986; Paillet et al , 1986;

Harding et al., 1987; Hornby et al., 1988). Theory and laboratory experiments developed to interpret the reflected Stoneley wave response show that the amplitude of the reflected Stoneley wave is related to the aperture of isolated fractures or in the case of multiple intersecting fractures the magnitude of the response is related to the total cross-sectional area of permeable fractures (Hornby et al., 1988).

Stoneley wave analyses discussed in this report pertain to three zones centered at depths of 105m, 185m and 1067m. The shallow zone contained a fracture that was reported to be impermeable during a straddle packer injection test (Statton personal communication; 1987). The zones located at 185m and 1064m are sites of water influx reported by the drillers (Naumoff personal communication; 1987).

Results

Wellbore Breakouts

Wellbore breakouts have been mapped over the depth range 306m to 1438m (Plumb et al., 1988). The depth distribution of the center azimuths of breakouts sampled at 30 cm intervals is shown in Figure 4. The majority of breakouts are located below the Honey Hill fault. (Figure 2) The frequency of breakout occurrence and the degree of azimuth clustering of breakout centers varies with depth. Above the Honey Hill fault breakouts are few and breakout azimuths are more widely scattered. Below the fault the scatter in breakout azimuth is reduced but a distinct zone from 1067m to 1175m appears systematically rotated with respect to the average breakout direction in adjacent zones. In several locations the breakout azimuth rotates within 2-3 meters of shallow dipping fractures suggesting that some sort of stress redistribution has occurred near these fractures (Figure 5).

The mean breakout azimuths computed over the entire well are 346° and 166° with a standard deviation of 5.5° and circular variance of .018. This indicates that the average directions for the minimum and maximum horizontal stress are 346°-166° and 76°-256° respectively. Breakout azimuth data indicate that the contemporary stress direction at Moodus is slightly rotated from to the mid-continent stress province. This result is consistent with other breakout data published for eastern North America including a recent study of a well located on Cape Ann Massachusetts (Figure 1).(Plumb and Cox, 1987; Fang et al., 1988)

Fracture Patterns

A reconnaissance study of the fractures imaged by the ultrasonic scanner indicate that

fracture dips are bimodally distributed with peaks at 0°-10 °and 80°-90° degrees (Figure 6). Shallow dipping planes probably include measurements on foliation planes that have been activated as slip surfaces (Chen and de Boer, 1988). Strikes of steeply dipping fractures show a single preferred orientation of N 45 W (Figure 7). The distribution of fractures with depth and shows several zones of high fracture intensity.(Figure 8).

The preferred strike of steeply dipping fractures is not consistent with fracture patterns expected from the contemporary stress. This preferred orientation is more readily explained as developing during Mesozoic time (de Boer personal communication). Analysis of fractures in outcrops near Moodus may help resolve this question.

Some fractures are consistent with the contemporary stress field. A particularly interesting structure is located at a depth of 840m (Figure 9). A 0.3 meter thick fracture zone is mapped which is oriented (37°, 090°) (dip angle, dip azimuth). Adjacent breakouts indicate that the azimuth of maximum compression is 085°-265° Thus this fracture-stress relationship is exactly what one expects for contemporary thrust faults. Recent seismic activity at Moodus is consistent with this result (Mrotek et al.,1988). This is an exciting result since to our knowledge no faults have been identified in New England which are capable of releasing stress associated with observed ENE-WSW maximum compressive stress. Fault plane solutions of recent earthquakes indicate that high angle reverse faulting may be occurring on steeply dipping N-S striking faults (Quittmeyer personal communication, 1988). This observation suggests that field mapping efforts to locate analogous structures should concentrate on shallow and steeply dipping structures striking about North-South. It is interesting to note that geomorphology in this region suggests the influence of a N-S rock fabric, such as the trend of Pickeral Lake and the course of the Salmon River. The N-S trend may reflect the geomorphologic expression of the contemporary stress. Plumb et al., (1984) noticed a similar geomorphologic expression of the contemporary stress near Blue Mountain Lake New York.

Stoneley Wave Analysis of Fractures

Strong Stoneley wave reflections were generated at the two water producing zones located at 185m and 1064m but no measurable reflections were detected from the impermeable fracture located at 105m. Processing techniques used in our Stoneley

wave analysis do not permit evaluation of single fractures with apertures less than about 200 microns. Therefore the lack of reflection from an isolated fracture only means that it has an aperture less than our detection level. Unfortunately the detection level for permeable fractures is not optimal in the Moodus well because of a problem with the down-hole waveform digitizer. As a result the noise level in the data correspond to a reflection coefficient of 0.008 or an effective aperture of about 500 microns. The noise limited our precision for quantifying effective fracture apertures but did not prevent our detection of water producing fracture zones. Some weak reflections observed in the Moodus well,but not shown, may be attributed to processing noise as discussed above or to borehole rugosity.

Fracture at 105m: Image analysis indicates that an isolated fracture located at 105m is oriented (68° 146°). The lack of Stoneley wave reflection indicates that the has very low permeability (Figure 10). The impermeable nature of the fracture is suggested by the fact that fluids could not be injected into the fracture under high pressure during an attempted hydrofracture stress test (Statton personal communication).

Fracture zone at 185m: The upper permeable zone identified by drillers at a depth of approximately 185m consists of at least 7 intersecting fractures (Figure 11). It is clear from the amplitude and transit time images that there are many more short non-planar fractures in this zone which are impractical to map. Fractures mapped between 186 m and 188 m, strike between ENE and SSW with dips ranging from 4 to 65 degrees. The geometry of this interval indicates that the fractures are highly interconnected.

In this example the Stoneley wave responds to the ensemble of fractures producing a reflection coefficient of 0.224. Theoretically this reflection coefficient would be observed from a single fracture whose hydraulic aperture is 3.5mm. Since the total flow area is distributed among several fractures and since permeability varies as the square of fracture aperture the permeability of this fracture zone will be less than that of a 3.5mm aperture fracture.

Fracture zone at 1057m: The deepest fracture zone probed by the Stoneley wave is located between 1057 m and 1072 m. This zone consists of NNW striking fractures dipping from 15 to 30 degrees toward the ENE intersected by WSW-ENE striking

fractures dipping 45 to 75 degrees toward NNW and SSE. Again we see a fracture system that is highly interconnected (Figure 12).

Five large Stoneley wave reflections are observed in this interval. The strongest reflector is number 5 located at about 1070m (3512'). Image analysis shows this reflector to be a fracture oriented (29, 342) the reflection coefficient is .06. Four weaker reflectors are located between 1057 m and 1068m. In general each reflection is associated with multiple intersecting fractures (Figure 12). The weaker reflections are observed from the interval that was grouted and redrilled. The stronger reflection is observed from a section of the well that was not grouted. Thus it appears that even though the fractures have been grouted their permeability was not completely eliminated.

Summary

Stress Directions:

The average azimuth of wellbore breakouts observed in the Moodus well indicates that the contemporary stress direction at Moodus is similar to the mid-continent stress province. This result is consistent with other breakout data published for eastern North America including a recent study of the Peter Britton #3 well located on Cape Ann Massachusetts (Plumb and Cox; 1987; Fang et al., 1988) (Figure 1). All breakouts measured in the Peter Britton #3 well occur in Avalonian rocks as do the majority of breakouts measured in the Moodus. Thus we see only a small clockwise rotation of stress direction upon crossing (entering?) this major tectonic boundary in eastern New England.

Fractures:

The majority of steeply dipping fractures are inconsistent with origin under the contemporary stress field. For a thrust faulting environment we would expect steeply dipping compression and release fractures to be oriented parallel and perpendicular to the maximum compressive stress, however these fractures are not prominent on our images. We can only conclude that the observed fractures originated under a different state of stress perhaps the one existing during Mesozoic.time (Chen and de Boer 1988).

Shallow dipping fractures are consistent with the contemporary stress. Statistically the horizontal fractures dominate the fracture population (Figure 6). Under the contemporary stress we would expect to find nearly horizontal compression fractures and perhaps shear fractures which dip between 20-40 degrees toward the East or West. Core analysis form a nearby well indicates that many subhorizontal surfaces have been active slip surfaces associated with NW tectonic transport (Chen and de Boer, 1988). Regional structural analysis suggests that this may have occurred during late Permian time.

Occasionally fractures oriented as potential shear planes are also observed (Figure 9). The existence of such favorably oriented surfaces does not mean that we intersected "an active fault" it only shows that such surfaces can be expected in the region. Analogous structures should be searched for in outcrops. A structure with a similar appearance seen on the ultrasonic images identified in the the Peter Britton #3

well is also correlated with the orientation of nearby faults (Fang et al., 1988). It is significant that potentially active faults have been observed in images from both the Moodus and in Peter Britton#3 wells. The Moodus structure may be associated with the contemporary stress but that the structure in Peter Britton #3 may be a suitably oriented preexisting structure

Borehole Stoneley wave reflections identified in the Moodus well are correlated with the locations of fractures. The strongest reflections are observed from fractures located in zones where the drillers reported significant water influx. Among the known water producing fracture zones the ungrouted fractures produce the larger reflections. We note that when reflections are observed there often is more than one fracture intersecting the well. In many cases intersecting fractures include shallow dipping fractures intersecting steeply dipping fractures. This geometry is favorable for a highly interconnected fracture network in the region surrounding the well. This high fracture connectivity indicates a potential for significant fracture system permeability (cf. Long and Witherspoon, 1985).

Our logs have shown that the Moodus well has intersected connected permeable fractures and a potentially active trust fault. Connected permeable fractures and the existence of potentially active faults are significant tectonic factors consistent with the current seismic activity in the region.

References

Aggarwal, Y. P., L. R. Sykes , D. W. Simpson, and P. G. Richards, Spatial and temporal variations in ts/tp and Pwave residuals at Blue Mountain Lake , New York: Application to earthquake prediction, J. Geophys. Res., 80, 718-732, 1975.

Chen Y-h, and J. Z. de Boer, Neotectonic deformation in the Honey Hill fault zone (Ct) by reactivation of Mesozoic normal faults, EOS, Trans AGU, 69, 491, 1988.

Costain, J. K., G.A. Bollinger and J. A. Speer, Hydroseismicity-A hypothesis for the role of water in the generation of intraplate seismicity, Geology,15, 618-621, 1987.

Evans, K., C. Scholz and T. Engelder, Horizontal fracturing during hyrofracture stress measurements in Conway granite, EOS Trans AGU, 67, 1206-1207, 1986.

Fang W., J. de Boer, R. A. Plumb, F. L. Paillet and P. Britton, Wellbore breakouts and Fracture Orientation: Cape Ann Massachusetts, EOS Trans AGU, 69, 492, 1988.

Gephart , J. W., and D. D. Forsyth, On the state of stress in New England as determined from earthquake focal mechanisms, Geology, 13, 70-72, 1885.

Hardin, E. L., C. H. Cheng, F. L. Paillet, and J. D. Mendelson, Fracture Characterization by means of attenuation and generation of tubewaves in fractured crystalline rock at Mirror Lake, New Hampshire, J. Geophys. Res., 92, 7989-8006, 1987.

Hornby, B. E., D. L. Johnson, K. W. Winkler, and R. A. Plumb, Fracture evaluation from the borehole Stoneley wave, Geophysics (in press).

Hsu, K., A. Brie, and R. A Plumb A new method for fracture identification using array sonic tools, Jour. Petroleum Technology, 677-683, 1987.

Long, C. S. and P. A. Witherspoon, The relationship of the degree of interconnection to permeability in fracture networks, J. Geophys. Res., 90, 3087-3098, 1985.

Mrotek, K., A., R.C. Quittmeyer, P. G. Naumoff and C. T. Statton, Observations of the earthquake swarm near Moodus Connecticut: September/October 1987, EOS, Trans AGU, 69, 16, p. 495, 1988.

Paillet F. L., C. H. Cheng, A. E. Hess, and E. L. Hardin, Comparison of fracture permeability estimates based on tube-wave generation in vertical seismic profiles, acoustic waveform-log attenuation, and pumping-test analysis, Transactions National Water Well Association Conference on Geophysics and Groundwater Instrumentation; Denver, pp. 18, October, 1986.

Plumb, R. A. , T. Engelder and M. Sbar, Near surface in-situ stress 2 . A comparison with stress directions inferred from earthquakes, joints, and topography near Blue Mountain Lake New York, J. Geophys. Res., 89, p. 9333-9349, 1984.

Plumb, R. A., T. Engelder and D. Yale, Near surface in-situ stress 3. Correlation with microcrack fabric within the New Hampshire Granites, J. Geophys Res.,89, p. 9350 -9364, 1984.

Plumb R.A., and S. M Luthi, Application of borehole images to geologic modeling of an eolian reservoir, Society of Petroleum Engineers, Paper #15487, 61st Annual Fall Technical Conference , New Orleans, LA, October 5-8, 1986, pp.11, (in press Formation Evaluation).

Plumb, R. A. , and J. W. Cox, Stress directions in eastern North America determined to 4.5 km from borehole elongation measurements, J. Geophys Res., 92, p 4805-4816, 1987.

Plumb, R. A., W. Fang, and J. de Boer, Preliminary wellbore breakout and fracture Orientations in the Moodus #1 well, EOS Trans AGU, 69, p. 492, 1988.

Quarrier, S., Moodus deep drill hole: News Note #6, Connecticut Geological and Natural History Survey Natural Resources Center News Note, n6, pp.2, June 23, 1987.

Quittmeyer, R. C., C. T. Statton, K. A. Mrotek, and M. Houlday, Possible implications of recent microearthquakes in southeastern New York State, Earthquake Notes, 56, 35-42, 1985.

Raleigh , C. B., J. H. Healy and J. D. Bredehoeft, Faulting and crustal stress at Rangely Colorado, in Flow and Fracture of Rocks, Geophys. Monogr. Ser., v,. 16, edited by H. C. Heard, I. Y. Borg, N. L. Carter and C. B. Raleigh, pp275-284, AGU, Washington D.C., 1972.

Sbar, M. L., and L. R. Sykes, Contemporary compressive stress and seismicity in eastern North America : An example of intra-plate tectonics, Geol. Soc. Am. Bull., 84, 1864-1882, 1973.

Sbar, M. L., and L. R. Sykes, Seismicity and lithospheric stress in New York and adjacent areas, J. Geophys. Res, 82, 5771-5786, 1977.

Seborowski, K. D., G. Williams, J. Kelleher, and C. T. Statton, Tectonic implications of recent earthquakes near Annsville, New York, Bull. Seismol. Soc. Am., &2, 1601-1609, 1982.

Wintsch, R. P., and J. N. Aleinikoff, U-Pb Isotopic and geologic evidence for late Paleozoic anatexis, deformation, and accretion of the late Proterozoic Avalon terrain southcentral Connecticut, Am. Jour. Sci., 287, 107-126, 1987.

Yang , J-P., and Y. P. Aggarwal, Seismotectonics of northeastern United States and adjacent Canada, J. Geophys. Res, 86, 4981-4998, 1981.

Zemanek, J., and R. L. Caldwell, The borehole televiewer- A new logging concept fro Fracture location and other types of borehole inspection, J. Pet. Tech., 25, 762-774, 1969.

Zoback, M. L. and M. D. Zoback, State of stress in the coterminous United States, J. Geophys. Res., 85, 6113-6156, 1980.

Zoback, M. D., R. N. Anderson, and D. Moos, In-situ stress measurements in a 1 km deep well near the Ramapo fault zone, EOS, Trans AGU, 66, 363, 1985.

Appendix 1:
BHTV Calibration

Field Calibration:

Field and laboratory calibration of the Schlumberger BHTV is done with the BHTV sonde disconnected from its electronics and telemetry cartridges Figure A1). Typically the BHTV sonde containing the ultrasonic assembly is positioned vertically and connected by a cable to the electronics which are positioned horizontally about two feet from the sonde. To establish the value of CROT we place the BHTV sonde inside a tank containing a target that we align to magnetic north (CROT is a computer program variable used to correct image orientations) . The target is a ridge about 0.125" wide on the inside of the test tank that is easily imaged using our transit time waveforms. At Moodus, we placed a marker about 60' from the BHTV sonde such that a line connecting the sonde and the marker is oriented magnetic north. The tool is then powered up and the transit time waveforms are monitored on the computer. If the transducers are exactly aligned with respect to the magnetometer the target ridge appears split between the right- and left-end of the transit time waveform.indicating CROT = 0 and If not the value of CROT is determined which will produce the correct orientation of the target on the image. The accuracy of BHTV image orientations is determined by how well we can realign our target to magnetic north. We estimate our accuracy to be about 1°. Field calibration at Moodus gave a value of 10.7° for CROT. That is, the ridge appeared on the waveforms at an apparent azimuth of 349.3° Therefore our image must be rotated + 10.7° to bring the ridge to its correct position. This is the value of CROT that was applied to field prints provided at the wellsite. Thus the field prints are calibrated to magnetic North. Computer processed data presented in this report have been corrected (-15°) for magnetic declination

Shop Calibration

Because orientation was critical for the scientific results at Moodus we have performed several additional tests of our BHTV calibration procedure at Tyller Texas After leaving Moodus we took the tool to Tyler Texas for another logging job. The Schlumberger shop at Tyler has an aluminum tower that enabled us to calibrate the tool in its fully assembled logging configuration. Three repeat calibrations indicated that the orientation of the north target was positioned 3.8° further west than determined by our field calibration procedure. Thus we appear to have found a systematic error in our value of CROT used at Moodus. Assuming that the fully

assembled configuration provides the best value for CROT, the revised value is 10.7° + 3.8° = 14.5 °. Applying this correction will have the effect of shifting objects 3.8° clockwise from the position displayed on our field prints. This correction was applied to images delivered to Tom Statton.in the fall of 1987.

At the Tyler shop we also performed a series of tests to determine whether the position of the electronics cartridges had any effect on the field calibration results. Following the normal field calibration procedure we sighted our target on magnetic north and viewed the position of target with the electronics cartridges placed at three different bearings; 076°, 135°, and 245° with respect to the sonde. If the position of the electronics has an influence on the calibration, then the position of north target would shift as we moved the electronics. In each test configuration, we observed the target with the high frequency and low frequency transducer giving a total of six measurements. We found no systematic shift in the position of the target. The standard deviation of the six different determinations of magnetic north was 1.39°. This difference is only slightly different from the magnetometer triggering uncertainty which has a standard deviation of 0.97°. Thus we find no more than a 0.5° error associated with the placement of our electronics cartridge during our field calibration procedure.

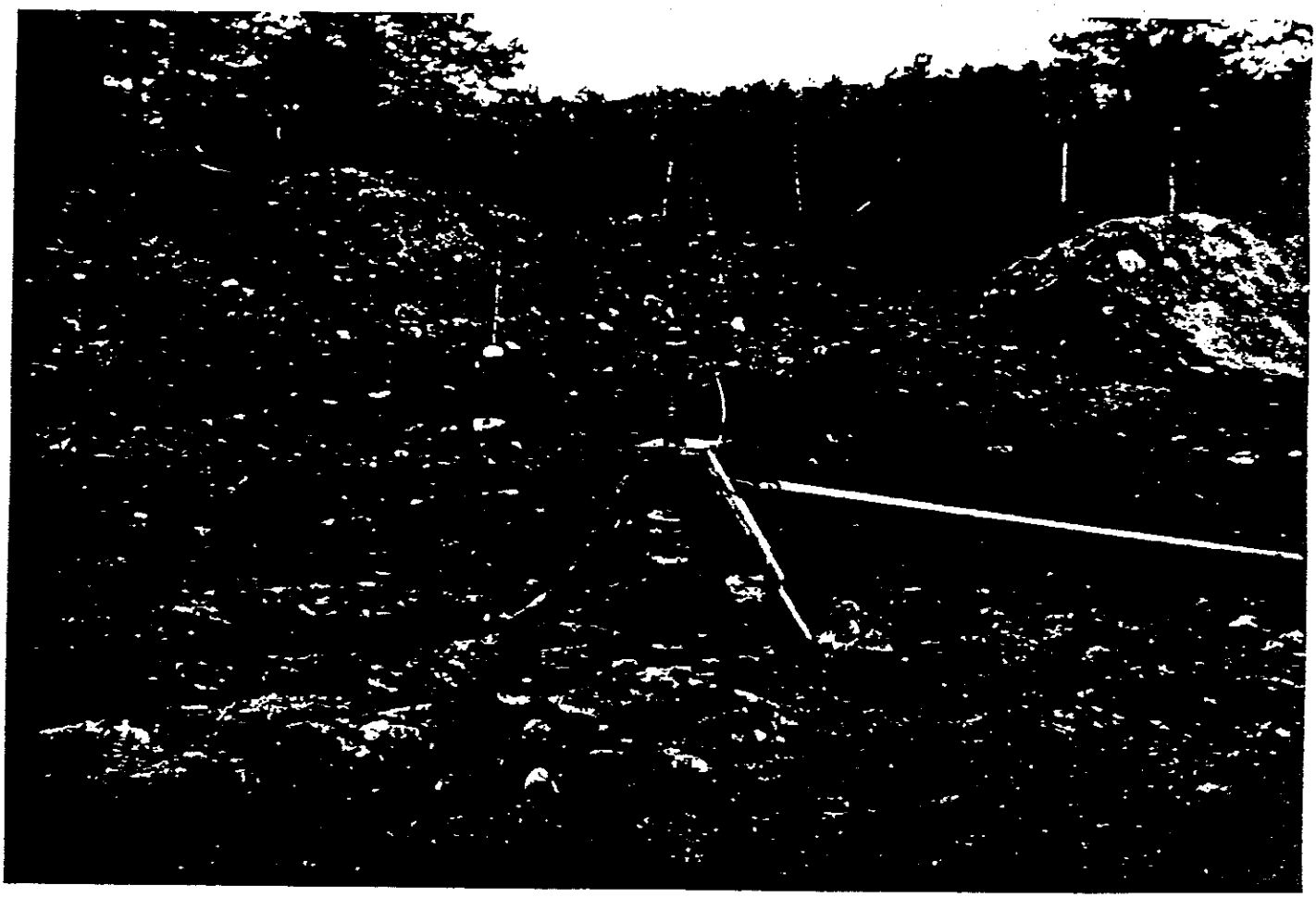

Figure Captions

Figure 1: Location of the Moodus Well.

Figure 2: Stratigraphy penetrated by the Moodus well.after Quarrier, (1987)

Figure 3: BHTV Amplitude image showing vertical fractures (3a) and dipping fractures and breakouts (3b).

Figure 4: Breakout azimuth vs depth in the Moodus well.

Figure 5: Example of breakout rotation near a sub-horizontal fracture

Figure 6: Histogram of fracture dip angle.

Figure 7: Rose diagram of fracture strikes (dips greater than 10 degrees).

Figure 8: Depth distribution of fractures.

Figure 9: Example of a potentially active thrust fault .

Figure 10: Absence of a Stoneley wave response to the fracture located at 105m (10a). Image of the fracture and lower hemisphere stereographic projection of the fracture (10b).

Figure 11: Stoneley wave response to fracture s located between 185m-188m(11a). Image of the fracture zone and lower hemisphere stereographic projection of the fractures (11b).

Figure 12: Stoneley wave response to fractures located between 1057m and 1072m.(12a). Images of the fractures correlated with reflectors 2-5 (12b) and lower hemisphere stereographic projections of each reflecting fracture zone (12c).

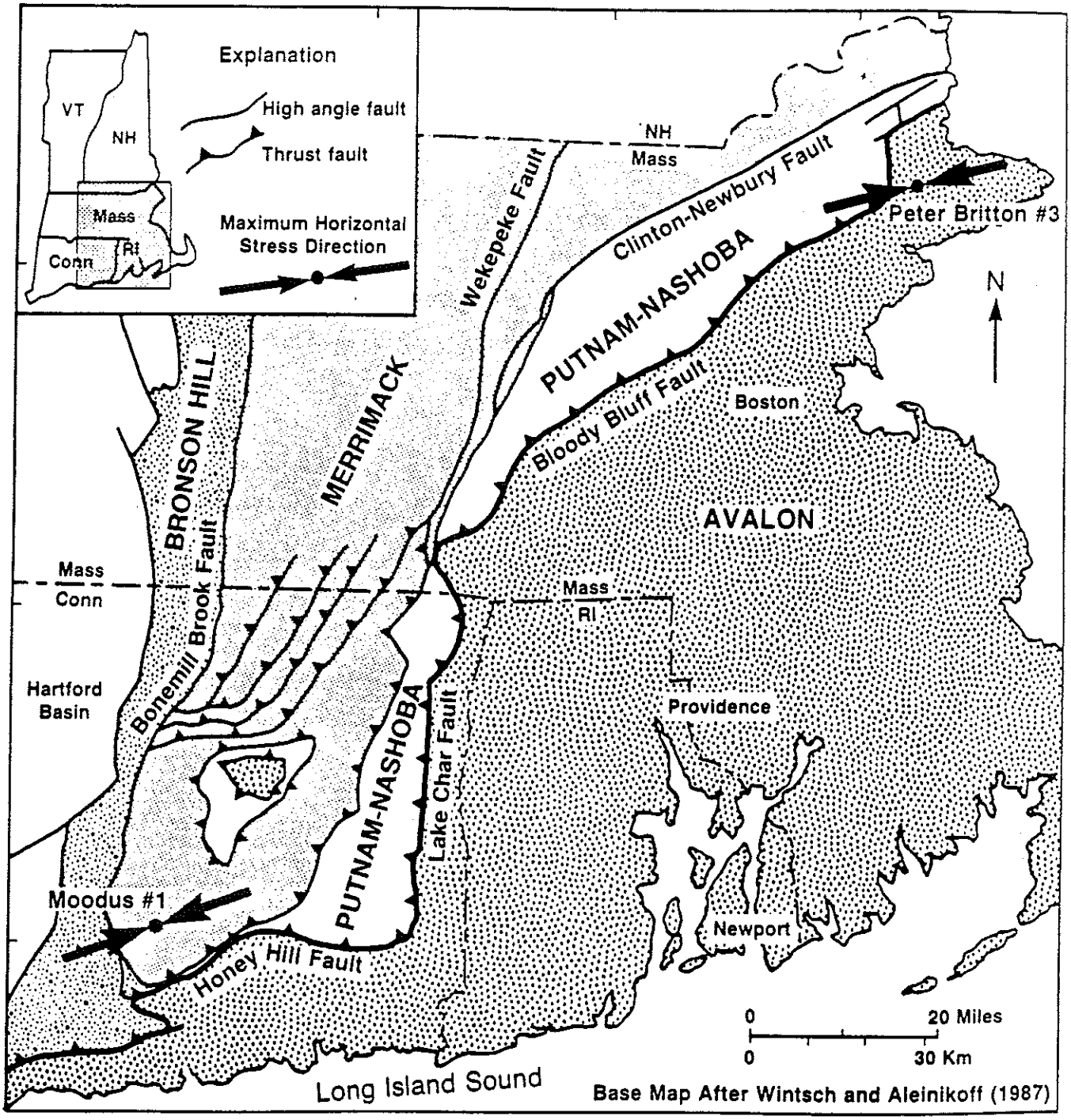
Explanation
High angle fault
Thrust fault
Maximum Horizontal Stress Direction
VT
NH
Mass
Conn
RI
NH
Mass
Wekepeke Fault
Clinton-Newbury Fault
Peter Britton #3
PUTNAM-NASHOBA
Bloody Bluff Fault
Boston
N
BRONSON HILL
Bonemill Brook Fault
MERRIMACK
AVALON
Mass
Conn
Mass
RI
Hartford Basin
Providence
PUTNAM-NASHOBA
Lake Char Fault
Moodus #1
Honey Hill Fault
Newport
0
20 Miles
0
30 Km
Long Island Sound
Base Map After Wintsch and Aleinikoff (1987)

Figure 1

Summary Log of the Moodus well

(after Quarrier, 1987)

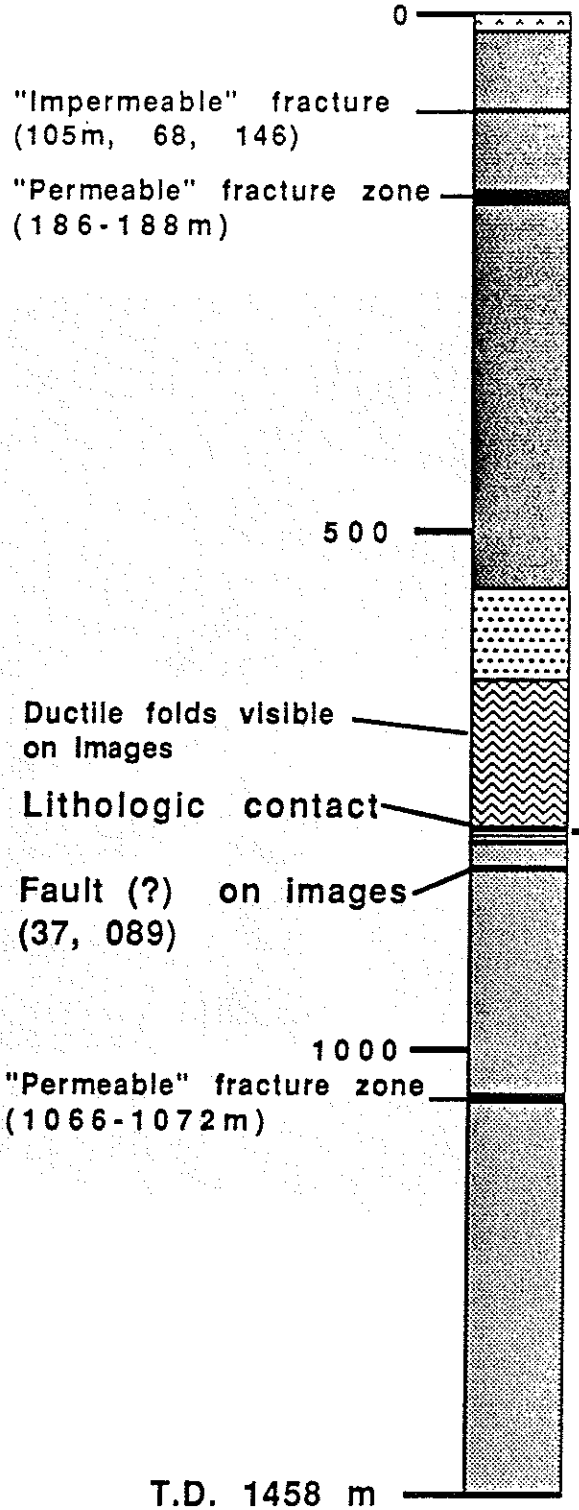

overburden

Hebron Gneiss (SOh)

clinopyroxene- (biotite/phlogopite) gneisses and schists

Canterbury Gneiss (?) (Dc)

biotite-garnet granitic gneiss

Tatnic Hill Formation (?) (Ota)

biotite (muscovite) gneiss and schists

Honey Hill Fault (?)

Waterford Group (?) (Zw)

grayish-white biotite-amphibolite-plagioclase-rich gneiss

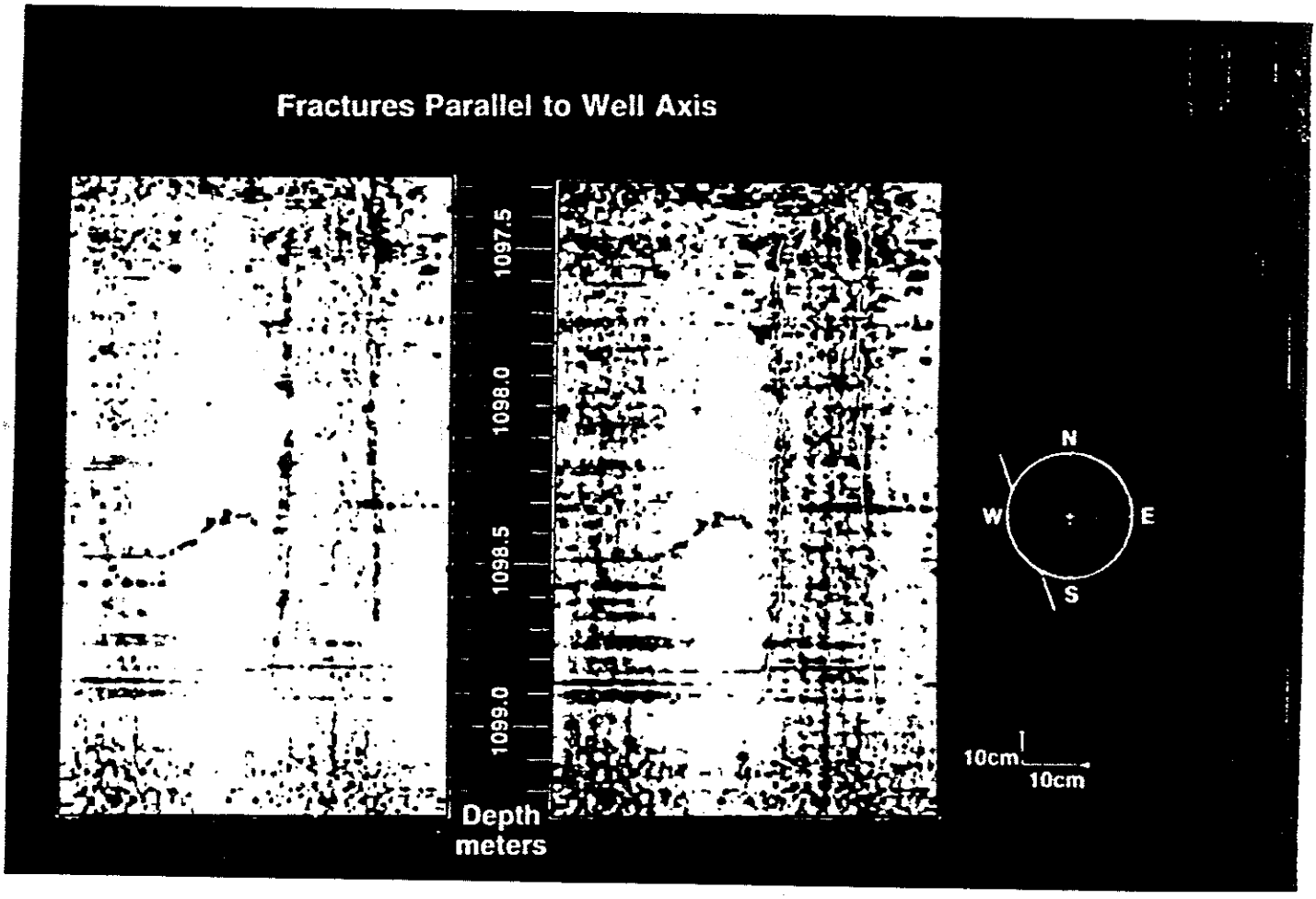
Fractures Parallel to Well Axis
1097.5
1098.0
1098.5
1099.0
Depth
meters
N
W
E
S
10cm
10cm

Fractures Inclined to Axis
1149.0
1150.0
1150.5

BREAKOUT AZIMUTH
MOODUS #1

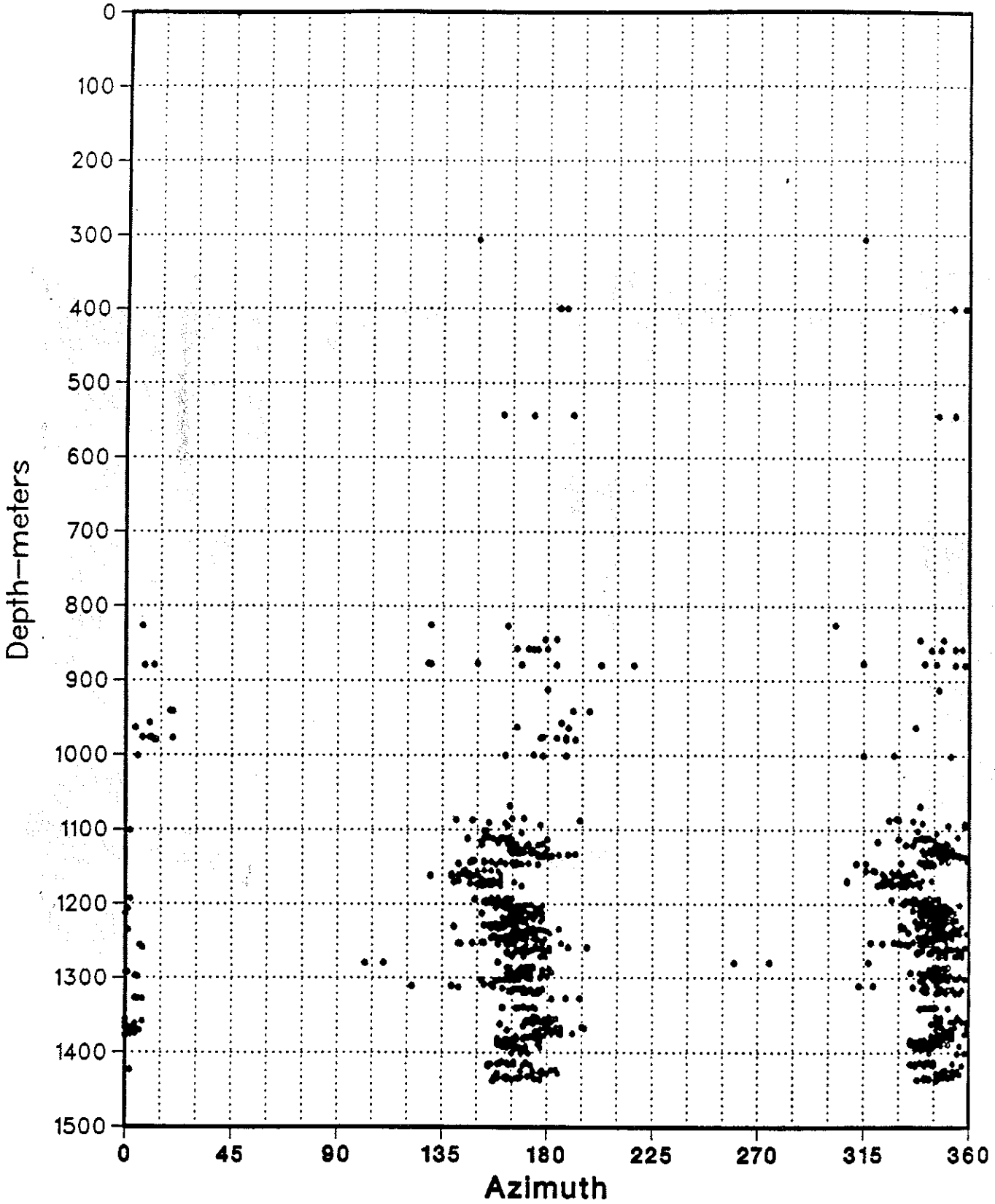

Circular Mean Breakout Azimuth = 346-166; Circ. Var. = .018; Stdv. = 5.5
Minimum Stress Azimuth = 346-166; Maximum Stress Azimuth = 76-256

RAP/SDR/4-19-88

Breakout Rotation

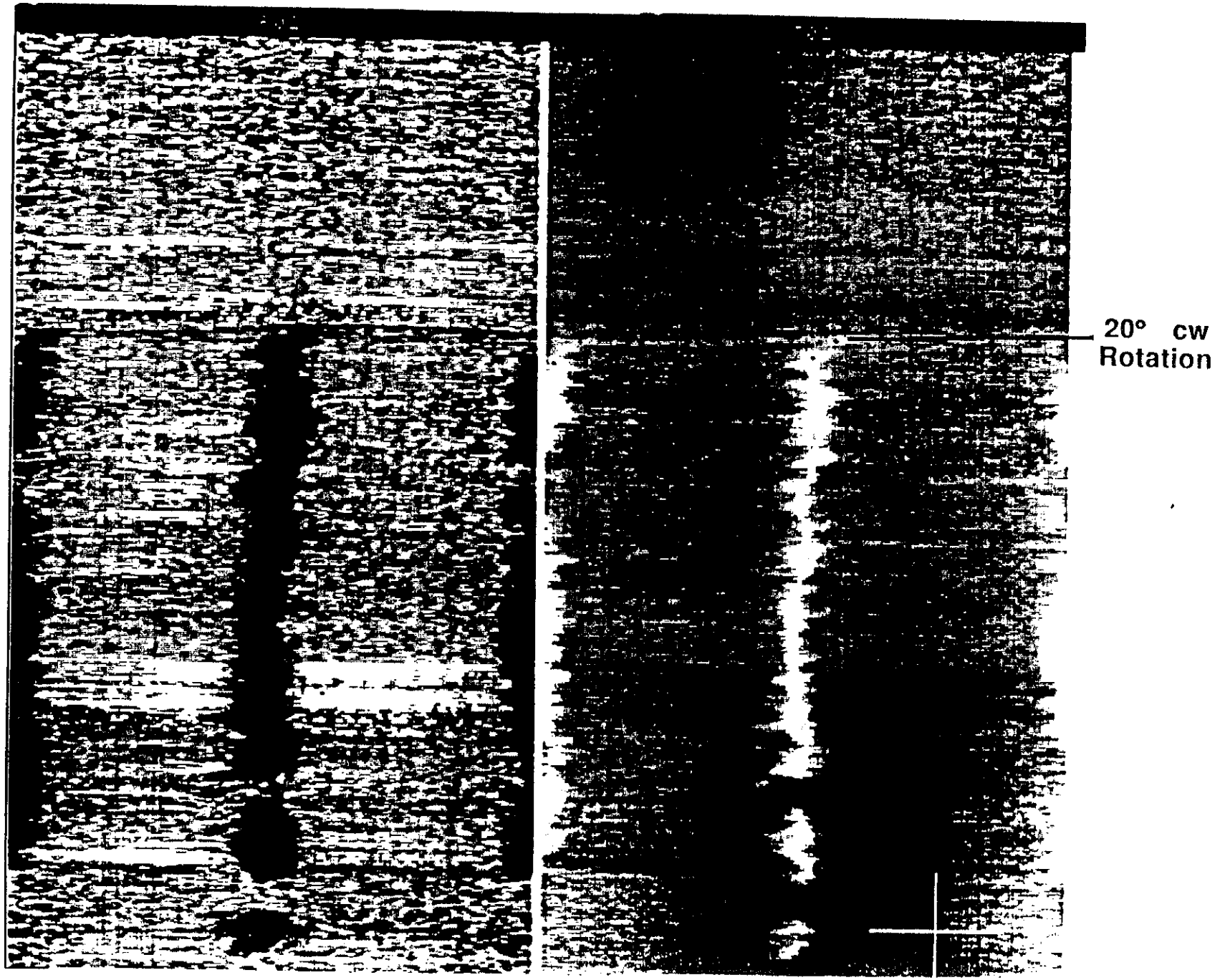

Preliminary Dip Distribution
Moodus#1

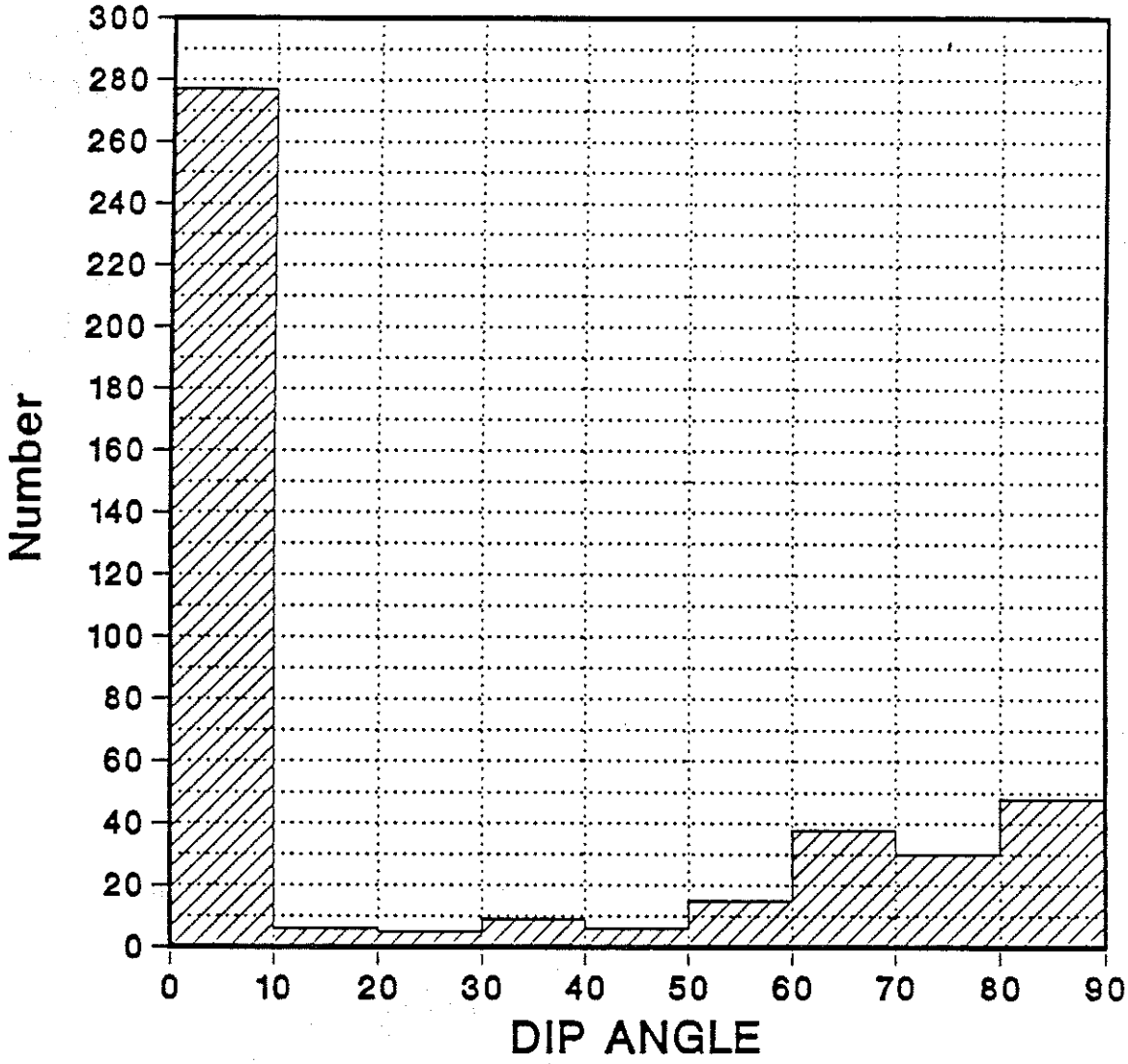

Fig 6

Fracture Strikes
Moodus #1

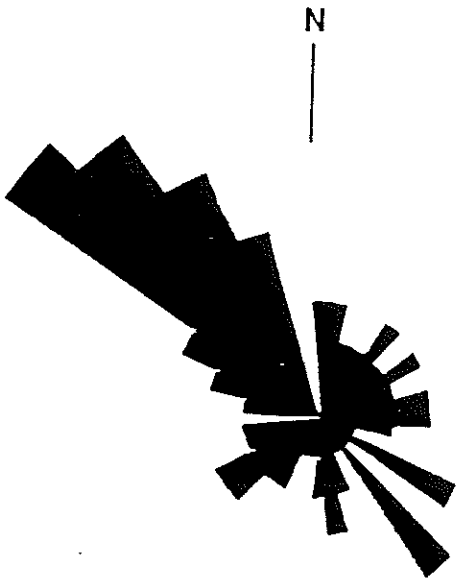

Fig 7

Distribution of the Fractures in Moodus #1 Hole

Histogram of Depth of All Fractures, N = 421
Increment = 40 Meters

Depth Midpoint (Meters)	Fracture Count (Obs.)	
80.0	3	***
120.0	1	*
160.0	0	
200.0	7	*******
240.0	3	***
280.0	5	*****
320.0	13	*************
360.0	7	*******
400.0	47	**
440.0	15	***************
480.0	15	***************
520.0	18	******************
560.0	8	********
600.0	17	*****************
640.0	20	********************
680.0	17	*****************
720.0	28	****************************
760.0	7	*******
800.0	11	***********
840.0	8	********
880.0	10	**********
920.0	6	******
960.0	15	***************
1000.0	23	************************
1040.0	17	*****************
1080.0	31	********************************
1120.0	13	*************
1160.0	15	***************
1200.0	17	*****************
1240.0	4	****
1280.0	13	*************
1320.0	7	*******
1360.0	2	**
1400.0	5	*****

Thrust Fault ?

Fault ?
(37,089)

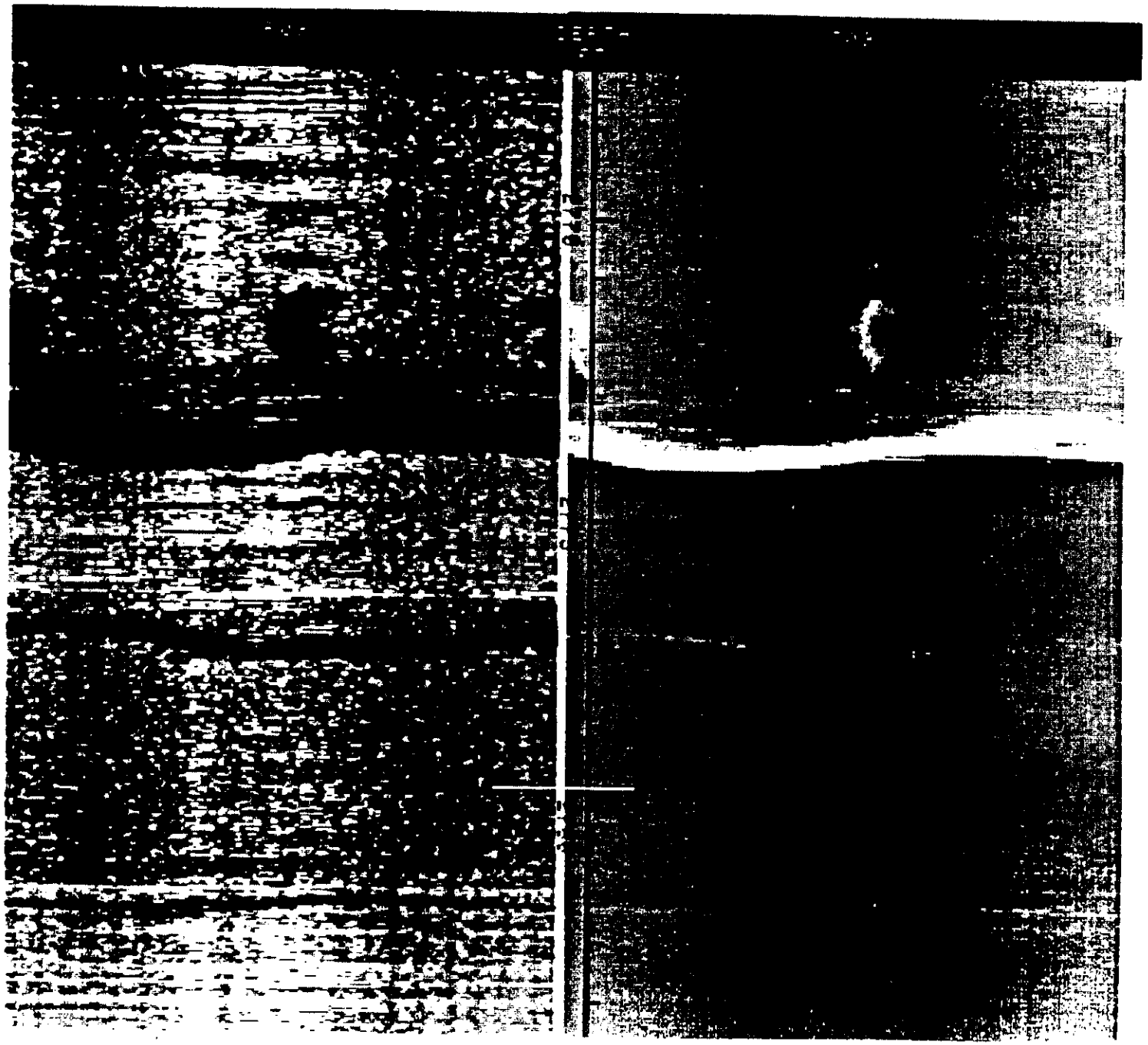

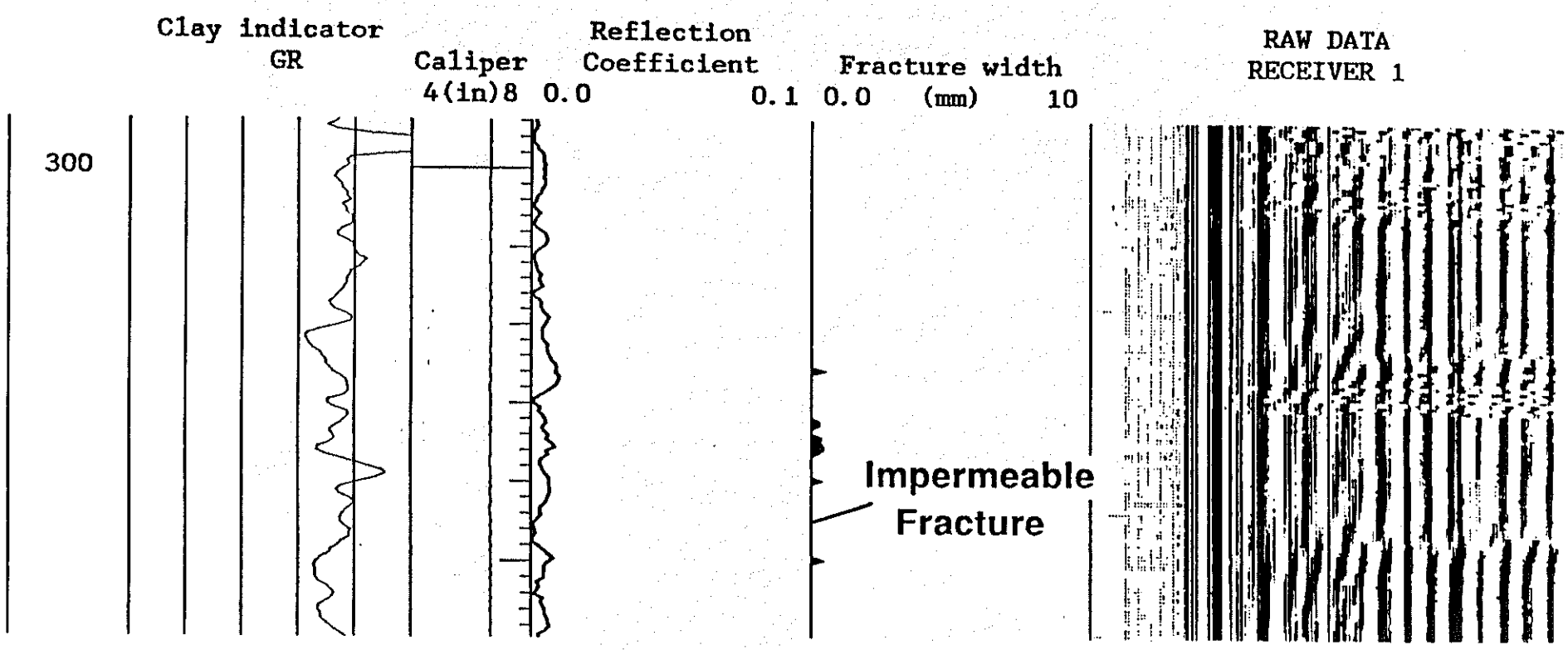
Clay indicator
GR
Caliper
4(in)8
Reflection
Coefficient
0.0
0.1
Fracture width
0.0
(mm)
10
RAW DATA
RECEIVER 1
300
Impermeable
Fracture

Reflecting Fractures

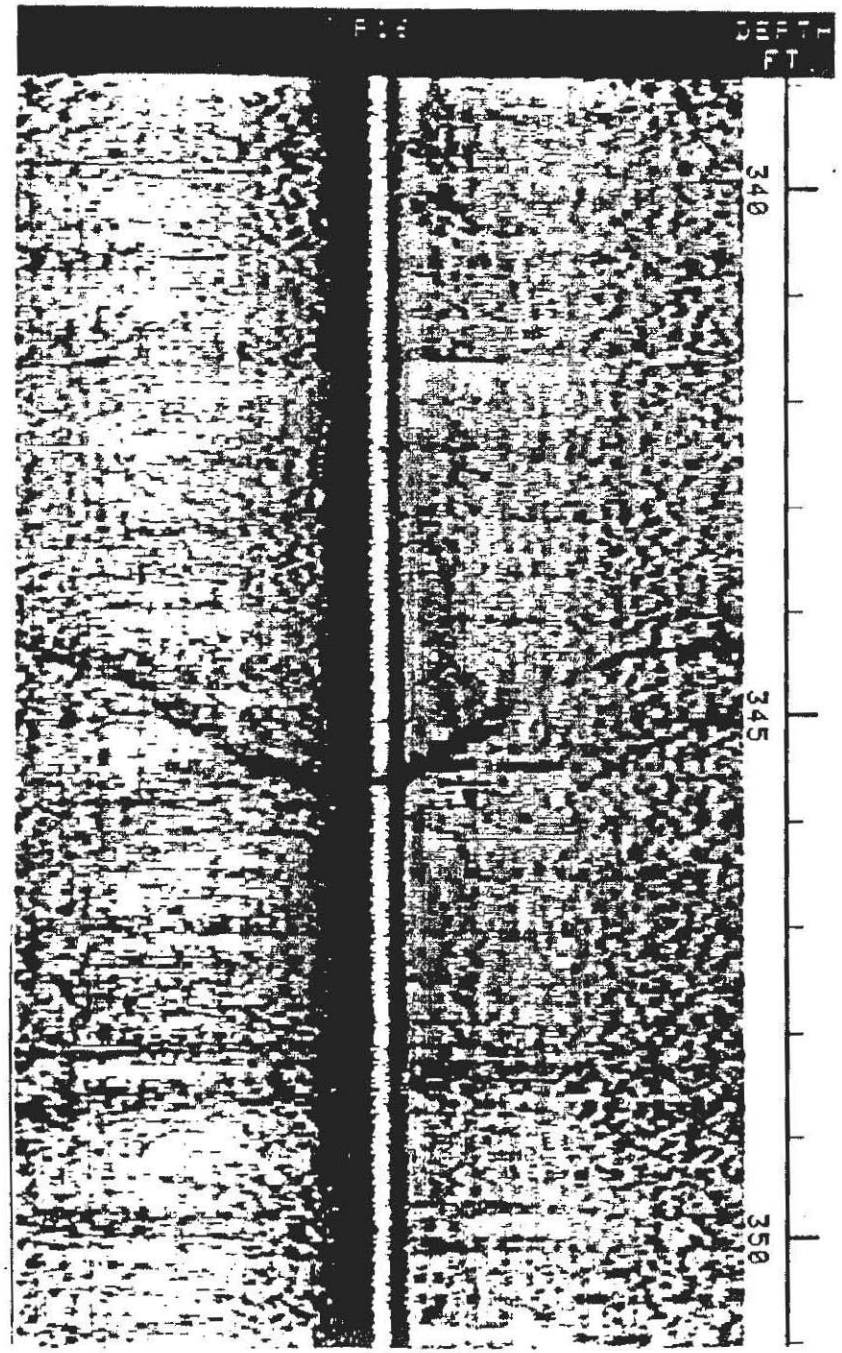

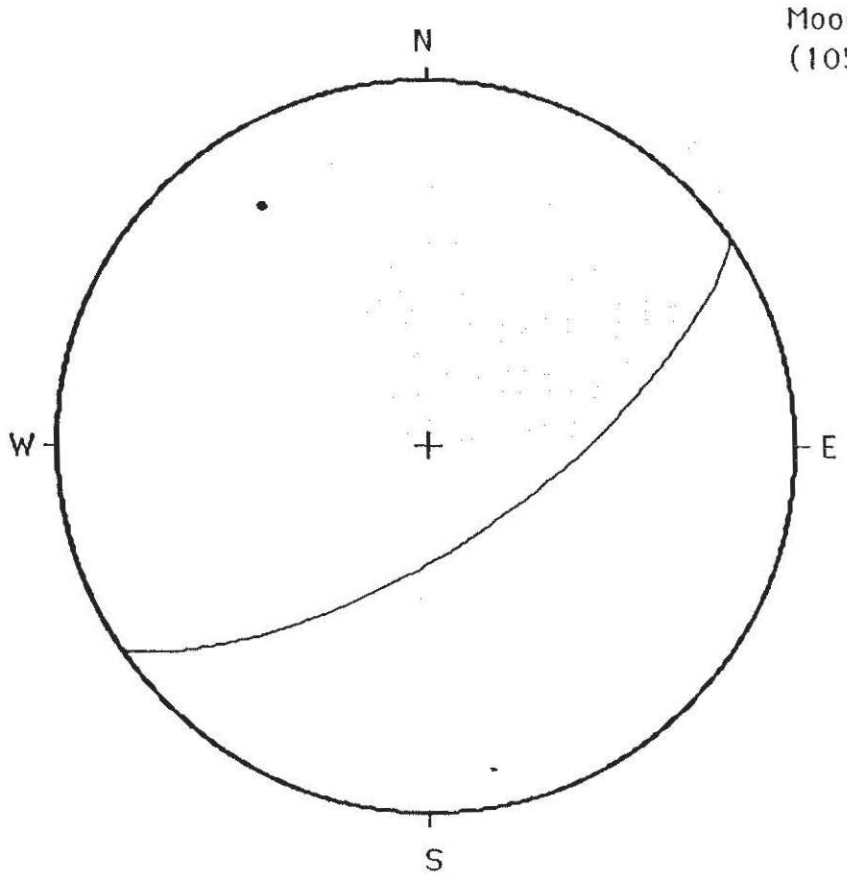

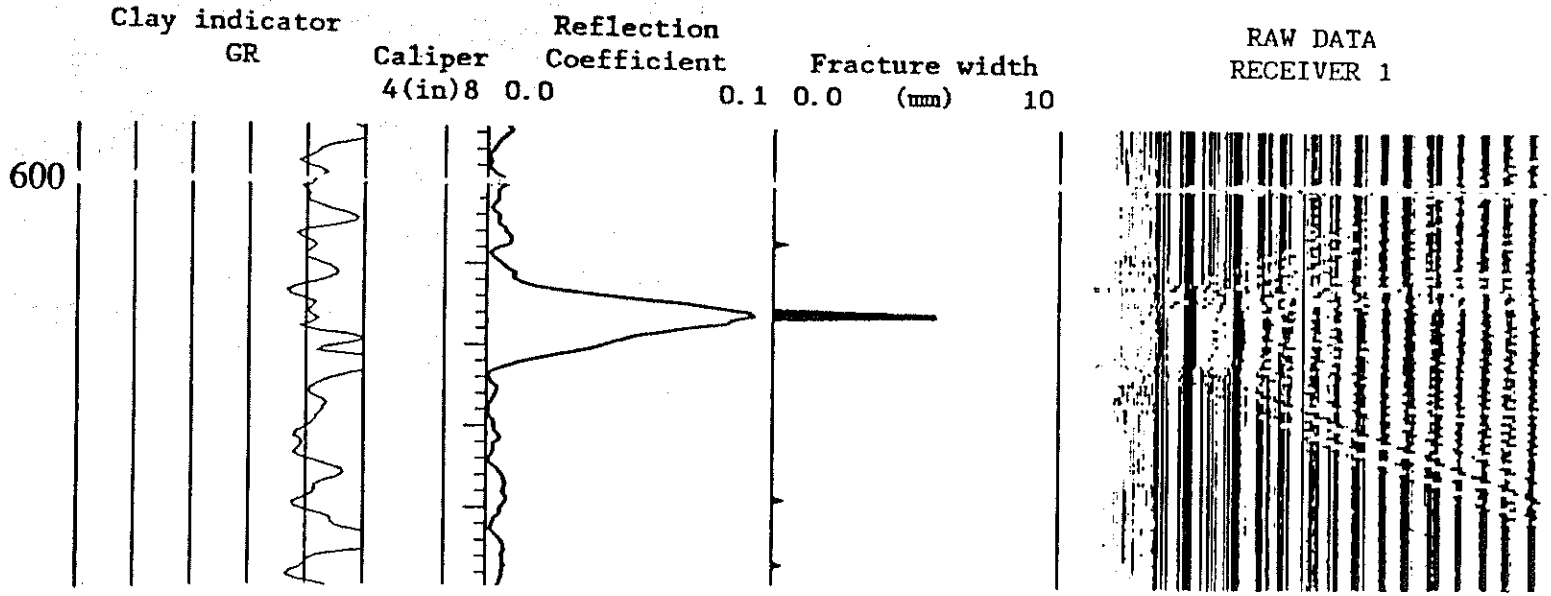
Clay indicator
GR
Caliper
4(in)8
0.0
Reflection
Coefficient
0.1
0.0
Fracture width
(mm)
10
RAW DATA
RECEIVER 1
600

Reflecting Fractures

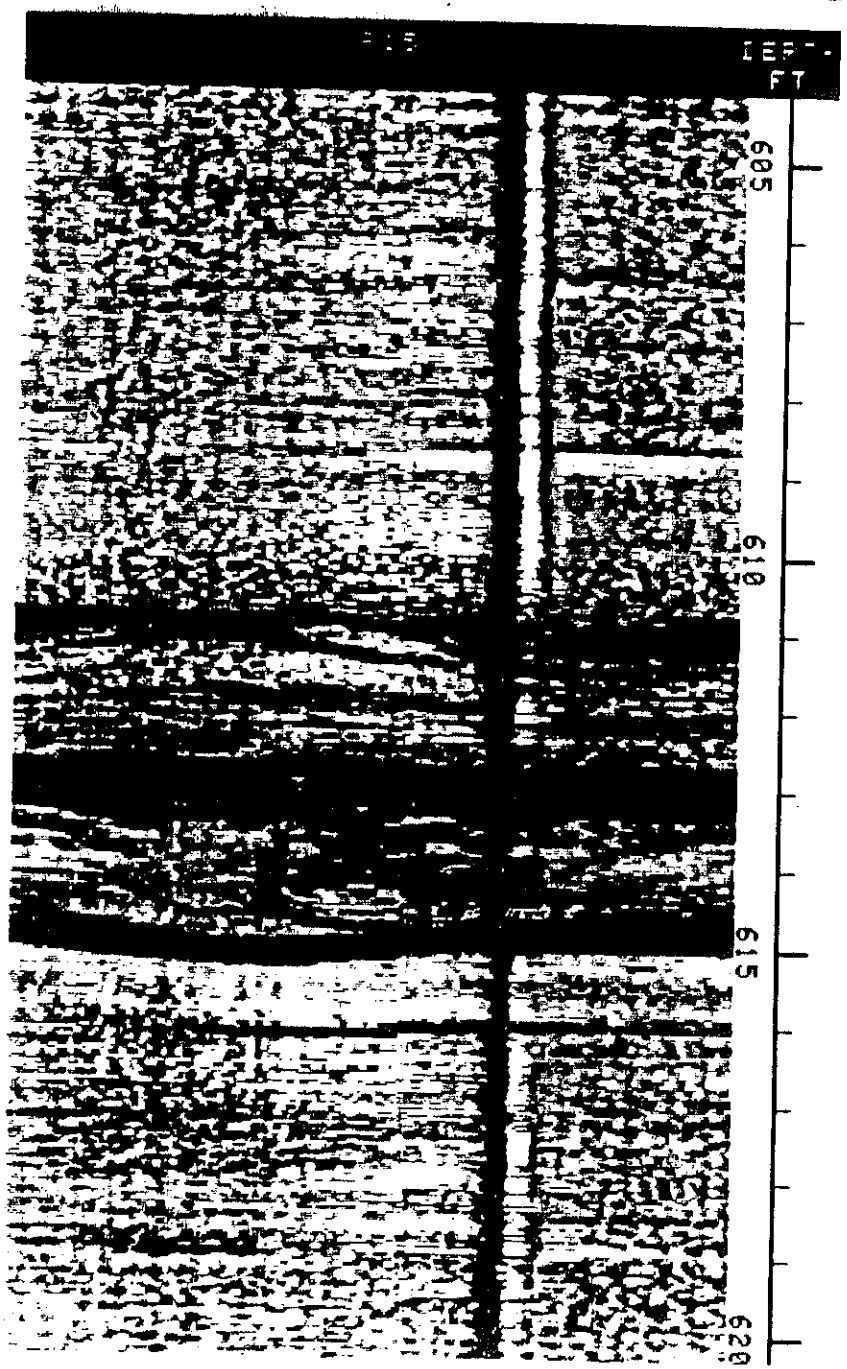

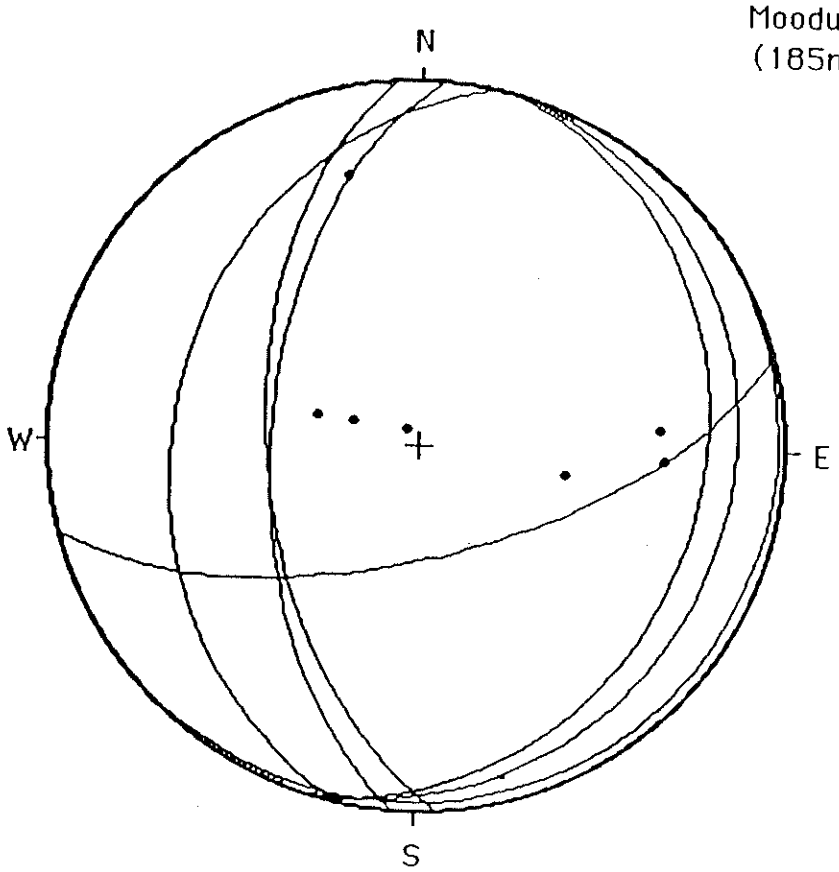

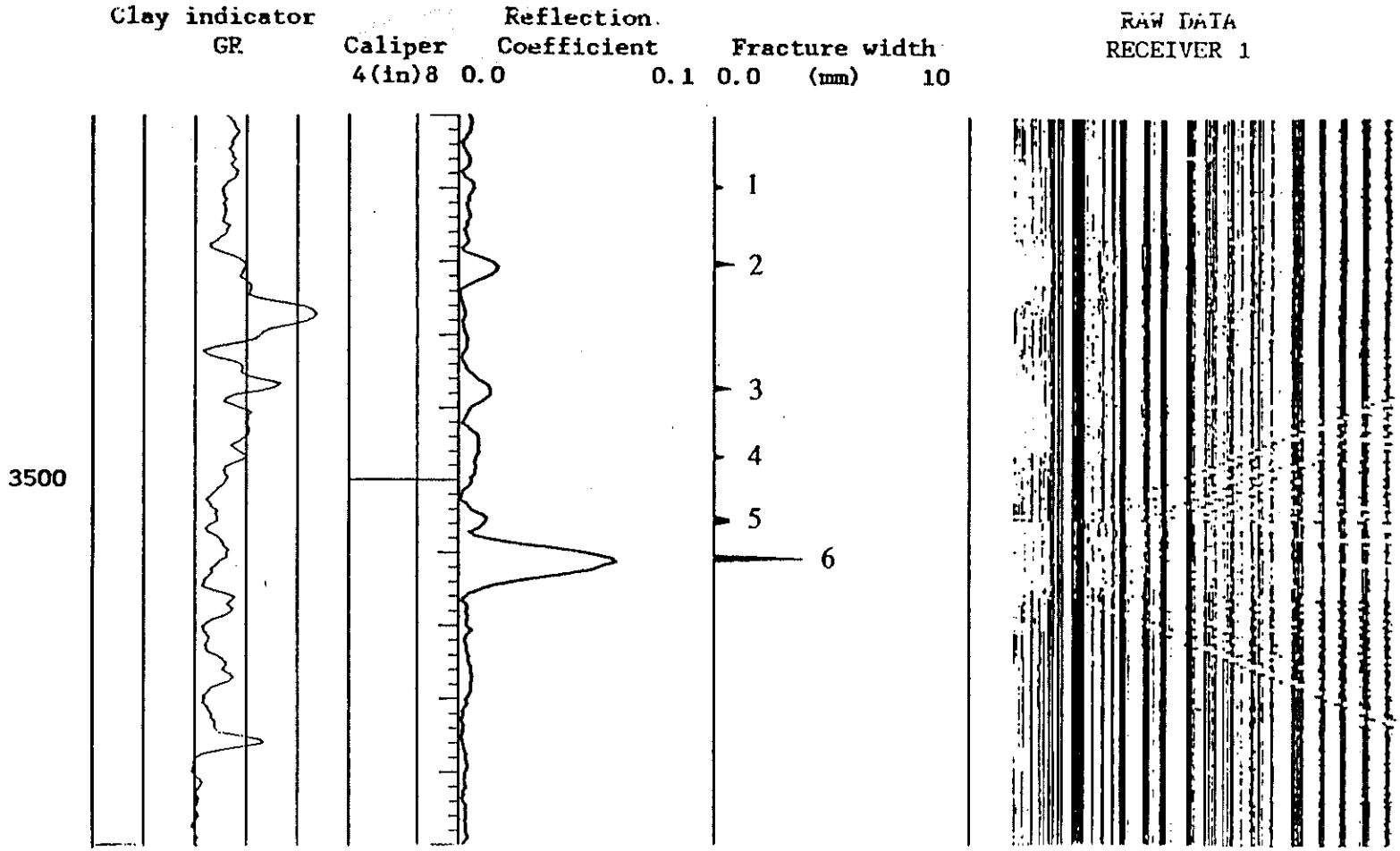
Clay indicator
GR
Caliper
4(in)8
Reflection
Coefficient
0.0
0.1
Fracture width
0.0
(mm)
10
RAW DATA
RECEIVER 1
3500
1
2
3
4
5
6

Reflecting Fractures

2B2

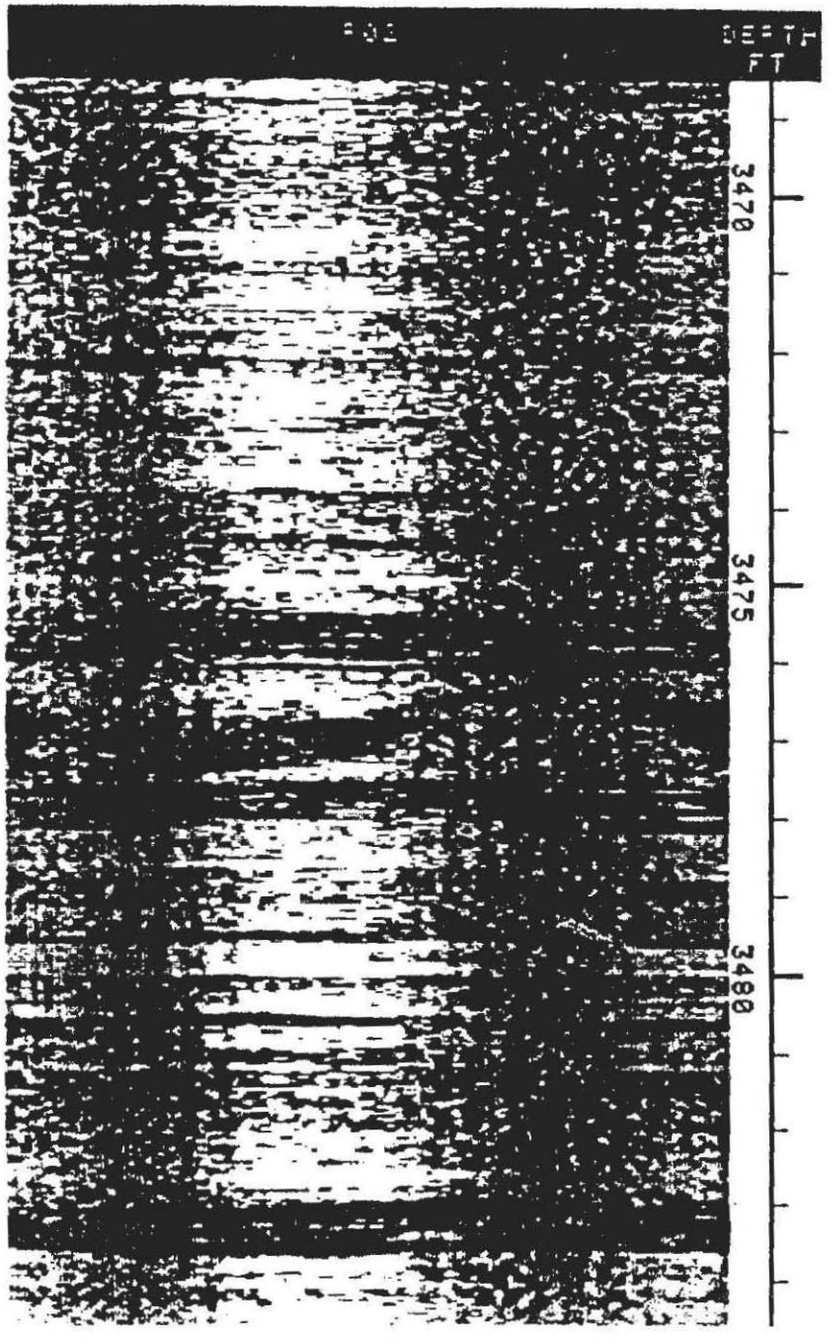

2B3

2B4

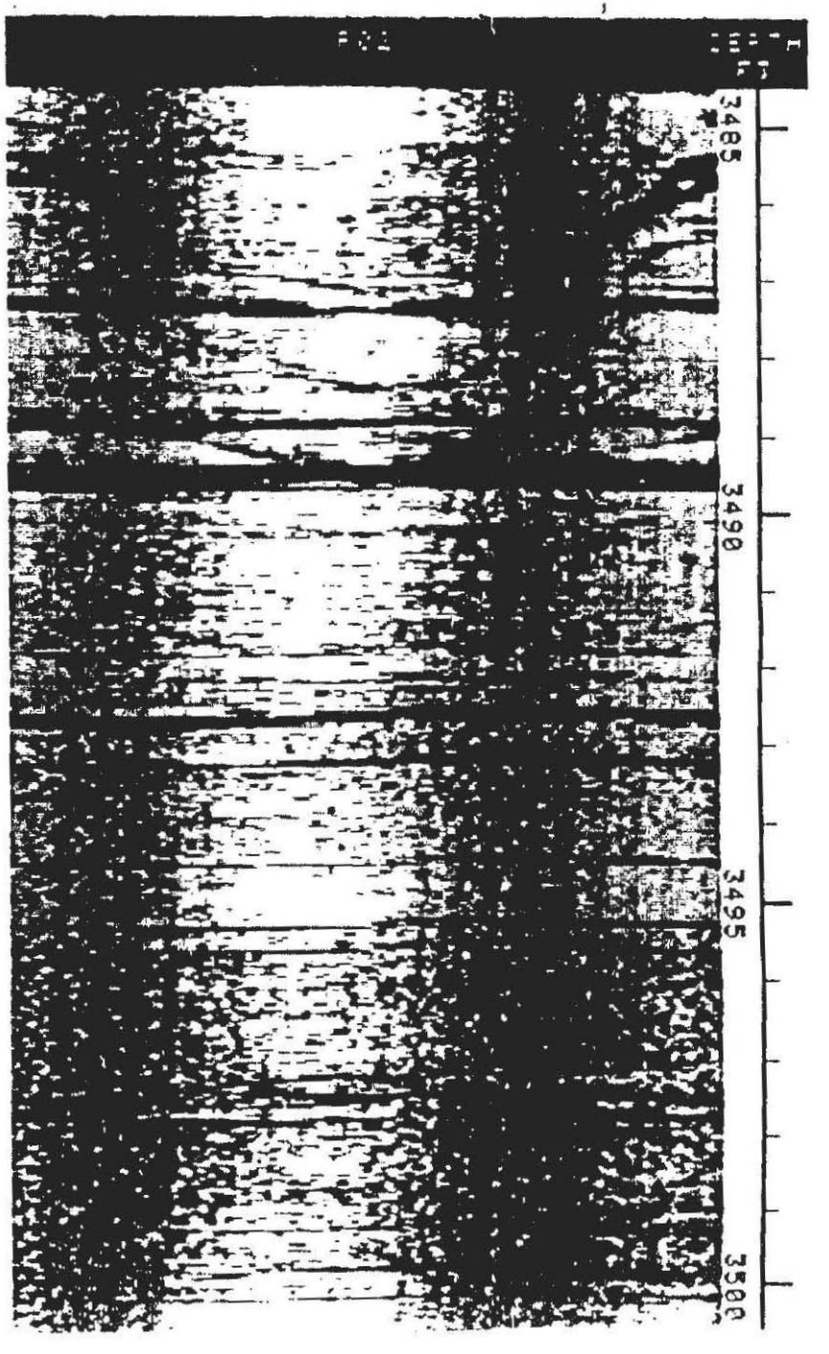

Reflecting Fractures

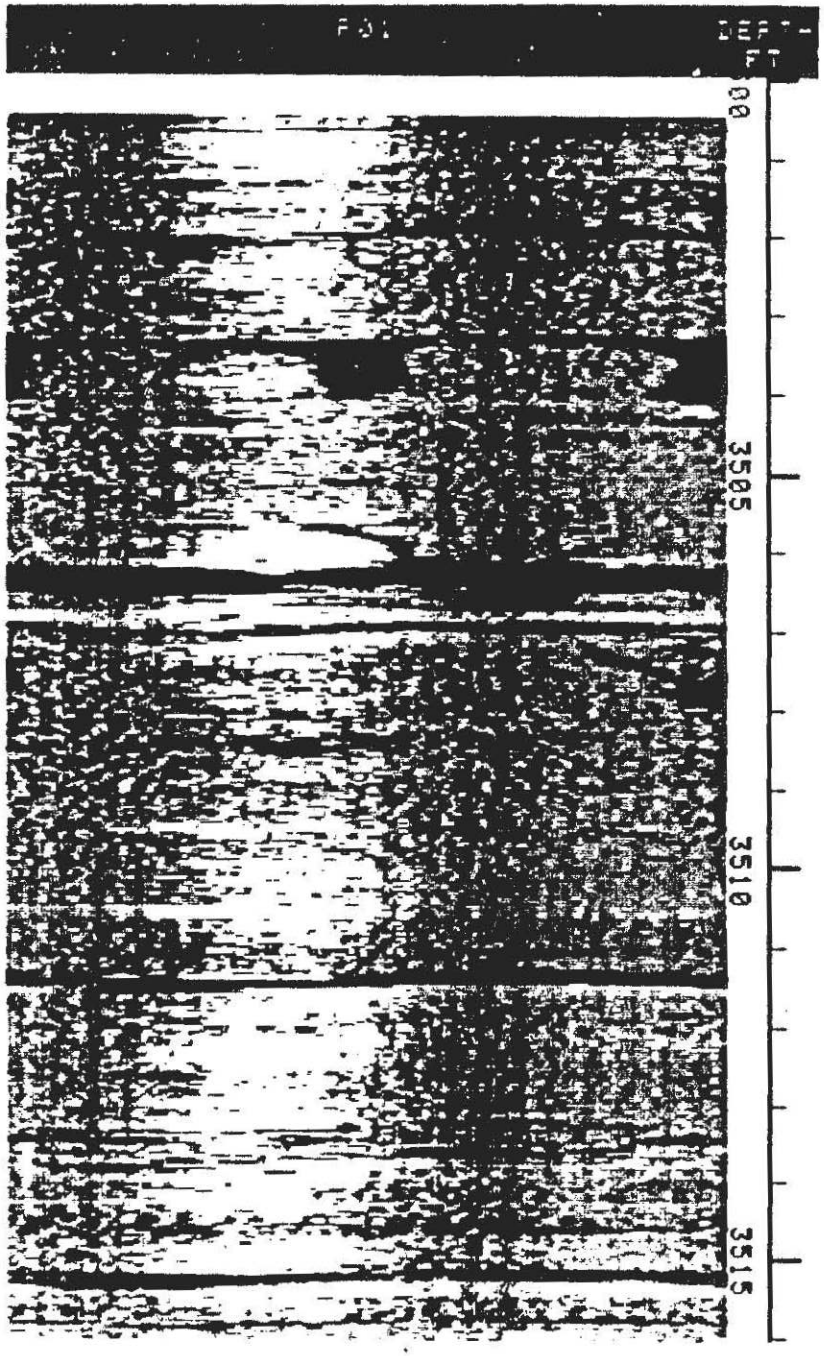

2B5

2B6

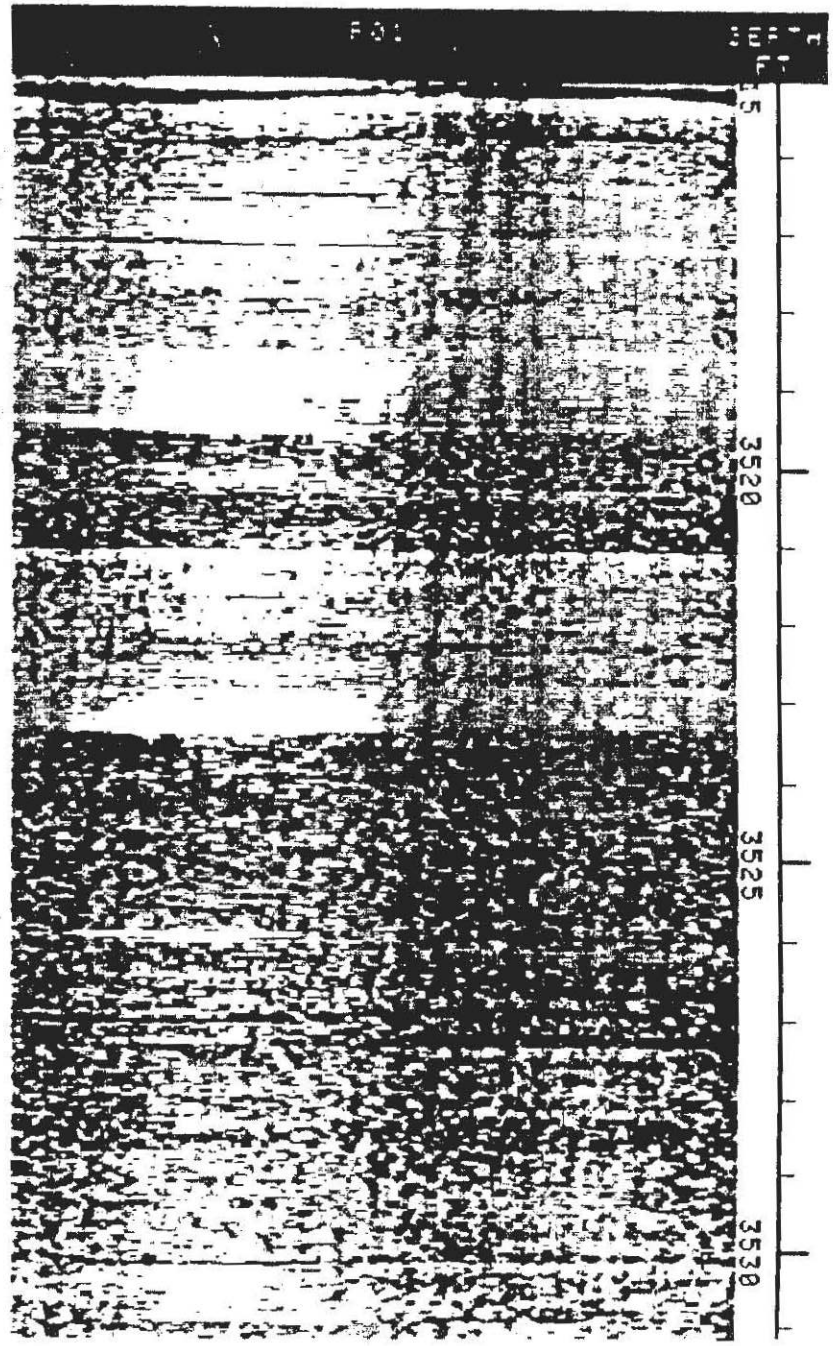

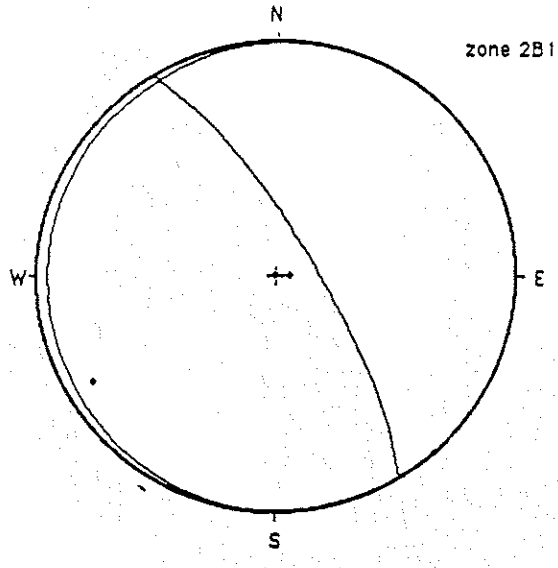
N
zone 2B1
W
E
S

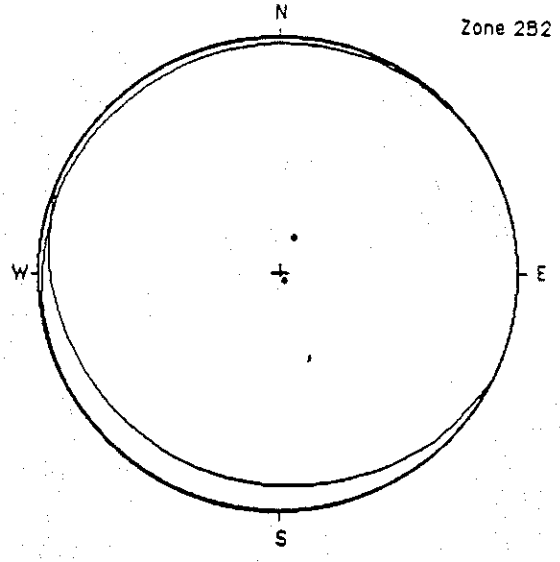
N
Zone 2B2
W
E
S

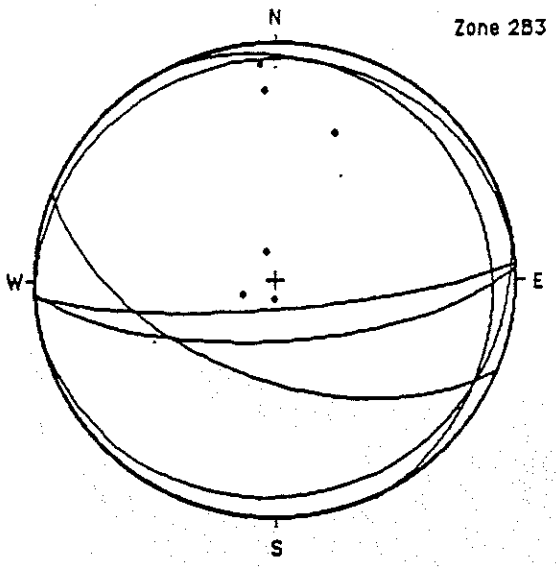
N
Zone 2B3
W
E
S

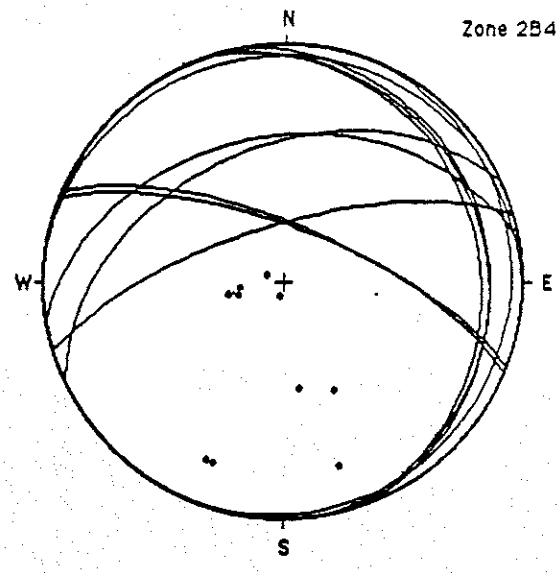
N
Zone 2B4
W
E
S

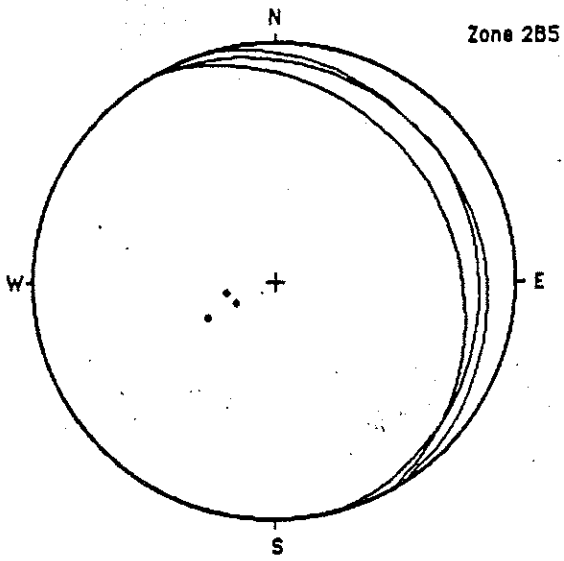
N
Zone 2B5
W
E
S

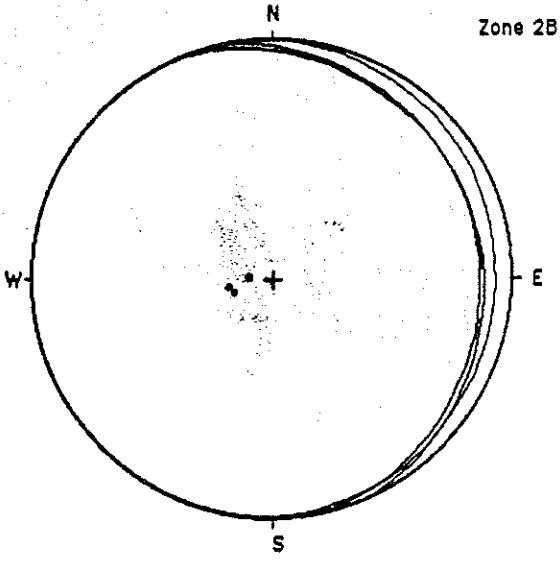
N
Zone 2B6
W
E
S

Appendix E

APPENDIX E

Geochemical analysis of Avalonian rocks from the Moodus borehole.

Identification and Interpretation of Chemical Cyclicity in Subsurface Avalonian Rocks, Moodus, Connecticut

R. P. Wintsch and C.P. Ambers
Department of Geology
Indiana University
Bloomington, Indiana 47405

Introduction

The structural geology of east-central Connecticut is dominated by a series of low amplitude domes and basins that deform metasedimentary and metavolcanic rocks. These stratified rocks have recently been assigned to the Avalon, Putnam-Nashoba, and Merrimack terranes (Zartman and Naylor, 1984) and are separated from one another by major ductile faults. The structure of the rocks within the lowest Avalon terrane has been interpreted to include a complicated set of recumbent nappes that fold layers of metaigneous rocks (Dixon and Lundgren, 1968). Recently Wintsch et al. (1987) have proposed that the stratigraphic correlations on which the interpretations of the fold nappes are based are invalid. The earlier workers correlated metaintrusive, sill-like, lithodemic bodies with extrusive, lithostratigraphic metavolcanics. The alternative interpretation is that the rocks constitute part of a normal sequence. The 4800 foot deep hole drilled in Moodus, Connecticut, provides important information that bears on these revised stratigraphic and structural interpretations.

Results

Cuttings collected every 20 feet were described and selected samples were analyzed petrographically (Ambers, 1988). The results show that the drill hole at Moodus penetrates all the rock types encountered in the outcrop area around the Willimantic dome and along the Honey Hill fault zone. A geochemical log of the

borehole (Anderson et al., this volume) helps constrain lithologic contacts by providing a chemical analysis every 6 inches. With this depth information, a cross section can be constructed (Figure 1) extending from the lithologic section exposed in the Hadlyme area, north to the Moodus hole, and northeast to the lithologic section exposed in the Willimantic dome.

The geochemical log reveals an irregular distribution of the rocks below 2690' assigned to the Avalon terrane. Calibration of the log for whole rock composition was accomplished by analyzing cuttings collected within selected intervals for major and minor elements (Table 1). The normative mineralogy of these gneisses and granofelses shows that the rocks classify as meta-granites and metagranodiorites. The granitic gneisses contain subequal K-feldspar, quartz and plagioclase, and accessory biotite. The granodioritic gneisses contain plagioclase, quartz, hornblende, biotite, and accessory magnetite, K-feldspar, sphene and zircon.

The geochemical log clearly shows the distribution of these two rock types with depth. It also indicates a strong chemical cyclicity in the gneisses. Zones up to 100 feet thick can be identified as having gradual increases, decreases or constancy in the concentration of some elements with depth. Boundaries between zones are marked by steep concentration gradients that produce breaks in slope in the log. Because the section contains compositional anomalies including amphibolites, quartz veins and pegmatites, both positive and negative compositional spikes are present throughout the log. In spite of this, a "baseline" of approximately uniform trend can be identified. The variation of the concentration of most components with SiO_2 concentration is systematic suggesting the rocks are metaigneous. Consequently, only intervals having systematic variations of several elements were considered meaningful in terms of identifying layered structure using chemical composition. Some sections have component distributions that suggest the units may be made up of several layers. The lack of consistency in compositional trends among the elements, however, makes it difficult to identify meaningful breaks within such sections. These are identified as composite layers.

The distribution of layers so identified with depth is given in Table 2. The depth of the compositional breaks, the variations in the concentrations of K_2O and Al_2O_3, the thickness of each zone, and the rock types are given. Some units have a saw-tooth or jagged pattern, while others are smooth (J and S, respectively, Table 2). The chemical cyclicity present in the log is found in the concentrations of K_2O, Al_2O_3, SiO_2,CaO and FeO (Total). The concentrations of K_2O and Al_2O_3 are selected to characterize this chemical variation because their concentrations were measured independently, and are slightly more reliable than the concentrations of the other elements (Hertzog, et al., 1987). Although K_2O is a mobile component in some geologic settings, K_2O contents of metaigneous rocks in eastern Connecticut have been shown to relate to igneous protolith compositions with little or no modification by metamorphism (Webster and Wintsch, 1987).

Three types of trends are present in the layers composing the Avalon section: (I) increasing K_2O and SiO_2 and decreasing Al_2O_3, FeO, and CaO with depth, (II) decreasing K_2O, and SiO_2 and increasing Al_2O_3, FeO, and CaO with depth, and (III) constant composition with depth. Most of the granitic layers show smooth compositional trends, and 7 of 10 are type III showing no variation with depth. The granodioritic rocks are much more heterogeneous. Only about half of the 28 layers show smooth variations, and again these are predominantly type III. Nine layers show increasing K_2O with depth (type I). These are commonly jagged, have many small spikes, and most are often interpreted as composite layers. Only six granodioritic layers show decreasing K_2O with depth, and four of these are smooth.

Discussion

The plagioclase gneisses exposed at the surface south of the Honey Hill fault near Hadlyme, and around the Willimantic dome (see Rodgers, 1985) have chemical compositions indicating that they are the metamorphic equivalents of

granodioritic igneous rocks (Wintsch et al., 1987). Limited chemical data, especially from Hadlyme, suggest many plagioclase gneisses of the Avalon terrane are metamorphosed ash flow tuffs. Evidence supporting this interpretation includes: layered structure in the gneisses from Hadlyme preserved in the bulk chemistry and metamorphic mineralogy, interlayering of these gneisses with layers of basaltic, rhyolitic, and pelitic composition, and individual layers showing chemical cyclicity similar to modern ash flow tuffs.

The chemical cyclicity revealed in the geochemical log at Moodus supports the interpretation that these rocks were also deposited as ignimbrites. The interpretation is much more compelling at Moodus, however, because the data are essentially continuous through 1990 feet of rock. All of the observations that can be made with the geochemical log are consistent with what is known about modern ash flow tuffs including: 1) The thickness of individual layers varies from a few feet (difficult to resolve in the log) to 90 feet or more. Such thicknesses are typical of distal portions of modern ash flows. 2) The granitic and granodioritic layers are intercalated with a few amphibolite (basaltic) layers. This is common in modern settings. 3) The trends of increasing K_2O and decreasing Al_2O_3 and other mafic components with depth is commonly found today (e.g. Bishop Tuff, Hildreth, 1979), and has been interpreted as reflecting the chemical stratification that should exist in a differentiating magma. This type of structure is common in the granodioritic layers in the Moodus subsurface which are sufficiently mafic that in situ fractionation of their parent magmas would be expected. Such zonation is not common, however, in the granitic layers. 4) The trends of decreasing K_2O and increasing mafic components with depth are the least common in both rock types at Moodus. They are also less common in modern flows, but are present (Smith, 1979, p. 18), and can be interpreted in two ways. They may be composite flows erupting over long periods of time, with each successive flow tapping a more highly fractionated magma, or they may result from eruption from a side vent of the magma chamber, where the deeper and more mafic magma compositions lie. The higher, more felsic compositions would then follow out the vent as the overlying cauldera collapsed. The smooth trends

identified in the geochemical log are more consistent with this second interpretation because the many flows of the first would likely produce a jagged geochemical trend. 5) Geochemical trends showing no compositional gradations with depth are also common in modern volcanics (e.g. Fish Canyon tuff, Whitney and Stormer, 1985). These are usually interpreted as resulting from the eruption of a magma of buffered eutectic composition, or an unfractionated magma of uniform composition. In the Moodus well, 16 of 20 layers that show no vertical compositional variation are smooth. The smoothness of the trends in the seven granitic layers is suggestive that their parent magmas were eutectic liquids. Most of the granodioritic layers that have smooth geochemical trends are thicker than 50 feet. These are consistent with large eruptions of homogeneous magmas.

Conclusions

The above thicknesses and chemical trends revealed in the geochemical log are consistent with the interpretation that the granitic and granodioritic layers present in the Moodus subsurface below 2690' were deposited as a pile of ash flow tuffs. Because of their wide surface exposures, these metavolcanic layers must underly most of the Merrimack terrane in eastern Connecticut. These results strengthen the interpretation of Wintsch et al. (1987) that rocks exposed in outcrop south of the Honey Hill fault zone are metavolcanic and thus cannot correlate with intrusive rocks of similar composition deeper in the terrane.

Acknowledgments

ESEERCO, EPRI, and NU, through Tom Statton, provided access to a field copy of the geochemical log. The field and laboratory work were partially supported by the State Geological and Natural History Survey of Connecticut, and by NSF Grant EAR-86-18305.

References

Ambers, C.P., 1988, Summary of logging conventions used in the description of core materials from 4764' deep well at Moodus, Connecticut; the 1000' well at Moodus, Connecticut; and 1500' well at Gillette Castle, Connecticut: State Geological and Natural History Survey of Connecticut, Open File Report.

Dixon, R.H. and Lundgren, L.W., 1968, Structure of eastern Connecticut, in Zen, E-an, White, W.S., Hadley, J.B., and Thompson, J.B., Jr., eds.: Studies of Appalachian Geology, northern and maritime: New York, Wiley Intersci. Publishers, p. 219-229.

Hertzog, R., Colson, L., O'Brien, M., Scott, H., McKeon, D., Wraight, P., Grau, J. Ellis, D., Schweitzer, J., and Herron, M., 1987, Geochemical logging with spectrometry tools: Soc. Petrol. Engr., Trans., v. 283, p. 447-460.

Rodgers, J., 1985, Compiler, Bedrock geologic map of Connecticut: Conn. Geol. Nat. Hist. Survey, scale 1:125,000.

Smith, R.L., 1979, Ash-flow magmatism: Geological Society of America, Special Paper 180, p. 5-27.

Webster, J.R. and Wintsch, R.P., 1987, Petrochemistry and origin of the Killingworth dome rocks, Bronson Hill anticlinorium, south-central Connecticut: Geological Society of America Bulletin, v. 98, p. 465-474.

Whitney, J.A. and Stormer J.C., 1985, Mineralogy, petrology, and magmatic conditions from the Fish Canyon Tuff, central San Juan Volcanic Field, Colorado: Journal of Petrology, v. 26, p. 726-762.

Wintsch, R.P., Webster, J.R., Bernitz, J.A., and Fout, J.S., 1987, Subdivision of the Rope Ferry Gneiss, Avalon terrane, and structural implications (abs.): Geol. Soc. America, Abs. with Prog., v. 19, p. 66.

Zartman, R.E. and Naylor, R.S., 1984, Structural implications of some radiometric ages of igneous rocks in southeastern New England: Geol. Soc. America Bulletin, v. 95, p. 522-539.

Figure 1. A cross section from south of Gillette Castle State Park (Hadlyme), along the Connecticut River, through the site of the borehole in Moodus, to outcrop areas around the Willimantic dome. Data from a hole drilled at the state park give the depth control of the lithologic boundaries on the left side of the section. Data from the 4800 foot deep hole at Moodus give depth control at about km 15. Both of these holes also mark bends in the cross section. The first 15 km are approximately due north, and from km 15 to 45 the section trends NE. Hope Valley Alaskite (Zsh) is not reached in the Moodus section; the question mark indicates the lack of certainty in the depth of this boundary. Abbreviations are as follows (after Rodgers, 1985; Wintsch et al., 1987):

Merrimack Terrane

Dc	Canterbury Gneiss (Intrusive into O?h)
Obr	Brimfield Formation
O?h	Hebron Formation

Putnam-Nashoba Terrane

Zty	Yantic Member, Tatnic Hill Formation
Ztl	Lower Member, Tatnic Hill Formation

Avalon Terrane

Zwhm	Mansfield Hollow Facies, Hadlyme Formation, Waterford Complex
Zwhn	North Plains Facies, Hadlyme Formation, Waterford Complex
Zwm	Mamacoke Formation
Zsh	Hope Valley Alaskite, Sterling Complex

Hopyard Basin Cross Section

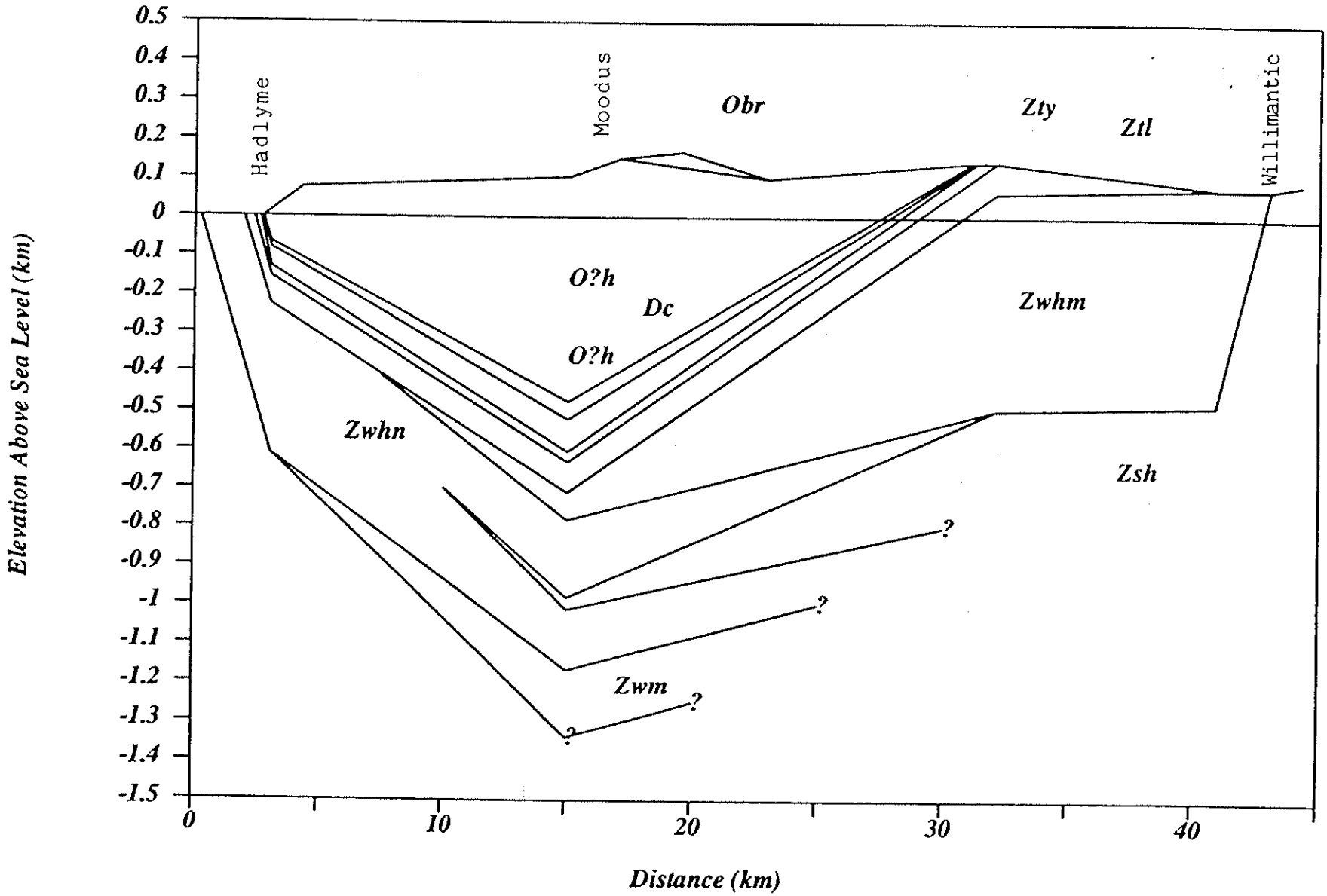

Figure 1

Table 1. Partial Chemical Analyses of Cuttings of Felsic Gneisses from the Deep Hole, Moodus, Connecticut.

Sample[1]	Label	S.G.[2]	SiO_2	TiO_2	Al_2O_3	FeO[3]	MnO	MgO	CaO	Na_2O	K_2O	BaO	SrO	LOI[4]	Total
1904	a	2.65	75.3	0.150	13.8	1.38	0.099	0.453	1.740	3.99	4.38	0.0371	0.0079	0.035	101.37
2024	b	2.64	74.3	0.182	13.8	1.20	0.028	0.334	1.250	3.82	5.15	0.0381	0.0064	0.479	100.59
2044	c	2.63	74.5	0.130	14.1	0.98	0.021	0.292	1.090	3.30	6.11	0.0446	0.0074	0.581	101.16
2744	d	2.69	68.6	0.319	16.5	1.99	0.048	0.735	3.520	4.82	2.18	0.0883	0.0366	0.494	99.33
2804	e	2.71	69.0	0.474	15.8	2.88	0.065	0.994	3.330	4.98	1.44	0.0459	0.0323	0.603	99.64
3304	f	2.77	68.1	0.708	14.1	4.86	0.090	2.140	4.540	3.36	2.71	0.0707	0.0253	0.644	101.35
3363	g	2.74	68.2	0.636	14.5	4.13	0.087	1.570	3.760	3.88	1.68	0.0410	0.0310	0.883	99.39
3463	h	2.73	66.0	0.560	15.6	3.73	0.082	1.680	3.350	4.07	2.34	0.0925	0.0315	1.119	98.66
3523	i	2.82	60.6	0.987	15.9	6.86	0.165	2.760	5.540	3.85	2.36	0.0692	0.0320	1.070	100.19
3583	j	2.64	76.0	0.155	11.8	2.09	0.029	0.205	0.888	3.60	4.87	0.0149	0.0026	0.284	99.94
3943	k	2.76	62.6	0.608	17.2	4.29	0.099	1.470	5.380	4.89	1.51	0.0672	0.0432	0.664	98.82
4043	l	2.69	71.0	0.438	14.3	2.62	0.040	0.702	2.430	4.00	2.76	0.1004	0.0292	0.550	98.97
4183	m	2.75	58.8	0.763	19.1	5.13	0.106	2.520	5.150	4.11	3.60	0.1251	0.0476	1.300	100.75
4243	n	2.72	67.4	0.509	16.1	3.29	0.098	1.080	3.350	4.75	1.67	0.0507	0.0243	0.575	98.90
4323	o	2.70	72.5	0.406	13.3	2.73	0.059	1.170	3.060	3.18	2.71	0.1435	0.0264	0.767	100.05
4544	p	2.69	71.3	0.425	12.7	2.60	0.058	0.883	2.580	3.43	2.91	0.0908	0.0232	0.891	97.89
4584 A	q	2.70	69.6	0.472	14.3	3.16	0.087	1.180	3.040	3.66	3.06	0.0873	0.0245	0.555	99.22
4584 B	r	2.89	52.0	1.040	17.3	8.25	0.212	4.770	8.490	3.81	1.79	0.0333	0.0429	1.330	99.07
4624	s	2.69	69.7	0.410	14.3	2.76	0.123	1.080	2.060	3.67	3.53	0.1848	0.0313	0.573	98.42
4744	t	2.75	64.8	0.623	15.6	4.90	0.132	1.580	3.050	4.06	2.35	0.1077	0.0229	0.871	98.10

1 Sample number is depth in feet
2 Specific gravity
3 FeO as total iron
4 Loss on ignition

Table 2. Summary of Geochemical Layering Identified in the Moodus Deep Well With Trends in K_2O and Al_2O_3 Content.

Contact Depth (ft)	K_2O[1]	Al_2O_3[1]	Trend Type[2]	Thickness (ft)	Rock Type[3]
2674					Upper Contact
2720	|	|	J	46	Dac > Amph (Comp)
2765	/	\	J	45	Rhy/Dac
2840	|	|	J	75	Dac w/Peg (Comp)
2935	|	\	S	95	Dac (Comp)
3005	|	|	S	70	Dac (Comp)
3085	|	|	S	80	Dac
3180	/	|	J	95	Dac > Rhy (Comp)
3290	|	\	J	110	Dac (Comp)
3342	\	/	S	52	Dac
3370	|	|	S	28	Rhy
3416	|	|	S	46	Dac
3485	\	/	S	69	Dac
3568	/	\	S	83	Dac
3660	|	|	S	92	Rhy
3716	\	|	J	56	Dac (Comp)
3760	\	/	S	44	Dac
3788	|	\	J	28	Dac (Comp)
	|	|	?	12	Rhy

Table 2. Summary of Geochemical Layering Identified in the Moodus Deep Well With Trends in K_2O and Al_2O_3 Content (continued).

Contact Depth (ft)	K_2O[1]	Al_2O_3[1]	Trend Type[2]	Thickness (ft)	Rock Type[3]
3800					
	|	|	S	20	Dac > Rhy (Comp)
3820					
	\	/	S	16	Rhy
3836					
	|	|	S	14	Dac
3850					
	\	\	S	15	Rhy
3865					
	/	\	J	20	Dac
3885					
	/	\	J	15	Dac
3900					
	/	\	J	24	Dac
3924					
	\	|	S	20	Rhy
3944					
	|	|	S	12	Amph
3956					
	|	|	?	2	Rhy
3958					
	|	|	?	8	Amph
3966					
	/	\	J	39	Dac > Rhy (Comp)
4005					
	?	?	J	16	Rhy > Amph (Comp)
4021					
	|	|	S	4	Amph
4025					
	|	\	J	53	Dac (Comp)
4078					
	?	|	S	38	Rhy
4116					
	\	|	S	54	Rhy
4170					
	|	\	J	55	And (Comp)

Table 2. Summary of Geochemical Layering Identified in the Moodus Deep Well With Trends in K_2O and Al_2O_3 Content (continued).

Contact Depth (ft)	K_2O[1]	Al_2O_3[1]	Trend Type[2]	Thickness (ft)	Rock Type[3]
4225					
	\	/	J	55	Dac
4280					
	\	/	S	80	Dac
4360					
	|	\	S	68	Dac
4428					
	\	/	S	62	And
4490					
	\	/	J	40	Dac
4530					
	|	|	S	55	Dac
4585					
	|	|	S	75	Dac
4660					
	|	|	J	50	Dac/And
4710				Log end	

1. Direction of variation of relative concentration with increasing depth: /, decreasing; |, constant; \, increasing; ?, erratic fluctuations. 2. Trend type describes shape of chemical variation; J, jagged; S, smooth. 3. Identification of rock type based on cuttings and selected chemical analysis; Rhy, metarhyolitic; Dac, metadacitic; Amph, amphibolite; and, metaandesitic; peg, pegmatite; Comp, thickness constitutes composite flow.

Appendix F

APPENDIX F

Results of geochemical and geophysical surveys in the Moodus Borehole. Field copies of the geophysical and geochemical logs, as well as high-resolution copies of the Formation Microscanner logs are archived at Woodward-Clyde Consultants, Wayne, N.J.

Geochemical and Geophysical Structure in the Moodus Deep Drillhole, Connecticut, and the Mass Flux Associated with Low-Angle Thrust Faults

by

Roger N. Anderson
Roy E. Dove
Gilles Ollier
Philippe E. Pezard
Colin F. Williams

Borehole Research Group
Lamont-Doherty Geological Observatory
Columbia University
Palisades, New York 10964

and

Peter Naumoff
Woodward-Clyde Consultants
Wayne, New Jersey 07470

Abstract

Introduction

The movement of great volumes of rock over large distances along shallow thrust faults is an integral part of the formation of continental terrains during collision events. Yet, the mechanics of thrusting along such decollement surfaces has remained one of the interesting problems in our understanding of compressional tectonics on the earth. The occurrence of such displacements is widespread (from the Nappes of the Alps, to the east coast of the

United States, to present-day displacement along the forelands of Pakistan and India), but the mode by which coherent blocks of rock slide long distances over very modest slopes has remained controversial. Hubbard and Ruby, (1956), have proposed the most widely held explanation for how such movements are possible: very high pore pressures along the fault decrease the frictional resistance to the point that small differential stresses result in large displacements.

While few direct measurements have been made that clearly demonstrate the past existence of such high fluid pressures along such thrust fault surfaces, the widespread metamorphism which accompanies such terrains requires large fluid and mass fluxes to have been active. Such geochemical fluxes must be present if differential pore pressures existed in the past since convection is inevitable in rock so out of buoyant equilibrium. Measurements that shed light on the timing of faulting versus hydrothermal alteration and metasomatism are crutial data-sets in our quest to understand compressional tectonics on the continents. Consequently, deep crustal drilling has targeted these low-angle thrust faults in a variety of geological environments around the world. It is clear that we must measure the geophysical, and particularly, the geochemical state of the fault zone *in situ* if we are to understand the mechanics of such movements. The West German KTB project and the American ADCOH program are two ultra-deep continental drilling plans that have plans to penetrate old decollement surfaces at 10-15 km depths.

We report here geochemical and geophysical logging results from a shallower penetration of such a low-angle thrust fault under eastern Connecticut at the Moodus deep drillhole. We examine the geophysical state of the rock near the fault zone, then attempt to trace the geochemical mass fluxes of elements along and across the fault zone and place some restrictions on the timing of that movement. A detailed understanding of the lithostratigraphy of the country rock is required before we can recognize mass fluxes which might be associated with widespread hydrothermal and metasomatic alteration. The timing of fluid flow versus fault movement, while inprecisely determined by such mass flux analyses, is constrained by

the observed elemental fluxes determined by geochemical logs. For example, the logs discriminate seperate Thorium and Uranium enrichment "events" above the fault that are likely to have involved significant flow of first high temperature and pressure metasomatic, then low temperature hydrothermal fluids along the fault zone.

The Moodus #1 Well

As part of a seismogenic risk analysis of the northeastern United States, the Empire State Electric Energy Research Corperation (ESEERCO), the Northeast Utilities (NU) and the Electric Power Research Institute (EPRI) funded Woodward-Clyde Consultants to drill a deep borehole through an area of small earthquake swarms near Moodus, Connecticut in 1987. The major purpose of the large experimental program carried out in the well was to measure the direction and magnitude of the regional stress field at seismogenic depths. The Borehole Research Group of Lamont-Doherty Geological Observatory contracted with Schlumberger Well Services for geochemical and geophysical logging of the 1.5 km deep well.

The Moodus #1 well penetrated 770 m of Merrimack Group Paleozoic metamorphic rocks, encountered the Honey Hill Fault from 750 m to 820 m depth, and bottomed in Waterford Group Precambrian metamorphic rocks. The Honey Hill Fault is the southern extension of the Lake Char thrust fault which represents the major decollement surface in eastern Connecticut (figure 1). The fault zone was the site of primary thrusting to the east of a Paleozoic terrain over Precambrian rocks in the Permian (Wintsch and LeFort, 1982), and may be the locus of the present day, low-level seismogenic activity in the area. The major mission of the logging program was to determine if there is evidence for large mass fluxes across the fault zone, in addition to the determination of the more traditional lithostratigraphic description of the rock surrounding the wellbore. Below, we show that elemental mass fluxes derived from the geochemical logs discriminate between metasomatic and hydrothermal alteration associated with past fluid motions near the fault zone and primary lithological variations caused by the superposition of different rock-types during the thrust movement along the fault.

Geophysical Logs

Electrical resistivity, neutron porosity, density and velocity logs were run from the surface to 1480 m depth in the Moodus #1 well. Deep (LLD) and shallow (LLS) laterolog electrical resistivity measurements were made in order to determine porosity and the location of fractures. A Cesium 126 gamma ray source was used to measure density (RHOB) and photoelectric capture cross-section (PEF). An Americeum-Berrylium neutron source was used to determine neutron porosity (NPHI). Natural radioactivity from Potasium, Uranium and Thorium were measured by a natural gamma ray spectrometer to give total radioactivity (SGR), and a caliper log was used to determine the size of the wellbore (CALI) (Figure 2). Major fracture zones are discriminated by very low resistivity, low density, high porosity, high radioactivity, and low photoelectric capture cross-section spikes found throughout the well (e.g., the Honey Hill Fault Zone from 750 to 820 m depth).

Electrical resistivities of the metamorphic rocks in the wellbore increased with depth from approximately 20,000 ohm-m in the Merrimack Group to greater than 200,000 ohm-m in the Waterford rocks in the lower section of the well. The latter values are some of the highest resistivities ever recorded from a laterolog. Consequently, porosities are generally low, ranging from 2 % in the Merrimack to < 1% in the Waterford rocks. Neutron porosities read higher (2-5 %) because the neutrons are slowed by all hydrogen in the formation, and therefore, NPHI reflects the total water content of the formation and pore spaces including hydroxyls bound within the metamorphic rocks. Chemical analyses of rock cuttings confirm the presence of up to 3 weight percent bound water (Wintsch and Ambers, 1988). The drop in porosity from Merrimack to Waterford rocks likely reflects a real drop in the abundance of pore spaces because the overall grade of metamorphism does not change downhole (Naumoff, 1988). Densities range from 2.6 to 2.8 gm/cm^3, with the more mafic biotite- and hornblende-rich amphibolites distinguishable not only from their high density, but by unusually high porosity as well (again reflecting the presence of abundant hydroxyl-bearing minerals) (figure 2).

The shallow laterolog resistivity value (LLS) is greater than that of the deep resistivity (LLD) throughout the well, indicating the strong anisotropy of these highly foliated metamorphic gneisses. The anisotropy is caused by horrizontal resistivities that are lower than the vertical, which allows for an easier, more conductive pathway for the deeply penetrating LLD current.

Fractures and bedding planes were imaged using a new generation dipmeter called the Formation Microscanner[1]. The Formation Microscanner consists of high-resolution, 27-button arrays of electrodes on two of the four dipmeter pads. The variation in electrical resistivity across each pad is then used to produce an image that differentiates foliation and fractures and measures strike and dip. A major fault zone appears on the Formation Microscanner as a thick zone of coherent fractures. Fault zones are also easily discriminated on the four orthogonal pads of the dipmeter.

The Honey Hill Fault was imaged by the Formation Microscanner as a series of discrete deformation zones up to several meters thick (figure 3). East dipping layers are recorded above and below the fault. West dipping formations delineate the fault itself, with dips above steepening toward the fault and those below shallowing away from the fault (figure 4). The deformation above and below the fault is caused by downturn along the hanging wall and upturn along the footwall because of motion along the thrust fault. Strike rather than dip is the main indicator that a fault plane has been crossed (figure 5). The Honey Hill Fault appears to be dipping at approximately 15 degrees to the west (figure 6). Several east dipping thrust faults are present in the Waterford Group rocks below the fault (e.g, figure 7), probably reflecting deformation in the Precambrian basement that preceeded continental collision.

Geochemical Logs

Neutron-source, gamma ray spectrometry logs were used in the Moodus #1 well to compute dry weight percent oxide abundances of

[1]Mark of Schlumberger

SiO_2, Al_2O_3, CaO, FeO, K_2O, and TiO_2, as well as trace elemental abundances of Sulfur, Uranium, Thorium and the heavy rare earth element (HREE) Gadolinium at 0.15 m intervals throughout the well (figure 8). The photoelectric capture cross-section and density curves were then used along with the measured elemental abundances to calculate the residual major element concentration of NaO+MgO (Herzog, et al, 1987, Anderson, et al, 1988a) (figure 8).

In order to make these measurements, the Geochemical Logging Tool[2] carries three measurement devices into the borehole: a) A NaI crystal, natural gamma ray spectral analyzer detects the energy levels of naturally emitted gamma rays from the formation. The weight percent of Potasium present in the rock, as well as the total content of Thorium and Uranium in parts-per-million, are determined by this sensor; b) A Californium neutron source/ NaI photoaccumulator combination activates Aluminum atoms in the formation and records the emitted gamma rays; and c) A **minitron** bursts neutrons into the formation to activate Silica, Calcium, Iron, and Titanium as well as Sulfur and Gadolinium. Hydrogen and Chlorine contents of the wellbore fluid and formation are also measured.

The variation of major elements in dry weight percent of the oxides is estimated by assuming that in all earth rocks, approximately 50 % is oxygen by weight (Herzog, et al, 1987). The geochemical logging measurements made in the well detect a fraction of the total spectrum for each activated element that is linearly proportional to the concentration of that element in the **volume** of the measurement. Thus, the relative yields from each element measured through thermal neutron capture reactions is renormalized to elemental oxides which must sum to 100 % at each sampling interval. Since the elements measured by either capture activation or natural spectroscopy make up almost all of the significant oxides comprising rock (particularly when sodium and magnesium are also estimated), the calculations should be reliable in any geological formation (Herzog, et al, 1987). **These elemental weight percent oxide values were calculated with no calibration or other reference to core analyses.**

[2]Mark of Schlumberger

The accuracies of the geochemical logging results in the metamorphic rocks of the Moodus #1 well were varified by comparing log and X-Ray Fluorescence analyses made on cuttings at 18 intervals within the well (Figure 8, analyses from Wintsch and Ambers, 1988). Although the geochemical log analyses are not as accurate in absolute terms as the laboratory analyses, they are made continuously throughout the well. In addition, the relative precision between depth points is far superior to their absolute accuracy (Anderson, et al, 1988b). The continuous nature of the geochemical logging measurements allows for the precise definition of not only lithologic units and their boundaries, but of quantitative geochemical mass fluxes throughout the wellbore.

Lithostratigraphy for Major Elemental Variations

The geochemical logs can be used to discriminate lithological units within the Moodus #1 wellbore. The simplest lithological determination can be derived using a discriminator analysis. Using the major elements and Gd, U and Th, we can perform a linear discriminant function analysis by choosing two extreme "Type Intervals" -- the most-felsic, granitic gneiss (810-870 m) and the most mafic, amphibolitic gneiss (1280-1300 m). The discriminant analysis proceedure assigns a quality factor to each measurement point in the well. The value of the quality factor depends upon where within the space defined by the 10 input logs (figure 8) the data at each depth point fall relative to the compositions of the two end-members. The end-member zones form two clouds of data points within the multi-dimensional space represented by ten axes (each element's log response at the end-member depths). The data at other depth points fall elsewhere within the space. The discriminator function equation defines an axis within the space which connects the two end-member clouds. All data from other depth points are projected onto the axis defined by the discriminator function and assigned a value which represents the relative position of the data points at each depth relative to that line connecting the data clouds of the two end-members.

By choosing the most granitic and mafic rocks as end-members, we discriminate relative granitic or amphibolitic gneiss

compositions at each depth point (figure 9). Beginning at the bottom of the well, we see that the Waterford Group below the fault consists of a mafic gneiss from 1280 to 1480 m, and a granitic unit from 810 to 1100 m. The unit between 1100 and 1280 m consists of thin interlayers of these two units. Above the Honey Hill Fault, we see a steady gradation upward from more mafic to granitic rock, culminating in a very felsic unit from 650 to 600 m. From that depth to the top of the well, the granitic gneisses become progressively less silicic, and there are distinct interlayers of mafic gneisses (e.g., 580-600 and 480-500 m).

Mineralogy Model for the Moodus Well

In order to establish a more sophisticated, mineralogy-based lithostratigraphy of the Moodus #1 well, the elemental concentrations from the geochemical logs were inverted using a correlation matrix to determine the volumes of ideal mineral compositions which might be present in the well (Herzog, et al, 1987). We identified average dry weight percent oxide chemical compositions of quartz, orthoclase, plagioclase (An 45), biotite, hornblende, and pyrite (Table 1). The mineral compositions were then input as end-members into an inversion matrix with the weight percent oxide compositions of Si, Al, Fe, Ca, K, Ti, Na+Mg, and S from the geochemical logs. The resulting best-fit mineralogy of the well is shown in figure 10. Reconstruction from the mineralogy determinations back to ideal elemental compositions indicates how well the model actually fits the observational data (compare dashed and solid curves of figure 8).

With mineralogy in hand, it is now possible to distinguish the detailed lithostratigraphy od geological units tentatively identified with the discriminant analysis (Anderson, et al, 1988c). A summary of the mineral variations of Figure 10 shows that the upper 600 m of the well consists of a quartz-biotite rich-rock in which the quartz content increases with depth at the expense of the plagioclase (figure 11). This mineralogy fits with that observed in cuttings, core and outcrop for the Hebron Formation (Naumoff, 1988). The quartz-orthoclase-plagioclase rock from 600 to 650 m is the Canterbury granitic gneiss. The remaining paleozoic rock unit above the Honey

Hill Fault is the quartz-biotite-amphibole rich Tatnic Hill Formation.

The Honey Hill Fault zone is composed of biotite-rich rocks similar to the Tatnic Hill formation, bounded at 750 m and 810 m by amphibolitic mylonites (figure 11). Beneath the fault zone, granitic gneisses grade downward into more biotite-rich gneisses of the Waterford Group. The interval from 1300 m to 1480 m is an amphibole-rich gneiss grading into a more quartzitic rock. An amphibolite interval is found at the very bottom of the wellbore. Within the Waterford Group is a zone from 1120 to 1270 m which appears to be interlayering of amphibolitic and felsic rocks, bounded top and bottom by pegmatitic dikes (figure 11).

Trace Elemental Variations in the Moodus Well

The lithostratigraphic classification from the log-derived mineralogy model did not consider the variations of U, Th or Gd. These trace elements further clarify the lithostratigraphic interpretation of the geochemical logs. The basal Waterford Gneiss contains very low abundances of U, Th, and Gd, for example, whereas the upper Waterford Formation is somewhat higher in Th content (figure 8). Of particular interest is the interlayered zone, which has very high Gd values even though the felsic and amphibolitic units immediately above and below (from which the interlayered rock presumably cam) have low HREE values. This zone and its bounding pegmatitic dikes are likely to have an intrusive origin rather than a structural origin. That is, variations in HREE content within rocks of similar major elemental compositions must come from magmatic fractionation rather than from hydrothermal overprinting during shearing. Hydrothermal temperatures are not believed to be high enough to mobilize Gd or other HREE.

The Honey Hill Fault contains high Th content biotite-rich rocks bounded by low Th amphibolites. The extremely high Th content continues upward into the Tatnic Hill Formation, though the U content is low. The granites of the Canterbury Gneiss have high U as well as high Th values (figure 8). High U content continues to the surface in the Hebron Formation, but the Th and HREE values are low. The so-called "silver bullet gneiss" from 340 to 420 m contains up

to 20 ppm Uranium. These variations in U and Th content will be further developed into quantitative geochemical fluxes below.

Heat Flow and Heat Production in the Moodus Well

The Moodus well lies within the New England Heat Flow Province of Birch, et al, (1968), a region characterized by a positive linear relationship between heat flow and near-surface radiogenic heat production. The remarkable consistency of this relationship througout New England allows for general correlations between heat flow and lithostratigraphy. Precambrian basement terrains, depleted in radiogenic elements through metamorphism and hydrothermal circulation throughout New England, have the lowest heat flow, the Paleozoic metamorphics have slightly higher values, and Mesozoic and Cenozoic intrusives, enriched in Uranium and Thorium, typically have high heat flow, often as high as in regions of active tectonics, such as the Basin and Range.

Situated as it is across a major low-angle thrust of Paleozoic strata over Precambrian basement, two heat flow concerns are predominant in the Moodus Well. First, is the heat flow consistent with the higher values typically associated with the Paleozoic rocks of New England or the lower Precambrian values? Heat flow controls the geothermal gradient, which in turn, determines the depth of the brittle-ductile transition, and thus has important implications for the nature of regional stress and strain accumulation. Second, is there evidence of fluid flow associated with high permeability fractures and faults? Given the widely recognized importance of crustal fluids as both instigators (through high pore pressure) and indicators (through tectonically-driven flow) of increased seismicity, the evidence provided by heat flow profiles for the presence or absence of fluid flow constrains the causes and effects of the local earthquakes occurring at Moodus.

Geothermal Data Acquisition and Analysis

Most of the calculations and estimates presented here are based upon the Schlumberger log measurements discussed above, especially the K, U, and Th contents available from the natural

spectral gamma tool (NGT). However, in order to obtain an equilibrium temperature log, a Lamont logging crew returned to the Moodus well in February, 1988, seven months after drilling ended, to run a self-contained temperature and pressure logging tool into the well. In addition, samples from 9 cores were taken to the U.S. Geological Survey in Menlo Park, California, where thermal conductivity measurements were made.

While the core measurements provided valuable calibration points, the average core spacing of 500 feet precluded their use for developing a profile of heat flow versus depth in the well. Instead, thermal conductivity profiles were calculated from the geochemical log-derived mineralogy via a method developed by Williams et al. (1988). The standard (and usually most successful) approach utilizes a geometric mean model for conductivity,

$$K = K_1^{V_1} * K_2^{V_2} * K_3^{V_3} * \ldots\ldots\ldots * K_n^{V_n} \qquad (1)$$

where K_n is the thermal conductivity of the nth constituent of volume fraction n. However, as the dual laterolog has already shown, the strong subhorizontal foliation of the formations present in the Moodus well produces a highly anisotropic thermal conductivity, with the vertical component as much as 40% less than the horizontal. While the geometric mean matches the horizontal conductivity, the appropriate model for the vertical thermal conductivity (which controls the heat flow) is a series model of the form:

$$1/K = V_1/K_1 + V_2/K_2 + V_3/K_3 + \ldots\ldots\ldots + V_n/K_n \qquad (2)$$

Figure 12 displays the results of this series computation as well as a comparison of the core measurements with the log-derived curves.

Heat Generation in the Moodus Well

Crustal heat production was calculated from the abundances of K, U, and Th according to the relation:

$$A = 0.26U + 0.07Th + 0.40K \qquad (3)$$

where A is the heat production in microwatts per cubic meter, U and Th are abundances in parts per million, and K is in dry weight percent (Wollenberg and Smith, 1987). All four curves in eq. (3) are displayed in Figure 13, with heat production averaging ~3.4 microwatts per cubic meter in the Paleozoic section above the Honey Hill Fault (which covers a zone from 750m to 820m) and ~2.1 microwatts per cubic meter in the Precambrian section below.

The numerous spikes in heat production result from Uranium peaks associated with pegmatitic intusions which are present throughout the section. The large abundance of Uranium which appears from 320m to 410m part of a thick section of the Silver Bullet Gneiss, which is not enriched in Th. All three radiogenic elements are enriched in the Canterbury Gneiss from 580m to 640m, while Thorium enrichment only continues from the Tantic Hill to the base of the Honey Hill Fault. In general, the Precambrian Waterford rocks are depleted in both Uranium and Thorium relative to other Precambrian rocks in the New England area, although Potassium remains relatively constant throughout the well, except for high values in the Silver Bullet Gneiss, Canterbury Granite, Tatnic Hill Gneiss and the interlayered zone from 1090m to 1270m within the Waterford Group (figure 13).

Geothermal Results and Interpretations

The temperature, temperature gradient, log-derived thermal conductivity and resulting heat flow in the Moodus #1 Well are shown in Figure 14 for the depth range 250m to 850m. In general, heat flow is relatively constant, averaging approximately 51 mW/m^2, except for the section from 750 m to 820 m (the Honey Hill Fault), where a lower thermal gradient combines with slightly lower thermal conductivity to decrease the heat flow to ~40 mW/m^2. Since heat flow returns to the higher value below the Honey Hill Fault, only two possible explanations can account for the decrease within the fault zone. Given the disturbed and deformed nature of the rocks near the fault, it is possible that the series-model for the calculation of thermal conductivity underestimates the conductivity

in the fault zone. However, the presence of heavily fractured rock probably decreases rather than increases the thermal conductivity. A more likely explanation is that drilling across the Honey Hill Fault opened previously isolated fractures to fluid from the wellbore. A first-order calculation of the intake flow rate needed to account for the depressed heat flow gives an approximate fluid velocity of 20 cm/year into the fault, a slow flow rate that could easily be driven by changes in the water column within the borehole.

There are no other detectable indications of fluid flow from the geothermal measurements in the Moodus well, suggesting that the high level of microseismicity has not altered the stable, hydrostatic pressure regime of formation fluids in the section of hole for which we have accurate temperature data. Water inflow was detected deeper than 1000 m, however, and cement was required to grout the well from 1000 to 1100 m depth. Unfortunately, the grouting prevented us from making accurate temperature measurements in this section of the well.

Mobilization of Heat Generating Elements

As noted above, there is ample evidence for the mobilization of radiogenic elements because of depletion in the Precambrian and enrichment in the Paleozoic rocks of the Moodus well. This is most easily seen by considering the relationship of Thorium to Uranium. Thorium, a relatively immobile element, can only be transported in significant quantities through high temperature metasomatic processes, whereas Uranium is most commonly leached from a host rock by relatively low temperature oxidizing fluids, and deposited as a low-temperature precipitate. In the Moodus area, both processes have been highly active in the past, accounting for systematic depletion of Thorium and Uranium below, and enrichment above the Honey Hill Fault. Figure 15 shows a plot of the Uranium to Thorium ratio versus Uranium content. Most basement rocks yield a nearly constant U/Th ratio of 1/4, but in the Moodus well the ratio is not constant. The plot in Figure 15 displays a c x (c is a constant) vs. x trend, which shows that changes in Uranium content do not correlate with changes in Thorium content, confirming the mobilization of Uranium relative to Thorium. If Thorium moved with Uranium, the Uranium to Thorium ratio would remain constant, and the data in

Figure 15 would plot on a horizontal line (slope equal to zero) instead of on a line with a positive slope, c.

Given the ease with which Uranium can be mobilized by low temperature fluids, the high levels of Uranium in the pegmatitic intervals suggest that very little hydrothermal circulation or metasomatism has taken place since emplacement of these units. Typical U-Pb isotopic ages for these pegmatites place them within the Permian collision event between North America and Africa at ~270 Ma (Wintsch et al., 1985). The survival of abundant U in these intervals indicates that the entire Moodus section has been free of significant fluid flow disturbances since that time. Thus, the intrusion and faulting associated with Triassic rifting must have been confined to areas immediately to the west such as the Hartford and Newark Basins. Rifting, seafloor spreading, and subsequent tectonic events have not left any hydrothermal imprint on the rocks of the Moodus well.

In the light of these results, what are the implications for heat flow and the geothermal gradient? Figure 16 shows a plot of heat flow and heat production data from New England (Birch et al., 1968), along with data from the Moodus well. If the Avalon rocks from below the Honey Hill fault are used for the reference heat production, the data from Moodus fall exactly on the New England trend. This identifies the Moodus region as an area of low heat flow, and despite uncertainty regarding thermal conductivity at depth in the crust, the low heat flow and heat production suggest that the brittle-ductile transition (which probably corresponds to the interval between the 300 deg C and 450 deg C isotherms) is at a depth of approximately 20 km. Thus, all of the upper crustal deformation in eastern Connecticut proceeds by brittle fracture, and the same strain responsible for microseismicity at Moodus is accumulating elastically at depth.

One of the possible implications of the linear heat flow-heat production relationship, (figure 16), is that within a given heat flow province, heat production decays with depth according to the relation:

$$A(z) = A(z=0)\, e^{-z/d} \qquad (4)$$

where d is the slope on the heat flow-heat production line, z is depth and A is heat generation. Since the Avalon terrain appears to fall within the same province as the Merrimack synclinorium, it is possible to calculate the amount of offscraping along the Honey Hill Fault required to reduce the Precambrian heat production to its current value from a value equivalent to the Paleozoic rock overlying it. With d = 7.5 km, a simple calculation yields z = 3.6 km, which is the amount of Avalon section missing relative to the Merrimack.

Geochemical Mass Fluxes

By normalizing the elemental compositions found within the well to those at the Honey Hill Fault, we can examine chemical variations which may have resulted from the overprinting of metasomatic or hydrothermal fluid alteration on top of the basic lithological variations of the original igneous and sedimentary rocks in the Moodus well. This analysis allows for the identification of the predominant changes in chemical abundances that are from the metamorphism versus those from variations in original composition. Obviously, there were initial igneous and sedimentary compositional differences between formations in the well, and we identify these as abrupt chemical transitions that occur exactly at the lithostratigraphic boundaries observed above.

Major elemental fluxes are predominantly from such lithological contrasts (figure 17), as can be seen from the variation in Si, Al, Ca, Mg, K, Fe and Ti across the interlayered zone within the Waterford Group. Trace elemental fluxes tell quite a different story, however, with general increases in abundances recorded upward in the well for U, Th and S (figure 18). Exceptions are not found at major lithologic units, but in pegmatitic and amphibolitic dikes which appear to have postdated metamorphism (see above). Evidence for fluxes of U , S and hi Th upward appear to be prevalent in this well. The fact that these elements do not move in concert further constrains the timing of such fluxes.

Quantification of the Geochemical Mass Fluxes in the Moodus Well

We divide the well into two segments; above versus below the Honey Hill fault, on the assumption that fluid pathways were likely different in the two cases. Below the fault, fluids were probably moving upward as bouyancy was driving dewatering of the Avalon metamorphic terrain. The related shallow thrusts along and above the Honey Hill Fault introduce a considerable horrizontal component to the permeability structure surrounding the upper part of the well. Therefore, the chemical system is not likely to have been closed (i.e., vertical), especially along and above the Honey Hill Fault. By seperating the two analyses, we can examine geochemical changes in spite of these different hydrological constraints. That is, the geochemical mass fluxes from the two intervals may be additive if the system was closed and dominated by vertical fluid flow. However, if horizontal fluxes entered the column at the fault zone, the chemical fluxes from the two zones will not be additive.

We can integrate the changes in composition with depth away from the Honey Hill Fault for major elements (figure 19) and minor elements (figure 20). We see that Al does not increase significantly across the fault, whereas Si increases dramatically. Ca and K changes are less severe. An examination of the mineralogy model (figures 10 and 11) shows that the increases in Si and K are primarily due to increases in quartz and orthoclase contents above versus below the fault. For example, the Canterbury granitic gneiss at 600 m is significantly enriched in quartz.

Hydrothermal alteration might have significantly changed the mafic content of the country rock, and indeed there appear to be very large differences in Mg, Fe and Ti across the fault. Fe and Ti increase toward the fault from both above and below (figure 19). Mg increases below the fault as hornblende content increases with depth substantially. Low temperature hydrothermal alteration should have resulted in increased Mg content coupled with a concommittant decrease in Ca content. Instead we find a small decrease in Ca as well as the large decrease in Mg content as the fault is approached. It is therefore probable that the Mg change is caused by primary

lithological contrast between units within the Waterford Group.

The minor element mass fluxes cross lithological boundaries more noticably than those of the major elements (figure 20). For example, Thorium is significantly enriched above versus below the fault, as are Uranium and Sulfur concentrations. S increases because of an increased occurrence of precipitated pyrite. Th content is highest in the Tatnic Hill formation, indicating significant mass transfer of Th either with emplacement of the Tatnic Hill, or from high-temoperature fluid movement along and upward from the Honey Hill Fault. There is significant depletion in Th below the fault, perhaps because of Th movement into the Tatnic Hill formation, but not enough Th is missing from the lower Precambrian rocks in the well to account for the magnitude of the Th increase in the Tatnic Hill formation.

This "Thorium-event" appears to be a critical fluid flow marker in the tectonic development of the Moodus terrain. The Precambrian and Paleozoic rocks of the Hebron and Waterford Groups appear to have been in place before emplacement of the Tatnic Hill formation, because there is uniform enrichment in Th upward throughout the well except for the Tatnic Hill formation. Permian thrusting along a ductile shear zone at 350-400 degrees C appears to have produced the mylonitization along the Honey Hill Fault at this time. Metasomatism accompanying this thrusting is the likely source of Thorium enrichment in the Tatnic Hill formation.

U and S must have moved upward across the Tatnic Hill after this "Thorium-event" because both elements increase uniformly upward in the well. These elements reacted with colder tempreature hydrothermal fluids to remove significant U and S from Tatnic Hill, suggesting it was already in place before this "cold-temperature event" occurred. That is, the Tatnic Hill formation has also been stripped of U just as with the units below the Honey Hill Fault (figure 20).

Intrusions at 270 ma of the Silver Bullet Gneiss, the Canterbury Granite, and the pegmatitic intrusuions that produced the large U spikes in figure 13 must have postdated both hot and cold fluid movements along and across the fault because these U peaks have

not been "washed away" by chemical reactions.

Integrated Mass Fluxes

We can further quantify the total geochemical mass fluxes of elements moved by these crustal fluids. To begin, we must calculate the total volume of each element moved by estimating the porosity (ϕ) and density (p) changes accompanying alteration, which appear from the porosity log to be from 1 to 4 % and from the density log to be from 2.8 % to 2.6 % (figure 18). The total integrated mass flux (F) of each element i (in grams) is then:

$$F_i = \frac{(1-\phi^b)}{(1-\phi^a)} (p^b/p^a) \int_{z_1}^{z_2} (X^b_i - X^a_i)\, dz \qquad (5)$$

where X^b_i is the weight fraction of element i in the altered rock and X^a_i is that in its protolith (from Lesher, et al, 1986). Figure 21 presents the integrated geochemical mass flux of each element, F_i. The mass fluxes, F_i, as a percentage of the total mass of each element available in the protolith, F_t, are shown in figure 22. The absolute mass flux in weight percent and grams for each element, along with the percentage of the mass flux relative to that of the total mass of each element available for mobilization, are also shown in Table 2.

Experimental error in the geochemical log data results in a probable +/- 0.3 % dispersion in the F_i calculation, somewhat higher than the 0.1 % value attributable to laboratory analysis error (Lesher, et al, 1986). This error can be varified by examining the Gd flux which should be zero because it is an incompatible element. The geochemical mass flux analysis suggests that Al and Ca have not moved substantially. Si appears large in relative terms (figure 21), but not in absolute terms because of the large number of Si cations available in silicic rocks (figure 22). As noted above, Mg moving alone without a concommittant decrease in Ca is likely to be of primary igneous origin, as are Fe and Ti changes.

More importantly, the geochemical mass flux calculations predict that 9.6 % of the available Sulfur, 9.7 % of the Uranium and 3.0 % of the Thorium has been enriched above the fault zone by fluid movements. The origin for the Uranium increase is not totally from beneath the fault, however, but from downslope along the fault plane, as well. Although the overall content of Uranium in the Avalon Group is somewhat low for Precambrian rocks (see above), these rocks are not depleted enough to account for the large enrichment in U above the fault (figure 22). Sulfur enrichment above the fault also must be derived from both along the fault and from below for the same mass balance arguements (figures 20 and 22). In contrast, Th displays enrichment upward throughout the well, indicating a source from below the total depth of the well as well as from along the fault plane (figures 20 and 22) .

Summary

The conclusion based upon the logging measurements is that an important geochemical overprinting of the Moodus well rocks has occurred from first hot, then cold fluid movements along and across the Honey Hill Fault. A major "Thorium-event" appears to have accompanied thrusting of the Tatnic Hill formation over Percambrian basement. Th enrichment was caused by the upward movement of hot, metasomatic fluids. Depletion below, and enrichment above the Honey Hill Fault of U, and S, appears to have accompanied a later cold-temperature hydrothermal event. All significant fluxes appear to have moved before the intrusion of the Silver Bullet Gneiss, the Canterbury Granite, and pegmatitic intrusives in the Waterford Group because these units each retain their primary Uranium concentrations.

Unfortunately, the geochemical mass fluxes calculated above represent an integrated result of all the previous history of these Paleozoic and older rocks, complete with structural and metamorphic changes which have occurred beneath eastern Connecticut from the time of implacement, through thrusting, subsequent fault movement, and alteration to the present day. Consequently, we do not have further constraints with which to

estimate additional useful time-dependant chemical parameters such as water-rock ratios from these logging measurements.

An important implication of the large-scale movement of geochemical fluxes along and across the Honey Hill Fault concerns the Hubbard and Rubey (1959) pore pressure hypothesis for the cause of low-angle thrusting. There has clearly been significant fluid movement along the Honey Hill Fault. The only non-convection mechanism for mass fluxes in the crust is diffusion, and even in such old terrains, the rates are too slow and at too small magnitudes to account for the mass exchange observed in the well. The geochemical logging results at the Moodus #1 well demonstrate that such fluid movements were certainly present on a large scale in the past. The discordance between the fluxes of Thorium and Uranium further constrain all of this mass transfer to have preceeded the emplacement of pegmatitic intrusives prior to 270 Ma. Therefore, these fluid movements have little relation to any possible mechanism for the cause of the swarms of earthquakes occurring today in the Moodus, Connecticut, area.

Acknowledgements

We wish to thank Mark Zoback and Tom Statton who saw the importance of geochemical and geophysical logging in the Moodus well, and allocated sufficient time and funds to carry out the work. This study was ultimately supported by ESEERCO, NU, and EPRI, and we thank them very much.

References

Anderson, R. N., R. Dove, L. Silver, and E. James, Geochemical Well Logs from the Cajon Pass Scientific Drillhole I: Elemental and mineralogical analyses from logs and their preliminary comparison with core analyses, Geophys. Res. Lett., 1988a.

Anderson, R.N., Dove, R.E., and Pratson, E., The calibration of geochemical well logs in basalt, granite and metamorphic rocks, and their use as a lithostratigraphic tool, Geol. Soc. London, in press, 1988b.

Anderson, R. N., C. Broglia, P.Pezard, and C. Williams, Geochemical Well Logs from the Cajon Pass Scientific Drillhole II: Discrimination of Distinct Lithostratigraphic Units within the Granitic Basement, Geophys. Res. Lett., 1988c.

Birch, F., Roy, R.F., and Decker, E.R., Heat flow and thermal history in New England and New York, in Studies of Appalachian Geology: Northern and Maritime, Zen, White and Hadley, eds, Wiley Interscience, 437-451, 1968.

Herzog, R., L. Colson, B. Seeman, M. O'Brien, H. Scott, D. McKeon, P. Wraight, J. Grau, J. Schweitzer, and M. Herron, Geochemical Logging with Spectrometry Tools, Soc. Pet. Engrs, SPE Paper 16792, 1987.

Hubbard, M.K. and Rubey, Role of fluid pressure in the mechanics of overthrust faulting, , Geol. Soc. Am. Bull, 70, 115-166,1959.

Lesher, C.M., H. L. Gibson, and I. H. Campbell, Composition-volume changes during hydrothermal alteration of andesitr at Buttercup Hill, Noranda District, Quebec, Geochem. Cosmochem. Acta., 50, 2693-2705, 1986.

Naumoff, P. G, Lithology and structure identified in a 1.5 km borehole near Moodus Connecticut, EOS, 69, 491, 1988.

Williams, CV.F., R.N. Anderson, and C, Broglia, In situ investigation of , Thermal Conductivity, Heat Generation, and Heat Flow in the Cajon Pas scientific drillhole, California, Geophys. Res. Lett., in press, 1988.

Wintsch, R. P. and J-P LeFort, A clockwise rotation of Variscan strain orientation in SE New England and regional implications, in Hutton, D.H.W. and Sanderson, D.J., eds, Variscan tectonics of the North Atlantic region, Oxford, Blackwell Sci. Publ., 245-251, 1982.
Wintsch, R.P., and Aleinikoff, J.N., U-Pb isotopic and geological evidence for late Paleozoic anatexis, deformation and accretion of the Late Proterozoic Avalon terrain, south central Connecticut, Am. J. Sci, 287, 107-126, 1987.

Wintsch, R.P., and Ambers, C.P., Regional correlation of subsurface lithologies and structures, Moodus, Connecticut, EOS, 69, 495, 1988.

Wollenberg, H.A. and Smith, Radiogenic heat production of crustal rocks: an assessment based on geochemical data, Geophys. Res. Lett., 14, 295-298, 1987.

Figure Captions

Figure 1. Schematic cross-section from west to east across the Moodus #1 well in east central Connecticut, and the relative location of the surface break of the Honey Hill and Lake Char Faults.

Figure 2. Geophysical logs from the Moodus #1 well. Units of density are gm/cm3, and SGR, API units.

Figure 3. Dipmeter and Formation Microscanner logs across the Honey Hill Fault. The Formation Microscanner gives a high resolution image of the resistivity contrast shown in large scale by the dipmeter. The fault is a series of en echelon fracture zones of low resistivity (black) dipping about 15 degrees to the west.

Figure 4. Dipmeter resistivities and strike-dip "tadpoles" indicating geometry of Honey Hill Fault zone (2535-2555 ft.).

Figure 5. Schmidt stereograms of strike and dip of Honey Hill Fault Zone (center), and Tatnic Hill formation above and below, from figure 4.

Figure 6. Cartoon of geometry of Honey Hill Fault zone indicated by figures 3, 4, and 5.

Figure 7. Formation Microscanner image of thrust fault dipping 37 degrees to the east in the Waterford Formation of the Precambrian Avalon Group.

Figure 8. Geochemical well log analyses from the Moodus #1 well. Dashed curves are dry weight percent oxide analyses for the major elements and ppm analyses for the trace elements. Solid lines are

the theoretical elemental abundances calculated from a matrix inversion model of mineralogy in the well (figure 7). Solid dots are X-ray Fluorescence chemical analyses from cuttings of the well (from Wintsch and Ambers, 1988).

Figure 9. Discriminant analysis of geochemical logs (figure 5). Two end-members were taken to be the mafic diorite at 4180-4250 feet and the granitic gneiss at 2700-2900 feet. Major lithostratigraphic units are shown as well.

Figure 10. Mineralogy logs from a matrix inversion of major elemental abundances from the geochemical logging results (figure 5). Ideal mineral compositions are given in table 2.

Figure 11. Simplified lithostratigraphy from mineralogy model of figure 10.

Figure 12. Plot of vertical (diamonds) and horizontal (squares) thermal conductivities from core, along with log-derived thermal conductivities for geometric mean model (eq. 1, in text), and series model (eq. 2 in text).

Figure 13. Potassium, Uranium and Thorium contents from geochemical well logs, and heat generation calculated from eq. 3 in text for the Moodus well.

Figure 14. Temperature, temperature gradient, log-derived thermal conductivity, and heat flow from 250 to 850 m in the Moodus well. Note the low heat flow across the Honey Hill Fault from 750 to 820 m.

Figure 15. Uranium to Thorium ratio plotted against Uranium for the Moodus well logs. The data points are 100 m averages taken within individual formations. Note the positive correlation that demonstrates the mobility of Uranium relative to Thorium.

Figure 16. New England heat flow and heat production data from Birch, et al, 1968 (solid triangles), along with heat flow from Moodus well plotted for heat production from the Precambrian and Paleozoic sections (solid circles). The Precambrian rocks extend

from 700 m to the base of the crust, so the Precambrian heat production is the preferred value for comparison to the Birch values (leftmost circle).

Figure 17. Smoothed major elemental abundances from figure 8. Vertical lines are protolith compositions from the Honey Hill Fault.

Figure 18. Minor elemental abundances from figure 8 smoothed and normalized to the composition of the Honey Hill Fault. Density and porosity from figure 2 are also smoothed to the same degree.

Figure 19. Integrated geochemical mass fluxes in dry weight percent of the major element oxides away from the Honey Hill Fault. To the left is depletion and to the right is enrighment. Horizontal bars are major lithological boundaries in the hole from figure 11.

Figure 20. Integrated geochemical mass fluxes for minor elements in th3e Moodus well. Symbols as in figure19.

Figure 21. Total geochemical mass flux (Fi from eq. 5, text) in grams above versus below the fault for each element (see Table 2).

Figure 22. Ratios of elemental mass fluxes calculated in Table 2 (figure 21) to the total amount of each element in the protolith. Such a plot gives an accurate estimate of the relative magnitudes of the geochemical mass fluxes for the elements.

Table 1

Cajon Pass Mineral Inversion Matrix

ELEMENTAL	SiO2	TiO2	Al2O3	FeO*	Na+MgO	CaO	K2O	S
Weight %								
MINERAL								
Quartz	115	0	0	0	0	0	0	0
Plagioclase	60	0	22	0	6	7	0	0
Orthoclase	64	0	18.6	0.5	1	0.1	10	0
Biotite	39	4.1	14	16	9	0.5	8.2	0
Hornblende	45	1.5	10	10	14	12	0.5	0
Sphene	30	20	0	0	0	10	0	0
Pyrite	0	0	0	47	0	0	0	53
Calcite	0	0	0	0	0	140	0	0

TABLE 2. Total Mass Flux from Metamorphism across the Honey Hill Fault in the Moodus #1 well.

Element	oxide wt %		Fi (gm) flux of element		F_T (gm) total element available		Fi/F_T (%)	
	BELOW	ABOVE	BELOW	ABOVE	610m BELOW	550m ABOVE	BELOW	ABOVE
Si	+635	+9,862	+9.2	+143.8	61,381	55,344	+.015%	+.26%
Al	-709	-2,679	-11.7	-44.4	14,149	12,757	-.08%	+.31%
Ca	-2,375	+224	-53.2	+5.1	5,466	4,928	-.97%	+.1%
Mg	-12,315	-659	-231.4	-12.4	2,732	2,067	-8.5%	-.6%
Fe	+11,782	-8,764	+272.6	-202.8	8,469	7,636	+3.2%	-2.6%
Ti	+1,428	1,080	+26.6	-20.2	1,025	924	+2.5%	-2.2%
K	+1,220	+1,812	+32.5	+48.3	5,693	5,133	+.6%	+.9%
Cd	+2,883	-1,156	-.007	-.003	1.36	1.23	+.5%	-.2%
U	-822	+12,893	-.002	+.032	.34	.31	-.5%	+10.3%
Th	+11,145	+9,171	+.028	+.023	1.70	1.54	+1.6%	+1.4%
S	-601	+1,602	-16.8	+44.8	342	30.8	-4.9%	+14.5%

FAULT

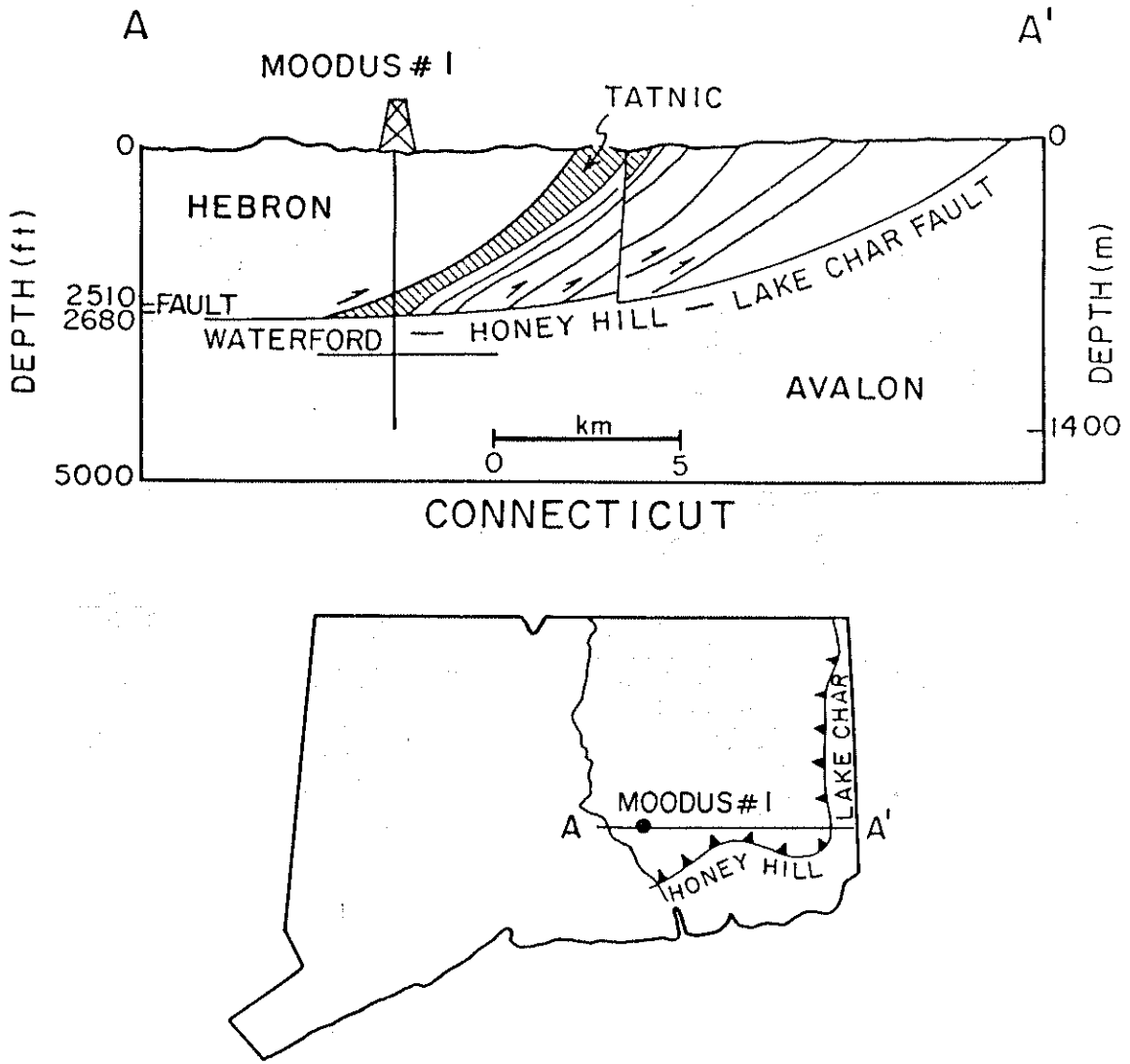
A
A'
MOODUS # 1
TATNIC
0
0
HEBRON
DEPTH (ft)
DEPTH (m)
2510
2680
FAULT
WATERFORD
HONEY HILL
LAKE CHAR FAULT
AVALON
km
0
5
1400
5000
CONNECTICUT
MOODUS#1
A
A'
LAKE CHAR
HONEY HILL

Figure 1

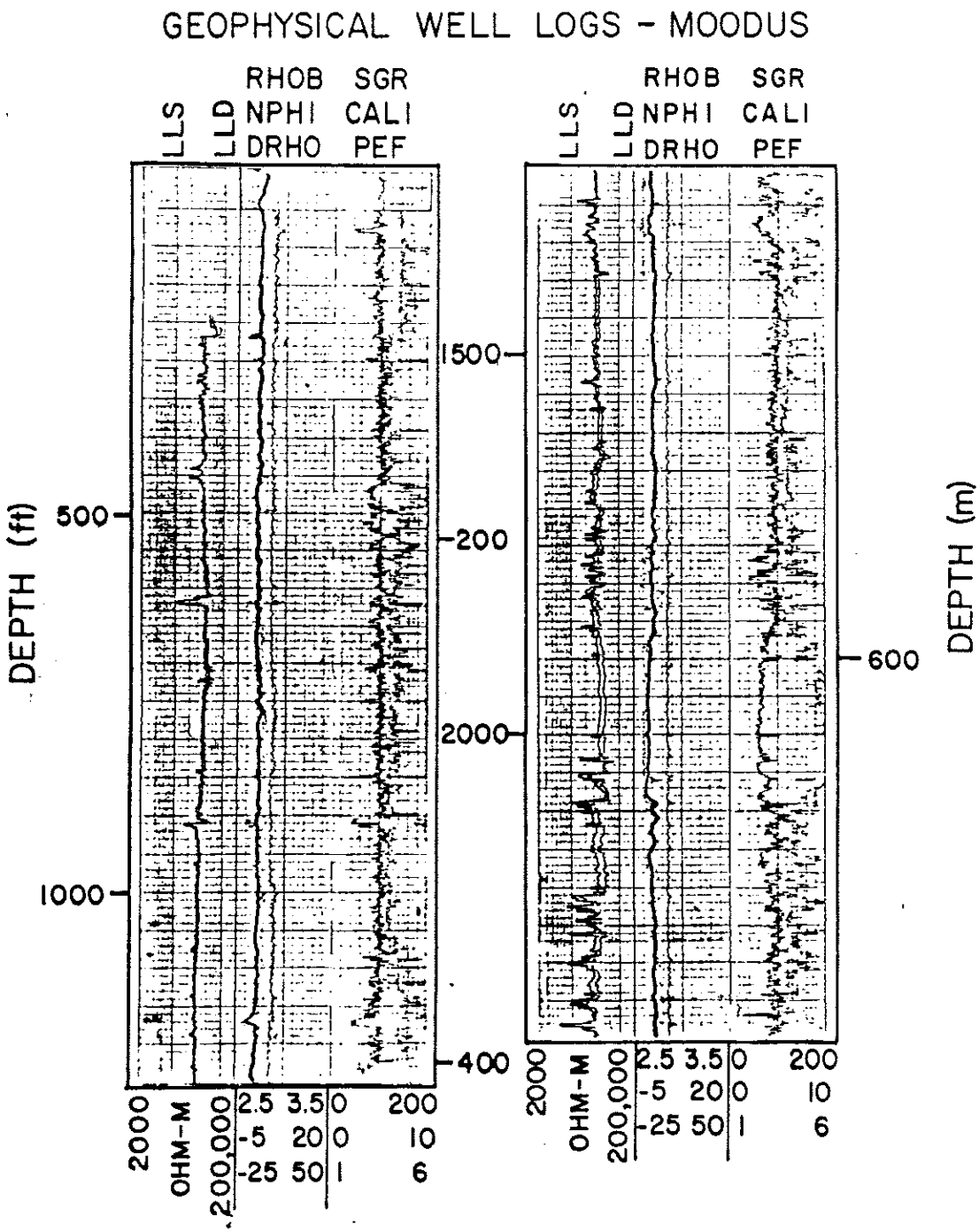
GEOPHYSICAL WELL LOGS - MOODUS
LLS
LLD
RHOB
NPHI
DRHO
SGR
CALI
PEF
DEPTH (ft)
DEPTH (m)
500
1000
1500
2000
200
400
600
2000
OHM-M
200,000
2.5 3.5
-5 20
-25 50
0 200
0 10
1 6

Figure 2

GEOPHYSICAL WELL LOGS - MOODUS

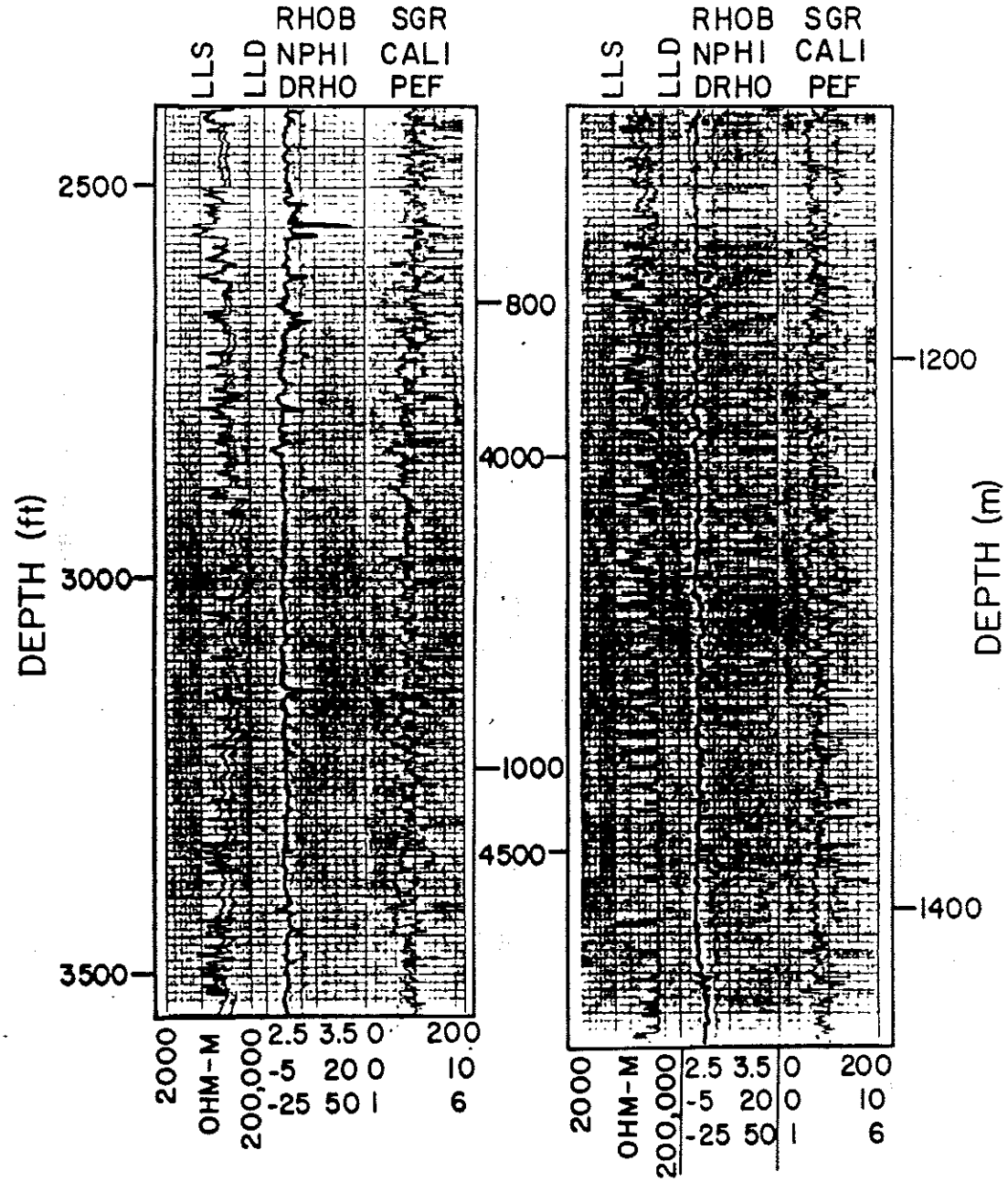

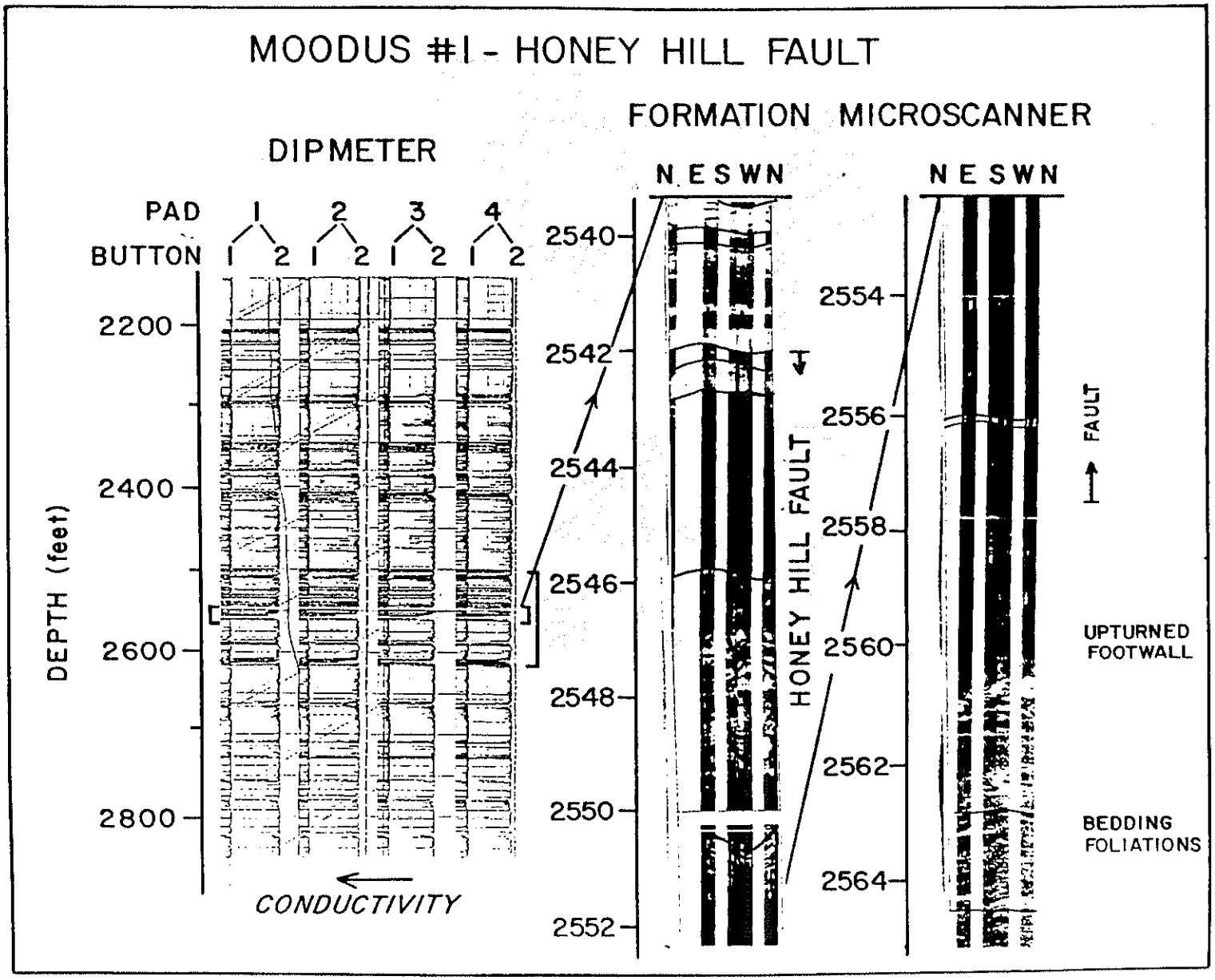
MOODUS #1 - HONEY HILL FAULT
DIPMETER
FORMATION MICROSCANNER
PAD 1 2 3 4
BUTTON 1 2 1 2 1 2 1 2
N E S W N
N E S W N
DEPTH (feet)
2200
2400
2600
2800
2540
2542
2544
2546
2548
2550
2552
2554
2556
2558
2560
2562
2564
HONEY HILL FAULT
FAULT
UPTURNED FOOTWALL
BEDDING FOLIATIONS
CONDUCTIVITY

Figure 3

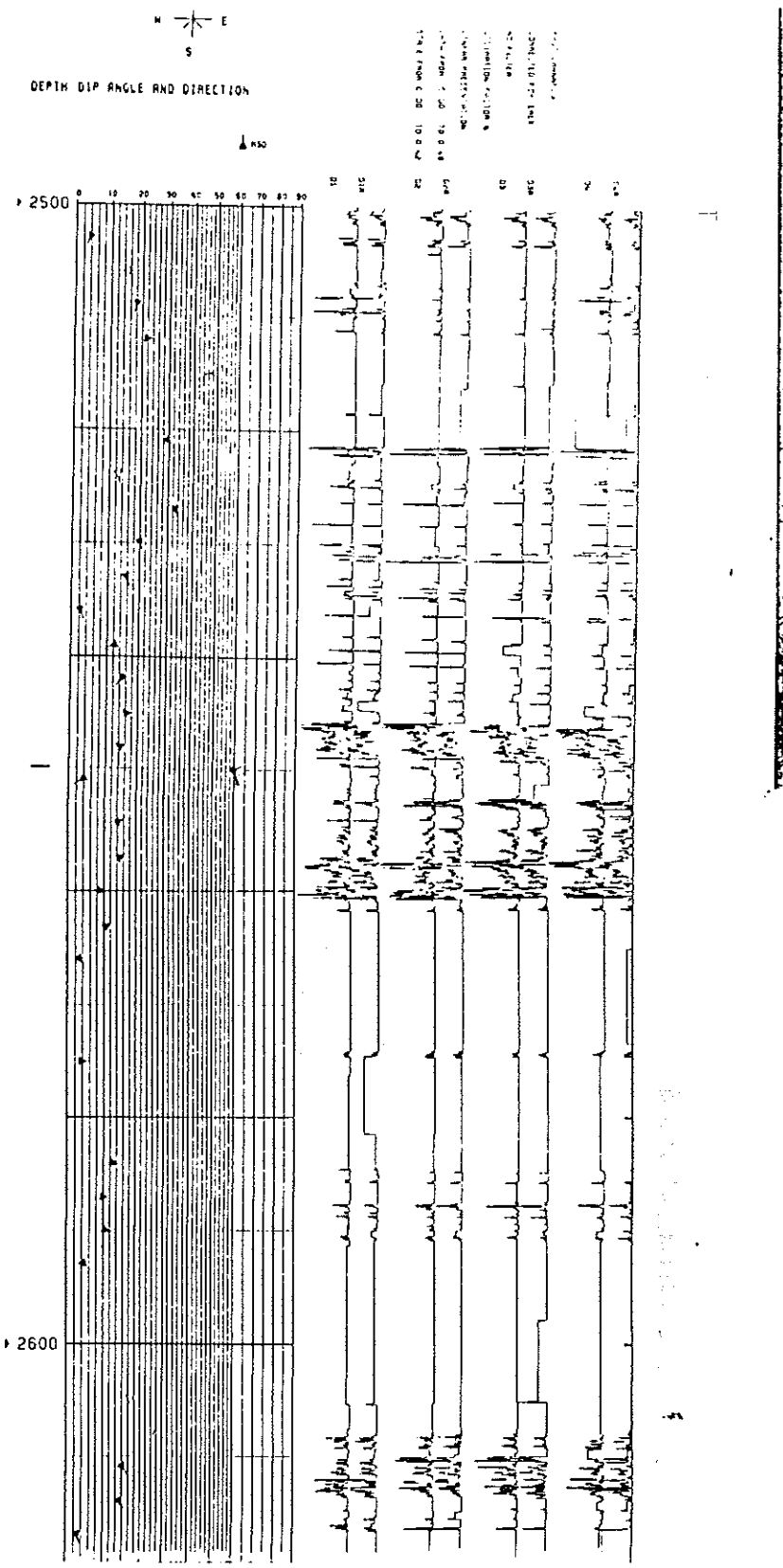

Figure 4

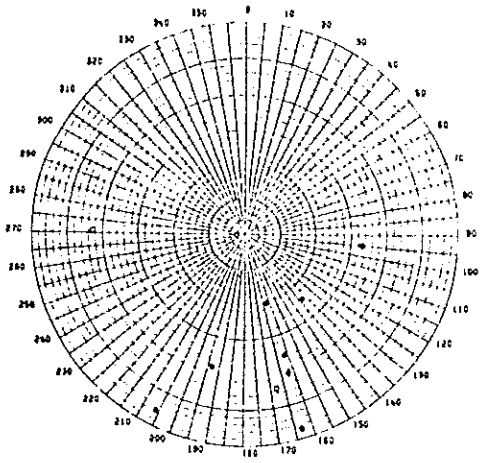

ZONE FROM 2503 FT TO 2536 FT
POLAR SCALE - FROM EDGE TO CENTER 50 DEGREES

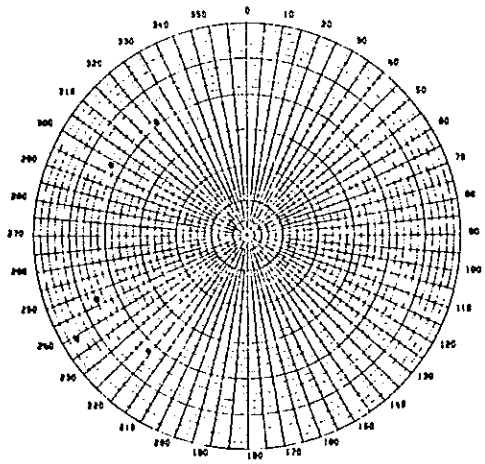

ZONE FROM 2539 FT TO 2551 FT
POLAR SCALE - FROM EDGE TO CENTER 50 DEGREES

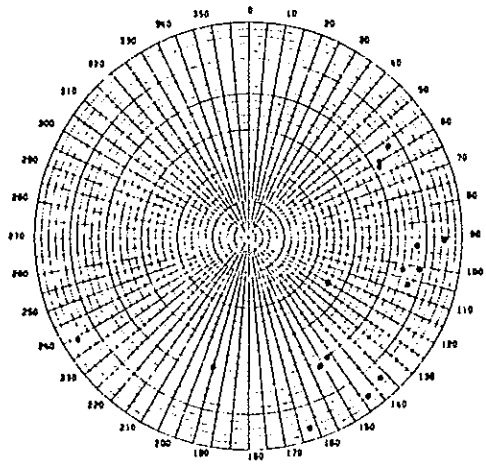

ZONE FROM 2551 FT TO 2620 FT
POLAR SCALE - FROM EDGE TO CENTER 50 DEGREES

Figure 5

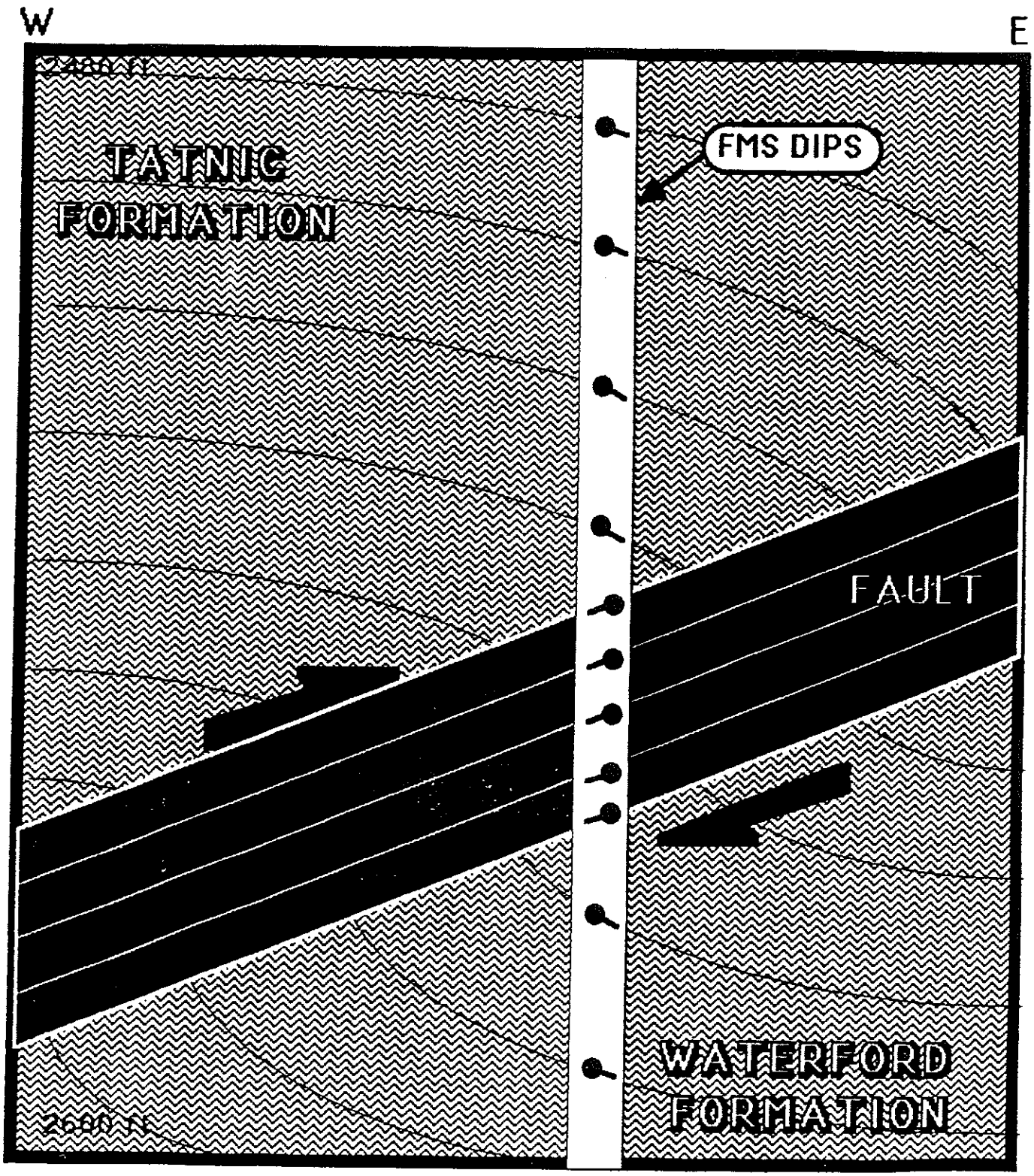

HONEY HILL FAULT ZONE

FMS-THRUST FAULT
PRECAMBRIAN

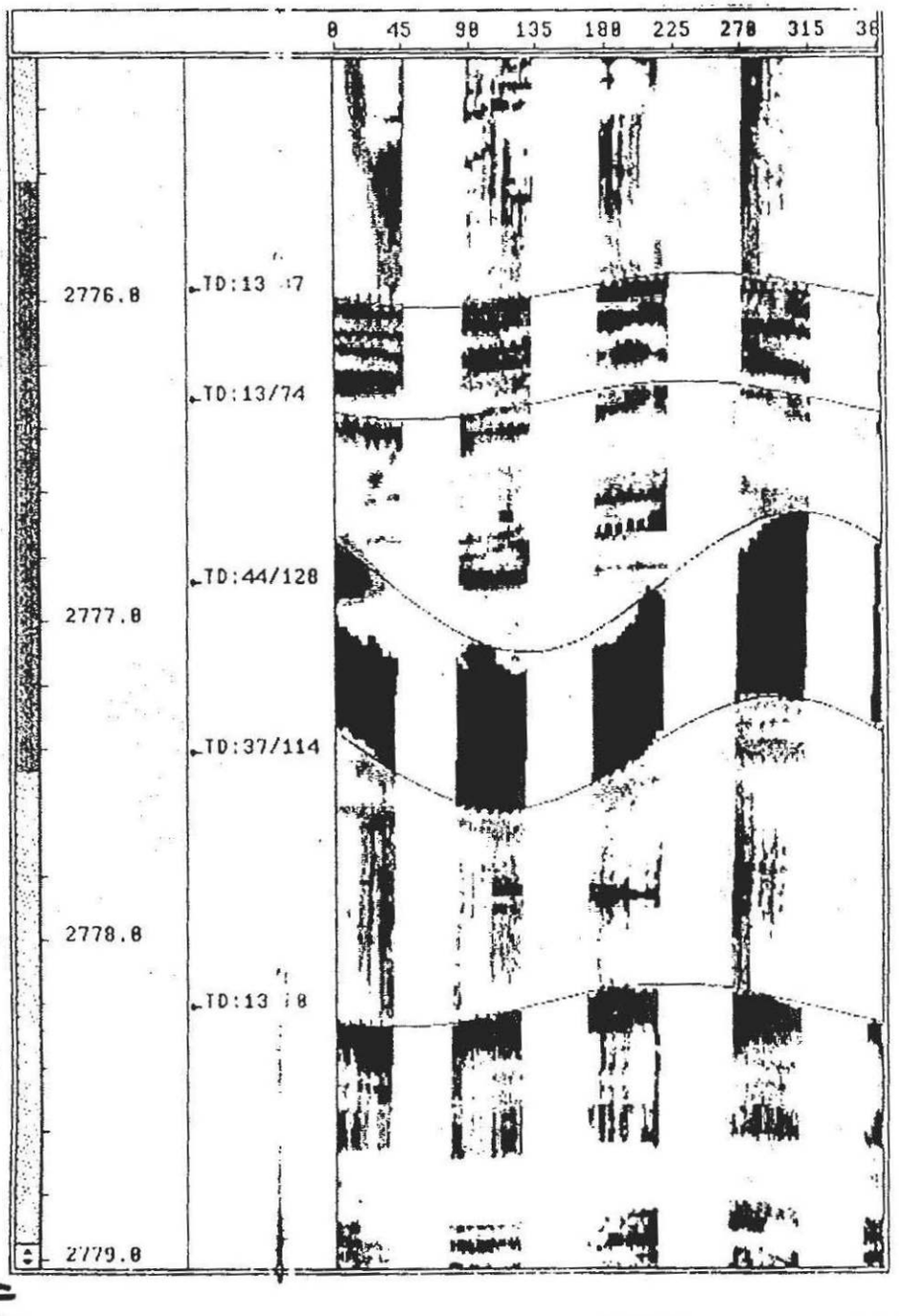

DEPTH: 2777 $\frac{1}{2}$'
STRIKE: 24° - 204°
FAULT ANGLE: 37°

Figure 7

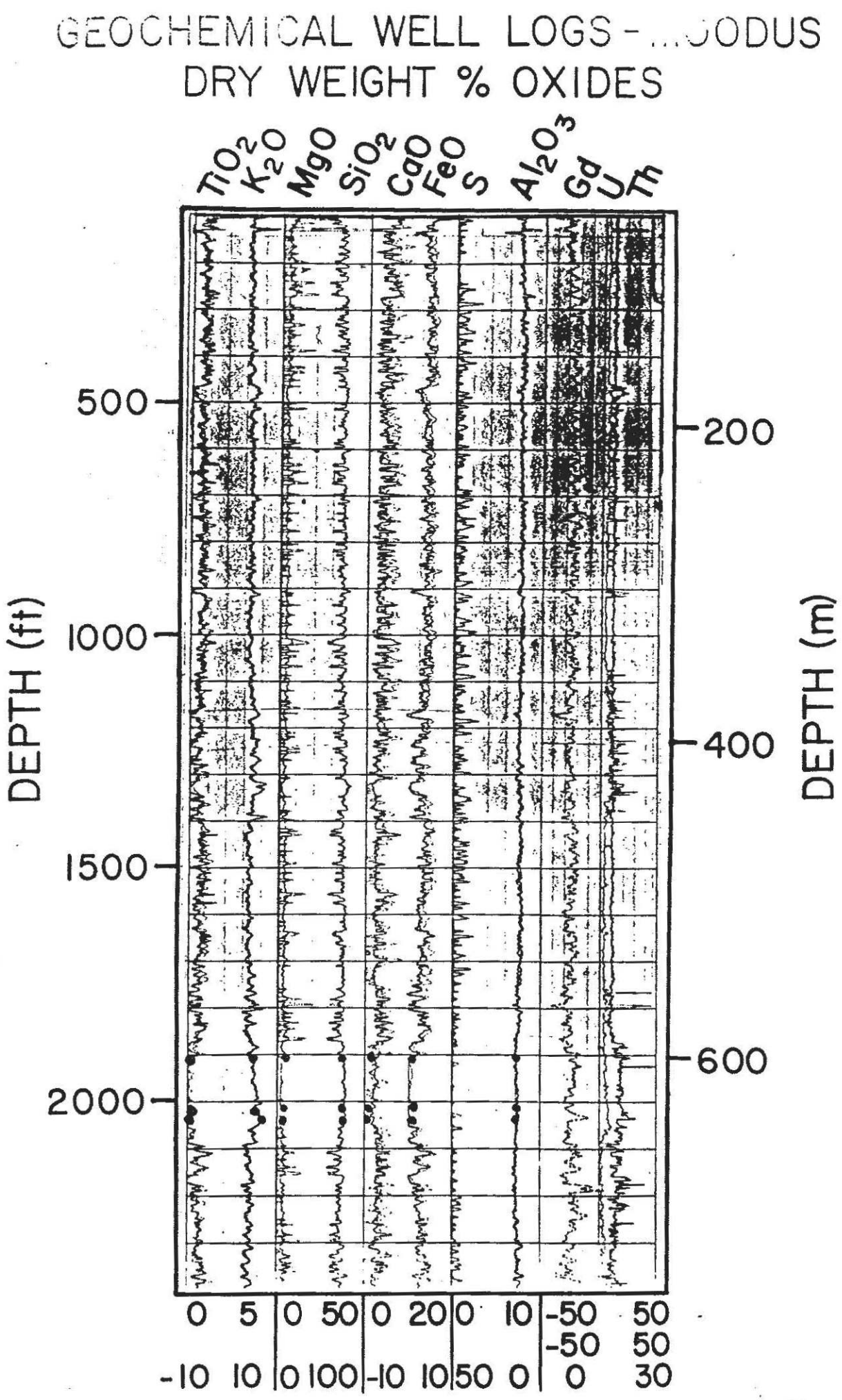
GEOCHEMICAL WELL LOGS - ...ODUS
DRY WEIGHT % OXIDES
TiO2
K2O
MgO
SiO2
CaO
FeO
S
Al2O3
Gd
U
Th
DEPTH (ft)
500
1000
1500
2000
DEPTH (m)
200
400
600
0 5
-10 10
0 50
0 100
0 20
-10 10
0 10
50 0
-50 50
-50 50
0 30

Figure 8

GEOCHEMICAL WELL LOGS - MOODUS
DRY WEIGHT % OXIDES

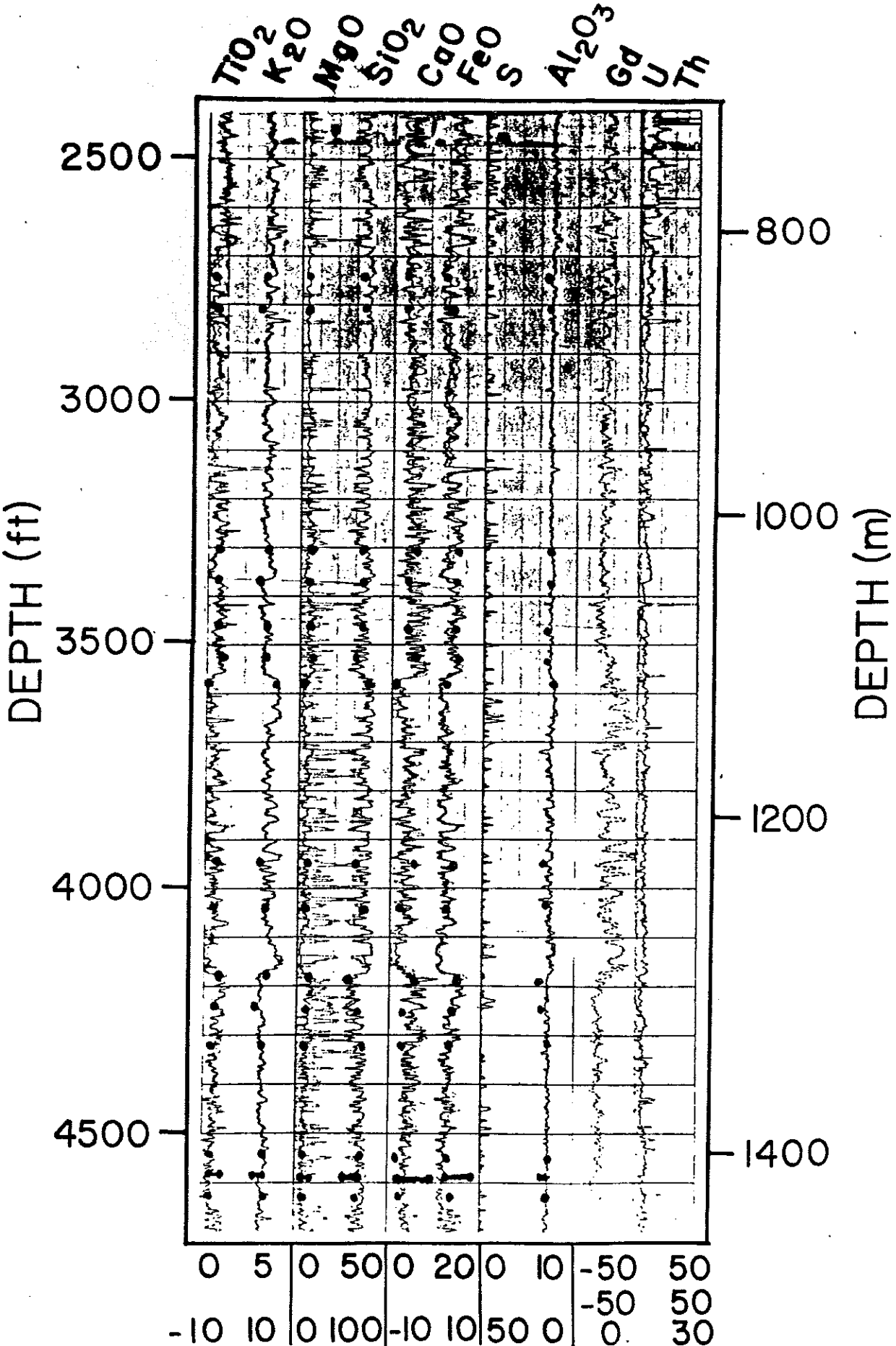

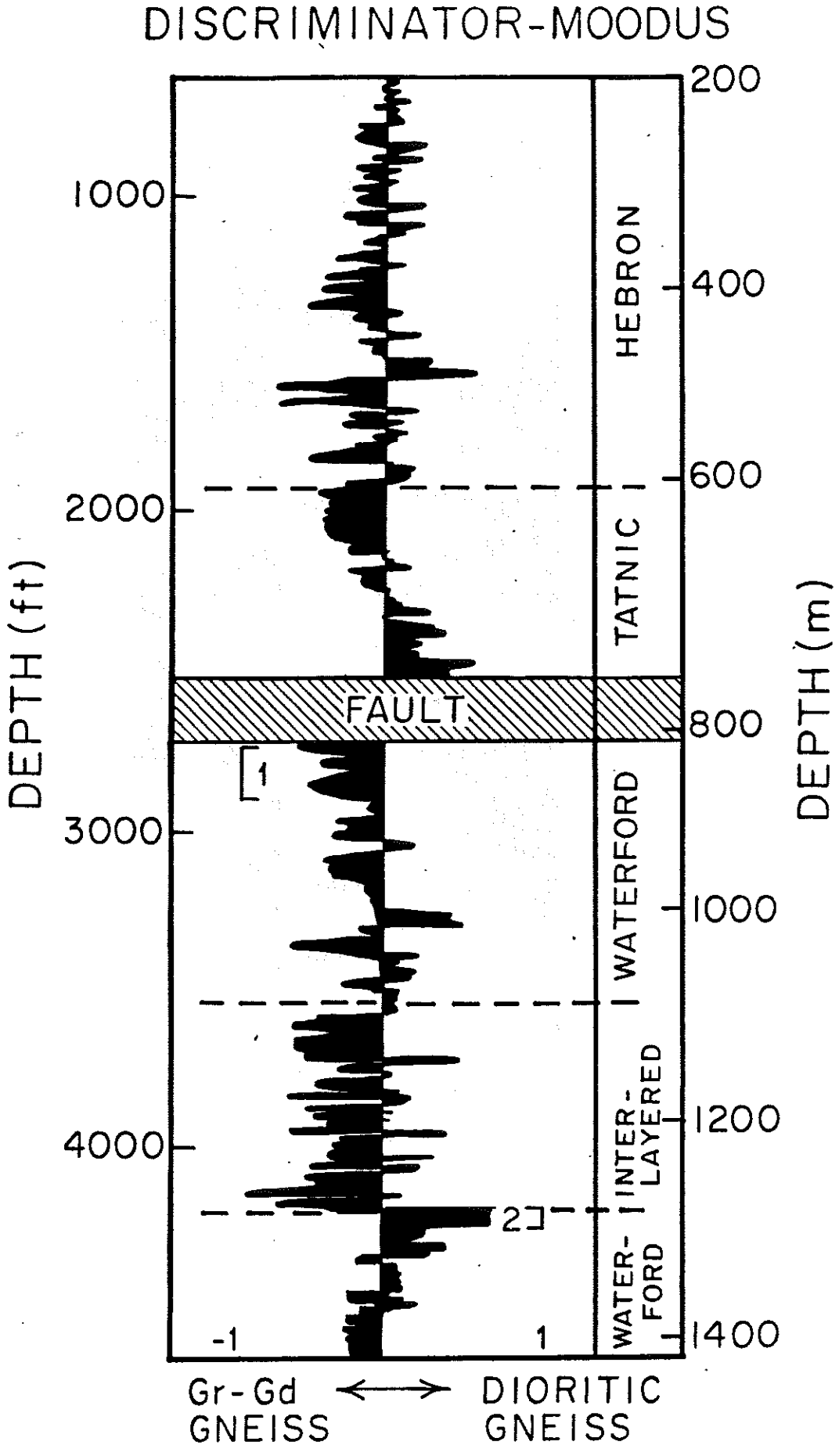
DISCRIMINATOR-MOODUS
DEPTH (ft)
1000
2000
3000
4000
200
400
600
800
1000
1200
1400
DEPTH (m)
HEBRON
TATNIC
FAULT
WATERFORD
INTER-LAYERED
WATER-FORD
1
2
-1
1
Gr-Gd GNEISS
DIORITIC GNEISS

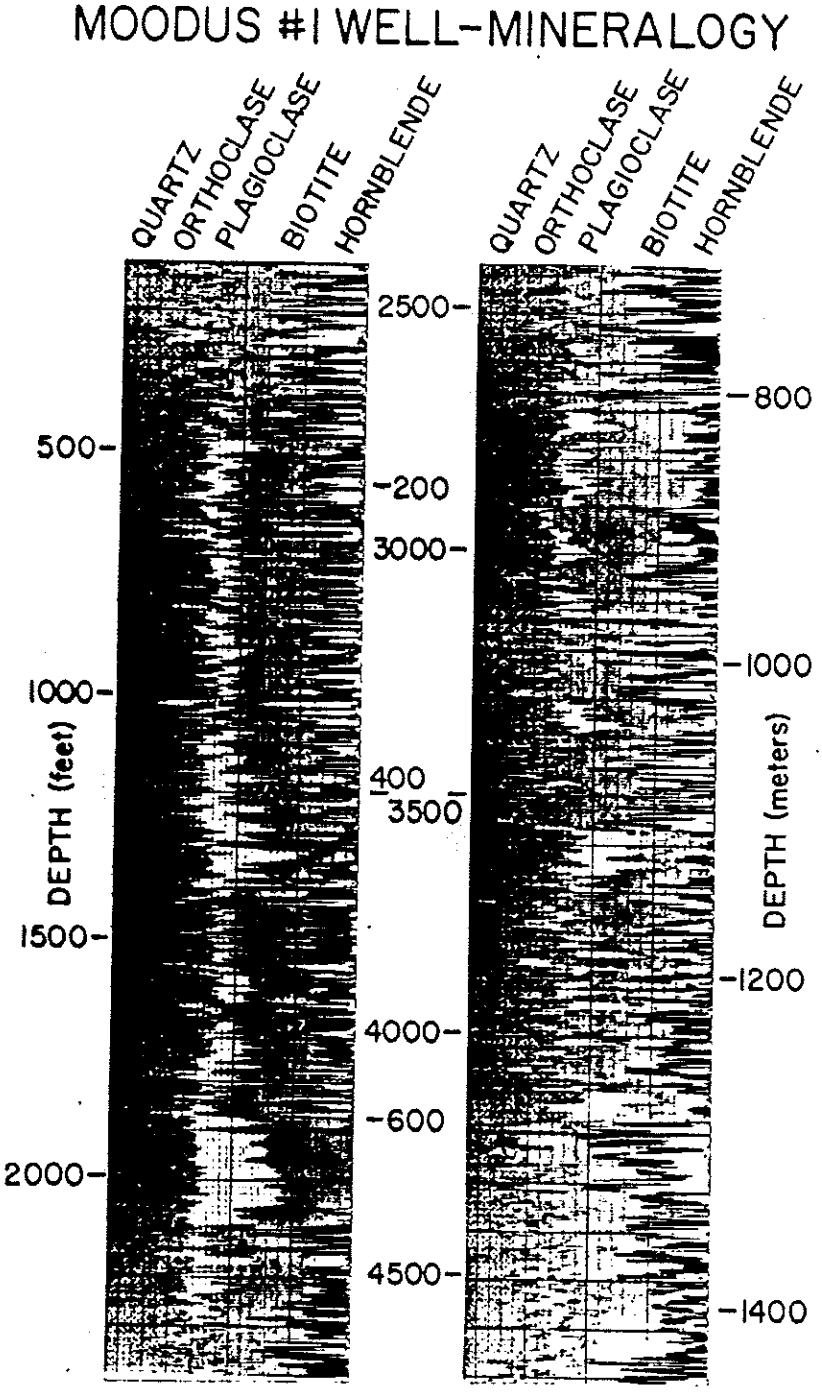
MOODUS #1 WELL-MINERALOGY
QUARTZ
ORTHOCLASE
PLAGIOCLASE
BIOTITE
HORNBLENDE
QUARTZ
ORTHOCLASE
PLAGIOCLASE
BIOTITE
HORNBLENDE
500-
1000-
1500-
2000-
DEPTH (feet)
2500-
-200
3000-
400
3500
4000-
-600
4500-
-800
-1000
-1200
-1400
DEPTH (meters)

Figure 10

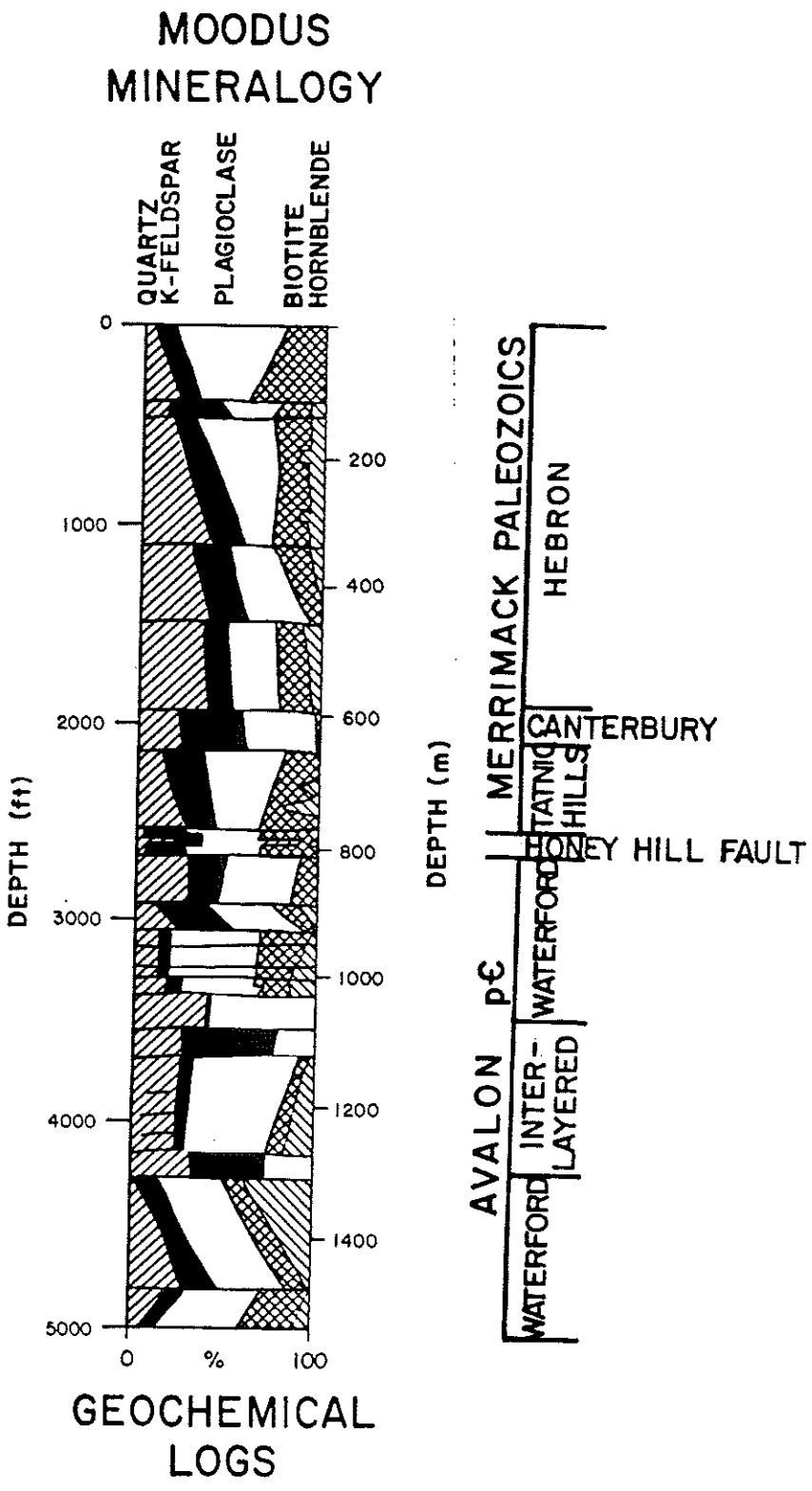
MOODUS
MINERALOGY
QUARTZ
K-FELDSPAR
PLAGIOCLASE
BIOTITE
HORNBLENDE
DEPTH (ft)
0
1000
2000
3000
4000
5000
200
400
600
800
1000
1200
1400
0
%
100
GEOCHEMICAL
LOGS
DEPTH (m)
MERRIMACK
PALEOZOICS
HEBRON
CANTERBURY
TATNIC
HILLS
HONEY HILL FAULT
WATERFORD
AVALON
pC
INTER-
LAYERED
WATERFORD

Figure 11

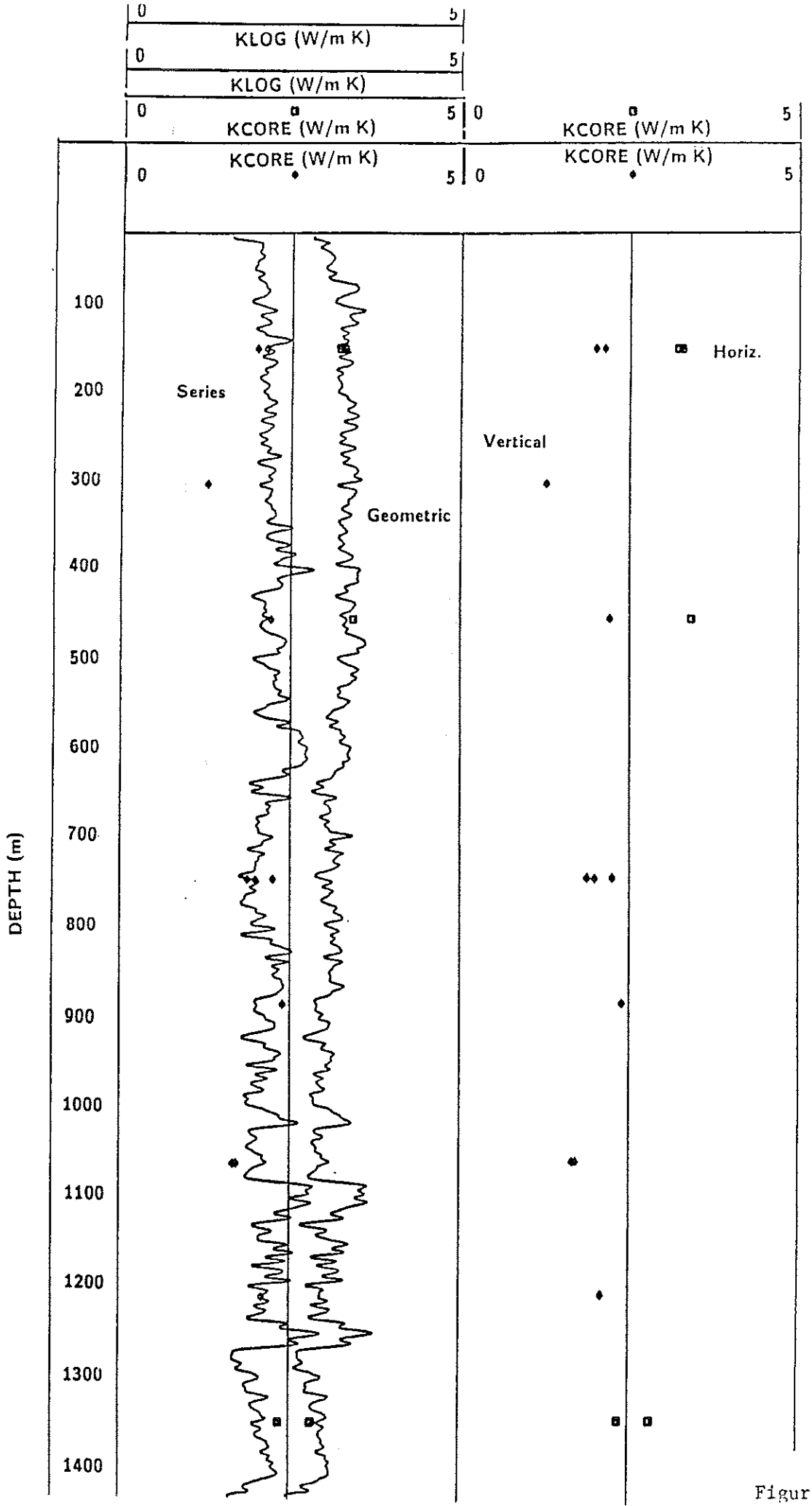
0
5
KLOG (W/m K)
0
5
KLOG (W/m K)
0
5
KCORE (W/m K)
0
5
KCORE (W/m K)
0
5
KCORE (W/m K)
0
5
KCORE (W/m K)
DEPTH (m)
100
200
300
400
500
600
700
800
900
1000
1100
1200
1300
1400
Series
Geometric
Vertical
Horiz.

Figure 12

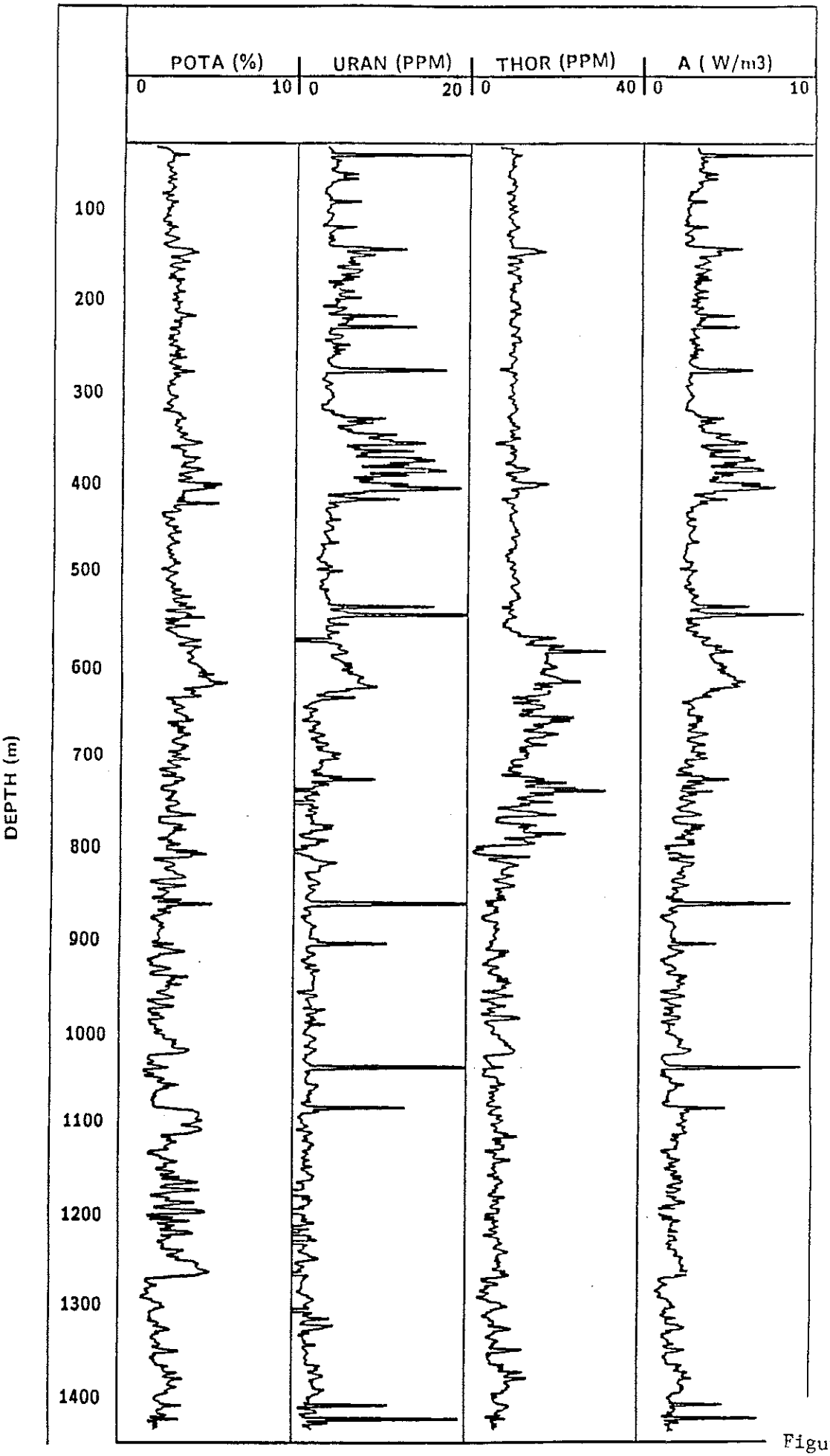
POTA (%)
0
10
URAN (PPM)
0
20
THOR (PPM)
0
40
A (W/m3)
0
10
DEPTH (m)
100
200
300
400
500
600
700
800
900
1000
1100
1200
1300
1400

Figure 13

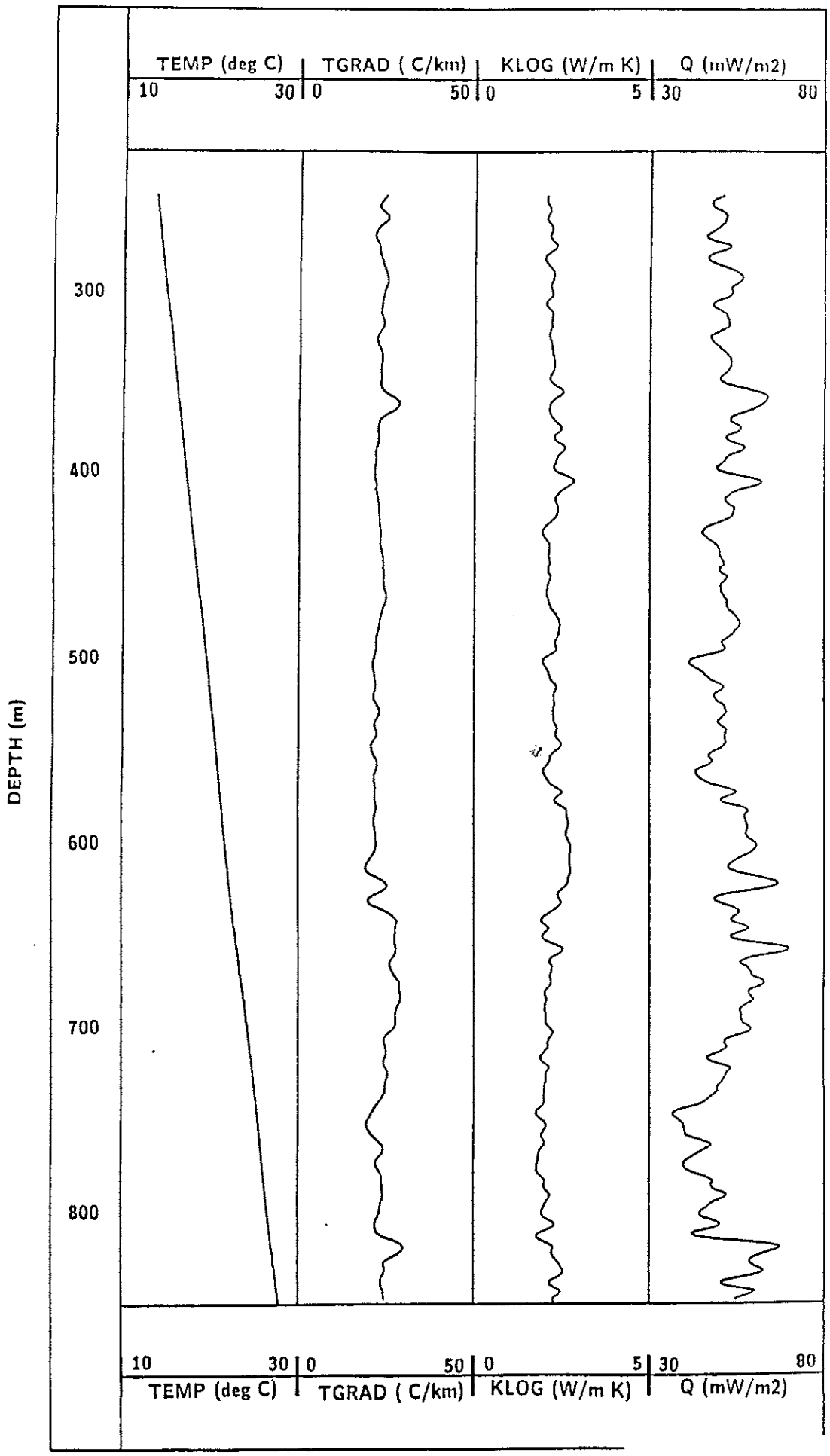
TEMP (deg C)
10
30
TGRAD (C/km)
0
50
KLOG (W/m K)
0
5
Q (mW/m2)
30
80
DEPTH (m)
300
400
500
600
700
800
10
30
TEMP (deg C)
0
50
TGRAD (C/km)
0
5
KLOG (W/m K)
30
80
Q (mW/m2)

Figure 14

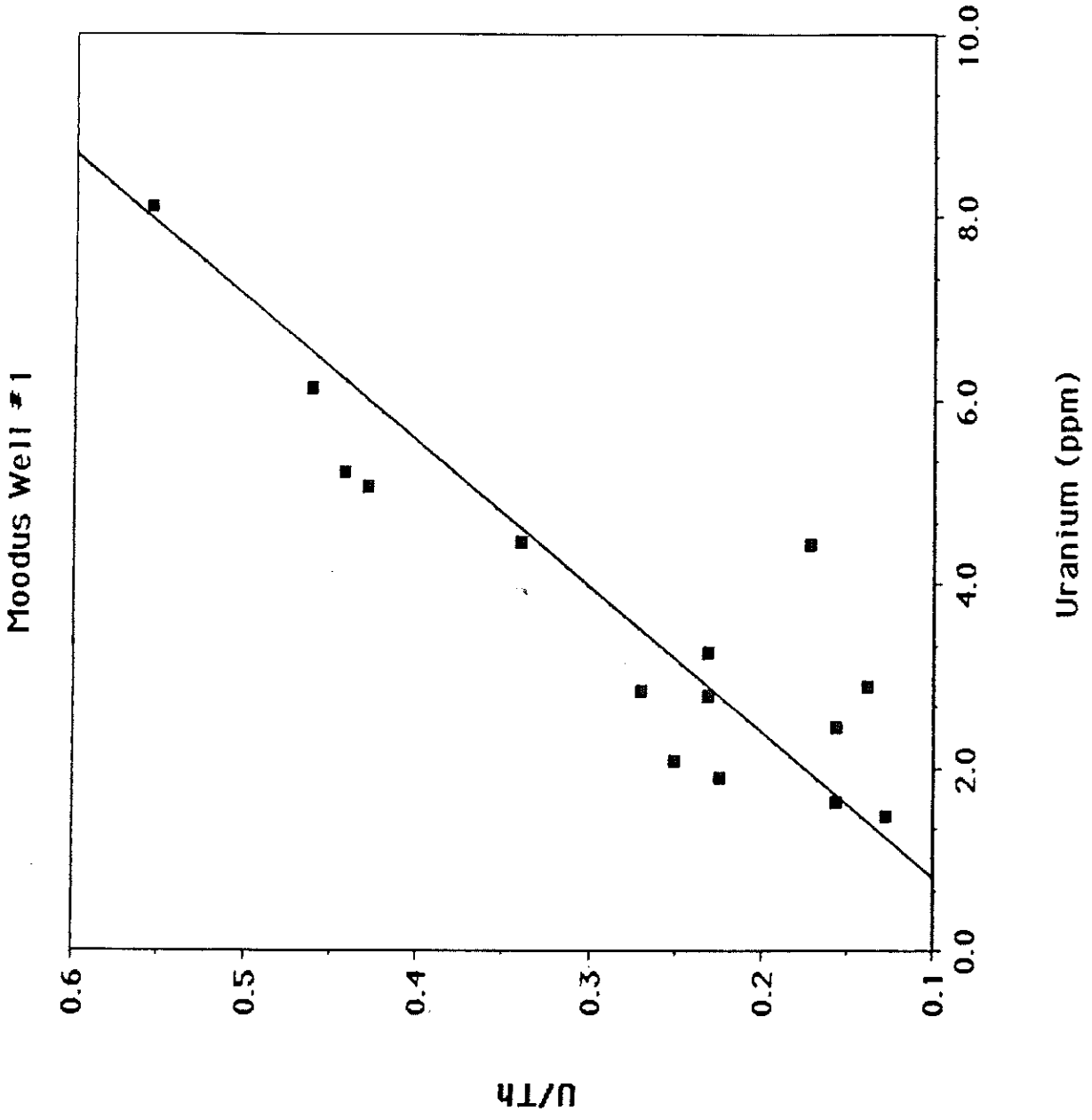

Figure 15

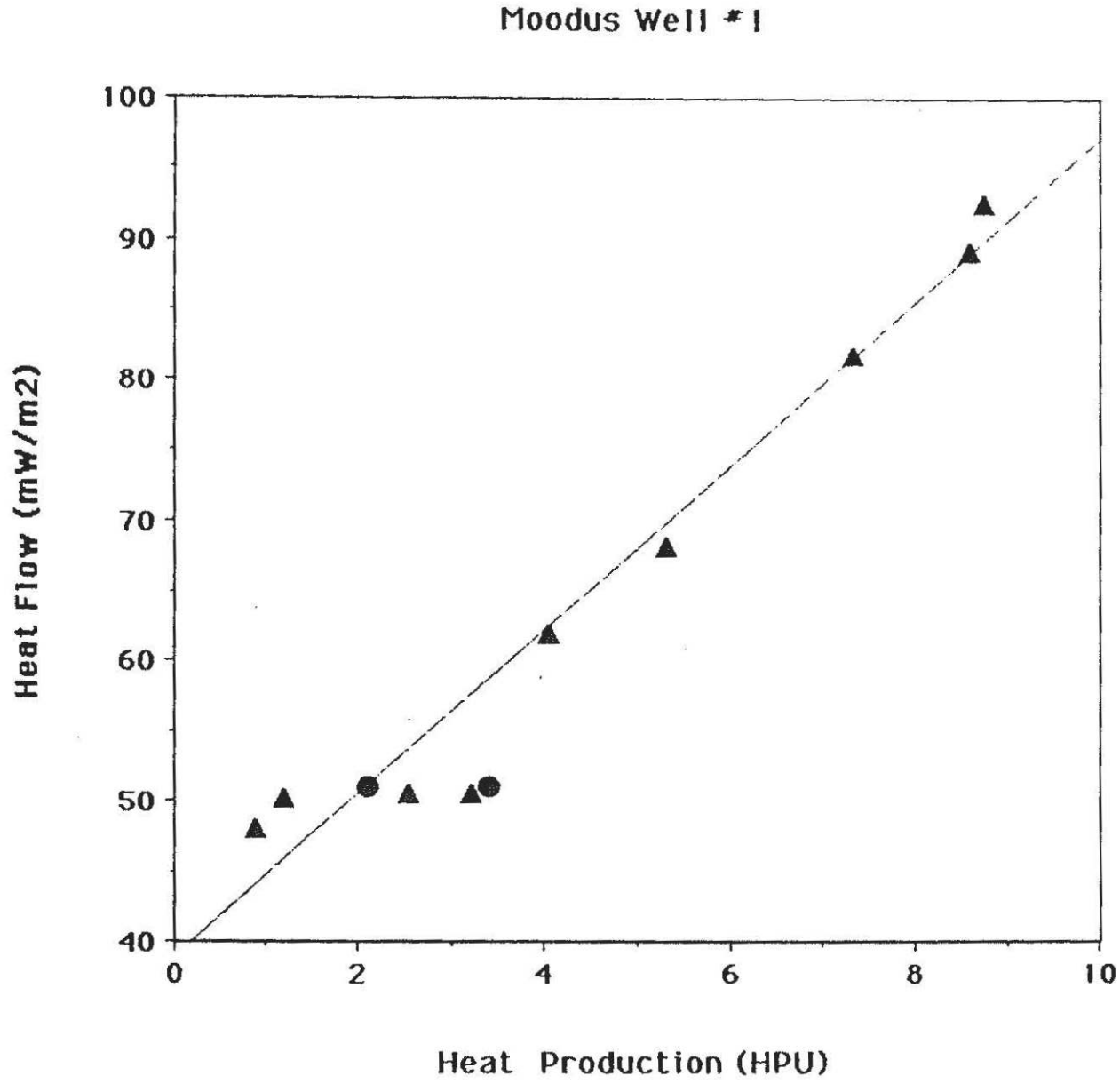
Moodus Well #1
Heat Flow (mW/m2)
100
90
80
70
60
50
40
0
2
4
6
8
10
Heat Production (HPU)

Figure 16

SMOOTHED ELEMENTAL LOGS - PRODUCTS
DEPTH (m)
200
400
600
800
1000
1200
1400
TiO2
FeO
MgO
CaO
Al2O3
SiO2
2
0
20
0
20
0
20
0
20
0
40
0
ENRICHMENT
DEPLETION
DEPTH (ft)
1000
2000
FAULT
3000
4000

Figure 17

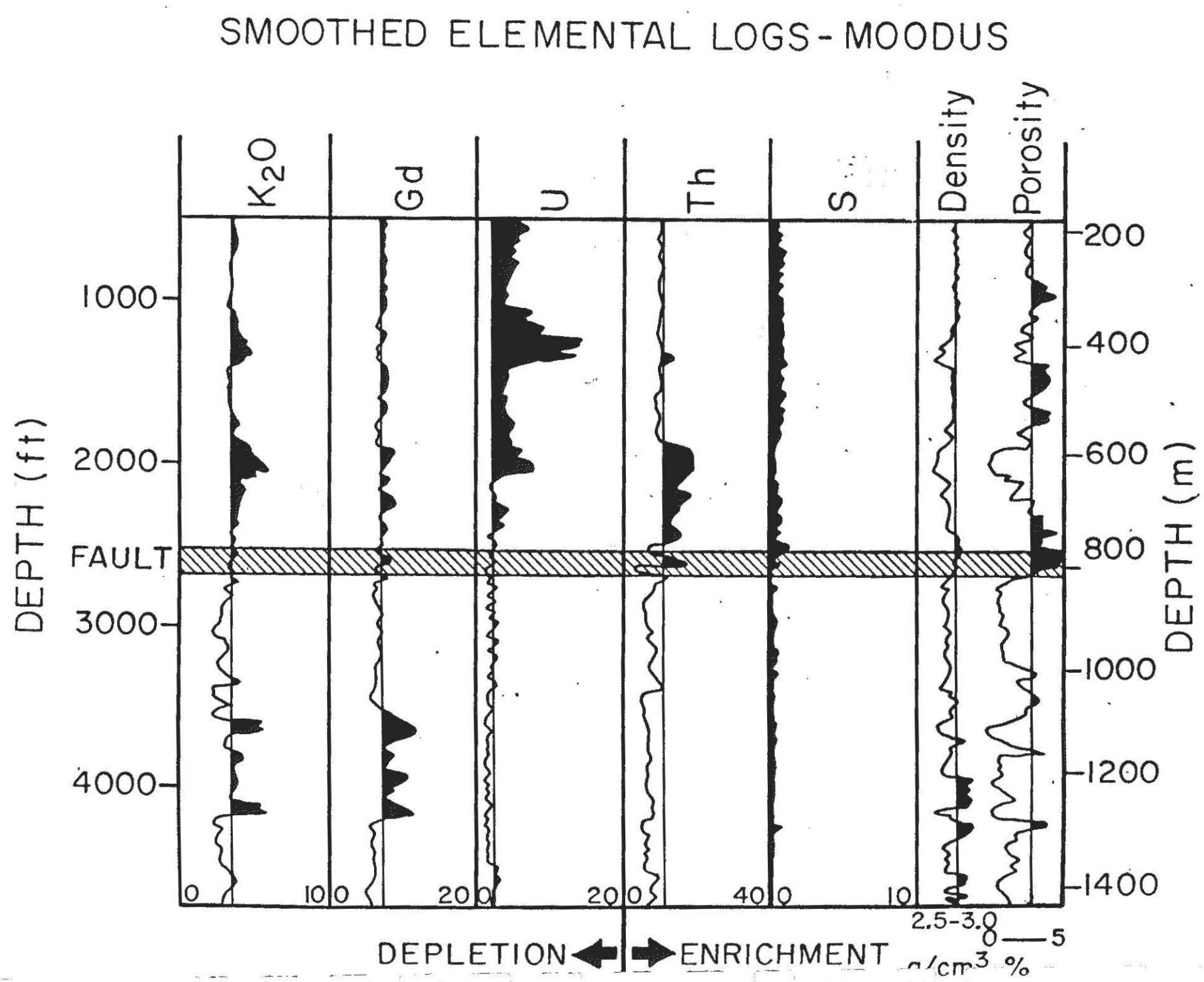
SMOOTHED ELEMENTAL LOGS - MOODUS
K2O
Gd
U
Th
S
Density
Porosity
DEPTH (ft)
1000
2000
FAULT
3000
4000
DEPTH (m)
200
400
600
800
1000
1200
1400
0
10
0
20
0
20
0
40
0
10
2.5-3.0
0
5
DEPLETION
ENRICHMENT
g/cm3
%

Figure 18.

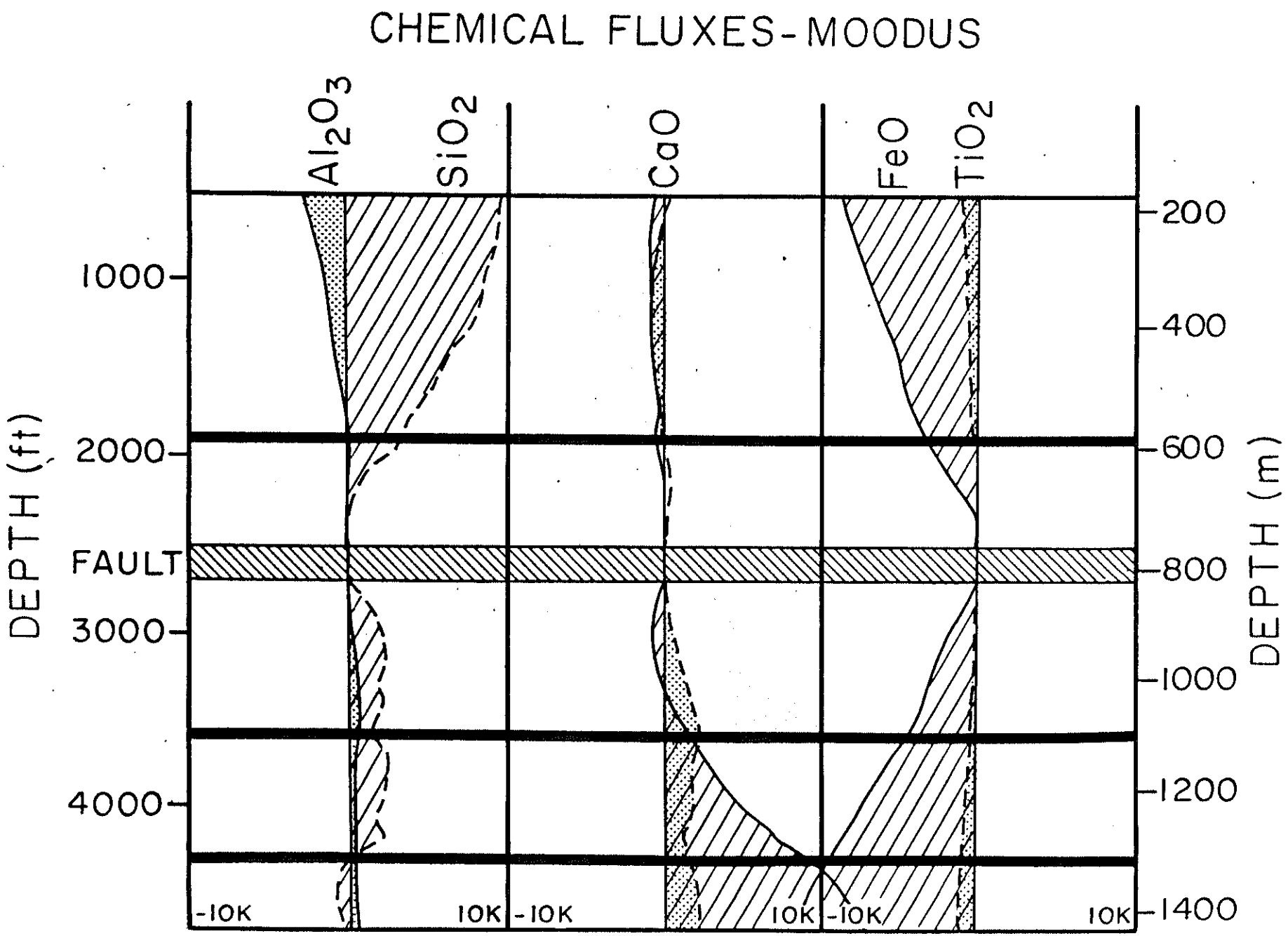
CHEMICAL FLUXES-MOODUS
Al2O3
SiO2
CaO
FeO
TiO2
DEPTH (ft)
1000
2000
FAULT
3000
4000
DEPTH (m)
200
400
600
800
1000
1200
1400
-10K
10K
-10K
10K
-10K
10K

Figure 19

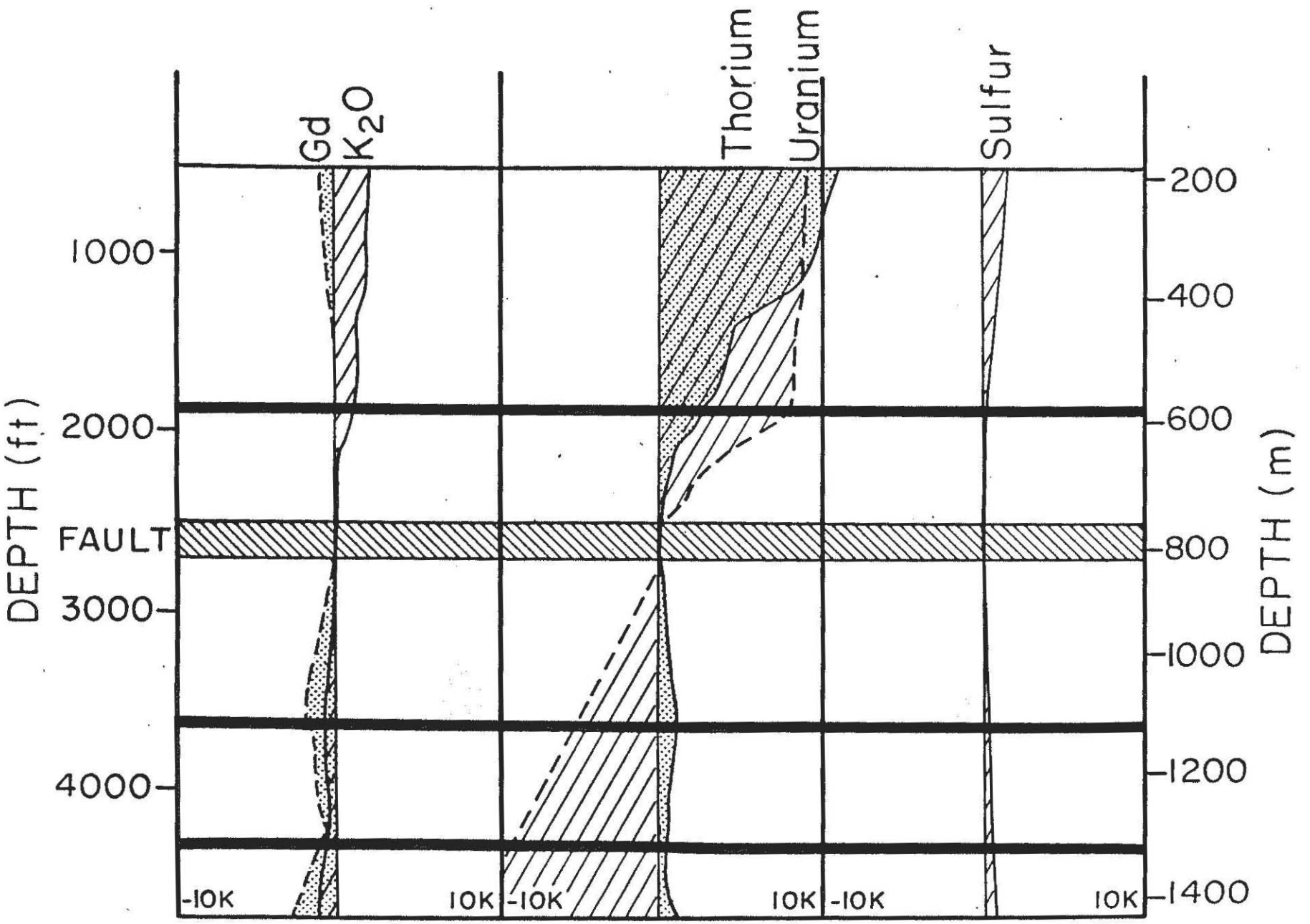
CHEMICAL FLUXES - MOODUS
Gd
K_2O
Thorium
Uranium
Sulfur
DEPTH (ft)
1000
2000
FAULT
3000
4000
DEPTH (m)
200
400
600
800
1000
1200
1400
-10K
10K
-10K
10K
-10K
10K

Figure 20

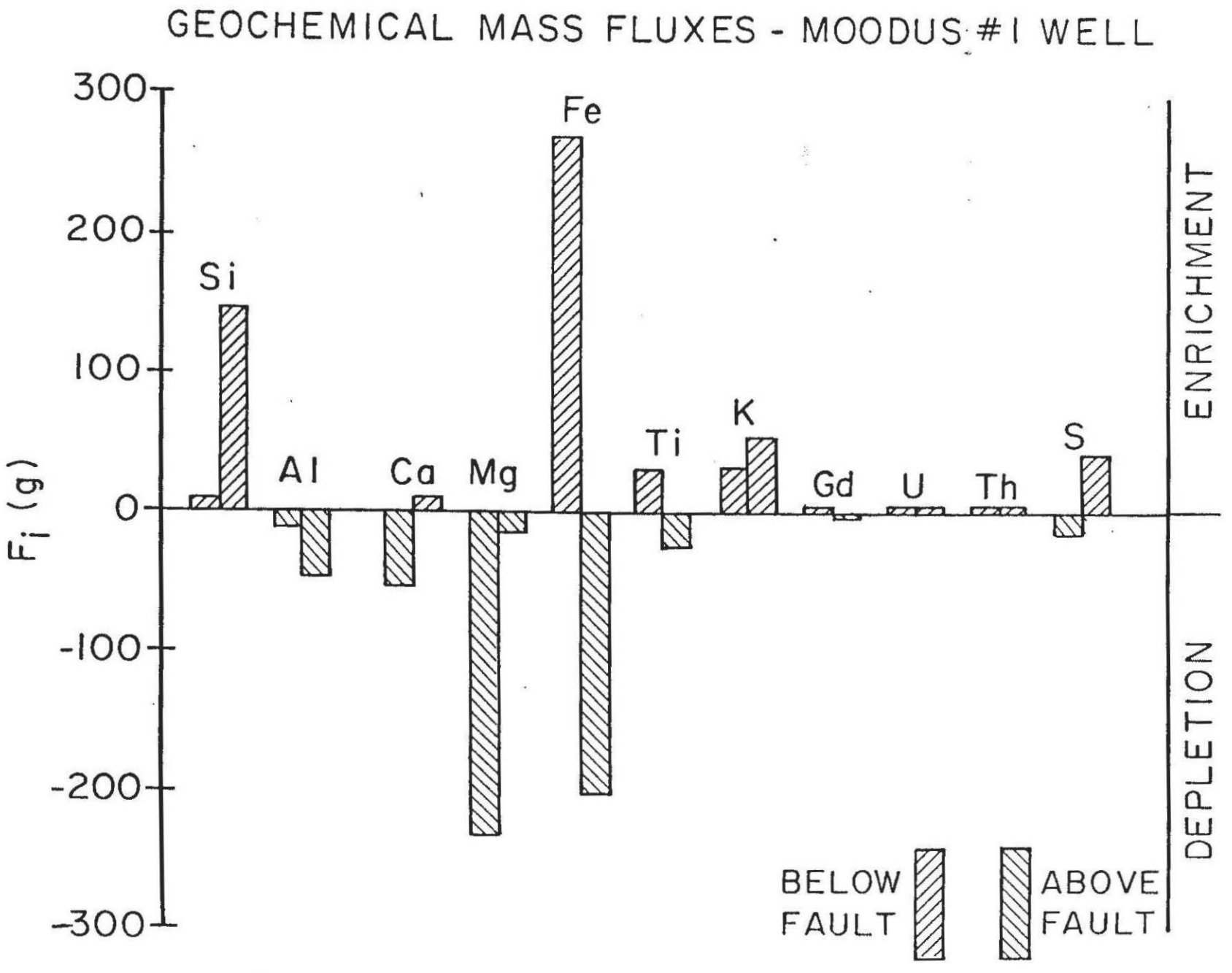
GEOCHEMICAL MASS FLUXES - MOODUS #1 WELL
300
200
100
0
-100
-200
-300
F_i (g)
Si
Al
Ca
Mg
Fe
Ti
K
Gd
U
Th
S
ENRICHMENT
DEPLETION
BELOW FAULT
ABOVE FAULT

Figure 21

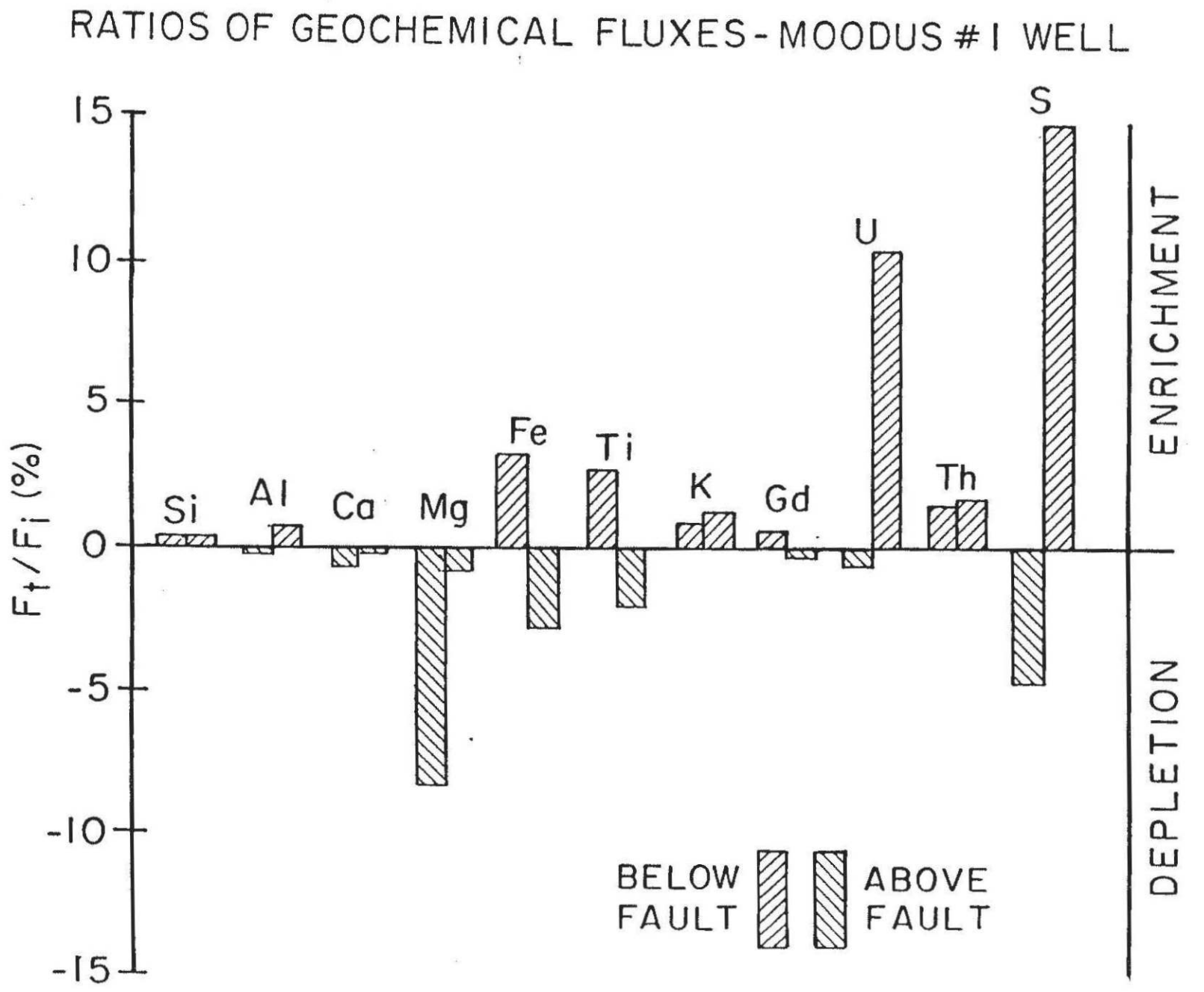
RATIOS OF GEOCHEMICAL FLUXES - MOODUS #1 WELL
15
10
5
0
-5
-10
-15
F_f / F_i (%)
Si
Al
Ca
Mg
Fe
Ti
K
Gd
U
Th
S
ENRICHMENT
DEPLETION
BELOW FAULT
ABOVE FAULT

Figure 22

Appendix G

APPENDIX G

Differential strain analysis of Moodus borehole core.

LABORATORY ANALYSIS

OF

MOODUS CORE SAMPLES

by

Irene Llewellyn Meglis

The Pennsylvania State University

Department of Geosciences

University Park, PA 16802

Prepared for

Woodward-Clyde Consultants

December, 1988

PROJECT OVERVIEW

The Moodus Test Well was drilled in the spring of 1987 to a depth of approximately 1.5 km. The site, located in south-central Connecticut, is of interest because of shallow, low-level earthquakes which occur in the area. The focus of the Moodus study is to determine the crustal stresses which produce these earthquakes. As part of that study, measurements of strain and ultrasonic velocities under hydrostatic confining pressure were made on cores recovered from depths as shown in Figure 1. The ultrasonic velocities are useful for comparison with in situ logs, while the strain data provide information on the nature of the crack populations present in the samples.

BACKGROUND

Microcracks in core samples have been used with success as indicators of in situ stress (Strickland and Ren, 1980). When cracks have formed purely from stress relief in mechanically isotropic rocks, the directions of maximum, intermediate and minimum crack strains correspond well with maximum, intermediate, and minimum principal stress directions in situ, as shown in Figure 2. The analysis is less straightforward when some portion of the crack population is present in situ (Kowallis et. al., 1982), or when the rocks are mechanically anisotropic (Meglis,

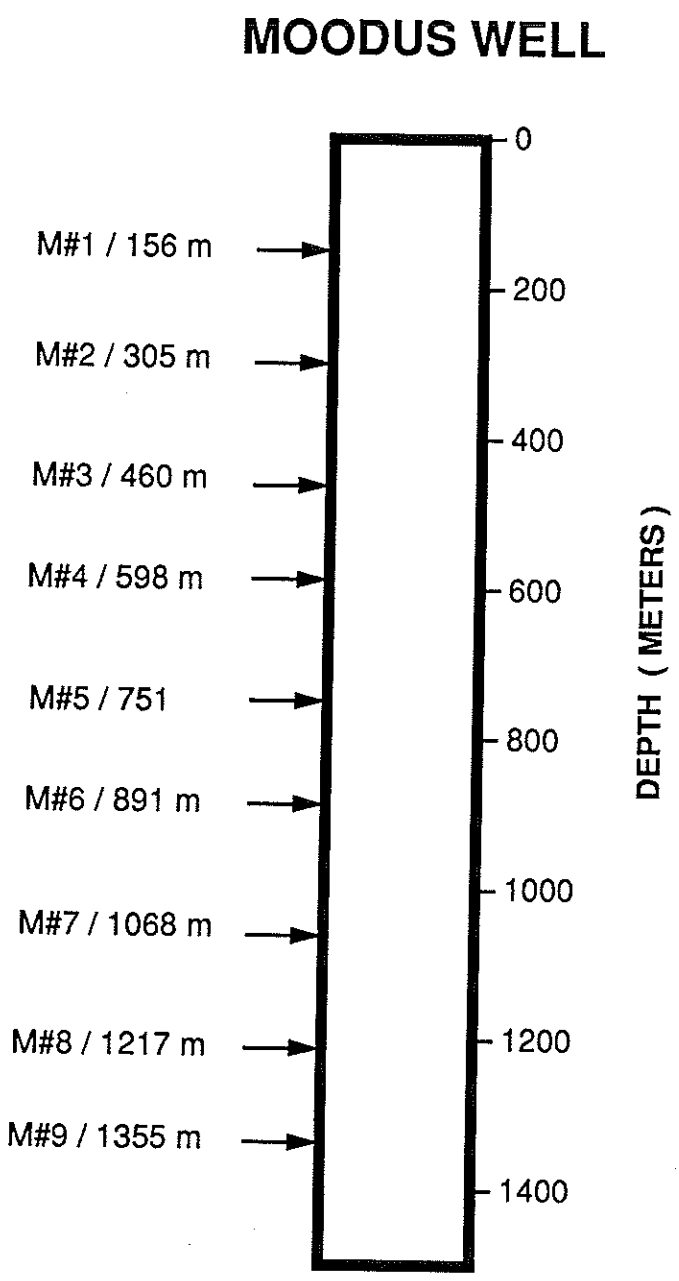

Figure 1 : Initial Depths of Core Samples

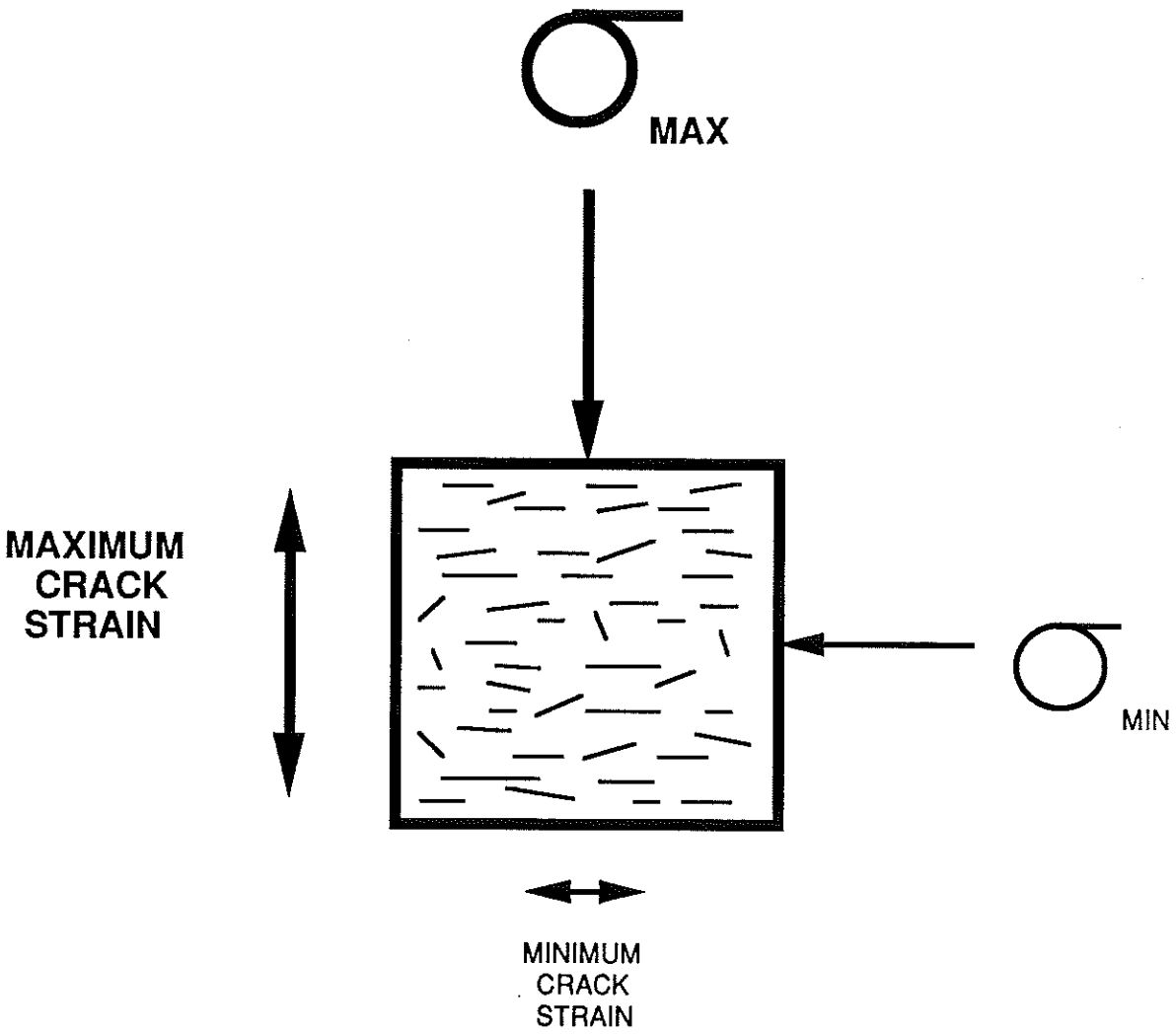

Figure 2 : Relationship between measured crack strains and in situ stresses for stress relief cracks (after Strickland and Ren.)

1987). In the case of the Moodus cores, the foliation in the samples dominates the physical properties. Since this foliation is predominantly horizontal, the possibility existed that sub-vertical crack planes may have had a fairly simple relationship to the stress field.

The technique for studying the crack population involves simultaneous measurements of strain in nine orientations on a sample as hydrostatic pressure is applied, as shown in Figure 3. The results of these measurements give the relative distribution of crack porosity in the cores.

PROCEDURE

Cubic samples of approximately 5 cm sides were prepared, oriented vertically, with sides parallel and perpendicular to north 80 degrees east (roughly the maximum horizontal stress orientation as determined by Zoback et. al.) The cubes were polished using a surface grinder, dried under a vacuum at low temperature, and strain gauges rosettes were applied on the top, north and east faces as shown. The samples were then coated with rubber sealant to exclude the confining medium (hydraulic oil.) Strain readings were taken every 10 MPa as the rocks were loaded hydrostatically from 0 to 140 MPa, and again as they were unloaded.

After the samples were unloaded, 1 MHz compressional and shear

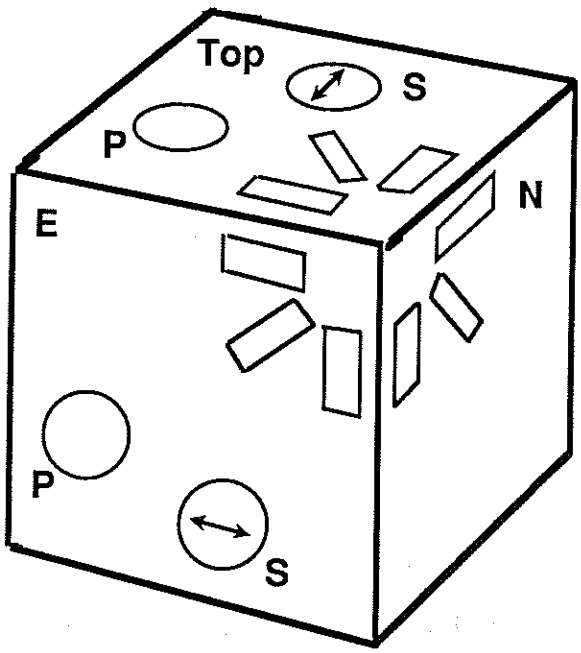

Figure 3 : Location of Strain Gauges and Velocity Transducers on Prepared Specimen

transducer pairs were attached, as shown in Figure 3. The samples were re-coated with rubber, and velocities were measured as the rocks were reloaded to 140 MPa. A shear wave with east/west polarization and a compressional wave were measured in the vertical propagation direction. A shear wave with north/south polarization and a compressional wave were measured in the horizontal, east/west propagation direction. A compressional wave in the north/east direction was measured as well on Moodus #5.

The strain gauge precision is quite high (plus or minus 0.15%); the precision of the pressure readings is plus or minus 0.5 MPa. The error in strain measurements due to temperature changes, instrument drift, and other factors may be on the order of a few percent. Results for vertical strains on the north and east faces are plotted with preliminary vertical strains measured on different segments of the core samples in the Spring of 1988. Measurement repeatability is within a few hundred microstrains. Allowing for sample inhomogeneities and different sample preparation procedures, this reproducibility is fairly good.

The difficulty in identifying the arrivals at the receiving transducers is the primary source of error in the velocity measurements, particularly when the signals are weak or scattered due to interactions with the microcracks. However, the consistency of the loading and unloading velocities at high pressures indicates the error is less than 0.05 km/sec for strong signals.

RESULTS

Strain Data

The results of the strain measurements are presented in Figures 4a through 4e. The rubber jackets were breached on four of the nine samples, thus these data were not usable. Several strain gauge signals are erratic (e.g. Moodus #4 Top-N/S) and several were lost completely. However, the bulk of the signals are useful. The system lost pressure at 50 MPa during the measurements on Moodus #4; the data are presented for the interval measured.

The curves shown are characteristic of the behavior of rocks containing microcracks when subjected to laboratory confining pressure. The large, non-linear strains exhibited at low pressures mark the closure of microcracks in the rocks. As confining pressure increases, the amount of strain decreases and follows a linear trend, reflecting primarily the elastic compression of matrix materials.

The linear portion of each loading curve was fit with a least squares regression. This represents the strain a sample would exhibit in the absence of the crack porosity. The difference between this curve and the observed strain at zero pressure is due to the presence of cracks and is termed the crack strain. A sample regression line is shown for Moodus #1. Crack strains for all samples are plotted against core depth in Figures 5a through 5c.

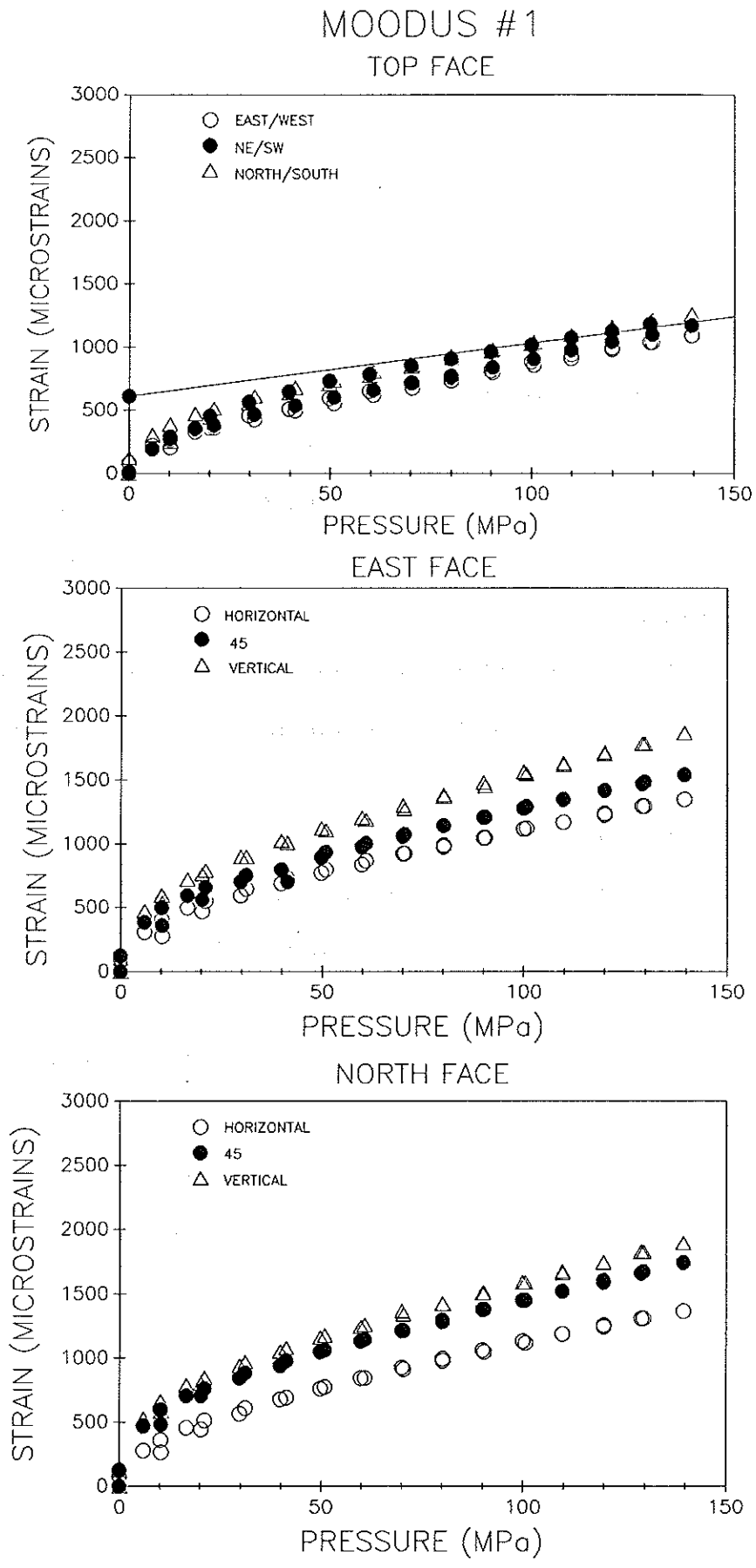

Figure 4 (a) : Moodus #1 Total Strain

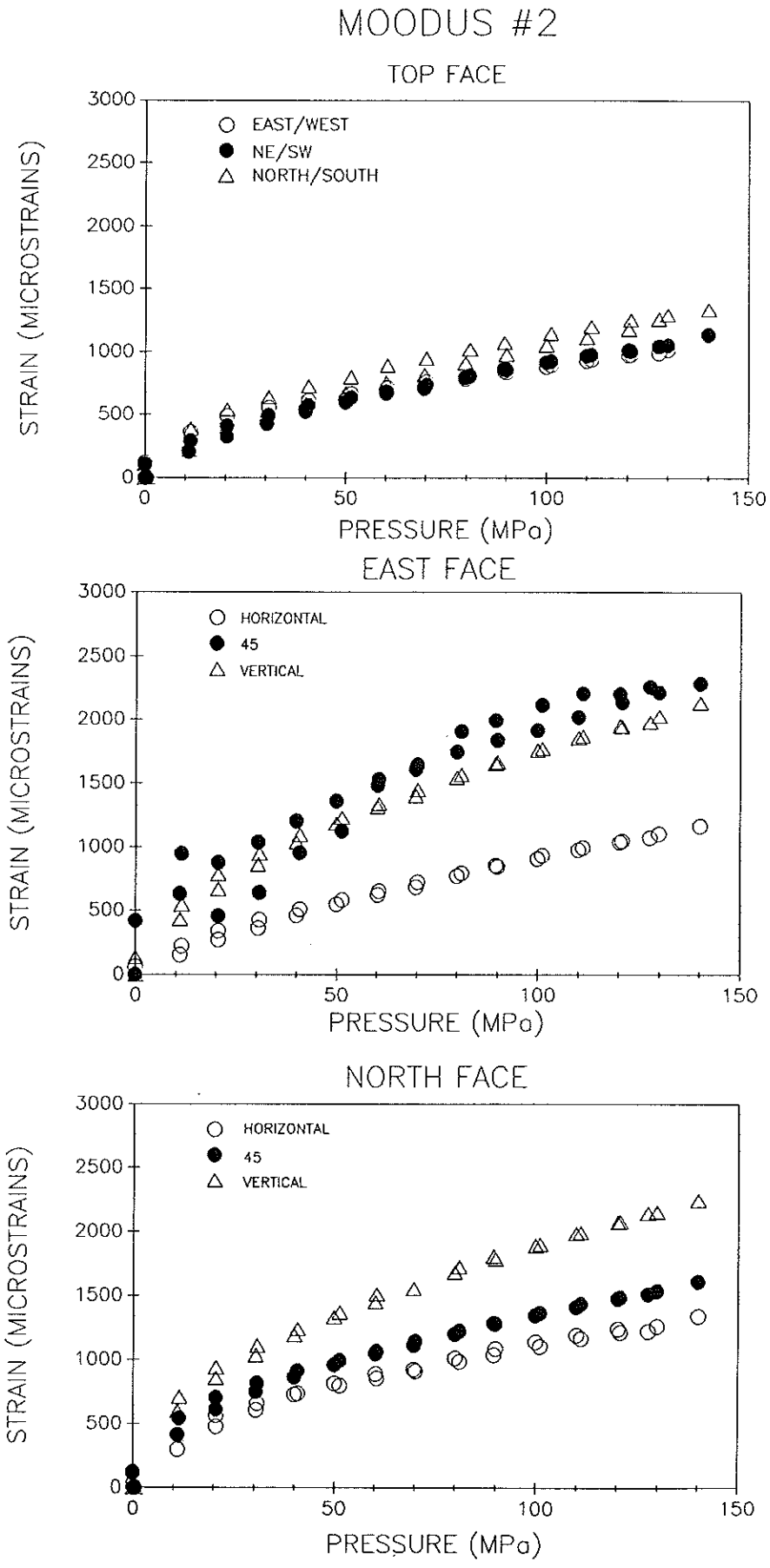

Figure 4 (b): Moodus #2 Total Strain

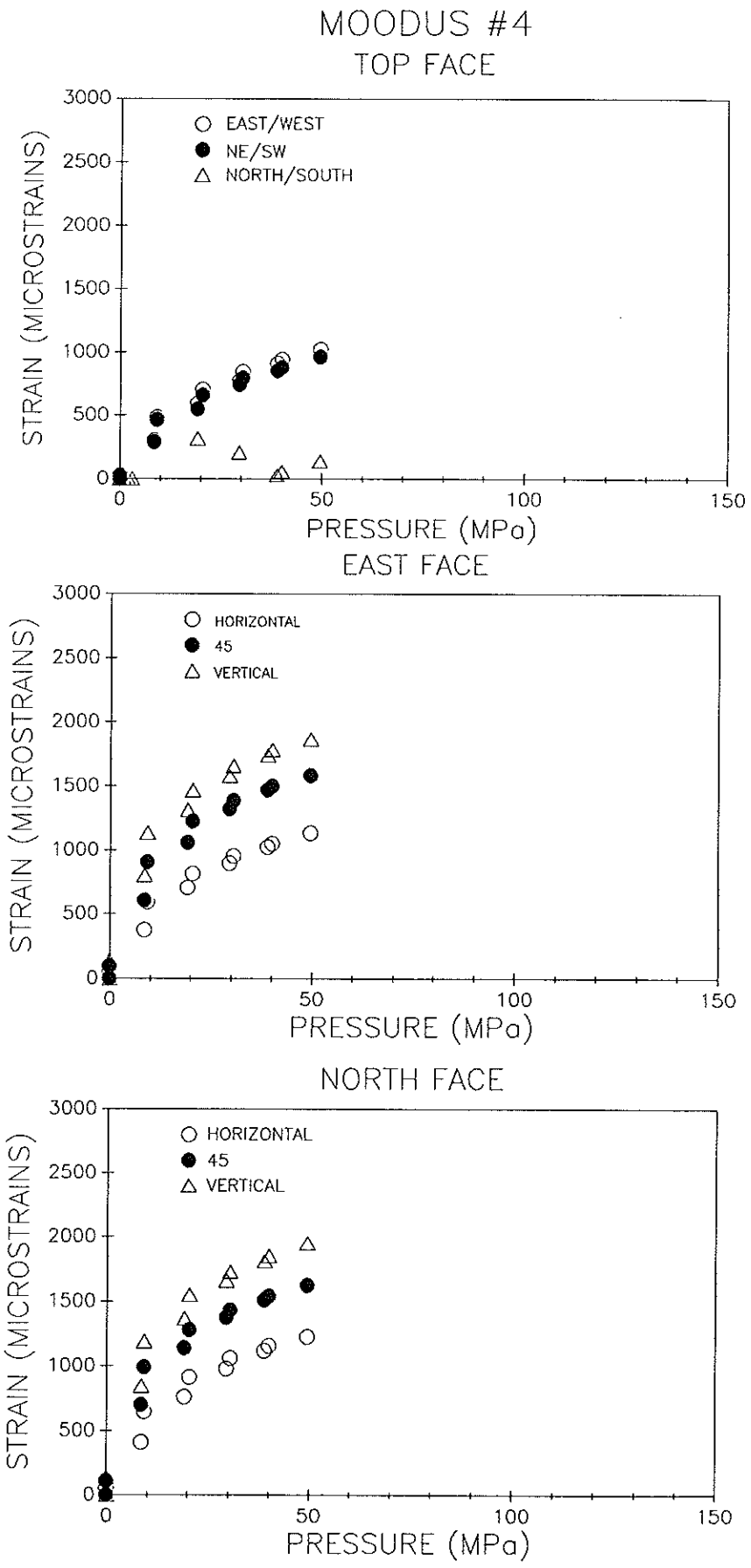

Figure 4 (c) : Moodus #4 Total Strain

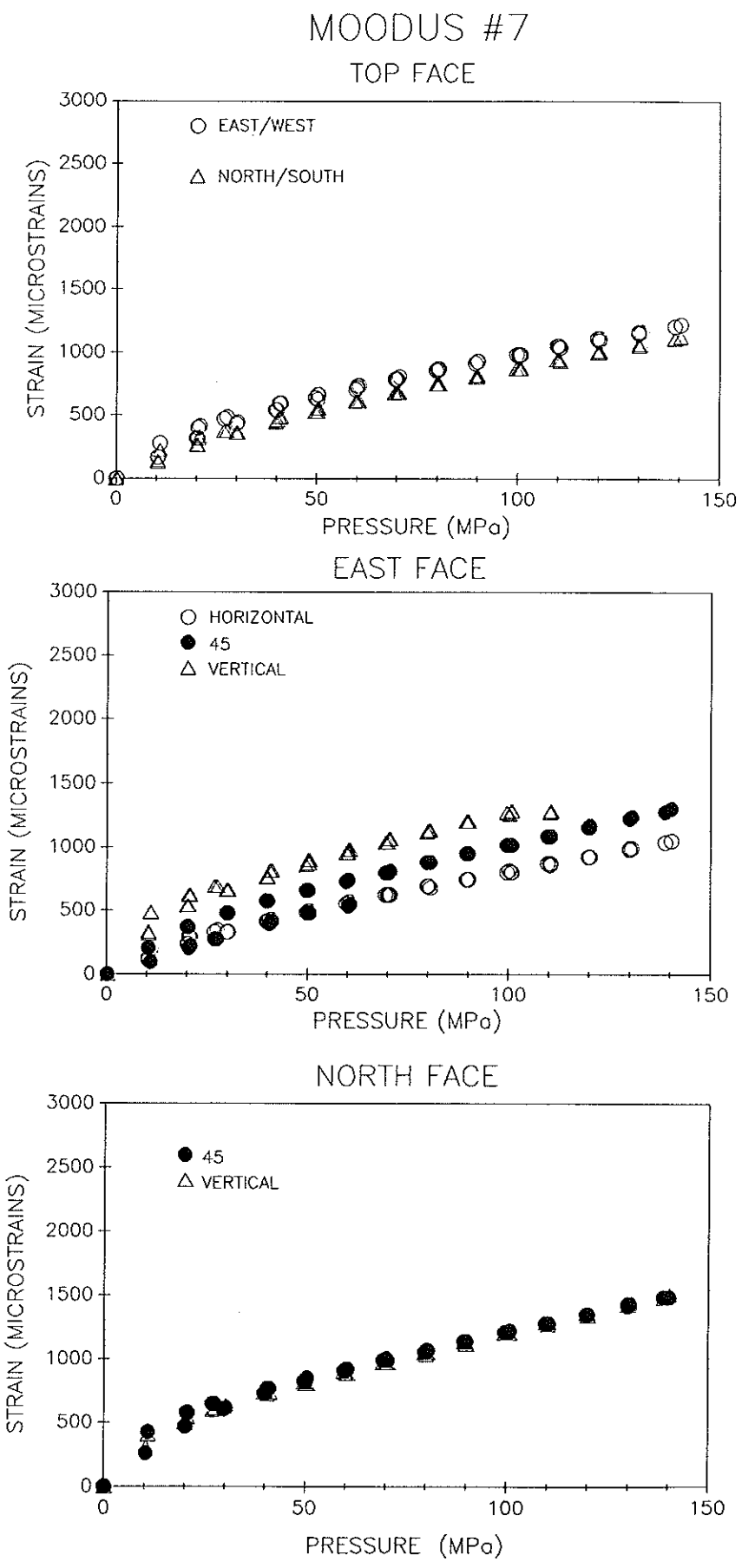

Figure 4 (d) : Moodus #7 Total Strain

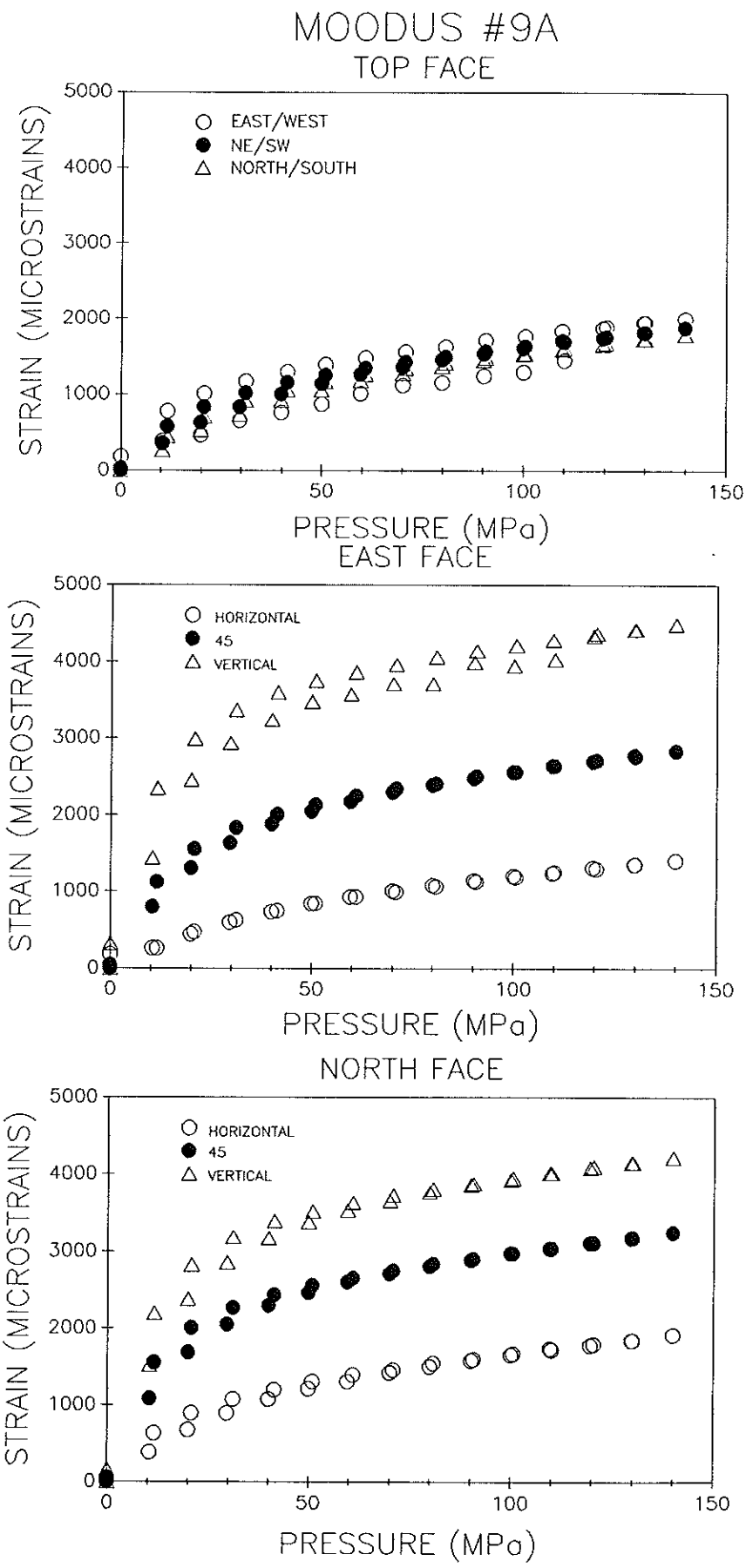

Figure 4 (e) : Moodus #9A Total Strain

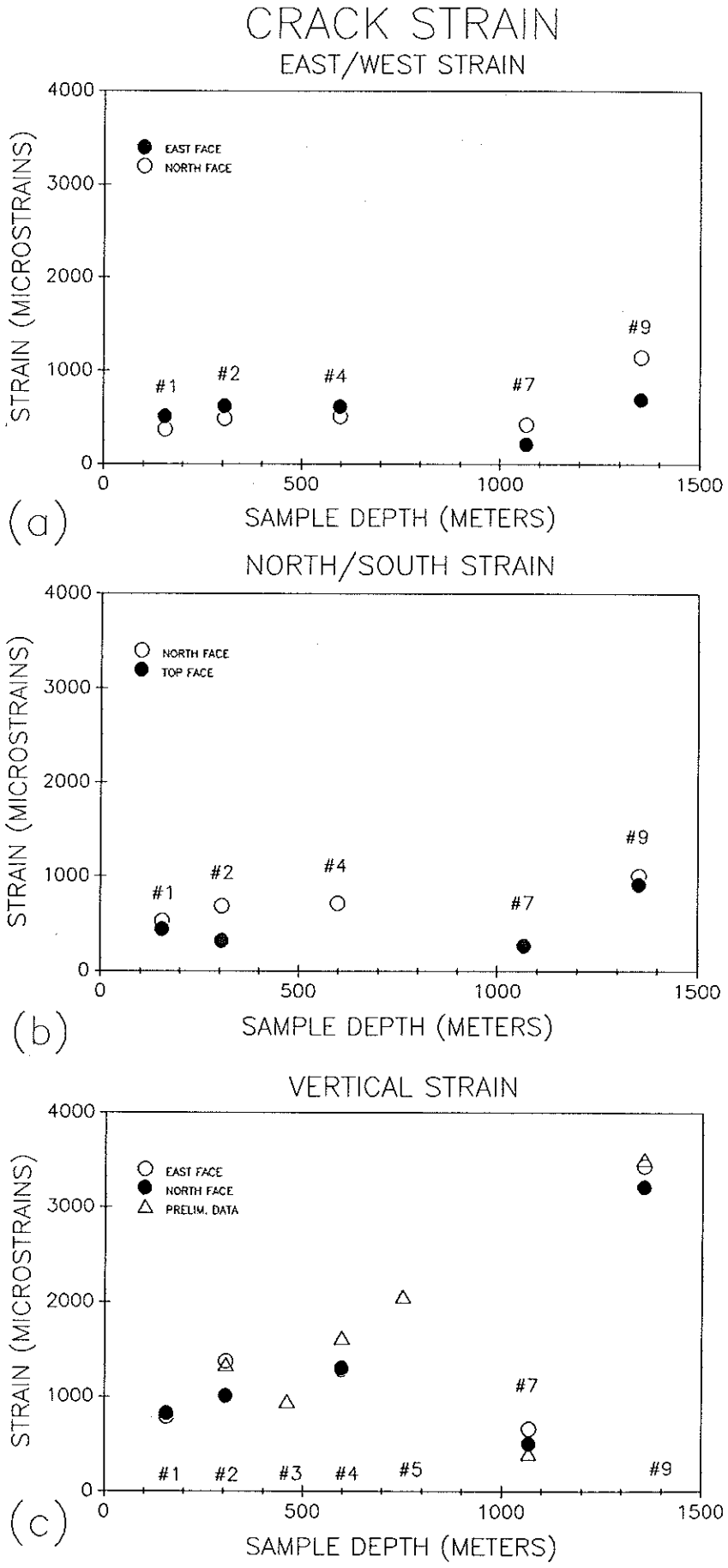

Figure 5 : Sample crack strains

Figures 5a and 5b are from theoretically redundant gauges, and should show identical strains. The observed variations result from inhomogeneities in the rock samples as well as possible variations in sample preparation, and thus are a reflection of the repeatability of the measurements.

Crack strains range from a few hundred to a few thousand microstrains, and tend to increase with increasing sample depth, with the marked exception of Core #7. This deep sample (1068 m) had the lowest crack strains of all the cores studied. Crack strains were invariably largest in the vertical direction. Horizontal crack strains were somewhat lower, and the difference between east/west strain and north/south strain is undetectable within the precision of the measurements.

Velocity Data

Velocity measurements made on the five unbreached samples are plotted in Figures 6a through 6e. The vertically propagating waves in the deepest sample (Moodus #9) were sufficiently attenuated, likely due to the very large crack strain in this direction, that no shear wave was detectable and the compressional wave was detectable only after the sample was pressurized slightly. Several measurement directions are absent, owing to loss of a transducer signal or obscuring of the arrival by transducer ringing.

The shapes of the velocity curves are similar to the strain

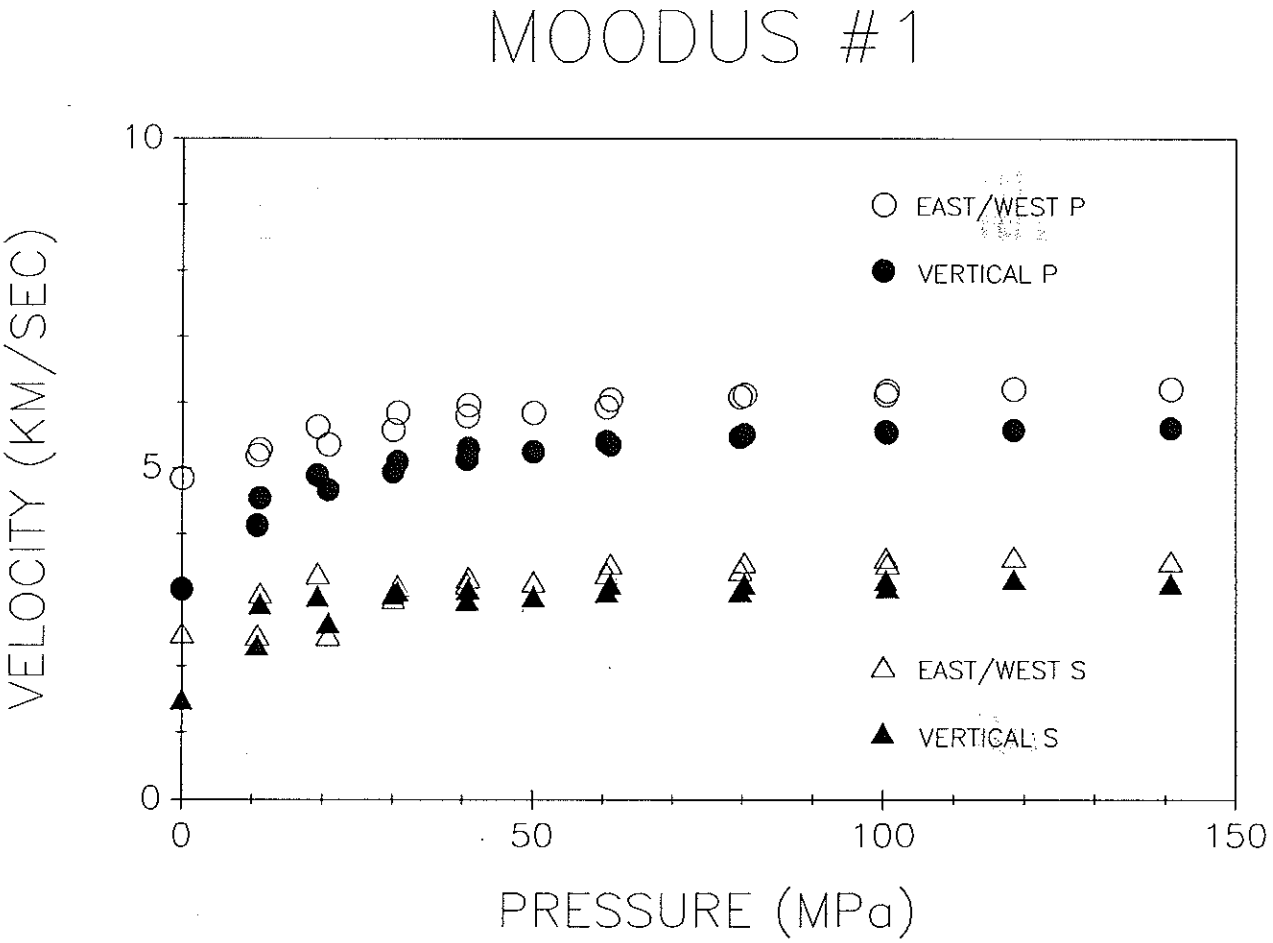

Figure 6 (a): Moodus #1 Measured Velocities

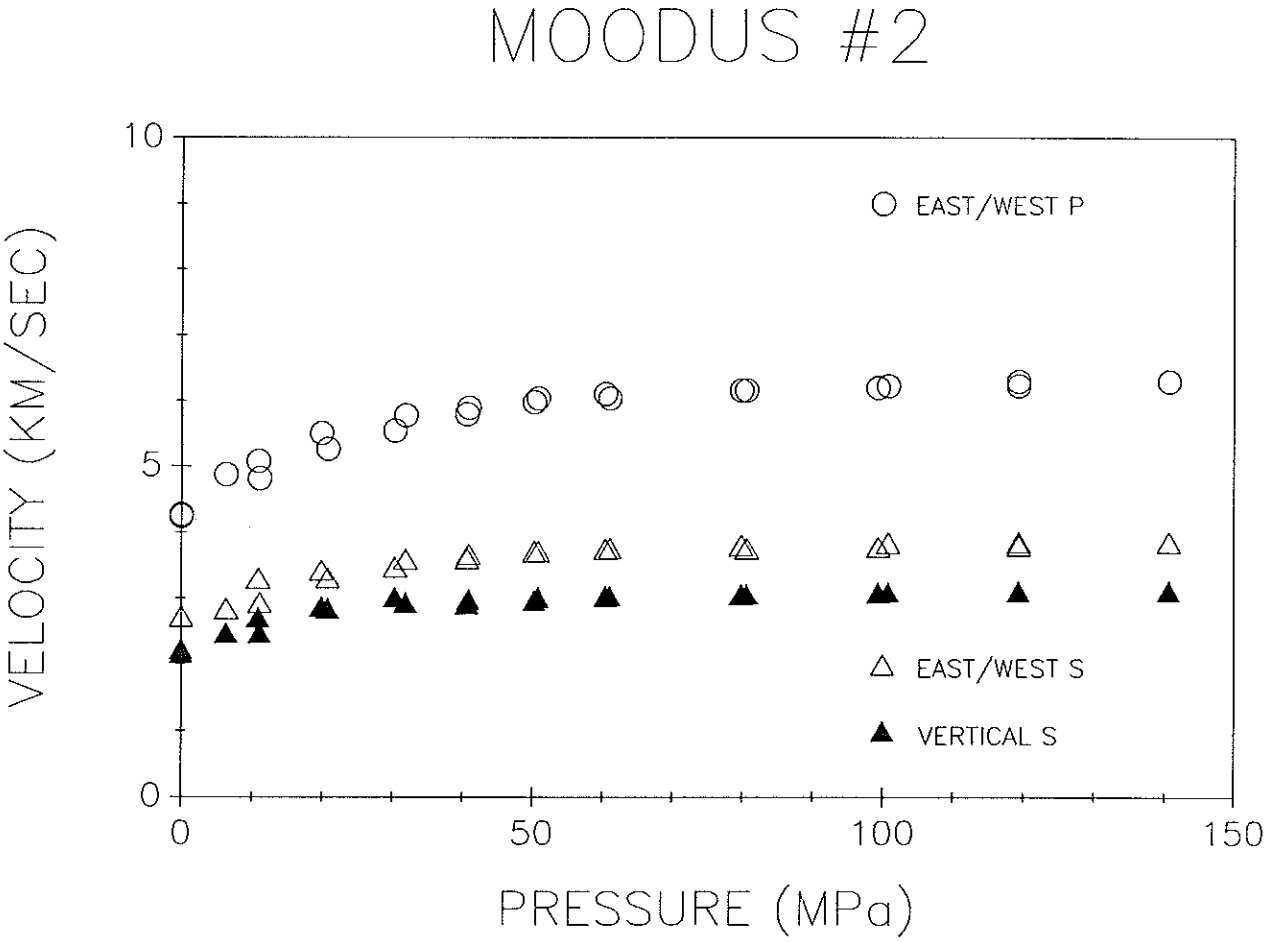

Figure 6 (b): Moodus #2 Measured Velocities

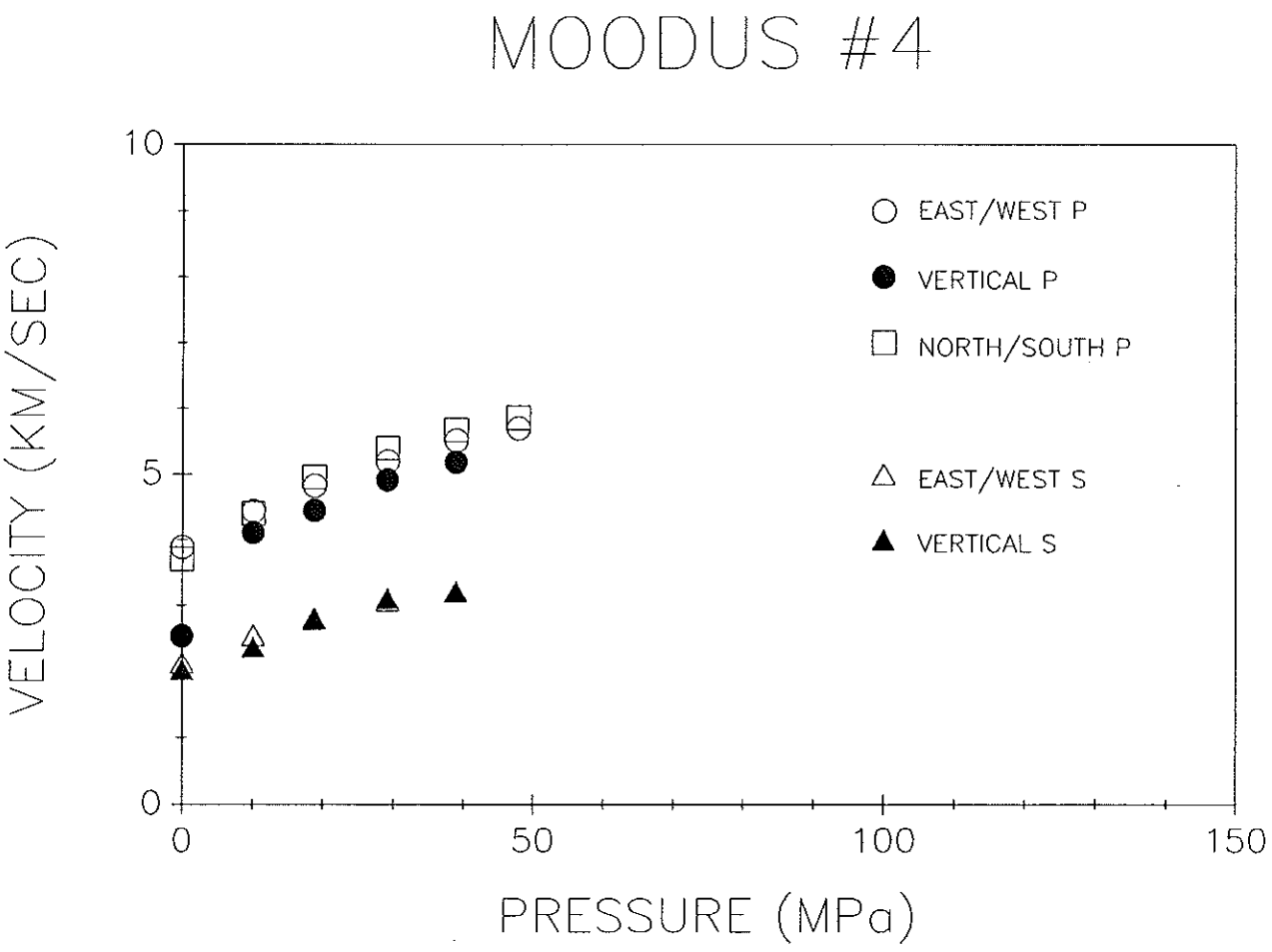

Figure 6 (c): Moodus #4 Measured Velocities

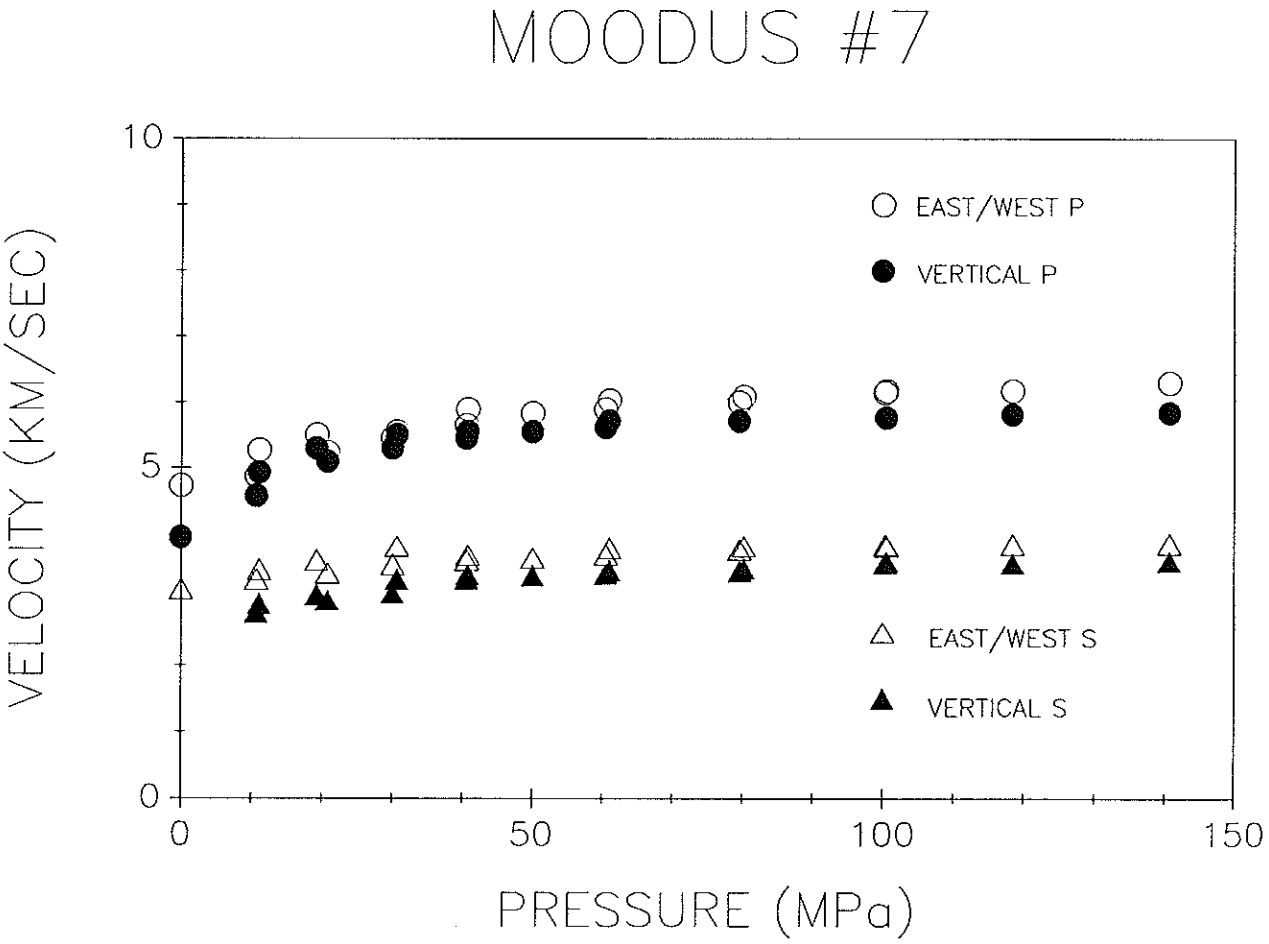

Figure 6 (d): Moodus #7 Measured Velocities

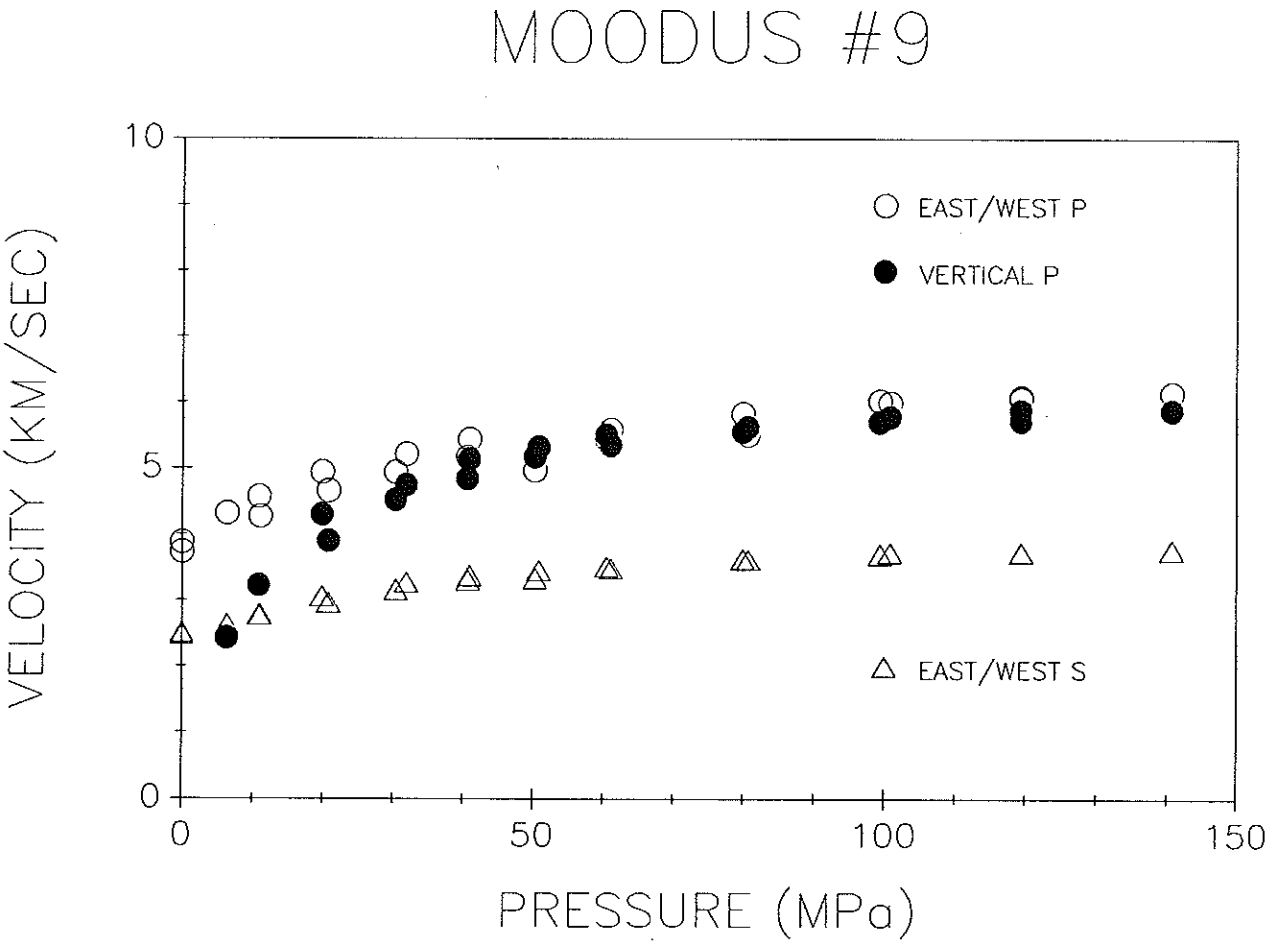

Figure 6 (e): Moodus #9 Measured Velocities

curves, reflecting the same closure of cracks with pressure. As shown in Figures 7a through 7d, the horizontally propagating compressional waves have significantly higher velocities than the vertically propagating waves at zero confining pressure. The differences between horizontal and vertical decrease markedly with confining pressure. The difference among shear waves is not quite so marked.

The zero-confining pressure velocities drop only slightly with increasing sample depth (with the exception of Core #7); this drop is apparent mainly in the vertical propagation direction. The velocities measured at the maximum pressure are similar among all the samples, indicating the matrix properties are similar.

DISCUSSION

The characteristics of the microcracks in these samples suggest strongly that the cracks have formed as a result of stress relief. The horizontal foliation in the samples studies has apparently dominated the formation of the cracks, thus obscuring any relationship between the crack strains and in situ deviatoric stresses in a given sample. It was hypothesized that horizontal crack strain variations may reflect in situ horizontal stress magnitude variations in spite of the effect of foliation. However the horizontal crack strains measured are not distinguishable within the error of the measurements. The striking linearity of

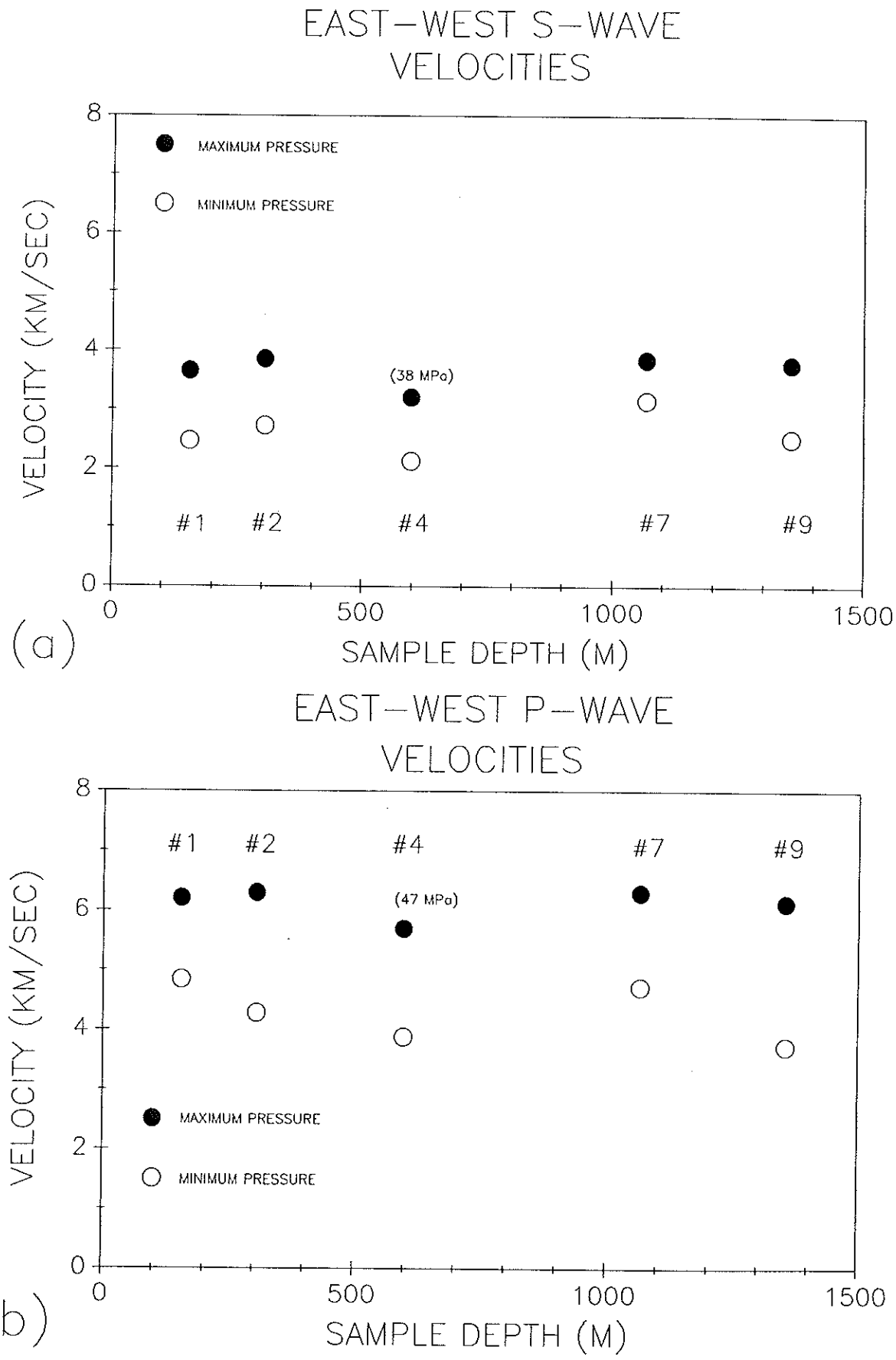

Figure 7: Sample Velocities with Initial Depth

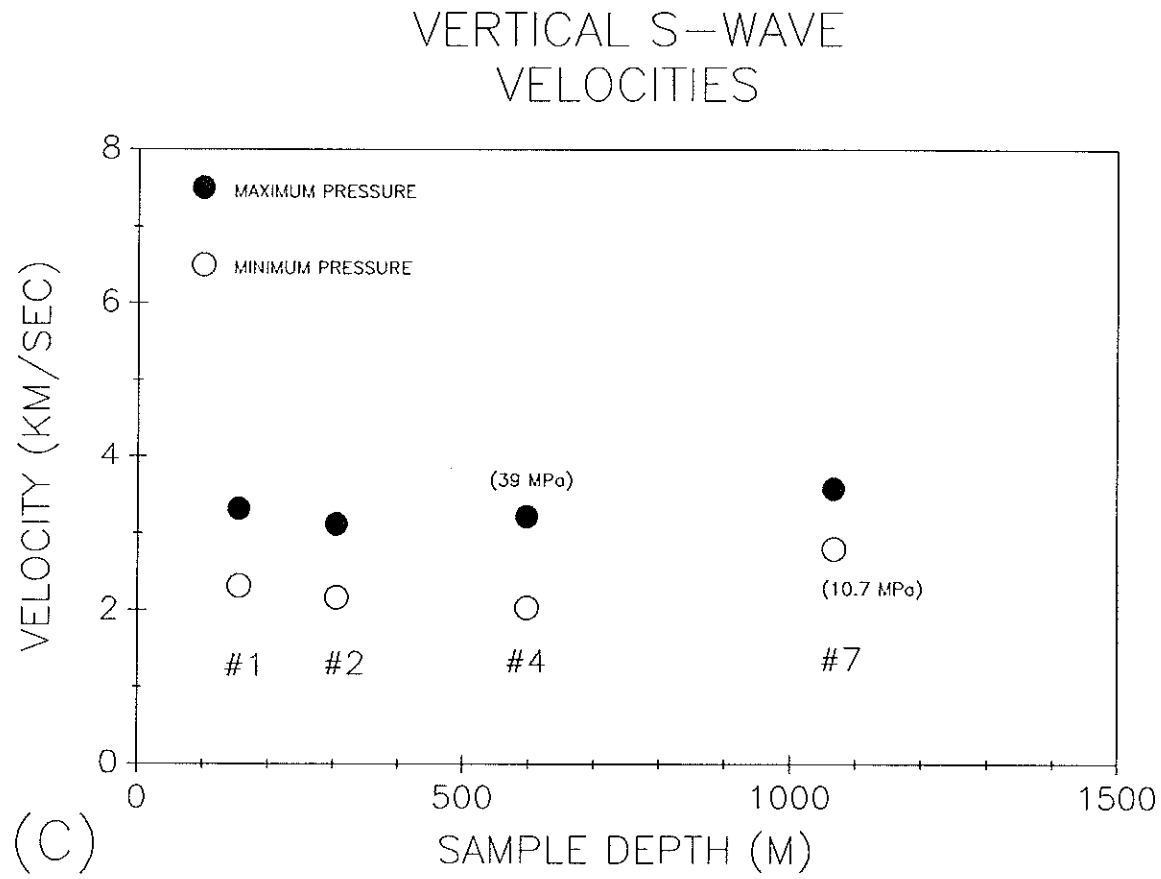

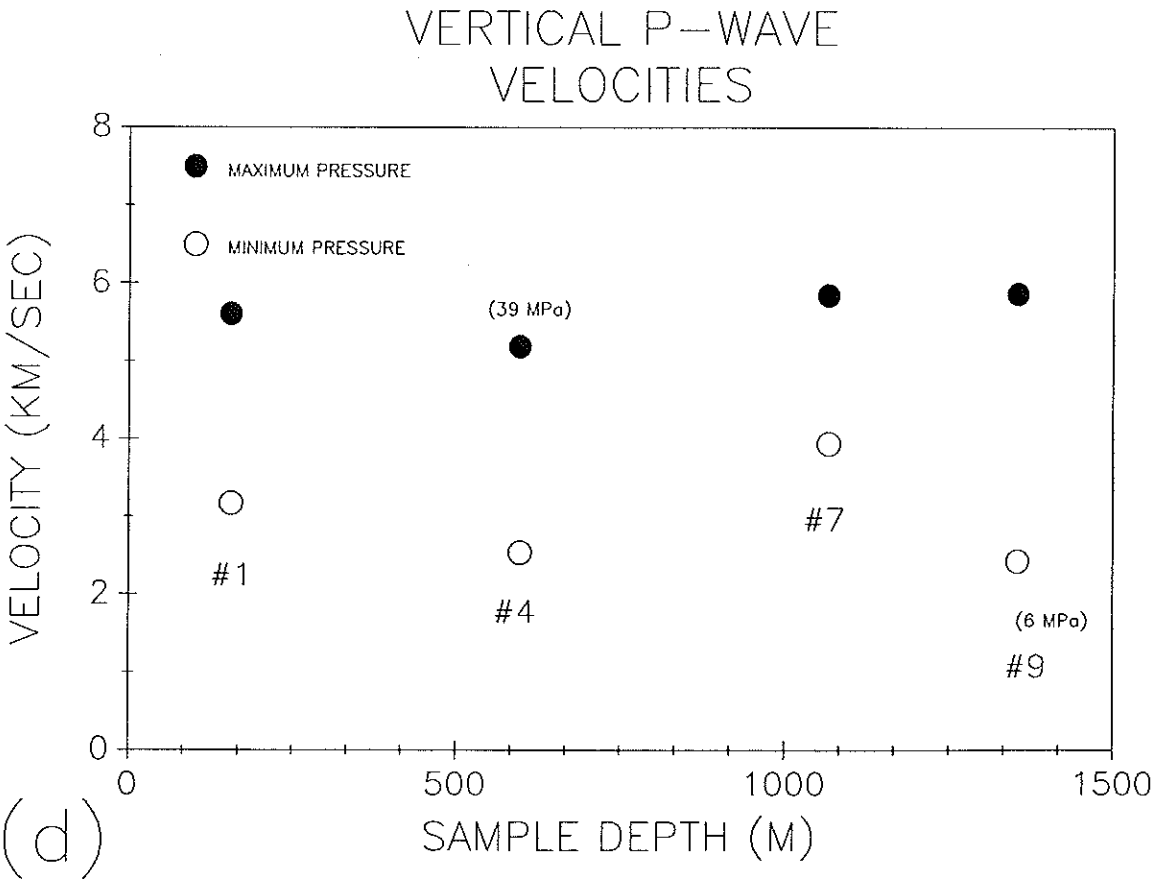

Figure 7 : Sample Velocities with Initial Depth

the vertical crack strain with sample depth, however, suggests that subhorizontal crack porosity is indeed proportional to the magnitude of the in situ stress.

The velocity properties of the samples are controlled by the microcrack population at low laboratory confining pressures. These measurements show no significant drop with depth in the horizontal propagation direction--reflecting the fairly low horizontal crack strains. The measurements made in the vertical propagation direction are affected by the vertical crack strains, which are larger and increase with depth more than the horizontal strains, and thus the drop in velocity with sample depth is somewhat more pronounced. At the highest laboratory confining pressures, the cracks have closed sufficiently that the matrix properties dominate the velocity properties of the rocks. At these pressures the velocities show no significant variations with depth.

Moodus Core #7 is anomalous in having both low crack strain and higher velocities, suggesting that the stress field has been locally relieved at the depth of Core #7. This explanation for anomalous core properties was first suggested by Carlson and Wang (1986) for core from Illinois borehole UPH-3. Core recovered from a highly fractured interval in that well had low stress-relief crack porosity and reoriented cracks. Those characteristics were observed as well in Kent Cliffs Core #6 (Meglis, 1987), which was recovered from a shear zone containing a major open fracture.

Examination of Figure 8, the fracture count and aperture with depth reported by Zoback and Moos (1988), indicates that this is a reasonable interpretation of the properties of Moodus Core #7. Core #7 was recovered from the highly fractured zone at roughly 1070 meters depth, which contained an open fracture of very large aperture. Thus, the properties of core samples may be useful for discerning fine-scale stress variations such as this.

SUMMARY

Measurements of strain and ultrasonic velocity have been made on five of the nine Moodus core samples. These results indicate that the crack porosity present is likely to be due to stress relief, thus rocks in situ should have low crack porosity. The crack populations in the cores appear to be sensitive to the in situ stress field, particularly evident in the sub-horizontal cracks (i.e. vertical strain) and the properties of Core #7 (recovered from a highly fractured zone.) However, the sub-vertical crack populations (horizontal crack strains) did not show a similar sensitivity to the horizontal in situ stress magnitudes. Thus the horizontal crack strains are not useful as stress indicators in this case.

The velocity properties of the cores are dominated at low laboratory confining pressures by the stress-relief crack porosity. Velocities are significantly lower than at the higher confining

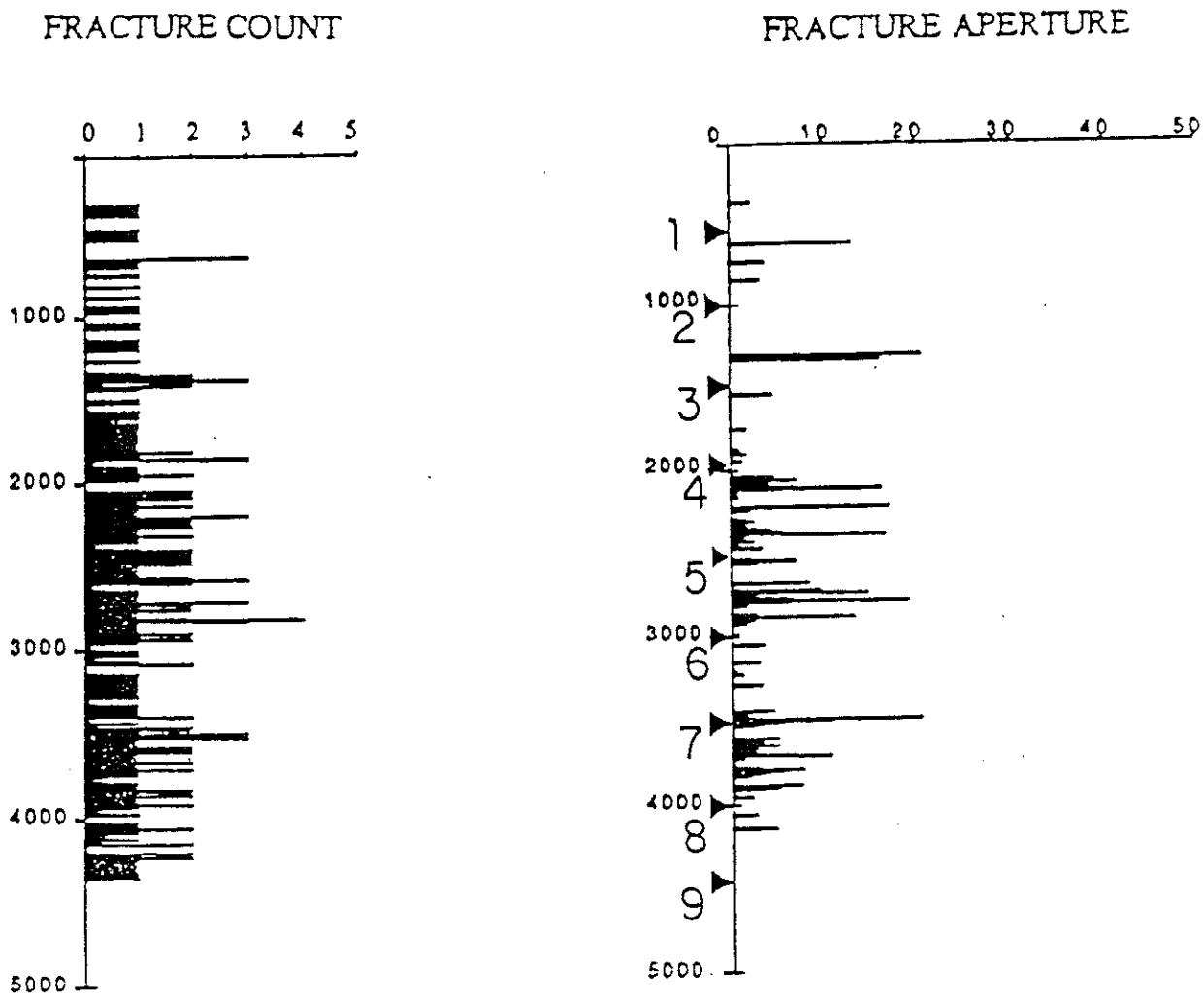

Figure 8: Moodus Sample Depths Shown on Plots of In Situ Fracture Count and Aperture (from Zoback and Moos, 1988.)

pressures, and show a slight drop with depth in the vertical propagation direction which is absent at high pressure. At maximum pressure the velocity properties of the cores are similar, indicating the matrix properties are similar. The in situ velocity properties of the cores are expected to be similar to the higher pressure laboratory properties.

BIBLIOGRAPHY

Carlson, S. and H. Wang, Microcrack Porosity and In Situ Stress in Illinois Borehole UPH-3, J. Geophys. Res., 91, 10,421-10,428, 1986.

Halleck, P., Anisotropic Stress-Strain Behavior of Drill Core Specimens from the Kent Cliffs Test Well, Kent Cliffs Borehole Research Project (Draft Final Report), 1986.

Kowallis, B., E. Roeloffs, and H. Wang, Microcrack Studies of Basalts from the Iceland Research Drilling Project, J. Geophys. Res., 87, 6650-6656, 1982.

Meglis, I., Ultrasonic Velocity and Porosity in the Kent Cliffs, N.Y. Test Well cores and the Application to In Situ Stress Determination, M.S. Paper, Pennsylvania State University, 1987.

Strickland, F. and N.-K. Ren, Use of Differential Strain Curve Analysis in Predicting In-situ Stress State for Deep Wells, Proc. U.S. Rock Mech. Symp., 21st, 523-532, 1980.

Zoback, M., In-Situ Stress Measurements in the Kent Cliffs Research Well, Kent Cliffs Borehole Research Project (Draft Final Report), 1986.

Zoback, M., and D. Moos, In Situ Stress, Natural Fracture and Sonic Velocity Measurements in the Moodus, Connecticut Scientific Research Well, Report to Woodward-Clyde, 1988.

Appendix H

APPENDIX H

Appendix H consists of magnetic susceptibility values for the 9 Moodus borehole cores.

MAGNETIC SUSCEPTIBILITY OF ROCK UNITS FROM THE MOODUS WELL

Weijiang Fang, Yuan-hsin Chen, and Jelle de Boer
Department of Earth and Environmental Sciences, Wesleyan University

Detailed measurements were made of the magnetic susceptibility in nine cored segments from the Moodus well.

The data shows that lithostratigraphic units above the Honey Hill fault are characterized by relatively low susceptibility values with little variation. Mean susceptibilities in the Hebron gneiss, Canterbury gneiss, and Tatnic Hill Formation range from 7 to 24 x 10^{-6} (c.g.s.) (Figure 1) with standard deviations ranging between 3 and 16 x 10^{-6}. The Canterbury gneiss stands out by its very low magnetic values.

The Waterford gneiss, directly below the Honey Hill fault zone is considerably more magnetic. Mean values are 63 and 76 x 10^{-6}, respectively (Figure 1). With the higher susceptibility comes a broader range of values. Much of the magnetic increase can be attributed to the presence of fine grained, relatively pure magnetite, which appears concentrated in streaks parallel to the foliation. A second major increase in magnetic susceptibility occurs at a depth between 1150 and 1200 meters. Mean susceptibility values below this zone are 252 and 303 x 10^{-6} (c.g.s.). Much of the variability here is due to the presence of relatively large (granular) magnetite masses which are widely distributed throughout the gneiss.

We believe the latter susceptibility increase to be relatively abrupt and to occur in a narrow zone, which is characterized also by major geochemical variations (1085 - 1274m) and a 20° counter-clock rotation of breakouts (1140 - 1176m) (Figure 2). Anderson et al. (this report) refer to this zone as the geochemical transformation between predominantly granitic and mafic gneisses.

The rotation of the breakouts suggests that we are dealing with a tectonic zone as well. This tectonic zone is probably similar to the Honey Hill fault zone, but occurs at greater depth below it.

Field evidence indicates the presence of several major (northward dipping), low angle fault zones in the Avalon terrane, south of the Honey Hill fault. The surface exposures of these fault zones have been located in several road cuts and can be traced using aeromagnetic and ground magnetic surveys.

The exposed faults are characterized by geochemical and geophysical anomalies.

The chemical changes include an increase in Fe, and Mg and a decrease in Si, K, and Na. The geophysical change is represented by significant demagnetization (Figure 3a and 3b).

It appears that the magnetic data are highly instructive in delineating tectonic units and specific fault zones.

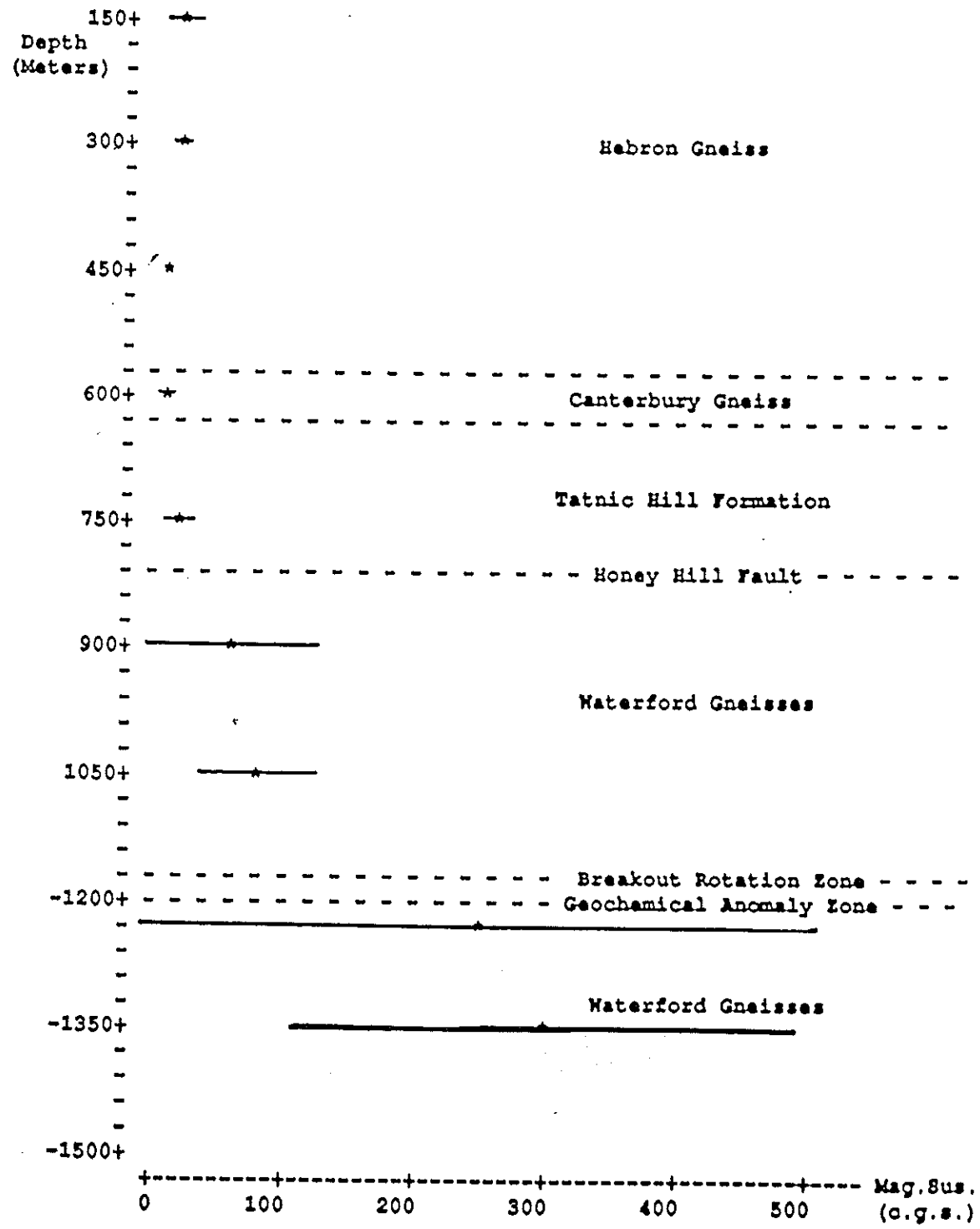

Fig. 1. Magnetic Susceptibilities of Core Sections from Deep Moodus Hole and its Geologic Interpretation

BREAKOUT AZIMUTH
MOODUS #1

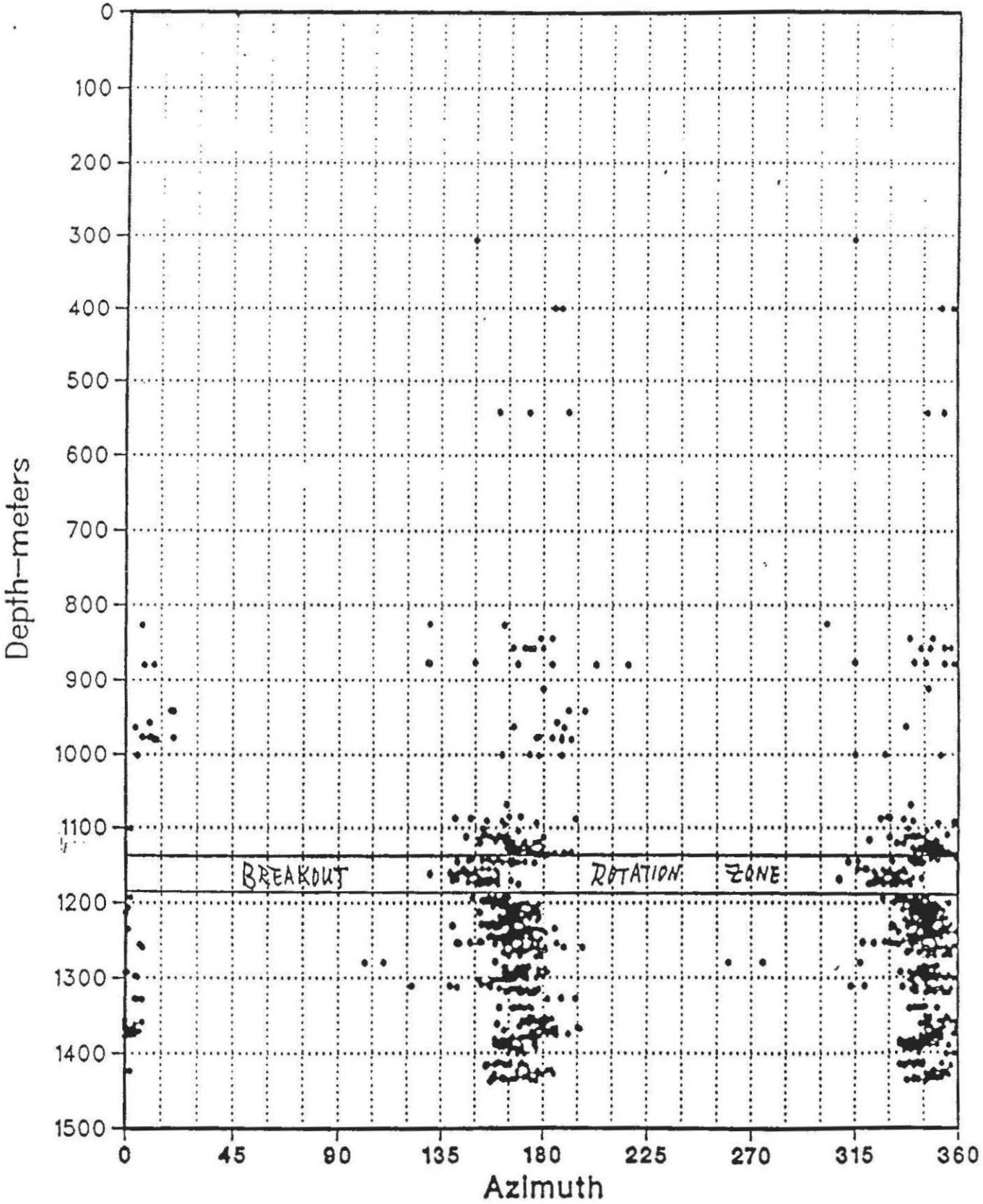

Fig. 2 Circular Mean Breakout Azimuth = 346-166; Circ. Var. = .018; Stdv. = 5.5
Minimum Stress Azimuth = 346-166; Maximum Stress Azimuth = 76-256

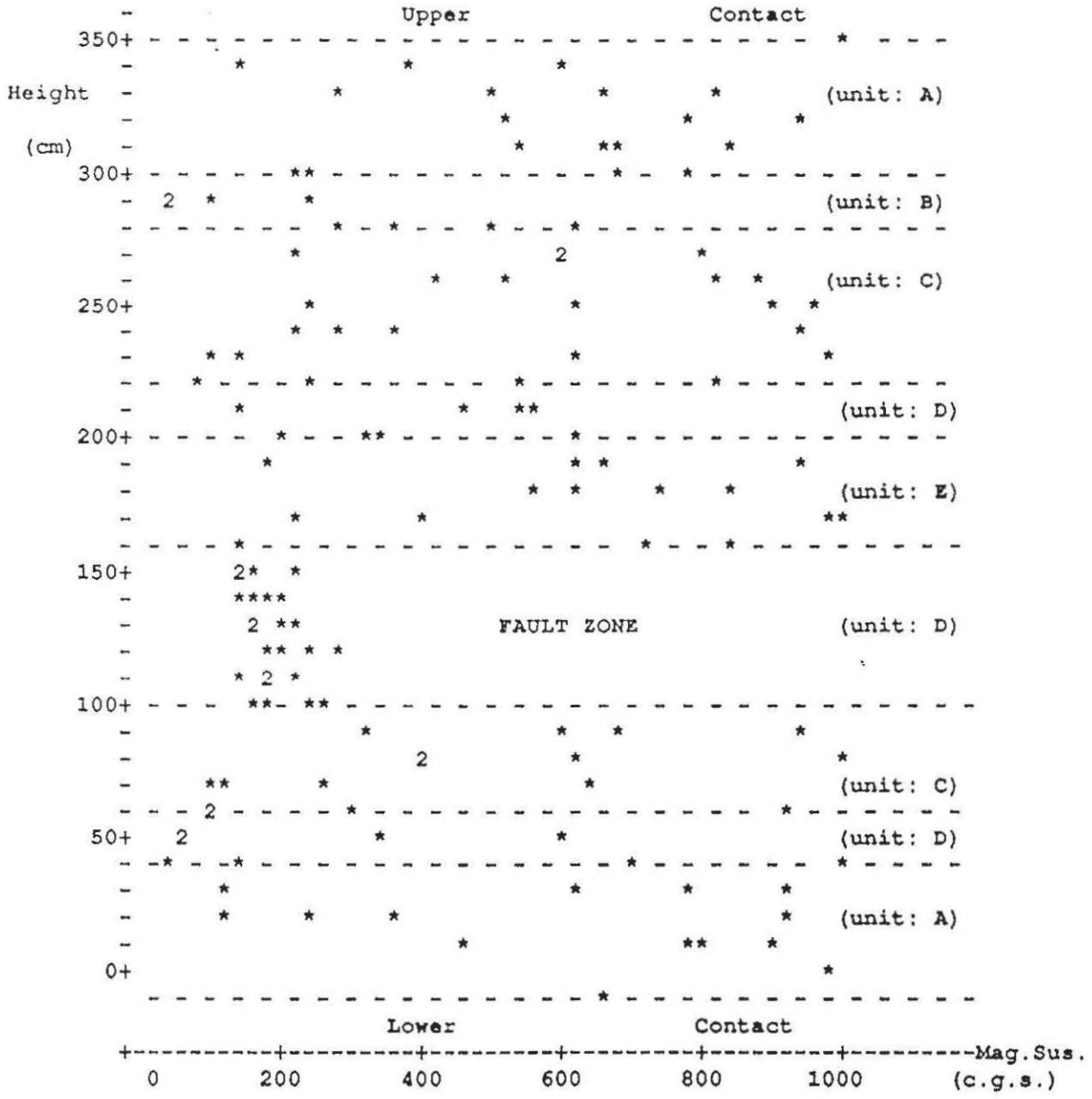

F16 3A Magnetic susceptibility of ENE-trending, NNW-dipping fault in Selden Neck State Park (CT). Unit A:granitic gneiss with biotite. Unit B:biotite gneiss with quartz veins and feldspar augen. Unit C: biotite gneiss. Unit D:biotite schist. Unit E:granitic gneiss.

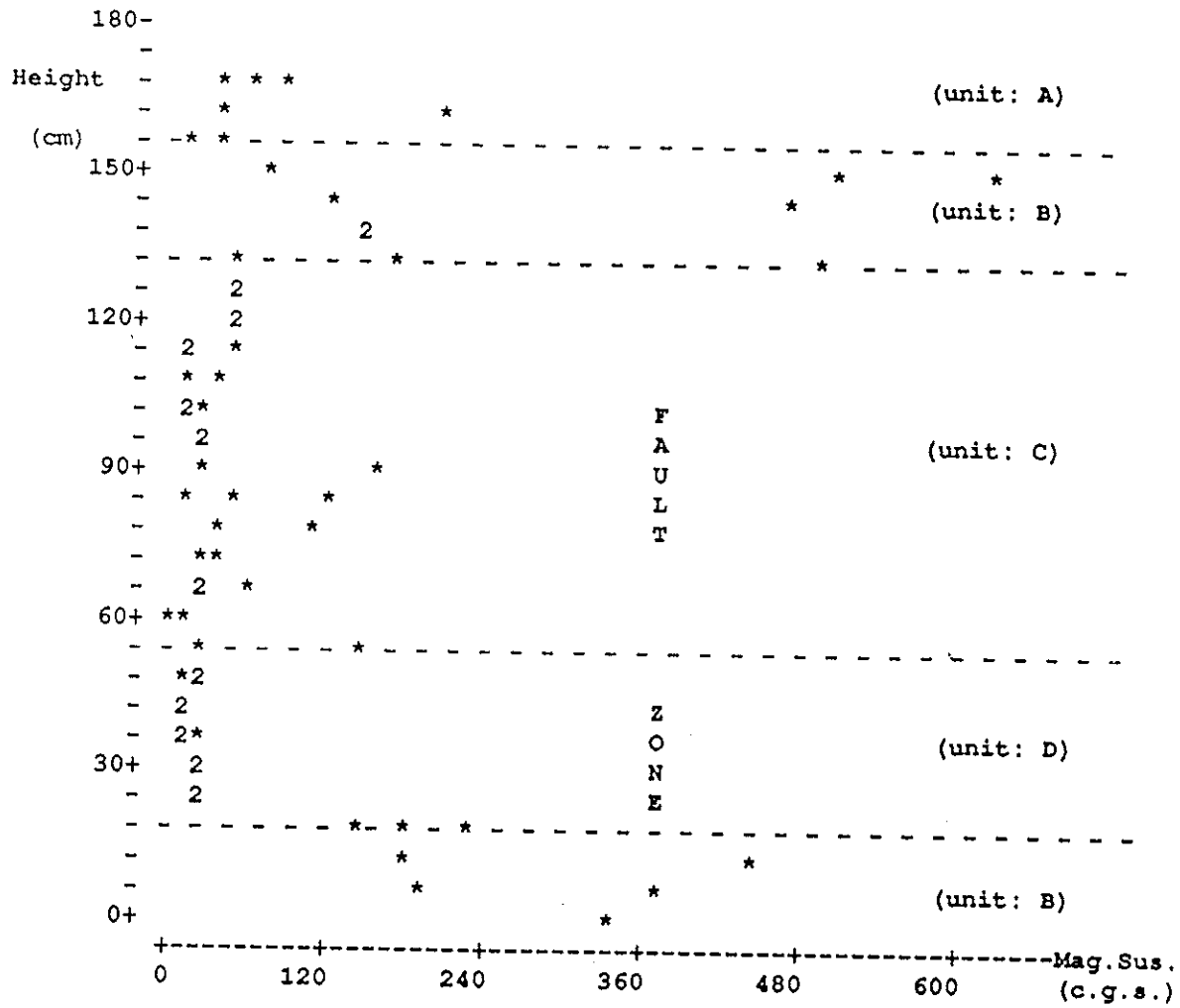

FIG. 3B Magnetic susceptibility of E-W trending, north-dipping fault at the site of the intersection of Route 11 and 82 (CT). Unit A: coarse-grained granitic gneiss. Unit B:coarse-grained granitic gneiss. Unit C:biotite gneiss with deformed pegmatite. Unit D: biotite schist.

Appendix I

APPENDIX I

Results of the seismic monitoring study of the Moodus 1987 earthquake swarm.

SEISMIC MONITORING NEAR MOODUS CONNECTICUT: SEPTEMBER THROUGH OCTOBER 1987

INTRODUCTION

The Moodus borehole research project was developed to investigate whether the orientation of the tectonic stress field changes between southeastern New York and New England. Measurements of stress direction in New York suggest a uniform orientation with the maximum principle stress trending northeast to east-northeast (e.g., Sbar and Sykes, 1977; Quittmeyer et al., 1985; Zoback, 1986). These results are based on inferences from earthquake fault plane solutions, direct measurements of stress by the hydrofracture method, and interpretation of borehole breakouts. In New England, where only fault plane solutions are available, more variability in orientation is reported with an average east-west trend (e.g., Yang and Aggarwal, 1981; Pulli and Toksoz, 1981; Pulli, 1983). To assess whether different stress regimes do indeed exist in New York and New England, the Empire State Electric Energy Research Corporation, in cooperation with Northeast Utilities and the Electric Power Research Institute, sponsored a research project to measure directly the stress field near Moodus, Connecticut. This site was chosen, in part, because it was hoped that the research would shed some light on the setting and cause of the Moodus earthquake source.

The historical record for the Moodus region includes numerous references to earthquake occurrence. In fact, the name Moodus comes from an Indian word, 'Morehemoodus', meaning "the place where noises come from the ground" (Brigham, 1871 quoted in Ebel et al., 1982). The recurrent nature of the seismicity and its proximity to a nuclear power plant have focused the attention of scientific and regulatory organizations on the cause of these earthquakes. In particular, one concern is the potential for significant damaging events originating from the Moodus source in the future.

Several weeks after the termination of the planned experiments in the Moodus borehole, a swarm of earthquakes began less than a kilometer from the borehole site. The Moodus Project was quickly expanded to include detailed monitoring of the swarm events. By carefully locating the earthquakes and determining the style of faulting that was occurring, the implications of the borehole stress measurements could be checked against the "ground truth" of the swarm results. This additional phase of the Moodus research project thus provided an opportune complement to the work that had already taken place.

This section of the Final Report describes the earthquake monitoring effort at Moodus and results obtained from the recorded data. After a brief discussion of past earthquake occurrence, the design and installation of the temporary network are presented. Then the data and methods of analysis are discussed. Finally, the results are shown to be in excellent agreement with the conclusions concerning earthquake generation that were drawn from the prior borehole experiments.

BACKGROUND

Seismic activity in the vicinity of Moodus, Connecticut is documented in the historical record as early as 1791 (Table I-1). Local Indian traditions, however, suggest that earthquakes occurred in this area prior to colonization by Europeans (Brigham, 1871 in Ebel et al., 1982). While seismicity is recurrent, none of the historical events has been large. The largest event in the historical record occurred on 16 May 1791. This earthquake produced damage of intensity level VI to VII on the Modified Mercalli (MM) scale (Electric Power Research Institute, 1986). Its magnitude (mb) was estimated at 4.30 on the combined basis of maximum intensity and total felt area (Veneziano and Van Dyck, 1986). Earlier, Street and Lacroix (1979), using only an estimate of total felt area, determined the magnitude of this event to be 4.35 (mbLg). Five other earthquakes with reported intensities of V (MM) are located within about 50 km of Moodus (Figure I-1).

During the 1970's, a number of high-gain seismic stations were installed near Moodus to investigate in more detail the recurring activity. By the end of the decade, six short-period vertical seismometers were being recorded in analog format. Station spacing averaged about 5 km, and provided detection of events as small as -2.0 (m_c) (Ebel et al., 1982). In the mid-1980's, the recording format for these stations was converted from analog to digital.

Recent earthquake activity generated by the Moodus source has been in the form of swarms from a very localized volume. Hypocenters for these events are clustered within an area on the order of one to two kilometers; all have been shallow (<2.3 km) (Ebel, 1986, oral communication; Ebel, 1988). Magnitudes of the largest events in each sequence range from about 2 to 3.

In 1981, a swarm began with a series of over 30 foreshocks. These events were all smaller than magnitude 1.0 and occurred during a two day period. During the following week the mainshock, of magnitude 2.1, was followed by more than 300 aftershocks. After this, activity continued at a low rate for several months, punctuated by occasional bursts in the rate of occurrence. In total, over 500 earthquakes were detected during the 1981 sequence. Because of their small size, however, only a few could be independently located (Ebel et al., 1982).

Swarms also occurred in 1982 and 1986. The 1982 swarm was similar in character to the one in 1981. A series of foreshocks preceded the mainshock which was followed by a typical aftershock sequence (Ebel, 1988). In 1986, however, the pattern differed. During this swarm, the largest shock occurred near the end of the sequence. Prior to that event, which had a magnitude of about 2-1/4, the swarm was characterized by small bursts of earthquakes.

TEMPORARY MONITORING NETWORK: 1987

A new swarm began on 11 September 1987 with the occurrence of a

magnitude 2.3 (m_C) earthquake. Local residents felt and heard the event. The epicenter for this shock placed it less than 1 kilometer from the Moodus research borehole. A check with Weston Observatory of Boston College indicated that this microearthquake had initiated a new swarm of activity. Spurred by recent work on stress measurements at the site, a temporary array of seismometers was deployed in the epicentral region to determine the locations, depths, and style of faulting that occur at Moodus.

The array, consisting of eight stations, was installed beginning on 17 September 1987. Four stations were operating by the end of the first day; the final network configuration was established on 01 October 1987. The stations were deployed in a tight array surrounding the region of activity (Figure I-2). Epicentral distances ranged from about 1/4 km to 2 km. Inter-station spacing averaged approximately 1 km. Site coordinates were determined for each station using aerial photographs and topographic maps. The monitoring stations ran for approximately five weeks. The time periods for which the different stations were operating are summarized in Figure I-5.

Moodus field stations were similar in most respects to those typically established for seismic network monitoring. All field stations except one (BORE) employed a short-period vertical seismometer (Geospace HS-10). At BORE, a three-component sensor (Spregnether S-6000) was installed. The signal generated by the seismometer was directed to a Spregnether Portable Telemetry System (PTS-3 or PTS-6) where it was amplified, filtered, and put onto a carrier tone for transmission. Data from all field stations were telemetered to a central receiving site using radios. At the central site, the signals were recorded on magnetic tape in analog format. Two Honeywell 101 recorders were employed; one for recording and one for playback. A common time base was recorded along with the seismic data on each tape. This time base was calibrated daily against the time signal from the U.S. Naval Observatory using a telephone link-up.

Data from three stations were displayed on drum recorders so that events

could be detected. For detected events, the seismograms were played back from the magnetic tape for analysis. Arrival times of P- and S-waves were scaled, and reading qualities were assigned to the measurements. For impulsive arrivals, times were scaled with a precision of 0.01 sec. In addition to arrival times, the duration of the seismic signal was also determined. These data were then used to locate the earthquake and estimate its size.

DATA ANALYSIS

Earthquakes were located using the computer program HYPOINVERSE (Klein, 1978). The plane-layered model of velocities used in the location procedure was derived from the sonic velocity log of the Moodus borehole (Figure I-3, Table I-2). The ratio of compressional to shear wave velocities was assumed to have a constant value of 1.75. The sonic velocity logs indicate this is a good average for the ray paths being traversed. Distance and residual weighting were not employed as all distances and residuals were small.

A magnitude was calculated for each event on the basis of signal duration using the relation derived by Chaplin et al. (1981):

$$mbLg = 2.21 \log10(t) - 1.70$$

in which t is the signal duration in seconds. This relation is derived from a set of New England earthquakes for which both durations and mbLg magnitudes were determined. The set of events they analyzed ranged in magnitude (mbLg) from about 1.8 to 4.4, and in duration from about 25 to 500 sec. It is assumed here that their relation can be extrapolated to shorter durations and smaller magnitude values than were used in the regression.

Fault plane solutions were determined for individual events, groups of events and for the entire composite data set. A grid-search procedure (Snoke et al., 1984) was used to assess objectively the range of possible solutions. The relative

polarities of field stations were checked by comparison of the signatures produced by teleseismic arrivals. Polarities were also compared with observations at Weston Observatory stations.

RESULTS

During the five weeks of monitoring, the network detected over 170 earthquakes. Data were sufficient to locate 168 of these events. They ranged in magnitude from 1.8 to -1.6 (m_c). The location program produced two quality ratings for each event according to the scheme originally set forth in HYPO71 (Lee and Lahr, 1975). The average of these two ratings forms the overall quality assessment. The first rating (QS) depends on the size of the standard errors of the solution. Station distribution determines the second rating (QD). This assessment procedure assigned an A quality to 93 of the located earthquakes, B to 24 events, C to 49 events, and D to 2 events. The high percentage of A and B quality locations results from the good distribution of nearby stations.

The relative accuracy of the C quality locations, for which the QS and QD ratings were A and D, respectively, was tested by degrading several A and B quality earthquakes such that their station distribution was similar to that for the C events. Horizontal and vertical differences in the calculated location for these two cases are less than 150 meters. Hence, plots of seismicity in this report include C-AD earthquakes, as well as all A and B quality events. Spatial patterns in the Moodus seismicity can be resolved, in a relative sense, at a characteristic length on the order of 100 to 200 meters.

During the period of monitoring, earthquakes occurred at a long-term rate that was fairly constant (Figure I-4a). Over the short-term (per day), however, the rate of occurrence showed substantial variations. Periods of reduced activity separate bursts of seismicity that are associated with the occurrence of the larger events in the swarm ($0<m_c<2$) (Figure I-5). During the period of monitoring, eight earthquakes with magnitude greater than 0.0 (m_c) were recorded. The maximum

number of events to occur in one day was 19; several days had no events. Energy release also showed large variations (Figure I-4b). The two major periods of energy release during the five weeks of monitoring occurred from 19 through 26 September, and from 10 through 12 October.

The calculated depths of the swarm events range from 1.3 to 1.9 km for the better quality locations (A,B, and C-AD). Based on the borehole lithology (Appendix B), these earthquakes occurred in Waterford Group rocks of the Avalonian terrane. They are located about 0.5 to 1.0 km below the wide zone of shearing associated with the Honey Hill fault.

The swarm events occupy a volume with a radius of approximately 1/4 kilometer (Figure I-9). While most hypocenters that plot outside of this volume are poorly determined, one event is well located about 1/2 kilometer to the north-northwest. The relation of this event to the present, previous, or future swarms is unclear. Its pattern of first motions is consistent with the style of faulting determined for the other swarm events.

As the swarm progressed, the earthquakes migrated spatially. Four phases of activity can be defined on the basis of the spatial distribution of events. This activity is displayed in two formats in Figures I-6 through I-13. Figures I-6 through I-9 are epicentral plots of the four phases of activity. Figures I-10 through I-13 are stereographic plots of the data from three orthogonal perspectives (top, a birds-eye view; middle, a cross-section looking from the south towards the north; bottom, a cross-section looking from the west towards the east). These latter four figures allow the data to be viewed in three dimensions with the aid of a stereoscope.

The first phase of activity lasted from 19 September through 30 September. During this phase, the southeastern half of the swarm volume experienced activity (Figure I-6 and I-10) that included four events of magnitude greater than 1.0 (m_C). The earthquakes are distributed along a northeast trend approximately 0.6

km long and 0.2 km wide. This trend does not coincide with the orientation of potential fault planes as identified in the composite fault plane solution.

The second phase of migration began on 02 October and extended through 09 October. During this period, activity moved to the northwest of the site of previous activity (Figures I-7 and I-11). All of the earthquakes during this phase were small with magnitudes less than -0.5 (m_c). This migration of activity coincided with the establishment of the final monitoring station to the west-southwest of the swarm. The locations of these events relative to previous activity, however, are insensitive to inclusion of data from this final station. The earthquakes occurring during this phase were spatially distinct from previous activity.

During the third phase of activity, which lasted from 10 October through 13 October, the southwestern portion of the swarm volume became active. In addition, activity continued near the intersection of the first and second phase. The activity in the southwestern part of the swarm volume included three earthquakes with magnitude greater than 1.0 (m_c).

The final phase of activity occurred primarily in the southern and northeastern portions of the swarm volume. This phase is defined from 14 October through 22 October when monitoring finished. The fourth phase of activity included two events with magnitude greater than 0.0, but none with magnitude greater than 1.0 (m_c). The events in the southern portion of the swarm volume are located near the epicenters of the larger events that occurred during the first phase of activity.

The spatial distribution of seismicity during the five weeks of monitoring defines an apparent concentration of events surrounding an area of reduced activity (Figure I-14). Three possibilities are offered to explain this observation. First, the region of reduced activity may represent the rupture zone of the large event (mainshock) that triggered the swarm. Under this hypothesis, only small

stress concentrations are left on the main rupture plane, and thus only a few aftershocks occur in that region. In the region surrounding the main fault plane stress is concentrated and many aftershocks occur.

The best estimate of the location of the mainshock does not support this hypothesis. The mainshock was located using only local stations operated by Weston Observatory of Boston College. Locations of other events during this swarm, using only this subset of stations, suggest that systematic shifts in location resulting from station distribution are insufficient to move the mainshock into the relatively aseismic zone.

A second hypothesis is that the aseismicity of the central zone results from some difference in rock properties, such as lithology or pore pressure. Lithology in this region, however, generally varies in a vertical direction. Dramatic horizontal changes in the lithology of the Waterford Group rocks, such as might be related to the reduced seismicity zone, are not observed in surface exposures. Variations in other rock properties at this depth are poorly documented. Hence it is difficult to assess the potential of this hypothesis to explain the observed seismicity pattern.

Finally, the region of reduced activity may be related to the period of observation. The monitoring effort began one week after the mainshock, and activity continued after monitoring ceased. Events may have occurred in the central portion of the swarm volume either before or after the monitoring took place. Data from the Weston Observatory network are insufficient to resolve this possibility. Most of the earthquakes recorded by the temporary stations were too small to be located based solely on data from the Weston network. Thus, events in the region of apparent reduced activity would likely not have been located unless they were greater than about magnitude 0.5 (m_c). Even for such events, locational uncertainties would probably be too large, relative to later locations using data from the temporary stations, to determine whether or not they occurred in the region of apparent reduced activity.

A composite fault plane solution was determined on the basis of all A and B quality events. These events provide a data set of over 550 first motion observations. For most stations the observed first motion is the same for all events. At two stations (BORE and DILL), however, the observed first motion changes depending on the location of the event. These changes constrain well the orientation of one nodal plane. The other nodal plane is also well constrained by the distribution of the data from other stations.

The composite solution indicates reverse faulting is occurring on planes that strike approximately N0E +- 15 degrees and dip either 25 to 30 degrees to the east or 60 to 65 degrees to the west (Figure I-15). The P-axes for these solutions plunge 15 to 20 degrees at an azimuth of N270E +- 5 to 10 degrees (Figure I-16). Fault plane solutions for single events, and composite solutions for subsets of the events, are more poorly constrained.

The direction of maximum compressive stress inferred from the P-axes of the composite fault plane solution agrees well with the estimates of stress determined from borehole experiments. Zoback and Moos (this report) obtain a value of 89 +- 5 degrees for the maximum compressive stress direction, while Plumb and Hornby (this report) report a value of 76 +- 6 degrees. The two estimates of maximum stress direction from borehole experiments, and the results of earthquake swarm monitoring, are all consistent with a maximum compressive stress direction of approximately N80E.

SUMMARY

A seismic monitoring array was deployed for five weeks in the vicinity of the 1987 Moodus swarm. This network has provided a wealth of new information on the earthquake process at Moodus. The 1987 swarm activity occupied a volume with a radius of about 1/4 km. The events were very shallow, ranging in depth from 1.3 to 1.9 km. The earthquakes migrated spatially during the monitoring

period, activating different portions of the eventual swarm volume. One portion of the volume showed a reduced level of activity relative to surrounding regions. This region may represent the mainshock rupture zone, a zone in which rock properties are not favorable for earthquake occurrence, or a region that was activated either before or after the period of station deployment.

A composite fault plane solution indicates that north-south striking faults are being activated in a reverse sense. One nodal plane dips to the west at about 60 to 65 degrees; the other dips easterly at 25 to 30 degrees. The westerly dipping nodal plane should intersect the borehole at about 2300 ft and surface about 0.9 km east of the epicentral area. The easterly dipping nodal plane would intersect the surface about 2.6 km west of the epicentral area. These areas merit future attention in the search for evidence of surface faulting near Moodus.

The earthquakes are clearly unrelated to the Honey Hill fault zone which lies 0.5 to 1.0 km above the zone of activity. The orientation of the Honey Hill is also inconsistent with the orientation and sense of faulting observed for the fault plane solution.

The orientation of the tectonic stress field at Moodus, as inferred from the earthquake data, is consistent with the conclusions of the Moodus borehole experiments. Both types of data indicate the direction of maximum compressive stress is approximately east-west. An orientation of N80E is within the error estimates of all indicators.

LIST OF FIGURES

LIST OF FIGURES
(continued)

LIST OF FIGURES
(Continued)

TABLE I-1

YEAR	ORIGIN TIME MO	DY	HR	MN	SEC	LAT (deg N)	LON (deg W)	DEPTH (km)	MAGN (mb)	DEPEND-ENCE
1791	5	16	13	22	.00	41.50	72.40	0	4.30	MAIN
1791	5	19	3	0	.00	41.50	72.50	0	3.11	DEPN
1792	8	29	3	0	.00	41.50	72.50	0	3.11	DEPN
1792	10	24	6	0	.00	41.50	72.50	0	2.51	*
1793	1	11	13	0	.00	41.50	72.50	0	2.51	*
1793	7	6	11	0	.00	41.50	72.50	0	2.51	*
1794	3	6	19	0	.00	41.50	72.50	0	3.11	MAIN
1794	3	7	4	0	.00	41.50	72.50	0	3.11	DEPN
1794	3	9	19	0	.00	41.50	72.50	0	3.11	DEPN
1794	3	10	4	0	.00	41.50	72.50	0	3.11	DEPN
1805	8	12	0	0	.00	41.50	72.50	0	2.51	*
1805	12	30	11	0	.00	41.50	72.50	0	3.11	MAIN
1811	7	0	0	0	.00	41.50	72.50	0	2.51	*
1812	2	9	14	0	.00	41.50	72.50	0	2.51	*
1812	7	5	13	0	.00	41.50	72.50	0	2.51	*
1813	12	28	21	0	.00	41.50	72.50	0	2.51	*
1827	8	23	0	0	.00	41.40	72.10	0	3.11	MAIN
1837	4	12	0	0	.00	41.70	72.70	0	3.70	MAIN
1844	6	0	1	0	.00	41.50	72.40	0	2.51	*
1845	1	1	0	0	.00	41.50	72.40	0	2.51	*
1852	8	1	0	0	.00	41.40	72.10	0	2.51	*
1856	3	13	3	0	.00	41.40	72.60	0	3.11	MAIN
1858	6	27	0	0	.00	41.40	72.80	0	3.42	MAIN
1860	3	12	0	0	.00	41.50	72.50	0	2.51	*
1862	2	3	1	0	.00	41.50	72.50	0	3.11	MAIN
1885	4	28	20	10	.00	41.30	72.70	0	2.51	*
1886	9	5	0	0	.00	41.50	72.50	0	3.11	MAIN
1894	4	10	0	0	.00	41.60	72.50	0	3.11	MAIN
1894	11	23	13	30	.00	41.40	72.20	0	2.51	*
1897	9	5	0	0	.00	41.50	72.50	0	3.11	MAIN
1899	5	17	1	15	.00	41.60	72.60	0	3.92	MAIN
1906	5	8	13	30	.00	41.50	72.50	0	3.11	MAIN
1913	11	15	0	0	.00	41.50	72.50	0	2.51	*
1916	12	2	9	0	.00	41.50	72.50	0	2.51	*
1917	2	16	9	0	.00	41.50	72.50	0	3.11	MAIN
1917	3	11	0	0	.00	41.50	72.50	0	2.51	*
1919	8	11	0	0	.00	41.50	72.50	0	2.51	*

TABLE I-1 (CONTINUED)

YEAR	ORIGIN TIME MO	DY	HR	MN	SEC	LAT (deg N)	LON (deg W)	DEPTH (km)	MAGN (mb)	DEPEND-ENCE
1925	10	30	0	0	.00	41.50	72.50	0	3.11	MAIN
1925	11	14	13	4	.00	41.70	72.40	0	3.69	DEPN
1934	1	30	10	30	.00	41.80	72.60	0	3.11	MAIN
1937	7	27	9	10	.00	41.80	72.40	0	2.51	*
1938	9	20	0	0	.00	41.50	72.20	0	2.51	*
1940	3	2	4	15	36.00	41.50	72.50	0	2.51	*
1940	3	13	1	29	.00	41.50	72.50	0	2.51	*
1944	12	14	3	15	.00	41.60	72.80	0	3.11	MAIN
1951	1	26	3	27	.00	41.50	72.50	0	3.11	MAIN
1968	11	3	8	33	.00	41.40	72.50	0	3.28	*
1976	4	24	10	22	22.10	41.46	72.49	0	2.18	*
1982	6	17	14	14	36.04	41.55	72.45	4	2.28	*

TABLE I-2

Velocity Model for Earthquake Locations

Velocity (km/sec)	Depth to Top of Layer (km)
05.15	00.00
05.40	00.12
05.60	00.33
05.90	00.82
06.60	13.00
08.10	34.00

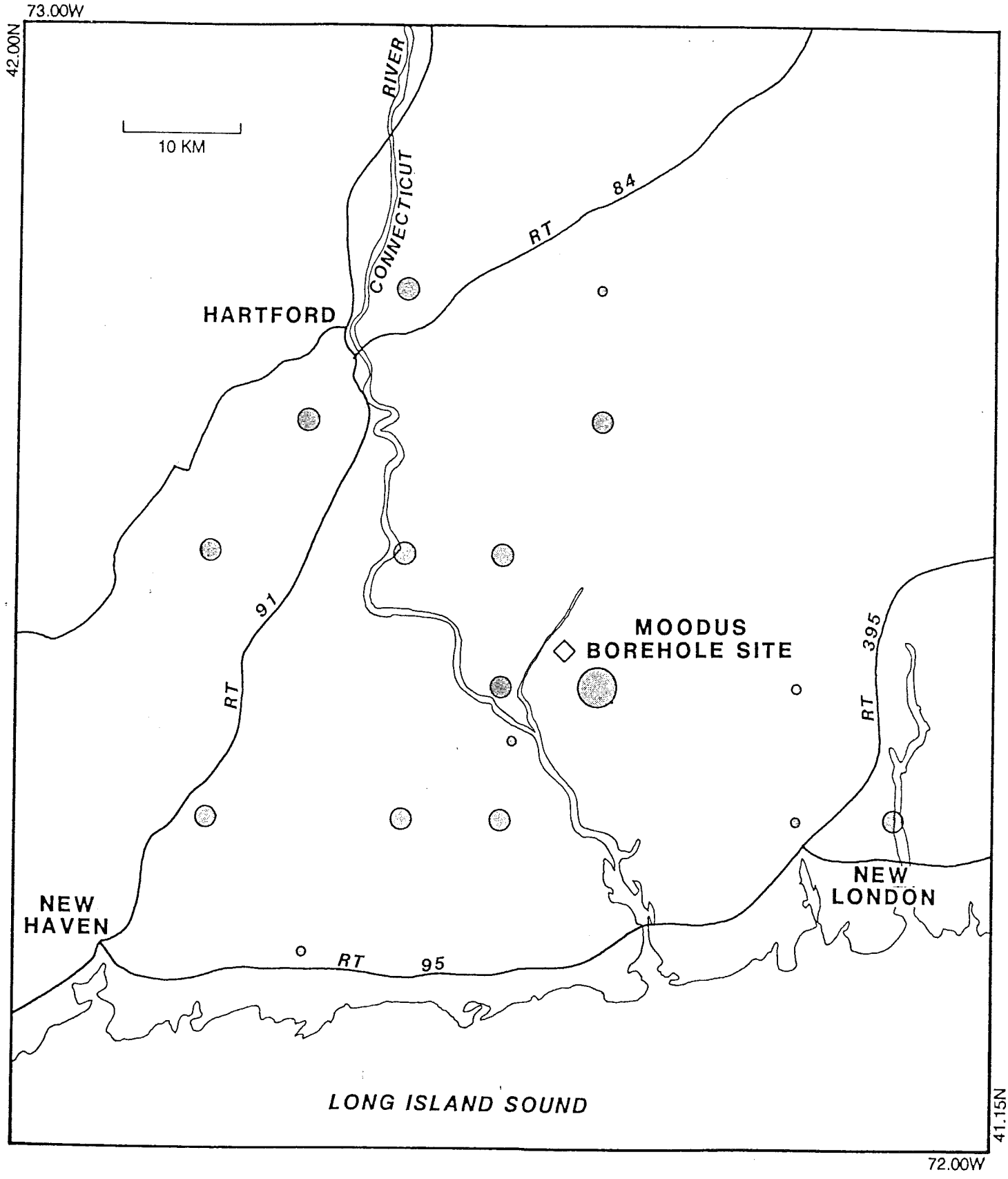
73.00W
42.00N
10 KM
CONNECTICUT RIVER
RT 84
HARTFORD
RT 91
MOODUS
BOREHOLE SITE
RT 395
NEW
HAVEN
RT 95
NEW
LONDON
LONG ISLAND SOUND
41.15N
72.00W

FIGURE I–1

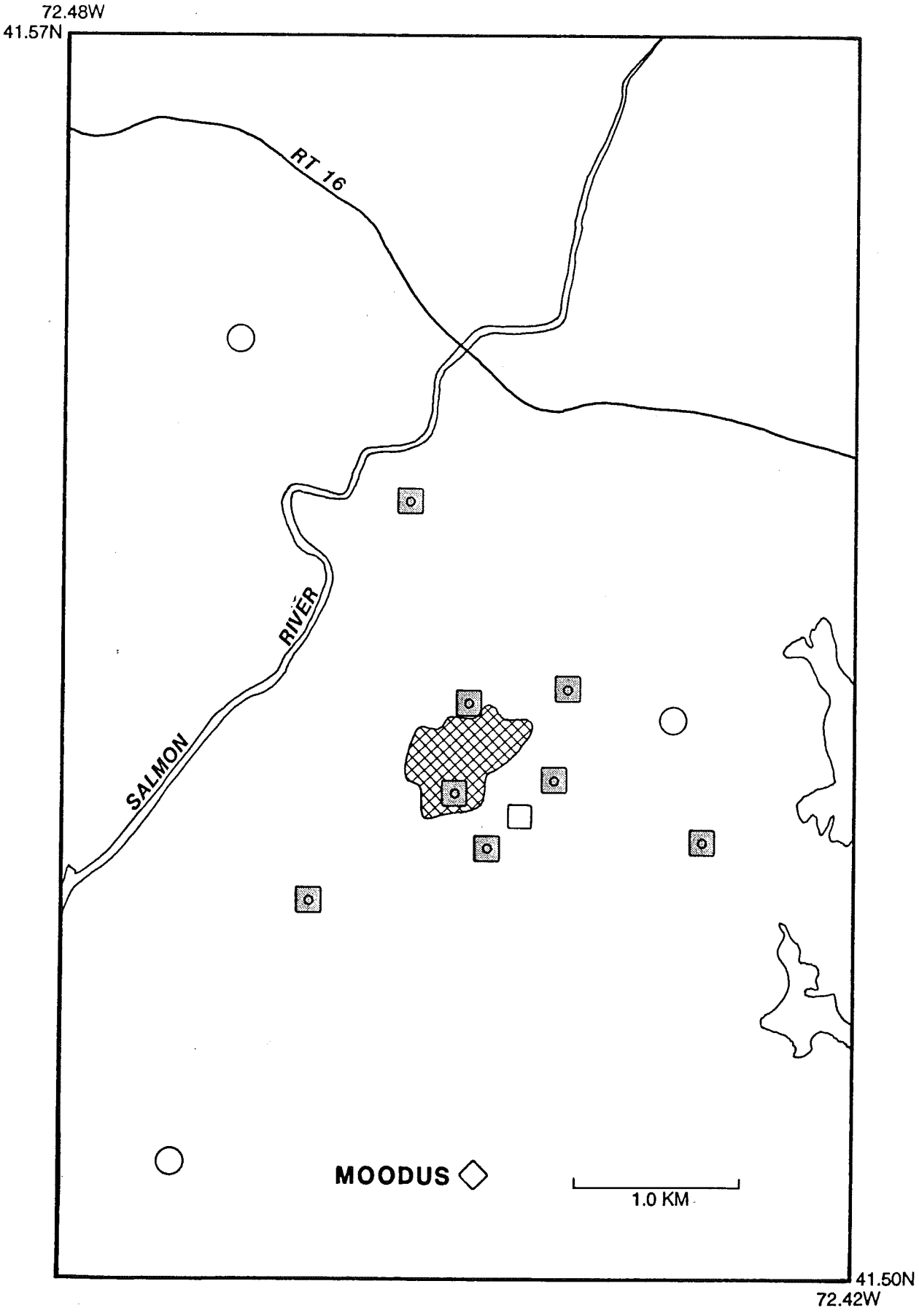

FIGURE I–2

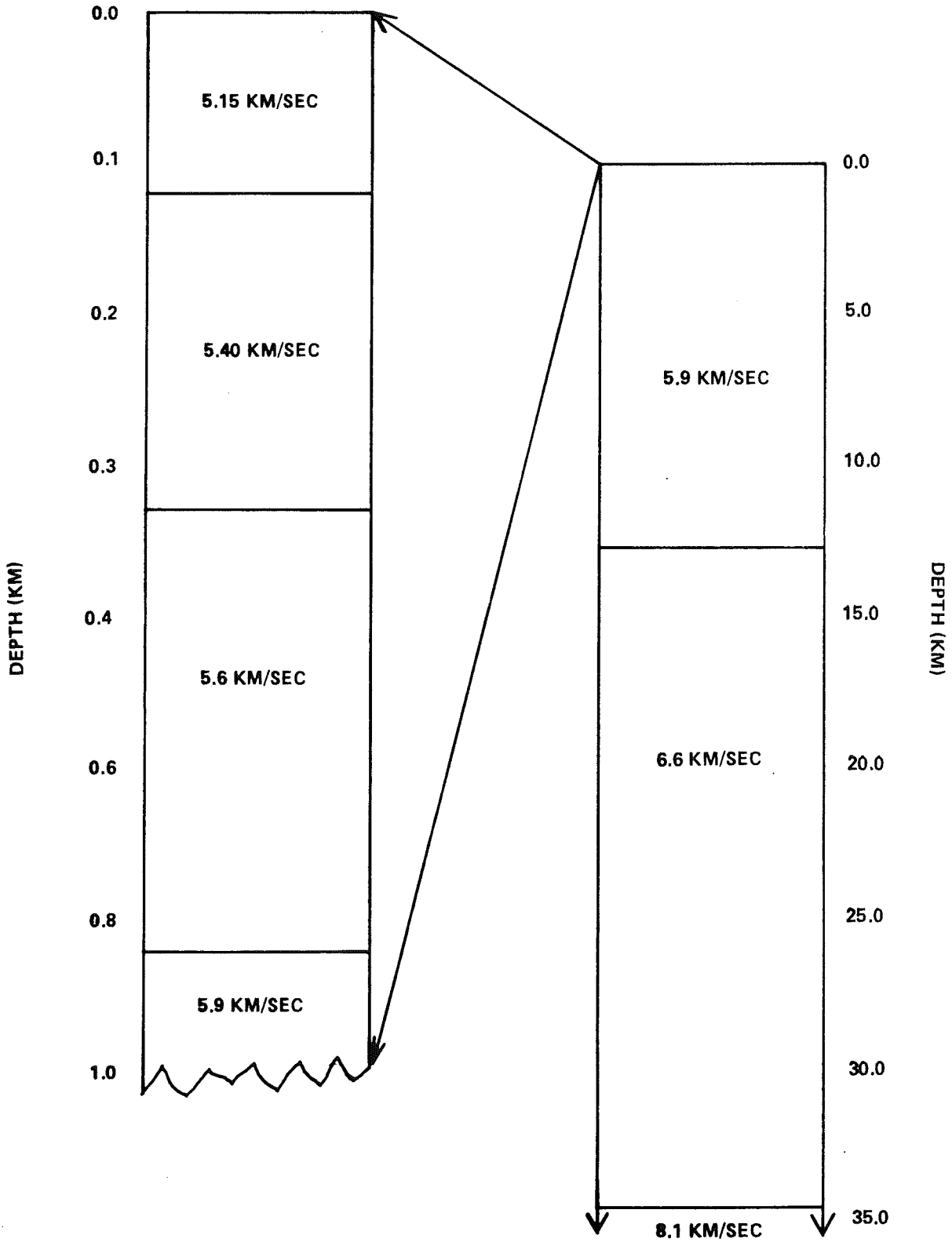
0.0
0.1
0.2
0.3
0.4
0.6
0.8
1.0
DEPTH (KM)
5.15 KM/SEC
5.40 KM/SEC
5.6 KM/SEC
5.9 KM/SEC
0.0
5.0
10.0
15.0
20.0
25.0
30.0
35.0
DEPTH (KM)
5.9 KM/SEC
6.6 KM/SEC
8.1 KM/SEC

FIGURE I–3

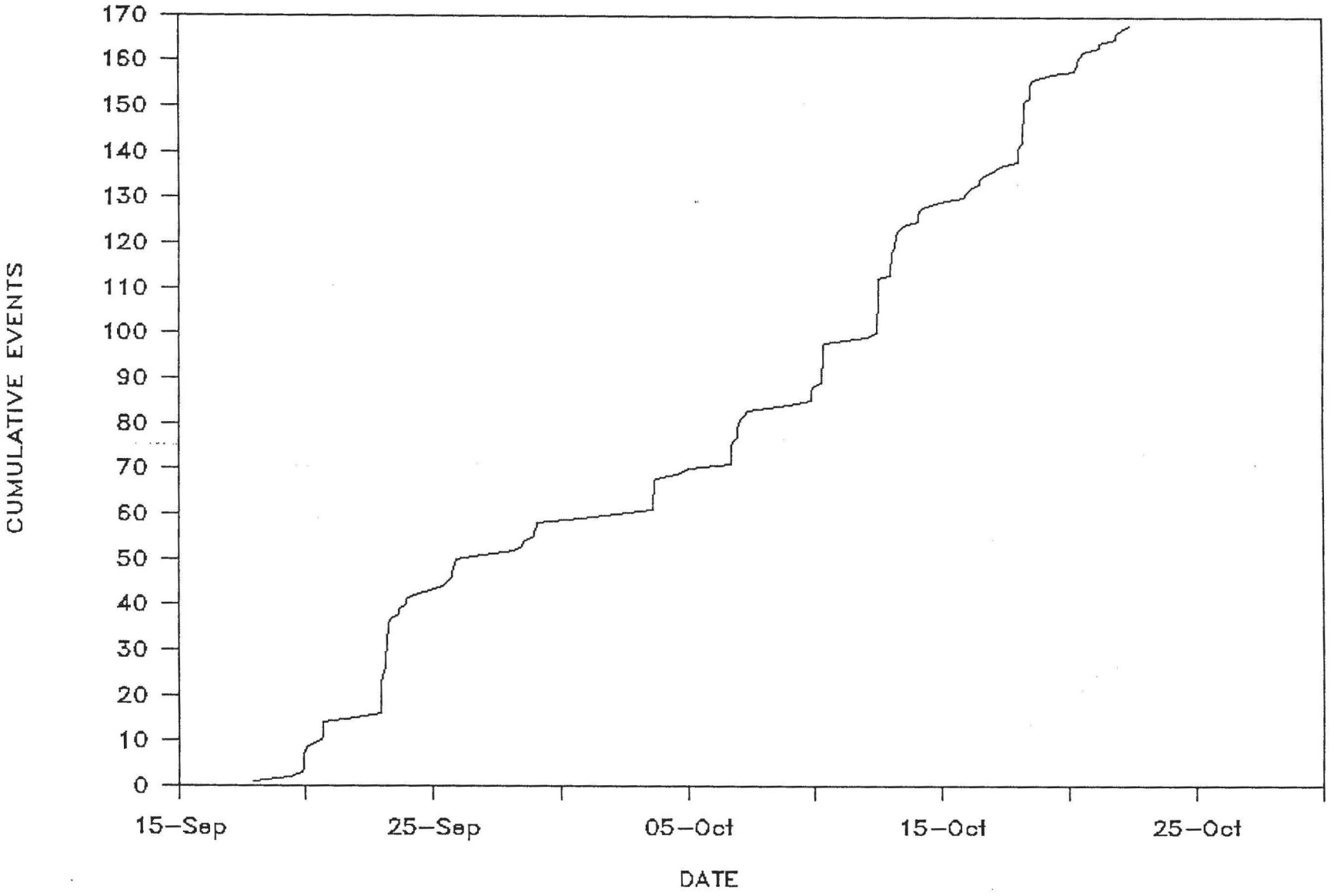
CUMULATIVE EVENTS
170
160
150
140
130
120
110
100
90
80
70
60
50
40
30
20
10
0
15–Sep
25–Sep
05–Oct
15–Oct
25–Oct
DATE

FIGURE I–4A

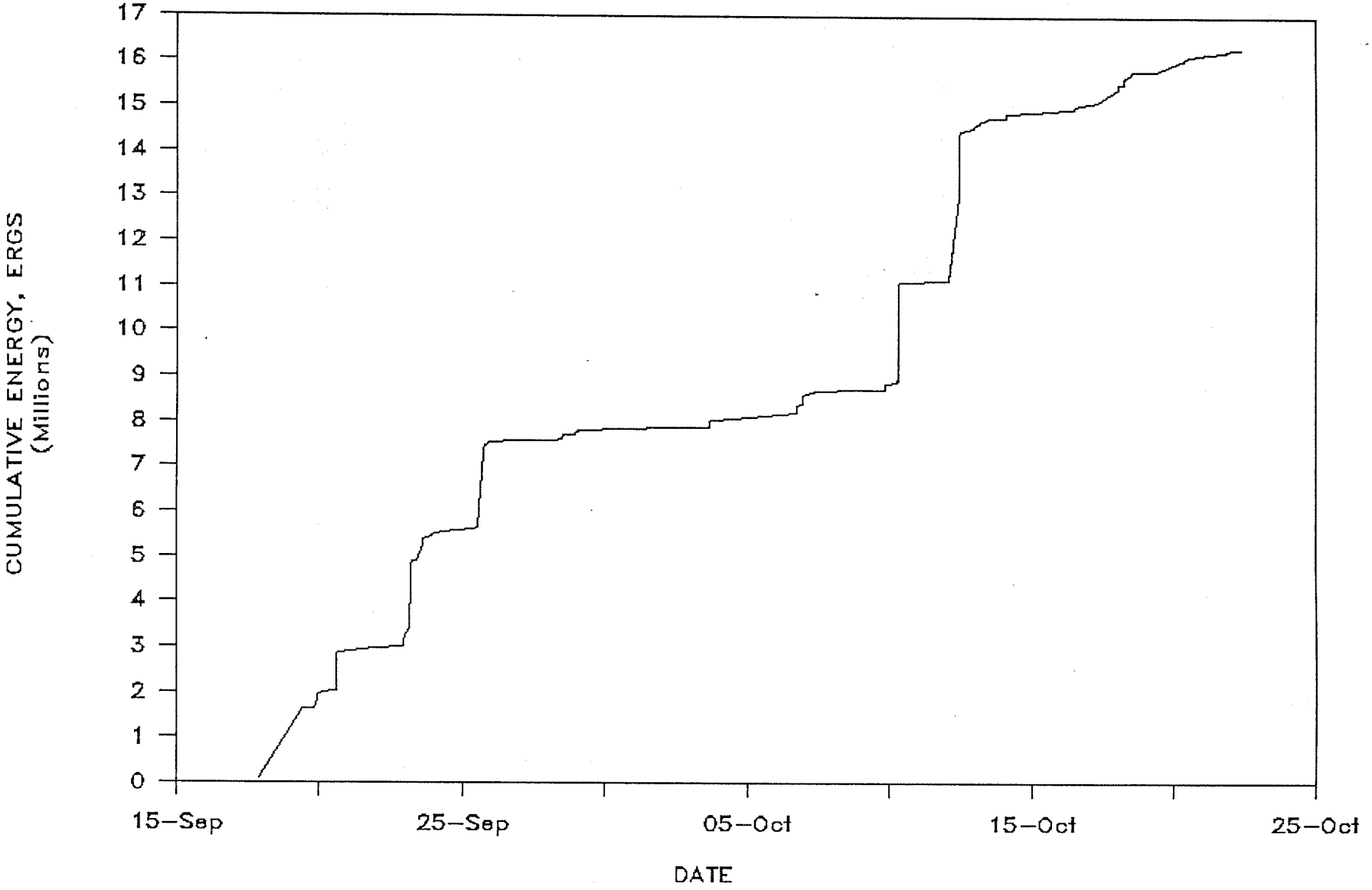
CUMULATIVE ENERGY, ERGS
(Millions)
17
16
15
14
13
12
11
10
9
8
7
6
5
4
3
2
1
0
15–Sep
25–Sep
05–Oct
15–Oct
25–Oct
DATE

FIGURE I–4B

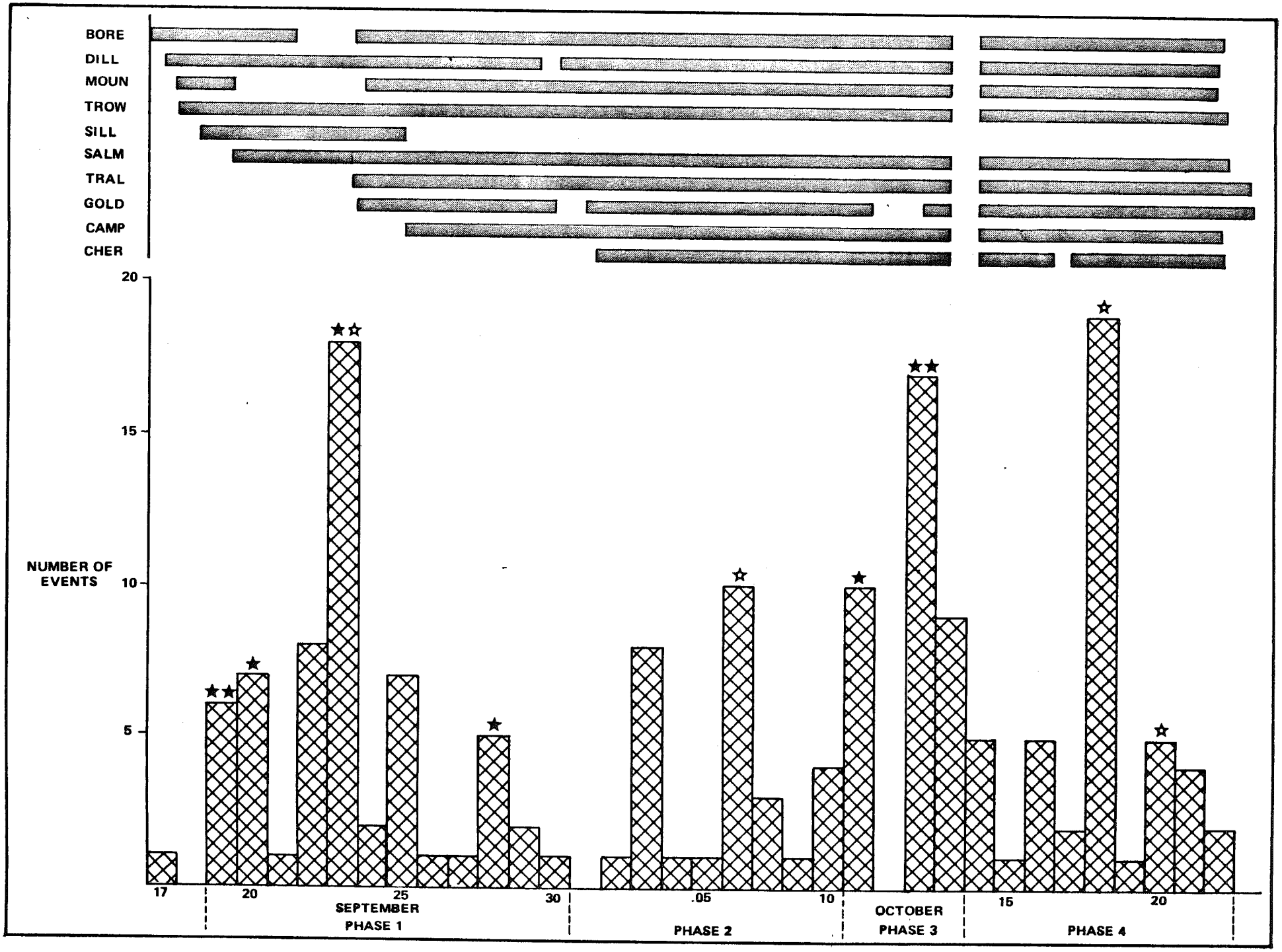
BORE
DILL
MOUN
TROW
SILL
SALM
TRAL
GOLD
CAMP
CHER
20
15
10
5
NUMBER OF EVENTS
17
20
25
30
.05
10
15
20
SEPTEMBER
PHASE 1
PHASE 2
OCTOBER
PHASE 3
PHASE 4

FIGURE I–5

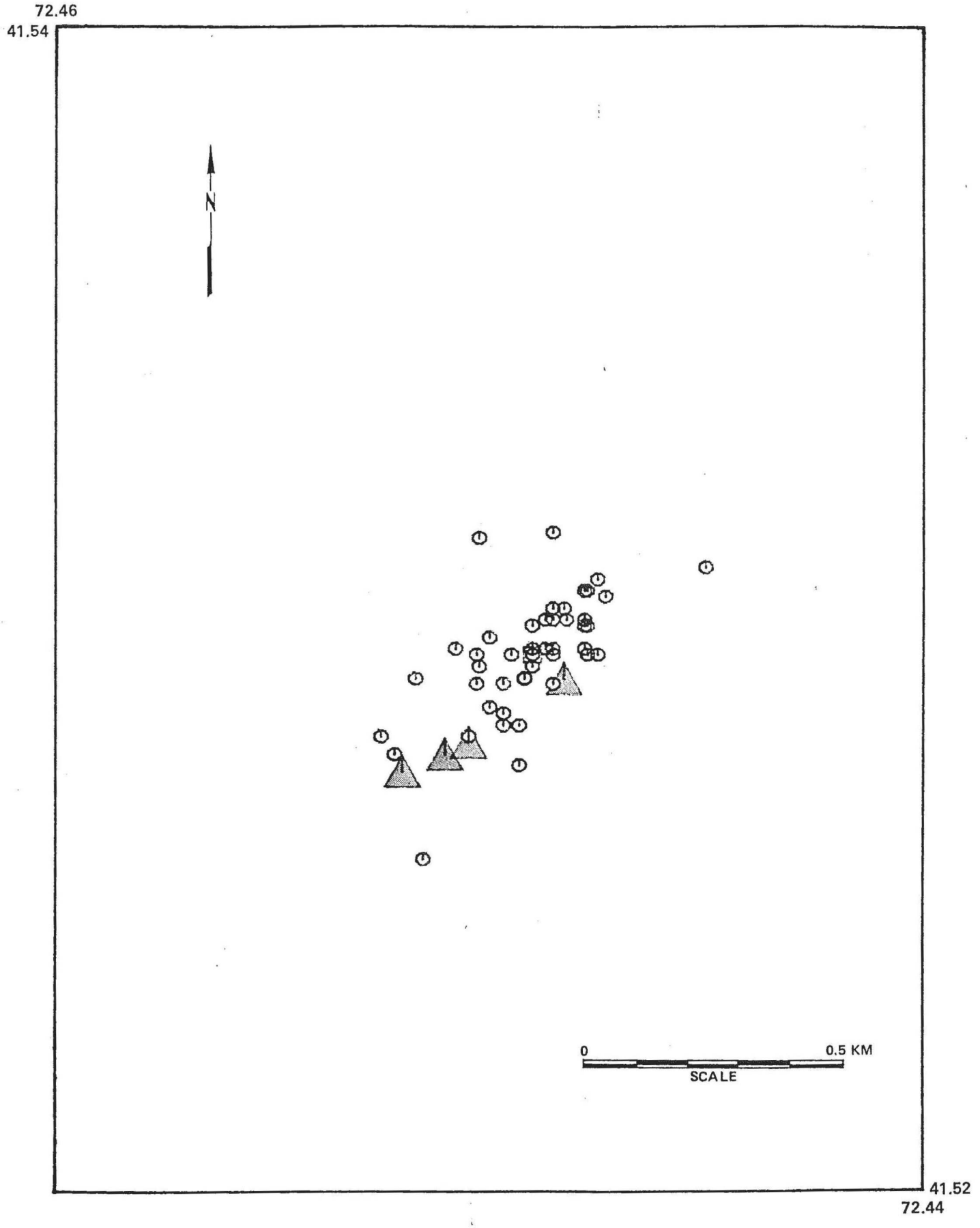

FIGURE I–6

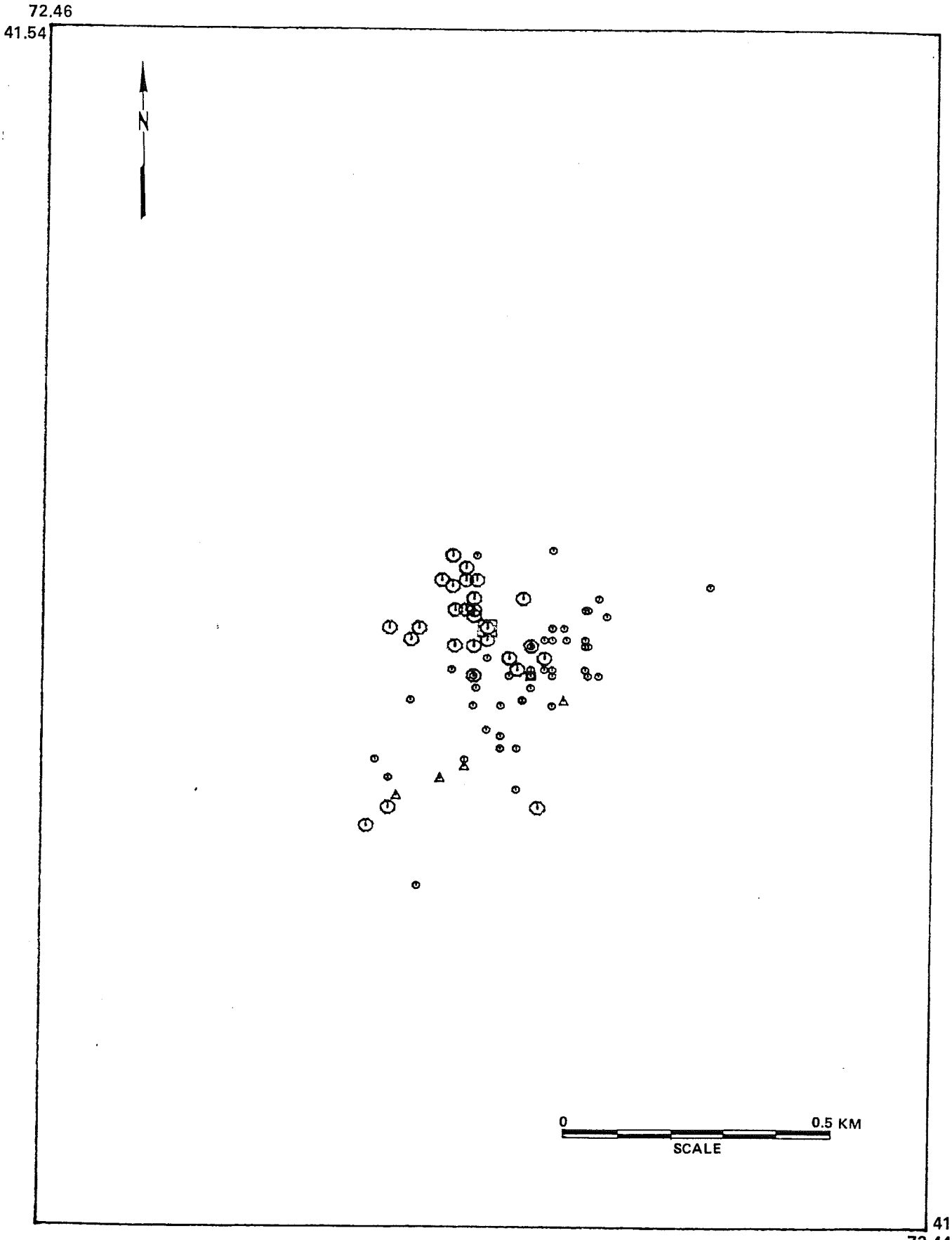

FIGURE I–7

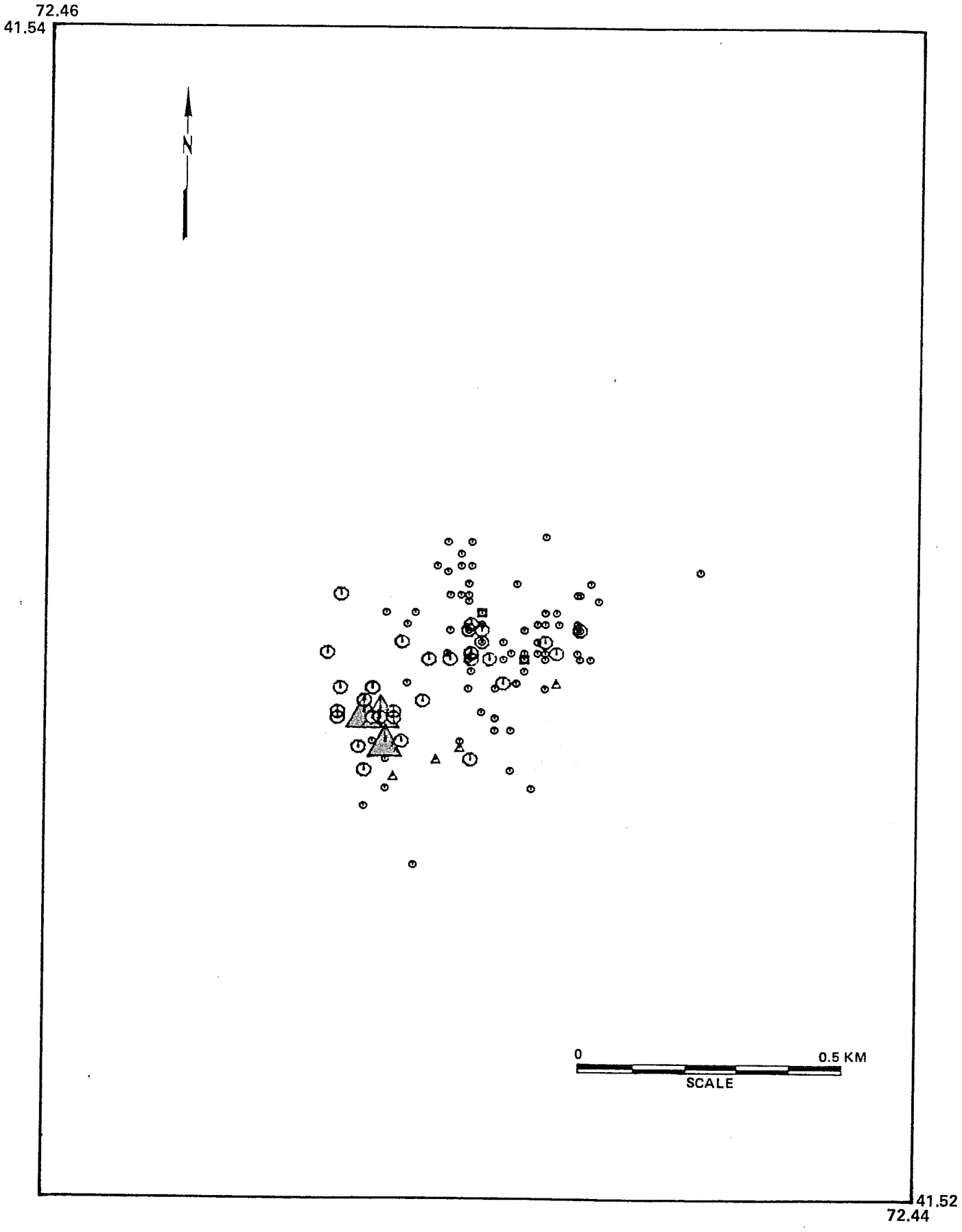

FIGURE I–8

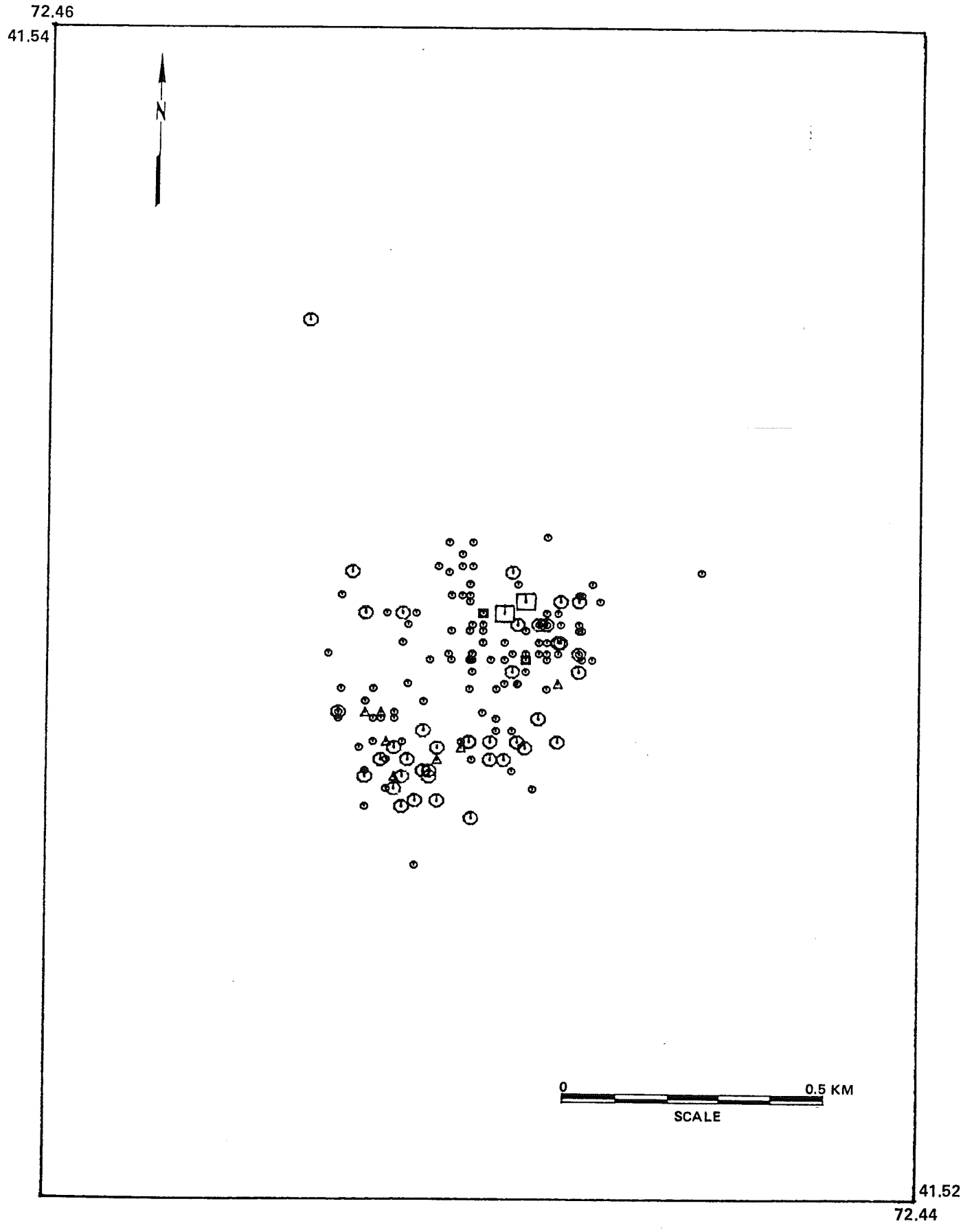

FIGURE I–9

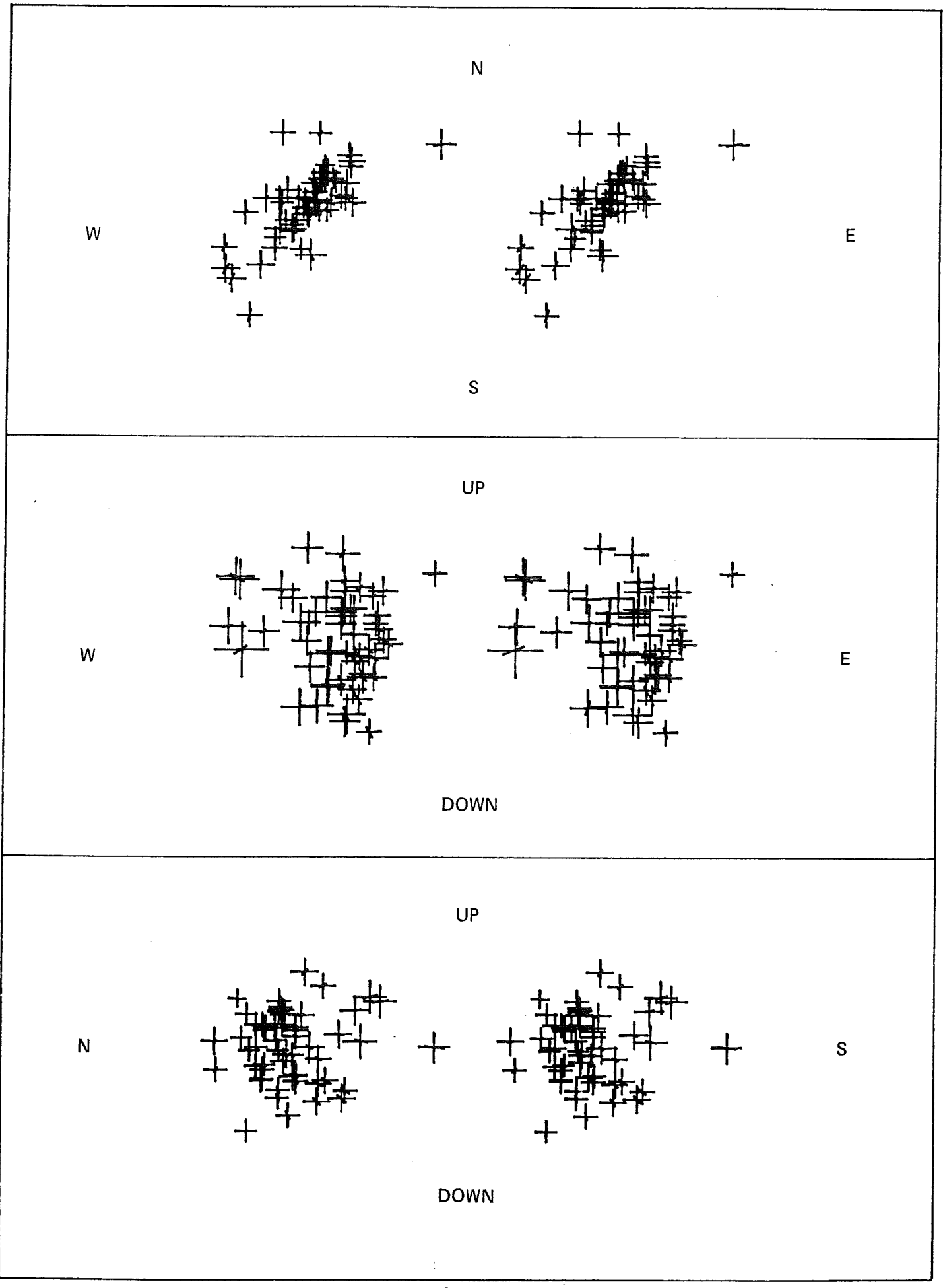

FIGURE I–10

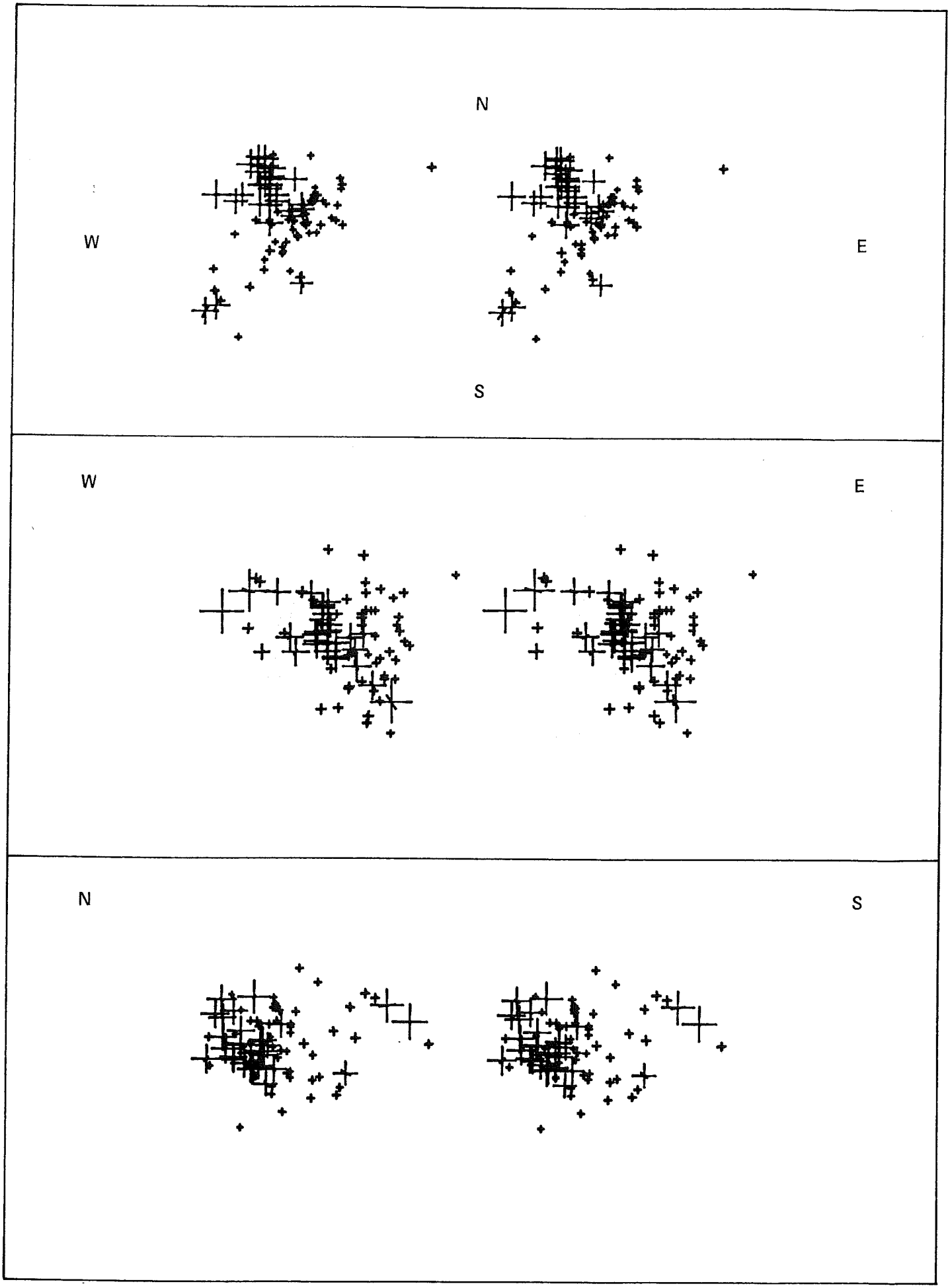

FIGURE I–11

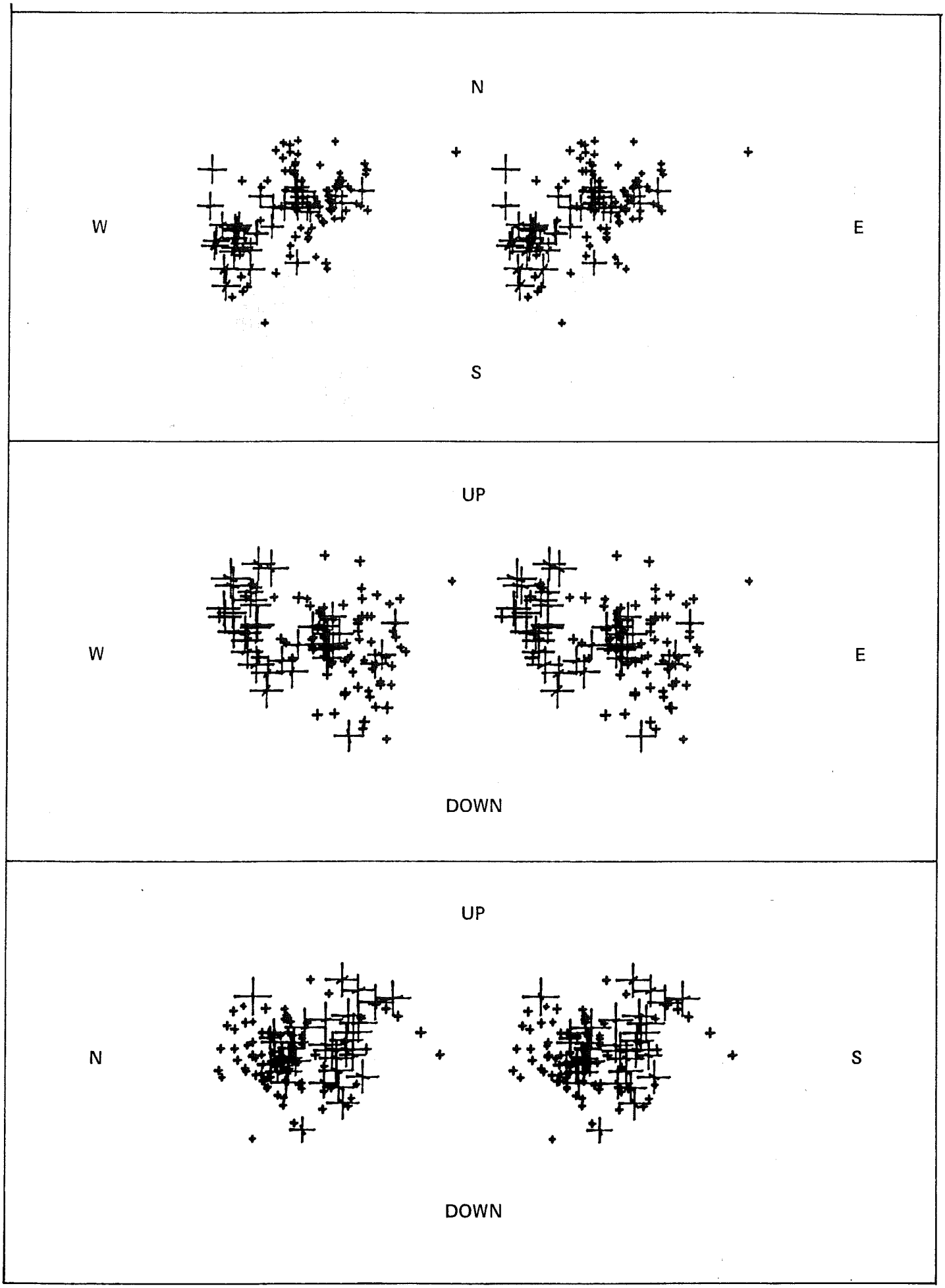

FIGURE I–12

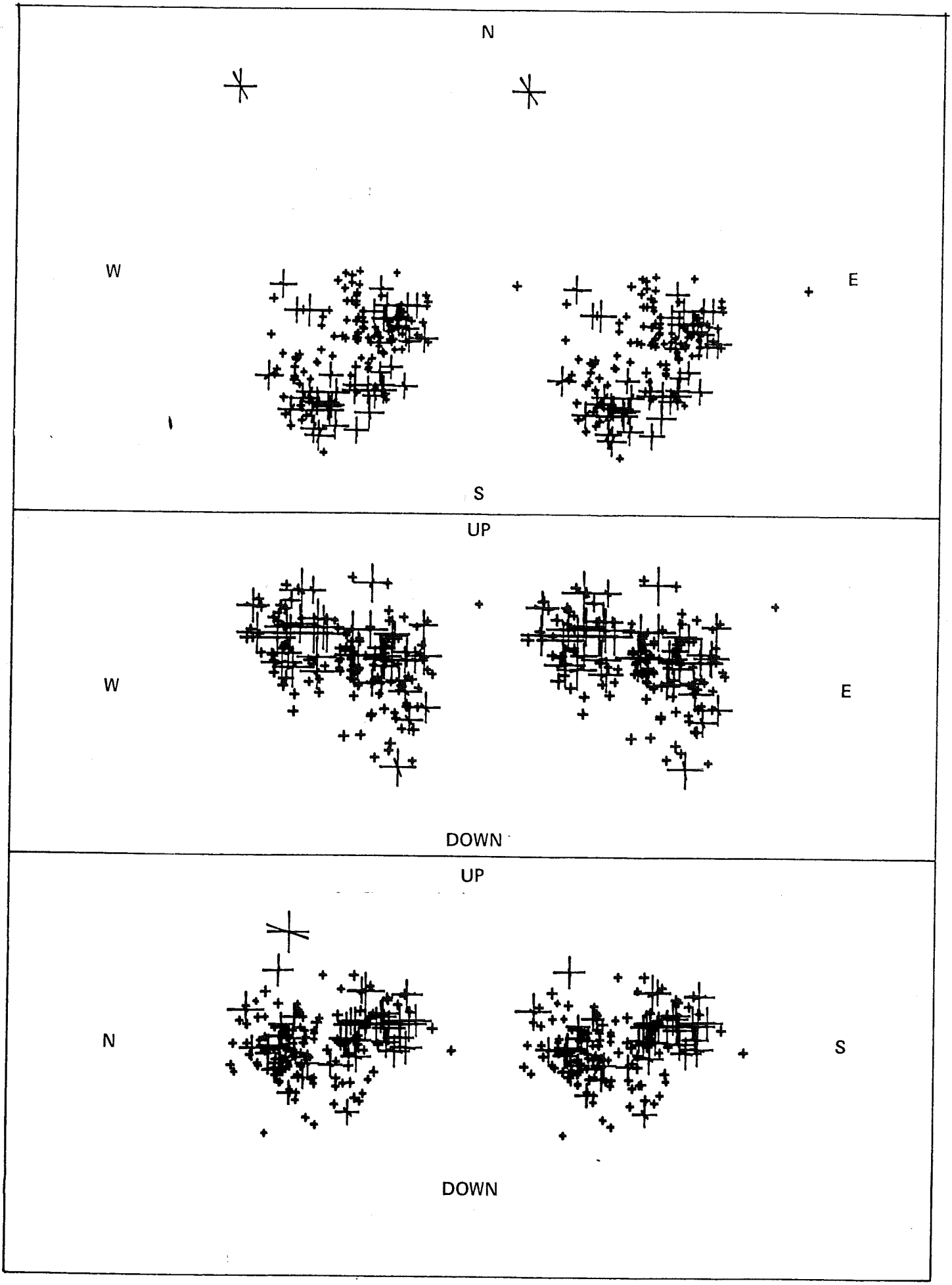

FIGURE I–13

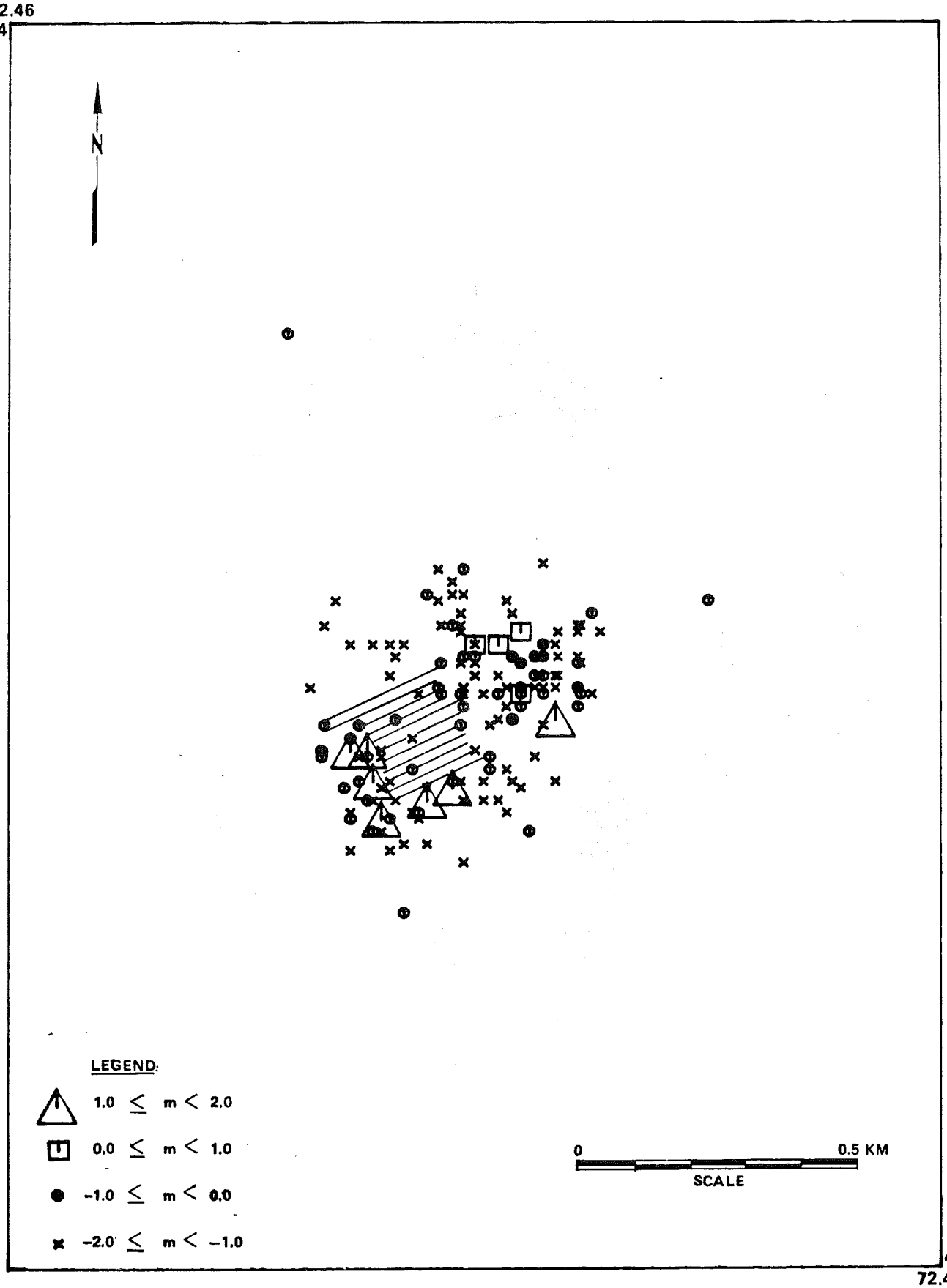
72.46
41.54
N
LEGEND:
1.0 ≤ m < 2.0
0.0 ≤ m < 1.0
-1.0 ≤ m < 0.0
-2.0 ≤ m < -1.0
0
0.5 KM
SCALE
41.52
72.44

FIGURE I–14

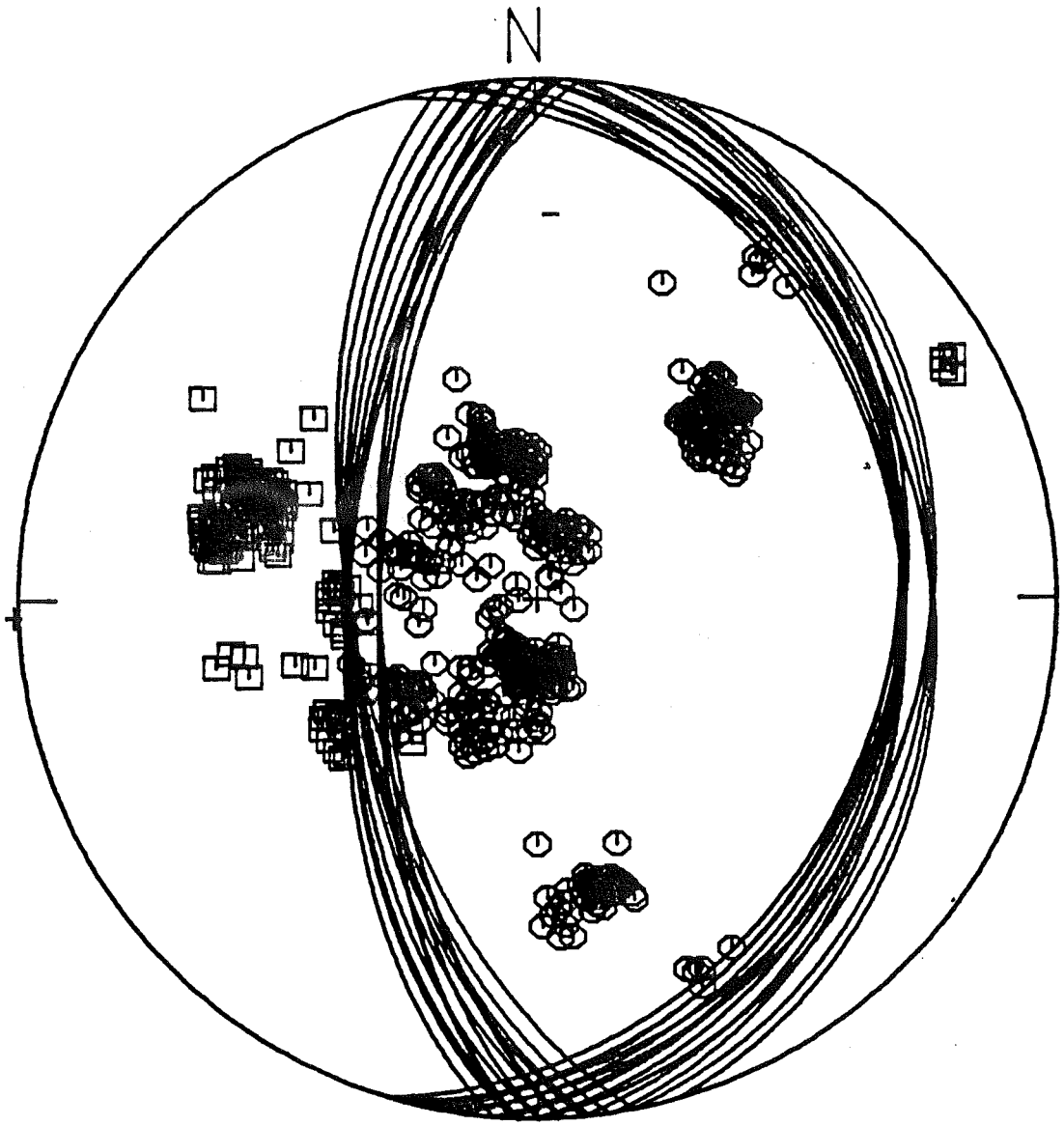

FIGURE I–15

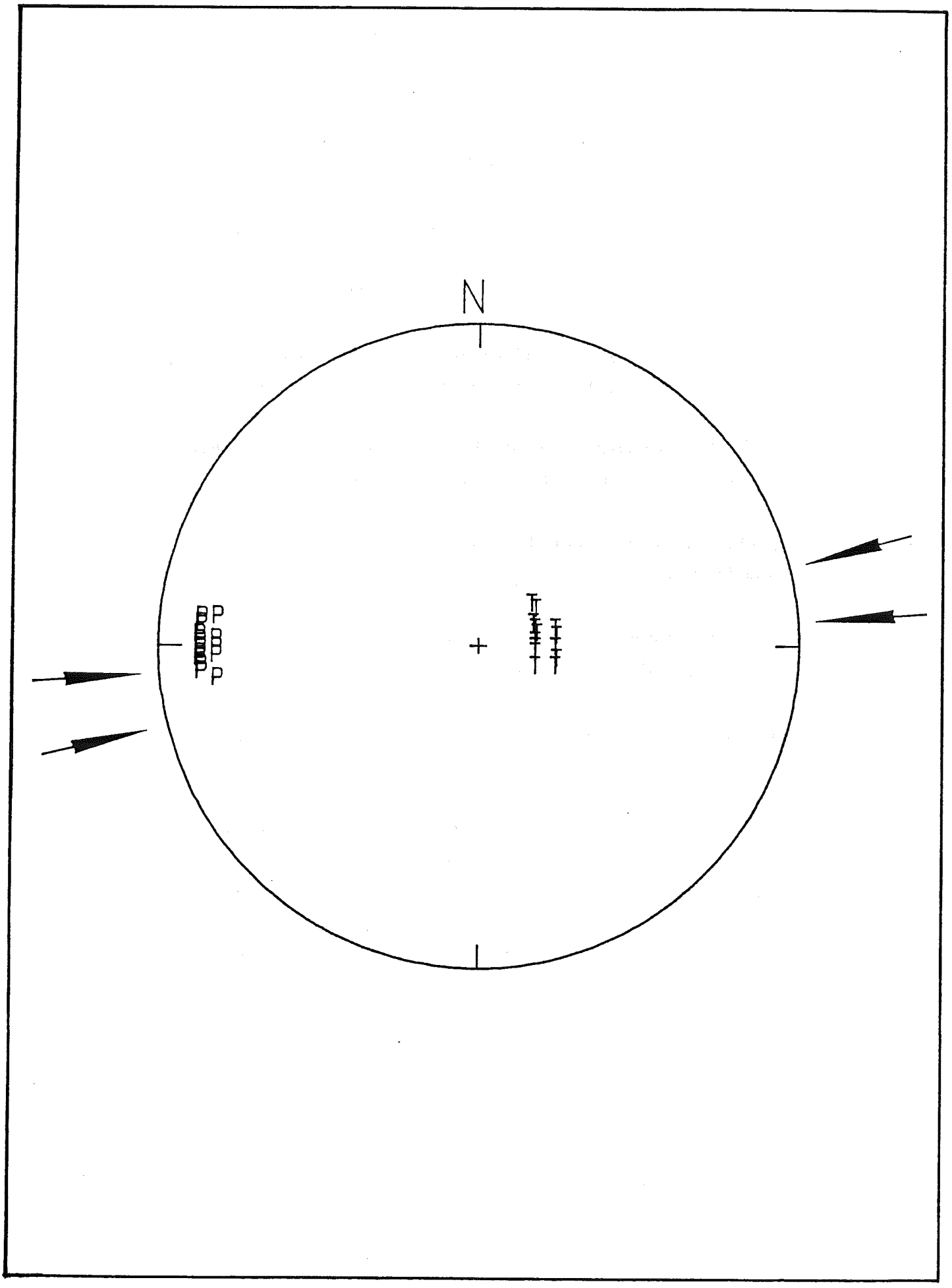

FIGURE I–16

REFERENCES

Chiburis, E.F. and T. Grahm, Seismic Networks in New England, in abstracts with Programs, Vol. 10, No. 2, Northeastern Section of the Geological Society of America, 13th Annual Meeting, p. 36 (abstract).

Chaplin, M.P., Taylor, S.R., and Toksoz, M.N., 1980, A Coda-Length Magnitude Scale for New England, Earthquake Notes, v. 51, No. 4, p. 15-22.

Ebel, J.E., 1988, Comparisons of the 1981, 1982, 1986 and 1987 Swarms at Moodus, Connecticut, Eos transactions, American Geophysical Union, v. 69, p. 495.

Ebel, J.E., Vudler, V., and Celata, M., 1982, The 1981 Earthquake Swarm Near Moodus, Connecticut, Geophysical Research Letters, v. 9, p. 397-400.

Electric Power Research Institute, 1986, Earthquake Catalog for the Central and Eastern United States, Version dated January 1986.

Klein, F.W., 1978, Hypocenter Location Program, HYPOINVERSE, U.S. Geological Survey Open File Report 78-694.

Lee, W.H.K, and Lahr, J.C., 1975, HYPO71 (Revised): A Computer Program for Determining Hypocenter, Magnitude, and First Motion Pattern of Local Earthquakes, U.S. Geological Survey Open File Report 75-311, 113 p.

Pulli, J.J., 1983, Seismicity, Earthquake Mechanisms, and Seismic Wave Attenuation in the Northeastern United States, Massachusetts Institute of Technology, Doctoral Dissertation, 390 pp.

Pulli, J.J., and Toksoz, M.N., 1981, Fault Plane Solutions for Northeastern United States Earthquakes, Bulletin of the Seismological Society of America, v. 71, p. 1875-1882.

REFERENCES
(continued)

Quittmeyer, R.C., Statton, C.T., Mrotek, K.A., and Houlday, M., 1985, Possible Implications of Recent Microearthquakes in Southeastern New York State, Earthquake Notes, v. 56, p. 35-42.

Sbar, M.L., and Sykes, L.R., 1977, Seismicity and Lithospheric Stress in New York and Adjacent Areas, Journal of Geophysical Research, v. 82, p. 5771-5786.

Snoke, J.A., Munsey, J.W., Teague, A.G., and Bollinger, G.A., A Program for Focal Mechanism Determination by Combined Use of Polarity and SV-P Amplitude Ratio Data, Earthquake Notes, v. 55, p. 15, (abstract).

Street, R., and Lacroix, A., 1979, An Empirical Study of New England Seismicity: 1727-1977, Bulletin of the Seismological Society of America, v. 69, p.159-175.

Veneziano, D., and Van Dyke, J., 1985, Magnitude Conversion and Cluster Analysis for the EPRI Catalog (12 Dec. 1985 version), Consulting Report to Risk Engineering, Inc., 20 Decemeber 1985, Electric Power Research Institute/Seismicity Owners Group Probabilistic Seismic Hazard Program for the Central and Eastern United States.

Yang, J.P., and Aggarwal, Y.P., 1981, Seismotectonics of Northeastern United States and Adjacent Canada, Journal of Geophysical Research, v. 86, p. 4981-4998.

Zartman, R.E., and Naylor, R.S., 1984, Structural Implications of Some Radiometric Ages of Igneous Rocks in Southeastern New England, Geological Society of America Bulletin, v. 95, p. 522-539.

REFERENCES
(continued)

Zoback, 1986, In-Situ Stress Measurements in the Kent Cliffs Research Well, in Kent Cliffs Borehole Research Project: A Determination of the Magnitude and Orientation of Tectonic Stress in Southeastern New York, Final Report to the Empire State Electric Energy Research Corporation, Research Report EP 84-27.

Zoback, M.D., Anderson, R.N., and Moos, D., 1985, In Situ Stress Measurements in a 1-Km-Deep Well Near the Ramapo Fault Zone, Eos Transactions, American Geophysical Union, v. 66, p. 363.

Zoback, M.L., and Zoback, M.D., 1980, State of Stress in the Conterminous United States, Journal of Geophysical Research, v. 85, p. 6113-6156.